

**Synthesis of Polyesters by Ring opening  
polymerization and Copolymerization using  
Aluminium and Titanium Complexes**

**Mohammed Ahmed Bahili**



**A thesis submitted to Cardiff University in accordance  
with the requirements for the degree of Doctor of  
Philosophy**

**School of Chemistry**

**Cardiff University**

**United Kingdom**

**November 2017**

## **DECLARATION**

This work has not been submitted in substance for any other degree or award at this or any other university or place of learning, nor is being submitted concurrently in candidature for any degree or other award.

Signed ..... (Mohammed A. Bahili)      Date .....

### **STATEMENT 1**

This thesis is being submitted in partial fulfillment of the requirements for the degree of (PhD)

Signed ..... (Mohammed A. Bahili)      Date .....

### **STATEMENT 2**

This thesis is the result of my own independent work/investigation, except where otherwise stated. Other sources are acknowledged by explicit references. The views expressed are my own.

Signed ..... (Mohammed A. Bahili)      Date .....

### **STATEMENT 3**

I hereby give consent for my thesis, if accepted, to be available for photocopying and for inter-library loan, and for the title and summary to be made available to outside organizations.

Signed ..... (Mohammed A. Bahili)      Date.....

### **STATEMENT 4: PREVIOUSLY APPROVED BAR ON ACCESS**

I hereby give consent for my thesis, if accepted, to be available online in the university's Open Access repository and for inter-library loans after expiry of a bar on access previously approved by the Academic Standards & Quality Committee.

Signed ..... (Mohammed A. Bahili)      Date.....

## ACKNOWLEDGMENTS

Firstly, I would like to express my sincere gratitude to my Supervisor Dr. Ben Ward who has been a tremendous mentor for me. I am truly grateful for his selfless time and care, for his excellent support, guidance and valuable knowledge. Without him none of this work would have been possible.

I would also like to thank Dr. Angelo Amoroso for his advice and help. I would like to thank all the members of staff in inorganic chemistry for their assistance and sharing their knowledge. I would also like to thank all the technical staff at Cardiff University especially Dr. Rob Jenkins for his assistance with special NMR spectroscopic experiments, Robin and Simon for their assistance with mass spectrometry; Sham and James are thanked for their services. I would like to acknowledge Dr. Sankar from Cardiff catalysis institute for allowing me to use his GPC machine. Special thanks should go to Susana, a PhD student with the Sankar group, for the time and efforts she spent with the GPC measurements. I would like to thank all the past and present colleagues and friends in the inorganic section: Mark Driver, Mauro Monti, Mohammed M. Hasson, Ali Al-Riyahee, Emily Langdon-Jones, Emily Stokes, Seni Chappai, Andy Woods, Geraint Roberts and Mark Sullivan for their help, sharing their knowledge and for the enjoyable time we spent in the university.

I am deeply indebted to my beloved parents for their sacrifice, love, care and support for me all my life. No words can express my gratitude towards them. This accomplishment would not have been possible without them. My Father, is sadly no longer with us to be able to see my achievements described in this thesis. I dedicate this thesis to his memory. A big thank you has to go to my brothers, sisters, father-in-law and mother-in-law for their support and encouragement.

I would like to express my deep gratitude to my wife for her unlimited support, encouragement and companionship which turned my time in Cardiff into a pleasure.

Last but not least, I would like to thank the ministry of higher education and scientific research-Iraq and University of Basrah for giving me this opportunity to study a PhD in the UK.

## Abstract

A series of new aluminium(III) and titanium(IV) complexes bearing a series of salen ligands have been prepared; the ligands have not been previously used to support Al or Ti. The complexes have been tested as initiators for polymerization reactions, including both ring-opening polymerization of cyclic esters, and the ring-opening copolymerization of cyclic anhydrides and epoxides.

This thesis has been divided into six chapters:

**Chapter 1** provides an overview of the use of Al and Ti complexes in the ring-opening polymerization of cyclic esters, and the use of Al complexes in the ring-opening copolymerization of cyclic anhydrides and epoxides. An introduction to these catalytic reactions is discussed, along with some background relating to polymer characterization.

**Chapter 2** provides details of the ligand synthesis, and the preparation of the monometallic metal complexes used in the rest of the thesis. A relatively new class of salen-type ligands bearing a hemi-labile pyridyl donor have been prepared and fully characterized. The challenges that accompanied the preparation of some derivatives of the ligand have been discussed, and the identity of the ligands has been supplemented by solid state analysis. Complexes based upon Al and Ti, derived from these ligands, have been reported in this thesis. Their synthesis and characterization in both solution and solid state are reported.

Three types of Al complex have been synthesized: alkyl, alkoxide/aryloxy, and chloride. These complexes have been characterized using NMR spectroscopy, which includes a discussion of the hemi-labile nature of the pyridyl; this was confirmed using variable temperature NMR spectroscopy and equilibrium analysis.

The synthesis and characterization of Ti(IV) isopropoxide complexes is described. NMR spectroscopy, including two dimensional experiments such as COSY, HSQC and HMBC, were instrumental in determining the structures of these complexes.

**Chapter 3** describes how to exploit the complexes described in Chapter 2 as catalysts for the ring-opening polymerization of cyclic esters such as *rac*-lactide and  $\epsilon$ -caprolactone. Both aluminium and titanium showed good to moderate activity in this type of polymerization. Various conditions were investigated in order to obtain the optimum conditions to afford polyester with acceptable molecular weights and polydispersity indices.

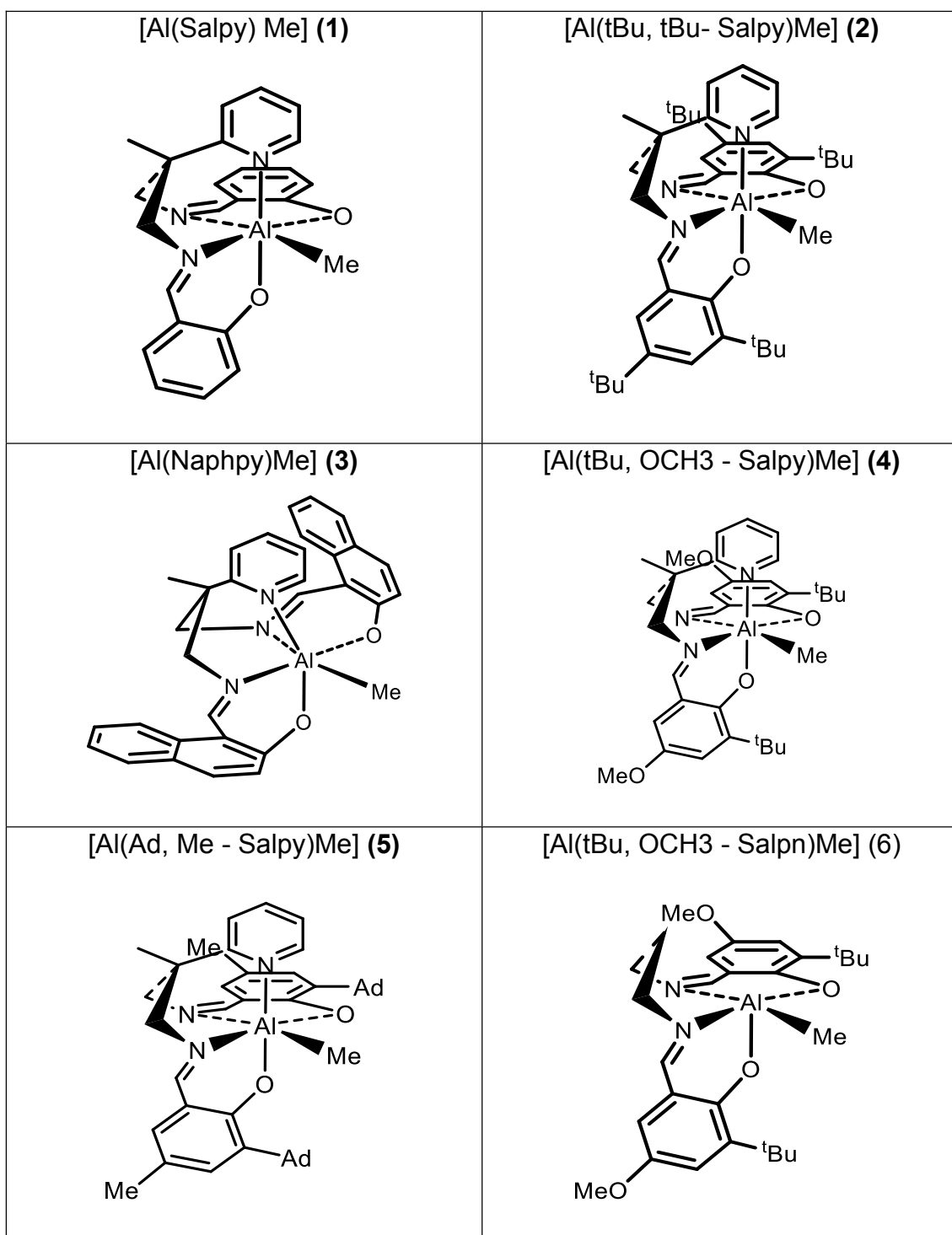
**Chapter 4** describes how to exploit the aluminium chloride complexes described in Chapter 2 in the ring-opening copolymerization of cyclic anhydrides and epoxides, thereby diversifying the range of available polymers (and associated properties) by incorporating various monomers. The copolymerization reaction was investigated under various conditions, including with and without cocatalyst, and the polymers were evaluated using  $^1\text{H}$  NMR spectroscopy and gel permeation chromatography.

**Chapter 5** describes the synthesis and characterization of bimetallic aluminium complexes using the Salpy ligand framework. Three bimetallic aluminium complexes were obtained and were characterized in both solution and in the solid state. The complexes were used as initiators in the ring-opening polymerization of  $\epsilon$ -caprolactone. The polymerization performance was evaluated and the polymers characterised using gel permeation chromatography.

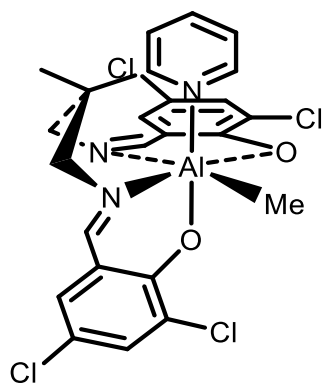
**Chapter 6** contains full experimental details and characterizing data for all ligands and complexes described within the thesis.

## The structures and names of the prepared complexes

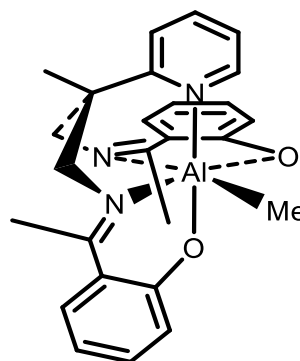
### 1. Aluminium methyl complexes



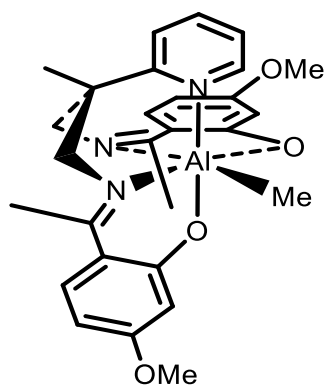
[Al(Cl, Cl - Salpy)Me] (7)



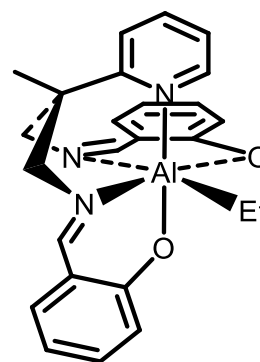
[Al(Acpy)Me] (8)



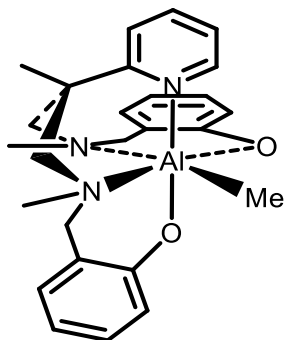
[Al(OMe- Acpy)Me] (9)



[Al(Salpy)Et] (10)

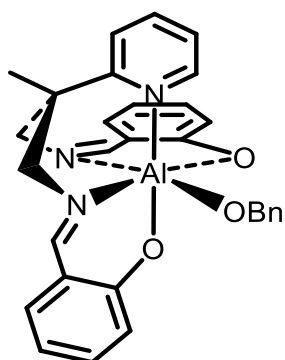


[Al(Salpy-Me)Me] (11)

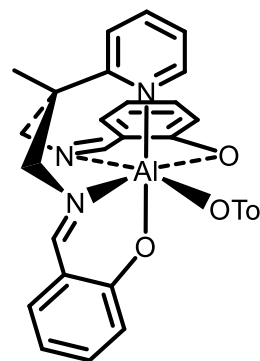


## 2. Aluminium benzyl and tolyl complexes

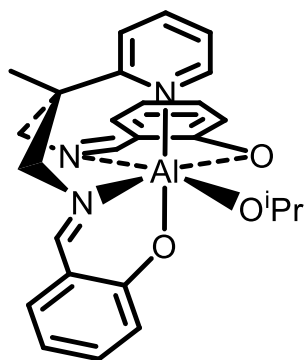
[Al(Salpy)(OBn)] (12)



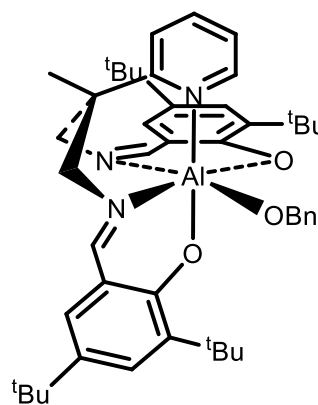
[Al(Salpy)(OTol)] (13)



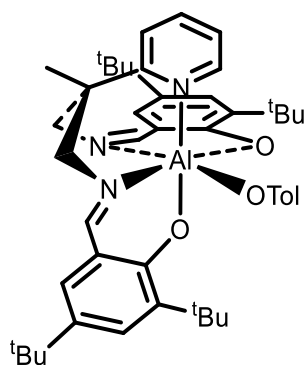
[Al(Salpy)(O<sup>i</sup>Pr)] (14)



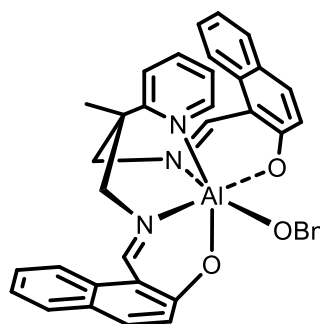
[Al(<sup>t</sup>Bu, <sup>t</sup>Bu-Salpy)(OBn)] (15)



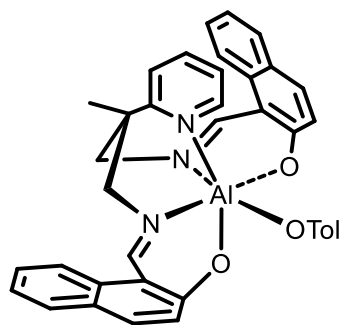
[Al(<sup>t</sup>Bu, <sup>t</sup>Bu-Salpy)(OTol)] (16)



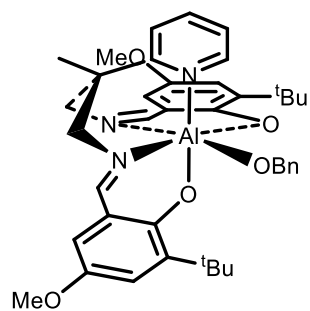
[Al(Naphpy)(OBn)] (17)



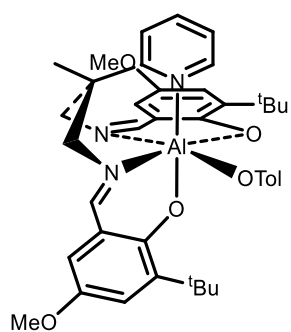
[Al(Naphpy)(OTol)] (**18**)



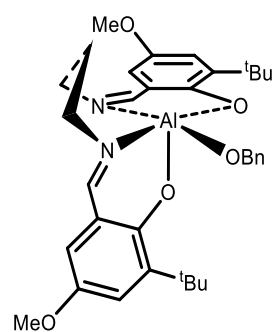
[Al(<sup>t</sup>Bu, OCH<sub>3</sub> - Salpy)(OBn)] (**19**)



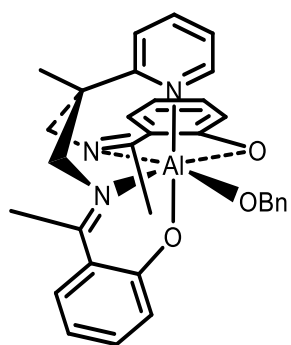
[Al(<sup>t</sup>Bu, OCH<sub>3</sub> - Salpy)(OTol)] (**20**)



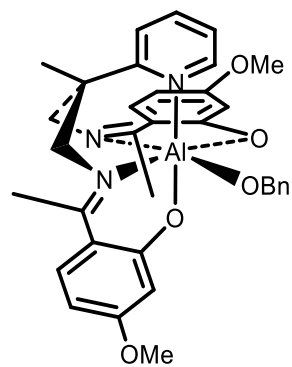
[Al(<sup>t</sup>Bu, OCH<sub>3</sub> - Salpn)(OBn)] (**21**)



[Al(Acpy)(OBn)] (**22**)

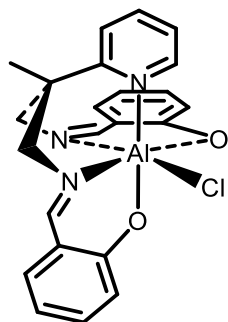


[Al(OCH<sub>3</sub>- Acpy)(OBn)] (**23**)

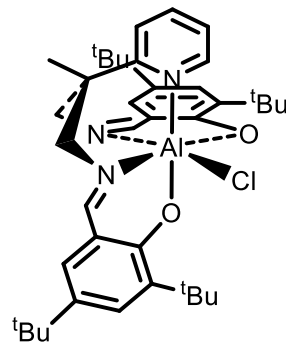


### 3. Aluminum Chloride complexes

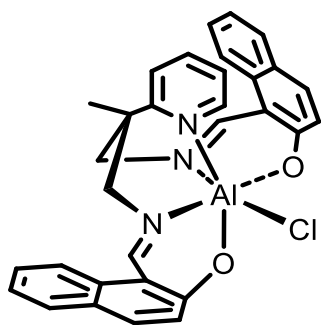
[Al(Salpy)Cl] (**24**)



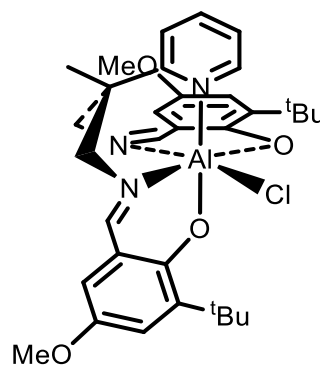
[Al(<sup>t</sup>Bu, <sup>t</sup>Bu-Salpy)Cl] (**25**)



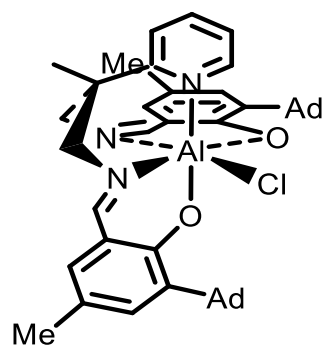
[Al(Naphpy)Cl] (**26**)



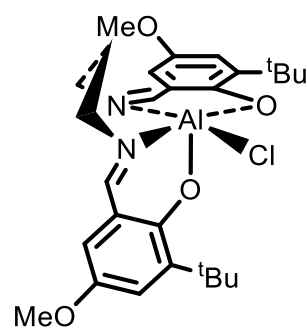
[Al(<sup>t</sup>Bu, OCH<sub>3</sub>-Salpy)Cl] (**27**)



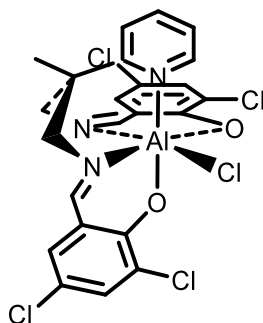
[Al(Ad, Me-Salpy)Cl] (**28**)



[Al(<sup>t</sup>Bu, OCH<sub>3</sub>-Salpn)Cl] (**29**)

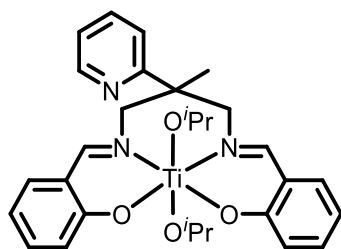


[Al(Cl, Cl - Salpy)Cl] (**30**)

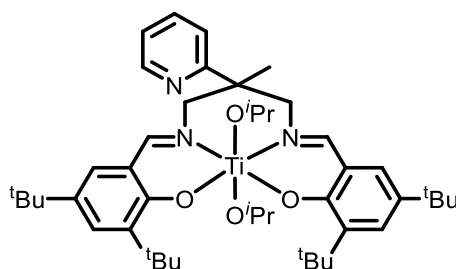


#### 4. Titanium Isopropoxide complexes

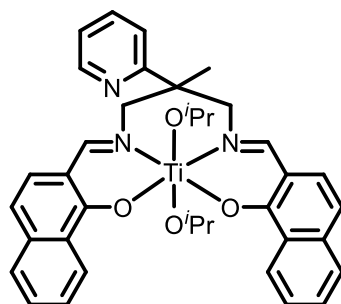
[Ti(Salpy)(O<sup>i</sup>Pr)<sub>2</sub>] (**31**)



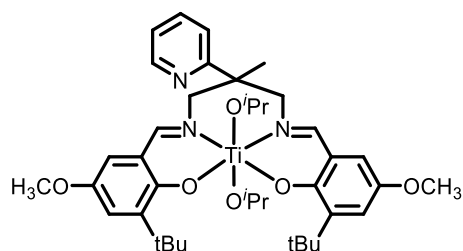
[Ti(<sup>t</sup>Bu, <sup>t</sup>Bu - salpy)(O<sup>i</sup>Pr)<sub>2</sub>] (**32**)

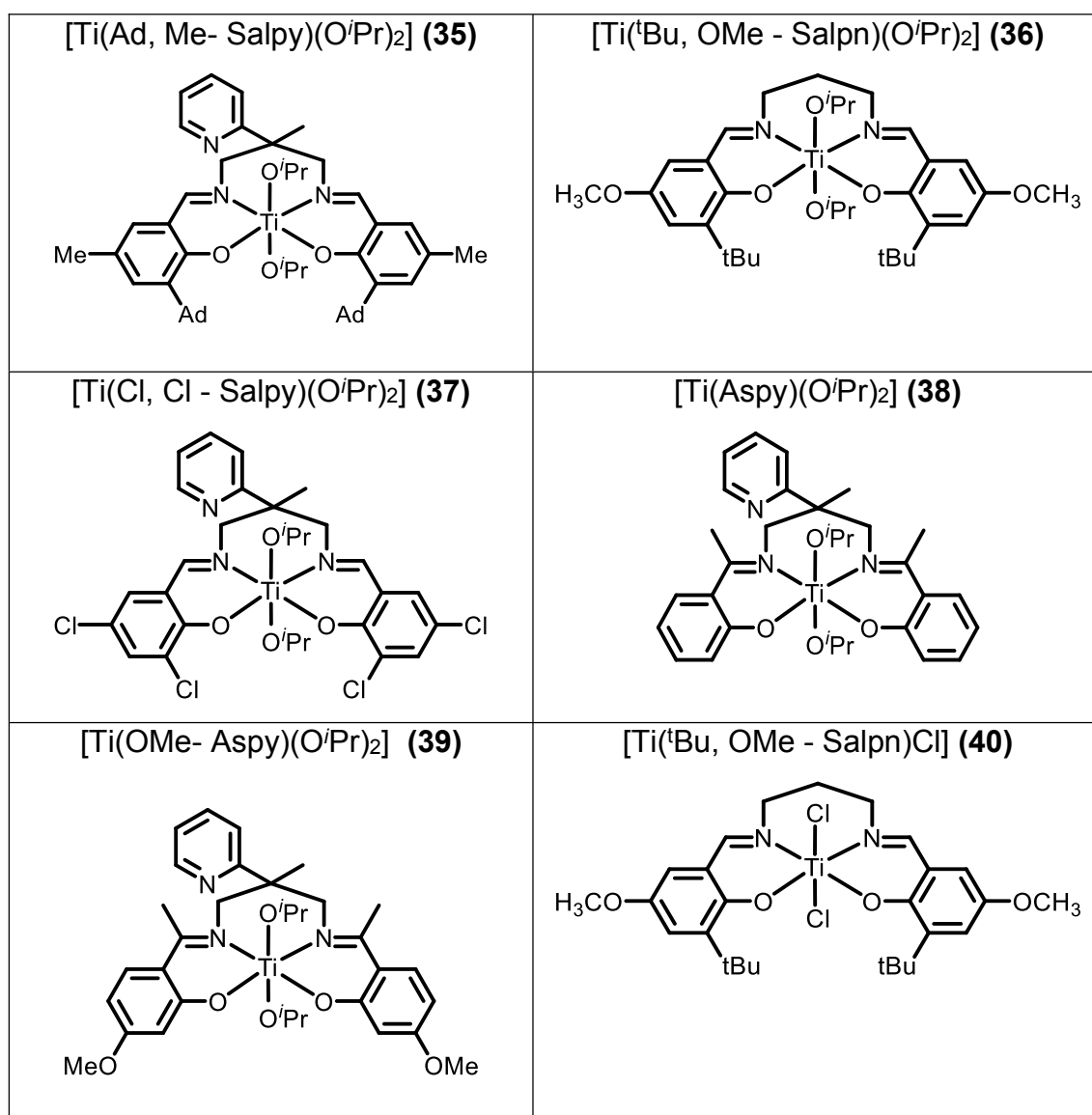


[Ti(Naphpy)(O<sup>i</sup>Pr)<sub>2</sub>] (**33**)



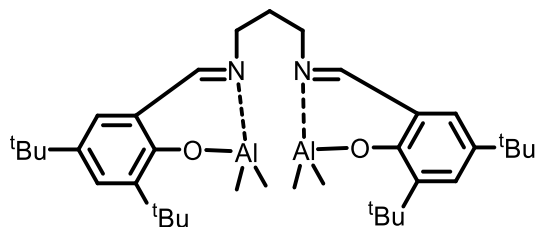
[Ti(<sup>t</sup>Bu, OMe - Salpy)(O<sup>i</sup>Pr)<sub>2</sub>] (**34**)



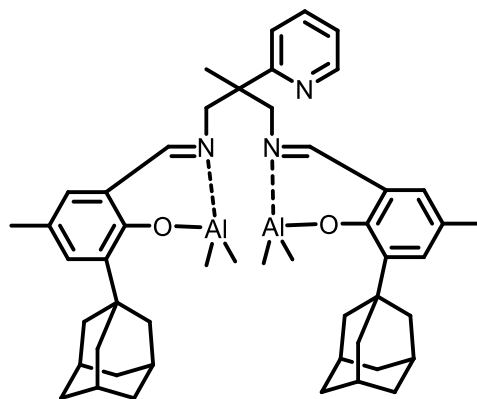


## 5. Bimetallic aluminum complexes

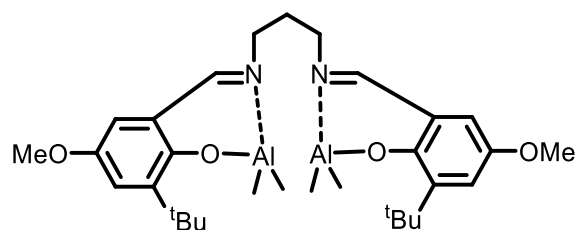
$[\text{Al}_2(\text{}^t\text{Bu}, \text{}^t\text{Bu} - \text{Salpy})\text{Me}_4]$  (41)



$[\text{Al}_2(\text{Ad}, \text{Me} - \text{Salpy})\text{Me}_4]$  (42)



$[\text{Al}_2(\text{}^t\text{Bu}, \text{OMe} - \text{salpn})\text{Me}_4]$  (43)



# Abbreviations

## 1. General

Å	Angstrom
Bn	Benzyl
°C	degrees Celsius
DCM	Dichloromethane
ε-CL	Epsilon-Caprolactone
Et	Ethyl
h	Hour(s)
iPr	Iso-propyl
Me	Methyl
min	Minute(s)
NBO	Natural Bonding orbital
py	Pyridyl
PPDA	2-methyl-2-pyridin-2-yl-propane-1,3-diamine
salen	bis(salicylaldimine)
THF	tetrahydrofuran
<sup>t</sup> Bu	tert-butyl
Tol	p-tolyl, 4-C <sub>6</sub> H <sub>4</sub> Me
vs	Versus

## 2. Spectroscopy

ASAP	Atmospheric Solids Analysis Probe
br	broad
δ	chemical shift in ppm
COSY	Correlation Spectroscopy
J	coupling constant
d	doublet
E.I.	Electron Impact
Hz	Hertz
HMBC	Heteronuclear Multiple Bond Connectivity
HSQC	Heteronuclear Single Quantum Coherence
MS	Mass Spectrometry
m	multiplet
MHz	Megahertz
NMR	Nuclear Magnetic Resonance
ppm	parts per million

q	quartet
sept	septet
s	singlet
t	triplet

### 3. Polymerization

OR	Alkoxy group
R	Alkyl group
CHO	Cyclohexene oxide
GPC	Gel permeation chromatography
I	Initiator
LA	Lactide
MA	Maleic anhydride
M	Monomer
$M_n$	Number-average molecular weight
$M_w$	Weight-average molecular weight
PA	Phthalic anhydride
PDLA	Poly(D-lactide)
PLA	Poly(lactide)
PO	Propylene oxide
<i>rac</i> -LA	Racemic lactide
ROCOP	Ring-opening copolymerization
ROP	Ring-opening polymerization
SEC	Size exclusion chromatography
SA	Succinic anhydride

# Contents

## Chapter 1- An Introduction

1 Introduction .....	2
1.1 Polymers .....	2
1.2 Thermodynamics of Ring-Opening Polymerization .....	5
1.3 Ring-opening polymerization of cyclic esters .....	6
1.3.1 Cationic ring-opening polymerization .....	6
1.3.2 Anionic ring-opening polymerization .....	7
1.3.3 Enzymatic ring-opening polymerization .....	9
1.3.4 Coordination-Insertion ring-opening polymerization .....	9
1.4 Transesterification reaction .....	10
1.5 Ring opening polymerization of caprolactone and lactide .....	12
1.6 Determination of the the stereosequence distribution in the PLA.....	16
1.7 Catalysts in ring opening polymerization of CL and LA and their reactivity .	19
1.8 Bimetallic aluminium complexes .....	26
1.9 Titanium complexes .....	29
1.10 Molecular weight determination.....	31
1.11 Ring opening copolymerization (ROCOP).....	34
1.12 Conclusions and objectives for this thesis.....	39
1.13 References.....	40

## Chapter 2- Synthesis, Characterization, and X-ray Crystal Structures of Salpy, Acpy and Salpn type Ligands, and their Complexes with Aluminium and Titanium

2.1 Introduction .....	51
2.2 Synthesis and characterization of Ligands .....	52
2.2.1 Synthesis and characterizations of dianionic salen type ligands .....	52

2.2.2 Reduction of Schiff base compounds (synthesis of secondary diamine H <sub>2</sub> - Salpy and alkylation of secondary amine CH <sub>3</sub> -Salpy).....	60
2.2.3 Synthesis of neutral symmetrical ligands .....	62
2.3 Synthesis and characterization of aluminium complexes .....	66
2.3.1 Aluminium methyl complexes .....	66
2.3.1.1 Synthesis and spectroscopic characterization .....	66
2.3.1.2 Crystallographic characterisation of aluminium methyl complexes ...	80
2.3.2 Alkoxide and phenoxide Aluminium complexes .....	89
2.3.2.1 Synthesis and spectroscopic characterization .....	89
2.3.2.2 Crystallographic characterisation of aluminium alkoxide and phenoxide complexes .....	94
2.3.3 Aluminium chloride complexes .....	102
2.3.3.1 Synthesis and spectroscopic characterization .....	102
2.3.3.2 Measurement of activation parameters.....	106
2.3.3.3 Crystallographic studies of aluminium Chloride complexes .....	111
2.4 Synthesis and characterization of titanium complexes.....	116
2.4.1 Titanium isopropoxide complexes .....	116
2.4.1.1 Synthesis and spectroscopic characterization .....	116
2.4.1.2 Crystallographic studies of titanium isopropoxide complexes.....	122
2.4.2 Titanium chloride complexes (synthesis and characterization of [Ti( <sup>t</sup> Bu, OCH <sub>3</sub> - salpn)(Cl) <sub>2</sub> ] ( <b>29</b> )).....	129
2.5 Conclusions .....	131
2.6 References.....	133

### **Chapter 3- Ring opening polymerization of $\epsilon$ -Caprolactone and *Rac*-Lactide**

3.1 Ring-opening polymerisation using aluminium complexes.....	138
3.1.1 Introduction .....	138
3.1.2 $\epsilon$ -caprolactone polymerization.....	139

3.1.2.1	General procedure for $\epsilon$ -caprolactone polymerization .....	139
3.1.2.2	Characterization and evaluation of the polymer products .....	139
3.1.2.3	Aluminium methyl complexes as initiator for ROP of Caprolactone	141
3.1.2.4	Polymerization of $\epsilon$ -CL Using aluminium benzyloxy complexes .....	153
3.1.2.5	Ring opening polymerization of Caprolactone using phenoxide complexes. ....	158
3.1.2.6	The effect of cocatalyst on the ROP of $\epsilon$ -CL using [Al(Salpy)Me] (1) .....	164
3.1.2.7	Density functional calculations of polymerization mechanism .....	169
3.1.3	Racemic lactide (Rac-LA) Polymerization .....	171
3.1.3.1	General procedure for Rac-LA polymerization.....	171
3.1.3.2	Characterization and evaluation of the polymer products .....	172
3.1.3.3	Aluminium methyl complexes as initiator for ROP of rac-lactide.....	173
3.1.3.4	Aluminium benzyloxy complexes as initiators for the ROP of rac-lactide .....	179
3.1.3.5	Stereochemistry of the prepared polylactides .....	181
3.2	Ring-opening polymerisation using titanium complexes.....	186
3.2.1	Introduction .....	186
3.2.2	General polymerisation procedure .....	187
3.2.3	Result and discussion .....	188
3.3	Conclusions .....	201
3.4	References.....	202

#### **Chapter 4- Copolymerization of epoxide with cyclic anhydride**

4.1	Introduction .....	210
4.2	Anhydrides, Epoxide and cocatalysts.....	212
4.3	General procedure for Copolymerization of Anhydrides and CHO.....	215
4.4	Result and discussion .....	217
4.5	Density functional calculations .....	238

4.6 Conclusion .....	242
4.7 References.....	243
<b>Chapter 5- Bimetallic aluminium complexes: Synthesis, characterization, X-ray crystal structures and ring opening polymerization</b>	
5.1 Introduction .....	249
5.2 Synthesis and characterization of bimetallic aluminium methyl complexes [Al <sub>2</sub> ( <sup>t</sup> Bu, <sup>t</sup> Bu-Salpy)Me <sub>4</sub> ] ( <b>41</b> ), [Al <sub>2</sub> (Ad,Me-Salpy)Me <sub>4</sub> ] ( <b>42</b> ), and [Al <sub>2</sub> ( <sup>t</sup> Bu,OMe- salpn)Me <sub>4</sub> ] ( <b>43</b> ).....	251
5.3 Crystallographic studies of bimetallic aluminium methyl complexes .....	255
5.4. Ring opening polymerization using Bimetallic aluminium complexes .....	260
5.5 Lactide polymerization .....	270
5.6 Conclusion .....	271
5.7 References.....	272

### Chapter 6- Experimental

Chapter 6 .....	274
Experimental .....	274
6.1 General Methods and Instrumentation .....	275
6.2 Ligand Synthesis.....	277
6.2.1 synthesis of Salpy <sup>(1)</sup> .....	277
6.2.2 Synthesis of Salpy-H <sub>2</sub> .....	278
6.2.3 Synthesis of Salpy-Me .....	279
6.2.4 Synthesis of <sup>t</sup> Bu, <sup>t</sup> Bu - Salpy .....	280
6.2.5 Synthesis of Naphpy .....	281
6.2.6 Synthesis of 3-tert-butyl-5-methoxy salicylaldehyde <sup>2</sup> .....	282
6.2.7 Synthesis of <sup>t</sup> Bu, OMe- Salpy .....	283
6.2.8 Synthesis of 2-Adamantyl-4-methylphenol <sup>3</sup> .....	284
6.2.9 Synthesis of 3-adamantyl-2-hydroxy-5- methylbenzaldehyde <sup>3</sup> .....	285

6.2.10 Synthesis of Ad, Me- Salpy.....	286
6.2.11 Synthesis of <sup>t</sup> Bu, OMe- Salpn .....	287
6.2.12 Synthesis of Cl, Cl- Salpy .....	288
6.2.13 Synthesis of Acpy .....	289
6.2.14 Synthesis of OMe- Acpy .....	290
6.2.15 Synthesis of Pypy .....	291
6.2.16 Synthesis of Qupy .....	291
6.3 Aluminum complexes .....	292
6. 3. 1. Aluminum methyl complexes .....	292
6.3.1.1 Synthesis of [Al(Salpy) Me] <b>(1)</b> .....	292
6.3.1.2 Synthesis of [Al( <sup>t</sup> Bu, <sup>t</sup> Bu- Salpy)Me] <b>(2)</b> .....	293
6.3.1.3 Synthesis of [Al(Naphpy)Me] <b>(3)</b> .....	294
6.3.1.4 Synthesis of [Al( <sup>t</sup> Bu, OCH <sub>3</sub> - Salpy)Me] <b>(4)</b> .....	294
6.3.1.5 Synthesis of [Al(Ad, Me - Salpy)Me] <b>(5)</b> .....	295
6.3.1.6 Synthesis of [Al( <sup>t</sup> Bu, OCH <sub>3</sub> - Salpn)Me] <b>(6)</b> .....	296
6.3.1.7 Synthesis of [Al(Cl, Cl - Salpy)Me] <b>(7)</b> .....	296
6.3.1.8 Synthesis of [Al(Acpy)Me] <b>(8)</b> .....	297
6.3.1.9 Synthesis of [Al(OMe- Acpy)Me] <b>(9)</b> .....	298
6.3.1.10 Synthesis of [Al(Salpy)Et] <b>(10)</b> .....	298
6.3.1.11 Synthesis of [Al(Salpy-Me)Me] <b>(11)</b> .....	299
6.3.2. Aluminium alkoxide and aryloxide complexes .....	299
6.3.2.1 Synthesis of [Al(Salpy)(OBn)] <b>(12)</b> .....	299
6.3.2.2 Synthesis of [Al(Salpy)(OTol)] <b>(13)</b> .....	300
6.3.2.3 Synthesis of [Al(Salpy)(OiPr)] <b>(14)</b> .....	301
6.3.2.4 Synthesis of [Al( <sup>t</sup> Bu, <sup>t</sup> Bu- Salpy)(OBn)] <b>(15)</b> .....	301
6.3.2.5 Synthesis of [Al( <sup>t</sup> Bu, <sup>t</sup> Bu- Salpy)(OTol)] <b>(16)</b> .....	302
6.3.2.6 Synthesis of [Al(Naphpy)(OBn)] <b>(17)</b> .....	303

6.3.2.7 Synthesis of [Al(Naphpy)(OTol)] <b>(18)</b> .....	304
6.3.2.8 Synthesis of [Al( <sup>t</sup> Bu, OCH <sub>3</sub> - Salpy)(OBn)] <b>(19)</b> .....	304
6.3.2.9 Synthesis of [Al( <sup>t</sup> Bu, OCH <sub>3</sub> - Salpy)(OTol)] <b>(20)</b> .....	305
6.3.2.10 Synthesis of [Al( <sup>t</sup> Bu, OCH <sub>3</sub> - Salpn)(OBn)] <b>(21)</b> .....	306
6.3.2.11 Synthesis of [Al(Acpy)(OBn)] <b>(22)</b> .....	306
6.3.2.12 Synthesis of [Al(OCH <sub>3</sub> - Acpy)(OBn)] <b>(23)</b> .....	307
6.3.3. Aluminum Chloride complexes .....	307
6.3.3.1 Synthesis of [Al(Salpy) Cl] <b>(24)</b> .....	307
6.3.3.2 Synthesis of [Al( <sup>t</sup> Bu, <sup>t</sup> Bu- Salpy)Cl] <b>(25)</b> .....	308
6.3.3.3 Synthesis of [Al(Naphpy)Cl] <b>(26)</b> .....	309
6.3.3.4 Synthesis of [Al( <sup>t</sup> Bu, OCH <sub>3</sub> - Salpy)Cl] <b>(27)</b> .....	310
6.3.3.5 [Al(Ad, Me - Salpy)Cl] <b>(28)</b> .....	311
6.3.3.6 Synthesis of [Al( <sup>t</sup> Bu, OCH <sub>3</sub> - Salpn)Cl] <b>(29)</b> .....	312
6.3.3.7 Synthesis of [Al(Cl, Cl - Salpy)Cl] <b>(30)</b> .....	312
6.4 Titanium Isopropoxide complexes .....	313
6.4.1 Synthesis of [Ti(Salpy)(O <sup>i</sup> Pr) <sub>2</sub> ] <b>(31)</b> .....	313
6.4.2 Synthesis of [Ti( <sup>t</sup> Bu, <sup>t</sup> Bu - salpy)(O <sup>i</sup> Pr) <sub>2</sub> ] <b>(32)</b> .....	314
6.4.3 Synthesis of [Ti(Naphpy)(O <sup>i</sup> Pr) <sub>2</sub> ] <b>(33)</b> .....	315
6.4.4 Synthesis of [Ti( <sup>t</sup> Bu, OMe - Salpy)(O <sup>i</sup> Pr) <sub>2</sub> ] <b>(34)</b> .....	316
6.4.5 Synthesis of [Ti(Ad, Me- Salpy)(O <sup>i</sup> Pr) <sub>2</sub> ] <b>(35)</b> .....	318
6.4.6 Synthesis of [Ti( <sup>t</sup> Bu, OMe - Salpn)(O <sup>i</sup> Pr) <sub>2</sub> ] <b>(36)</b> .....	319
6.4.7 Synthesis of [Ti(Cl, Cl - Salpy)(O <sup>i</sup> Pr) <sub>2</sub> ] <b>(37)</b> .....	320
6.4.8 Synthesis of [Ti(Aspy)(O <sup>i</sup> Pr) <sub>2</sub> ] <b>(38)</b> .....	322
6.4.9 Synthesis of [Ti(OMe- Aspy)(O <sup>i</sup> Pr) <sub>2</sub> ] <b>(39)</b> .....	323
6.5 Titanium Chloride complex.....	324
6.5.1 Synthesis of TiCl <sub>4</sub> (thf) <sub>2</sub> <sup>7</sup> .....	324
6.5.2 Synthesis of [Ti( <sup>t</sup> Bu, OMe - Salpn)Cl] <b>(40)</b> .....	325

6.6. Bimetallic aluminum complexes .....	325
6.6.1 Synthesis of $[\text{Al}_2(\text{}^t\text{Bu}, \text{}^t\text{Bu} - \text{Salpy})\text{Me}_4]$ <b>(41)</b> .....	325
6.6.2 Synthesis of $[\text{Al}_2(\text{Ad}, \text{Me} - \text{Salpy})\text{Me}_4]$ <b>(42)</b> .....	326
6.6.3 Synthesis of $[\text{Al}_2(\text{}^t\text{Bu}, \text{OMe} - \text{salpn})\text{Me}_4]$ <b>(43)</b> .....	327
6.7 References.....	328
<b>7 General Conclusions</b> .....	<b>330</b>
<b>Appendices</b> .....	<b>335</b>

# **Chapter 1**

## **An**

### **Introduction**

## 1 Introduction

### 1.1 Polymers

Polymers are pervasive in every aspect of modern society. As macromolecules principally derived from organic monomers, they are lightweight, inexpensive, and can have a high mechanical strength; they are therefore useful in a wide variety of applications, from packaging to aeronautical components. Since the advent of synthetic polymers in the 1950s, their production has grown exponentially and, despite a minor aberration due to the 2008 financial downturn, there is no sign of any decrease in this trend (Figure 1.1).

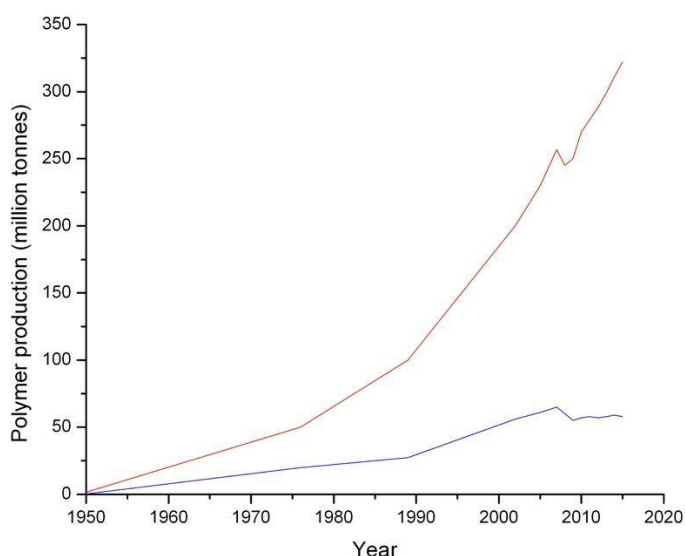


**Figure 1.1:** Production of polymers, 1950-present (red: global; blue: Europe)<sup>1</sup>

The success of synthetic polymers has come with a great environmental cost. The most common polymers, such as poly(ethylene) (PE), poly(propylene) (PP), and poly(styrene) (PS), are derived from crude oil. Crude oil is a finite terrestrial resource and this makes polymers a non-sustainable commodity. Many polymers (including, but not limited to, poly(alkenes)) are comparatively unreactive (e.g. poly(alkenes consist of only C–C and C–H single bonds). This makes them attractive for their applications, but it also makes them environmentally persistent. It is estimated that as of 2015, 6300 million metric tons of plastic waste has been generated, of which 79% has ended up either in

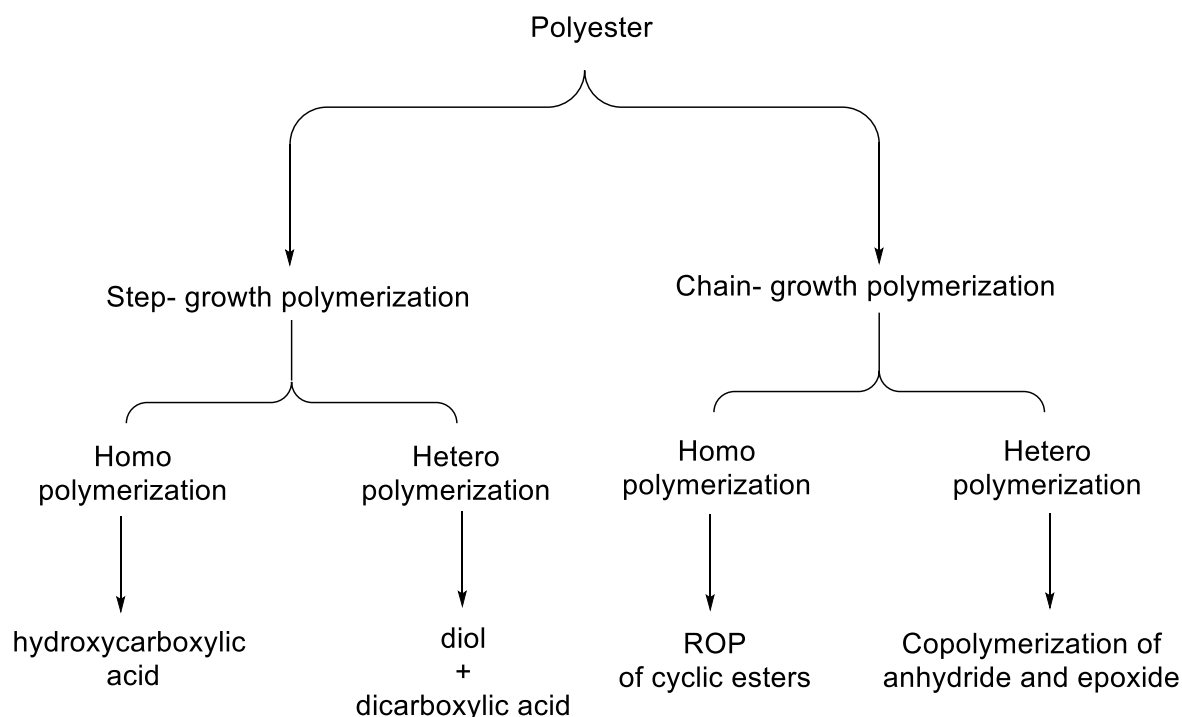
## **Chapter 1 - An Introduction**

landfill or in the natural environment.<sup>2</sup> These polymers are frequently non-biodegradable and can therefore take hundreds of years to decompose.

In an era of increased environmental awareness, society seeks to reduce the environmental footprint of human activity; scientists are therefore seeking to develop alternative polymers that are either biodegradable, or else industrially compostable, so as to avoid the quantity of polymer contained in landfill.<sup>3</sup> In order to achieve this, polymers must be developed that are not only easier to degrade, but they must also have properties that are comparable to traditional polymers, otherwise they will not find widespread application; society will only adopt new polymer technology if it does not need to compromise on performance.

Polyesters are among the more versatile of synthetic polymers in that they find a wide range of application as fibres, plastics, and coatings. Polyesters from renewable sources has been considered as essential materials; poly(lactic acid) (PLA) is an example of such a polyester, which has attractive properties such as biodegradability, and has broad potential applications in biomedical, pharmaceutical and agricultural fields.

There are two important routes for the synthesis of polyesters: step-growth polymerization (SGP) and chain growth polymerization (CGP) (Scheme 1.1). Step-growth polymerization involves the condensation reaction between a dicarboxylic acid or ester, with a diol. With chain growth polymerization the polymer chain grows by adding subsequent monomers to the growing polymer chain. Scheme 1 describes these two routes.



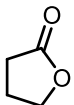
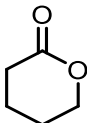
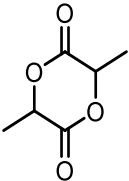
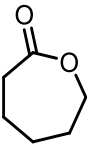
**Scheme 1.1:** The two routes for the synthesis of polyesters

In recent years, substantial attention has been given to the production of polyesters utilizing chain-growth polymerization methods, such as ring-opening polymerization (ROP) and ring-opening copolymerization (ROCOP). Step-growth polymerization involves a higher energy consumption compared to chain-growth polymerization; consequently, milder conditions are sufficient to achieve the polymerization reaction. A side product of water or alcohol (which is very important to remove in order to improve the polymerization reaction rate and to increase the conversion) is produced in step-growth polymerization, whereas no side product with chain-growth polymerization. Regarding the range of polymers that can be produced, a diverse number of monomers can be used with CGP to obtain polyesters for specific applications, whereas a more limited number of monomers are generally available for SGP. There is also a lack of control over the polymer microstructure and molecular weight for SGP, in comparison to CGP which can be more readily controlled by the catalyst.<sup>4</sup>

## 1.2 Thermodynamics of Ring-Opening Polymerization

Thermodynamics represent the single most important factor that determines whether a cyclic monomer can be converted to linear polymer. Table 1.1 compares the thermodynamic parameters characterizing the polymerization ability of the most important cyclic esters.<sup>5,6</sup>

**Table 1.1:** Standard thermodynamic parameters of polymerization of selected cyclic esters monomer

Monomer					
Ring size	4	5	6	6	7
$\Delta H/ \text{KJ mol}^{-1}$	-82.3	5.1	-27.4	-22.9	-28.8
$\Delta S/ \text{J mol}^{-1} \text{K}^{-1}$	-74 <sup>a</sup>	-29.9 <sup>a</sup>	65.0 <sup>a</sup>	-25.0 <sup>b</sup>	-53.9 <sup>a</sup>

<sup>a</sup>[Monomer] = 10 M conducted in liquid monomer, <sup>b</sup>[Monomer] = 1 M conducted in solution.

Equation 1 shows that, it is possible to polymerize cyclic monomers at any temperature when  $\Delta H < 0$  and  $\Delta S > 0$  at standard conditions, whereas the monomers with  $\Delta H > 0$  and  $\Delta S < 0$  cannot be converted into linear macromolecules.<sup>7</sup>

$$\dots\dots\dots(1)$$

In the most ideal case, an increase in the polymerization temperature leads to an increase in  $[M]_{\text{eq}}$  when  $\Delta H < 0$  and  $\Delta S < 0$  (Equation 2).

$$\text{---} \text{---} \dots\dots\dots(2)$$

Where  $[M]_{\text{eq}}$  = Monomer concentration when polymerization is completed).

### 1.3 Ring-opening polymerization of cyclic esters

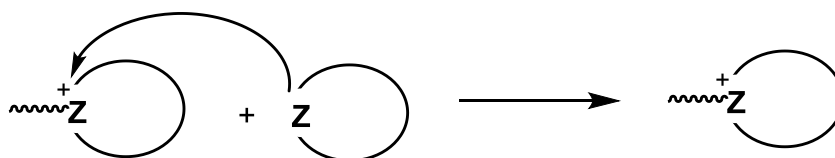
An important process in polymer chemistry is the formation of polymers through ring-opening reactions of cyclic compounds. Chain growth, in such polymerizations, takes place through successive additions of the ring-opened monomers to the polymer chain.<sup>8</sup>



A diverse range of cyclic monomers have been shown to undergo ring-opening polymerization reactions. Examples include lactones, lactams, and many heterocyclics with multiple heteroatoms in the ring. Lactones, and some other cyclic esters, are generally polymerized by three different mechanisms, namely cationic, anionic, and coordination-insertion; enzymatic mechanisms have also been reported.<sup>9</sup>

#### 1.3.1 Cationic ring-opening polymerization

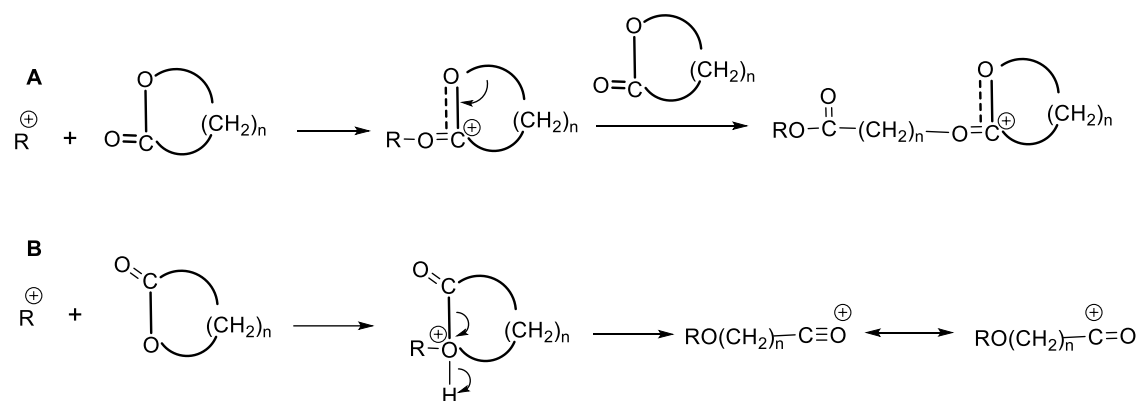
Most cationic ring-opening polymerizations occur via the activation, and subsequent opening of oxonium ion centres; the reaction tends to proceed via the nucleophilic attack of a monomer monomer on the oxonium ion.<sup>10</sup>



Z represents a functional group, such as O, NH, Si-O, CO-O, and CO-NH, present in ethers, amines, siloxanes, esters, and amides, respectively.

Hofman and co-workers revealed that two different kinds of active species can be formed in the cationic polymerization of lactones, namely oxonium and/or acylium cations. This results from the existence of two nucleophilic centres (oxygen atoms in the lactone monomer). The identity of the active species depends on whether the cation is attacked by the exocyclic oxygen (the carbonyl) or the endocyclic oxygen (the ring-oxygen); the identity of the active species will

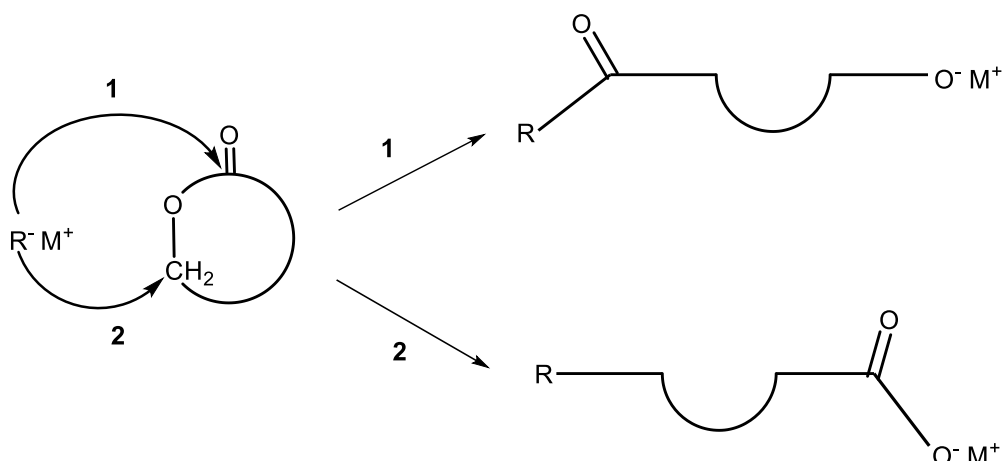
dictate the subsequent bond scission.<sup>11</sup> If the oxonium cation is formed by attack at the exocyclic oxygen atom in the lactone monomer, the cationic species undergoes bond scission between the acyl-oxygen and the alkyl-carbon (Scheme 1.2-A), i.e. acyl C–O bond scission is not possible. Conversely, if the oxonium cation is formed by attack at the endocyclic oxygen atom, bond scission occurs at the acyl- C–O (Scheme 1.2-B).



**Scheme 1.2:** Mechanism for cationic ROP of cyclic esters

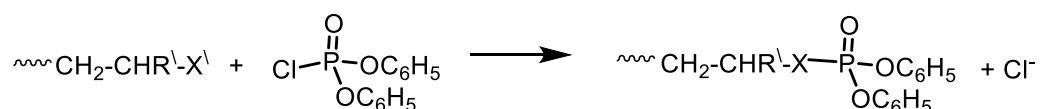
### 1.3.2 Anionic ring-opening polymerization

Anionic ring-opening polymerization occurs via the formation and propagation of anionic centres. For unsymmetrically substituted rings there are formally two ways in which the monomer can be ring-opened. For example, the polymerization of  $\beta$ -lactones can proceed via nucleophilic attack of a negatively charged initiator either on the carbon of the carbonyl group (acyl-oxygen cleavage) or on the alkyl-oxygen (alkyl-oxygen cleavage). In both cases, carboxylate and alkoxide end groups will be formed (Scheme 1.3).<sup>12</sup>



**Scheme 1.3:** Anionic Mechanism of ROP of cyclic esters.

The preferred route can be identified by end group analysis for a prematurely terminated reaction (“short-stop” polymerization reaction), for example with diphenyl chlorophosphite. Using a phosphorus-containing group means that the samples can be analyzed using  $^{31}\text{P}$  NMR spectroscopy ( $^{31}\text{P}$  has  $I = \frac{1}{2}$ ; 100% abundance). Scheme 1.4 shows an example of this reaction.<sup>13</sup>



**Scheme 1.4:** Short-stop polymerization with diphenyl chlorophosphite (X = O or S)

The most efficient catalysts for the anionic polymerization of lactones tend to be based upon alkali metals, alkali metal alkoxide, and alkali metal naphthalenide complexes containing crown ethers.<sup>14,15</sup> Moreover, it is possible to obtain polyesters with molecular weights up to 30,000 using anionic initiators such as alkali metal alkoxides<sup>16–18</sup> and carboxylates.<sup>19–21</sup>

### **1.3.3 Enzymatic ring-opening polymerization**

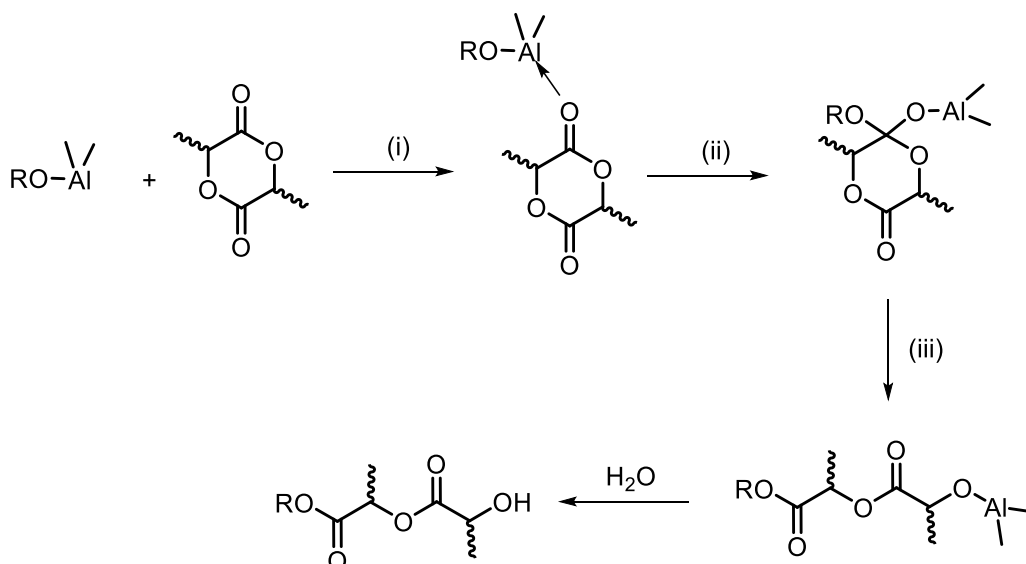
The lipase enzymes induce the ROP of  $\epsilon$ -caprolactone ( $\epsilon$ -CL, 7-membered cyclic ester) and  $\gamma$ -valerolactone ( $\gamma$ -VL, 6-membered cyclic ester); this was first discovered independently by the Uyama and Knani groups in 1993.<sup>22-24</sup> The ROP of  $\epsilon$ -CL by lipase *Pseudomonas fluorescens* (lipase PF) in bulk at 75 °C for 10 days gave poly( $\epsilon$ -CL) in 92% yield with  $M_n$  value of 7,700 and PDI of 2.4. In the same way the polymerization of  $\gamma$ -VL at 60 °C afforded poly( $\gamma$ -VL) with  $M_n$  of 1,900 and PDI of 3.04. Subsequently a wide range of enzymes were reported to be active initiators for the ROP of cyclic esters.<sup>25-27</sup>

The mechanism for the ROP of cyclic esters promoted by enzymes is thought to involve the ring-opening of the monomer by nucleophilic attack of the serine residue of lipase, followed by hydrolysis of the acyl-enzyme intermediate, or its esterification with low molar mass alcohol or hydroxy-terminated polyester chains.<sup>25,28</sup> Therefore, the mechanism has much in common with the anionic ROP mechanism.

### **1.3.4 Coordination-Insertion ring-opening polymerization**

The ROP of cyclic esters using coordination complexes is thought to proceed via a coordination-insertion mechanism. The ROP of  $\epsilon$ -CL and LA has been reported to operate via three individual steps. This mechanism was first experimentally validated in two independent studies by Kricheldorf and coworkers,<sup>29</sup> and by Teyssie and coworkers,<sup>30</sup> using  $\text{Al}(\text{O}i\text{-Pr})_3$  as the initiator for the ROP of  $\epsilon$ -CL and LA.

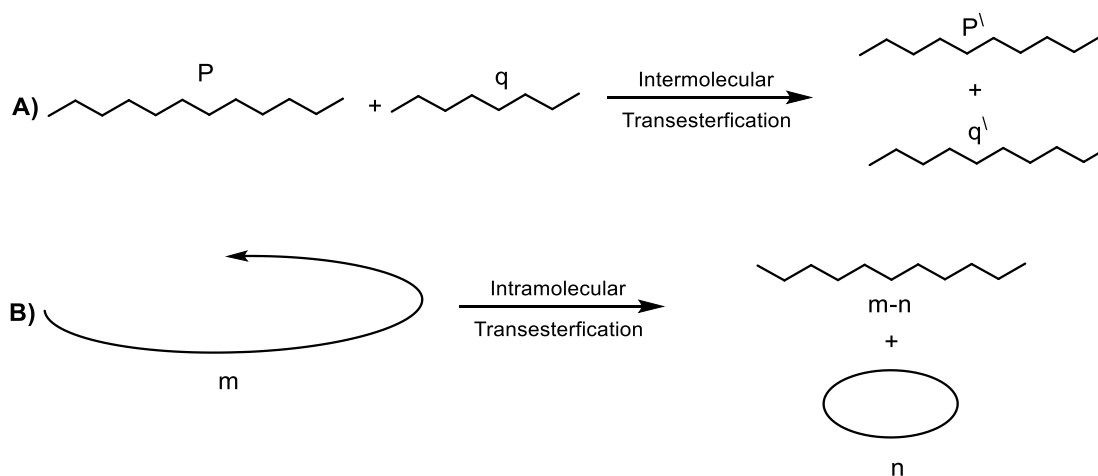
The three steps of the coordination-insertion mechanism involve (i) coordination of the monomer to the catalyst metal centre, and subsequent insertion of a metal-alkoxide ligand into the carbonyl group of the monomer by nucleophilic addition of the alkoxide oxygen to the carbonyl carbon; (ii) ring-opening of the monomer via acyl-oxygen cleavage; (iii) formation of a hydroxyl end group via hydrolysis of the active metal-alkoxide bond. The second chain end is capped with an isopropyl ester, since an isopropoxide complex was used (Scheme 1.5).<sup>9</sup>



**Scheme 1.5:** coordination- insertion mechanism

### 1.4 Transesterification reaction

One of the main side reactions, during the ring-opening polymerization of lactides and lactones, is transesterification. Such reactions affect the polymerization by giving poor control over the number-average molecular weight ( $M_n$ ), as well as a decreasing trend of number-average molecular weight.<sup>31–33</sup> Two types of transesterification reaction, intermolecular (**A**) and intramolecular (**B**), are represented in Scheme 1.6.<sup>34</sup>



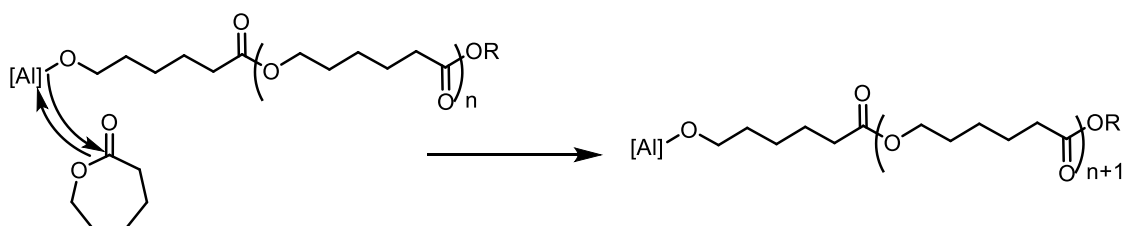
**Scheme 1.6:** inter- and intramolecular transesterification

## Chapter 1 - An Introduction

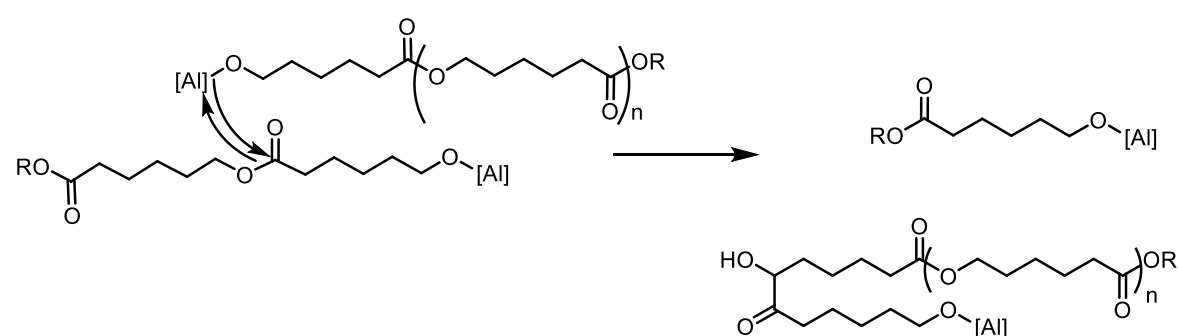
In addition to degradation of the polymer chain (Scheme 1.6A), the intramolecular transesterification leads to the formation of cyclic polymers by the back-biting reaction, affording a mixture of linear and cyclic molecules (Scheme 1.6B). Intermolecular transesterification causes a broadening of the molecular weight distribution (MWD) by virtue of increasing the number of chain-termination steps.<sup>35,36</sup> An example of such side reactions was reported by Nomura and coworkers, when they demonstrated the ROP of  $\epsilon$ -CL using a series of Al complexes containing phenoxyimine ligands. Transesterification side reactions accompanied the ROP when initiated by some of the complexes studied. The coordination-insertion and transesterification are shown in Scheme 1.7.<sup>37</sup>

Transesterification reactions can be identified by the molecular weight ( $M_n$ ), molecular weight distribution (MWD)<sup>30,38</sup> and by  $^{13}\text{C}$  NMR analysis.<sup>36</sup>

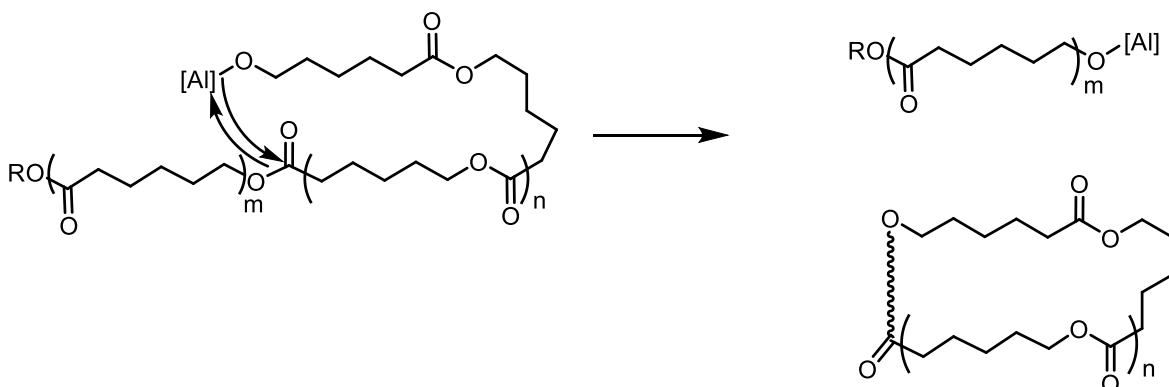
### Coordination-Insertion



### i- Intermolecular transesterification



ii- Intramolecular transesterification (back-biting)

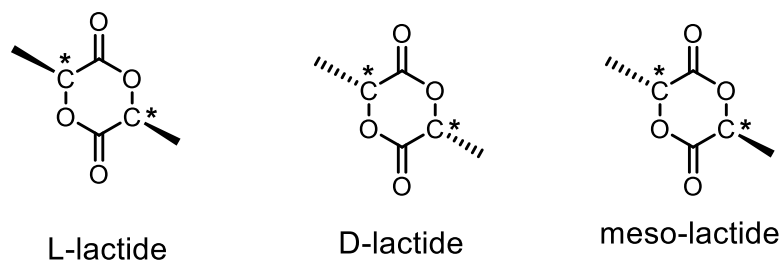


**Scheme 1.7:** coordination-insertion and transesterification in  $\epsilon$ -CL ROP

## 1.5 Ring opening polymerization of caprolactone and lactide

The most important cyclic ester monomers, among a diverse range of cyclic esters available, are  $\epsilon$ -caprolactone and lactide. These two monomers have been known since the 1930s, when initial work on their preparation was carried out by Carothers.<sup>39</sup> The polyester formed from  $\epsilon$ -caprolactone ( $\epsilon$ -CL) and lactide (LA) benefited from their biocompatible, biodegradable, and renewable properties.<sup>40–44</sup>

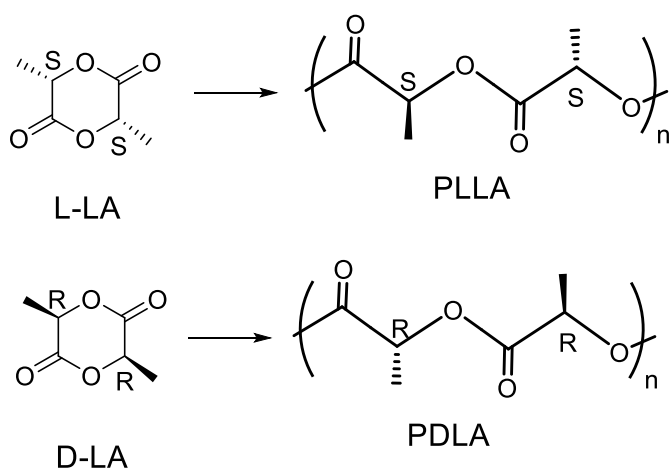
Lactic acid possesses one asymmetric carbon, and therefore exists in one of two configurations, *R* and *S*, depending upon the arrangement of substituents around the chiral carbon. Lactide, which is a cyclic dimer of lactic acid has two chiral carbons, so it has three possible configurations, D-lactide (RR), L-lactide (SS) and meso-lactide (RS) (Figure 1.2). Racemic lactide (rac-lactide) or DL-lactide is a 50/50 mixture of L- and D-lactide.

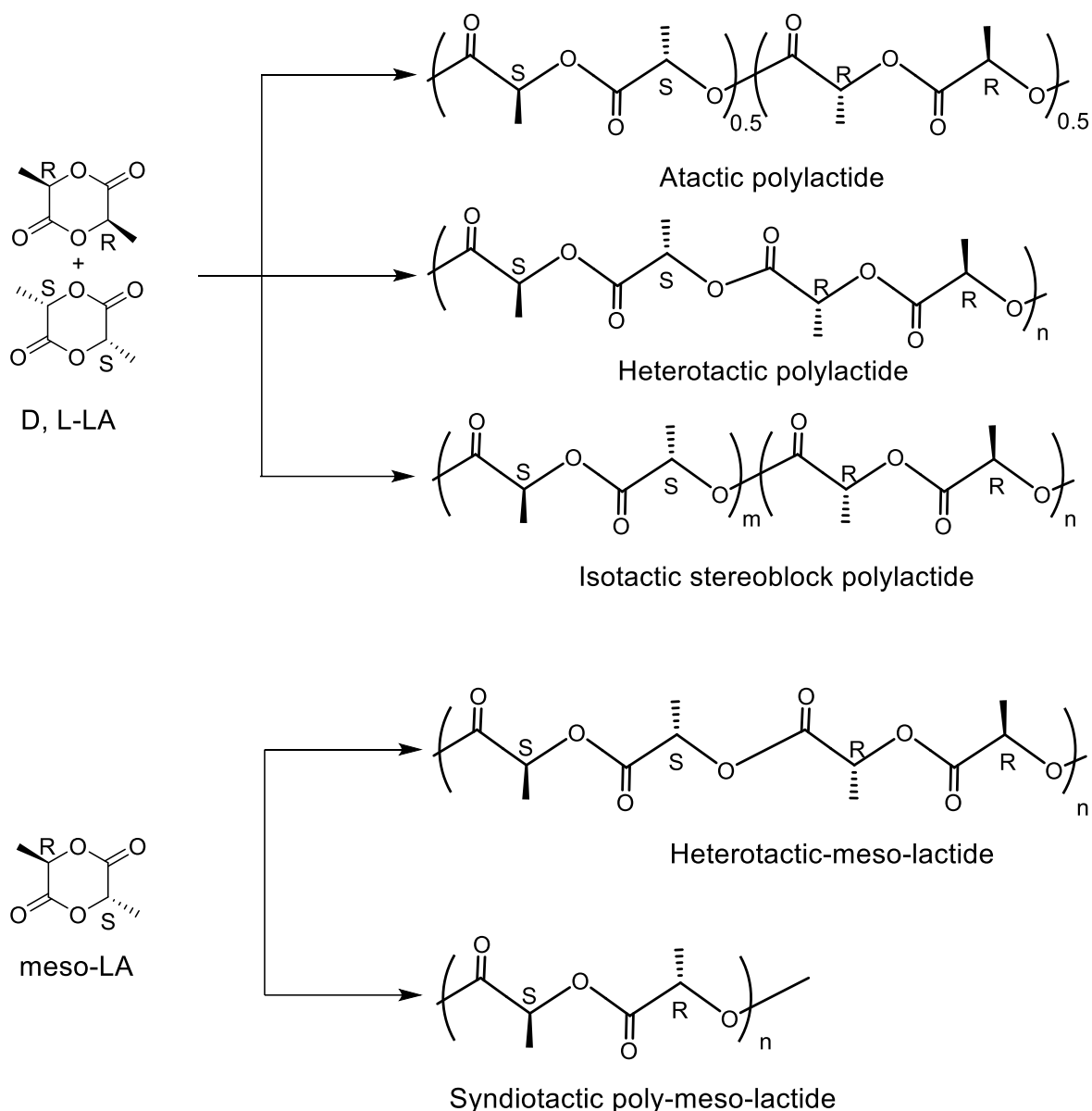


**Figure 1.2:** D, L and meso-lactide structures

Polymerization of D-LA or L-LA leads to the formation of isotactic PDLA and PLLA respectively. Many of the physical and mechanical and degradation properties of PLA are influenced by the amount and distribution of the *R* and *S* stereocenters in the polymer chain.<sup>45,46</sup> The distribution of stereocentres is determined by the relative probability that a specific sequence of stereocenters will be present in the polymer (i.e., *RRRR*, *RSSR*, etc.). Polymers with high stereoregularity can form highly crystalline polymers.<sup>47,48</sup> the challenge in PLA synthesis is the synthesis of thermally stable polymers, which can be achieved by controlling the stereoregularity.<sup>49</sup>

The stereocomplex between PLLA and PDLA has a melting temperature ( $T_m$ ) (230 °C ) higher than the  $T_m$  of homochiral PLLA and PDLA which is 162-180 °C.<sup>50,51</sup> The microstructures of the polymer produced from L, D, meso and *rac*-lactide are represented in Scheme 1.8.



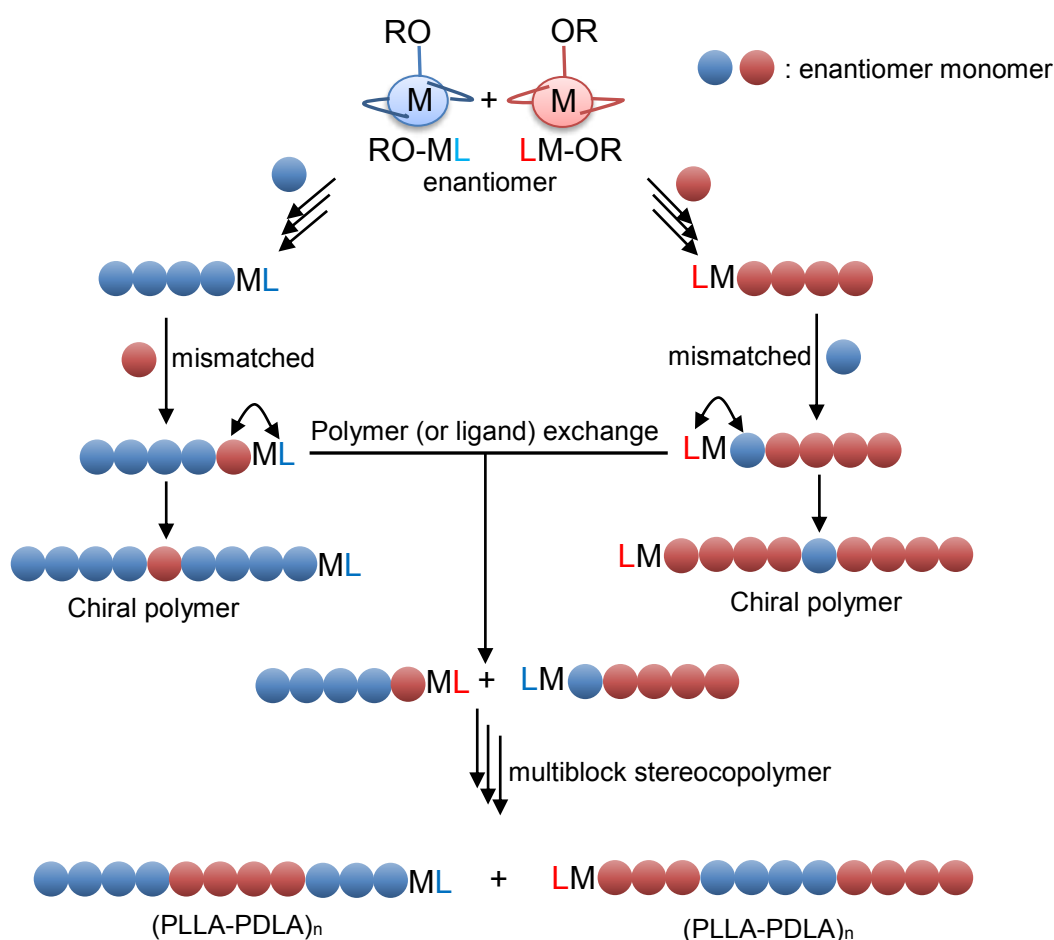


**Scheme 1.8:** the stereosequences in PLA

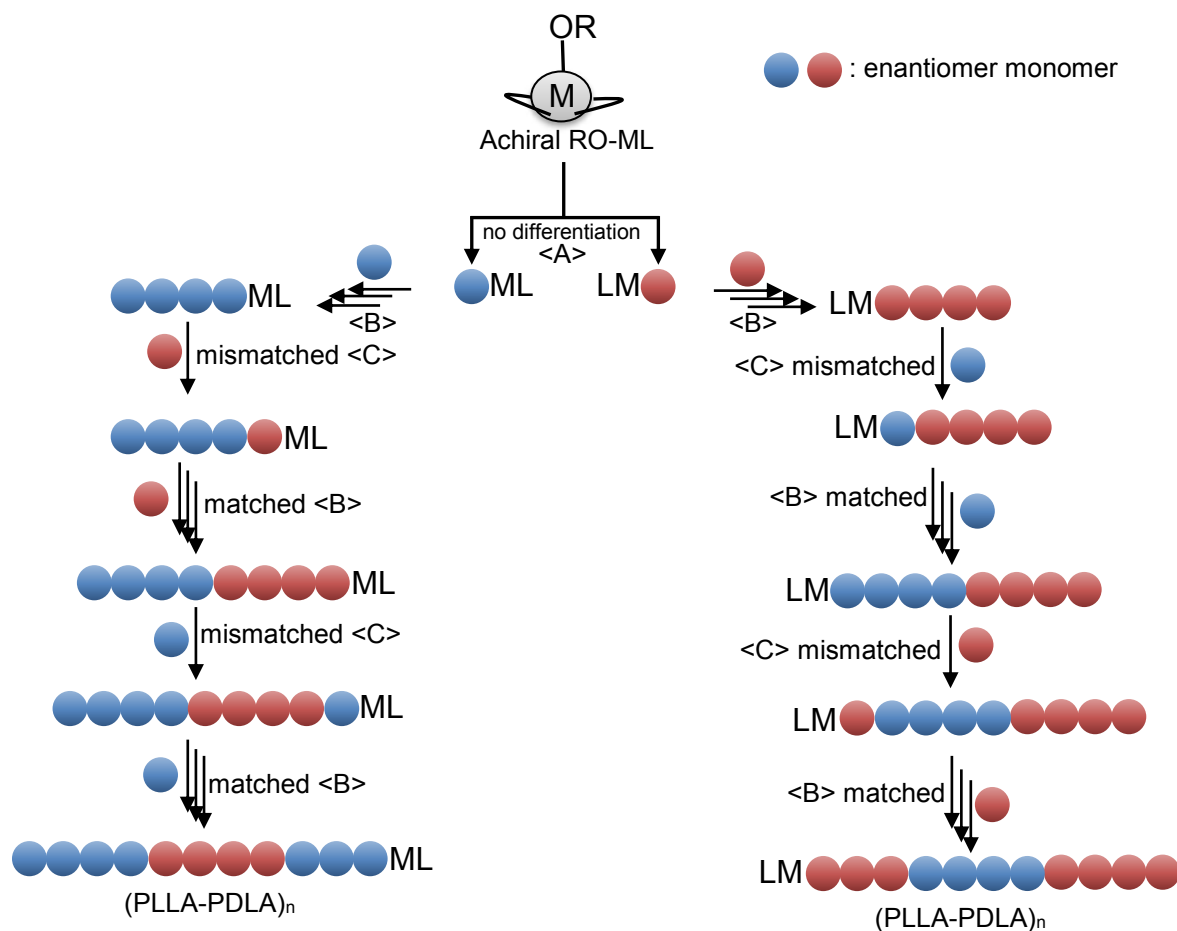
There are two suggested mechanisms by which the stereoselectivity of polymers can be achieved: site-control mechanism (SCM), and chain-end control mechanism (CEM) (Scheme 1.9 and Scheme 1.10).<sup>52</sup> The key step in the SCM is the consistent differentiation of LLA and DLA during the polymerization by a complex that possesses a chiral environment, constructed by the supporting ligand(s) around the metal centre. With CEM both the ligand and the complex are achiral and the initiation reaction occurred without any differentiation between the two enantiomers; the stereogenic centre of the last unit in the growing polymer chain to be added, influences which enantiomeric monomer is incorporated next.<sup>53,54</sup>

## Chapter 1 - An Introduction

The initiation reaction by the CEM occurs without enantiomeric differentiation of the racemic monomer (<A>, Scheme 1.10). In this case, the chirality is incorporated into the propagating chain end. The monomer with the same chiral sense as that of the inserted monomer is then preferentially incorporated into the propagating chain end (<B>). When a mismatched monomer has been incorporated (<C>), the monomer with the same chirality as the propagating chain end, in other words the mismatched monomer just before it, changes to a matched monomer in the next propagation step (<B>).<sup>52</sup>



**Scheme 1.9:** Isotactic polymer sequences by a site control mechanism (SCM)



**Scheme 1.10:** Isotactic polymer sequences via a chain-end control mechanism (CEM).

## 1.6 Determination of the the stereosequence distribution in the PLA

The stereosequence distribution in PLA can be identified by NMR spectroscopy. Two signals are seen for the LA monomer in  $^1\text{H}$  NMR spectroscopy; the first appears as a doublet at approx. 1.5 ppm and is attributed to the methine proton. The second signal appears as a quartet at about 5 ppm. The PLA signals shift slightly to low field. Both  $^1\text{H}$  NMR spectra of PDLA, which contain *R* configuration monomers, and PLLA, which contain *S* configuration monomers, are identical, since the polymers are enantiomers; the methyl and methine protons are in the same relative configuration, in other word, in the same environments. The homonuclear decoupled  $^1\text{H}$  NMR spectra of such polymers gives only two singlets (no coupling between the methyl and methine protons), although in practice the experiment involves irradiation of the methyl signal at 1.5 ppm,

saturating this signal which disappears from the NMR spectrum; the methine signal remains but is observed as a singlet.

Polymerization of *rac*-LA gives polymers with a different microstructure, as shown in Scheme 1.8. The chemical shifts of the signals in the  $^1\text{H}$  and  $^{13}\text{C}$  NMR spectra of PDLLA are slightly affected by the stereoconfiguration of 1-3 adjacent stereogenic centres on either side (i.e. the adjacent monomers within the polymer chain). This gives rise to multiple signals for the methine and methyl groups, that are differentiated by very small difference in chemical shift. The affected signals will appear as overlapping multiplets and a complicated spectrum will be consequently obtained. This problem can be overcome by using homonuclear decoupled  $^1\text{H}$  NMR spectroscopy, since the signals are observed as singlets, and are therefore easier to distinguish in the resulting spectrum. In such cases, the observed resonances can be assigned to various stereosequence combinations in the polymer. Depending on the linkage between the adjacent stereocentres, the assignments are designated as various combinations: (*i*) for isotactic pairwise relationships (*-RR-* and *-SS-*), when the two adjacent stereogenic centres are the same; and (*s*) for *syndiotactic* pairwise relationships (*-RS* and *-SR-*) when the two adjacent stereocentres are different (Figure 1.3).<sup>55</sup> According to a Bernoullian statistical distribution of insertion sequences, the intensities will result in a 3:2:1:1:1 distribution of probabilities. For example *iii*: *isi*:*sis*:*iis*:*sii* tetrads in poly(*rac*-lactide).<sup>56</sup>

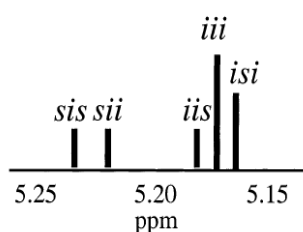


**Figure 1.3:**  $^1\text{H}$  stereosequence assignments for *rac*-PLA

Regarding the stereosequence sensitivity for a polymer with  $n$  stereocentre pairs, there are  $2^{(n-1)}$  possible combinations of pairwise relationships that can be theoretically observed in the NMR spectra. For example, there are  $2^3 = 8$  possible combinations for tetrads. However, only five out of these eight possible signals

are actually observed for tetrad sensitivity, suggesting that not all of the possible stereosequence combinations can be observed in the NMR spectra, or else that some of them are found as overlapping signals.<sup>57</sup> The isotacticity of PLA can be determined from the following relation between  $P_i$  and intensity of the tetrads, where  $P_i$  is the probability of the stereochemistry a monomer unit is the same as the previously inserted one:  $[iii] = P_i(P_i + 1)/2$ ,  $[isi] = (1 - P_i)/2$ ,  $[iis] = P_i(1 - P_i)/2$ ,  $[sii] = P_i(1 - P_i)/2$ ,  $[sis] = (1 - P_i)^2/2$ .<sup>58</sup> Figure 1.4 shows the five tetrads obtained from *rac*-lactide.

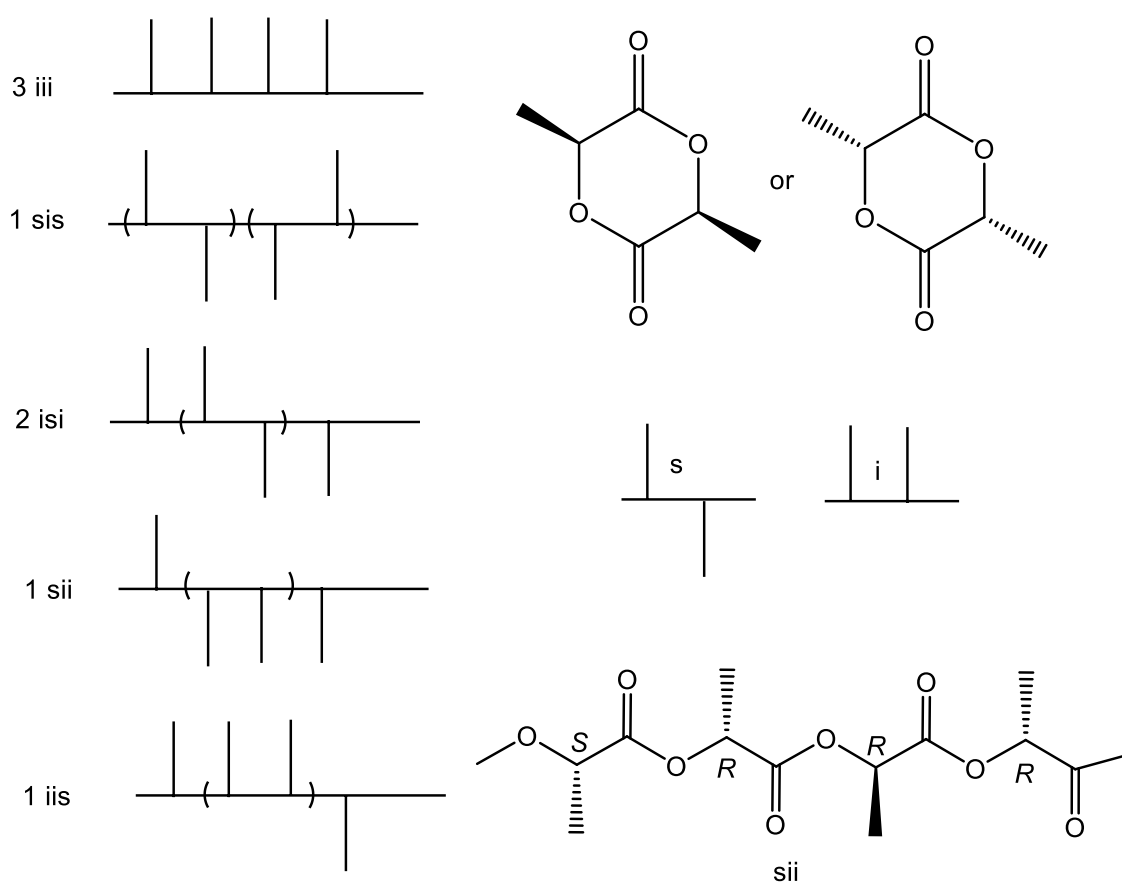
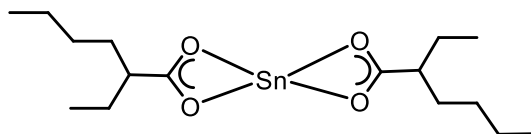


Figure 1.4: Tetrads obtained from *rac*-lactide

## 1.7 Catalysts in ring opening polymerization of CL and LA and their reactivity

The most important complex used for the industrial production of PCL and PLA is tin(II) bis(2-ethylhexanoate) which is usually referred to as tin(II) octanoate,  $\text{Sn}(\text{Oct})_2$  (Figure 1.5). The importance of this catalyst is a result of several features: it is commercially available, easy to handle, and soluble in common organic solvents and in melt monomers. It is highly reactive, and so typical reaction times in bulk at 140-180 °C range from minutes to a few hours, and high molecular weight of polymers (up to 105 or even 106 Da in the presence of an alcohol) can be obtained.<sup>59</sup>



**Figure 1.5:** The structure of tin(II) octanoate  $[\text{Sn}(\text{Oct})_2]$

Another type of catalysts which have been widely studied are aluminium alkoxides; such catalysts been shown efficient reactivity in the ROP of cyclic esters. The homoleptic complex  $\text{Al}(\text{O}^i\text{Pr})_3$  is an example; as well as being active, it has been used for mechanistic studies. Its reactivity for the ROP of cyclic esters was first reported by Teyssie and coworkers;<sup>30</sup> aluminium triisopropoxide is generally less reactive than  $\text{Sn}(\text{Oct})_2$ . Long reaction times, usually several days, are required. Moreover, polymers of lower molecular weight are commonly obtained. ROP reactions with this catalyst show an induction period of a few minutes.

Due to the advantages of well-controlled molecular weight and low polydispersity index (PDI), many researchers have concentrated on the development of new catalysts for the ring-opening polymerization of cyclic esters. As a result, a wide range of organometallic complexes have been investigated as initiators, in order to achieve polymers with the desired properties (or the ability to control the polymer properties). In this manner, coordination complexes with variable supporting ligands play a key role, not only in molecular weight and molecular weight distribution, but also in the production of stereoregular polyesters.<sup>49</sup> Many

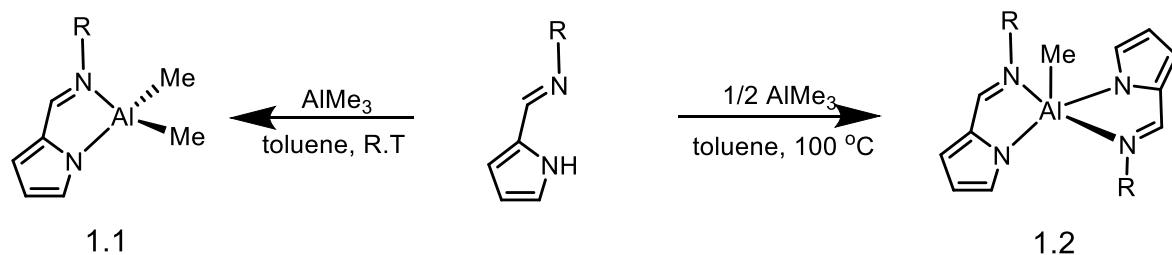
factors affect the reactivity of the catalysts; a generalized formula for catalytic initiators is [LMR], where L is an ancillary ligand, M represents a metal and R is the initiating group such as methyl, ethyl, alkoxy..etc. Changing any of these parameters, especially the metal or the supporting ligand, will affect the behaviour of the catalyst and the properties of the resulting polymer.

Since there are a large number of metals that have been used in this arena of chemistry, such as Zn, Mg,<sup>60,61</sup> Ga, In,<sup>62-64</sup> Zr, Hf,<sup>65-67</sup> Sn,<sup>68-70</sup> to name only a few, this review will focus on catalysts based upon aluminium and titanium, and their effect on the ring opening polymerization of  $\epsilon$ -caprolactone and lactide.

Aluminium complexes have received particular attention among metal-based initiators; they are known for giving excellent control over the polymerization reaction, have high Lewis acidity, and low toxicity. Over the past two decades, particular attention has been given to aluminium complexes supported by ligands such as Salen,<sup>71-74</sup> Salan,<sup>75</sup> and Salalen.<sup>76</sup> Aluminum catalysts which are used for the ROP of cyclic esters can be classified into three types, alkyl (organometallic), alkoxy, and bimetallic complexes.

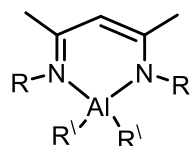
Alkyl complexes can be obtained by the stoichiometric reaction of the appropriate pro-ligand with trialkyl aluminium. An example of this route was reported by Hornmiron and coworkers (**1.1** and **1.2**, Scheme 1.11).<sup>77</sup> These complexes, containing various ligand substituents, were used for the polymerization of *rac*-LA in the presence of 1 equivalent of benzyl alcohol. All complexes exhibited molecular weights in close agreement with theoretical values, and with narrow molecular weight distributions in accord with controlled living polymerizations.

Enhancing the steric hindrance at the *ortho* position of the aniline derivatives had a positive effect on the stereoselectivity; exchanging the substituted phenyl unit with an adamantyl group resulted in the production of isotactic enriched PLA with a *P* value of 0.63.



**Scheme 1.11:** Aluminium methyl complexes prepared by Hornmiron and coworkers

Another type of aluminium methyl complexes was reported by Dexu Kong and coworkers when they used a series of complexes derived from N-substituted  $\beta$ -diketiminate ligands (**1.3a-h**, Figure 1.6). All the complexes showed poor to good activity in the absence of benzyl alcohol, with an activity highly dependent on the N-substituent on the ligand manifold. For instance, when a *tert*-butyl group was introduced, good catalytic activities were obtained in comparison to initiators possessing either smaller or larger groups, indicating that suitable steric hindrance is beneficial for optimizing the catalytic activity.<sup>78</sup>



- 1.3a: R= R<sup>1</sup>= Me
- 1.3b: R= <sup>i</sup>Pr, R<sup>1</sup>= Me
- 1.3c: R= <sup>t</sup>Bu, R<sup>1</sup>= Me
- 1.3d: R= Bn, R<sup>1</sup>= Me
- 1.3e: R= CH<sub>2</sub>CH<sub>2</sub>Ph, R<sup>1</sup>= Me
- 1.3f: R= CHPh<sub>2</sub>, R<sup>1</sup>= Me
- 1.3g: R= <sup>t</sup>Bu, R<sup>1</sup>= Et
- 1.3h: R= <sup>t</sup>Bu, R<sup>1</sup>= <sup>i</sup>Bu

**Figure 1.6:** Aluminium (III) initiators prepared by Dexu Kong and coworkers

Salen-type ligands are diionic ligands combining N- and O-donors. Such ligands have been widely employed in the preparation of well-defined complexes for lactide and  $\epsilon$ -caprolactone ROP.<sup>79</sup> The free ligands are readily prepared from the direct condensation of diamines and salicyl carbonyl derivatives, and a large number of structural variants can be obtained. The aluminium alkyl complexes can be obtained by the reaction of the protio-ligands with trialkyl aluminium under

dry and inert conditions. Two paths can be followed to synthesise the alkoxy complexes. The first method is a ligand exchange with trialkoxy aluminium precursors such as aluminium triisopropoxide. The second method involve alcoholysis of pre-formed alkyl aluminium complexes. According to X-ray analyses, the geometries at aluminium in these complexes is either square pyramidal (sqb) or trigonal bipyramidal (tbp).

Achiral salen aluminium complexes (**1.4** series) have been reported by Spassky and coworkers as active initiators for the ROP of lactide and *rac*-BBL (Figure 1.7).

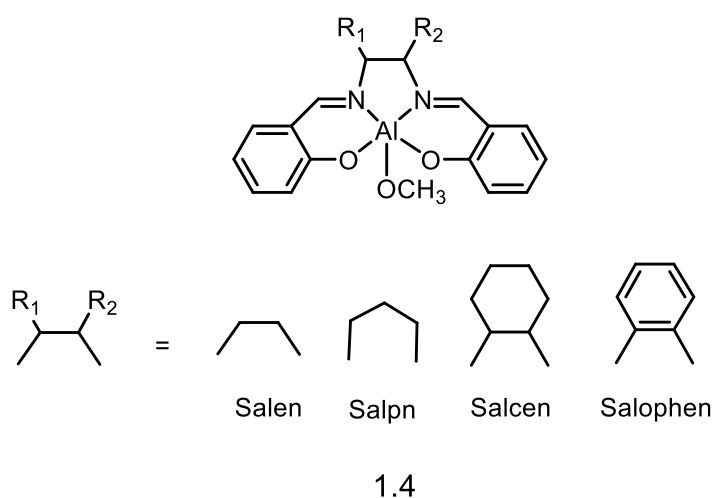
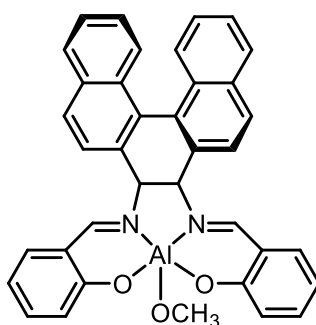


**Figure 1.7:** Achiral salen aluminium complexes prepared by Spassky and coworkers

In 1993, the Spassky group oligomerized racemic and (L) enantiomerically enriched lactides with [(salen)Al(OCH<sub>3</sub>)], in toluene and dichloromethane solutions at different temperatures. The authors reported that transesterification reactions increased with temperature and reaction time. The polydispersity index of the polymers, in dichloromethane, increased with time, from 2.3 after 15.5 hours, to 3.5 and 4.0 after 56 and 40 hours respectively, while the conversion remained almost the same. They attributed the high polydispersity observed to the partial insolubility of the initiator in toluene at the beginning of polymerization which can be reduced by replacing the dichloromethane solvent with toluene (giving PDI=1.14).<sup>80</sup>

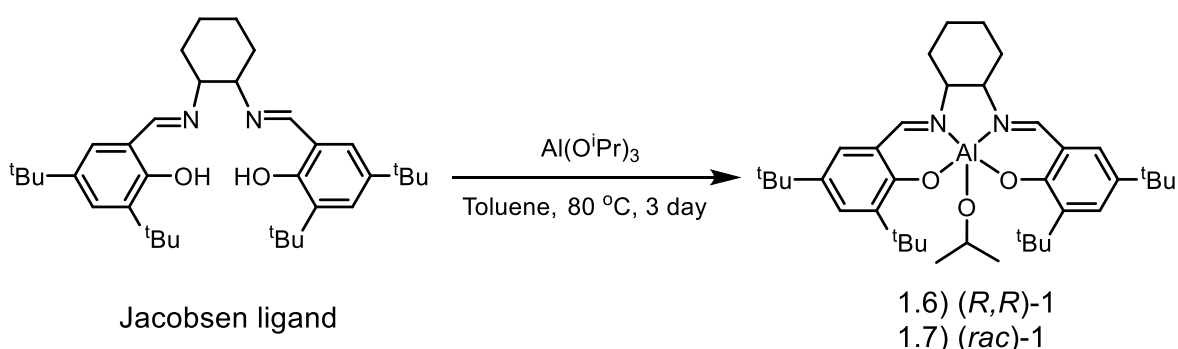
## Chapter 1 - An Introduction

In 1996, Spassky and coworkers first reported the formation of highly isotactic and crystalline PLA by the ROP of rac-lactide using the enantiopure *R*-salbinap aluminium(III) methoxide complex (**1.5**) with less than 50% conversions, mainly poly(D-lactide) was formed whereas the unreacted L-lactide remained in solution. With higher conversions, the degree of isotactic enrichment started to decrease. The authors attributed the decrease in isotactic enrichment to an increase in concentration of the unfavoured monomer enantiomer as the reaction proceeded.<sup>81</sup>



1.5

In 2002, Zhong and coworkers reported that enantiopure *RR*-configured aluminum isopropoxide complex with the Jacobsen ligand (Complexes **1.6** and **1.7**, Scheme 1.12).<sup>82</sup>



**Scheme 1.12:** enantiopure aluminum isopropoxide complexes reported by Zhong and coworkers

## Chapter 1 - An Introduction

The first experiments conducted in toluene at 70 °C ( $[M]_0/[I]_0 = 62:1$ ,  $[M]_0 = 0.8 \text{ molL}^{-1}$ ) revealed that both **1.6** and **1.7** provided PLA with well-controlled  $M_n$  and very low polydispersity indices. A  $P_i$  value of 0.93 was obtained for the polymerization of *rac*-LA initiated by **1.7**.

In 2007, Nomura and coworkers documented the preparation of isotactic stereoblock PLA using achiral aluminium-Salen complexes with rigid backbones (**1.8**, **1.9** and **1.10** in **Figure 1.8**). Introducing  $^t\text{BuMe}_2\text{Si}$  substituents at the 3-positions of the salicylidene moieties gave the highest selectivity for this class of complex, with a  $p_i$  value of 0.98 and a  $T_m$  of 210 °C.

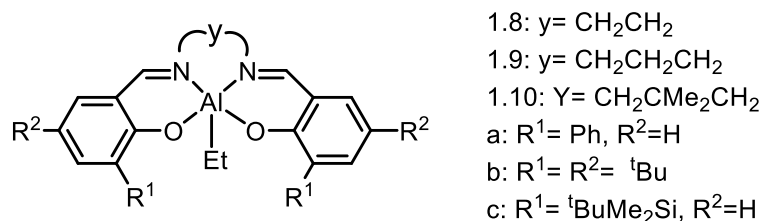


**Figure 1.8:** Aluminium ethyl complexes prepared by Nomura and coworkers

Nomura and coworkers reported a series of Al complexes containing phenoxyimine ligands which, in the presence of benzyl alcohol, were active in the ROP of  $\epsilon$ -CL. High conversion (91-94%) was achieved after 45 min when using the fluorine derivatives (**1.11a-d** in **Figure 1.9**).

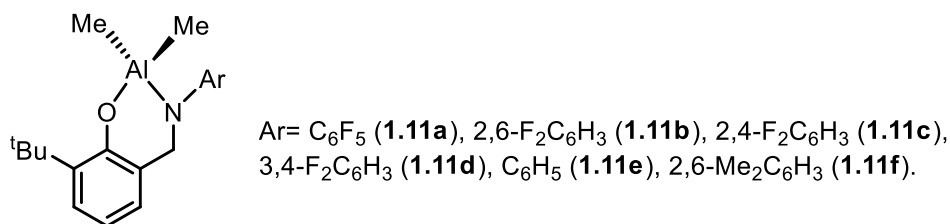


**Figure 1.9:** Phenoxyimine aluminium methyl complexes prepared by Nomura and coworkers

The results clearly indicate that substitution of the ortho-position, especially by adding a fluorine substituent, can strongly affect the catalytic activity. It has also

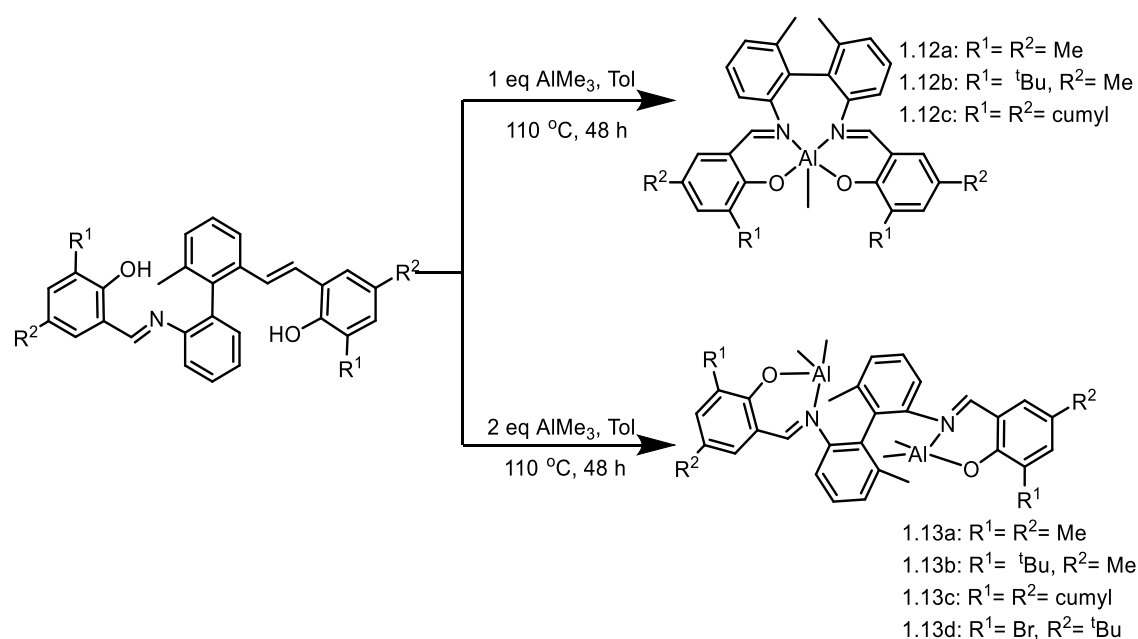
been reported that ROP by the C<sub>6</sub>F<sub>5</sub> analogue (**1.11a**) proceeded in a living manner; a linear relationship between the monomer conversions and the  $M_n$  values with consistently with low Mw/Mn values was observed. Changing the substituent to C<sub>6</sub>H<sub>5</sub> (**1.11e**) lead to broader molecular weight distributions (PDI values), suggesting that transesterification processes become more prominent (Table 1.2).<sup>83</sup>

**Table 1.2:** ROP of  $\epsilon$ -CL initiated by **1.11a-d**/ BnOH

<b>Complex</b>	<b>Time/min</b>	<b>Conv. %</b>	<b><math>M_n</math> (GPC)X10<sup>-4</sup></b>	<b>PDI</b>
<b>1.11a</b>	15	48	3.15	1.19
<b>1.11a</b>	30	81	4.87	1.21
<b>1.11a</b>	45	94	5.53	1.22
<b>1.11b</b>	30	21	1.06	1.12
<b>1.11b</b>	60	49	2.16	1.24
<b>1.11b</b>	90	73	2.99	1.42
<b>1.11b</b>	120	89	3.35	1.50
<b>1.11c</b>	60	25	1.20	1.11
<b>1.11c</b>	120	59	2.45	1.18
<b>1.11c</b>	180	87	3.47	1.32
<b>1.11c</b>	240	97	3.94	1.48
<b>1.11d</b>	60	19	0.95	1.13
<b>1.11d</b>	120	46	1.92	1.17
<b>1.11d</b>	180	73	2.82	1.41
<b>1.11d</b>	240	89	3.24	1.58

## 1.8 Bimetallic aluminium complexes

Another class of aluminium complexes which has given interesting results regarding the ROP of cyclic esters, is based upon bimetallic aluminium complexes. Such types of complex have been reported for different types of reactions, including the synthesis of cyclic carbonates from the reactions of epoxides and carbone dioxide,<sup>84–87</sup> the ROP of epoxide,<sup>88</sup> as well as  $\epsilon$ -CL and LA polymerization.<sup>53,89</sup> For Salen-type ligands in particular, mono- and bimetallic complexes can often be afforded by using the same ligand, taking into account that the formation one of them (mono- or bimetallic) can be preferred over the other, depending on the nature of the ligand. Theoretically, adding different equivalents of  $\text{AlMe}_3$  into the solution of salen-type ligands having  $\text{N}_2\text{O}_2$ -donors may afford two types of aluminum complexes. Five-coordinated complexes with the Al centre coordinated by the salen  $\text{N}_2\text{O}_2$  donors may be obtained when 1 equivalent of  $\text{AlMe}_3$  is added; introducing 2 equivalents of  $\text{AlMe}_3$  can produce bimetallic complexes with each Al atom coordinated by one N and one O donor of a single salen “arm”. An example is shown in Scheme 1.13.<sup>90</sup>



**Scheme 1.13:** preparation route of mono- and bimetallic aluminium complexes.

Yao and coworkers reported the preparation of binuclear aluminium piperazine-bridged bis(phenol) complexes as initiators for the ROP of  $\epsilon$ -CL (1.14a-c in Figure 1.10). The authors showed the the dinuclear complexes were

## Chapter 1 - An Introduction

2–8 times more active than their mononuclear counterparts. All the complexes showed moderate to good yields of 34–92% when they tested at 70 °C for 4 hours in toluene, with the monomer to Al ratio of 200:1 without using a cocatalyst. However, the resulting polymers had relatively broad distributions (PDI = 1.47–2.04), which means that the polymerization reaction is not as well controlled as some other examples in the literature.<sup>91</sup>

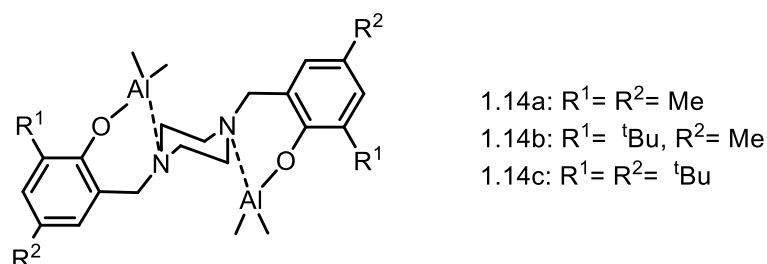
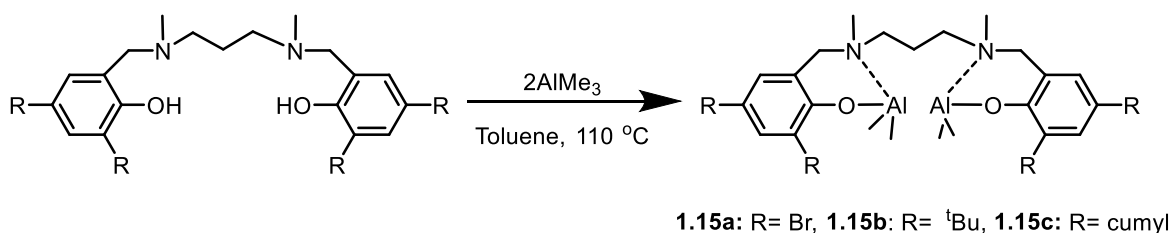


**Figure 1.10:** Binuclear aluminium piperazine initiators synthesized by Yao and coworkers

Ma and Wang studied the reactivity of binuclear aluminium complexes (**1.15a-c** in **scheme 1.14**) towards the ROP of LA and  $\epsilon$ -CL in the presence of alcohol cocatalyst.



**Scheme 1.14:** binuclear aluminium complexes reported by Ma and Wang

Complexes **1.15a-c** showed catalytic activity for the ROP of both *rac*-lactide and L-lactide. The isopropanol cocatalyst had a significant influence on the catalytic efficiency of the polymerization reaction; relatively long reaction times were required when 2 equivalents of 2-propanol were used, whereas higher conversions were obtained in shorter times when 4 equivalents was added. Examples are shown in Table 1.3

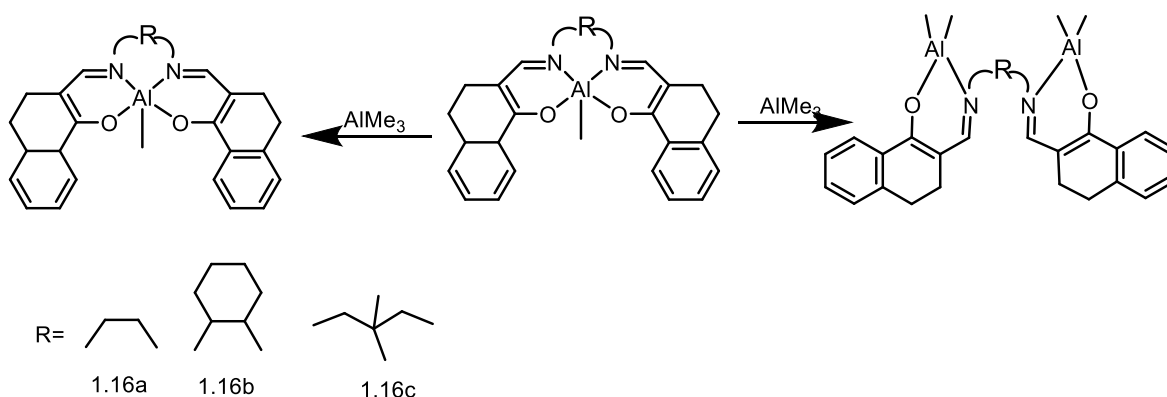
Table 1.3: ROP of *rac*-lactide initiated by **1.15a-c**

Initiator (I)	Feed ratio	Time/min	Conv. %	$M_n$ ( $10^3$ )	PDI	$P_i$
<b>1.15a</b>	100:1:2	18	88	6.9	1.10	0.57
<b>1.15a</b>	100:1:4	7	93	3.5	1.09	0.41
<b>1.15b</b>	100:1:2	96	86	5.7	1.13	0.62
<b>1.15b</b>	100:1:4	24	81	2.9	1.09	0.4
<b>1.15c</b>	100:1:2	96	83	5.6	1.12	0.62

Feed ratio =  $[LA]_0 : [Cat.]_0 : [iPrOH]_0$

The introduction of bulky groups such as *tert*-butyl and cumyl into the *ortho* position of the ligands resulted in a remarkable decrease in the polymerization rate. Generally, With  $\epsilon$ -CL, the catalyst showed high reactivity since all experiments were conducted at room temperature.<sup>75</sup>

Recently, Huang and coworkers prepared a series of new binuclear aluminium complexes containing  $\beta$ -ketiminato ligands (Scheme 1.15).<sup>92</sup>



**Scheme 1.15:** Mono and binuclear aluminium initiators prepared by Huang and coworkers

The ROP of  $\epsilon$ -CL by the binuclear aluminium complexes **1.16a-c** was investigated in the presence of isopropanol. These complexes promoted the ROP

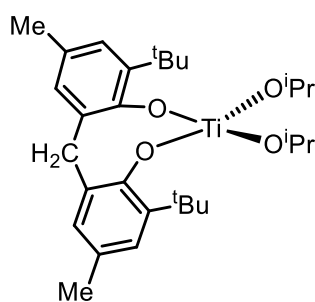
of  $\epsilon$ -CL effectively, and initiated rapid polymerization. **1.16c** exhibited impressively high catalytic activity, and 83% of the monomer conversion was converted in just 3 min. The order of activity of these catalysts is **1.16b** < **1.16a** < **1.16c**. The authors attribute the higher activity of **1.16c** to the flexible bridge group. An approach of the two metal centres can occur in solution, resulting in an improvement in cooperativity, and hence in the catalytic activity.

## 1.9 Titanium complexes

Considerable attention has been paid recently in the polymerization of cyclic esters utilizing titanium alkoxides because of their low toxicity and the possibility to synthesize medium to high molecular weight polymers with relatively narrow molecular weight distributions.

A successful application of titanium-based catalysts is for the living polymerization of olefins.<sup>93</sup> Outside of olefin polymerization, titanium complexes bearing bulky alkoxo,<sup>94</sup> amine(bisphenolate)<sup>95,96</sup> or bis(aryloxo)<sup>97,98</sup> ligands and half-metallocenes ( $\text{CpTiCl}_3$ )<sup>99,100</sup> (amongst other complexes) have been shown to exhibit distinctively high activity in the polymerization of  $\epsilon$ -caprolactone or lactide.

Many investigations of titanium complexes' activity in the ROP of cyclic esters suggest that titanium alkoxy complexes show rather low activities, especially for LA polymerisation. For example, bulky methylene-bridged bis(phenolate) complexes of titanium alcoholates such as complex **1.17** are able to initiate the living polymerisation of more reactive lactones, with each metal centre affording two propagating polyester chains. However, in comparison to main group or lanthanide-based initiators, they show lower propagation rate.<sup>98</sup>



## Chapter 1 - An Introduction

A series of bis(dialkylamido) titanium complexes was reported by Harada and coworkers (Figure 1.11).<sup>101</sup> These complexes are coordinated by O–E–O (E= S, CH<sub>2</sub>) chelating bis(aryloxo) ligands. The polymerization was conducted at high temperature (100 °C). The sulfur-bridged complex **1.18b** catalyzed the polymerization of  $\epsilon$ -CL in 90% yield within 32 hours, to afford PCL with an  $M_n$  of 18,800 and PDI of 1.31; with methylene bridge, the conversion reached 91% in only 8 h and an  $M_n$  of 56,200 was reported.

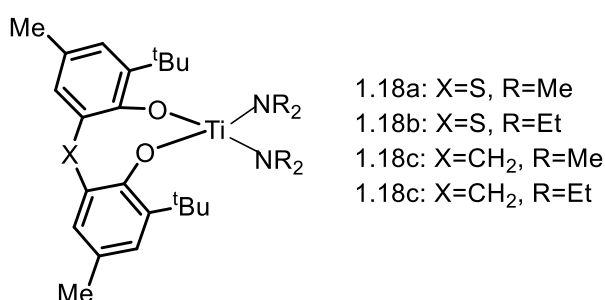


**Figure 1.11:** Bis(dialkylamido) titanium catalysts prepared by Harada and coworkers

Chien and coworkers prepared a series of tridentate aminebiphenolate titanium complexes (Figure 1.12), which were studied for activity in the ROP of  $\epsilon$ -CL.

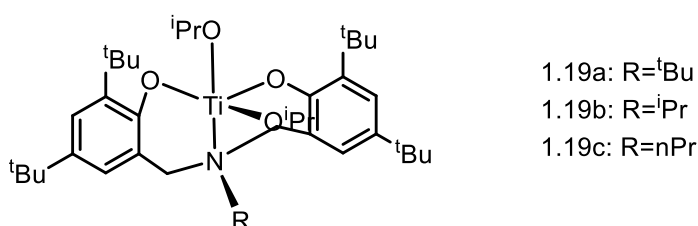


**Figure 1.12:** aminebiphenolate titanium prepared by Chien and coworkers

In all cases, **1.19c** showed higher reactivity than **1.19a** and **1.19b**; the polymerization rate followed the order **1.19a** < **1.19b** < **1.19c**. While **1.19c** completely reacts with 300 equiv. of  $\epsilon$ -CL to produce PCL after 24 hours, both **1.19a** and **1.19b** react much slower and they gave low conversion. An explanation was given by the author regarding the reactivity of **1.19a**, which they

attributed to the stronger electron-releasing *N-tert*-butyl, which presumably lowers the electrophilicity of the titanium and thus disfavours monomer coordination. The difference in the reactivity of the isopropyl-substituted **1.19b** and the *n*-propyl-derived **1.19c** was attributed to the relative sterics of the *N*-alkyls in these complexes.

Tseng and coworkers documented synthesis of (Ti) complexes bearing hydrazine-bridged Schiff base ligands, and investigated them as catalysts for the ring-opening polymerization (ROP) of L-lactide (LA).<sup>102</sup> These complexes were found to give high conversions within 30- 3000 minutes, with low to moderate molecular weights ranging from 2400-18500 and the PDI ranging from 1.09-1.98.

In general, it can be seen from the above examples that Schiff base ligands are highly suitable supporting environments for both aluminium and titanium, in the ROP of cyclic esters. The influence of relatively subtle changes in the ligand structure can have a profound influence on the catalytic activity, and much can therefore be learnt from these examples.

## **1.10 Molecular weight determination**

Synthetic polymers are composed of macromolecules having a distribution of molecular weights; they do not contain macromolecules of only one single molecular weight. Different techniques can be used to determine the distribution curve using different averages of the molecular weight such as  $M_n$  and  $M_w$ .<sup>103</sup>

There are various physical methods to determine the molecular weight of the polymer. The more prominent ones are ebullioscopy, cryoscopy, osmotic pressure measurements, light scattering, ultracentrifugation, and gel permeation chromatography (also called size exclusion chromatography). All of these determinations are carried out on solutions of polymers.<sup>8</sup>

The term *number-average molecular weight* ( $M_n$ ) refers to a measure of chain length of the polymer chains. The  $M_n$  is defined as:

---

## Chapter 1 - An Introduction

where  $n_i$  is the number of molecules or the number of moles in the sample having the molecular weight  $M_i$ . Physically, the number-average molecular weight can be measured by any technique that “counts” the molecules. These techniques include vapour phase and membrane osmometry, freezing point lowering, boiling point elevation, and end-group analysis.<sup>104</sup> In contrast to number average molecular weight which is the summation of mole fraction of  $M_i$ , the summation of each molecules times its molecular weight, the summation of the weight fraction of each polymer molecules times its molecular weight give a value which is called the weight average molecular weight,  $M_w$  which is defined as:

$$M_w = \frac{\sum n_i M_i^2}{\sum n_i M_i}$$

Gel Permeation Chromatography (GPC), also known as Size Exclusion Chromatography (SEC), is a very powerful method of polymer fractionation and has become a standard method for determination of molecular-weight distribution and relative molar masses. The molecular weight distribution is an important characteristic of polymers. The polymer properties are significantly affected by the molecular-weight distribution of the polymer.<sup>105</sup>

The GPC is a technique used to determine the average molecular weight distribution of a polymer sample. Using the appropriate detectors and analysis procedure it is also possible to obtain qualitative information on long chain branching or determine the composition distribution of copolymers.<sup>106</sup>

In a GPC experiment, the polymer is separated in a column which is packed with swollen, uniformly packed resin. Such material usually consists of polymeric porous spheres, often composed of polystyrene crosslinked by addition of varying amounts of divinylbenzene. This material represents the stationary phase which called the “gel”. The mobile phase corresponds to the solvent which passes through the column. A solution of the polydisperse polymer in the same solvent as was used to swell the resin is passed through the top of the column and eluted in the same way as HPLC chromatography. In GPC, however, the separation is based on separation by molecular size rather than chemical properties. Another

way of describing this is that the GPC experiment differentiates the different hydrodynamic volumes of the polymers associated with their different molecular weights. Smaller molecules can penetrate the pores and are therefore retained to a greater extent than the larger molecules, which elute faster.<sup>103,104,106</sup> Figure 1.13 shows the separation process.<sup>107</sup>

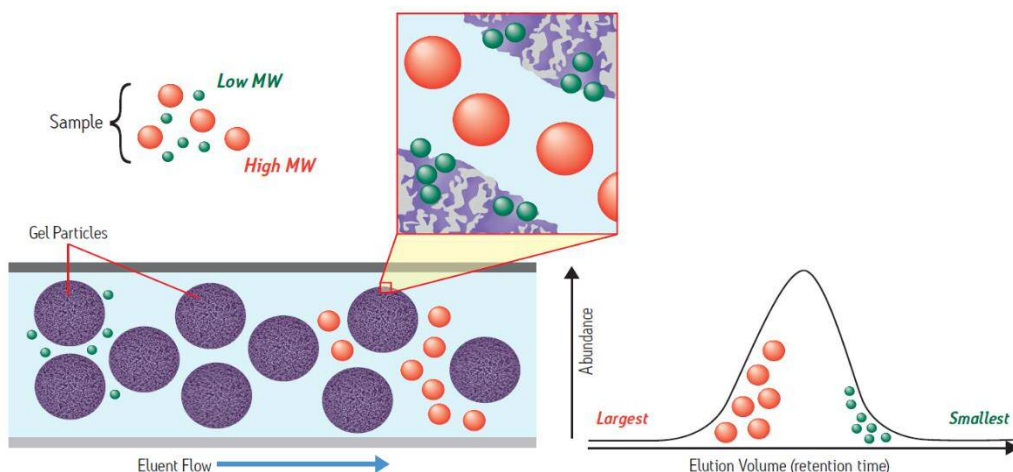


**Figure 1.13:** Polymer separation according to the size in SEC.<sup>107</sup>

No individual molecular weight can be obtained by gel permeation chromatography (GPC). However, it must be calibrated against polymer samples whose molecular weight are defined as an absolute molecular weight by another technique (polystyrene for example). After calibration with polystyrene fractions using the same solvent and temperature, the molecular weight can be determined. If we refer to the reference polymer (e.g., polystyrene) as polymer 1 and the polymer to be analyzed as polymer 2, following that:<sup>105</sup>

$$\dots\dots\dots(1)$$

From Mark- Houwink-Sakurada relationship,

$$\dots\dots\dots(2)$$

$$\dots\dots\dots(3)$$

By substituting equation 2 and 3 in equation 1 and solving for  $\log M_2$ , we obtain

$$\log M_2 = \frac{1}{a} \left( \log \frac{K}{M_1} + \log \frac{[\eta]}{[\eta]_0} \right)$$

$M_1$  = the molecular weight obtained from GPC analysis.

$M_2$  = the corrected molecular weight

$K$  and  $a$  = Mark–Houwink parameters for standard and measured polymer (can obtain from a polymer handbook or from the primary literature).

## **1.11 Ring opening copolymerization (ROCOP)**

The ring-opening copolymerization of cyclic anhydrides and epoxides is one of the most promising next-generation methods for production of polyester, following chain-growth polymerization. Such importance comes from the diversity of polyester which can be produced from such polymerization, since a wide range of anhydrides and epoxides are available commercially and in some cases easy to synthesize or isolate from natural sources. A simple search on the web page of a common commercial supplier (Sigma-Aldrich) reveals 500 epoxides (the search limit) and 257 cyclic anhydrides. This gives the theoretical number of *different* polymers (i.e. not including cross-linking, varying tacticity, molecular weights, etc) as 128,500. Whilst this is a crude analysis, it cannot be doubted that ROCOP is a method that can give a highly diverse range of polymers to match many different applications.

The development of the field has covered many parameters and factors around the copolymerization. A wide range of catalysts have been demonstrated as initiators for the ROCOP of anhydride and epoxide, based on several metals including (but not limited to) aluminium,<sup>108–110</sup> chromium,<sup>108,111–114</sup> cobalt,<sup>108,114–116</sup> magnesium,<sup>117,118</sup> and zinc.<sup>115,117,119,120</sup> A diverse array of both epoxides and anhydrides have been reported for this polymerization procedure. Among all epoxides demonstrated by researchers in the area, propylene oxide (PO) and cyclohexene oxide (CHO) have dominated. Changing the cyclic anhydride

backbone plays a key role in changing the thermal and mechanical properties of the resulting polyester; a large number of anhydrides have been demonstrated, ranging from aliphatic, aromatic, unsaturated, monocyclics, bicyclics, and tricyclics. A list of most popular anhydrides used in ROCOP studies are listed in Figure 1.15.

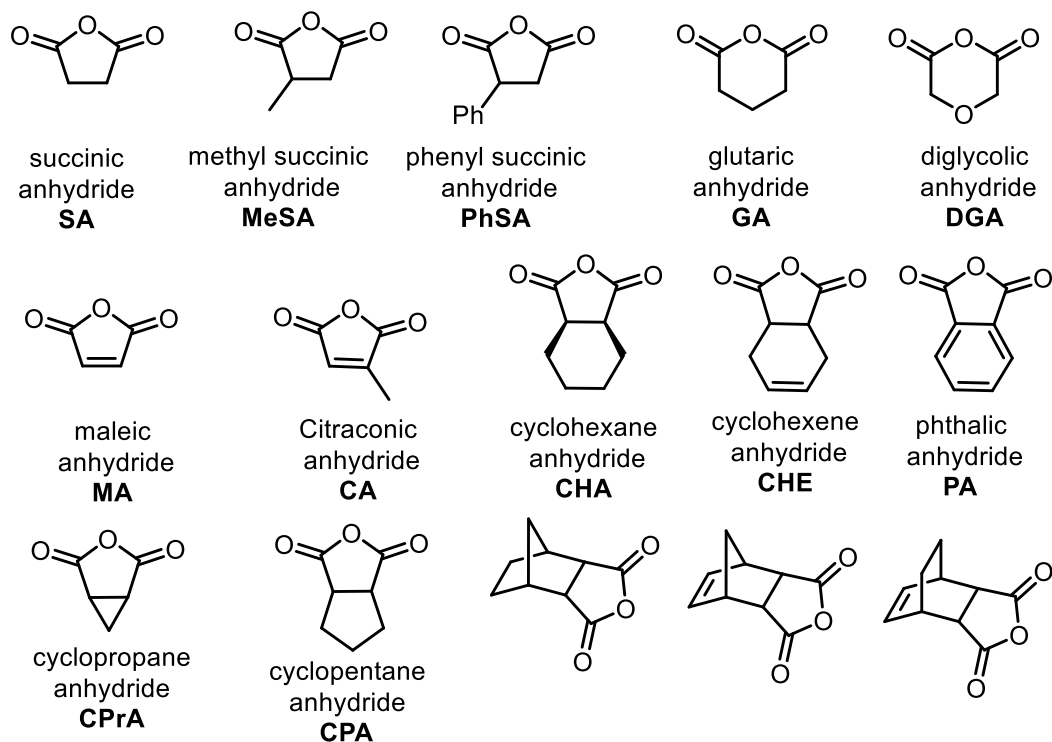
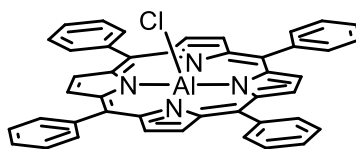


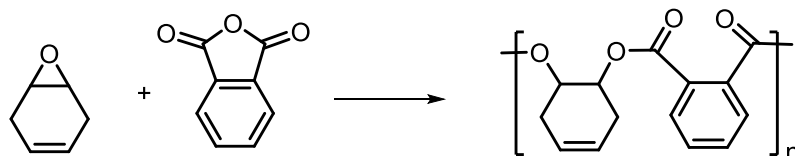
**Figure 1.15:** cyclic anhydride commonly used in ROCOP

In 1985, Inoue and co-workers reported the first successful copolymer with high degree of regulation in the sequences of the repeating unit, using an aluminium porphyrin, (5,10,15,20-tetraphenylporphinato)aluminium chloride **1.20**, coupled with a halide salt (Ethyltriphenylphosphonium bromide) as a novel initiator for the alternating copolymerization of phthalic anhydride (PA) and a series of epoxides.<sup>121</sup>



**1.20**

Whilst many copolymers are considered renewable since the anhydrides are derived from renewable sources, this is not the only claim to these polymers being renewable. An unsaturated polyester was synthesized using epoxides derived from 1,4-cyclohexadiene (CHD), which is often produced from renewable resources via self-metathesis of plant oil derivatives; the copolymerization partner was carbon dioxide or phthalic anhydride (Scheme 1.16).<sup>118</sup>



**Scheme 1.16:** polyester from 1,4-cyclohexadiene oxide (CHDO) and phthalic anhydride

Salen-type complexes have been widely studied as reactive initiators for ROCOP, for the synthesis of polyesters and polycarbonate with several metals. The nature of the polyesters resulting from the copolymerization reaction depends on the nature of the catalyst, the presence or absence of a cocatalyst, the solvent, the polymerization conditions, and the type of anhydride/epoxide. Duchateau and coworkers reported two types of chromium complexes, chromium tetraphenylporphyrinato (TPPCrCl, **1.21**) and salophen (SalophenCrCl, **1.22**). The copolymerization of CHO and SA in bulk without cocatalysts show a polyester with low ester content; an alternating polymer was formed when 4-(N,N-dimethylamino) pyridine (DMAP) was used, with  $M_n$  values between 700-2300 g mol<sup>-1</sup> being obtained. With a different anhydride, cyclopropane-1,2-dicarboxylic acid anhydride (CPrA), cyclopentane-1,2 dicarboxylic acid anhydride (CPA), and phthalic anhydride (PA), completely alternating polymers were obtained with catalyst **1.21**. Catalyst **1.22** gave low ester content polymers with both CPrA and SA.<sup>122</sup>

Coates and DiCiccio reported the ring-opening copolymerization of MA with various types of epoxide shown in Figure 1.16, using chromium (III) salen complexes as a catalyst (**1.23**).<sup>111</sup>

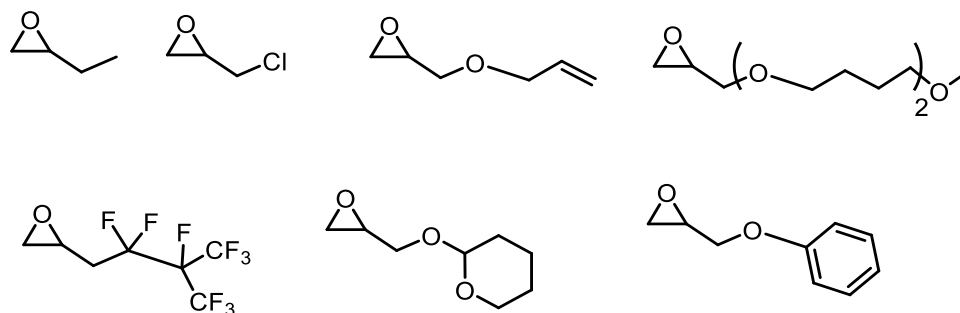
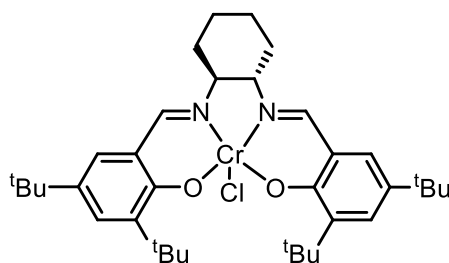


**Figure 1.16:** epoxides used by Coats and coworkers for copolymerization

Under mild conditions, all the ethylene oxide derivatives gave completely alternating polyesters with no evidence of polyether linkage. Interestingly, no cocatalyst was used; the presence of a cocatalyst is normally requisite for promoting an alternating microstructure of the polyester. The authors obtained high molecular weight polyesters ( $M_n > 15$  kDa). To control the molecular weight of the polyester, a chain transfer agent was demonstrated to afford low-molecular-weight unsaturated resins.



**1.23**

Escobedo and coworkers reported the same catalyst as an initiator for the ROCOP of various anhydrides and epoxides.<sup>112</sup> Unlike the previous study of Coates *et al.* who studied the copolymerization of MA and epoxide without any cocatalysts, Escobedo and coworker found that the chromium(III) catalyst alone was ineffective for the ROCOP of PA and CHO. The cocatalysts alone were less effective than a combination of both catalyst and cocatalyst. The researchers concluded that the relative reactivities of the copolymerization of CHO with various cyclic anhydrides are  $\text{CHA} > \text{PA} > \text{CHE}$ . Moreover, utilising CHA with

## Chapter 1 - An Introduction

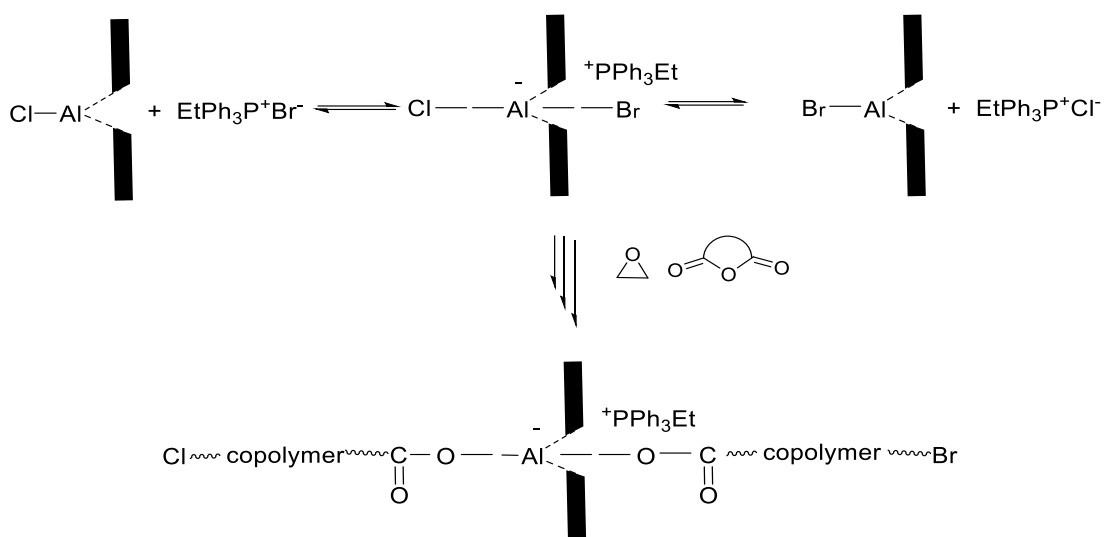
three diverse types of epoxide under identical reaction conditions afforded a reactivity trend of PO > CHO ≥ SO. No further explanation about the different reactivity of both cyclic anhydride and epoxide was given.

In 2012, Duchateau and coworkers demonstrated the reactivity of metal salen chloride complexes (M= Al, Cr and Co) with different ligand-diamine backbones, as catalysts for the ROCOP of CHO with SA, CPA and PA, employing a variety of cocatalysts. The aluminium catalysts were the least active while the chromium catalyst were the most reactive. Regarding the ligand moiety, salophen complexes were the best performing. Some bulk polymerization tests exhibited the formation of poly(ester-co-ether)s, whereas solution polymerization afforded alternating polyester.<sup>123</sup> Regarding the sterically demanding groups on the diamine backbone, more sterically demanding substituents, such as two phenyl groups on the diimine backbone, decreased the catalytic activity, compared to when less sterically demanding linkers such as ethylenediimine and cyclohexylenediimine were introduced. A similar trend was observed by Darensbourg and coworkers when they examined the activity of chromium salen systems.<sup>124</sup>

Although the study by DiCiccio and Coates demonstrated that the copolymerization of propylene oxide and maleic anhydride (MA) catalyzed by chromium(III) salen complexes, conducted in petroleum ether without the need of a cocatalyst, it is believed that in most cases the cocatalyst is crucial to improve the catalytic activity and ester content of the copolymers. A wide range of cocatalysts have been probed by researchers, which include PPNCI, DMAP, Et<sub>4</sub>N<sup>+</sup>CH<sub>3</sub>COO<sup>-</sup>, Et<sub>4</sub>N<sup>+</sup>Cl<sup>-</sup>, Et<sub>4</sub>N<sup>+</sup>Br<sup>-</sup>, EtPh<sub>3</sub>P<sup>+</sup>Br<sup>-</sup>

Inoue and coworkers suggested the mechanism of the copolymerization of phthalic anhydride and epoxides using (5,10,15,20-tetraphenyl porphinato) aluminium chloride (TPP)AlCl as a catalyst and ethyltriphenylphosphonium bromide (EtPh<sub>3</sub>PBr) as a cocatalyst. The combination of the catalyst and cocatalysts affords (TPP)AlCl-EtPh<sub>3</sub>PBr system) and the copolymerization reaction of the PA and epoxide proceeds simultaneously on both sides, respectively, of a metalloporphyrin plane (Scheme 1.17).<sup>121</sup> The molecular weight of the copolymer obtained by GPC analysis is higher than the calculated one by

almost a factor of two. The same authors used quaternary ammonium salt as a cocatalysts and the same observation was obtained.<sup>125,126</sup>



**Scheme 1.17:** Proposed mechanism of ROCOP of anhydride and epoxide suggested by Inoue and coworkers

## 1.12 Conclusions and objectives for this thesis

This overview has demonstrated that there is much need to develop the chemistry of polyesters via the ring-opening polymerization of cyclic esters, and that aluminium / titanium complexes have been proved to be active in this area. The effect of altering the periphery of the supporting ligand cannot be underestimated, and this is an area of further study. There is also much scope to diversify the production of polyesters using the ring-opening copolymerization of cyclic anhydrides and epoxides; this area has been much less studied, and primarily with 4-coordinate salen-type ligands, and porphyrins. There is much scope to develop this chemistry further.

As a result of these observations, the aim of this thesis involves:

- 1- Synthesis of new class of salen-type ligands bearing a pendant pyridyl donor. These ligands are referred to as the “Salpy” ligands.

- 2- To prepare a variety of complexes derived from earth abundant metals; in this study these were aluminium and titanium. The synthesis of multiple derivatives of the aluminium complexes was a specific target, which included changing the ligand substituents or the backbone of the ligand, as well as the ancillary ligand attached to the metal centre.
- 3- To use the Salpy complexes to produce polyester that are useful in, for example, biodegradable polymers, and those that find use in the medical sector. The aim was to study different cyclic esters, and to investigate the reactivity and selectivity of these initiators toward these polymerization reactions.
- 4- To study the Salpy aluminium complexes in the synthesis of polyesters with different properties via the ring-opening copolymerization of cyclic anhydrides and epoxides.
- 5- To probe the effect of the pyridyl on polymerization reactions when employed with bimetallic aluminium complexes.

### **1.13 References**

- 1 *Data obtained from [www.plasticseurope.org](http://www.plasticseurope.org).*
- 2 R. Geyer, J. R. Jambeck and K. L. Law, *Sci. Adv.*, 2017, **3**, e1700782.
- 3 *[www.newplasticseconomy.org](http://www.newplasticseconomy.org) .*
- 4 A. M. Diccio, J. M. Longo, G. G. Rodríguez-Calero and G. W. Coates, *J. Am. Chem. Soc.*, 2016, **138**, 7107–7113.
- 5 A. Duda and S. Penezek, *Macromolecules*, 1990, **23**, 1636–1639.
- 6 C. K. Williams, *Chem. Soc. Rev.*, 2007, **36**, 1573.
- 7 P. Dubois, O. Coulembier and J.-M. Raquez, *Handbook of ring-opening polymerization*, WILEY-VCH Verlag GmbH & Co., KGaA, Weinheim, 2009.
- 8 A. Ravve, *Principles of Polymer Chemistry*, Springer Science+Business Media, LLC, New York, 1st ed., 1995.

## Chapter 1 - An Introduction

- 9 O. Dechy-Cabaret, B. Martin-Vaca and D. Bourissou, *Chem. Rev.*, 2004, **104**, 6147–6176.
- 10 G. Odian, *Principles of Polymerization*, John Wiley & Sons, Hoboken, New Jersey, 4th ed., 2004.
- 11 A. Hofman, R. Szymański, S. Słomkowski and S. Penczek, *Makromol. Chemie*, 1984, **185**, 655–667.
- 12 A. C. Albertsson and I. K. Varma, *Biomacromolecules*, 2003, **4**, 1466–1486.
- 13 O. Nuyken and S. D. Pask, *Polymers (Basel)*, 2013, **5**, 361–403.
- 14 Z. J. Marek Kowalczyk, Piotr Kurcok, Wojciech GIBwkowsk, *J. Org. Chem.*, 1992, **57**, 389–391.
- 15 Z. Jedlinski, *J. Polym. Sci. Part A Polym. Chem.*, 2002, **40**, 2158–2165.
- 16 S. Sosnowski, S. Słomkowski and S. Penczek, *Macromolecules*, 1993, **26**, 5526–5527.
- 17 P. Kurcok, M. Kowalczyk, K. Hennek and Z. Jedliński, *Macromolecules*, 1992, **25**, 2017–2020.
- 18 P. Kurcok, Z. Jedliński and M. Kowalczyk, *J. Org. Chem.*, 1993, **58**, 4219–4220.
- 19 A. Duda, *J. Polym. Sci. Part A Polym. Chem.*, 1992, **30**, 21–29.
- 20 Z. Jedlinski, P. Kurcok and R. W. Lenz, *Macromolecules*, 1998, **31**, 6718–6720.
- 21 K. L. Liu, S. H. Goh and J. Li, *Polymer (Guildf)*, 2008, **49**, 732–741.
- 22 H. Uyama, K. Takeya and S. Kobayashi, *Proc. Japan Acad. Ser. B-Physical Biol. Sci.*, 1993, **69**, 203–207.
- 23 D. Knani, A. L. Gutman and D. H. Kohn, *J. Polym. Sci. Part A Polym. Chem.*, 1993, **31**, 1221–1232.

## Chapter 1 - An Introduction

- 24 Hiroshi Uyama; Shiro Kobayashi, *Chem. Lett.*, 1993, **22**, 1149–1150.
- 25 A. Duda, A. Kowalski, S. Penczek, H. Uyama and S. Kobayashi, *Macromolecules*, 2002, **35**, 4266–4270.
- 26 R. A. Gross, A. Kumar and B. Kalra, *Chem. Rev.*, 2001, **101**, 2097–2124.
- 27 S. Kobayashi, *J. Polym. Sci. Part A Polym. Chem.*, 1999, **37**, 3041–3056.
- 28 H. Uyama, K. Takeya, N. Hoshi and S. Kobayashi, *Macromolecules*, 1995, **28**, 7046–7050.
- 29 H. R. Kricheldorf, M. Berl and N. Scharnagl, *Macromolecules*, 1988, **21**, 286–293.
- 30 P. Dubois, C. Jacobs, R. Jérôme and P. Teyssté, *Macromolecules*, 1991, **24**, 2266–2270.
- 31 S. L. Hancock, M. F. Mahon and M. D. Jones, *New J. Chem.*, 2013, **37**, 1996–2001.
- 32 N. Ikpo, S. M. Barbon, M. W. Drover, L. N. Dawe and F. M. Kerton, *Organometallics*, 2012, **31**, 8145–8158.
- 33 M. Chen, H. Sun, W. Li, Z. Wang, Q. Shen and Y. Zhang, *J. Organomet. Chem.*, 2006, **691**, 2489–2494.
- 34 G. Montaudo, M. S. Montaudo, C. Puglisi, F. Samperi, N. Spassky, A. LeBorgne and M. Wisniewski, *Macromolecules*, 1996, **29**, 6461–6465.
- 35 A. Duda, Z. Florjanczyk, A. Hofman, S. Slomkowski and S. Penczek, *Macromolecules*, 1990, **23**, 1640–1646.
- 36 N. Spassky, V. Simic, M. S. Montaudo and L. G. Hubert-Pfalzgraf, *Macromol. Chem. Phys.*, 2000, **201**, 2432–2440.
- 37 N. Iwasa, S. Katao, J. Liu, M. Fujiki, Y. Furukawa and K. Nomura, *Organometallics*, 2009, **28**, 2179–2187.
- 38 A. Duda and S. Penczek, *Macromolecules*, 1995, **28**, 5981–5992.

## Chapter 1 - An Introduction

- 39 W. H. Carothers, G. L. Borough and F. J. Natta, *J. Am. Chem. Soc.*, 1932, **54**, 761–772.
- 40 J. K. Oh, D. I. Lee and J. M. Park, *Prog. Polym. Sci.*, 2009, **34**, 1261–1282.
- 41 J. R. Link, T. Gao, R. E. Betts, S. H. Reiver, V. Chin, S. N. Bhatia and M. J. Sailor, *Science (80-. )*, 2003, **299**, 2045–2047.
- 42 R. A. Gross, *Science (80-. )*, 2002, **297**, 803–807.
- 43 R. E. Drumright, P. R. Gruber and D. E. Henton, *Adv. Mater.*, 2000, **12**, 1841–1846.
- 44 B. Jeong, Y. H. Bae, D. S. Lee and S. W. Kim, *Nature*, 1997, **388**, 860–862.
- 45 J.-R. Sarasua, R. E. Prud'homme, M. Wisniewski, A. Le Borgne and N. Spassky, *Macromolecules*, 1998, **31**, 3895–3905.
- 46 M. S. Reeve, S. P. McCarthy, M. J. Downey and R. A. Gross, *Macromolecules*, 1994, **27**, 825–831.
- 47 M. T. Zell, B. E. Padden, A. J. Paterick, K. A. M. Thakur, R. T. Kean, M. A. Hillmyer and E. J. Munson, 2002, 7700–7707.
- 48 E. M. Woo and L. Chang, *Polymer (Guildf.)*, 2011, **52**, 6080–6089.
- 49 K. Nakano, N. Kosaka, T. Hiyama and K. Nozaki, *Dalt. Trans.*, 2003, 4039–4050.
- 50 H. Tsuji, F. Horii, S. H. Hyon and Y. Ikada, *Macromolecules*, 1991, **24**, 2719–2724.
- 51 Y. Ikada, K. Jamshidi, H. Tsuii and S. H. Hyon, *Macromolecules*, 1987, **20**, 904–906.
- 52 N. Nomura, R. Ishii, Y. Yamamoto and T. Kondo, *Chem. - A Eur. J.*, 2007, **13**, 4433–4451.
- 53 Z. Qu, R. Duan, X. Pang, B. Gao, X. Li, Z. Tang, X. Wang and X. Chen, *J.*

## Chapter 1 - An Introduction

- Polym. Sci. Part A Polym. Chem.*, 2014, **52**, 1344–1352.
- 54 N. Nomura, R. Ishii, M. Akakura and K. Aoi, *J. Am. Chem. Soc.*, 2002, **124**, 5938–5939.
- 55 K. A. M. Thakur, R. T. Kean, E. S. Hall, J. J. Kolstad and E. J. Munson, *Macromolecules*, 1998, **31**, 1487–1494.
- 56 M. H. Chisholm, S. S. Iyer, D. G. McCollum, M. Pagel and U. Werner-Zwanziger, *Macromolecules*, 1999, **32**, 963–973.
- 57 K. A. M. Thakur, R. T. Kean, E. S. Hall, J. J. Kolstad, T. A. Lindgren, M. A. Doscotch, J. I. Siepmann and E. J. Munson, *Macromolecules*, 1997, **30**, 2422–2428.
- 58 J. Coudane, G. Schwach and M. Vert, *J. Polym. Sci. Part A Polym. Chem.*, 1997, **35**, 1651–1658.
- 59 P. Degee, P. Dubois, R. Jerome, S. Jacobsen and H. G. Fritz, *Macromol. Symp.*, 1999, **144**, 289–302.
- 60 Y. L. Hsieh, Y. C. Lin, G. H. Lee and C. H. Peng, *Polym. (United Kingdom)*, 2015, **56**, 237–244.
- 61 A. Garcés, L. F. Sánchez-Barba, C. Alonso-Moreno, M. Fajardo, J. Fernández-Baeza, A. Otero, A. Lara-Sánchez, I. López-Solera and A. M. Rodríguez, *Inorg. Chem.*, 2010, **49**, 2859–2871.
- 62 G. G. Briand, S. A. Cairns, A. Decken, C. M. Dickie, T. I. Kostelnik and M. P. Shaver, *J. Organomet. Chem.*, 2016, **806**, 22–32.
- 63 L. E. N. Allan, G. G. Briand, A. Decken, J. D. Marks, M. P. Shaver and R. G. Wareham, *J. Organomet. Chem.*, 2013, **736**, 55–62.
- 64 S. Dagorne, M. Normand, E. Kirillov and J. F. Carpentier, *Coord. Chem. Rev.*, 2013, **257**, 1869–1886.
- 65 R. Lapenta, A. Buonerba, A. De Nisi, M. Monari, A. Grassi, S. Milione and C. Capacchione, *Inorg. Chem.*, 2017, **56**, 3447–3458.

## Chapter 1 - An Introduction

- 66 E. Luciano, A. Buonerba, A. Grassi, S. Milione and C. Capacchione, *J. Polym. Sci. Part A Polym. Chem.*, 2016, **54**, 3132–3139.
- 67 F. Della Monica, E. Luciano, G. Roviello, A. Grassi, S. Milione and C. Capacchione, *Macromolecules*, 2014, **47**, 2830–2841.
- 68 C. Sattayanon, W. Sontising, J. Jitonnorn, P. Meepowpan, W. Punyodom and N. Kungwan, *Comput. Theor. Chem.*, 2014, **1044**, 29–35.
- 69 L. Wang, C. E. Kefalidis, S. Sinbandhit, V. Dorcet, J. F. Carpentier, L. Maron and Y. Sarazin, *Chem. - A Eur. J.*, 2013, **19**, 13463–13478.
- 70 L. Wang, V. Poirier, F. Ghiotto, M. Bochmann, R. D. Cannon, J. F. Carpentier and Y. Sarazin, *Macromolecules*, 2014, **47**, 2574–2584.
- 71 E. D. Cross, L. E. N. Allan, A. Decken and M. P. Shaver, *J. Polym. Sci. Part A Polym. Chem.*, 2013, **51**, 1137–1146.
- 72 B. Gao, D. Li, Y. Li, Q. Duan, R. Duan and X. Pang, *New J. Chem.*, 2015, **39**, 4670–4675.
- 73 Y. A. Rulev, Z. Gugkaeva, V. I. Maleev, M. North and Y. N. Belokon, *Beistein J. Org. Chem*, 2015, **11**, 1614–1623.
- 74 K. Y. Hwang, M. H. Lee, H. Jang, Y. Sung, J. S. Lee, S. H. Kim and Y. Do, *Dalton Trans.*, 2008, **49**, 1818–20.
- 75 Y. Wang and H. Ma, *Chem. Commun.*, 2012, **48**, 6729.
- 76 P. Mckeown, M. G. Davidson, G. Kociok-ko and M. D. Jones, *Chem. Commun.*, 2016, **52**, 10431–10434.
- 77 S. Tabthong, T. Nanok, P. Kongsaree, S. Prabpai and P. Hormnirun, *Dalt. Trans.*, 2014, **43**, 1348–1359.
- 78 D. Li, Y. Peng, C. Geng, K. Liu and D. Kong, *Dalt. Trans.*, 2013, **42**, 11295–11303.
- 79 O. Dechy-cabaret, B. Martin-vaca and D. Bourissou, *Chem.Rev.*, 2004, **104**, 6147–6176.

## Chapter 1 - An Introduction

- 80 A. L. E. Borgne, V. Vincens, M. Jouglard and N. Spassky, *Makromol. Chem., Macromol. Symp.*, 1993, **73**, 37–46.
- 81 N. Spassky, M. Wisniewski, C. Pluta and A. Le, *Macromol. Chem. Phys.*, 1996, **197**, 2627–2637.
- 82 Z. Zhong, P. J. Dijkstra and J. Feijen, *Angew. Chemie - Int. Ed.*, 2002, **114**, 4692–4695.
- 83 K. Nomura, *Organometallics*, 2009, **28**, 2179–2187.
- 84 A. Lara-sa, M. North and P. Villuendas, *Catal. Sci. Technol.*, 2012, **2**, 1021–1026.
- 85 J. A. Castro-osma, M. North, W. K. Offermans and W. Leitner, 2016, 791–794.
- 86 M. North, P. Villuendas and C. Young, *Tetrahedron Lett.*, 2012, **53**, 2736–2740.
- 87 J. Martínez, J. A. Castro-osma, A. Earlam, C. Alonso-moreno, A. Otero, A. Lara-sunchez, M. North and A. Rodríguez-, *Chem. Eur. J.*, 2015, **21**, 9850–9862.
- 88 W. Li, H. Ouyang, L. Chen, D. Yuan, Y. Zhang and Y. Yao, *Inorg. Chem.*, 2016, **55**, 6520–6524.
- 89 V. A. Online, X. Pang, R. Duan, X. Li and X. Chen, *Polym. Chem.*, 2014, **5**, 3894–3900.
- 90 C. Kan, J. Ge and H. Ma, *Dalt. Trans.*, 2016, **45**, 6682–6695.
- 91 L. Chen, W. Li, D. Yuan, Y. Zhang, Q. Shen and Y. Yao, *Inorg. Chem.*, 2015, **54**, 4699–4708.
- 92 H. Huang, B. Wang, Y. Zhang and Y. Li, *Polym. Chem.*, 2016, **7**, 5819–5827.
- 93 G. J. P. Britovsek, V. C. Gibson and D. F. Wass, *Angew. Chemie Int. Ed.*, 1999, **38**, 428–447.

**Chapter 1 - An Introduction**

- 94 I. Sierra, P. Go, Y. Pe, M. Fajardo and A. Otero, *J. Organomet. Chem.*, 2006, **691**, 3053–3059.
- 95 S. Gendler, S. Segal, I. Goldberg, Z. Goldschmidt and M. Kol, *Inorg. Chem.*, 2006, **45**, 4783–4790.
- 96 A. J. Chmura, M. G. Davidson, M. D. Jones, M. D. Lunn, M. F. Mahon, A. F. Johnson, P. Khunkamchoo, S. L. Roberts and S. S. F. Wong, *Macromolecules*, 2006, **39**, 7250–7257.
- 97 P. S. Umare, G. L. Tembe, K. V. Rao, U. S. Satpathy and B. Trivedi, *J. Mol. Catal. A Chem.*, 2007, **268**, 235–243.
- 98 D. Takeuchi, T. Nakamura and T. Aida, *Macromolecules*, 2000, **33**, 725–729.
- 99 D. Priftis, N. Petzetakis, G. Sakellariou, M. Pitsikalis, D. Baskaran, J. W. Mays and N. Hadjichristidis, *Macromolecules*, 2009, **42**, 3340–3346.
- 100 A. Touris, K. Kostakis, S. Mourmouris, Y. Kotzabasakis, M. Pitsikalis and N. Hadjichristidis, *Macromolecules*, 2008, **41**, 2426–2438.
- 101 Y. Takashima, Y. Nakayama and T. Hirao, *J. Organomet. Chem.*, 2004, **689**, 612–619.
- 102 H. Tseng, H. Chen, Y. Huang, W. Lu, Y. Chang, M. Y. Chiang, Y. Lai and H. Chen, *Inorg. Chem.*, 2016, **55**, 1642–1650.
- 103 B. V. D. Braun, H. Cherdrón, M. Reham, H. Ritter, *Polymer Synthesis: Theory and Practice*, Springer, Berlin, 4th ed., 2005.
- 104 C. Carraher, *Polymer Chemistry*, Marcel Dekker, Inc., New York, 6th ed., 2003.
- 105 M. P. Stevens, *Polymer Chemistry: An Introduction*, Oxford University Press, Oxford, 3rd ed., 1999.
- 106 N. P. Cheremisinoff, *Polymer Characterization: Laboratory Techniques and Analysis*, Noyes Publications, New Jersey, 1996, vol. 22.

## Chapter 1 - An Introduction

- 107 K. Jenkins, *Beginner's Guide to Size-Exclusion Chromatography*, Waters Corporation, Milford, 2013.
- 108 A. Bernard, C. Chatterjee and M. H. Chisholm, *Polym. (United Kingdom)*, 2013, **54**, 2639–2646.
- 109 N. J. Van Zee, M. J. Sanford and G. W. Coates, *J. Am. Chem. Soc.*, 2016, **138**, 2755–2761.
- 110 A. Takasu, T. Bando, Y. Morimoto, Y. Shibata and T. Hirabayashi, *Biomacromolecules*, 2005, **6**, 1707–1712.
- 111 A. M. Diccio and G. W. Coates, *J. Am. Chem. Soc.*, 2011, **133**, 10724–10727.
- 112 D. J. Darensbourg, R. R. Poland and C. Escobedo, *Macromolecules*, 2012, **45**, 2242–2248.
- 113 J. Liu, Y.-Y. Bao, Y. Liu, W.-M. Ren and X.-B. Lu, *Polym. Chem.*, 2013, **4**, 1439–1444.
- 114 E. Hosseini Nejad, A. Paoniasari, C. E. Koning and R. Duchateau, *Polym. Chem.*, 2012, **3**, 1308.
- 115 C.-Y. Yu, H.-J. Chuang and B.-T. Ko, *Catal. Sci. Technol.*, 2016, **6**, 1779–1791.
- 116 J. M. Longo, A. M. Diccio and G. W. Coates, *J. Am. Chem. Soc.*, 2014, **136**, 15897–15900.
- 117 P. K. Saini, C. Romain, Y. Zhu and C. K. Williams, *Polym. Chem.*, 2014, **5**, 6068–6075.
- 118 M. Winkler, C. Romain, M. A. R. Meier and C. K. Williams, *Green Chem.*, 2015, **17**, 300–306.
- 119 D. F. Liu, L. Y. Wu, W. X. Feng, X. M. Zhang, J. Wu, L. Q. Zhu, D. Di Fan, X. Q. Lü and Q. Shi, *J. Mol. Catal. A Chem.*, 2014, **382**, 136–145.
- 120 Y. Zhu, C. Romain and C. K. Williams, *J. Am. Chem. Soc.*, 2015, **137**,

**Chapter 1 - An Introduction**

12179–12182.

- 121 T. Aida, K. Sanuki and S. Inoue, *Macromolecules*, 1985, **18**, 1049–1055.
- 122 S. Huijser, E. Hosseininejad, R. Sablong, C. De Jong, C. E. Koning and R. Duchateau, *Macromolecules*, 2011, **44**, 1132–1139.
- 123 E. Hosseini Nejad, C. G. W. Van Melis, T. J. Vermeer, C. E. Koning and R. Duchateau, *Macromolecules*, 2012, **45**, 1770–1776.
- 124 D. J. Darensbourg, R. M. Mackiewicz, J. L. Rodgers, C. C. Fang, D. R. Billodeaux and J. H. Reibenspies, *Inorg. Chem.*, 2004, **43**, 6024–6034.
- 125 T. Aida and S. Inoue, *J. Am. Chem. Soc.*, 1985, **107**, 1358–1364.
- 126 T. Aida, M. Ishikawa and S. Inoue, *Macromolecules*, 1986, **19**, 8–13.

# **Chapter 2**

## **Synthesis, Characterization, and X-ray Crystal Structures of Salpy, Acpy and Salpn type Ligands, and their Complexes with Aluminium and Titanium**

## 2.1 Introduction

Ligands play very important roles in organometallic and coordination chemistry, since they can bring about drastic changes in the chemical and physical properties of transition metal complexes. Thus, in many reactions catalyzed by transition metals, the products and/or product distributions depend on the ligand employed.<sup>1</sup>

When two equivalents of salicylaldehyde are combined with a diamine, a particular chelating Schiff base is obtained, the so-called Salen ligands. The first salen ligand was prepared by Pfeiffer *et al.* in 1933, by the direct condensation of salicylaldehyde with ethylene diamine.<sup>2</sup> These types of ligands have four coordinating atoms, often forming an N<sub>2</sub>O<sub>2</sub> plane in their complexes; for octahedral complexes this leaves two axial sites available for ancillary ligands. In this regard, they are very much like porphyrins, but are more easily prepared. Although the term Salen was used originally only to describe the tetradentate Schiff bases derived from ethylenediamine, the more general term “Salen-type” is used in the literature to describe the class of [O,N,N,O] tetradentate bis(iminophenol) Schiff base ligands. Depending on the aromatic substituents, and the nature of the diamine used in the synthesis, the structure of these ligands can vary enormously, since the number of possible substituents for both the aromatic rings and diamine moieties are vast, and can be prepared using simple chemical techniques (Figure 2.1).<sup>3-6</sup>

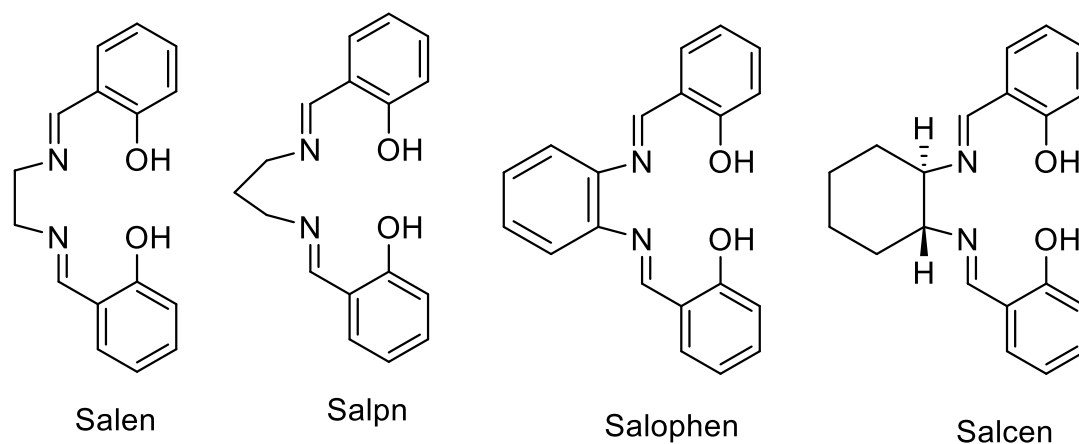


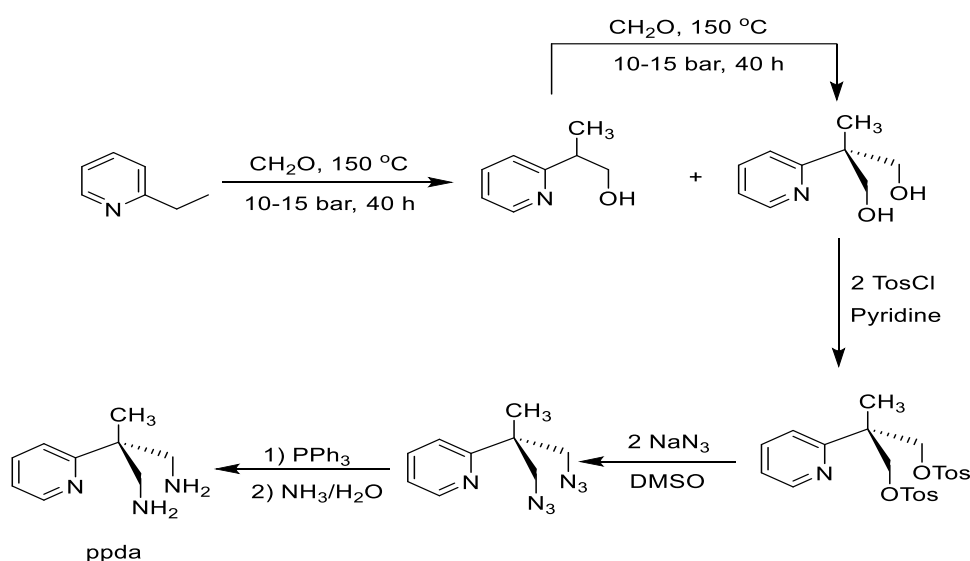
**Figure 2.1:** Different types of Salen ligands

## 2.2 Synthesis and characterization of Ligands

### 2.2.1 Synthesis and characterizations of dianionic salen type ligands

This thesis is principally concerned with complexes bearing salen-type ligands, bearing an additional pyridyl donor. These ligands were prepared using a common precursor of 2-methyl-2-pyridin-2-yl-propane-1,3-diamine, the synthesis of which is described below.

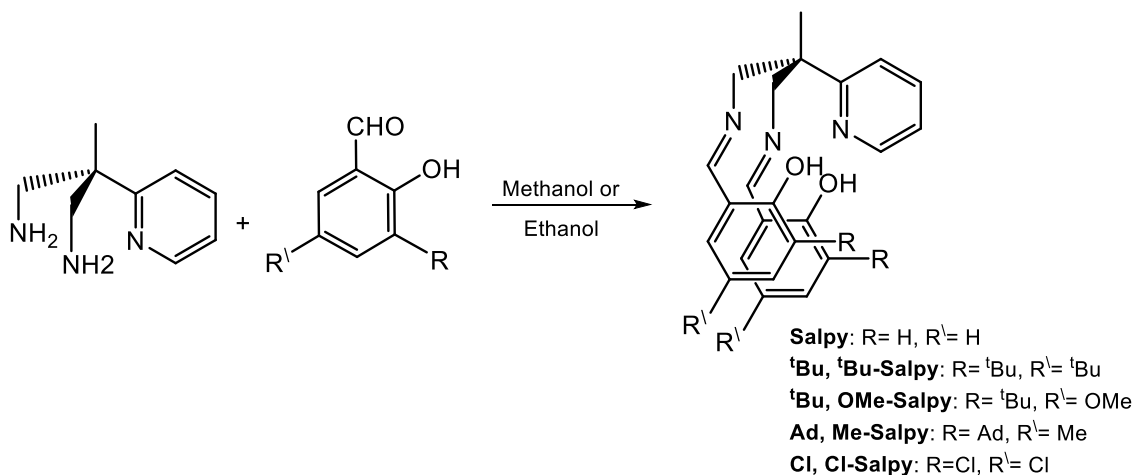
2-Methyl-2-pyridin-2-yl-propane-1,3-diamine (ppda) was synthesized using a modified procedure based on the published procedure by Gade and co-workers.<sup>7</sup> The preparation was carried out in 4 steps (Scheme 2.1). The first step involved the reaction of 2-ethylpyridine with formaldehyde solution (37%) in a mechanically-stirred autoclave at 150 °C for 40 h to afford both mono- and bis-alcohol derivatives. The bis-alcohol was separated by vacuum distillation as an orange viscous oil in low yield (18%). The yield was increased to 51% by further reaction of mono-alcohol with formaldehyde under the same conditions. The second step was the tosylation of bis-alcohol with p-toluenesulfonyl chloride (tosyl chloride), which allows conversion into an organic azide by reaction with sodium azide in the third step. Finally, 2-methyl-2-pyridin-2-yl-propane-1,3-diamine (ppda) was obtained as a colourless, viscous oil, by treatment with triphenylphosphine followed by aqueous ammonia.



**Scheme 2.1:** Synthesis of 2-methyl-2-pyridin-2-yl-propane-1,3-diamine (ppda)

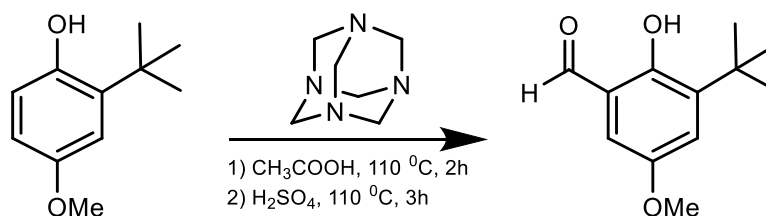
**Chapter 2 - Synthesis, Characterization, and X-ray Crystal Structures of Salpy, Acpy and Salpn type Ligands, and their Complexes with Aluminium and Titanium**

The Salpy protio-ligands were synthesized using ppda as the precursor. The ligands, (<sup>t</sup>Bu, <sup>t</sup>Bu - Salpy), (<sup>t</sup>Bu, OCH<sub>3</sub>- Salpy), (Ad, CH<sub>3</sub>- Salpy) and (Cl, Cl-Salpy) were synthesized via Schiff base condensation of ppda with the appropriate salicylaldehyde derivatives (Equation 2.1).



**Equation 2.1:** Synthesis of (R, R<sup>1</sup> - Salpy) ligands

In some instances, the appropriate salicylaldehyde derivative was not commercially available; in such cases they were prepared using published procedures. The <sup>t</sup>Bu, OCH<sub>3</sub>- salicylaldehyde was synthesized according to literature procedure<sup>8</sup> by using the Duff reaction or hexamine aromatic formylation. In this reaction 2-tert-butyl-4-methoxyphenol and hexamethylenetetramine were heated at 110 °C in glacial acetic acid, and then treated with aqueous sulfuric acid (Equation 2.2).

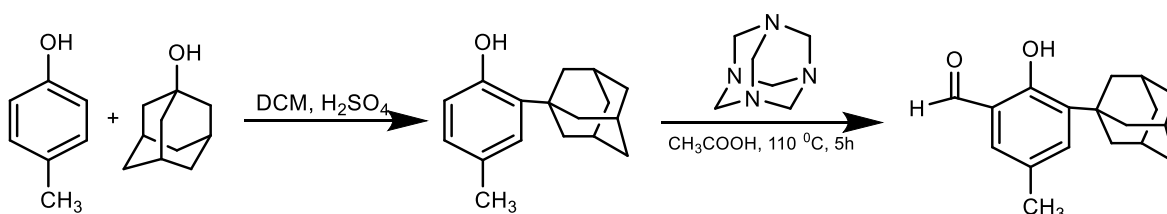


**Equation 2.2**

The aldehyde precursor of (Ad, CH<sub>3</sub>- Salpy) was prepared in two steps, the first being the reaction of p-cresol with 1-adamantanol and catalytic concentrated

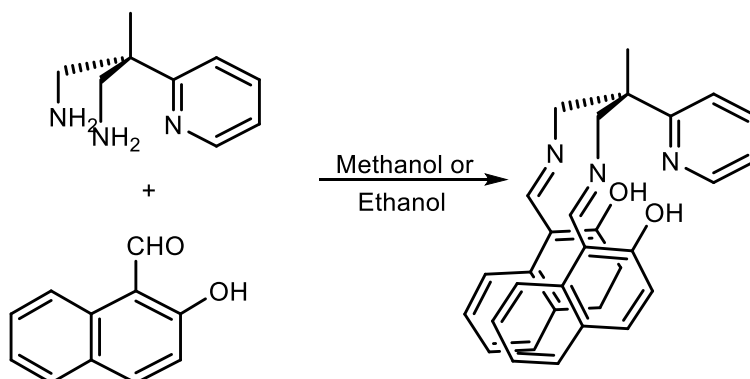
**Chapter 2 - Synthesis, Characterization, and X-ray Crystal Structures of Salpy, Acpy and Salpn type Ligands, and their Complexes with Aluminium and Titanium**

sulfuric acid to give 2-adamantyl-4-methylphenol. The second step involved reacting 2-adamantyl-4-methylphenol with hexamine and glacial acetic acid to give 3-(1-adamantyl)-5-methylsalicylaldehyde (Equation 2.3).<sup>9</sup>



**Equation 2.3**

The Naphpy ligand differs from the other ligands in that phenolic moiety is derived from hydroxynaphthalene (Equation 2.4), whereas the others are derived from variously substituted salicylaldehydes.



**Equation 2.4: Synthesis of Naphpy ligand**

The synthesis of the Naphpy ligand was found to be more problematic than the other ligand derivatives discussed, and its successful preparation was only achieved under the strict observance of specific conditions. The first step of the preparation was the recrystallization of the commercially-obtained aldehyde precursor, 2-hydroxy-1-naphthaldehyde. Comparison of the <sup>1</sup>H NMR spectra of the aldehyde before and after recrystallization indicated no apparent differences, however when the crude (non-recrystallized) aldehyde was reacted with ppda, a

**Chapter 2 - Synthesis, Characterization, and X-ray Crystal Structures of Salpy, Acpy and Salpn type Ligands, and their Complexes with Aluminium and Titanium**

sticky viscous oil was obtained, which defied purification. This problem persisted despite employing a variety of reaction conditions, such as reaction times, temperatures, and solvents. In the successful procedure, the reaction was conducted under an argon atmosphere at 40 °C overnight, using the recrystallized aldehyde. This gave a clean golden coloured solid. Figure (2.2) shows the <sup>1</sup>H NMR spectra of (Naphpy) prepared under both sets of conditions.

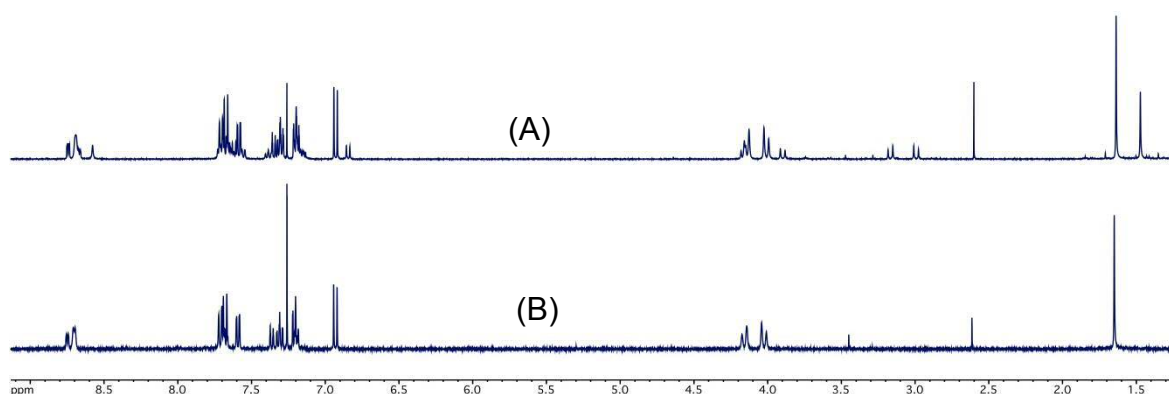
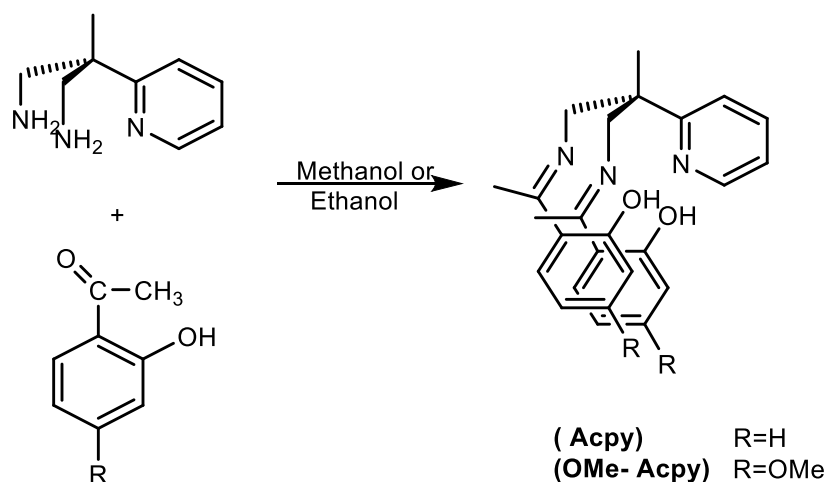


**Figure 2.2:** <sup>1</sup>H NMR spectra (400 MHz, CDCl<sub>3</sub>, 293 K) of the Naphpy protio-ligand, prepared under two reaction conditions: (A) using aldehyde as purchased, and (B) with recrystallized aldehyde.

(Acpy) and (OMe- Acpy) were synthesized via the Schiff base condensation of ppda with 2-hydroxyacetophenone and 2-hydroxy-4-methoxyacetophenone respectively (Equation 2.5).



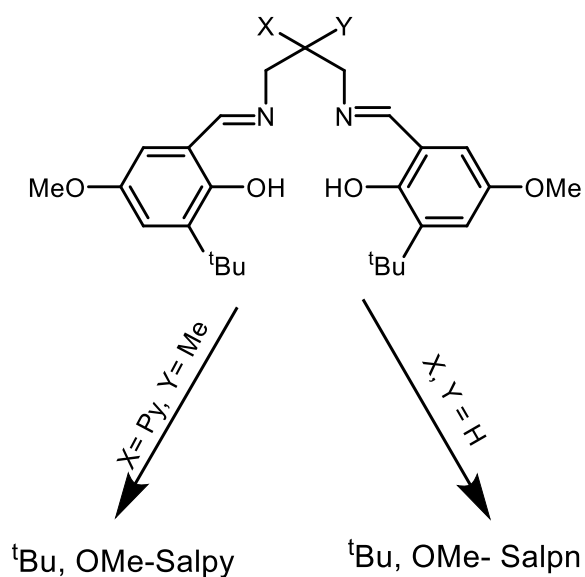
**Equation 2.5:** Synthesis of (R- Acpy) ligands

**Chapter 2 - Synthesis, Characterization, and X-ray Crystal Structures of Salpy, Acpy and Salpn type Ligands, and their Complexes with Aluminium and Titanium**

Both these two ligands were prepared using different conditions to the aldehyde ligand derivatives (Salpy and Naphpy). For these more sterically demanding derivatives, higher temperatures and longer reaction times were needed to complete the reactions. Generally, aldehydes are more reactive towards nucleophilic substitutions than ketones because of both steric and electronic effects. In aldehydes, the relatively small hydrogen atom is attached to one side of the carbonyl group, while a larger R group is affixed to the other side. In ketones, however, R groups are attached to both sides of the carbonyl group. Thus, steric hindrance is less in aldehydes than in ketones. Electronically, aldehydes have only one R group to supply electrons toward the partially positive carbonyl carbon (inductive effect), while ketones have two. The greater the electron density being supplied to the carbonyl carbon, the less electrophilic it is, which makes it less reactive towards nucleophiles. In both the Acpy and OMe-Acpy ligand syntheses, the ppda and ketone were stirred at 70 °C in dry ethanol for 20 h. After removing the solvent, the product was oily for Acpy; the protio-ligand was obtained as a solid after crystallization from DCM/hexanes. Crystals were formed upon cooling to -18 °C in a freezer.

In order to investigate the role of the central pyridyl donor, a comparable ligand was prepared, except where the pyridyl donor was omitted; such ligands have been reported previously and have been named as Salpn. The <sup>t</sup>Bu, OMe- Salpn derivative was synthesized by the Schiff base condensation of 1,3-propanediamine with 3-tert-butyl-5-methoxysalicylaldehyde (Scheme 2.2).

**Chapter 2 - Synthesis, Characterization, and X-ray Crystal Structures of Salpy, Acpy and Salpn type Ligands, and their Complexes with Aluminium and Titanium**



**Scheme 2.2:** The difference between <sup>t</sup>Bu, OMe- Salpy and <sup>t</sup>Bu, OMe- Salpn

This strategy allows essentially identical chemistry to be carried out, with identical synthetic pathways to aluminium and titanium complexes, where the only difference is in the donor group at the bridge, and therefore providing a means to study the behaviour of pyridyl group to afford a pentadentate ligand, as opposed to a tetradentate ligand.

All the prepared ligands were characterized by <sup>1</sup>H and <sup>13</sup>C NMR, and IR spectroscopies, and by mass spectrometry. 2D NMR spectra were measured where necessary to verify connectivity and assignment, especially in the aromatic region. The most diagnostic <sup>1</sup>H NMR signals for ligands Salpy, <sup>t</sup>Bu,<sup>t</sup>Bu-Salpy, Naphpy, <sup>t</sup>Bu,OMe-Salpy, Ad,Me-Salpy, <sup>t</sup>Bu,OMe-Salpn, Cl,Cl-Salpy, Acpy, and OMe-Acpy, are listed in Table 2.1

**Table 2.1:** Important signals for the prepared ligands

Compound	OH	H <sup>6</sup>	N=CH	CH <sub>2</sub>	CH <sub>3</sub>
Salpy	13.21	8.63	8.31	4.13, 4.0	1.53
Salpy-Me	10.46	8.60	-	3.65, 3.56	1.68
<sup>t</sup> Bu, <sup>t</sup> Bu - Salpy	13.57	8.64	8.36	4.07	1.58
Naphpy	14.42	8.59	8.54	3.98, 3.85	1.48
<sup>t</sup> Bu, OMe- Salpy	13.31	8.53	8.19	3.98	1.49
Ad, Me- Salpy	13.57	8.62	8.27	4.05	1.60
<sup>t</sup> Bu, OMe- Salpn	13.59	-	8.36	3.73	-
Cl, Cl- Salpy	14.12	8.60	8.17	4.15, 4.04	1.55
Acpy	15.73	8.50	-	4.19, 4.05	1.58
OMe- Acpy	16.6	8.61	-	4.15, 4.01	1.70

Most of the resonances were observed in the expected regions, e.g. 8.1–8.4 ppm for the imine CH resonances, with subtle but insignificant variations between ligand derivatives. These signals therefore warrant little further comment. More interestingly however, the <sup>1</sup>H resonances of the two methylene (CH<sub>2</sub>) groups were observed as two doublets between approximately 3.5 and 4.2 ppm, with corresponding geminal coupling of <sup>2</sup>J<sub>HH</sub> = 12–15 Hz. The reason for this is because these protons are diastereotopic, being positioned *cis* to either the apical methyl or to the pyridyl (Figure 2.3).

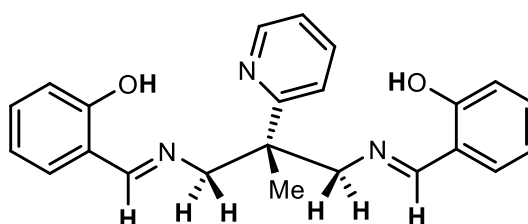


**Figure 2.3:** the diastereotopic CH<sub>2</sub> protons

This renders the protons inequivalent, with different chemical shifts. In these ligands, the mirror plane in the molecule renders the two methylene groups equivalent, hence why two doublets are observed. These signals can be used to identify the symmetry of their complexes; complexes bearing C<sub>s</sub> symmetry will

**Chapter 2 - Synthesis, Characterization, and X-ray Crystal Structures of Salpy, Acpy and Salpn type Ligands, and their Complexes with Aluminium and Titanium**

show two doublets as in the protio-ligand, whereas  $C_1$  symmetric complexes (i.e. those where the two “arms” are inequivalent) will show four doublets.<sup>10–12</sup> The difference between the chemical shifts of the methylene protons is strongly influenced by their precise chemical environment. Depending on this difference, these signals can be observed as two very distinct doublets, roofed doublets, highly second order multiplets, or even a singlet, in the rare case where the chemical shifts are coincidental (Figure 2.4). This makes these signals highly diagnostic, since two similar species are highly unlikely to show the same signal separation. This feature is particularly useful in the characterization of metal complexes, and will be discussed in due course.

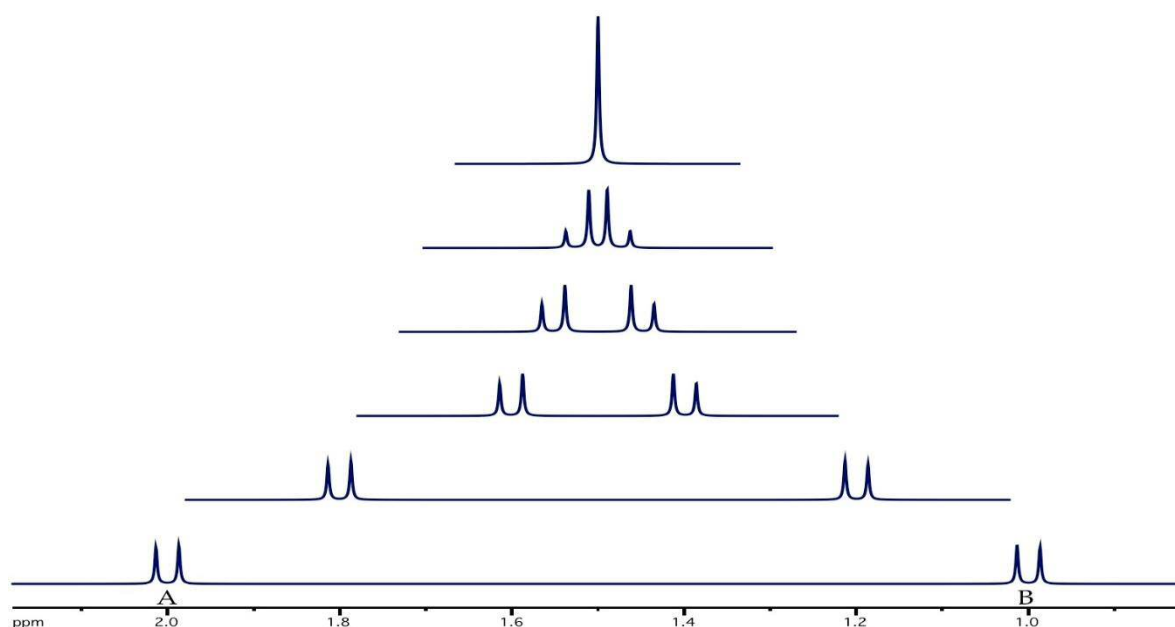


**Figure 2.4:** Simulated signals (300 MHz) of mutually-coupled doublets and their variation as a function of chemical shift difference

The  $C_s$ -symmetry of the Salpy, Salpn and Naphpy ligands result in simple  $^1H$  NMR spectra. Only one singlet between 8.17-8.54 ppm for the two imine protons was observed in each case; these are very distinctive due to there being only one proton of the pyridyl ring ( $H^6$ ) which appears in the range 8.50-8.64 ppm. All other aromatic and pyridyl protons were observed at low chemical shift relative to the imine protons.

**Chapter 2 - Synthesis, Characterization, and X-ray Crystal Structures of Salpy, Acpy and Salpn type Ligands, and their Complexes with Aluminium and Titanium**

The other remarkable feature is the phenol OH chemical shifts. As shown in Table 2.1, the chemical shift of the OH signal in the imine ligands (13.2–16.6 ppm) is significantly higher than the corresponding signal in the amine one (10.4 ppm). This presumably originates from the internal hydrogen bonding between the imine nitrogen and the phenol OH being more efficient in comparison to that in the amine ligand. The ligands derived from ketones have high OH chemical shifts in comparison with the salicylaldehyde ligands.

The infrared spectra of the ligands show an extremely broad O–H stretching vibration between 3100-3300  $\text{cm}^{-1}$ , which is indicative of strong hydrogen bonding. An intramolecular hydrogen bond can form in these ligands resulting in formation of a stable 6-membered as shown in Figure 2.5; this is also evident from the X-ray structure displayed in Figure 2.9.

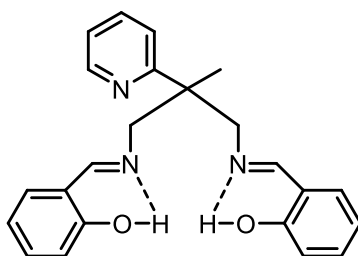


**Figure 2.5:** hydrogen bonding in Salpy ligand

This being the case, no absorption bands due to the free O-H stretching were observed in the infrared spectra of any of the ligands, which are typically in the range of 3700–3584  $\text{cm}^{-1}$ .<sup>13</sup> A strong C=N stretching vibration band was observed between 1600-1639  $\text{cm}^{-1}$ .

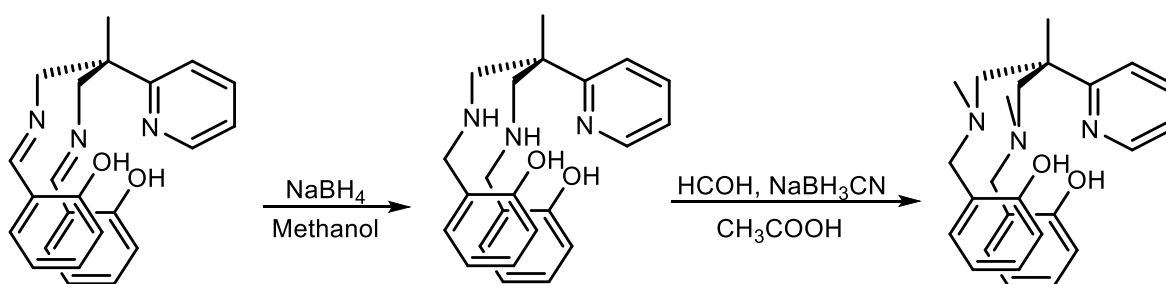
### **2.2.2 Reduction of Schiff base compounds (synthesis of secondary diamine H<sub>2</sub> - Salpy and alkylation of secondary amine CH<sub>3</sub>-Salpy)**

Like the carbon-oxygen double bond, the carbon-nitrogen double bond of a Schiff base can be readily reduced by complex metal hydrides. One of the most efficient and convenient methods for the conversion of C=N into amino compounds is the reduction of this double bond. The diamine derivatives of the ligands discussed above were synthesized by reduction with sodium borohydride in methanol at

**Chapter 2 - Synthesis, Characterization, and X-ray Crystal Structures of Salpy, Acpy and Salpn type Ligands, and their Complexes with Aluminium and Titanium**

room temperature. This reducing agent smoothly reduces Schiff bases to secondary amines in good yield. Sodium borohydride is preferred to lithium aluminium hydride because of its inertness to a wider range of solvent media, and because of its greater specificity in that other substituents such as nitro or chloro, which are reducible by lithium aluminium hydride, are unaffected by sodium borohydride.

The reduced product, Salpy-H<sub>2</sub> was soluble in most organic solvents such as dichloromethane, and so it was easy to extract it after aqueous workup to obtain the pure product. Salpy-Me was subsequently prepared by reaction of Salpy-H<sub>2</sub> with formaldehyde and sodium cyanoborohydride (Equation 2.6). After workup, the product was obtained as a white solid.



**Equation 2.6**

One of the advantages of this method for methylation of the amine, over the other available methods, is that the reaction occurs at room temperature, reducing the possibility of redistribution or decomposition of some of our ligands at high temperature. An alternative method employs formaldehyde and formic acid to provide the methyl group; however, the reaction is conducted at 98 °C, and at this temperature, in the presence of formaldehyde and formic acid, a polymerization reaction can occur. In addition, this method requires the use of a strong base such as sodium hydroxide in the extraction step, which is unsuitable for the relatively acidic phenolic groups.

The differences between imine and amine ligands centre on the nature, but not the identity, of the coordinating atoms, as well as ligand rigidity: The Salpy imine-containing ligands contain rigid C=N double bonds and a potential N<sub>3</sub>O<sub>2</sub> donor set (except for <sup>t</sup>Bu,OMe-Salpn, which contains a N<sub>2</sub>O<sub>2</sub> donor set). Conversely, Salpy-Me contains more flexible C-N single bonds; whilst these ligands also contain a potential N<sub>3</sub>O<sub>2</sub> donor set, the coordinative nature of an imine and amine are inherently different. All of the salen-type ligands in the above discussion contain two ionizable phenol groups, making them dianionic ligands when deprotonated.

### **2.2.3 Synthesis of neutral symmetrical ligands**

The second type of ligands is Pypy which were synthesized by the condensation of ppda with 2-acetylpyridine. Many attempts were made to prepare a symmetrical ligand from the condensation of 1 equivalent of ppda with 2 equivalents of 2-acetylpyridine but the pure symmetrical ligand Pypy<sup>a</sup> could not be obtained. Instead, after recrystallization, a cyclic hexahydropyrimidine compound Pypy<sup>b</sup> was obtained as a yellow solid (Scheme 2.3) which is not the expected neutral ligand. Many experiments were conducted, including changing the temperature, time and solvents to get Pypy<sup>a</sup>, however the main product was always Pypy<sup>b</sup>. This structure was verified by <sup>1</sup>H NMR spectroscopy (Figure 2.6), two-dimensional NMR spectroscopy, and X-ray crystallography (Figure 2.7). X-ray data for this structure, and all other in this thesis, were measured by the EPSRC National Crystallography Service<sup>14</sup> at the University of Southampton, and the structure solved and refined by Dr. Benjamin Ward.

**Chapter 2 - Synthesis, Characterization, and X-ray Crystal Structures of Salpy, Acpy and Salpn type Ligands, and their Complexes with Aluminium and Titanium**

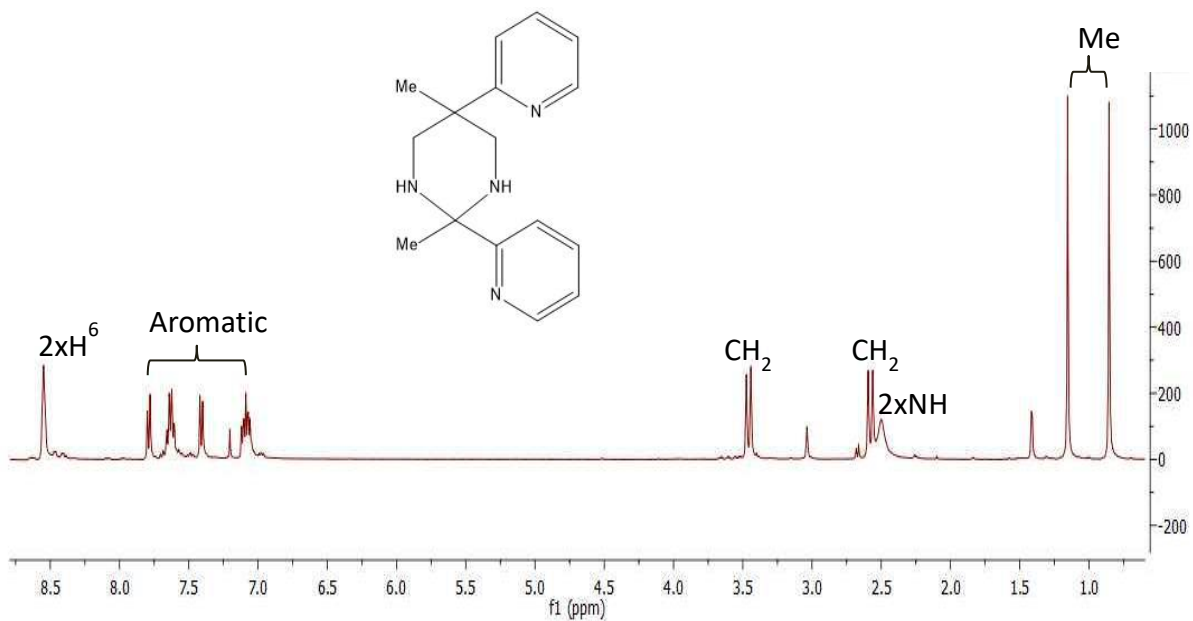


**Figure 2.6:** <sup>1</sup>H NMR spectrum (400 MHz, 293 K, CDCl<sub>3</sub>) of Pypy<sup>b</sup>

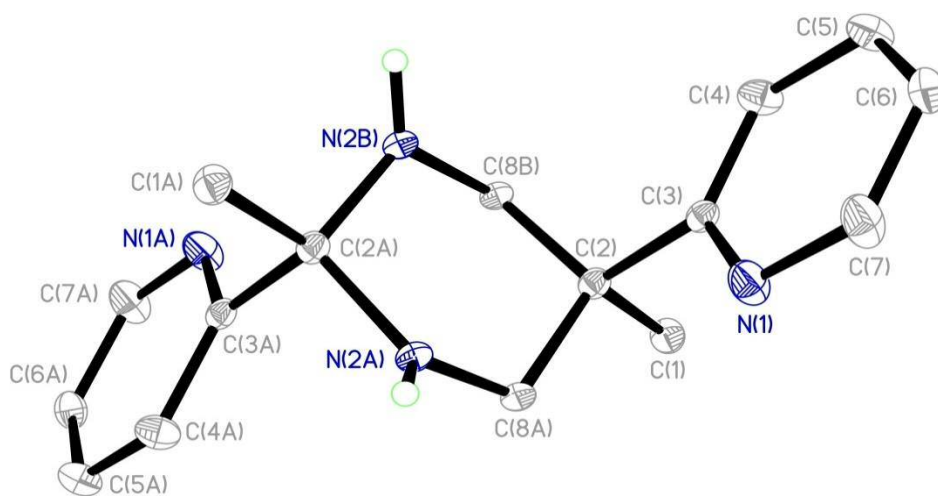
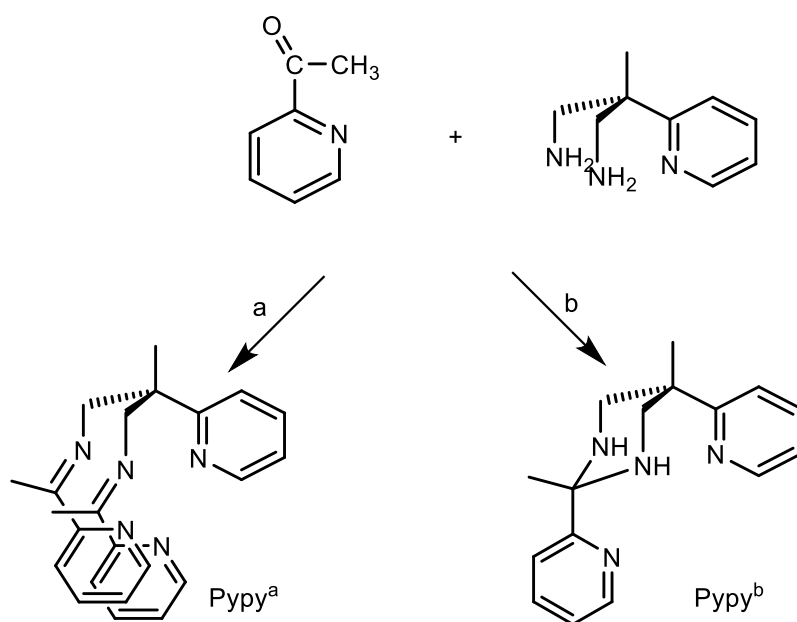


**Figure 2.7:** Molecular structure of Pypy<sup>b</sup>. Displacement ellipsoids are drawn at 30% probability and H atoms other than NH have been omitted for clarity. NH hydrogens are drawn as spheres of arbitrary radius



**Scheme 2.3:** The products of the reaction of ppda with 2-acetylpyridine

The molecular motif of Pypy<sup>b</sup> has been reported by Houser *et al.* In their report, Houser and co-workers used it as an intermediate in the step-wise condensation of different aldehydes with ppda, ultimately forming asymmetric bis(imine) and bis(amine) ligands.<sup>15,16</sup> Its formation presumably has implications for the mechanism of ligand formation from ppda. It is reasonable to suggest that the Schiff base condensation proceeds via the hexahydropyrimidine intermediate, which under “normal” reaction conditions (*i.e.* in the presence of a second equivalent of aldehyde or ketone) spontaneously undergoes ring-opening to afford the bis(imine) protio-ligand. In the case of 2-acetylpyridine, the ring-opening reaction is presumably disfavoured, which prevents further reaction. Steric arguments would be reasonable (*i.e.* the 2-acetylpyridine is too sterically crowded to permit the ring-opening reaction without forcing conditions), but it is surprising, and unexpected, that this should be the case when other ketones afford the bis(imine) ligands without apparent hindrance, as described in Section 2.3.

The extent to which this observation pertains was investigated by changing the aldehyde precursor, using 2-quinolinecarboxaldehyde instead of 2-acetylpyridine

**Chapter 2 - Synthesis, Characterization, and X-ray Crystal Structures of Salpy, Acpy and Salpn type Ligands, and their Complexes with Aluminium and Titanium**

(Qupy). Unfortunately, the resulting ligand was not clean and more than one component appeared in the NMR spectrum. Crystallization with different solvents, or separation by column chromatography was not able to give a pure product. With all different reaction conditions attempted, an impure dark brown product was obtained. The  $^1\text{H}$  NMR spectrum of Qupy is shown in Figure 2.8.

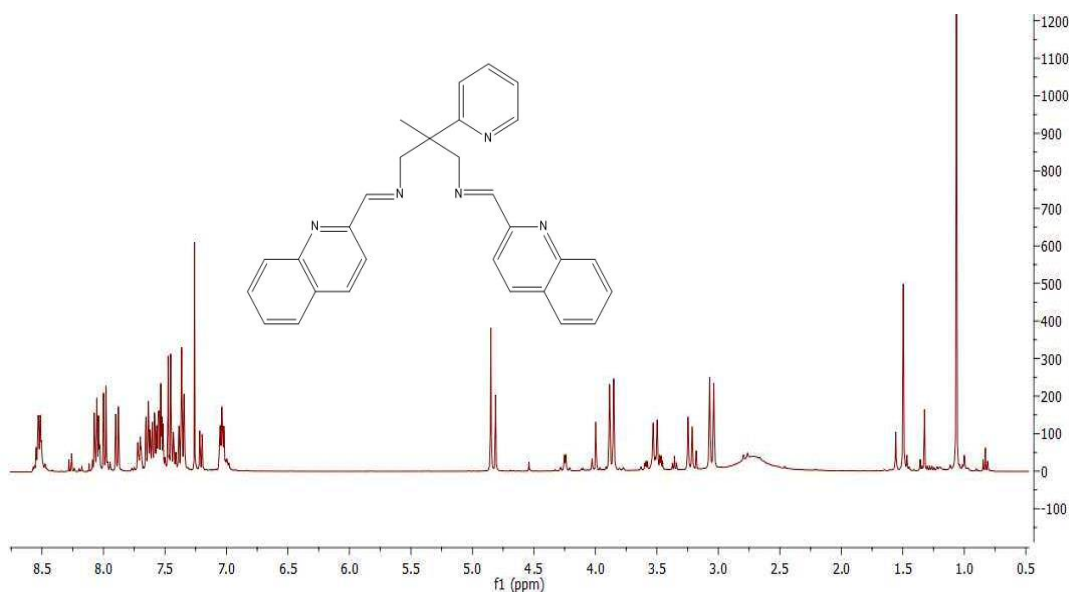


**Figure 2.8:**  $^1\text{H}$  NMR spectrum (400 MHz, 293 K,  $\text{CDCl}_3$ ) of Qupy

Houser *et al.* demonstrated the challenges in the synthesis of asymmetric ligands derived from ppda with two types of aldehyde. The first challenge is, as described above, the tendency to form hexahydropyrimidines (through cyclization) with the first equivalent of aldehyde. The second challenge is the hydrolysis of asymmetric bis(imine) followed by condensation to their symmetric analogues.<sup>17</sup> Locke *et al.* reported the preference of the formation of hexahydropyrimidines with electron deficient aldehydes (e.g. 2-pyridinecarboxaldehyde), and the tendency to form bis(imine)s with electron rich aldehydes like 2-hydroxybenzaldehyde.<sup>18</sup>

Many attempts were performed to isolate a pure asymmetric ligand from the reaction of Pypy<sup>b</sup> with salicylaldehyde, but all attempts were unsuccessful; a solid separated from the reaction mixture, which was isolated and purified. The NMR spectra indicated the formation of the symmetrical Salpy ligand. Crystals suitable

**Chapter 2 - Synthesis, Characterization, and X-ray Crystal Structures of Salpy, Acpy and Salpn type Ligands, and their Complexes with Aluminium and Titanium**

for single crystal X-ray diffraction were grown directly from the reaction (Figure 2.9), which indicated the formation of Salpy, consistent with the  $^1\text{H}$  NMR data.

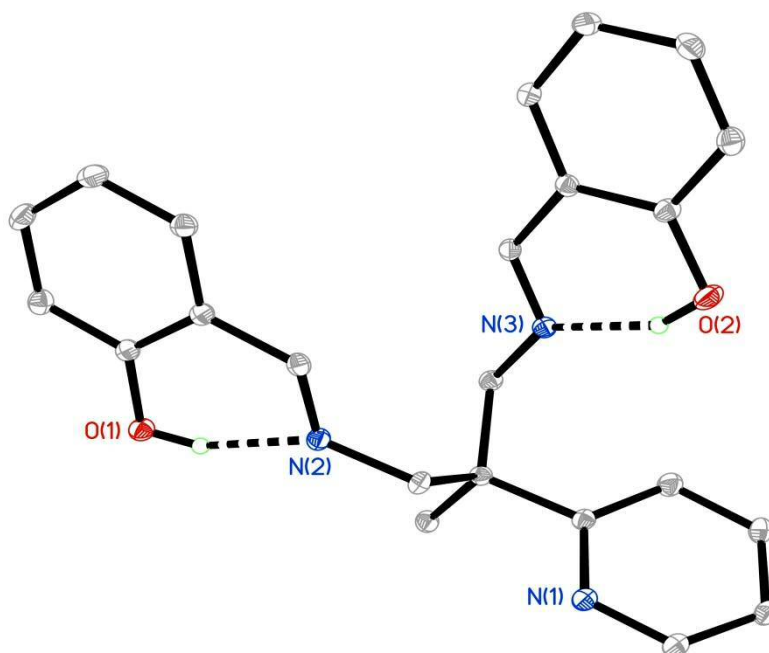


**Figure 2.9:** Molecular structure of Salpy. Displacement ellipsoids are drawn at 30% probability, and H atoms other than OH have been omitted for clarity. OH hydrogens are drawn as spheres of arbitrary radius

## 2.3 Synthesis and characterization of aluminium complexes

### 2.3.1 Aluminium methyl complexes

#### 2.3.1.1 Synthesis and spectroscopic characterization

The use of salen and salan-type ligands has facilitated significant advances in the field of aluminium-mediated catalysis. Their four-coordinate structure enables the ligands to adopt a planar motif in their complexes, whilst allowing a degree of conformational flexibility that is compatible with closed-shell metals, which have little or no geometrical preference. Different varieties of salen-type ligands have been reported to support aluminium complexes, which are usually afforded as five-coordinate species.

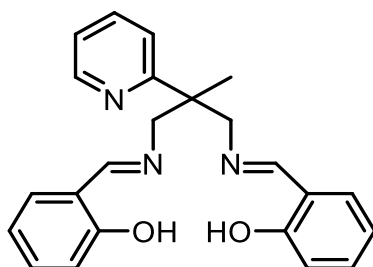
With this in mind, we sought to study derivatives of these ligands, that incorporate an extra donor moiety into the ligand manifold, since it is likely that such a donor could have a profound effect on the observed reactivity in a catalytic context. We

**Chapter 2 - Synthesis, Characterization, and X-ray Crystal Structures of Salpy, Acpy and Salpn type Ligands, and their Complexes with Aluminium and Titanium**

therefore employed the pyridyl-bis(iminophenolate) ligands (Salpy) described above, the core of which was first reported by Shakya *et al.*,<sup>19</sup> and is derived from the diamido-pyridine core of Gade.<sup>7</sup> The advantage of using these ligand types is that in the diamido-pyridine complexes, the pyridyl has been shown to be hemi-labile, and can facilitate novel reaction pathways; the incorporation of such a pyridyl donor into a ligand of higher denticity is likely to enhance the hemi-labile effect, particularly for aluminium, which favours lower coordination numbers.

Despite these ligands having been reported, to the best of our knowledge, no report has been found so far focusing on the synthesis of Salpy complexes with metals other than copper<sup>19</sup> and iron.<sup>20</sup> With Cu(II), the ligand is unable to adopt a  $\kappa^5$ -coordination arrangement due to the Jahn-Teller distortion at the Cu(II) centre; this study is therefore the first one in which this class of ligands can, in principle, afford five- and six-coordinate metal complexes with a variable coordinative state of the pyridyl donor, assisted by the zero LFSE of main group and  $d^0$  metal ions. All previous studies of aluminium with salen types ligands provide tetradentate ligands and five coordinate metal complexes.

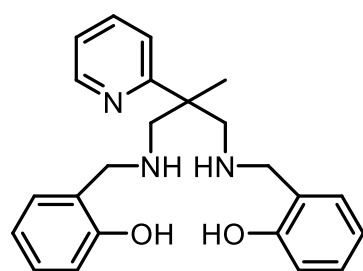
The first study of this class of ligands was reported by Houser *et al.*, who prepared the Salpy ligand by the Schiff base condensation of ppda with salicylaldehyde **2.1**, which was subsequently used to prepare copper complexes. By treatment of the imine ligand with copper(II) in the presence of base, a mononuclear copper complex [Cu(Limine)(MeOH)] was produced.<sup>19</sup>



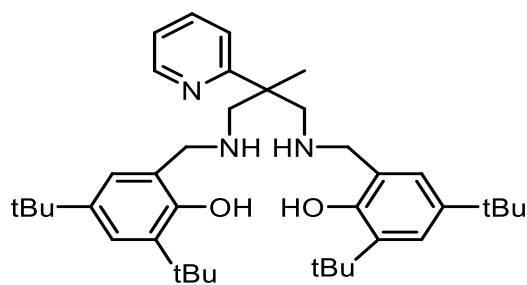
**2.1** H<sub>2</sub>L<sup>imine</sup>

**Chapter 2 - Synthesis, Characterization, and X-ray Crystal Structures of Salpy, Acpy and Salpn type Ligands, and their Complexes with Aluminium and Titanium**

The authors reported the complexation of the reduced version ( $L^{\text{amine}}$  **2.2** and  $L^{\text{tBu-amine}}$  **2.3**) with iron to form unsupported hydroxo- and oxo-bridged diiron(III) and mononuclear iron(III) complexes. Dimeric  $[(FeL^{\text{amine}})_2(\mu\text{-OH})]BPh_4$  and  $[(FeL^{\text{tBu-amine}})_2(\mu\text{-O})]$ , and monomeric  $[FeL^{\text{tBu-amine}}(OMe)]$  were synthesized from ferric perchlorate, whilst monomeric  $[FeL^{\text{amine}}Cl]$  and  $[FeL^{\text{tBu-amine}}Cl]$  were synthesized from ferric chloride.<sup>20</sup>



**2.2**  $H_2L^{\text{amine}}$



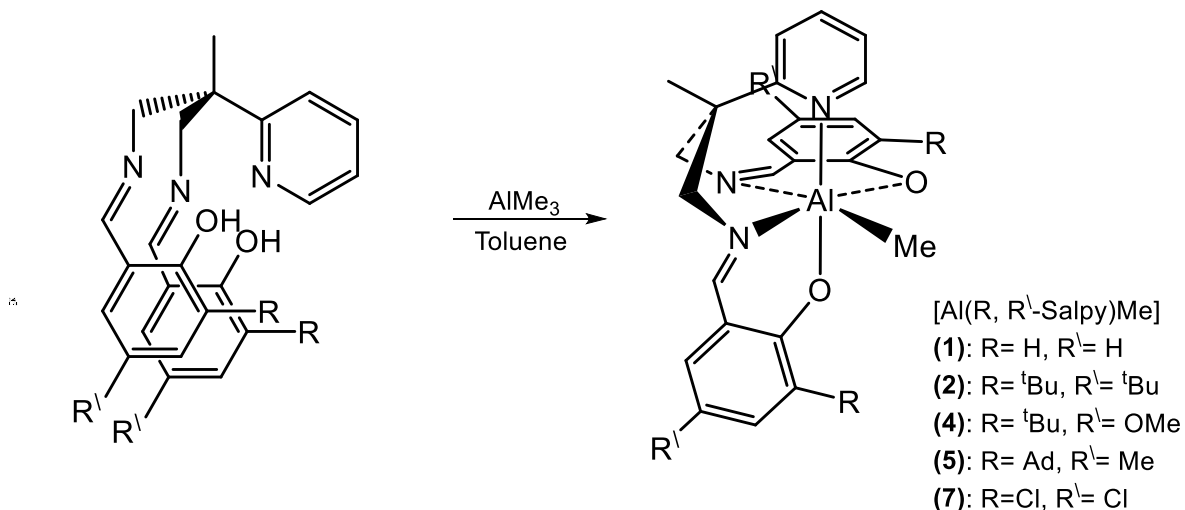
**2.3**  $H_2L^{\text{tBu-amine}}$

These reduced ligands, when combined with copper(II) salts and base, afforded either tricopper(II) or monocopper(II) species, depending on the nucleophilicity of the phenol groups in the ligands.<sup>21</sup> It was reported that the ligands in the trimeric complexes  $\{[CuL^{\text{amine}}(CH_3CN)]_2Cu\}(ClO_4)_2$  and  $\{[CuL^{\text{amine}}Cl]_2Cu\}$ , and in the monomeric complex  $[CuL^{\text{tBu-amine}}(CH_3OH)]$ , coordinate in a tetradentate mode via the amine N atoms and the phenolato O atoms. The pyridyl donors in these complexes do not coordinate.

Reaction of the protio-ligands, R,R'-Salpy, Naphpy, <sup>t</sup>Bu,OMe-Salpn, and R-Acpy, with 1 equivalent of AlMe<sub>3</sub> in toluene at ambient temperature yielded the methyl aluminium complexes  $[Al(R,R'\text{-Salpy})Me]$  (**1,2,4,5** and **7**),  $[Al(Naphpy)Me]$  (**3**),  $[Al(^t\text{Bu,OMe-Salpn})Me]$  (**6**) and  $[Al(R\text{-Aspy})Me]$  (**8** and **9**) respectively (as shown for Salpy derivatives, equations 2.7). These reactions were effectively quantitative (by NMR spectroscopy) and occurred instantaneously; the complexes were isolated as off-white, pale yellow or yellow powders in good yields (73–92%). Characterization by <sup>1</sup>H and <sup>13</sup>C NMR spectroscopy revealed the formation of the expected methyl aluminium complexes and was consistent with the mononuclear structures (Except  $[Al(Ad, Me\text{-Salpy})Me]$  (**5**)). For instance, the

**Chapter 2 - Synthesis, Characterization, and X-ray Crystal Structures of Salpy, Acpy and Salpn type Ligands, and their Complexes with Aluminium and Titanium**

OH peak of the free ligands (between 10.4-16.6 ppm) disappeared upon reaction, and the  $^1\text{H}$  NMR signals for aluminum methyl protons were observed in the upfield region between -1 to -0.3 ppm as singlets with integration of 3 H.



**Equation 2.7:** Synthesis of  $[\text{Al}(\text{R}, \text{R}^1\text{-Salpy})\text{Me}]$

Interestingly, in early experiments for the preparation of  $[\text{Al}(\text{Salpy})\text{Me}]$  (1) using THF as a solvent and 1 : 1.2 ratio of ligand :  $\text{AlMe}_3$ , the NMR spectra were rather broad and complex, and consistent with a mixture of isomers. It was therefore difficult to unambiguously assign the spectra or to identify the nature of the resulting complex(s) (Figure 2.10).

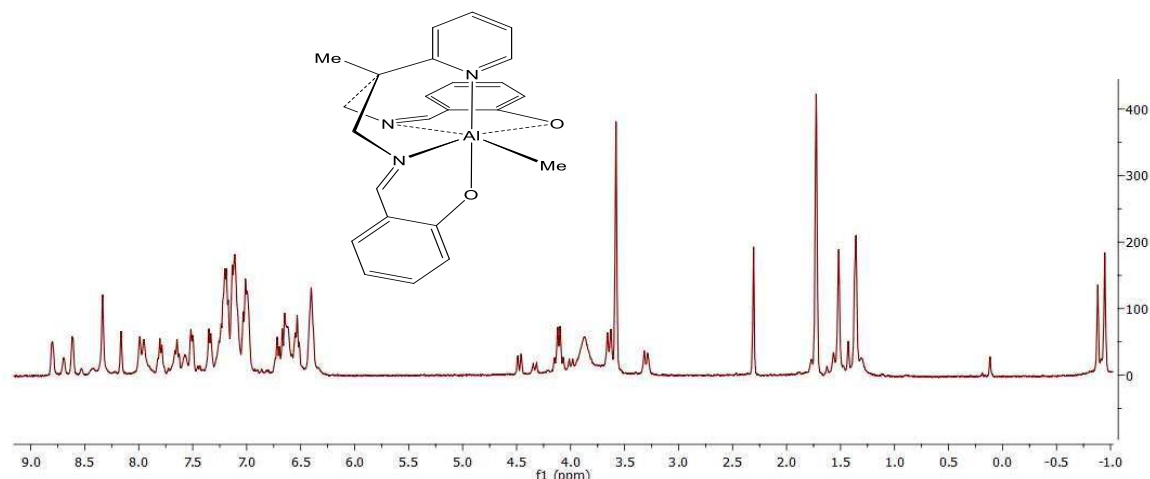


**Figure 2.10:**  $^1\text{H}$  NMR spectrum (400 MHz, 293 K,  $\text{THF-d}^8$ ) for the  $[\text{Al}(\text{Salpy})(\text{Me})]$  (more than two isomers)

**Chapter 2 - Synthesis, Characterization, and X-ray Crystal Structures of Salpy, Acpy and Salpn type Ligands, and their Complexes with Aluminium and Titanium**

Nevertheless, elemental combustion analyses and mass spectrometry data were consistent with the proposed formula, and crystals of **1** were grown from the reaction mixture which confirm that one of the isomers corresponds to the expected structure (*vide infra*). Many experiments were performed, in order to reduce the apparent isomerization, and to obtain clearer NMR data. The conditions of the reaction were changed, starting from changing the solvent to a non-coordinating variant, so toluene replaced THF, and the ratio of ligand to trimethylaluminium was changed to 1 : 1. The temperature of the reaction was manipulated, the reaction was conducted at low temperature for the addition of AlMe<sub>3</sub> before warming to room temperature. The optimized conditions for this reaction included adding AlMe<sub>3</sub> at room temperature and heating the solution to 80 °C overnight. Comparison of the spectra in Figures 2.10 and 2.11 shows significant differences: in that obtained from the optimized conditions there were only two components.

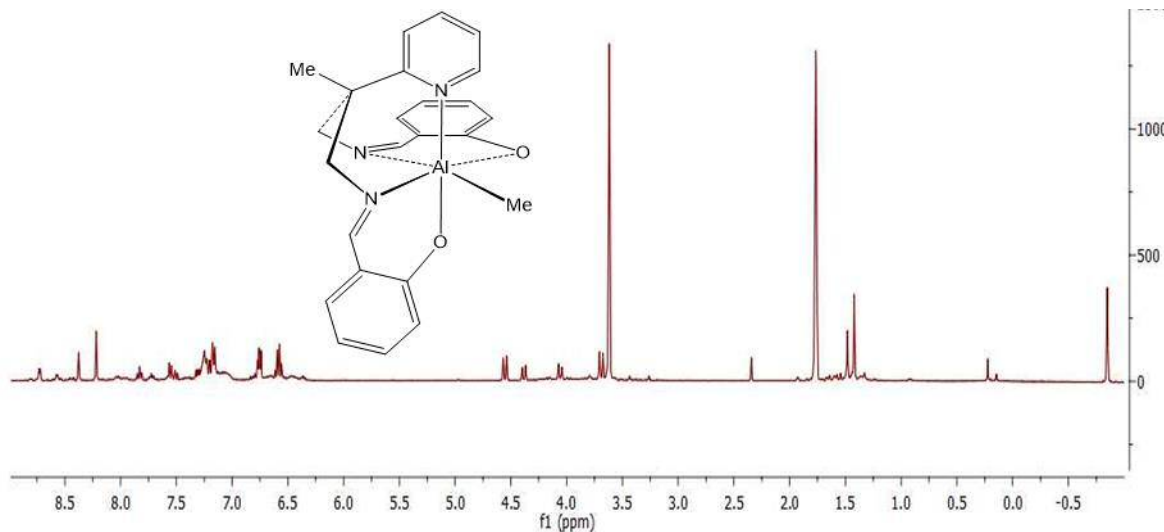
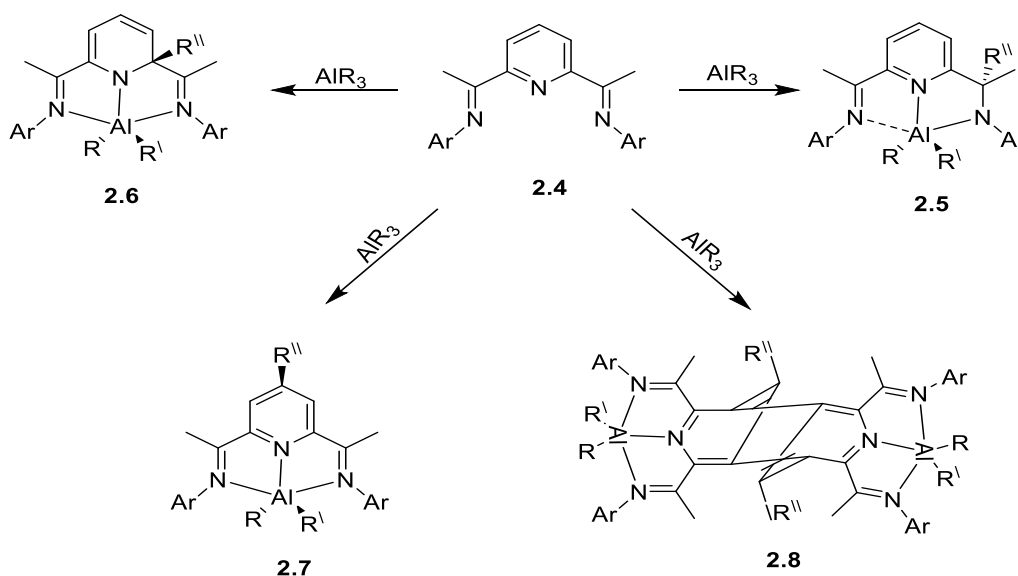


**Figure 2.11:** <sup>1</sup>H NMR spectrum (400 MHz, 293 K, THF-d<sup>8</sup>) for the [Al(Salpy)(Me)] (two species)

Knijnenburg *et al.* investigated the stoichiometric reactions of aluminium alkyls (Me<sub>3</sub>Al, Et<sub>3</sub>Al, iBu<sub>3</sub>Al, iBu<sub>2</sub>AlH, Et<sub>2</sub>AlCl) with the neutral ligand **2.4**. A mixture of products was formed initially in these reactions, but the composition of the mixture

**Chapter 2 - Synthesis, Characterization, and X-ray Crystal Structures of Salpy, Acpy and Salpn type Ligands, and their Complexes with Aluminium and Titanium**

changed upon prolonged heating, although never in such a way that only a single product remained (Scheme 2.4).<sup>22</sup>



**Scheme (2.4):** Alkylation products obtained from  $\text{AlR}_3$  reacting with a pyridine-bis(imine) ligand

In this thesis, not only were the reaction conditions changed to get a more well-defined complex but also the aluminium alkyl ligand could be varied. Triethyl aluminium  $\text{AlEt}_3$  was used as a comparison with  $\text{AlMe}_3$ , to see if employing an ethyl group would affect the coordination chemistry.  $\text{AlEt}_3$  was added to a stirred solution of Salpy in equimolar ratio, in toluene. The stirring was continued overnight, and the solvent was removed to obtain the complex  $[\text{Al}(\text{Salpy})(\text{Et})]$  (**10**) after washing with hexane and drying in high vacuum. The  $^1\text{H}$  NMR spectrum of **10** shows two principal species in a ratio (obtained by integration of the  $\text{H}^6$  resonance) of 1 : 0.58, along with minor traces of other species (Figure 2.12). It can be concluded from this experiment that both ethyl and methyl groups have the same coordination chemistry in these systems.

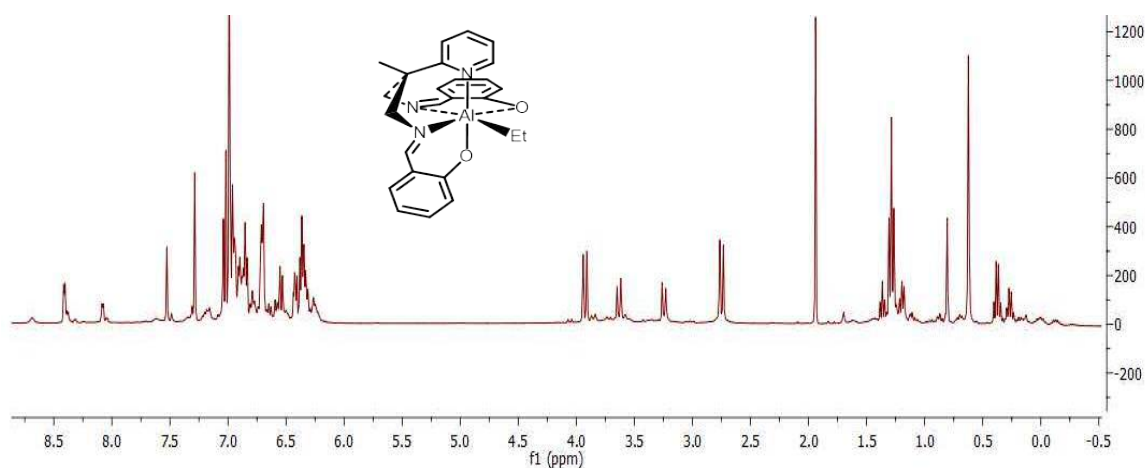


**Figure 2.12:** <sup>1</sup>H NMR spectrum (400 MHz, 293 K, C<sub>6</sub>D<sub>6</sub>) of [Al(Salpy)(Et)] (**10**)

Introducing bulky groups in ortho and para position of the phenol groups restricts the formation of multiple isomers; the minor components described above for [Al(Salpy)R] (R = Me (**1**) or Et (**10**)) were not observed for other derivatives of the Salpy ligand. Nevertheless, the observance of two principal species was not limited to the salicylaldehyde-derived ligand; even with ligands bearing substituted phenol rings, [Al(<sup>t</sup>Bu, <sup>t</sup>Bu -Salpy)Me] (**2**) for instance, two components were observed when the ligand reacts with AlEt<sub>3</sub> or AlMe<sub>3</sub> (Figure 2.13). The <sup>1</sup>H NMR spectrum shows two species with ratio of 1:0.7. There are two signals attributed to the pyridyl H<sup>6</sup> and two for the imines. The CH<sub>2</sub> groups appear as two well-separated doublets for each species, the minor isomer having a slightly lower separation between the two doublets. The Al-CH<sub>3</sub> protons for both isomers have coincidental chemical shifts below 0 ppm (Figure 2.13).

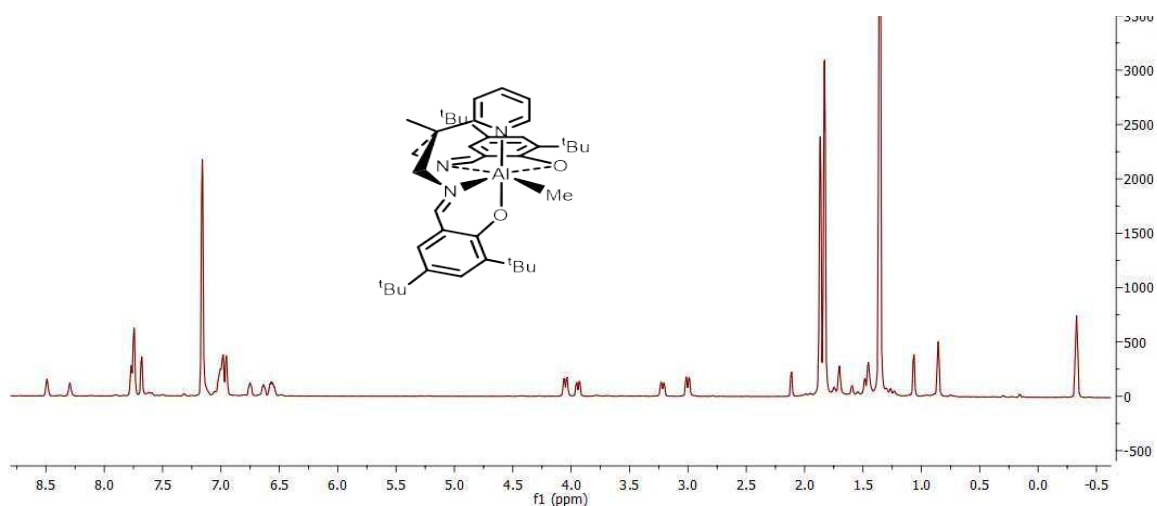


**Figure 2.13:**  $^1\text{H}$  NMR spectrum (400 MHz, 293 K,  $\text{C}_6\text{D}_6$ ) of  $[\text{Al}(\text{tBu}, \text{tBu-Salpy})\text{Me}]$  (**2**)

The salicylaldehyde substituents have a significant influence on the stoichiometric ratio of the two species observed in the aluminium Salpy complexes. This effect may be partially electronic, e.g. by introducing electron withdrawing or electron donating groups, but may also be steric-derived: large groups will alter the most favoured coordination modes of the ligand around the relatively small aluminium ion. The NMR spectra of  $[\text{Al}(\text{tBu}, \text{OCH}_3\text{-Salpy})\text{Me}]$  (**4**) indicated the presence of two species in a 1:0.8 ratio. The  $^1\text{H}$  NMR spectrum of **4** is shown in Figure 2.14. Many attempts have been made to obtain only one species, however, all attempts failed and the two isomers ubiquitously observed in these complexes could not be separated or purified. Interestingly, where possible the species were probed using 2D NMR spectroscopy, including COSY, HSQC, and HMBC. Where data were available (*i.e.* not obscured by the overlapping of signals) it was clear that the two species contain the same groups, and have an essentially identical connectivity.

**Chapter 2 - Synthesis, Characterization, and X-ray Crystal Structures of Salpy, Acpy and Salpn type Ligands, and their Complexes with Aluminium and Titanium**

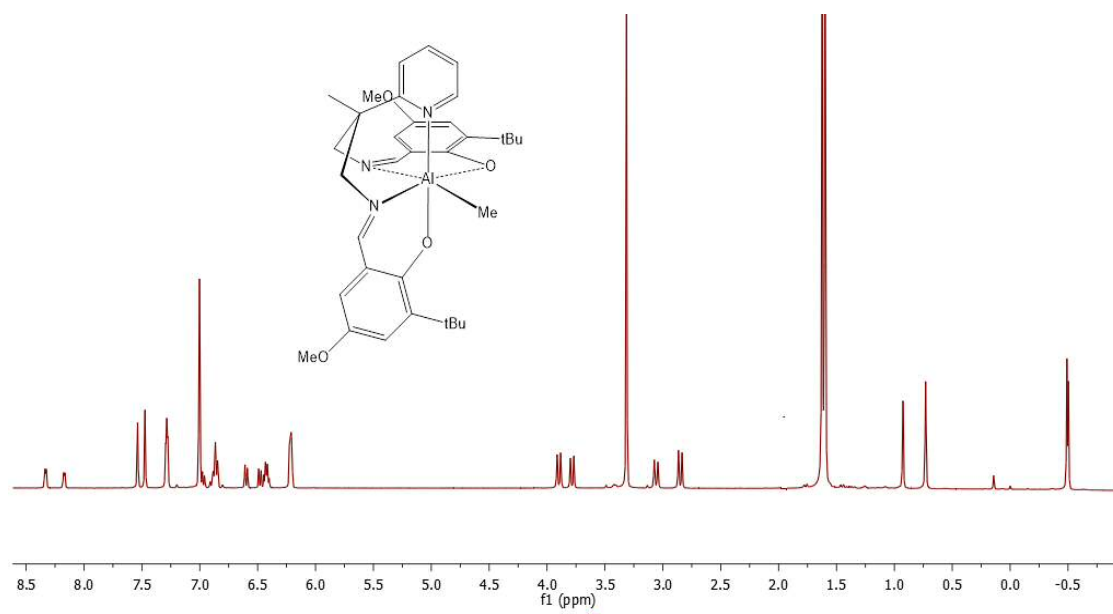


**Figure 2.14:** <sup>1</sup>H NMR spectrum (400 MHz, 293 K, C<sub>6</sub>D<sub>6</sub>) of [Al(tBu, OCH<sub>3</sub>-Salpy)Me] (**4**)

The intriguing presence of two inseparable isomers with identical ligand connectivity is suggestive of a hemi-labile pyridyl donor, the two isomers corresponding to coordinated-pyridyl (6-coordinate), and pendant-pyridyl (5-coordinate) isomers. Since the <sup>1</sup>H NMR spectrum of **4** indicated the presence of two species, and the spectrum was particularly well-defined, variable temperature spectra were measured between 20 and 70 °C in C<sub>6</sub>D<sub>6</sub> in order to obtain some insight into the identity of the two species. The relative proportion of the two isomers showed a subtle temperature dependence; integration of the spectra (H<sup>6</sup> resonance) allowed the equilibrium coefficients to be extracted, which were used to construct a Van't Hoff plot (Figure 2.15), using the following equation:



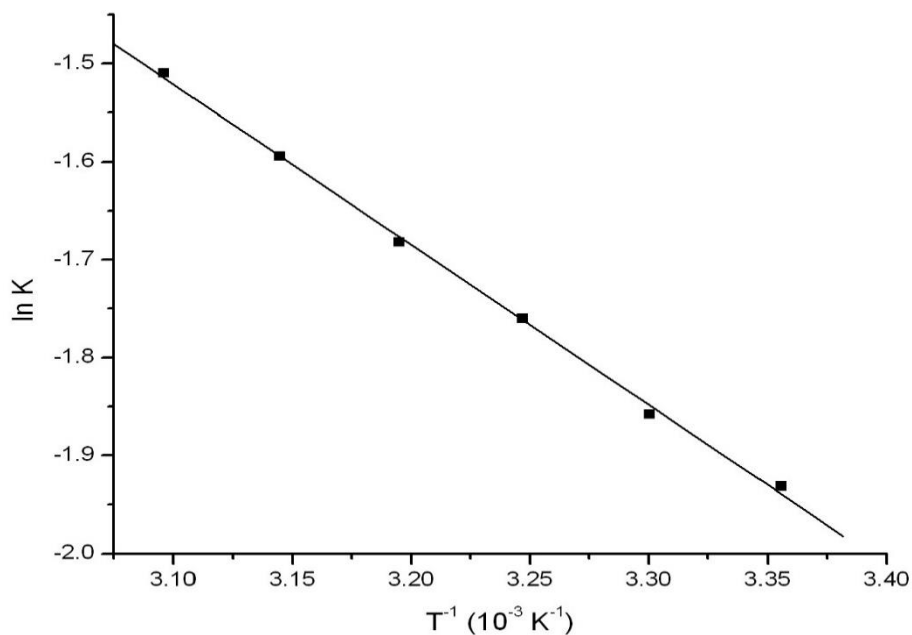


**Figure 2.15:** Van't Hoff plot for the isomer equilibrium in  $[Al(tBu, OCH_3\text{-Salpy})Me]$  (**4**)

Thermodynamic parameters were extracted from the Van't Hoff plot, giving  $\Delta H = 1.4 \pm 1.2 \text{ kJ.mol}^{-1}$  and  $\Delta S = 2.9 \pm 3.9 \text{ J.mol}^{-1} \text{ K}^{-1}$ . The small energies involved are consistent with the isomers being observed in an approximately equal ratio, and the entropic contribution of close to zero is consistent with an intramolecular equilibrium process, as we have proposed.

The reaction of stoichiometric  $AlMe_3$  with the Ad,Me-Salpy protio-ligand in toluene lead to the formation of a bimetallic aluminium complex  $[Al_2(Ad,Me\text{-Salpy})Me_4]$  (**42**) as the major product, with the anticipated monometallic complex  $[Al(Ad,Me\text{-Salpy})Me]$  (**5**) being formed as a minor product; the two complexes were formed in 1 : 0.5 respectively (Figure 2.16). The synthesis and characterization of the bimetallic complexes are discussed fully in Chapter five. All attempts to isolate the monometallic complex were unsuccessful, although single crystals suitable for X-ray diffraction were grown from a concentrated solution in benzene. The difficulty in preparing  $[Al(Ad,Me\text{-Salpy})Me]$  (**5**) presumably arises as a result of the excessive steric demands of the adamantyl groups in the ortho positions; this makes it less favourable for the phenol rings to exist in close proximity, as they necessarily are in a monometallic complex.

**Chapter 2 - Synthesis, Characterization, and X-ray Crystal Structures of Salpy, Acpy and Salpn type Ligands, and their Complexes with Aluminium and Titanium**

Several experiments were undertaken to preferentially form the monometallic complex: The reaction time was increased to 24 h, and the ratio of free ligand to aluminium reagent was changed from 1 : 1 to 1 : 1.1 but preference to form a bimetallic complex was unchanged. The reaction temperature was also varied, from ambient temperature to 80 °C, again with no influence on the reaction outcome.

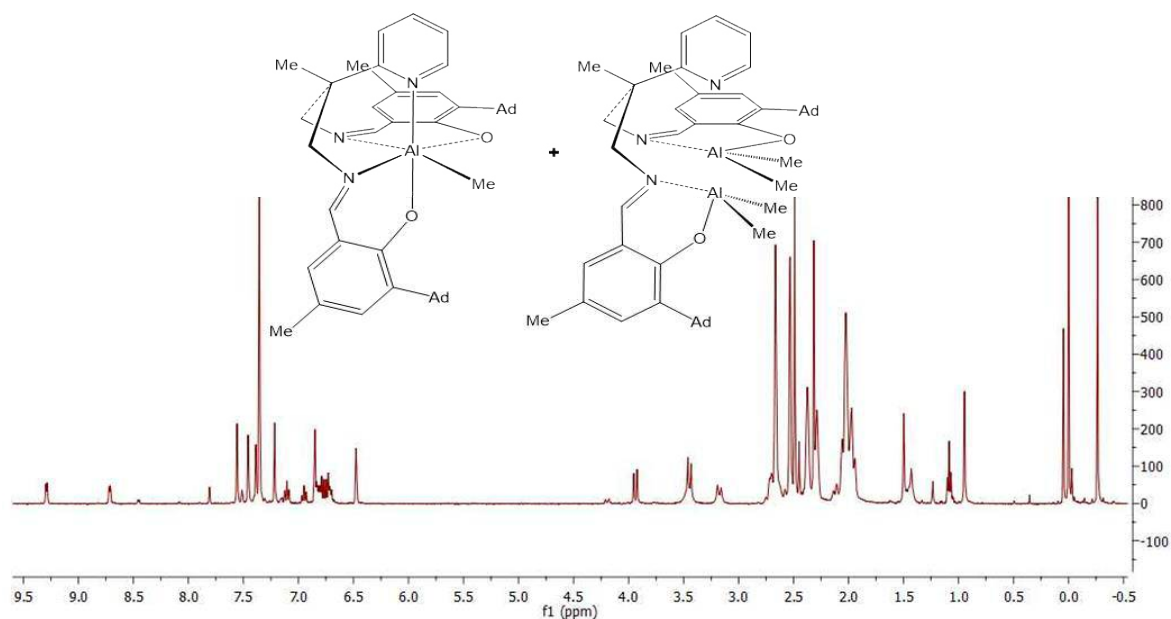
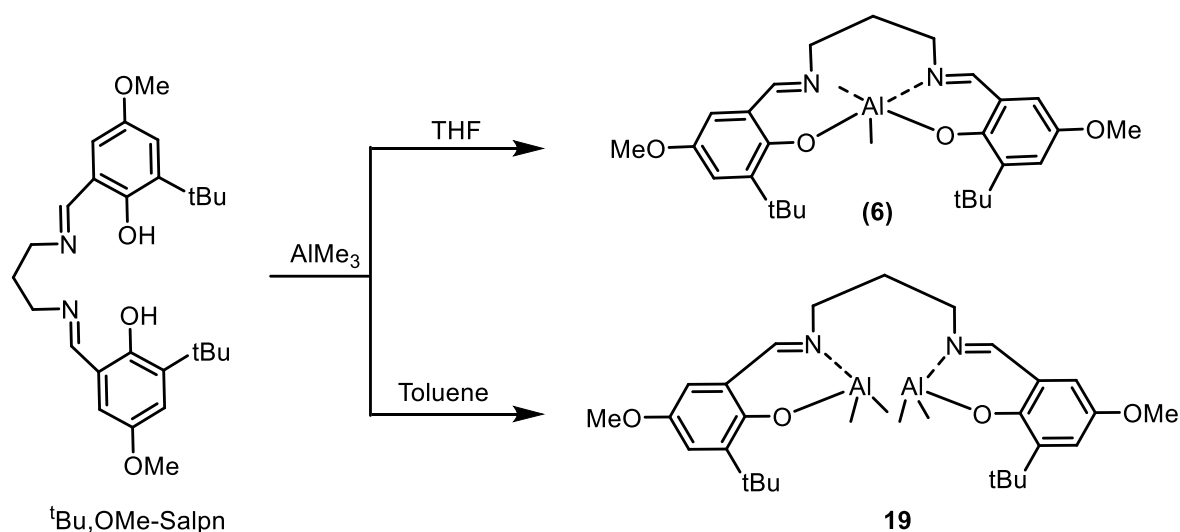


**Figure 2.16:**  $^1\text{H}$  NMR spectrum (400 MHz, 293 K,  $\text{C}_6\text{D}_6$ ) of the  $[\text{Al}(\text{Ad},\text{Me-Salpy})\text{Me}]$  and  $[\text{Al}_2(\text{Ad},\text{Me-Salpy})\text{Me}_4]$  mixture

To examine the effect of the pyridyl and methyl group on the diamine backbone, we prepared a three-carbon salen-type ligand, but without any substituents on the diamine, *i.e.* replace the apical methyl and pyridyl with hydrogens. This ligand,  $^t\text{Bu},\text{OMe-Salpn}$ , was used to make this comparison with  $^t\text{Bu},\text{OMe-Salpy}$ , thereby ensuring that the substituents on the phenol rings are identical in both ligands. Reaction of one equivalent of the  $^t\text{Bu},\text{OMe-Salpn}$  protio-ligand with  $\text{AlMe}_3$  in THF afforded  $[\text{Al}(^t\text{Bu},\text{OMe-Salpn})\text{Me}]$  (**6**) as a pure white powder. When the reaction was conducted in toluene, under otherwise identical conditions, a bimetallic complex was isolated, *i.e.* changing the solvent from non-polar to polar changed the preference of the ligand toward the complexation reaction from mono to bimetallic (Scheme 2.5).

**Chapter 2 - Synthesis, Characterization, and X-ray Crystal Structures of Salpy, Acpy and Salpn type Ligands, and their Complexes with Aluminium and Titanium**



**Scheme 2.5:** synthesis of mono- and bimetallic aluminium complexes of (*t*Bu, OMe- Salpn) **(6)**

The  $^1\text{H}$  NMR spectrum of **6** indicates a symmetrical complex with one singlet at 7.0 ppm for the imine protons. A significant shift of this peak upfield in comparison to the free ligand which appears as a singlet at 8.36 ppm. The two doublet peaks at 7.26 and 6.17 were assigned to the aromatic ring of the phenoxide ring. One sharp singlet was observed at 3.36 for six protons of two methoxy groups while the two tert-butyl groups appeared at 1.56 as a singlet.

The two Acen aluminium complexes were prepared using the ligands derived from 2-hydroxyacetophenone, via the reaction with  $\text{AlMe}_3$ ; in these cases,  $[\text{Al}(\text{Acpy})\text{Me}]$  (**8**) and  $[\text{Al}(\text{OMe-Acpy})\text{Me}]$  (**9**) show the same behaviour as the salen derivatives. The only difference is with complex **9** in which the two methylene groups in the ligand backbone are inequivalent; the  $^1\text{H}$  NMR spectrum of the complex shows four doublets integrating to 1 H for each isomer.

**Table 2.2:** The important  $^1\text{H}$  NMR chemical shifts for the Salpy (and related) ligands and their aluminium complexes

Ligand or Complex	H <sup>6</sup>	CH=N	CH <sub>2</sub>	CH <sub>3</sub>	Al-CH <sub>3</sub>
(Salpy)	8.63	8.31	4.13, 4.00	1.53	-
[Al(Salpy) Me]	8.69	8.18	4.52, 3.65	1.38	-0.89
( <sup>t</sup> Bu, <sup>t</sup> Bu- Salpy)	8.64	8.36	4.07	1.58	-
[Al( <sup>t</sup> Bu, <sup>t</sup> Bu- Salpy)Me]	8.49	7.67	4.05, 3.00	0.85	-0.32
(Naphpy)	8.59	8.54	3.98, 3.85	1.48	-
[Al(Naphpy)Me]	8.66	8.02	3.73, 3.45	1.44	-0.3
( <sup>t</sup> Bu, OCH <sub>3</sub> - Salpy)	8.53	8.19	3.98	1.49	-
[Al( <sup>t</sup> Bu, OCH <sub>3</sub> - Salpy)Me]	8.49	7.65	4.06, 3.47	0.9	-0.35
( <sup>t</sup> Bu, OCH <sub>3</sub> - Salpn)	-	8.36	3.73	-	-
[Al( <sup>t</sup> Bu, OCH <sub>3</sub> - Salpn)Me]		7.00	2.91, 2.61		-0.53
(Cl, Cl - Salpy)	8.60	8.17	4.15, 4.04	1.55	-
[Al(Cl, Cl - Salpy)Me]	8.95	7.97	3.98, 3.89	1.56	-0.9

The pyridyl group in the Salpy and related ligands has two effects upon the coordination chemistry of the resulting complexes. The first effect, as described above, is that the hemi-labile pyridyl switches the denticity of the ligand between tetradentate and pentadentate, and this will allow the ligand to become involved in catalytic reactions, by virtue of allowing a variable coordination number, and by tuning the Lewis acidity of the metal centre. The second effect of the pyridyl group coordination is in the stereochemistry of the complex. In most of the known Salen-type complexes, the Salen ligands adopts a planar N<sub>2</sub>O<sub>2</sub> coordination mode, in which the imine and phenoxide donors make an approximate square

**Chapter 2 - Synthesis, Characterization, and X-ray Crystal Structures of Salpy, Acpy and Salpn type Ligands, and their Complexes with Aluminium and Titanium**

plane; any co-ligands present in the complex occupy coordination sites above and below this plane. In principle, the pyridyl donor in the Salpy ligands can adopt the same coordination mode, with an N<sub>2</sub>O<sub>2</sub> equatorial plane and the pyridyl adopting an axial position, giving complexes with C<sub>s</sub>-symmetry. Figure 2.17 shows the two possible conformational stereoisomers of five coordinated aluminium methyl complexes

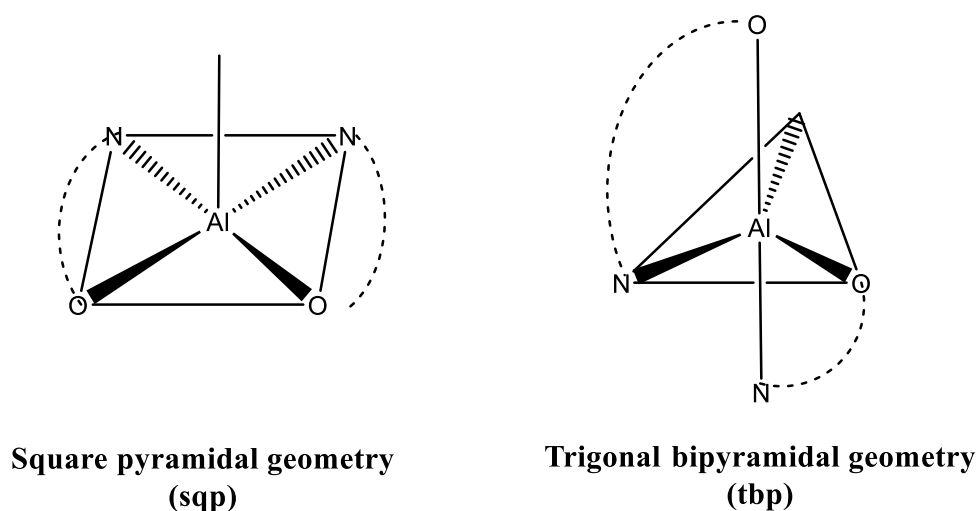


**Figure 2.17:** the two possible conformational stereoisomers of aluminium methyl complexes

However, the aluminium complexes reported in this thesis exhibit C<sub>1</sub>-symmetry with inequivalent phenol groups, and whilst some CH<sub>2</sub> groups appear equivalent, most show four doublets for these groups.

Structural characterization using solution-state <sup>1</sup>H NMR spectroscopy showed notable differences in the imine proton signals of the methyl aluminium complexes. Although all of these complexes featured a single resonance, consistent with a symmetric structure due to equivalence of the two imine protons,<sup>23</sup> based upon X-ray data (see below), both the CH<sub>2</sub> and imine groups should be inequivalent, thereby giving twice the number of signals (e.g. two imine signals per species). It is likely, based upon data obtained on other complexes (see below), that the two “arms” of the complexes are able to exchange at

ambient temperature, thus giving rise to averaged signals in their  $^1\text{H}$  NMR spectra. Exchange parameters have been obtained for other complexes and will be discussed in due course.

### **2.3.1.2 Crystallographic characterisation of aluminium methyl complexes**

Single crystals of  $[\text{Al}(\text{Salpy})(\text{Me})]$  (**1**) suitable for X-ray diffraction studies were successfully grown by the slow evaporation of benzene solutions under a nitrogen atmosphere. The molecular structure is shown in Figure 2.18. Selected bond lengths and angles are provided in Table 2.3. The Al atom contains a  $\kappa^5$ -Salpy ligand in which the pyridyl moiety is coordinated to the aluminium centre; the added presence of a methyl co-ligand gives a six-coordinate structure. The geometry around the Al atom is best described as distorted octahedral, with the two phenoxy groups, the pyridyl and one of the imine donors in salen ligand occupying the four equatorial positions and the methyl group and the remaining imine in the axial positions. The equatorial angles are closer to the ideal  $90^\circ$  between the oxygens [ $\text{O-Al-O} = 90.30(4)^\circ$ ] around aluminium and more acute for the nitrogens [ $\text{N-Al-N} = 78.65(4)$  to  $87.82(4)^\circ$ ]. The  $\text{C}(24)\text{-Al}(1)\text{-N}(2)$  angle is consequently bent slightly toward the open space between O1 and N1, and away from the ligand backbone leading to a less than ideal angle of  $166.52(5)^\circ$ .

The aluminium-pyridyl bond  $\text{Al}(1)\text{-N}(1)$  is significantly longer –  $2.1375(10)$  – than both aluminium-imine bonds  $\text{Al}(1)\text{-N}(2)$  and  $\text{Al}(1)\text{-N}(3)$  –  $2.0692(10)$  and  $2.0829(10)$  respectively – which is consistent with there being a weaker interaction between the pyridyl and aluminium, and therefore this donor being subject to hemi-labile donation.

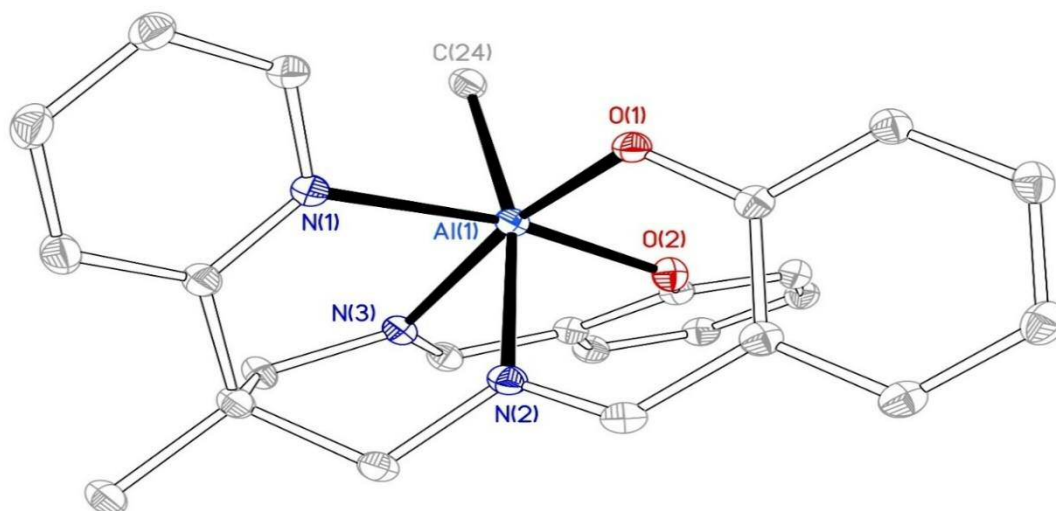


**Figure 2.18:** Molecular structure of [Al(Salpy)Me] (**1**) with thermal ellipsoids drawn at 30% probability and hydrogen atoms omitted for clarity.

The nitrogen bonds Al(1)-N in **1** (2.0692(10)- 2.1375(10)) are significantly longer than the Al-O bonds (1.8533(9)- 1.8550(8)) due to the greater atomic size of nitrogen.<sup>24</sup>

The coordination of phenoxy-imine to aluminium displays a structure in which both the two nitrogen atoms and two oxygen atoms are in mutually cis positions. It is important to realize that several isomers are possible, and the stability and reactivity are functions of the substituents of the Schiff bases, including the backbone joining the two phenoxyimine “arms”. The introduction of bulky groups in the phenoxy ring near to the oxygen is important, in order to stabilize these Schiff bases. Interestingly, the octahedral and  $C_1$ -symmetric aluminium-bis(phenoxyimine) complexes are chiral at metal, assuming a fluxional  $\Lambda$  or  $\Delta$  configuration (Figure 2.19), which explains why some of the complexes are  $C_1$  symmetric by NMR spectroscopy, and some have apparently higher symmetry.<sup>25</sup> All X-ray data recorded for aluminium complexes in this thesis are chiral at metal.

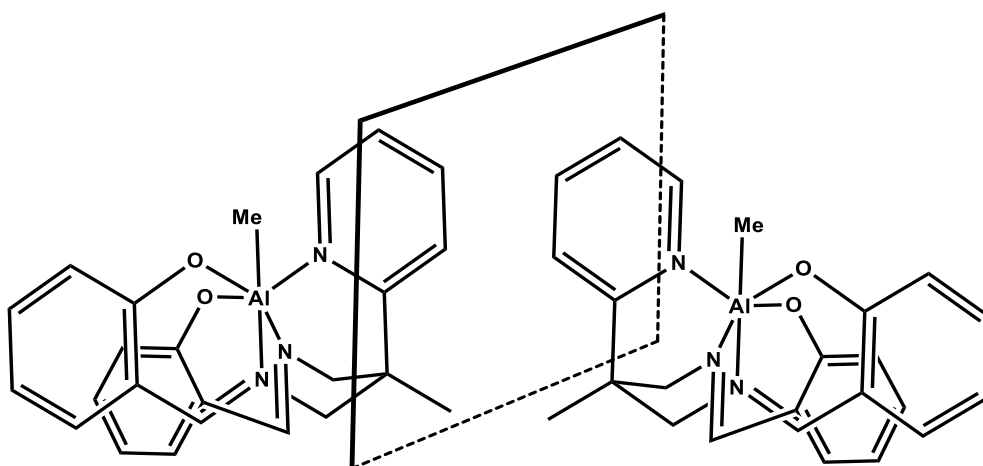


**Figure 2.19:** Isomers of octahedral [Al(Salpy)Me] (**1**)

**Table 2.3:** Selected bond lengths (Å) and bond angles (°) for [Al(Salpy)Me] (**1**)

Al(1)-O(2)	1.8533(9)	Al(1)-N(2)	2.0692(10)
Al(1)-O(1)	1.8550(8)	Al(1)-N(3)	2.0829(10)
Al(1)-C(24)	2.0260(12)	Al(1)-N(1)	2.1375(10)
O(2)-Al(1)-O(1)	90.30(4)	C(24)-Al(1)-N(3)	91.99(4)
O(2)-Al(1)-C(24)	99.56(5)	N(2)-Al(1)-N(3)	81.03(4)
O(1)-Al(1)-C(24)	100.50(4)	O(2)-Al(1)-N(1)	169.76(4)
O(2)-Al(1)-N(2)	91.67(4)	O(1)-Al(1)-N(1)	92.44(4)
O(1)-Al(1)-N(2)	86.78(4)	C(24)-Al(1)-N(1)	89.64(4)
C(24)-Al(1)-N(2)	166.52(5)	N(2)-Al(1)-N(1)	78.65(4)
O(2)-Al(1)-N(3)	87.38(4)	N(3)-Al(1)-N(1)	87.82(4)
O(1)-Al(1)-N(3)	167.52(4)		

Suitable crystals for structural determination of [Al(<sup>t</sup>Bu,OMe-Salpy)Me] (**4**) were obtained from a concentrated benzene solution. The molecular structure of **4** is depicted in Figure 2.20; selected bond lengths and angles are listed in Table 2.4. Complex **4** crystallizes in the monoclinic space group C2/c and contains 8

**Chapter 2 - Synthesis, Characterization, and X-ray Crystal Structures of Salpy, Acpy and Salpn type Ligands, and their Complexes with Aluminium and Titanium**

complex units within the unit cell. The asymmetric unit also contains a disordered benzene molecule. The structure shows that complex **4** is mononuclear with a five-coordinate aluminium centre; besides the methyl group, the Salpy ligand adopts a  $\kappa^4$ -N<sub>2</sub>O<sub>2</sub> coordination mode.

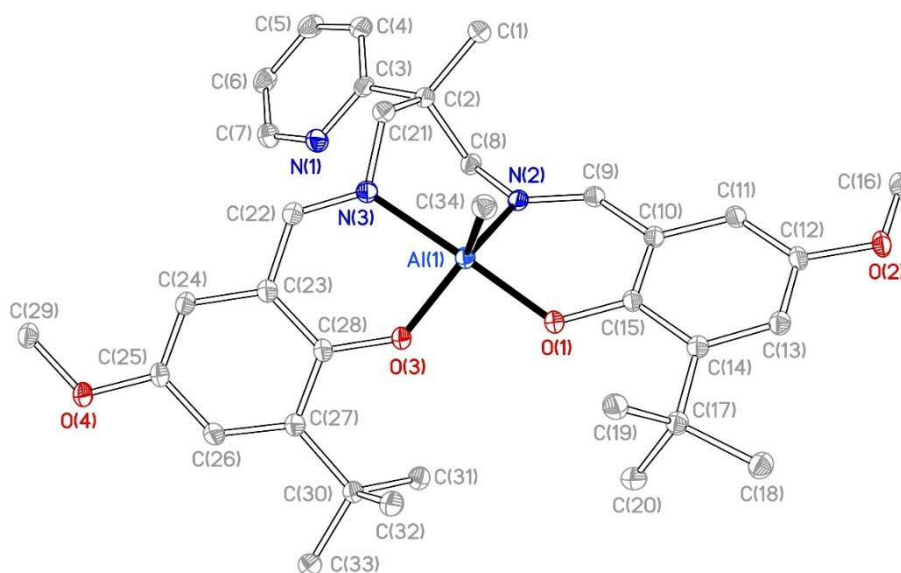


**Figure 2.20:** Thermal ellipsoid plot (30 %) of [Al(<sup>t</sup>Bu,OMe-Salpy)Me] (**4**), H atoms and solvent of crystallization omitted for clarity

A quantitative measure has been devised to determine the extent to which observed geometries resemble *tpb* or *sqp*.<sup>26</sup> The  $\tau$  (Tau) value is an index of the degree of trigonality, that can be used to determine how closely a distorted compound approximates either a *tpb* or *sqp* geometry. From the Figure 2.21,  $\alpha$  (D-E) and  $\beta$  (B-C) are the angles that are opposite each other in the *xy* plane. ideally square-pyramidal geometry is associated with  $\alpha = \beta = 180^\circ$ , for A as the axial ligand ( $\beta$  is the greater of the basal angles, BMC). For perfectly trigonal-bipyramidal geometry,  $\alpha$  becomes  $120^\circ$  and BMC the principal axis.

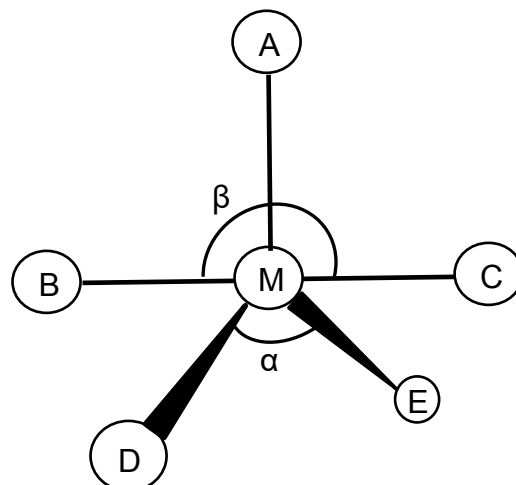


**Figure 2.21:** Index of the degree of trigonality diagram.

The formula for  $\tau$  is

$\beta$  is the largest angle at the metal centre.

$\alpha$  is the second-largest angle at the metal centre.

The  $\tau$  value ranges from 0 to 1. A value of zero identifies a compound as perfectly square pyramidal and a value of one as perfectly trigonal bipyramidal.<sup>26</sup>

The  $\tau$  value for complex **4** is 0.70, which indicates more trigonal bipyramidal geometry in the solid state. The atoms O(1) and N(3) occupy the axial sites and form an angle of  $172.11(8)^\circ$  with the aluminium. The atoms C(34), O(3), and N(2) define the equatorial plane, with angles subtended at aluminium being  $124.92(6)^\circ$  for O(3)-Al(1)-C(34),  $124.05(6)^\circ$  for O(3)-Al(1)-N(2), and  $110.81(6)^\circ$  for C(34)-Al(1)-N(2). The bond distances of the two Al-O bonds were significantly different. The axial Al(1)-O(1) bond length [ $1.8084(17)\text{\AA}$ ] was noticeably longer than that of the equatorial counterpart [Al(1)-O(3),  $1.7921(12)\text{\AA}$ ]. Likewise with the two Al-O bonds, the equatorial bond was shorter than the axial one.

**Table 2.4:** Selected bond lengths (Å) and bond angles (°) for [Al(<sup>t</sup>Bu,OMe-Salpy)Me] (**4**)

Al(1)-O(3)	1.7921(12)	Al(1)-N(2)	2.0075(14)
Al(1)-O(1)	1.8378(11)	Al(1)-N(3)	2.0470(14)
Al(1)-C(34)	1.9898(17)		
O(3)-Al(1)-O(1)	88.24(5)	C(34)-Al(1)-N(2)	110.81(6)
O(3)-Al(1)-C(34)	124.92(6)	O(3)-Al(1)-N(3)	87.85(5)
O(1)-Al(1)-C(34)	98.88(6)	O(1)-Al(1)-N(3)	166.98(6)
O(3)-Al(1)-N(2)	124.05(6)	C(34)-Al(1)-N(3)	93.54(6)
O(1)-Al(1)-N(2)	87.90(5)	N(2)-Al(1)-N(3)	84.02(5)

Crystals of [Al(Ad,Me-Salpy)Me] (**5**) that were suitable for X-ray structure determination were grown from a benzene solution. The solid-state geometry of complex **5** was confirmed by X-ray diffraction analysis. The molecular structure is shown in Figure 2.22, with selected bond distances and angles listed in Tables 2.5. The asymmetric unit contains, in addition to a molecule of **5**, three molecules of benzene of solvation. The analysis revealed that the aluminium in complex **5** is hexa-coordinate, the aluminium adopting a distorted octahedral geometry. As for the previously described 6-coordinate complexes in this series, the aluminium ion is coordinated by a  $\kappa^5$ -Salpy ligand due to the coordinating pyridyl group. In complex **5**, the Al(1)–N(1) bond length, 2.1679(10) (Å), is the longest among the Al–N bond lengths, as expected, and the trans angle between C(46) and N(3) are distorted away from the ideal 180°, C(46)-Al(1)-N(3) being 170.47(4)°. The aluminium-pyridyl bond distances for complexes **1** and **5** are within the expected range based upon examples in the Cambridge structural database (1.804–2.262, mean 2.033 Å for 448 examples).<sup>27</sup>

**Chapter 2 - Synthesis, Characterization, and X-ray Crystal Structures of Salpy, Acpy and Salpn type Ligands, and their Complexes with Aluminium and Titanium**

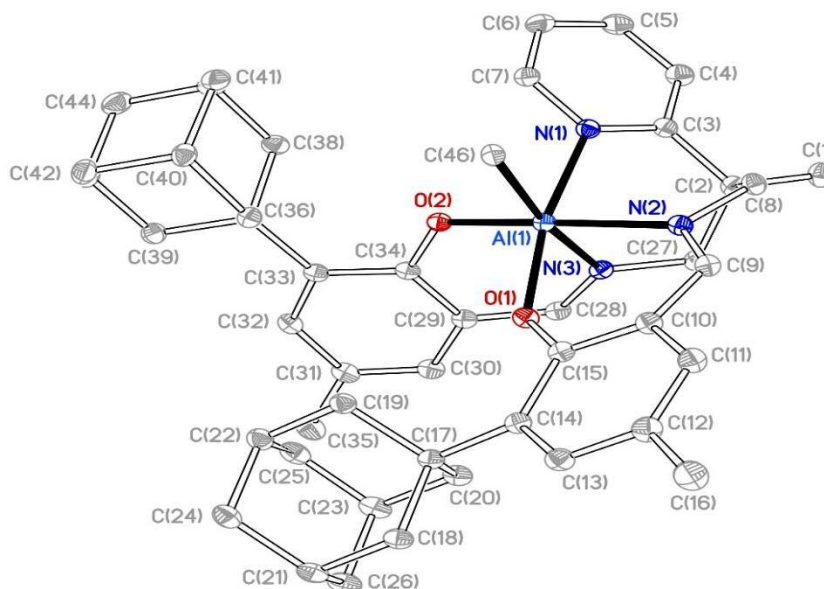


**Figure 2.22:** Thermal ellipsoid plot (30%) of  $[\text{Al}(\text{Ad,Me-Salpy})\text{Me}]$  (**5**). H atoms omitted for clarity

**Table 2.5:** Selected bond lengths (Å) and angles (°) for  $[\text{Al}(\text{Ad,Me-Salpy})\text{Me}]$  (**5**)

Al(1)-O(2)	1.8508(8)	Al(1)-N(2)	2.0488(10)
Al(1)-O(1)	1.8555(8)	Al(1)-N(3)	2.0663(10)
Al(1)-C(46)	2.0367(11)	Al(1)-N(1)	2.1679(10)
O(2)-Al(1)-O(1)	96.13(4)	C(46)-Al(1)-N(3)	170.47(4)
O(2)-Al(1)-C(46)	96.64(4)	N(2)-Al(1)-N(3)	83.00(4)
O(1)-Al(1)-C(46)	99.68(4)	O(2)-Al(1)-N(1)	87.74(4)
O(2)-Al(1)-N(2)	167.15(4)	O(1)-Al(1)-N(1)	166.68(4)
O(1)-Al(1)-N(2)	88.13(4)	C(46)-Al(1)-N(1)	92.49(4)
C(46)-Al(1)-N(2)	94.56(4)	N(2)-Al(1)-N(1)	85.51(4)
O(2)-Al(1)-N(3)	84.92(4)	N(3)-Al(1)-N(1)	78.15(4)
O(1)-Al(1)-N(3)	89.47(4)		

Crystal structure determination was carried out on  $[\text{Al}(\text{tBu,OMe-Salpn})\text{Me}]$  (**6**). This structure makes an interesting comparison with the previously discussed structures since **6** has no pyridyl to coordinate. Crystals of **6** were obtained by

**Chapter 2 - Synthesis, Characterization, and X-ray Crystal Structures of Salpy, Acpy and Salpn type Ligands, and their Complexes with Aluminium and Titanium**

the slow evaporation of a benzene solution. This complex crystallizes in the triclinic space group . The structure is included in Figure 2.23, and selected bond distances and angles are given in Table 2.6. The structure adopts a five-coordinate distorted trigonal bipyramidal (TBP) geometry at the aluminium centre and the degree of trigonality index ( ) is 0.76. the aluminium atom shares a plane with C(28), N(2) and O(2), with equatorial bond angles subtended at Al of  $122.57(8)^\circ$ ,  $122.47(7)^\circ$  and  $114.75(8)^\circ$ ; the axial sites are occupied by N(1) and O(3), with N(1)-Al(1)-O(3) being  $168.41(7)^\circ$ . The coordination geometry exhibits the same features as for the Salpy complexes with pendant pyridyl groups, the axial bond lengths are longer than the equatorial one, in this case, Al(1)-N(1) is longer than Al(1)-N(2) by 0.1 Å.

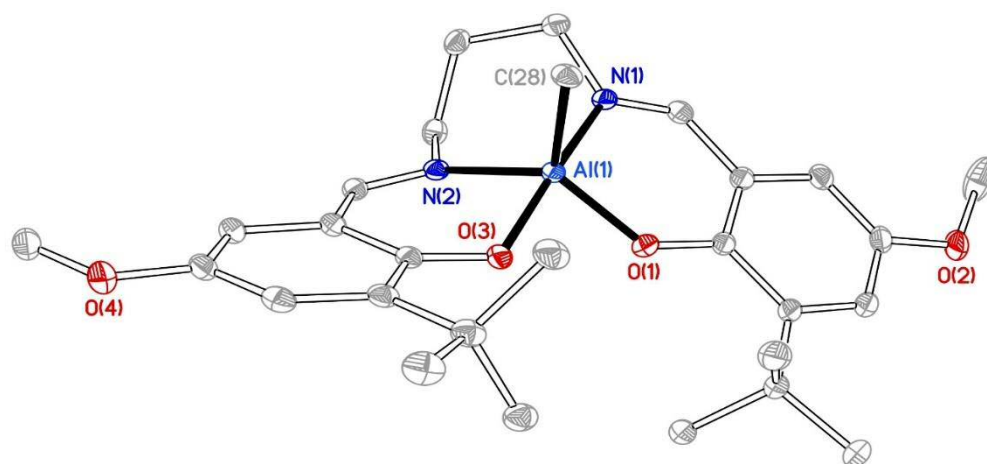


**Figure 2.23:** Thermal ellipsoid plot (30%) of [Al('Bu,OMe-Salpn)Me] (**6**). H atoms omitted for clarity

**Table 2.6:** Selected bond lengths (Å) and angles (°) for [Al(<sup>t</sup>Bu,OMe-Salpn)Me] (**6**)

Al(1)-O(1)	1.7827(15)	Al(1)-N(2)	1.9888(17)
Al(1)-O(3)	1.8375(15)	Al(1)-N(1)	2.0932(18)
Al(1)-C(28)	1.982(2)		
O(1)-Al(1)-O(3)	87.96(7)	C(28)-Al(1)-N(2)	114.75(8)
O(1)-Al(1)-C(28)	122.57(8)	O(1)-Al(1)-N(1)	87.18(7)
O(3)-Al(1)-C(28)	97.90(8)	O(3)-Al(1)-N(1)	168.41(7)
O(1)-Al(1)-N(2)	122.47(7)	C(28)-Al(1)-N(1)	93.58(8)
O(3)-Al(1)-N(2)	88.91(7)	N(2)-Al(1)-N(1)	84.84(7)

For complexes **1**, **4**, **5** and **6** The aluminium-N(imine) bond distances are all within the expected range based upon examples in the Cambridge structural database (1.734–2.891, mean 1.990 Å for 897 examples). The same with Al-C(CH<sub>3</sub>) bond (1.629–2.458, mean 1.991 Å for 4165 examples) and aluminium-O bond (1.542–2.739, mean 1.823 Å for 2608 examples).<sup>27</sup>

To study the correlation between the backbone of the ligand and the bond lengths, angles and the geometry of the resulting complex, complexes were chosen with identical substituents on the Salpy / Salpn phenoxide rings so that the only variation is associated with the backbone substituents; the structures of [Al(<sup>t</sup>Bu,OMe-Salpy)Me] **4** and [Al(<sup>t</sup>Bu,OMe-Salpn)Me] (**6**) are ideal for this purpose. Although complex **4** has a hemi-labile donor, the crystal structures of both complexes possess five coordinate distorted trigonal bipyramidal geometries. There is the possibility of a correlation between and the bite angle of the central N, N' chelate because such chelate in each complex connects an axial donor to an equatorial donor. The bite angle of less than 90° would be expected to minimize the transaxial angle  $\beta$ , and thus reduce (Table 2.7).

**Table 2.7:** the trigonal bipyramidal parameter for the solid state structures of [Al(<sup>t</sup>Bu,OMe-Salpy)Me] (**4**) and [Al(<sup>t</sup>Bu,OMe-Salpn)Me] (**6**)

Complex	A*	$\alpha$ , °	$\beta$ , °		N – N bite, °
4	N2	124.92(6)	166.98(6)	0.70	84.02(5)
6	N2	122.57(8)	168.41(7)	0.76	84.84(7)

\* A = The donor atom not involved in the two largest angles at the aluminium centre.

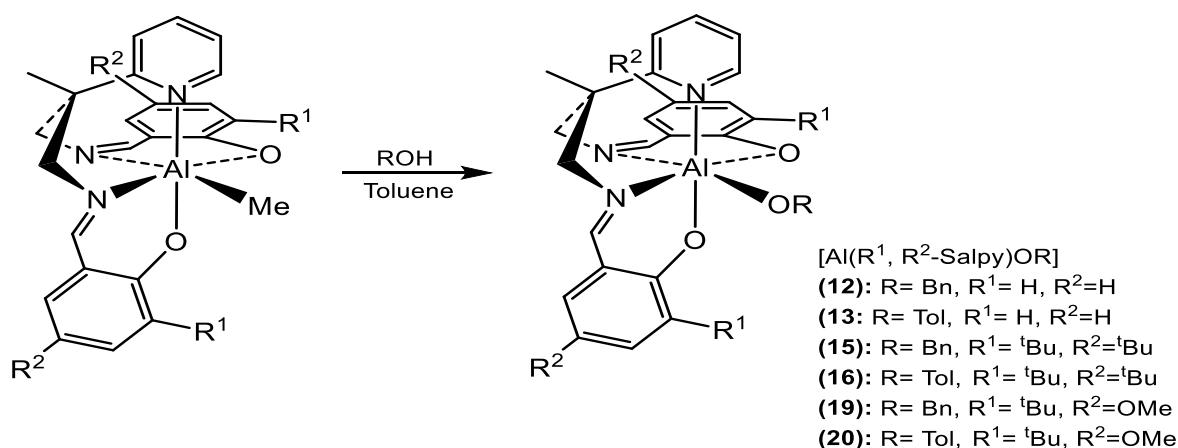
Hormnirun et al<sup>28</sup> presented that such a correlation is only present at the extreme ends of the range. They presented a list of aluminium methyl complexes with a different backbone and phenoxide substituent. They concluded that the flexibility of the linkage between the two nitrogen centres, and thus their ability to adopt a bite angle approaching 90°, is not the only factor affecting the geometry at the metal centre. From the data, which were obtained from the X-ray data for different diamines and substituents on the phenoxy rings, they claimed that electronic effects also play a vital role in geometrical variations.

## 2.3.2 Alkoxide and phenoxide Aluminium complexes

### 2.3.2.1 Synthesis and spectroscopic characterization

In the catalytic polymerization reactions discussed in this thesis, such as ring-opening polymerization of cyclic esters, alkoxide complexes are often more efficient initiators than organometallic precursors. It was therefore of interest to prepare alkoxide and phenoxide derivatives of the complexes reported in Section 2.3.1. To this end, treatment of the previously described aluminium methyl complexes with stoichiometric dry benzyl alcohol in toluene yielded benzyl aluminium complexes, [Al(L)(OBn)], with the concomitant release of CH<sub>4</sub>. In a similar manner, phenoxide complexes [Al(L)(OTol)] were obtained from the reaction of aluminium methyl complexes with p-cresol (Equation 2.8 for Salpy complexes).

**Chapter 2 - Synthesis, Characterization, and X-ray Crystal Structures of Salpy, Acpy and Salpn type Ligands, and their Complexes with Aluminium and Titanium**



**Equation 2.8:** Synthesis of [Al(R<sup>1</sup>, R<sup>2</sup>- Salpy)(OR)] complexes

Interestingly, it was initially apparent that one component was obtained from this reaction, although in one example, [Al(Salpy)(OBn)] (**12**), the expected second isomer was observed as a much smaller component than seen for the methyl complexes (1 : 0.12 based upon integration of the H<sup>6</sup> proton signals). The signals were often obscured by the signals attributed to the major component; combined with their necessary low intensity all signals could not be fully assigned. Nevertheless, the unobscured signals were consistent with the species containing the same components (i.e. O<sub>2</sub>N<sub>2</sub>Npy and OCH<sub>2</sub>Ph ligands) but with the pyridyl H<sup>6</sup> signal being observed at 8.60 ppm, comparable to that in the uncoordinated protio-ligand. This contrasts with that of the major component where the H<sup>6</sup> signal was observed at 9.10 ppm. From these data we infer that both components are likely to be present for all complexes, but the minor component may be present in too small a quantity for NMR detection for most of the derivatives. As for the methyl complexes, <sup>1</sup>H NMR spectra of **12** were measured at six temperatures from 298–323 K, and the relative integration of the two components used to determine the equilibrium coefficient at each temperature. These data were used to construct a van't Hoff plot (Figure 2.24), which was used to obtain the thermodynamic parameters for the equilibrium process, giving ΔH° = 13.6±4.3 kJ.mol<sup>-1</sup> and ΔS° = 29.5±13 J.mol<sup>-1</sup>.K<sup>-1</sup>. These parameters allowed us to estimate ΔG<sub>298</sub> as 4.8±4.8 kJ.mol<sup>-1</sup>. The parameters are consistent with those obtained for [Al(<sup>t</sup>Bu,OMe-Salpy)Me] discussed above, showing a relatively small energy difference between the two isomers. In the

case of **12** the value of  $\Delta S^\circ$  is slightly higher, and consistent with a slight increase in molecular disorder on de-coordinating the pyridyl donor.

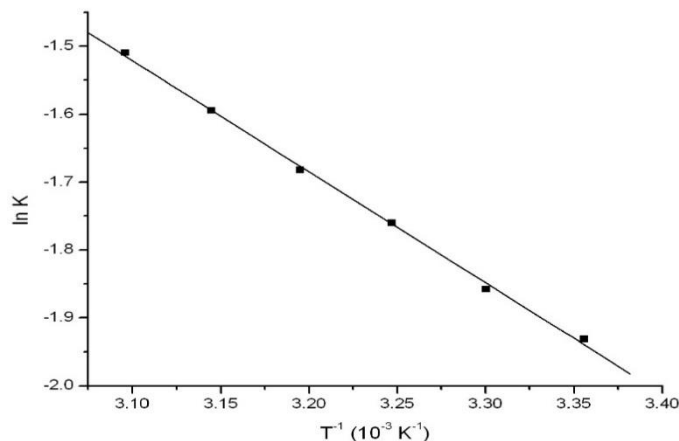


**Figure 2.24:** Van't Hoff plot for  $[Al(Salpy)(OBn)]$  (**12**)

Comparison of the  $^1H$  NMR spectra of complex **1** and **12** shows the disappearance of the  $AlCH_3$  signal in **12** and a new single resonance at 4.68 ppm. The  $H^6$  proton signal was shifted from 8.69 ppm in complex **1** to 9.10 in complex **12** which suggests that the pyridyl is coordinated in the major isomer in both cases.

$[Al(Salpy)(OTol)]$  **13** was synthesized by the direct reaction of complex **1** with freshly sublimed p-cresol in toluene under a nitrogen atmosphere; a pure complex was obtained using this route. The  $^1H$  NMR spectrum shows one species, the  $H^6$  resonance at 9.12 ppm suggesting that this is the six coordinate complex. In previous work with complexes of the structurally related diamido-pyridine ligands  $[MeC(2-C_5H_4N)(CH_2NR)_2]^{2-}$ , it has been established that the chemical shift corresponding to  $H^6$  can be indicative of the coordinative state of the pyridyl moiety. A significant downfield shift indicates that the pyridyl is coordinated to the metal ion, whereas a chemical shift similar to that of the free protio-ligand is suggestive of a pendant pyridyl donor. Again, the signal at -0.89 for  $Al-CH_3$  was not observed and a new resonance at 2.17 ppm appeared for  $CH_3$  of the tolyl methyl. Table 2.8 shows the important proton chemical shifts for the aluminium benzyl and tolyl complexes.

**Table 2.8:** The important chemical shift of <sup>1</sup>H NMR for the prepared aluminium benzyl and tolyl complexes

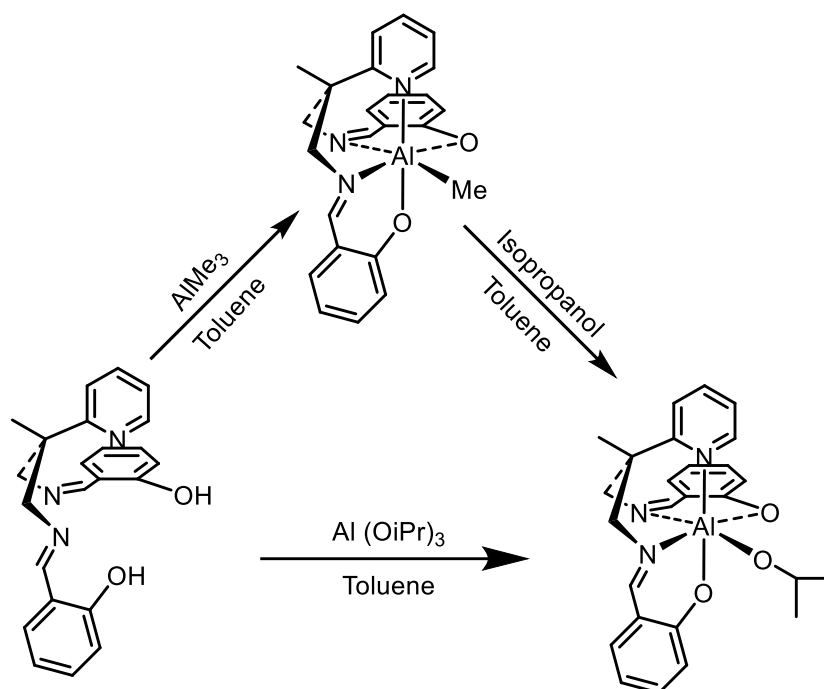
Complex	H <sup>6</sup>	CH=N	CH <sub>2</sub>	CH <sub>3</sub>
[Al(Salpy)(OBn)] (12)	9.10	7.84	3.80, 3.71	1.42
[Al(Salpy)(OTol)] (13)	9.12	7.92	3.80	1.58
[Al( <sup>t</sup> Bu, <sup>t</sup> Bu- Salpy)(OBn)] (15)	9.20	7.82	3.91, 3.61	1.43
[Al( <sup>t</sup> Bu, <sup>t</sup> Bu- Salpy)(OTol)] (16)	9.27	7.59	3.52	1.31
[Al(Naphpy)(OBn)] (17)	9.13	8.70	4.01-3.87	1.54
[Al(Naphpy)(OTol)] (18)	9.09	8.68	3.95	1.57
[Al( <sup>t</sup> Bu, OCH <sub>3</sub> - Salpy)(OBn)] (19)	9.21	7.82	3.94,3.62	1.19
[Al( <sup>t</sup> Bu, OCH <sub>3</sub> - Salpy)(OTol)] (20)	9.39	7.71	3.74,3.66	1.45
[Al( <sup>t</sup> Bu, OCH <sub>3</sub> - Salpn)(OBn)] (21)	-	8.05	3.91,3.50	-
[Al(Acpy)(OBn)] (22)	9.21	-	3.79	1.54
[Al(OCH <sub>3</sub> - Acpy)(OBn)] (23)	9.43	-	3.87	1.71

The <sup>1</sup>H NMR spectrum of [Al(<sup>t</sup>Bu, <sup>t</sup>Bu- Salpy)(OTol)] (**16**) shows an analogous signal at 9.27 ppm for the H<sup>6</sup> proton resonance, with corresponding <sup>13</sup>C resonances at 155.3 ppm for C<sup>6</sup>; this feature was common for all of the alkoxide complexes in this chapter, which all show high chemical shift for proton H<sup>6</sup>. Again, the higher chemical shift of this proton is a good indication that the pyridyl group is coordinated to the aluminium as part of a κ<sup>5</sup>-Salpy ligand.

The identity of the co-ligand has a remarkable effect on the isomer energetics of, and therefore the data observed for, the complexes. The spectra for all benzyl (except for **12**) and tolyl complexes showed only a single compound while those for all methyl complexes indicated multiple species. To investigate any effect of

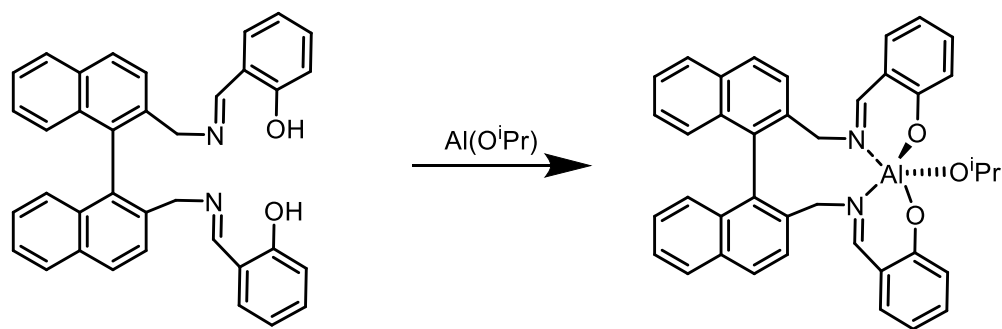
**Chapter 2 - Synthesis, Characterization, and X-ray Crystal Structures of Salpy, Acpy and Salpn type Ligands, and their Complexes with Aluminium and Titanium**

the O-substituent (e.g. steric) on the proportion of two isomers, an isopropoxide complex  $[\text{Al}(\text{Salpy})(\text{O}^i\text{Pr})]$  (**14**) was prepared. Complex **14** was prepared using two alternative routes, the first includes the direct reaction between the protio-ligands and aluminium isopropoxide. The other way involved the reaction of isopropanol with the corresponding aluminium methyl complex (Scheme 2.6).



**Scheme 2.6:** The two pathways for synthesis of  $[\text{Al}(\text{Salpy})(\text{O}^i\text{Pr})]$  (**14**)

The first route was by far the most challenging of the two. Aluminium isopropoxide is less reactive than trialkyl aluminium, presumably due to its oligomeric structure, which means that its reactions need longer reaction times and higher temperatures to complete. For example, Coates and Ovitt<sup>29</sup> prepared a new complex from salen-type ligands and Aluminium isopropoxide by stirring the reaction mixture at 70 °C for 2 days (equation 2.9). No complex was formed after stirring the Salpy protio-ligand with aluminium isopropoxide, so the reaction was conducted at 80 °C for two days, a milky suspension was formed and complicated NMR spectrum was obtained. Unfortunately, no pure complex was obtained from this method even when the free ligand was replaced with (<sup>t</sup>Bu, <sup>t</sup>Bu- Salpy).



**Equation 2.9**

The indirect reaction takes a short time and it was possible to run the reaction with or without heating. Dry Isopropyl alcohol was used as an aliphatic alcohol and was mixed with complex **1** in toluene, the complex [Al(Salpy)(O<sup>i</sup>Pr)] (**14**) was obtained, with only one isomer observed in the <sup>1</sup>H NMR spectrum.

The aluminium alkoxide and phenoxide complexes are much more stable in air than the corresponding methyl complexes, which are extremely air sensitive. Jegier *et al.* reported that Penta-coordinated aluminium complexes containing salen ligands tend to show low chemical stability and readily dissociate into other species in the air, or in the presence of Lewis bases, especially when an alkyl or halide unit is employed as an ancillary ligand.<sup>30</sup> Hwang *et al.* demonstrated the effect of the presence of *tert*-butyl groups in the salen ligands using aryloxide as the ancillary ligand. According to their study, these two groups enhance the stability of the resulting complex by encapsulating the metal centre, and by strengthening the bonding too. In addition, the presence of *tert*-butyl groups increases the solubility of the complexes in common organic solvents.<sup>31</sup>

### **2.3.2.2 Crystallographic characterisation of aluminium alkoxide and phenoxide complexes**

Crystals of [Al(Salpy)(OTol)](**13**) were obtained from concentrated solution in toluene. Selected bond distances and bond angles are given in Table 2.9. This tolyl complex crystalizes in the triclinic space group . A closer look at the

**Chapter 2 - Synthesis, Characterization, and X-ray Crystal Structures of Salpy, Acpy and Salpn type Ligands, and their Complexes with Aluminium and Titanium**

coordination sphere of Al shows a distorted octahedral geometry (Figure 2.25). With the same behaviour of complex 1, the complex contains a  $\kappa^5$ -Salpy ligand and one OTol ligand. The bond between the Al atom and the 4-methylphenoxy group is nearly perpendicular to the salen–Al coordination plane, revealing hexacoordination geometry around the Al centre. The three oxygens are bonded to the Al with slightly obtuse O–Al–O angles, whilst the N–Al–N angles are more acute. In aryloxyde / alkoxide complexes, it is common for O atom of the alkoxide/aryloxyde ligand to be formally  $sp$  hybridized, giving an approximately linear M–O–C angle. This, in principle, allows the  $p$ -based lone pairs to  $\pi$ -donate into empty metal-based  $d$  orbitals;<sup>32</sup> this is especially important in early transition metals with vacant  $d$  orbitals. In the structure of **13**, the Al(1)–O(3)–C(24) angle is  $137.9(2)^\circ$ , and cannot be reasonably considered as linear; the  $3d$  orbitals of aluminium are likely to possess an inaccessibly high energy, thus disfavours  $\pi$  donation of the lone pairs, and rendering the oxygen  $sp^3$  hybridized.

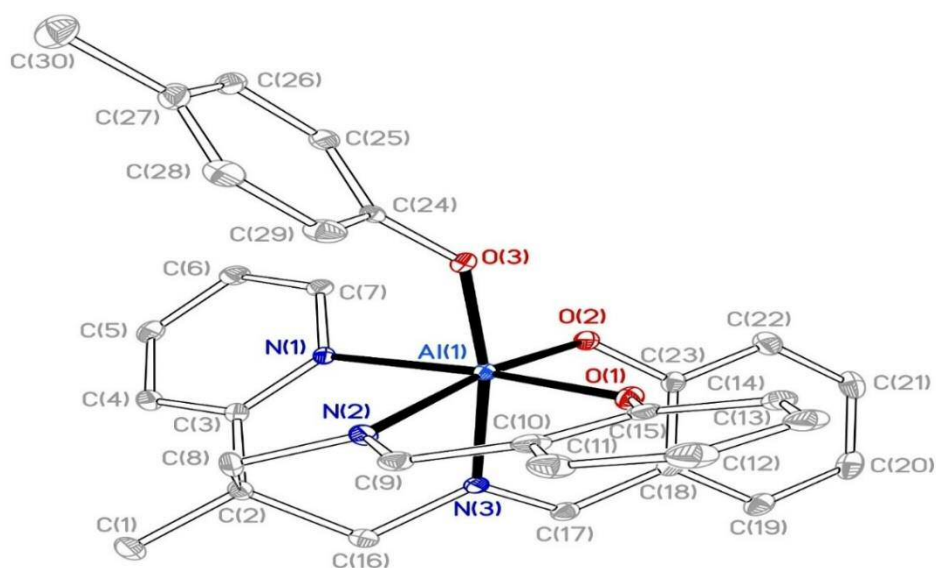


**Figure 2.25:** Molecular structure of [Al(Salpy)(OTol)] (**13**) with thermal ellipsoids drawn at 30% probability and hydrogen atoms omitted for clarity.

**Table 2.9:** Selected bond lengths (Å) and bond angles (°) for [Al(Salpy)(OTol)] (13)

Al(1)-O(3)	1.814(2)	Al(1)-N(2)	2.033(3)
Al(1)-O(1)	1.837(2)	Al(1)-N(3)	2.071(3)
Al(1)-O(2)	1.843(2)	Al(1)-N(1)	2.128(3)
O(3)-Al(1)-O(1)	96.79(11)	O(2)-Al(1)-N(3)	86.39(11)
O(3)-Al(1)-O(2)	92.14(11)	N(2)-Al(1)-N(3)	81.72(12)
O(1)-Al(1)-O(2)	91.34(11)	O(3)-Al(1)-N(1)	87.69(11)
O(3)-Al(1)-N(2)	99.60(11)	O(1)-Al(1)-N(1)	174.79(12)
O(1)-Al(1)-N(2)	89.26(12)	O(2)-Al(1)-N(1)	91.15(11)
O(2)-Al(1)-N(2)	168.09(12)	N(2)-Al(1)-N(1)	87.36(12)
O(3)-Al(1)-N(3)	167.14(11)	N(3)-Al(1)-N(1)	79.57(10)
O(1)-Al(1)-N(3)	96.02(11)		

X-ray quality crystals of [Al(<sup>t</sup>Bu,<sup>t</sup>Bu-Salpy)(OTol)] (16) were obtained by the slow evaporation of a concentrated toluene solution at ambient temperature. Complex 16 crystallizes in the triclinic space group . The solid-state structure is shown in Figure 2.26; selected bond lengths and angles are given in Table 2.10. The most notable feature in complex 16 is that the pyridyl is pendant, the aluminium centre adopting a 5-coordinate distorted trigonal bipyramidal geometry. This is especially noteworthy, since the NMR data for this complex did not suggest the presence of a pendant-pyridyl isomer; only one isomer was observed and the chemical shift of the H<sup>6</sup> proton suggested that the pyridyl was coordinated. This reinforces the suggestion that both isomers are present in all complexes, where they are absent more than likely denotes that they are present in a concentration that is too small to be detected spectroscopically. In literature examples, the geometry of five-coordinate salen-type aluminium complexes is either square pyramidal (sqp) or trigonal bipyramidal (tbp), depending on the nature of the connection between the two nitrogens of the ligand (the ligand “backbone”). A sqp geometry of the complex tends to be adopted with an ethyl, (CH<sub>2</sub>)<sub>2</sub>, or o-aryl backbone. With more flexible backbones, (CH<sub>2</sub>)<sub>n</sub> n > 2, a tbp geometry is often

**Chapter 2 - Synthesis, Characterization, and X-ray Crystal Structures of Salpy, Acpy and Salpn type Ligands, and their Complexes with Aluminium and Titanium**

obtained.<sup>33</sup> An explanation of this observation was demonstrated by Donald and Damon, who reported the crystal structures of four aluminium salen complexes.<sup>34–41</sup> In their report, the solid-state structures show that all four complexes display the distorted square pyramidal geometry typical of group 13 salen complexes, where the backbones are benzene or cyclohexane which are less flexible (Figure 2.27).

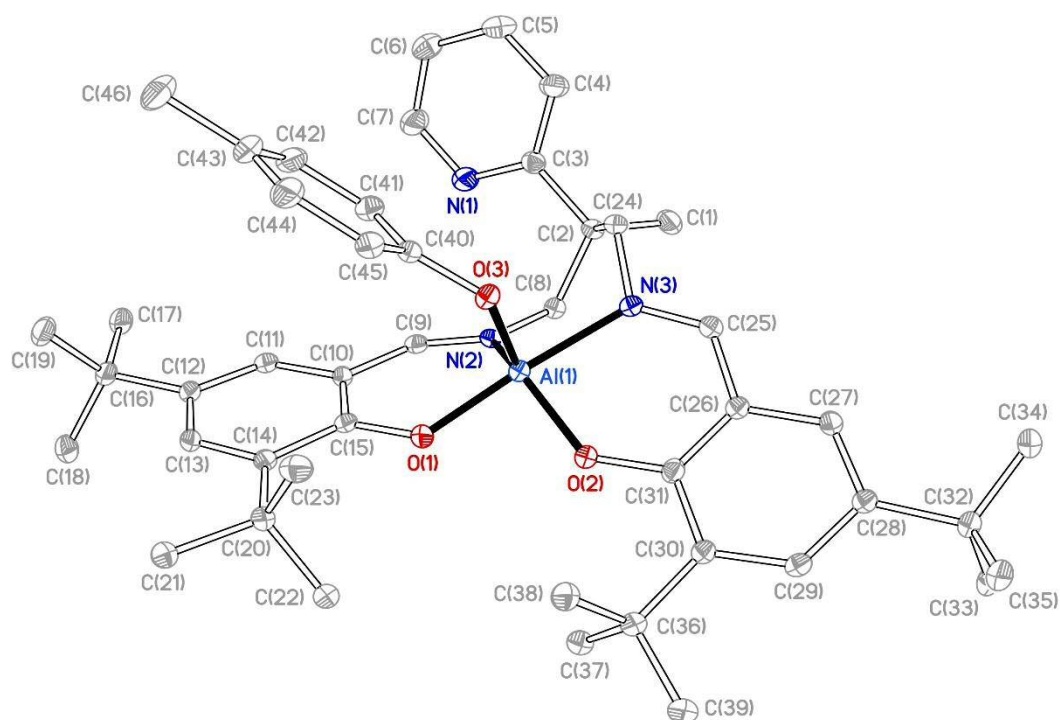
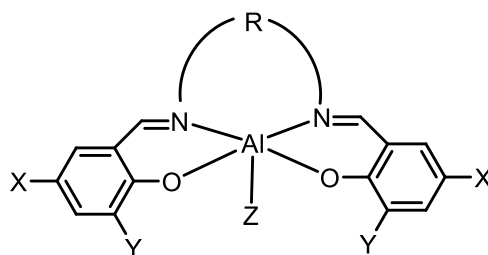


**Figure 2.26:** Molecular structure of [Al(ᵀBu,ᵀBu-Salpy)(OTol)] (16) with thermal ellipsoids drawn at 30% probability and hydrogen atoms omitted for clarity.



- A: X = H; Y = H; Z = Et; R = C<sub>6</sub>H<sub>4</sub><sup>-</sup>  
 B: X = <sup>t</sup>Bu; Y = <sup>t</sup>Bu; Z = Et; R = C<sub>6</sub>H<sub>10</sub><sup>-</sup>  
 C: X = <sup>t</sup>Bu; Y = <sup>t</sup>Bu; Z = C<sub>6</sub>H<sub>3</sub>(CH<sub>3</sub>)<sub>3</sub>; R = C<sub>6</sub>H<sub>10</sub><sup>-</sup>  
 D: X = <sup>t</sup>Bu; Y = <sup>t</sup>Bu; Z = C<sub>6</sub>H<sub>5</sub>; R = C<sub>6</sub>H<sub>10</sub><sup>-</sup>

**Figure 2.27:** The complexes prepared by Donald and Damon

In **16** the preference for a tbp geometry with the CH<sub>2</sub>{C(CH<sub>3</sub>)(Py)}CH<sub>2</sub> backbone is probably due to the fact that a sqp geometry would cause the methylene hydrogens to be eclipsed; in the tbp geometry they are staggered. The  $\tau$  values of the complex **16** is 0.72. From this number, it is readily observed that this complex, which is made from ligand containing a relatively long ligand backbone, achieves a distorted tbp geometry.

**Table 2.10:** Selected bond lengths (Å) and bond angles (°) for [Al(<sup>t</sup>Bu, <sup>t</sup>Bu-Salpy)(OTol)] (**16**)

Al(1)-O(3)	1.7627(17)	Al(1)-N(2)	1.970(2)
Al(1)-O(2)	1.7673(16)	Al(1)-N(3)	2.024(2)
Al(1)-O(1)	1.8084(17)		
O(3)-Al(1)-O(2)	116.79(8)	O(1)-Al(1)-N(2)	89.64(8)
O(3)-Al(1)-O(1)	98.99(8)	O(3)-Al(1)-N(3)	88.61(8)
O(2)-Al(1)-O(1)	89.83(7)	O(2)-Al(1)-N(3)	88.62(8)
O(3)-Al(1)-N(2)	114.21(8)	O(1)-Al(1)-N(3)	172.11(8)
O(2)-Al(1)-N(2)	128.41(8)	N(2)-Al(1)-N(3)	85.27(8)

**Chapter 2 - Synthesis, Characterization, and X-ray Crystal Structures of Salpy, Acpy and Salpn type Ligands, and their Complexes with Aluminium and Titanium**

The Al-O bond lengths in **13** are longer than the corresponding ones in **16**. One of the Salpy phenoxide oxygens, O(1), is located in an axial position, along with one of imine nitrogens, (N3). The aluminium atom shares an approximate plane with the two remaining oxygen atoms, one from the tolyl group and the other from the Salpy ligand, and one nitrogen atom of imine; these atoms form the equatorial plane with distorted 120° angles. From the data in Table 2.10, and from Figure 2.26, the Al-O<sub>axial</sub> bond length Al(1)-O(1) (1.8084(17)) is longer than Al-O<sub>equatorial</sub> (Al(1)-O(2) = 1.7673(16) and Al(1)-O(3) = 1.7627(17)). This is understandable, since an axial position is more crowded because each axial atom has three neighbouring equatorial atoms (on the same central atom) at 90° bond angles, while an equatorial atom has only two neighbouring axial atoms at 90° bond angles. For tbp molecules with five identical ligands, the axial bond lengths tend to be longer because of the different bonding situation in these ligands (3-centre, 4-electron bonding).

The molecular structure of **20** was determined from the X-ray diffraction data obtained from a single crystal grown by slow evaporation from toluene solution. The structure of compound **20** is shown in Figure.2.28; selected bond lengths and angles are given in Table 2.11. The asymmetric unit contains, in addition to a molecule of **20**, a molecule of toluene of solvation. This complex crystallizes in the triclinic space group . As for the previously reported structures, the tolyl Al-O bond distance is shorter than the Salpy Al-O distances and both the Al-N<sub>imine</sub> are shorter than the Al-N<sub>py</sub>.

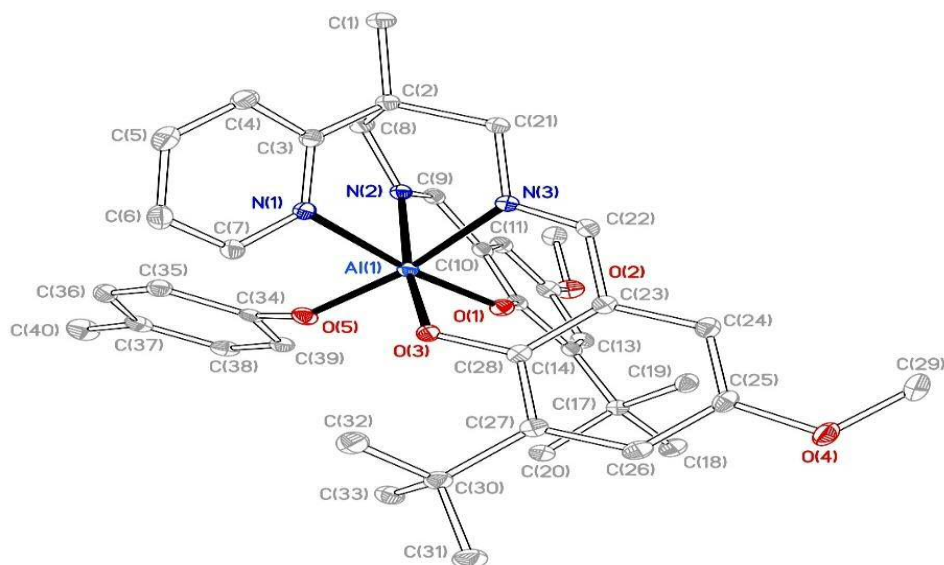


**Figure 2.27:** Thermal ellipsoid plot (30%) of [Al(*t*Bu,OMe-Salpy)(OTol)] (**20**). H atoms and solvent of crystallization omitted for clarity.

**Table 2.11:** Selected bond lengths (Å) and bond angles (°) for [Al(*t*Bu,OMe-Salpy)(OTol)] (**20**)

Al(1)-O(5)	1.7876(8)	Al(1)-N(2)	2.0168(9)
Al(1)-O(3)	1.8248(8)	Al(1)-N(3)	2.0370(9)
Al(1)-O(1)	1.8312(8)	Al(1)-N(1)	2.1293(9)
O(5)-Al(1)-O(3)	92.60(3)	O(1)-Al(1)-N(3)	93.33(4)
O(5)-Al(1)-O(1)	99.70(4)	N(2)-Al(1)-N(3)	83.01(4)
O(3)-Al(1)-O(1)	93.78(3)	O(5)-Al(1)-N(1)	87.32(4)
O(5)-Al(1)-N(2)	97.36(4)	O(3)-Al(1)-N(1)	88.52(3)
O(3)-Al(1)-N(2)	169.17(4)	O(1)-Al(1)-N(1)	172.49(4)
O(1)-Al(1)-N(2)	88.73(4)	N(2)-Al(1)-N(1)	87.72(4)
O(5)-Al(1)-N(3)	166.97(4)	N(3)-Al(1)-N(1)	79.67(3)
O(3)-Al(1)-N(3)	86.33(3)		

**Chapter 2 - Synthesis, Characterization, and X-ray Crystal Structures of Salpy, Acpy and Salpn type Ligands, and their Complexes with Aluminium and Titanium**

[Al(OMe-Acpy)(OBn)] (**23**) was the only aluminium O-benzyl complex that gave crystals suitable for X-ray structural determination. The triclinic crystals were grown from a concentrated toluene solution. Complex **23** crystallizes in space group . The structure of **23** is shown in Figure 2.29, and important bond lengths and angles are given in Table 2.12. The structure consists of a central six-coordinate aluminium atom in a distorted octahedral geometry, with the OMe-Acpy ligand adopting a  $\kappa^5$ -coordination mode. The structure is similar to those previously described, in which the pyridyl moiety coordinates to the aluminium centre. As seen previously, the O-Al-O angles are more obtuse [ $93.88(5)^\circ$  to  $97.13(5)^\circ$ ], whereas the N-Al-N angles are more acute [ $82.92(5)^\circ$  to  $86.99(5)^\circ$ ].

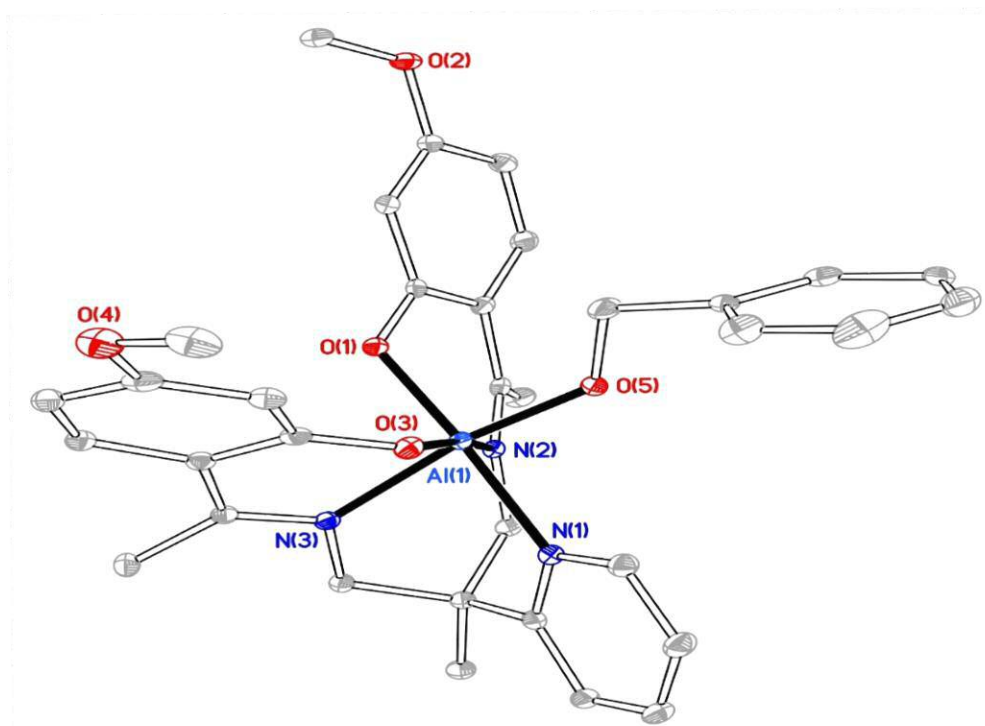


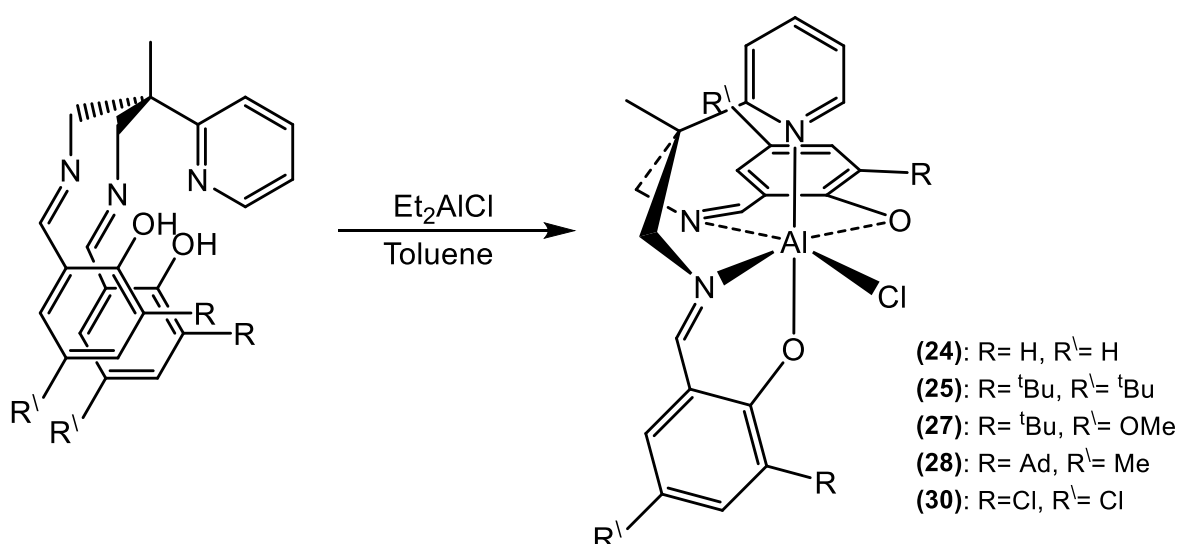
**Figure 2.29:** Thermal ellipsoid plot (30%) of [Al(OMe-Acpy)(OBn)] (**23**). H atoms omitted for clarity

**Table 2.12:** Selected bond lengths (Å) and bond angles (°) for [Al(OMe-Acpy)(OBn)] (**23**)

Al(1)-O(5)	1.7975(10)	Al(1)-N(2)	2.0509(12)
Al(1)-O(1)	1.8436(10)	Al(1)-N(3)	2.0551(12)
Al(1)-O(3)	1.8525(10)	Al(1)-N(1)	2.0829(12)
O(5)-Al(1)-O(1)	97.13(5)	O(3)-Al(1)-N(3)	85.28(5)
O(5)-Al(1)-O(3)	95.48(5)	N(2)-Al(1)-N(3)	85.06(5)
O(1)-Al(1)-O(3)	93.88(5)	O(5)-Al(1)-N(1)	87.38(5)
O(5)-Al(1)-N(2)	93.81(5)	O(1)-Al(1)-N(1)	173.42(5)
O(1)-Al(1)-N(2)	87.94(5)	O(3)-Al(1)-N(1)	90.44(5)
O(3)-Al(1)-N(2)	170.24(5)	N(2)-Al(1)-N(1)	86.99(5)
O(5)-Al(1)-N(3)	170.27(5)	N(3)-Al(1)-N(1)	82.92(5)
O(1)-Al(1)-N(3)	92.49(5)		

### 2.3.3 Aluminium chloride complexes

#### 2.3.3.1 Synthesis and spectroscopic characterization



**Equation 2.10:** Synthesis of [Al(R,R'-Salpy)Cl] complexes

**Chapter 2 - Synthesis, Characterization, and X-ray Crystal Structures of Salpy, Acpy and Salpn type Ligands, and their Complexes with Aluminium and Titanium**

Many catalysts, used in the co-polymerization of epoxides and either CO<sub>2</sub> or cyclic anhydrides, contain a chloride co-ligand. Since the co-polymerization of epoxides and cyclic anhydrides are of relevance to this thesis, it was of importance to prepare chloride derivatives of the aluminium complexes previously described. To this end, chloride complexes of the general formula [Al(R,R'-Salpy)Cl] were prepared according to equation 2.10, by reacting the (R,R'-Salpy) protio-ligands with diethylaluminium chloride in toluene, affording complexes in high yield. With all ligand derivatives, the reaction with Et<sub>2</sub>AlCl was rapid, with evolution of 2 equivalents of ethane gas evolved, and the product forming as a precipitate. To maximize the yield, the reaction time was lengthened to guarantee that all the ligand had been converted to the complex. The reaction was conducted under an inert atmosphere of argon or nitrogen, although the chloride complexes are expected to be significantly less sensitive than their organometallic congeners. The aluminium precursor was added dropwise to a solution of ligand at ambient temperature. The solvent was concentrated and full precipitation was achieved by adding dry hexanes. Yields were typically 83-93%.

The spectroscopic data for these complexes are consistent with monomeric complexes bearing a  $\kappa^5$ -coordinated Salpy ligand; there are no signature signals for the chloride co-ligand, but its presence is inferred by the elemental analysis, X-ray analyses (*vide infra*), and analogous complexes discussed above. The <sup>1</sup>H NMR spectra of all complexes show only one species [Al(R,R'-Salpy)Cl], and as for the alkoxide complexes, it is likely that the complexes exist in two isomeric forms, where one component (pyridine de-coordinated) is present in a concentration that is too small to be detected using NMR spectroscopy. The most diagnostic indication of complex formation is the disappearance of the phenol OH proton signal. The signals attributed to the imine protons of all complexes were extremely broad, to the extent that they often merged into the baseline. This behaviour was only observed with the chloride complexes containing a pyridyl donor which could potentially refer to a slow exchange of the two coordinative states of the pyridyl donor.

**Chapter 2 - Synthesis, Characterization, and X-ray Crystal Structures of Salpy, Acpy and Salpn type Ligands, and their Complexes with Aluminium and Titanium**

When a molecule exchanges between two or more conformations, the exchange processes can lead to broadening of the NMR spectra. Because many conformational exchange processes are so fast on the NMR time-scale, only averaged spectra are observed. Sterics can play an important role in the shape of NMR signals; in molecules which are not subject to excessive steric demand, some inequivalent nuclei give single sets of signals with an apparently higher symmetry than expected, due to the averaging of the various conformers. In molecules where there are very bulky groups, steric hindrance can slow the exchange down to the point at which the signals are broadened, or in extreme circumstances, where the exchange is altogether prevented and inequivalent signals are observed.

To examine the exchange process in detail,  $^1\text{H}$  NMR spectra were measured between  $+60^\circ\text{C}$  and  $-40^\circ\text{C}$  for  $[\text{Al}(\text{tBu},\text{OMe-Salpy})\text{Cl}]$  (**27**), as a representative example. Changing the temperature gave rise to a significant alteration in the appearance of the spectra (Figure 2.30). As the sample was heated above room temperature, the  $\text{H}^6$  signal broadened, whereas the broad signal attributed to the *tert*-butyl groups was found to sharpen; this signal remained rather broad at  $+60^\circ\text{C}$ , and would presumably have become very sharp with higher temperatures than were achievable in this experiment ( $\text{CDCl}_3$  boils at  $61^\circ\text{C}$ ). This is consistent with the system reaching a fast exchange and a consequent averaging of signals. At low temperatures however, all signals were found to sharpen, and signals associated with the phenol “arms” (including the *tert*-butyl and methoxy groups) and the backbone methylene groups were observed to decoalesce into two sets of signals of equal intensity. A second component also became apparent, by virtue of a second  $\text{H}^6$  signal at *ca.* 9.3 ppm, but the intensity was too small to allow the other signals to be adequately reported. Due to the small intensity of the second component, and a careful consideration of the integration values of the principal pyridyl vs. recoalesced signals, the spectra are consistent with a  $\text{C}_1$ -symmetric complex with inequivalent Salpy “arms”, as observed in the X-ray structures described above for the organometallic and alkoxide complexes, and below for the chloride congeners.

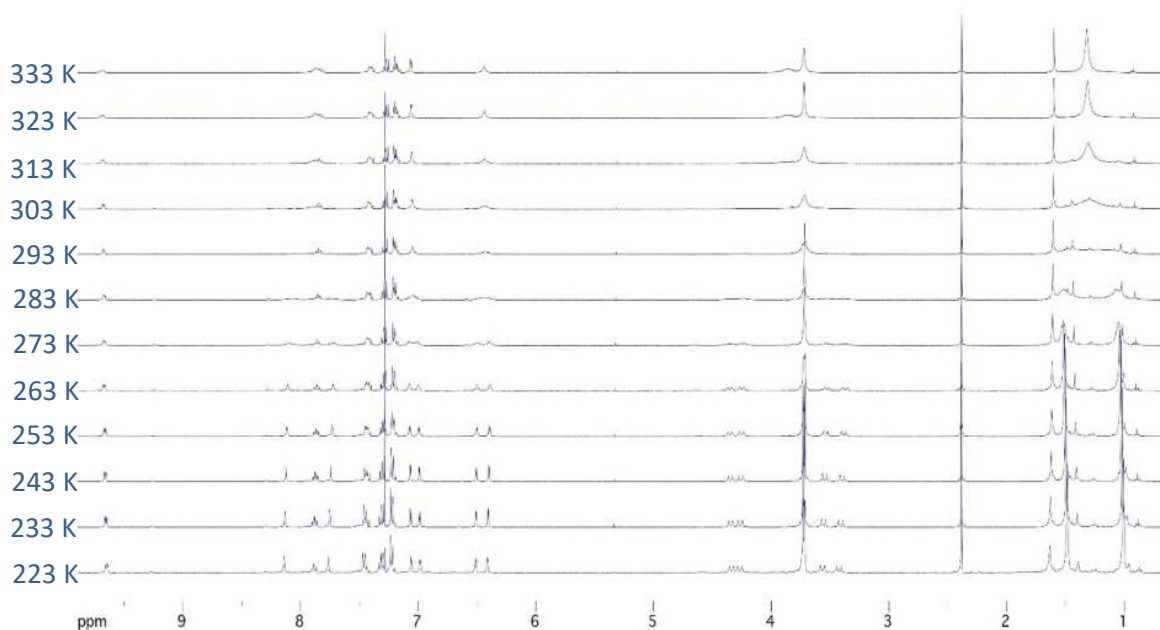


**Figure 2.30:** Variable temperature (VT)  $^1\text{H}$  NMR spectra (400 MHz,  $\text{CDCl}_3$ ) for  $[\text{Al}(\text{tBu},\text{OMe-Salpy})\text{Cl}]$  (**27**)

The  $^1\text{H}$  NMR spectrum of  $[\text{Al}(\text{tBu},\text{OMe-Salpn})\text{Cl}]$  (**29**) is consistent with higher symmetry, with one sharp singlet corresponding to both imine groups (Figure 2.31). As expected, the signals attributed to the methylene groups are significantly different to those  $[\text{Al}(\text{R},\text{R}'\text{-salpy})\text{Cl}]$ , such that they appear as a often-broad multiplets over a wider chemical shift range. The extended coupling is readily understood due to the presence of  $^3J$  coupling, and the extra flexibility of the backbone could readily give rise to fluxional processes, and therefore broader signals.

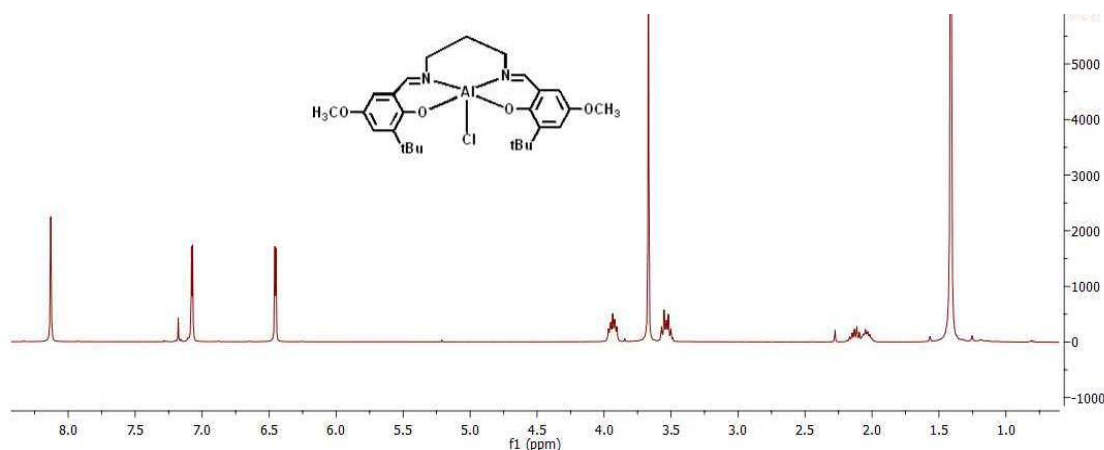


**Figure 2.31:**  $^1\text{H}$  NMR spectrum (400 MHz, 293 K,  $\text{CDCl}_3$ ) for  $[\text{Al}(\text{tBu},\text{OMe-Salpn})\text{Cl}]$  (**29**)

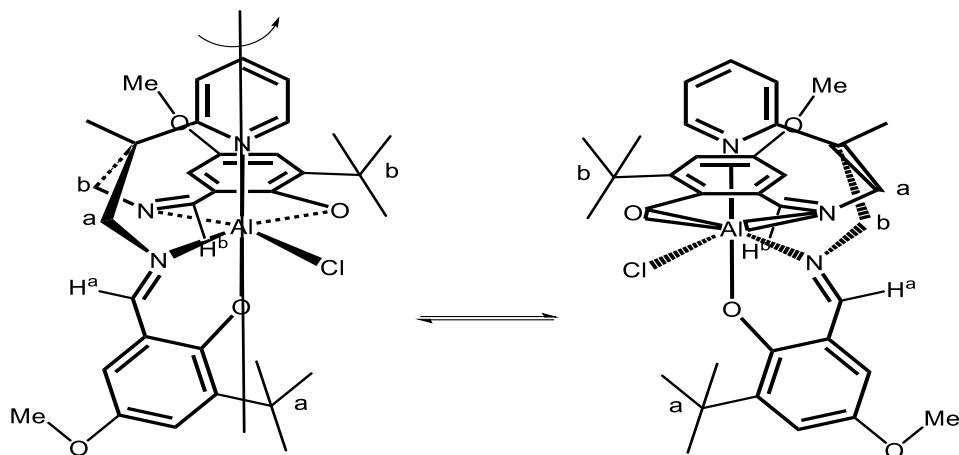
### 2.3.3.2 Measurement of activation parameters

Activation parameters for the exchange of the Salpy “arms” in  $[\text{Al}(\text{tBu},\text{OMe-Salpy})\text{Cl}]$  (**27**) (Equation 2.11) were obtained by the lineshape analysis of five measurements, at 10 K intervals in  $\text{CDCl}_3$ , of the  $^1\text{H}$  NMR data (400 MHz) taken from the variable temperature spectra discussed above. The higher temperature spectra, after coalescence, did not allow for accurate analysis, and so only spectra  $\leq 293$  K were used. The spectra of complex **27** were unusual in that the data allowed the activation parameters to be determined from three separate sets of resonances: those being the imine, the *tert*-butyl, and methylene resonances. For the imine and *tert*-butyl resonances, where singlets were observed, the linewidths at half height  $\nu_{1/2}(\text{obs})$  were corrected by subtracting the natural linewidths obtained from the low temperature limit  $^1\text{H}$  NMR spectrum recorded at 233 K. The values of  $\nu_{1/2}(\text{corr})$  were used to calculate the observed rate constants ( $k$ ) for the processes  $\text{N}=\text{C}-\text{H}_a \rightarrow \text{N}=\text{C}-\text{H}_b$ ,  ${}^t\text{Bu}^a \rightarrow {}^t\text{Bu}^b$   $\{k_{\text{obs}}(a \rightarrow b)\}$  and  $\text{N}=\text{C}-\text{H}_b \rightarrow \text{N}=\text{C}-\text{H}_a$ ,  ${}^t\text{Bu}^b \rightarrow {}^t\text{Bu}^a$   $\{k_{\text{obs}}(b \rightarrow a)\}$  according to the formula:<sup>42</sup>

For the methylene groups, where doublets were observed, the low temperature limit spectrum was simulated using the iNMR software package, and the rate constants obtained by modelling the exchange of the signals, and comparing against the experimental spectra iteratively. The values of all rate constants

**Chapter 2 - Synthesis, Characterization, and X-ray Crystal Structures of Salpy, Acpy and Salpn type Ligands, and their Complexes with Aluminium and Titanium**

thereby obtained are provided in Table 2.13 (imine), Table 2.14 (<sup>t</sup>Bu), and Table 2.15 (methylene).



**Equation 2.11**

**Table 2.13:** Corrected linewidths and rate constants for the exchange of imine environments in the complex [Al(<sup>t</sup>Bu, OCH<sub>3</sub> - Salpy)(Cl)]

Temperature (K)	N=C-H <sub>a</sub> → N=C-H <sub>b</sub>		N=C-H <sub>b</sub> → N=C-H <sub>a</sub>	
	$\nu_{1/2}$ (corr ab)	$k_{\text{obs}}$ (a→b)	$\nu_{1/2}$ (corr ba)	$k_{\text{obs}}$ (b→a)
243	0.270	0.848	0.326	1.024
253	1.195	3.755	1.476	4.638
263	3.320	10.431	3.898	12.248
273	15.201	47.762	15.104	47.457
283	33.825	106.278	32.256	101.348

**Table 2.14:** Corrected linewidths and rate constants for the exchange of <sup>t</sup>Bu environments in the complex [Al(<sup>t</sup>Bu, OCH<sub>3</sub> - Salpy)(Cl)]

Temperature (K)	<sup>t</sup> Bu <sub>a</sub> → <sup>t</sup> Bu <sub>b</sub>		<sup>t</sup> Bu <sub>b</sub> → <sup>t</sup> Bu <sub>a</sub>	
	$\nu^{1/2}$ (corr ab)	$k_{obs}$ (a→b)	$\nu^{1/2}$ (corr ba)	$k_{obs}$ (b→a)
253	1.717	5.395	1.561	4.905
263	2.436	7.654	2.923	9.184
273	12.300	38.647	15.665	49.219
283	37.083	116.515	41.749	131.175
293	108.194	339.946	99.343	312.136

**Table 2.15:** Rate constants for the exchange of (CH<sub>2</sub>) environments in the complex [Al(<sup>t</sup>Bu, OCH<sub>3</sub> - Salpy)(Cl)]

Temperature (K)	$k_{obs}$
253	4.400
263	12.400
273	37.400
283	110.600
293	368.480

These data have been used to construct Eyring plots (Figure 2.32) using the Eyring equation:

$$\ln \frac{k_c}{T} = \ln \frac{K_b}{h} + \frac{\Delta S^\ddagger}{R} - \frac{\Delta H^\ddagger}{RT}$$

[ $k_c$  = chemical exchange rate constant, T = absolute temperature,  $K_b$  = Boltzmann Constant ( $1.381 \times 10^{-23} \text{ JK}^{-1}$ ),  $h$  = Planck constant ( $6.626 \times 10^{-34} \text{ Js}$ ), R = gas constant ( $8.314 \text{ JK}^{-1} \text{ mol}^{-1}$ ),  $\Delta S^\ddagger$  = entropy of activation,  $\Delta H^\ddagger$  = enthalpy of activation].

**Chapter 2 - Synthesis, Characterization, and X-ray Crystal Structures of Salpy, Acpy and Salpn type Ligands, and their Complexes with Aluminium and Titanium**

where the chemical exchange rate constant  $k_c$  is equal to twice the observed rate constant  $k_{obs}$  since the conversion of environment 'a' to 'b' occurs at the same rate as the conversion from environment 'b' to 'a'.<sup>42</sup>

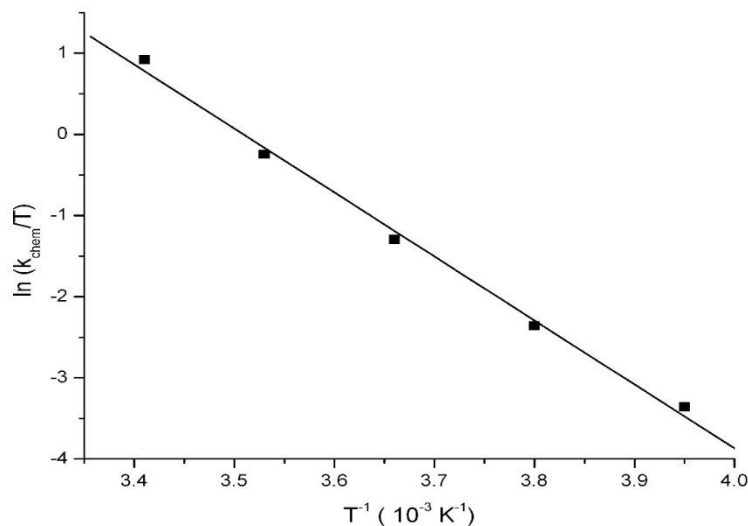


**Figure 2.32:** Eyring plot for methylene group exchange for  $[Al(tBu, OCH_3 - Salpy)(Cl)]$

It has been possible, using these Eyring plots (Figure 2.32), to extract the values for  $\Delta H^\ddagger$  and  $\Delta S^\ddagger$ , and their corresponding values of  $\Delta G^\ddagger_{298}$  (Gibbs free energy of activation at 298 K) shown in Table 2.16.

**Table 2.16** Activation parameters for the exchange of imine, methylene and  $tBu$  environments in the  $[Al(tBu, OCH_3 - Salpy)(Cl)]$  complex

	$\Delta H^\ddagger (KJ mol^{-1})$	$\Delta S^\ddagger (J K^{-1} mol^{-1})$	$\Delta G^\ddagger_{298} ((KJ mol^{-1}))$
$N=C-H_a \rightarrow N=C-H_b$	$67.7 \pm 5.4$	$39.7 \pm 19.9$	$55.8 \pm 0.5$
$N=C-H_b \rightarrow N=C-H_a$	$63.8 \pm 5.4$	$25.8 \pm 19.9$	$56.1 \pm 0.5$
Averaged values	65.8	32.8	56.0
$CH_{2a} \rightarrow CH_{2b}$	$65.6 \pm 0.5$	$32.7 \pm 0.8$	$56.0 \pm 0.3$
$tBu_a \rightarrow tBu_b$	$65.3 \pm 4.6$	$31.0 \pm 15.2$	$56.1 \pm 0.1$
$tBu_b \rightarrow tBu_a$	$65.3 \pm 4.6$	$31.5 \pm 15.2$	$55.9 \pm 0.1$
Averaged values	65.3	31.3	56.0

The values of  $\Delta S^\ddagger$  give the most insight into the exchange process. The positive values suggest that the transition state for the exchange contains more disorder (higher entropy) than the ground state, and could therefore be regarded as a dissociative mechanism. Since the spectra indicate an exchange of the inequivalent “arms” with each other giving a high temperature average of an apparently higher symmetry, if we define the phenoxide donors as *cis* and *trans* relative to the pyridyl, then it is likely that the  $O_{cis}$  becomes  $O_{trans}$ , whilst  $O_{trans}$  simultaneously becomes  $O_{cis}$ . It is hard to see how this exchange could be possible, owing to the rigid structure of the Salpy ligand, but if the process is dissociative, as the measured value of  $\Delta S^\ddagger$  suggests, then it is entirely possible that the pyridyl decoordinates, thereby allowing the  $O_2N_2$  core to adopt a planar (or nearly planar) arrangement and thus facilitating the exchange.

The chemical shifts of the  $H^6$  signals in  $[Al(R,R^1\text{-Salpy})Cl]$  are higher than the chemical shift of free ligand which is a good indication that the pyridyl is coordinated in the major isomer, giving a six-coordinate complex. The complexes were much less soluble than their organometallic and alkoxy counterparts;  $[Al(\text{Salpy})Cl]$  (**24**) was especially poorly soluble in chloroform, and so  $DMSO-d_6$  was used for NMR samples and it therefore inappropriate to compare this chemical shift to other complexes measured in  $CDCl_3$ .

Introducing an alkyl group to the phenol ring in the ligand enhances the solubility of the chloride complex in most solvents. The complexes  $[Al(tBu,tBu\text{-Salpy})Cl]$  (**25**),  $[Al(tBu,OMe\text{-Salpy})Cl]$  (**27**) and  $[Al(Ad,Me\text{-Salpy})Cl]$  (**28**) are more soluble than  $[Al(\text{Salpy})Cl]$  (**24**) in toluene or chloroform.  $[Al(tBu,OMe\text{-Salpn})Cl]$  (**29**) has a higher solubility than the Salpy complexes, presumably due the alkyl group on the phenol ring and the comparatively flexible aliphatic chain in the diamine backbone.  $[Cl,Cl\text{-Salpy})Cl]$  (**30**), which has two chloride atoms in the phenol ring, shows very low solubility.

The  $^{13}C\{^1H\}$  NMR spectra of the aluminium chloride complexes show a disappearance of the  $CH=N$  and  $CH_2$  signals for all pyridyl complexes. A downfield shift from 165.7ppm in the free ligand to 171.2 ppm in **29** was observed for the carbon of the imine group. There are no significant differences between

the chemical shifts relating to the methylene groups of **29**, in both free ligand and the complex. The absence of these signals in the Salpy complexes is likely due to broadening caused by the same exchange process, as described above for the  $^1\text{H}$  NMR spectra.

### **2.3.3.3 Crystallographic studies of aluminium Chloride complexes**

Suitable crystals for structural determination of  $[\text{Al}(\text{salpy})\text{Cl}]$  (**24**),  $[\text{Al}(\text{tBu},\text{OCH}_3\text{-salpy})\text{Cl}]$  (**27**) and  $[\text{Al}(\text{Ad},\text{CH}_3\text{-salpy})\text{Cl}]$  (**28**) were obtained by the slow evaporation of dichloromethane-toluene solutions. Complexes **24** and **27** crystallized in the monoclinic space groups  $P2_1/c$  and  $P2_1/n$  respectively, while complex **28** crystallized in the triclinic space group . The structures of the complexes **24**, **27**, **28** and **29** are included in Figures 2.33, 2.34, 2.35 and 2.36 respectively. Selected bond distances and angles are given in Tables 2.17, 2.18, 2.19, 2.20 respectively. The structures feature six-coordinate distorted octahedral geometries at the aluminium centre for **24**, **27** and **28**. For complex **29** the structure features a five-coordinate distorted trigonal bipyramidal geometry at the aluminium centre with a  $\tau$  value of 0.76. The coordination chemistry of the Salpy ligand, including the relative bond lengths and angles, are all as seen, and discussed in detail, for the methyl and alkoxide/phenoxide complexes discussed previously, and do not warrant further discussion. The aluminium-chloride bond distances are all within the expected range based upon examples in the Cambridge structural database (1.978–2.681, mean 2.150 Å for 1356 examples).<sup>27</sup>

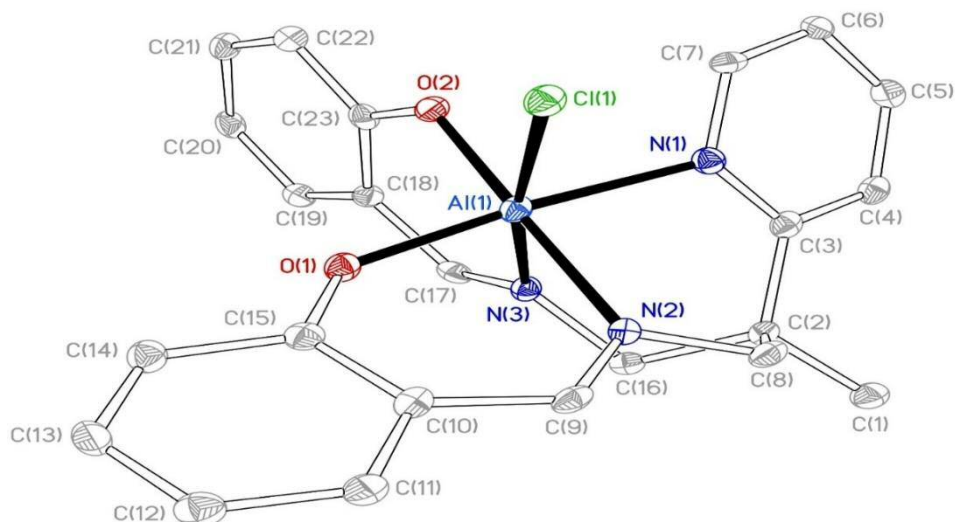


**Figure 2.33** Molecular structure of [Al(salpy)Cl] (**24**). Ellipsoids are shown at 30% probability level; hydrogens atoms are omitted for clarity

**Table 2.17:** Selected bond lengths (Å) and bond angles (°) for [Al(salpy)Cl]

Cl(1)-Al(1)	2.2752(16)	Al(1)-N(2)	2.013(3)
Al(1)-O(2)	1.829(3)	Al(1)-N(3)	2.035(3)
Al(1)-O(1)	1.840(3)	Al(1)-N(1)	2.119(3)
O(2)-Al(1)-O(1)	92.69(12)	N(2)-Al(1)-N(1)	87.05(13)
O(2)-Al(1)-N(2)	174.26(14)	N(3)-Al(1)-N(1)	79.69(13)
O(1)-Al(1)-N(2)	90.16(13)	O(2)-Al(1)-Cl(1)	92.86(10)
O(2)-Al(1)-N(3)	89.49(13)	O(1)-Al(1)-Cl(1)	95.42(10)
O(1)-Al(1)-N(3)	93.60(13)	N(2)-Al(1)-Cl(1)	91.83(10)
N(2)-Al(1)-N(3)	85.35(13)	N(3)-Al(1)-Cl(1)	170.56(10)
O(2)-Al(1)-N(1)	89.54(13)	N(1)-Al(1)-Cl(1)	91.18(10)
O(1)-Al(1)-N(1)	172.91(14)		

**Chapter 2 - Synthesis, Characterization, and X-ray Crystal Structures of Salpy, Acpy and Salpn type Ligands, and their Complexes with Aluminium and Titanium**

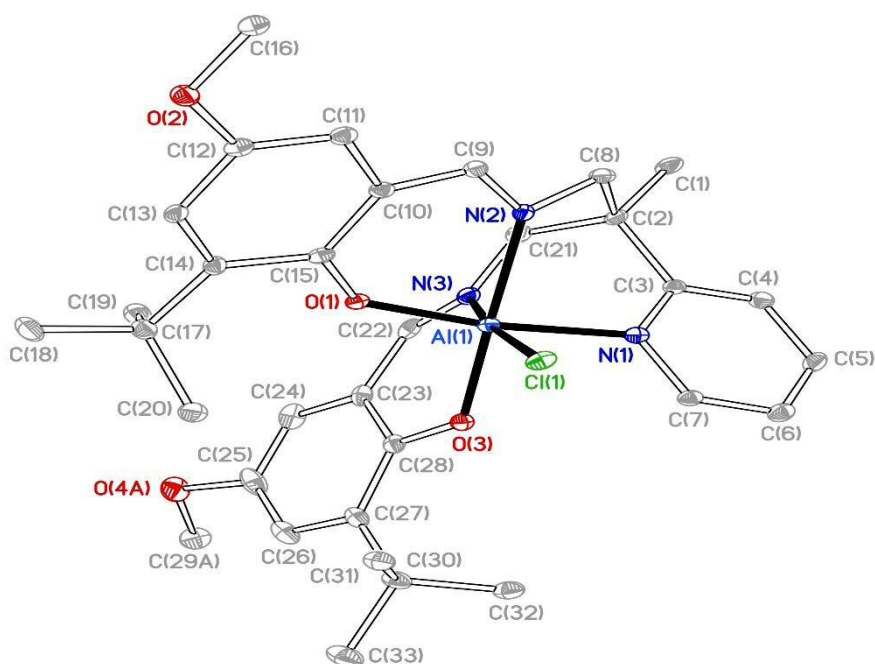


**Figure 2.34** Molecular structure of [Al(<sup>t</sup>Bu, OCH<sub>3</sub> - salpy)Cl]. Ellipsoids are shown at 30 % probability level; hydrogens are omitted for clarity

**Table 2.18:** Selected bond lengths (Å) and bond angles (°) for [Al(<sup>t</sup>Bu, OCH<sub>3</sub> - salpy)Cl]

Cl(1)-Al(1)	2.2835(15)	Al(1)-N(3)	2.009(3)
Al(1)-O(3)	1.824(3)	Al(1)-N(2)	2.026(3)
Al(1)-O(1)	1.828(3)	Al(1)-N(1)	2.098(3)
O(3)-Al(1)-O(1)	95.44(12)	N(3)-Al(1)-N(1)	81.67(13)
O(3)-Al(1)-N(3)	88.03(13)	N(2)-Al(1)-N(1)	85.77(13)
O(1)-Al(1)-N(3)	93.15(13)	O(3)-Al(1)-Cl(1)	93.66(9)
O(3)-Al(1)-N(2)	173.90(14)	O(1)-Al(1)-Cl(1)	94.83(10)
O(1)-Al(1)-N(2)	87.15(13)	N(3)-Al(1)-Cl(1)	171.65(12)
N(3)-Al(1)-N(2)	86.31(14)	N(2)-Al(1)-Cl(1)	91.62(10)
O(3)-Al(1)-N(1)	91.16(12)	N(1)-Al(1)-Cl(1)	90.11(10)
O(1)-Al(1)-N(1)	171.48(13)		

**Chapter 2 - Synthesis, Characterization, and X-ray Crystal Structures of Salpy, Acpy and Salpn type Ligands, and their Complexes with Aluminium and Titanium**

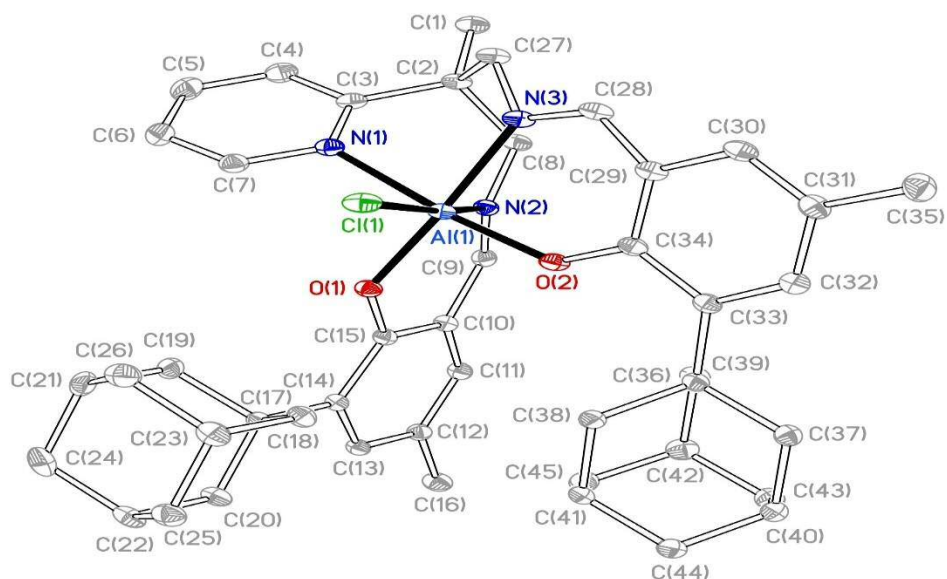


**Figure 2.35** Molecular structure of [Al(Ad, CH<sub>3</sub> - salpy)Cl]. Ellipsoids are shown at 30 % probability level; hydrogens are omitted for clarity

**Table 2.19:** Selected bond lengths (Å) and bond angles (°) for [Al(Ad, CH<sub>3</sub> - salpy)Cl]

Cl(1)-Al(1)	2.2854(6)	Al(1)-N(3)	2.0059(13)
Cl(2)-Al(2)	2.2807(6)	Al(1)-N(2)	2.0235(13)
Al(1)-O(1)	1.812.2844(11)	Al(1)-N(1)	2.1301(14)
Al(1)-O(2)	1.8235(12)		
O(1)-Al(1)-O(2)	95.72(5)	N(3)-Al(1)-N(1)	85.89(5)
O(1)-Al(1)-N(3)	173.48(6)	N(2)-Al(1)-N(1)	79.95(5)
O(2)-Al(1)-N(3)	89.11(5)	O(1)-Al(1)-Cl(1)	91.45(4)
O(1)-Al(1)-N(2)	88.51(5)	O(2)-Al(1)-Cl(1)	97.01(4)
O(2)-Al(1)-N(2)	92.89(5)	N(3)-Al(1)-Cl(1)	92.30(4)
N(3)-Al(1)-N(2)	86.88(5)	N(2)-Al(1)-Cl(1)	170.06(4)
O(1)-Al(1)-N(1)	88.78(5)	N(1)-Al(1)-Cl(1)	90.10(4)
O(2)-Al(1)-N(1)	171.47(6)		

**Chapter 2 - Synthesis, Characterization, and X-ray Crystal Structures of Salpy, Acpy and Salpn type Ligands, and their Complexes with Aluminium and Titanium**

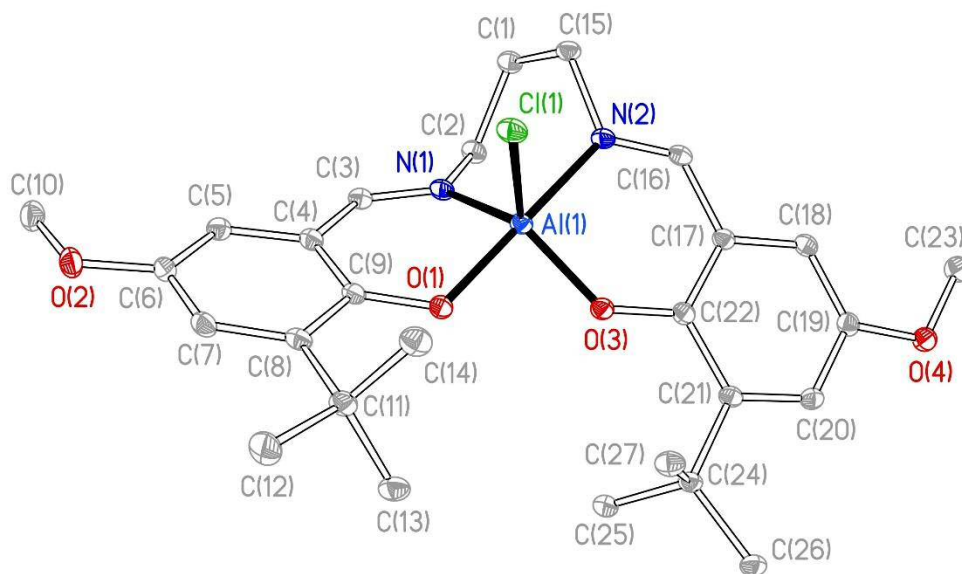


**Figure 2.36** Molecular structure of [Al(<sup>t</sup>Bu, OCH<sub>3</sub> - salpn)Cl]. Ellipsoids are shown at 30 % probability level; hydrogens are omitted for clarity

**Table 2.20:** Selected bond lengths (Å) and bond angles (°) for [Al(<sup>t</sup>Bu, OCH<sub>3</sub> - salpn)Cl]

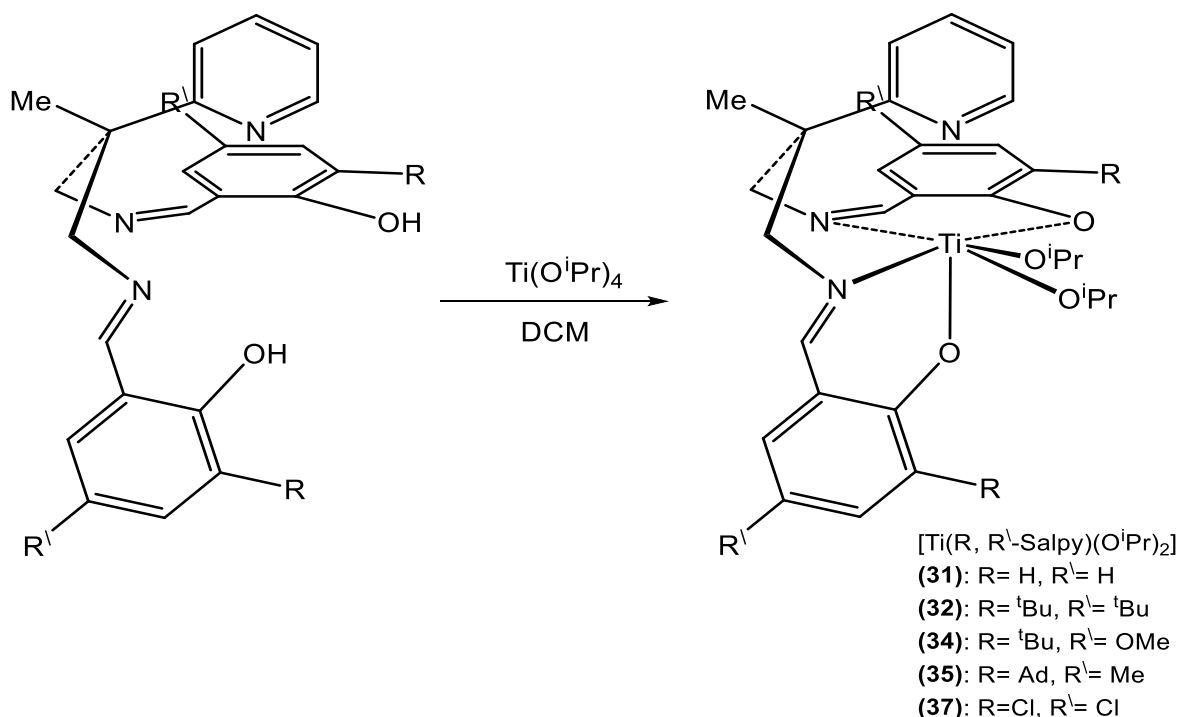
Cl(1)-Al(1)	2.1898(6)	Al(1)-O(3)	1.7608(11)
O(1)-Al(1)	1.8070(11)	Al(1)-N(2)	2.0222(13)
N(1)-Al(1)	1.9679(13)		
O(3)-Al(1)-O(1)	90.38(5)	N(1)-Al(1)-N(2)	84.88(5)
O(3)-Al(1)-N(1)	127.15(6)	O(3)-Al(1)-Cl(1)	119.73(4)
O(1)-Al(1)-N(1)	89.81(5)	O(1)-Al(1)-Cl(1)	94.56(4)
O(3)-Al(1)-N(2)	89.31(5)	N(1)-Al(1)-Cl(1)	112.92(4)
O(1)-Al(1)-N(2)	173.09(6)	N(2)-Al(1)-Cl(1)	91.58(4)

## 2.4 Synthesis and characterization of titanium complexes

### 2.4.1 Titanium isopropoxide complexes

#### 2.4.1.1 Synthesis and spectroscopic characterization

Titanium complexes are commonly used in polymerization catalysis.<sup>43</sup> It was therefore of interest to prepare titanium complexes of the Salpy and related ligands, and to test them for their potential in polymerization catalysis. Titanium isopropoxide complexes were the focus of these studies. The preparation of these complexes, and subsequent manipulations, were performed under an inert atmosphere of nitrogen or argon using standard Schlenk or glovebox techniques. Titanium complexes  $[\text{Ti}(\text{R},\text{R}^{\text{\'{i}}}\text{-Salpy})(\text{O}^i\text{Pr})_2]$ ,  $[\text{Ti}(\text{tBu},\text{OMe-Salpn})(\text{O}^i\text{Pr})_2]$  and  $[\text{Ti}(\text{R-Acpy})(\text{O}^i\text{Pr})_2]$  (**31-39**) were prepared via the alcoholysis reaction between stoichiometric quantities of  $\text{Ti}(\text{O}^i\text{Pr})_4$  with the corresponding protio-ligand, liberating 2 equivalents of isopropyl alcohol (Equation 2.12 for Salpy derivatives). The reaction was conducted by adding a dichloromethane solution of titanium(IV) isopropoxide to a stirred solution of the ligand, also in dichloromethane. Removal of the solvent and crystallization from hexanes afforded the products as yellow solids in moderate to high yields (77-84%).



**Equation 2.12:** Synthesis of  $[\text{Ti}(\text{R},\text{R}^{\text{\'{i}}}\text{-Salpy})(\text{O}^i\text{Pr})_2]$  complexes

**Chapter 2 - Synthesis, Characterization, and X-ray Crystal Structures of Salpy, Acpy and Salpn type Ligands, and their Complexes with Aluminium and Titanium**

All titanium complexes were characterized by  $^1\text{H}$  and  $^{13}\text{C}\{^1\text{H}\}$  NMR spectroscopy, and elemental analysis. The  $^1\text{H}$  NMR spectrum of  $[\text{Ti}(\text{tBu},\text{OMe-Salpy})(\text{O}^i\text{Pr})_2]$  (**34**) in  $\text{CDCl}_3$  is shown in Figure 2.37 as a representative example with Salpy ligands. 2D NMR experiments were used to fully assign all resonances in both  $^1\text{H}$  and  $^{13}\text{C}\{^1\text{H}\}$  NMR spectra. The  $^1\text{H}$  NMR spectrum shown in Figure 2.37 indicates that two  $\text{C}_1$ -symmetric diastereomers are formed in an approximately 2:1 ratio, determined by integration of the  $\text{H}^6$  proton of the pyridyl ring. The two species showed clearly separated signals for  $\text{H}^6$ . As suggested by Gade and coworkers,<sup>7</sup> and described for the aluminium complexes, the chemical shift of the  $\text{H}^6$  resonance can be indicative of the coordinative state of the pyridyl arm. Thus, little or no shift of the  $\text{H}^6$  resonance relative to the protio ligand ( $\delta = 8.53$  ppm) indicates that the pyridyl arm is not coordinated to the metal centre. In the spectra of **34**, the  $\text{H}^6$  proton resonance was observed as a doublet of doublets at 8.56 ppm for the major isomer, and 8.43 for the minor isomer, which suggests that the pyridyl remains pendant in both species. Moreover, the broad singlet (13.31 ppm) for the phenol OH protons was not observed, consistent with successful coordination of the Salpy ligand to the titanium.

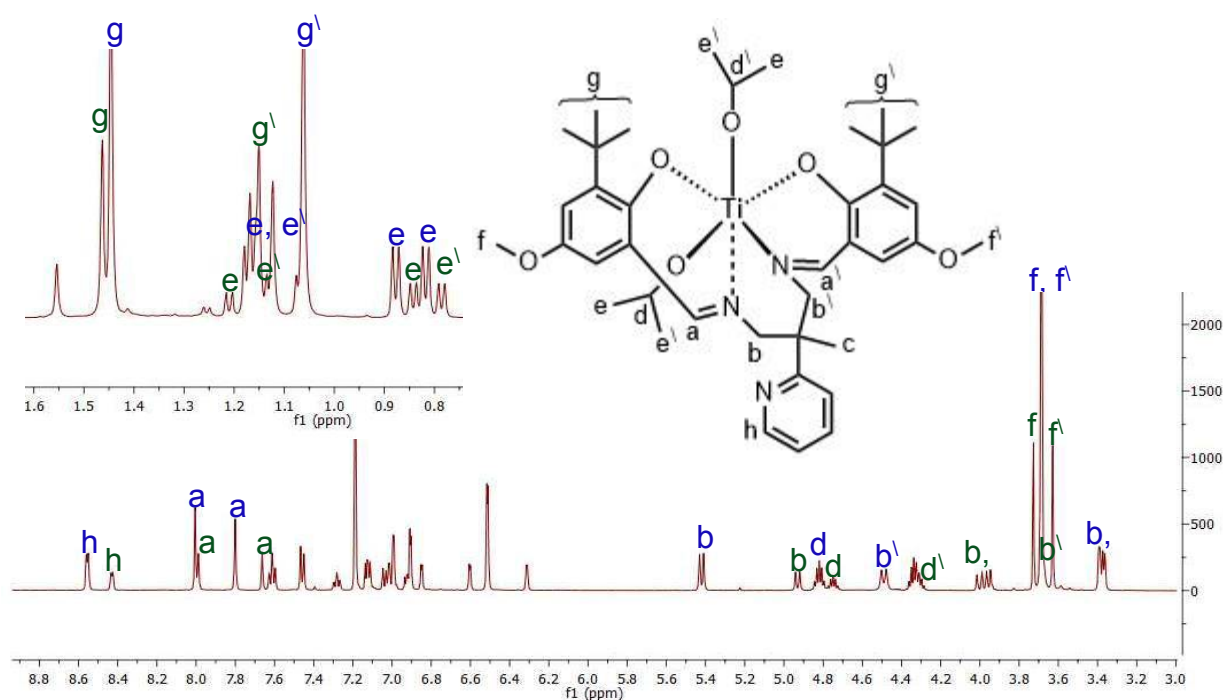


**Figure 2.37:**  $^1\text{H}$  NMR spectrum (400 MHz, 293 K,  $\text{CDCl}_3$ ) of  $[\text{Ti}(\text{tBu},\text{OMe-Salpy})(\text{O}^i\text{Pr})_2]$  (**34**)

**Chapter 2 - Synthesis, Characterization, and X-ray Crystal Structures of Salpy, Acpy and Salpn type Ligands, and their Complexes with Aluminium and Titanium**

Unlike the free ligand, both “arms” of the ligand in **34** are inequivalent, and as a result both isomers show two sets of iminophenoxide resonances. For example, the imine signals were observed as singlets at 8.00 and 7.80 ppm for the major isomer, and 7.99 and 7.66 ppm for the minor. The methylene protons are observed as four proton environments. Each proton was observed as an AX doublet; the signals are observed over a large chemical shift range (5.42-3.38 ppm). It therefore appears that the solution state geometry of **34** is  $\beta$ -cis, rather than the trans or  $\alpha$ -cis possibilities illustrated in Figure 2.38. In a similar manner, the  $^1\text{H}$  NMR spectrum showed two 1 H septets at 4.83 and 4.34 ppm along with four 3 H doublets at 1.07 (2 x  $\text{CH}_3$  overlapping), 0.80 and 0.74 ppm, corresponding to the isopropyl methine and methyl protons for the major isomer respectively.

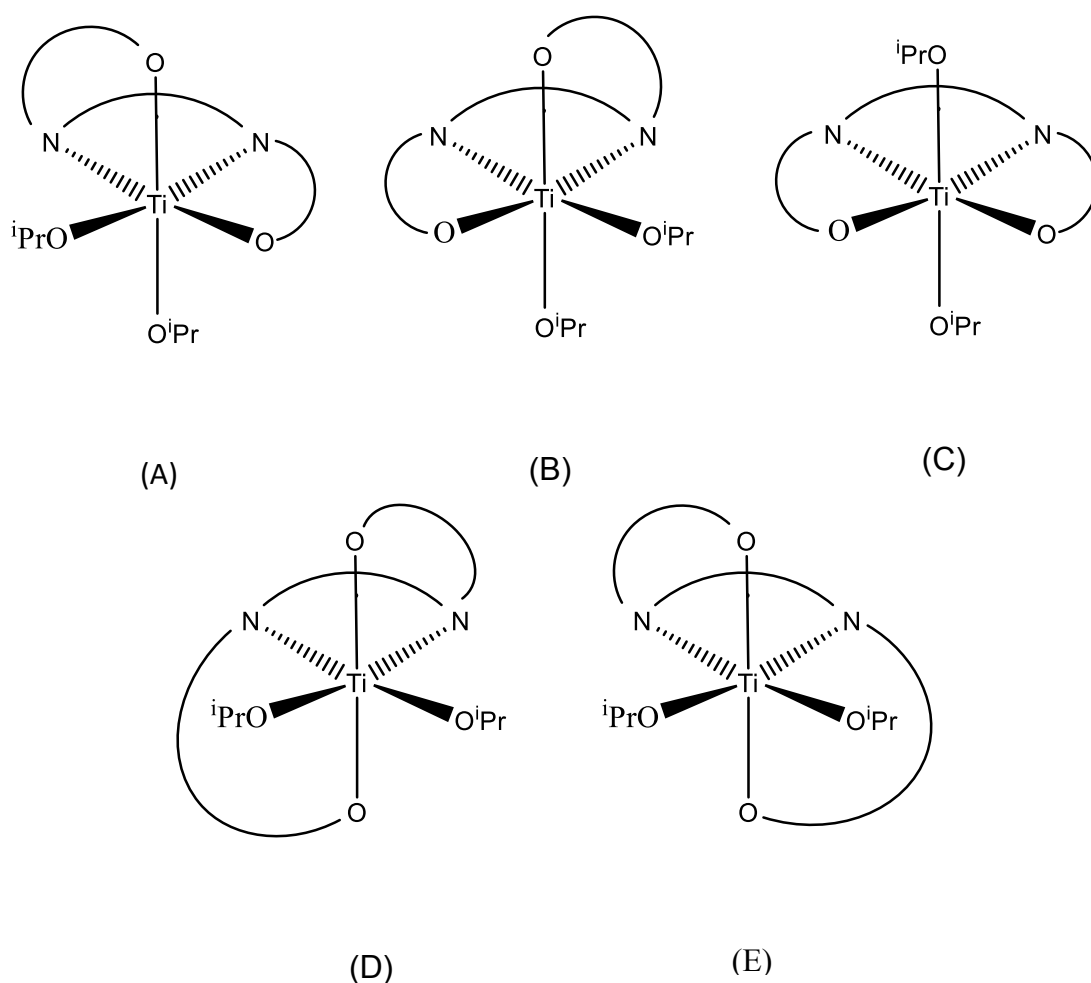


**Figure 2.38:** Possible conformations of  $\text{L}^x\text{Ti}(\text{O}^i\text{Pr})_2$  complexes, where  $\text{L}^x = \text{N}_2\text{O}_2$  tetradentate ligand

**Chapter 2 - Synthesis, Characterization, and X-ray Crystal Structures of Salpy, Acpy and Salpn type Ligands, and their Complexes with Aluminium and Titanium**

Similarly, the minor isomer shows four 1 H doublets at 4.93, 4.0, 3.96 and 3.64 ppm. The signals for the methine protons of isopropoxide groups appear as two septet resonances at 4.75 and 4.33 ppm while the four isopropyl methyl groups appear as four doublets at 1.06, 1.0, 0.77 and 0.71 ppm. As a comparison, the <sup>1</sup>H NMR chemical shifts for the two isomers of **34** are listed in Table 2.21.

**Table 2.21:** Chemical shifts of the two isomers of [Ti(<sup>t</sup>Bu,OCH<sub>3</sub>-salpy)(O<sup>i</sup>Pr)<sub>2</sub>]

Assignment	Chemical shift of major isomer (ppm)	Chemical shift of minor isomer (ppm)
H <sup>6</sup>	8.56	8.43
Imine (CH=N)	8.0 1H, 7.80 1H	7.99 1H, 7.66 1H
Pyridine group	7.61 1H, 7.46 1H, 7.12 1H	7.28 1H, 7.04 1H, 6.93 1H
Aromatic ring	6.99 1H, 6.91 1H, 6.51 2H	7.01 1H, 6.85 1H, 6.60 1H, 6.31 1H
Methylene (CH <sub>2</sub> )	5.42 1H, 4.49 1H, 3.38 2H	4.93 1H, 4.0 1H, 3.96 1H, 3.64 1H
Isopropyl (CH(CH <sub>3</sub> ) <sub>2</sub> )	4.83 1H, 4.34 1H	4.75 1H, 4.33 1H
Methoxy (OCH <sub>3</sub> )	3.69 6H	3.73 3H, 3.63 3H
<sup>t</sup> Bu (C(CH <sub>3</sub> ) <sub>3</sub> )	1.1.37 9H, 0.99 9H	1.08 18H
Isopropyl (CH(CH <sub>3</sub> ) <sub>2</sub> )	1.07 6H(Overlapping), 0.80 3H, 0.74 3H	1.06 3H, 1.0 3H, 0.77 3H, 0.71 3H
Methyl (CH <sub>3</sub> )	1.39	1.48

To compare the <sup>1</sup>H NMR spectra of [Ti(<sup>t</sup>Bu,OMe-Salpy)(O<sup>i</sup>Pr)<sub>2</sub>] (**34**) with that of [Ti(<sup>t</sup>Bu,OMe-Salpn)(O<sup>i</sup>Pr)<sub>2</sub>] (**36**), the spectrum of **36** has two sets of signals attributable to the iminophenoxide “arms”; these signals were present in a 1:1 ratio, and their relative intensities did not vary with temperature. This is therefore consistent with a single isomer, which is C<sub>1</sub>-symmetric.

The presence of only a single isomer in the spectra of **36**, and two for **34** suggests that the pyridyl has a role to play. There are two isomers possible for the β-cis arrangement, but these are enantiomers and are therefore indistinguishable by

**Chapter 2 - Synthesis, Characterization, and X-ray Crystal Structures of Salpy, Acpy and Salpn type Ligands, and their Complexes with Aluminium and Titanium**

NMR spectroscopy. However, as can be seen in the diagrams in Figure 2.37, the axial ligands perpendicular to the N–Ti–N plane are different: in diagrams A and B the iminophenoxide O-donor is ‘up’, whilst the isopropoxide is ‘down’. In the Salpy ligands, the central carbon of the backbone contains two *different* substituents, a pyridyl and a methyl; it is therefore clear to see that there are two possible isomers, based upon the relative orientation of these two substituents relative to the two axial ligands. For example, the pyridyl may lie *cis* to the iminophenoxide, or *cis* to the isopropoxide. These two arrangements correspond to two diastereoisomers and would therefore be expected to give different chemical shifts in their NMR spectra. This is a somewhat simplified explanation, since the backbone is twisted such that the pyridyl and methyl substituents do not eclipse the M–L bonds (Figure 2.39). Nevertheless, the X-ray structures discussed below do show that the substituents are closer to either the iminophenoxide or the isopropoxide, and the above description is therefore validated. Additional evidence is obtained from the crystallographic studies, in that the structure of  $[\text{Ti}(\text{}^t\text{Bu},\text{}^t\text{Bu-Salpy})(\text{O}^i\text{Pr})_2]$  crystallized as one isomer (pyridyl *cis* to isopropoxide) whereas all other examples crystallized as the other isomer (pyridyl *cis* to iminophenoxide). The solution-state NMR spectra for the remaining titanium Salpy complexes show that they all adopt two conformations in solution.

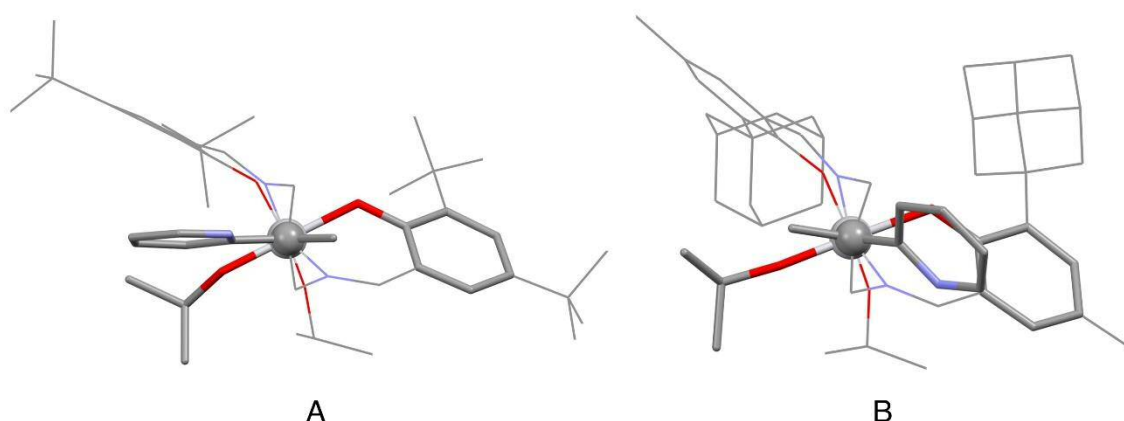


**Figure 2.39:** the two possible isomers for titanium complexes (29-37), A: the pyridyl *cis* to isopropoxide and B: the pyridyl *cis* to iminophenoxide.

**Chapter 2 - Synthesis, Characterization, and X-ray Crystal Structures of Salpy, Acpy and Salpn type Ligands, and their Complexes with Aluminium and Titanium**

Whilst it is assumed that these complexes adopt  $\beta$ -cis configurations, it is possible that one of the isomers corresponds to one of the other configurations given in Figure 2.37. Although all X-ray structures for these ligands in an octahedral environment (Al and Ti) are consistent with the  $\beta$ -cis configurations, care should be taken since a crystal structure is not necessarily representative of the bulk sample. Nevertheless, both the  $\alpha$ -cis and trans isomers would give complexes in which the two “arms” of the Salpy ligand are equivalent, and are therefore inconsistent with the data measured on the complexes in this thesis; the conclusion therefore stands, that all complexes are those in a  $\beta$ -cis arrangement.

Equilibrium  $\Delta G$  values can be obtained from the relative proportion of the two isomers (obtained by integration of the  $H^6$  resonance) and by applying the following equation:

$$\Delta G = - R T \ln K_{eq}$$

$\Delta G$  = Free energy difference between the two isomers

$K_{eq}$  = equilibrium constant

R = gas constant ( $8.314 \text{ JK}^{-1} \text{ mol}^{-1}$ )

As can see in table 2.22, these values are very small, suggesting that the group causing a difference in relative stability is somewhat removed from the main steric bulk of the ligand-*i.e.* the pyridyl does not interfere with the phenol alkyl group to a significant extent.

**Table 2.22:** the  $\Delta G$  values of the titanium complexes isomers

Complex	Isomer1/Isomer2	KJ mol <sup>-1</sup>
	ratio	
[Ti(Salpy)(O <sup>i</sup> Pr) <sub>2</sub> ] ( <b>31</b> )	2 : 1.1	1.45
[Ti( <sup>t</sup> Bu, <sup>t</sup> Bu - salpy)(O <sup>i</sup> Pr) <sub>2</sub> ] ( <b>32</b> )	2 : 0.72	2.48
[Ti(Naphpy)(O <sup>i</sup> Pr) <sub>2</sub> ] ( <b>33</b> )	2 : 1.04	1.6
[Ti( <sup>t</sup> Bu, OMe - Salpy)(O <sup>i</sup> Pr) <sub>2</sub> ] ( <b>34</b> )	2 : 1	1.68
[Ti(Ad, Me- Salpy)(O <sup>i</sup> Pr) <sub>2</sub> ] ( <b>35</b> )	2: 1.5	0.7
[Ti(Cl, Cl - Salpy)(O <sup>i</sup> Pr) <sub>2</sub> ] ( <b>37</b> )	1:0.3	2.93
[Ti(Aspy)(O <sup>i</sup> Pr) <sub>2</sub> ] ( <b>38</b> )	2 : 1.75	0.31
[Ti(OMe- Aspy)(O <sup>i</sup> Pr) <sub>2</sub> ] ( <b>39</b> )	2 : 1.9	0.12

#### 2.4.1.2 Crystallographic studies of titanium isopropoxide complexes

Crystals of **32** that were suitable for X-ray structural determination were grown by cooling a hexane solution to -30 °C. The solid-state structure of complex **32** was confirmed by X-ray diffraction analysis. The molecular structure is shown in Figure 2.40. The selected bond distances and angles are listed in Table 2.23. The analysis revealed that complex **32** was mononuclear and the central titanium atom displays a distorted octahedral geometry with *cis* angles in the range 77.27(7)–103.97(7)°.

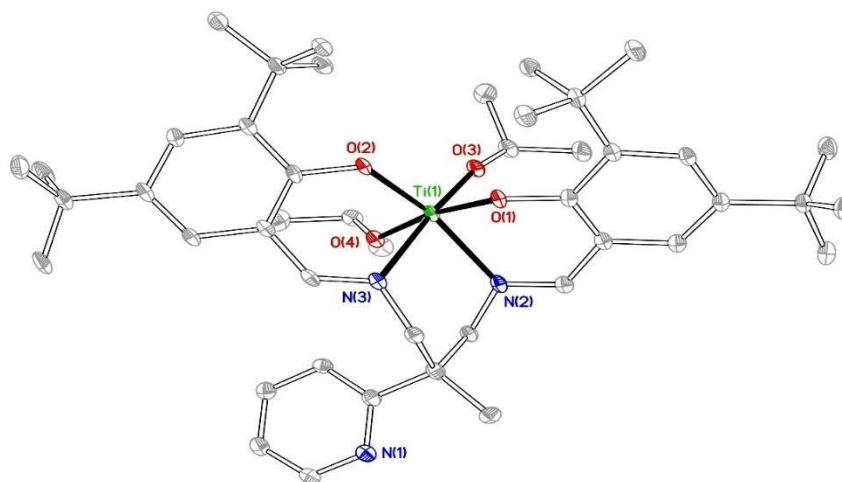


**Figure 2.40:** Molecular structure of  $[\text{Ti}(\text{tBu}, \text{tBu} - \text{salpy})(\text{O}'\text{Pr})_2]$  (**32**). Ellipsoids are shown at 30% probability; hydrogen atoms are omitted for clarity

**Table 2.23:** Selected bond lengths (Å) and bond angles (°) for  $[\text{Ti}(\text{tBu}, \text{tBu} - \text{salpy})(\text{O}'\text{Pr})_2]$  (**32**)

Ti(1)-O(3)	1.7899(16)	Ti(1)-O(1)	1.9701(15)
Ti(1)-O(4)	1.8594(15)	Ti(1)-N(2)	2.181(2)
Ti(1)-O(2)	1.9035(17)	Ti(1)-N(3)	2.2376(19)
O(3)-Ti(1)-O(4)	95.15(7)	O(2)-Ti(1)-N(2)	156.86(7)
O(3)-Ti(1)-O(2)	103.97(7)	O(1)-Ti(1)-N(2)	80.53(7)
O(4)-Ti(1)-O(2)	96.43(7)	O(3)-Ti(1)-N(3)	173.62(8)
O(3)-Ti(1)-O(1)	91.72(7)	O(4)-Ti(1)-N(3)	82.06(7)
O(4)-Ti(1)-O(1)	169.72(7)	O(2)-Ti(1)-N(3)	82.09(7)
O(2)-Ti(1)-O(1)	89.31(7)	O(1)-Ti(1)-N(3)	90.32(7)
O(3)-Ti(1)-N(2)	97.10(7)	N(2)-Ti(1)-N(3)	77.27(7)
O(4)-Ti(1)-N(2)	91.02(7)		

The X-ray structure of  $[\text{Ti}(\text{tBu}, \text{tBu} - \text{salpy})(\text{O}'\text{Pr})_2]$  indicates a  $C_1$ -symmetrical complex with two *cis* isopropoxide groups, and with the two phenoxy groups of

the tetradentate ligand in a *cis* configuration<sup>44</sup>. The titanium was coordinated by two imine N atoms and two O atoms from the Schiff base ligand and two O atoms from the isopropoxy groups. The pyridyl group is pendant, as expected from an analysis of the H<sup>6</sup> proton resonance, discussed above. The solid state structure also displayed that the quadridentate ligand adopted a  $\beta$ -*cis* geometry. The O3 and N3 donors are arranged in the *trans* position (O(3)–Ti(1)–N(3): 173.62(8) (Å)). The Ti(1)–N(3) bond length, 2.2376(19) (Å), is the longest among the Ti–A bond lengths. The Ti–A bond lengths reflects the donor's strengths of three different types of coordinated atoms. The Ti–O(phenoxy) bonds: Ti(1)–O(1) (1.9701(15) Å) and Ti(1)–O(2) (1.9035(17) Å), which were in the normal range found in related titanium complexes were longer than the Ti–O(iso-propoxy) bonds: Ti1–O3 (1.7899(16) Å) and Ti(1)–O(4) (1.8594(15) Å).<sup>45–47</sup> In complex **21**, the short bond lengths between the oxygen of isopropoxide group and titanium can be attributed to an additional  $\pi$ -type interaction of an oxygen lone pair of the O<sup>i</sup>Pr moiety with an empty d <sub>$\pi$</sub>  orbital of titanium, this type of interaction is less between the oxygen of the phenoxy group and titanium, which makes the bond length longer.<sup>48</sup> In all cases, the Ti–O bond distances were within the sum of the individual covalent radii of Ti and O (1.984 Å).<sup>49</sup> This observation is common in many related titanium isopropoxide complexes.<sup>50</sup> Additionally, the presence of an obtuse bond angle subtended at one of the O<sup>i</sup>Pr oxygen atoms [Ti–O–C = 162.26(16)°] further testified toward the presence of  $\pi$ -type interactions between the isopropoxy group and the titanium metal. The equivalent bond angles in the corresponding aluminium alkoxide/aryloxy complexes were less than 140°.

Single crystals of complexes **35–39** suitable for X-ray analyses were grown from saturated hexane solutions. The structures are analogous to those of **32**, in that the geometry around each Ti is distorted from an octahedral environment, with the metal centre hexacoordinated by two N atoms and two O atoms from the ligand and by two O atoms from two isopropoxide groups. Molecular structures, along with atomic numbering scheme for the coordinating sites, are shown in Figures 2.41- 2.45 , with selected bond distances and angles in Tables 2.24 and 2.25.

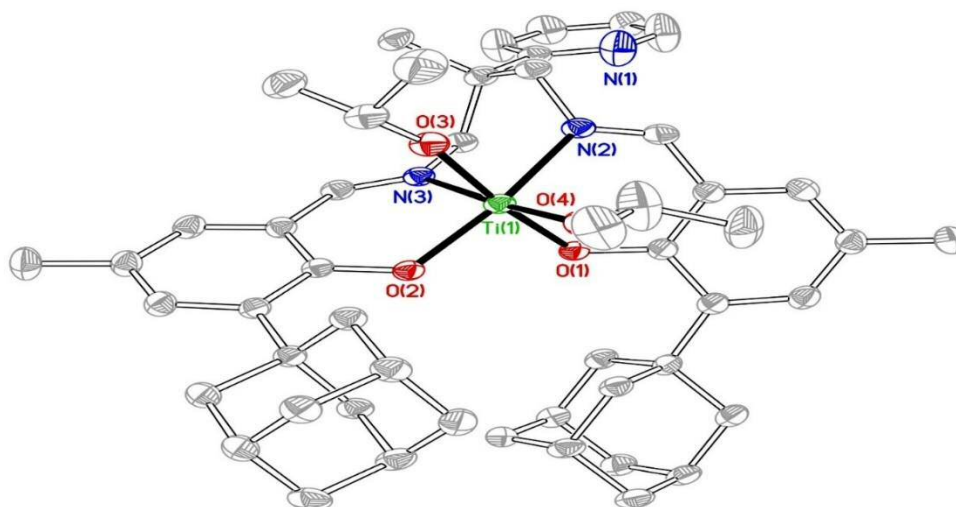


**Figure 2.41:** Molecular structure of  $[\text{Ti}(\text{Ad}, \text{CH}_3\text{-salpy})(\text{O}^i\text{Pr})_2]$  (**35**). Ellipsoids are shown at 30 % probability level; hydrogens are omitted for clarity

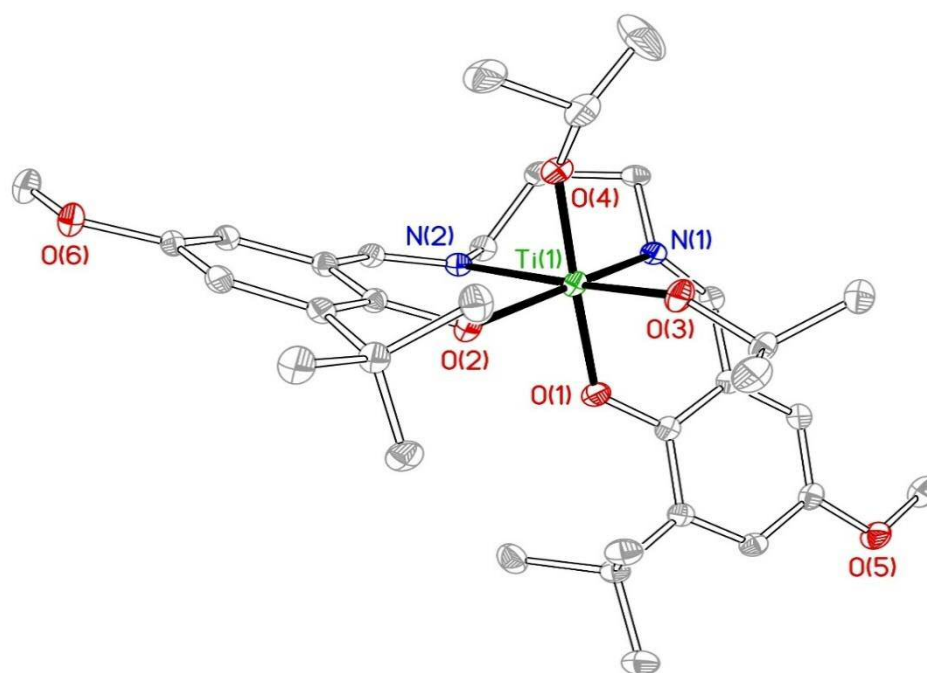


**Figure 2.42:** Molecular structure of  $[\text{Ti}(\text{'Bu}, \text{OCH}_3\text{-salpn})(\text{O}^i\text{Pr})_2]$  (**36**). Ellipsoids are shown at 30 % probability level; hydrogens are omitted for clarity

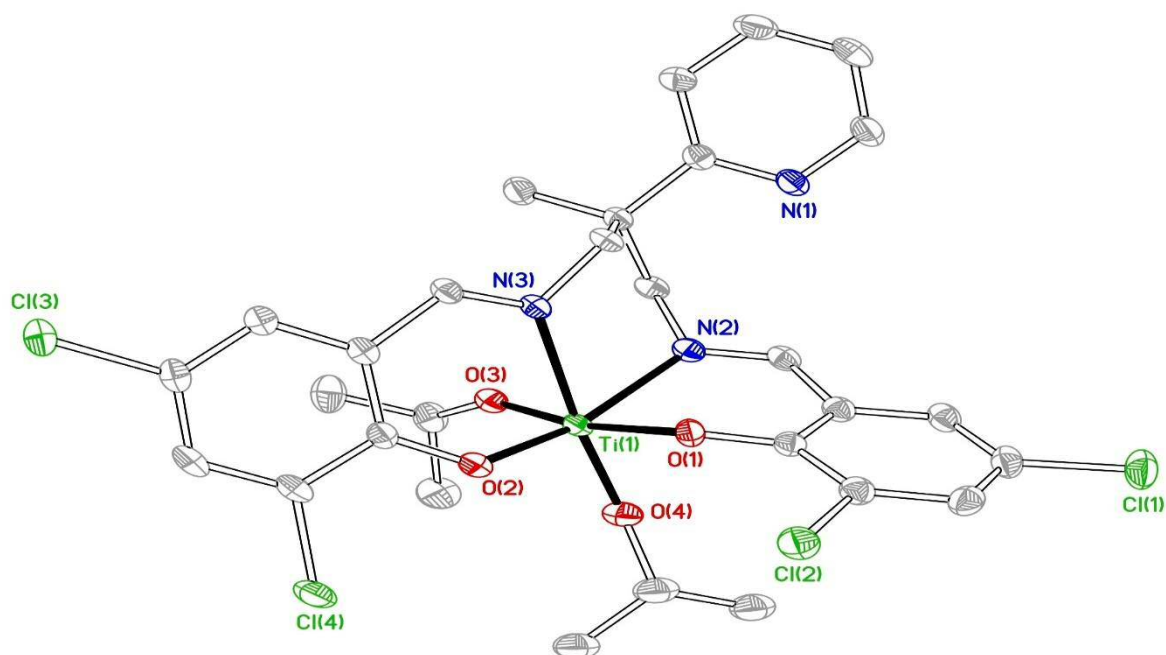


**Figure 2.43:** Molecular structure of  $[\text{Ti}(\text{Cl}, \text{Cl} - \text{salpy})(\text{O}^i\text{Pr})_2]$  (**37**). Ellipsoids are shown at 30 % probability level; hydrogens are omitted for clarity

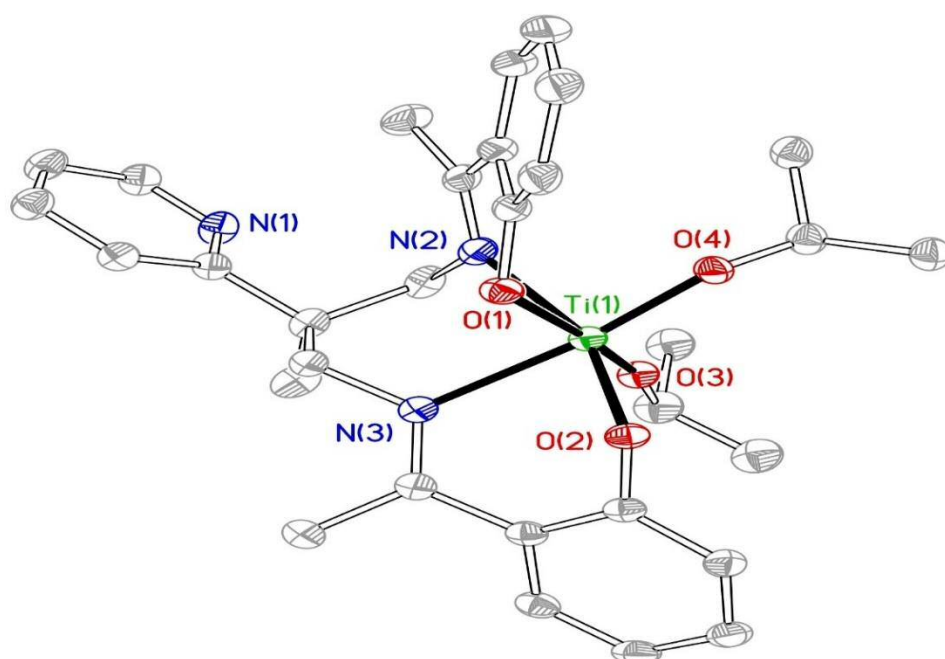


**Figure 2.44:** Molecular structure of  $[\text{Ti}(\text{Acpy})(\text{O}^i\text{Pr})_2]$  (**38**). Ellipsoids are shown at 30 % probability level; hydrogens are omitted for clarity

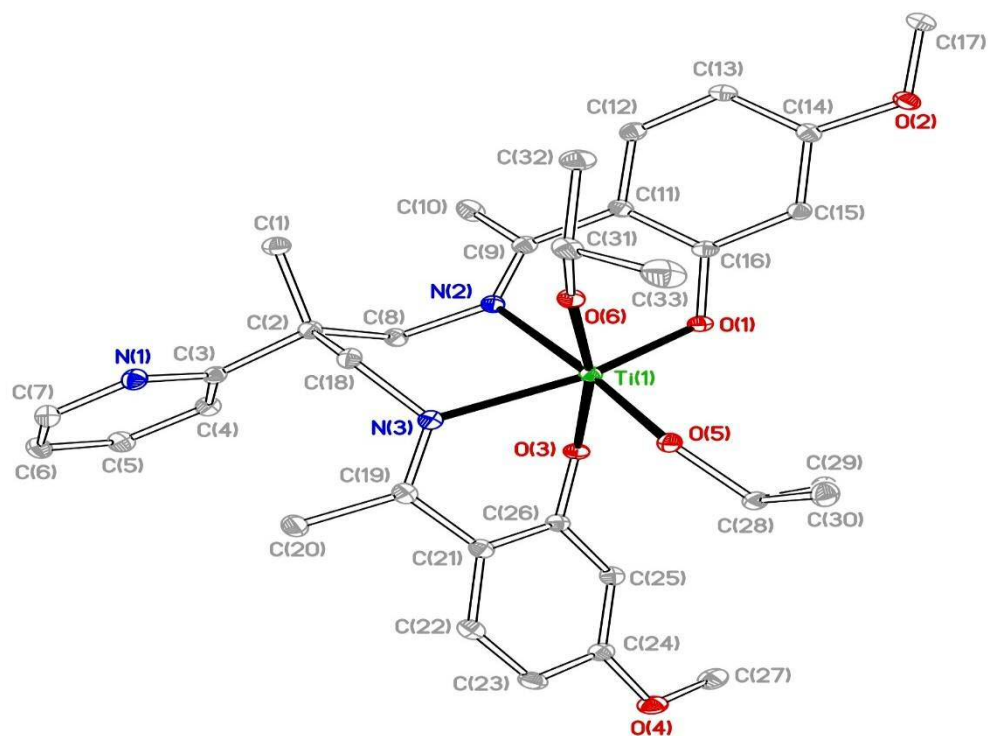


**Figure 2.45:** Molecular structure of  $[\text{Ti}(\text{OCH}_3\text{-Acpy})(\text{O}'\text{Pr})_2]$  (**39**). Ellipsoids are shown at 30 % probability level; hydrogens are omitted for clarity

**Table 2.24:** Selected bond lengths (Å) for  $[\text{Ti}(\text{Ad}, \text{CH}_3\text{-salpy})(\text{O}'\text{Pr})_2]$  (**35**),  $[\text{Ti}(\text{tBu}, \text{OCH}_3\text{-salpn})(\text{O}'\text{Pr})_2]$  (**36**),  $[\text{Ti}(\text{Cl}, \text{Cl-salpy})(\text{O}'\text{Pr})_2]$  (**37**),  $[\text{Ti}(\text{Acpy})(\text{O}'\text{Pr})_2]$  (**38**) and  $[\text{Ti}(\text{OCH}_3\text{-Acpy})(\text{O}'\text{Pr})_2]$  (**39**)

	Complex				
	35	36	37	38	39
Ti(1)-O(3)	1.819(2)	1.8026(12)	1.795(3)	1.8092(16)	1.8007(11)
Ti(1)-O(4)	1.801(3)	1.8383(12)	1.806(3)	1.8079(16)	1.8044(11)
Ti(1)-O(2)	1.922(2)	1.8987(12)	1.928(3)	1.9212(15)	1.9223(12)
Ti(1)-O(1)	1.973(2)	1.9704(12)	2.022(3)	1.9640(15)	1.9945(11)
Ti(1)-N(2)	2.173(3)	2.1880(13)	2.180(3)	2.1723(19)	2.1787(14)
Ti(1)-N(3)	2.252(3)	2.25234(14)	2.262(3)	2.2742(19)	2.2994(14)

**Chapter 2 - Synthesis, Characterization, and X-ray Crystal Structures of Salpy, Acpy and Salpn type Ligands, and their Complexes with Aluminium and Titanium**

**Table 2.25:** Selected bond angles (°) for [Ti(Ad, CH<sub>3</sub> - salpy)(O<sup>i</sup>Pr)<sub>2</sub>], [Ti(<sup>t</sup>Bu, OCH<sub>3</sub> - salpn)(O<sup>i</sup>Pr)<sub>2</sub>], [Ti(Cl, Cl - salpy)(O<sup>i</sup>Pr)<sub>2</sub>], [Ti(Acpy)(O<sup>i</sup>Pr)<sub>2</sub>] and [Ti(OCH<sub>3</sub>-Acpy)(O<sup>i</sup>Pr)<sub>2</sub>]

	Complex				
	35	36	37	38	39
<b>O(3)-Ti(1)-O(4)</b>	97.70(13)	98.87(14)	96.08(8)	97.35(5)	95.03(6)
<b>O(3)-Ti(1)-O(2)</b>	95.07(11)	96.56(13)	97.10(7)	90.46(5)	101.76(5)
<b>O(4)-Ti(1)-O(2)</b>	103.67(11)	100.48(12)	104.39(7)	167.10(5)	98.06(5)
<b>O(3)-Ti(1)-O(1)</b>	167.94(10)	169.32(11)	170.17(7)	100.48(5)	91.45(6)
<b>O(4)-Ti(1)-O(1)</b>	89.58(11)	89.02(13)	89.54(7)	96.63(5)	168.09(5)
<b>O(2)-Ti(1)-O(1)</b>	92.52(10)	89.01(11)	89.27(6)	91.99(5)	90.37(5)
<b>O(3)-Ti(1)-N(2)</b>	89.38(11)	91.10(13)	91.93(7)	173.56(5)	97.55(5)
<b>O(4)-Ti(1)-N(2)</b>	96.49(12)	98.14(12)	95.13(7)	88.75(5)	89.45(5)
<b>O(2)-Ti(1)-N(2)</b>	158.54(11)	158.49(11)	157.41(7)	83.17(5)	158.53(5)
<b>O(1)-Ti(1)-N(2)</b>	80.21(10)	80.60(11)	79.51(7)	80.77(5)	79.78(5)
<b>O(3)-Ti(1)-N(3)</b>	85.74(11)	85.80(12)	87.77(7)	98.69(5)	176.31(5)
<b>O(4)-Ti(1)-N(3)</b>	172.81(12)	174.21(13)	172.85(7)	89.75(5)	83.20(5)
<b>O(2)-Ti(1)-N(3)</b>	82.23(10)	82.28(11)	81.02(6)	78.89(5)	81.72(5)
<b>O(1)-Ti(1)-N(3)</b>	86.02(10)	85.93(11)	85.82(7)	158.82(5)	89.74(5)
<b>N(2)-Ti(1)-N(3)</b>	77.17(11)	78.26(11)	78.68(7)	79.20(5)	79.23(5)
<b>Ti-O(<sup>i</sup>Pr)-C-O(<sup>i</sup>Pr)</b>	158.8(2)	153.7(3)	172.6(7)	166.59(11)	149.06(12)
			137.76(19)		
<b>Ti-O(<sup>i</sup>Pr)-C-O(<sup>i</sup>Pr)</b>	150.9(4)	139.7(3)	170.9(2)	147.83(11)	134.52(11)
			150.5(5)		

Interestingly, the Ti–N bond lengths are not the same for both of the Salpy “arms” in a given complex. As we can see from Table 2.21, when the N atom lies *trans* to the O<sub>phenoxide</sub> atom, the Ti–N bond length is shorter than the Ti–N located *trans* to the O<sup>i</sup>Pr atom. This observation is consistent across all of these structures.

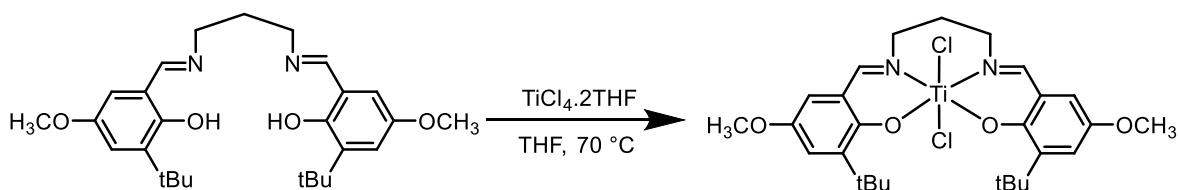
Amanda et al.,<sup>44</sup> Jaume et al.,<sup>47</sup> Stanislav et al.,<sup>51</sup> and Adi et al.<sup>52</sup> have reported titanium complexes that exhibit C<sub>2</sub>-symmetry, with two *cis* isopropoxide groups

and where the phenoxide groups are located in a mutually trans configuration. The structures of  $[\text{Ti}(\text{R}, \text{R}'\text{-Salpy})(\text{O}^i\text{Pr})_2]$  feature different symmetry, namely  $C_1$ -symmetrical complex with the two phenoxide groups of the tetradentate ligand in a *cis* configuration, along with two *cis* isopropoxide groups.

#### 2.4.2 Titanium chloride complexes (synthesis and characterization of $[\text{Ti}(\text{tBu}, \text{OCH}_3\text{-salpn})(\text{Cl})_2]$ (**29**))

The comparison between the coordination chemistry of  $[\text{Ti}(\text{tBu}, \text{OMe-Salpy})(\text{O}^i\text{Pr})_2]$  and  $[\text{Ti}(\text{tBu}, \text{OMe-Salpn})(\text{O}^i\text{Pr})_2]$ , both in solution and in the solid state, effectively measures the effect of the pyridyl donor on the coordination chemistry, the conclusion being that it has none, the structures adopting a  $\beta$ -*cis* motif regardless. A different comparison has been made to study the effect of the co-ligands with the four-coordinate Salpn ligand.

To this end, a chloride complex of titanium was prepared by the direct reaction between of (tBu,OMe-Salpn) and  $\text{TiCl}_4(\text{THF})_2$  in THF at 70 °C. After removing the solvent and washing with diethyl ether, the product was isolated as a brown solid in 94% yield.  $\text{TiCl}_4 \cdot 2\text{THF}$  was prepared according to literature procedure.<sup>53</sup>



**Equation 2.13**

The  $^1\text{H}$  NMR spectrum of  $[\text{Ti}(\text{tBu}, \text{OCH}_3\text{-salpn})\text{Cl}_2]$  (**40**) (Figure 2.46) showed only one isomer, and on comparison with the spectrum of the protio-ligand, all protons in the complex were shifted downfield except the imine proton which was shifted upfield from 8.36 ppm to 8.20 ppm (Table 2.26).

**Chapter 2 - Synthesis, Characterization, and X-ray Crystal Structures of Salpy, Acpy and Salpn type Ligands, and their Complexes with Aluminium and Titanium**

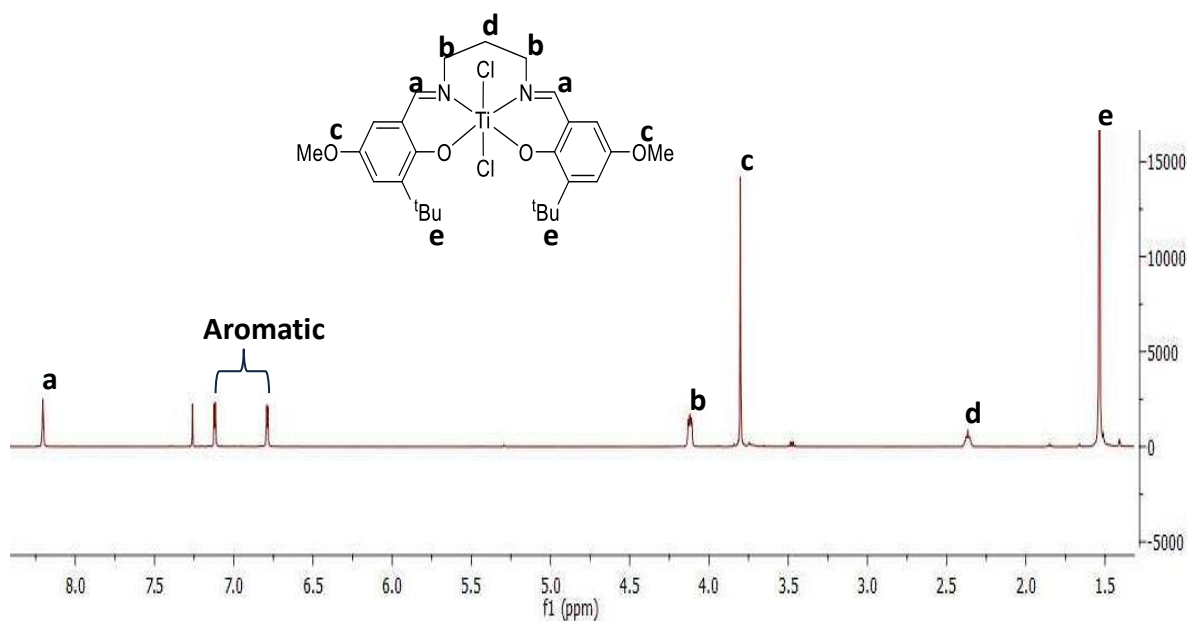


**Figure 2.46:**  $^1\text{H}$  NMR spectrum (400 MHz, 293 K,  $\text{CDCl}_3$ ) for the  $[\text{Ti}(\text{tBu}, \text{OCH}_3\text{-salpn})(\text{Cl})_2]$  (**40**)

**Table 2.26:**  $^1\text{H}$  NMR chemical shift of the  $(\text{tBu}, \text{OCH}_3\text{-salpn})$  and  $[\text{Ti}(\text{tBu}, \text{OCH}_3\text{-salpn})\text{Cl}_2]$

Ligand or Complex	OH	CH=N	Aromatic	CH <sub>2</sub>	OCH <sub>3</sub>	CH <sub>2</sub>	tBu
(tBu, OCH <sub>3</sub> -salpn)	13.57	8.36	6.98, 6.61	3.74	3.78	2.15	1.44
$[\text{Ti}(\text{tBu}, \text{OCH}_3\text{-salpn})\text{Cl}_2]$	-	8.20	7.11, 6.79	4.12	3.80	2.37	1.54

The signal for the imine carbons, remains largely unchanged, shifting only slightly upfield from 165.7 ppm to 165.6 ppm. Interestingly, the spectrum is consistent with  $C_s$ -symmetry, with the two Salpn “arms” being identical. This could suggest that a different ligand conformation is adopted with chloride ligands, although it cannot be unambiguously ruled out that a  $\beta$ -cis conformation is obtained, but where the rate of exchange, as described for the aluminium chloride complexes,

is much faster owing to less steric demand of the chloride ligands, compared to isopropoxide ligands.

## **2.5 Conclusions**

Three types of Schiff base ligands have been prepared. These are the Salpy ligands, which were synthesized from the reaction of salicylaldehyde derivatives and 2-Methyl-2-(2-pyridyl) propane-1, 3-diamine (ppda) in 2: 1 ratio; Acpy ligands, which were prepared from the condensation of 2 equivalent of acetophenone derivatives with one equivalent of ppda; and finally one Salpn ligand obtained from the treatment of 3-tert-butyl-5-methoxysalicylaldehyde with 1,3-diaminopropane. All the prepared ligands are symmetrical, with both “arms” being identical.

Many attempts were undertaken to prepare asymmetric or neutral ligands derived from ppda; unfortunately, the results were unsuccessful. The asymmetric ligands rapidly redistributed the arms to afford the corresponding symmetrical products. With the neutral symmetrical ligands, a cyclic compound was isolated as a main product instead of diamine Schiff base. All the prepared ligands were fully characterized by  $^1\text{H}$  and  $^{13}\text{C}\{^1\text{H}\}$ , and where necessary, 2D NMR spectroscopy, mass spectrometry and IR spectroscopy. IR spectra for all ligands indicated no bands for the OH groups of the phenol because of the strong hydrogen bonding between the imine group and phenol.

A series of aluminium and titanium complexes was prepared. The first group of complexes was a series of methyl aluminium complexes, aimed for use in ring-opening polymerization reactions. Many difficulties accompanied the preparation of such complexes, with multiple species being detected in solution. Two conformational isomers were found in the solution, by virtue of the hemi-labile pyridyl donor.

The second set of complexes were alkoxide and phenoxide aluminium derivatives. These complexes were obtained from the reaction of the methyl aluminium complexes with benzyl alcohol or p-cresol, a single product was

**Chapter 2 - Synthesis, Characterization, and X-ray Crystal Structures of Salpy, Acpy and Salpn type Ligands, and their Complexes with Aluminium and Titanium**

obtained from these reactions in most cases, although in one case a second species was detected, analogous to those observed for the methyl complexes.

The third type of aluminium complex was a series of chloride aluminium complexes, to be used as a catalyst for co-polymerization reactions. A single product was evident in solution. The NMR spectra of the complexes were invariably broad, and reflect the fast exchange of the two ligand “arms”. Variable temperature NMR spectra were measured to study their dynamic behaviour, and to calculate the activation parameters  $\Delta G^\ddagger$ ,  $\Delta H^\ddagger$  and  $\Delta S^\ddagger$  for this process.

The solid state structures of all of the above aluminium complexes were probed extensively using single crystal X-ray diffraction. The methyl and alkoxide/phenoxide complexes gave a mixture of  $\kappa^4$  and  $\kappa^5$  Salpy ligands, whereas all of the chloride complexes all exhibited a  $\kappa^5$  Salpy ligand.

Finally, titanium complexes were prepared, bearing isopropoxide and chloride co-ligands. The complexes bearing the Salpy ligands were observed as two conformation isomers in solution. Both  $^1\text{H}$  NMR and  $^{13}\text{C}$  NMR spectra revealed that both isomers have inequivalent iminophenoxide “arms”, giving  $C_1$ -symmetric complexes. All the complexes show a hexacoordinated titanium complexes with a pendant pyridyl group. These complexes exhibit  $\beta$ -*cis* geometry rather than trans or  $\alpha$ -*cis* geometries. The solid state structures and NMR data support this conclusion. One complex of titanium chloride was prepared as a comparison with isopropoxide complexes. The NMR spectra revealed higher symmetry than for the isopropoxide complexes.

In this chapter, the fine details of the coordination chemistry of the Salpy and related ligands has been investigated in complexes that are suitable for use as polymerization catalysts. The most novel feature of this chapter is almost certainly the role of a hemi-labile donor in the aluminium complexes; forthcoming chapters will probe the effect of this feature on the catalysts' performance in a variety of polymerization and co-polymerization reactions.

## 2.6 References

- 1 S. Komira, *Synthesis of Organometallic Compounds*, John Wiley & Sons, 1997.
- 2 C. C. H. Harvey Diehl, *Inorganic Synthesis*, Mcgraw-hill Book Company, 1950, vol. 3.
- 3 H. Chen, S. Dutta, P. Huang and C. Lin, *Organometallics*, 2016, **31**, 2016–2025.
- 4 A. L. E. Borgne, V. Vincens, M. Jouglard and N. Spassky, *Makromol. Chem., Macromol. Symp.*, 1993, **73**, 37–46.
- 5 and T. K. Nobuyoshi Nomura, Ryohei Ishii, Yoshihiko Yamamoto, *Chem. Eur. J.*, 2007, **13**, 4433–4451.
- 6 Z. Tang, X. Chen, X. Pang, Y. Yang, X. Zhang and X. Jing, *Biomacromolecules*, 2004, **5**, 965–970.
- 7 S. Friedrich, M. Schubarta, L. H. Gade, I. J. Scowenb, A. J. Edwardsb and M. Mcpartlinb, *Chem. Ber/ Recl.*, 1997, **130**, 1751–1759.
- 8 T. Kurahashi and H. Fujii, *J. Am. Chem. Soc.*, 2011, **133**, 8307–8316.
- 9 A. Sattler, J. A. Labinger and J. E. Bercaw, *Organometallics*, 2013, **32**, 6899–6902.
- 10 B. D. Ward, S. R. Dubberley, L. H. Gade and P. Mountford, *Inorg. Chem.*, 2003, **42**, 4961–4969.
- 11 B. D. Ward, G. Orde, E. Clot, A. R. Cowley, L. H. Gade, P. Mountford, M. Cedex and A. Institut, *Organometallics*, 2004, **23**, 4444–4461.
- 12 B. D. Ward, G. Orde, E. Clot, A. R. Cowley, L. H. Gade and P. Mountford, *Organometallics*, 2005, **24**, 2368–2385.
- 13 K. J. D. Silverstein M.Robert, Webster X. Francis, *Spectrometric Identification of Organic Compounds*, John Wiely & Sonc, INC, 7th ed., 2005.
- 14 Simon J. Coles and Philip A. Gale, *Chem. Sci.*, 2012, **3**, 683.
- 15 A. Biswas, M. G. B. Drew and A. Ghosh, *Polyhedron*, 2010, **29**, 1029–1034.
- 16 E. Kwiatkowski and M. Kwiatkowski, *Inorganica Chim. Acta*, 1986, **117**, 145–149.

**Chapter 2 - Synthesis, Characterization, and X-ray Crystal Structures of Salpy, Acpy and Salpn type Ligands, and their Complexes with Aluminium and Titanium**

- 17 A. Jozwiuk, Z. Wang, D. R. Powell and R. P. Houser, *Inorganica Chim. Acta*, 2013, **394**, 415–422.
- 18 J. M. Locke, R. Griffith, T. D. Bailey and R. L. Crumbie, *Tetrahedron*, 2009, **65**, 10685–10692.
- 19 R. Shakya, A. Jozwiuk, D. R. Powell and R. P. Houser, *Inorg. Chem.*, 2009, **48**, 4083–4088.
- 20 R. Shakya, D. R. Powell and R. P. Houser, *Eur. J. Inorg. Chem*, 2009, 5319–5327.
- 21 R. Shakya, Z. Wang, D. R. Powell and R. P. Houser, *Inorg. Chem.*, 2011, 11581–11591.
- 22 Q. Knijnenburg, J. M. M. Smits and P. H. M. Budzelaar, *Organometallics*, 2006, **25**, 1036–1046.
- 23 C. Agatemor, A. E. Arnold, E. D. Cross, A. Decken and M. P. Shaver, *J. Organomet. Chem.*, 2013, **745–746**, 335–340.
- 24 B. Cordero, V. Gómez, A. E. Platero-Prats, M. Revés, J. Echeverría, E. Cremades, F. Barragán and S. Alvarez, *Dalt. Trans.*, 2008, 2832–2838.
- 25 P. G. Cozzi, C. G. Ciamician and V. Selmi, *Chem. Soc. Rev.*, 2004, **33**, 410–421.
- 26 A. W. Addison, T. N. Rao, J. Reedijk, J. van Rijn and G. C. Verschoor, *J. Chem. Soc. Dalt. Trans.*, 1984, **251**, 1349–1356.
- 27 D. A. Fletcher, R. F. McMeeking and D. Parkin, *J. Chem. Inf. Model.*, 1996, **36**, 746–749.
- 28 P. Hornmiron, E. L. Marshall, V. C. Gibson, R. I. Pugh and A. J. P. White, *Proc. Natl. Acad. Sci. U. S. A.*, 2006, **103**, 15343–8.
- 29 T. M. Ovitt, G. W. Coates, C. U. V and N. York, *J. Am. Chem. Soc.*, 1999, **121**, 4072–4073.
- 30 J. A. Jegier and D. A. Atwood, *J. Chem. Soc., Dalt. Trans.*, 1999, 2583–2587.
- 31 K. Y. Hwang, M. H. Lee, H. Jang, Y. Sung, J. S. Lee, S. H. Kim and Y. Do, *Dalton Trans.*, 2008, **49**, 1818–20.
- 32 M. H. Chisholm, *J. Organomet. Chem.*, 2014, **751**, 55–59.
- 33 M. A. Munoz-Hernandez, T. S. Keizer, P. Wei, S. Parkin and D. A. Atwood, *Inorg. Chem.*, 2001, **40**, 6782–6787.

**Chapter 2 - Synthesis, Characterization, and X-ray Crystal Structures of Salpy, Acpy and Salpn type Ligands, and their Complexes with Aluminium and Titanium**

- 34 A. C. A. H. X. C. Structures, A. I. Oc, P. L. Gurian, L. K. Cheatham, J. W. Zillerb and A. R. Barron, *J. Chem. Soc., Dalt. Trans.*, 1991, **705**, 1449–1456.
- 35 D. a. Atwood, M. S. Hill, J. a. Jegier and D. Rutherford, *Organometallics*, 1997, **16**, 2659–2664.
- 36 D. J. Darensbourg and D. R. Billodeaux, *Inorg. Chem.*, 2005, **44**, 1433–1442.
- 37 S. Dzugan and V. Goedken, *Inorg. Chem.*, 1986, **20**, 2858–2864.
- 38 P. a Cameron, D. Jhurry, V. C. Gibson, A. J. P. White, D. J. Williams and S. Williams, *Macromol. Rapid Commun.*, 1999, **20**, 616–618.
- 39 J. P. Duxbury, *Organometallics*, 2000, **19**, 4445–4457.
- 40 M.-A. Munoz-Hernandez, T. S. Keizer, S. Parkin, Y. Zhang and D. A. Atwood, *J. Chem. Crystallogr.*, 2000, **30**, 219–222.
- 41 C.-A. Huang and C.-T. Chen, *Dalton Trans.*, 2007, 5561–5566.
- 42 Malcolm L. H. Green and Luet-Lok Wong, *Organometallics*, 1992, **11**, 2660–2668.
- 43 R. A. Collins, A. F. Russell and P. Mountford, *Appl. Petrochem. Res.*, 2015, **5**, 153–171.
- 44 A. J. Chmura, M. G. Davidson, M. D. Jones, M. D. Lunn, M. F. Mahon, A. F. Johnson, P. Khunkamchoo, S. L. Roberts and S. S. F. Wong, *Macromolecules*, 2006, **39**, 7250–7257.
- 45 B. Gao, X. Li, R. Duan and X. Pang, *New J. Chem.*, 2015, **39**, 2404–2408.
- 46 C. K. a Gregson, I. J. Blackmore, V. C. Gibson, N. J. Long, E. L. Marshall and A. J. P. White, *Dalt. Trans.*, 2006, 3134–3140.
- 47 J. Balsells, P. J. Carroll and P. J. Walsh, *Inorg. Chem.*, 2001, **40**, 5568–5574.
- 48 M. K. Panda, S. Kaur, A. R. Reddy, M. M. Shaikh, R. J. Butcher, V. Gupta and P. Ghosh, *Dalton Trans.*, 2010, **39**, 11060–8.
- 49 L. Pauling, *The Nature of The Chemical Bond*, Cornell University Press, Ithaca, NY, 3rd edn., 1960.
- 50 M. K. Panda, M. Shaikh and P. Ghosh, *Dalt. Trans.*, 2010, **39**, 2428–2440.
- 51 S. Groysman, E. Sergeeva, I. Goldberg and M. Kol, *Eur. J. Inorg. Chem.*, 2005, 2480–2485.

**Chapter 2 - Synthesis, Characterization, and X-ray Crystal Structures of Salpy, Acpy and Salpn type Ligands, and their Complexes with Aluminium and Titanium**

- 52 A. Yeori, S. Groysman, I. Goldberg and M. Kol, *Inorg. Chem.*, 2005, **44**, 4466–4468.
- 53 E. Manzer, *Inorg. Synth*, 1982, **21**, 135.

# Chapter 3

## Ring opening polymerization of $\epsilon$ -Caprolactone and *rac*-Lactide

## 3.1 Ring-opening polymerisation using aluminium complexes

### 3.1.1 Introduction

Biocompatible and biodegradable polymers have become leading candidates in biomedical and pharmaceutical industries. Environmentally friendly polyesters such as poly( $\epsilon$ -caprolactone) (PCL) and poly(lactic acid) (PLA), as well as their copolymers, are suitable for these applications.<sup>1</sup> The production of well-controlled polymers has been fuelled by the development of catalysts based upon main group and transition metal complexes, which act as initiators/catalysts for the ring-opening polymerization of  $\epsilon$ -caprolactone ( $\epsilon$ -CL) and lactide (LA). This area has been extensively studied, and the reader is directed to appropriate reviews for information pertaining to magnesium,<sup>2–4</sup> calcium,<sup>5–7</sup> titanium,<sup>8–10</sup> lanthanides,<sup>11–13</sup> iron,<sup>14,15</sup> zinc,<sup>16,17</sup> tin,<sup>18,19</sup> and aluminum.<sup>20–22</sup> Aluminium complexes are among the most efficient catalysts for lactone and lactide polymerizations and are established using N- and/or O-donor ligands. The “big picture” scientific interest is to obtain polymers with good mechanical properties, and well-defined polymer architectures. To achieve this aim, catalysis is used to control the microstructure of the polymeric chain, including their molecular weight, polydispersity, and tacticity.

Diverse examples of structurally similar dianionic tetradentate ONNO-type ligands such as *salan*,<sup>23–25</sup> *salalen*,<sup>21,26</sup> and dialkoxy–diimino<sup>27,28</sup> ligands have been reported as coordination environments for monometallic five-coordinate aluminium complexes. These complexes have been shown to be active in the ring-opening polymerization (ROP) of cyclic esters, and it is therefore of interest to use to probe the modification of such ligands by appending additional donor groups, to investigate the effect on the catalytic activity of such complexes.

In this study, the alkoxide / aryloxy complexes described in Chapter 2 were used in the catalytic ring-opening polymerization of (ROP) of both  $\epsilon$ -caprolactone and *rac*-lactide. Attempts were made to polymerize  $\gamma$ -butyrolactone and  $\beta$ -butyrolactone under various conditions; all attempts were unsuccessful and are therefore not discussed further in this thesis. Benzyl alcohol was used to generate the benzyloxy aluminium complexes *in situ* from the corresponding methyl

complexes. When pre-prepared benzyloxy and phenoxy complexes were used (for comparison to those made *in situ*), no additional benzyl alcohol was used.

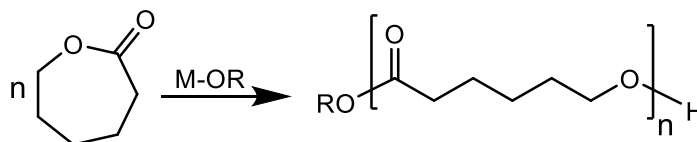
### 3.1.2 $\epsilon$ -caprolactone polymerization

#### 3.1.2.1 General procedure for $\epsilon$ -caprolactone polymerization

The chemicals used in the  $\epsilon$ -CL polymerization reactions were weighed in a nitrogen-filled glove box. In general, polymerization reactions were carried out in toluene (3 ml) at a prescribed temperature. The ratio of the monomer : catalyst : cocatalyst was 100:1:0 or 100:1:1. Benzyl or isopropyl alcohol was added to the catalyst solution (0.015 mmol) (although some entries were conducted without alcohol). After stirring for 5 min,  $\epsilon$ -caprolactone (1.5 mmol) was added. Polymerization experiments were conducted in a screw-cap vial that was removed from the glove box only after the reaction was fully assembled and the vial sealed. The reaction mixture was stirred at the prescribed temperature for the required time. The conversion was determined by  $^1\text{H}$  NMR spectroscopy. The reaction was quenched by the addition of 10 mL acetic acid solution (0.35 N). The resulting mixture was poured into 25 mL of n-hexane to precipitate the polymer. Crude products were recrystallized from THF/ hexane and dried *in vacuo* to a constant weight.

#### 3.1.2.2 Characterization and evaluation of the polymer products

The general reaction of the ring-opening polymerization (ROP) of  $\epsilon$ -CL is given in equation 3.1.



**Equation 3.1:** Ring-opening polymerization of  $\epsilon$ -CL by metal alkoxides

$^1\text{H}$  NMR spectroscopy and gel Permeation Chromatography (GPC) were used to evaluate the polymers, which were produced using aluminium complexes as initiators. The  $^1\text{H}$  NMR spectra of  $\epsilon$ -caprolactone ( $\epsilon$ -CL) and poly( $\epsilon$ -caprolactone) (PCL) are shown in Figures 3.1 and 3.2 respectively.

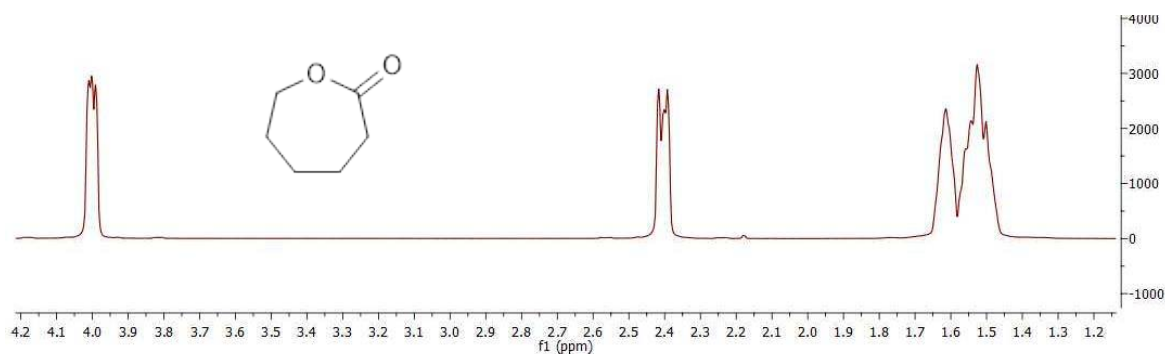


**Figure 3.1:**  $^1\text{H}$  NMR spectrum (400 MHz,  $\text{CDCl}_3$ , 293 K) of  $\epsilon$ -caprolactone ( $\epsilon$ -CL)

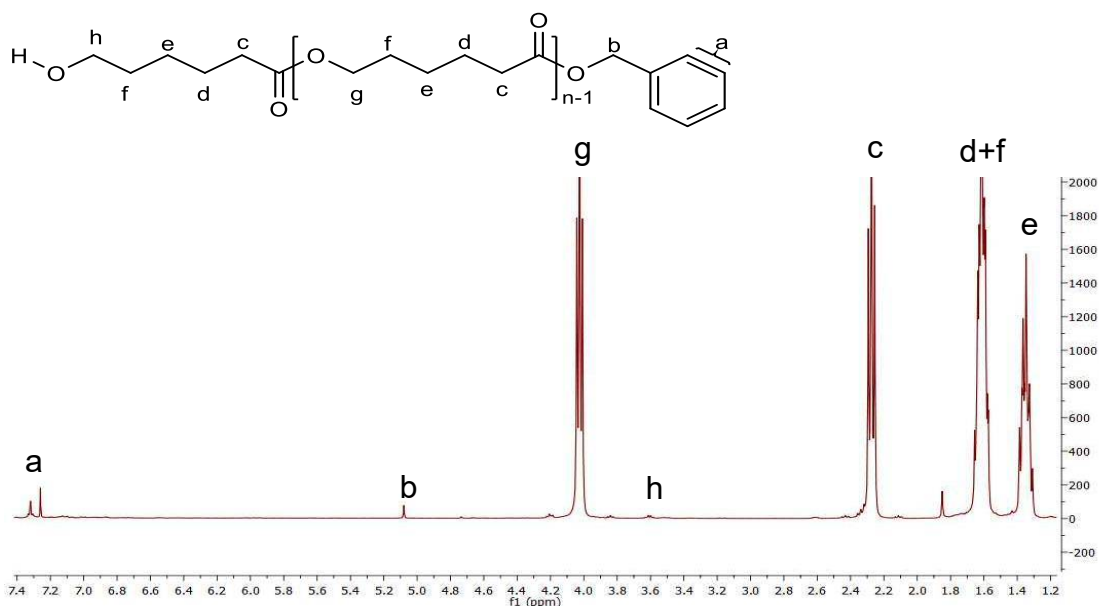


**Figure 3.2:**  $^1\text{H}$  NMR of poly( $\epsilon$ -caprolactone) (PCL) initiated by  $1/\text{BnOH}$

The multiplet attributed to the protons adjacent to the ester oxygen,  $\text{H}_f$ , is the most diagnostic signal in both the monomer and polymer; it shifts from around 4.0 ppm in the  $^1\text{H}$  NMR spectrum of the monomer, to near 3.9 ppm in the polymer. The relative integration of this signal (in crude reaction mixtures) was therefore used to calculate the percentage conversion of monomer to polymer.

The theoretical number average molecular weight  $M_n$  was calculated using the following equation, assuming one polymer chain per metal centre:<sup>29</sup>

$$M(\text{monomer}) \times [M]_0/[Al]_0 \times [\text{conversion}] + M(\text{BnOH})$$

The observed molecular weights and polydispersity indices (PDIs,  $M_w/M_n$ ) were determined by GPC using the appropriate Mark-Houwink corrections as described in Chapter 1.

### **3.1.2.3 Aluminium methyl complexes as initiator for ROP of Caprolactone**

A good catalyst / initiator for the ROP of cyclic esters will typically contain three components: a redox-inactive metal centre, ideally one that is colourless so that the resulting polymer is white – main group and  $d^0$  transition metals are thus suitable; an inorganic supporting ligand, often referred to  $L_n$ , which should be inert towards undesirable side-reactions and should be stable under the catalytic reaction conditions; and finally a labile co-ligand able to undergo an insertion reaction with C-X multiple bonds. Typically alkoxides are some of the most efficient initiators in ROP catalysis but others, such as amide, hydride, tetrahydroborate, and alkyl have also been used. In this context, aluminium complexes bearing dianionic Schiff base ligands (complexes that therefore invariably contain a single labile co-ligand) have become important catalysts, displaying good catalytic activity in the ROP of cyclic esters; most of these catalysts are aluminium alkoxide or alkyl complexes that are used in conjunction with added cocatalyst such as benzyl alcohol or isopropanol. Some alkyl complexes, used without a cocatalyst, have been reported as successful catalysts for the ROP of cyclic esters.<sup>30–33</sup>

In our study, three types of complexes were used to examine their efficacy in the ROP of  $\epsilon$ -caprolactone. The first type of catalysts were methyl aluminium complexes, e.g.  $[Al(R,R\text{-Salpy})Me]$ ; for these catalysts the polymerization experiments were undertaken with and without co-catalyst (benzyl alcohol or isopropyl alcohol). The second sets of catalysts were pre-synthesized aluminium benzyloxy complexes, e.g.  $[Al(R,R\text{-Salpy})(OCH_2Ph)]$ , which should be identical to the methyl complexes with added benzyl alcohol cocatalyst. The final catalyst type were the corresponding p-tolyloxy derivatives, e.g.  $[Al(R,R\text{-Salpy})(O-4-C_6H_4Me)]$ . All catalyst types were tested under identical conditions (except for the addition of co-catalyst) in order to determine the effect of the co-ligand identity.

### Chapter 3 - Ring opening polymerization of $\epsilon$ -Caprolactone and rac-Lactide

Since the alkyl complexes were used as a route to the alkoxide congeners, the complexes [Al(R,R-Salpy)Me] were initially used in the ROP of  $\epsilon$ -caprolactone. Selected examples were used for this preliminary study: [Al(Salpy)Me] (**1**), [Al(<sup>t</sup>Bu, <sup>t</sup>Bu-Salpy)Me] (**2**) and [Al(<sup>t</sup>Bu,OMe-Salpy)Me] (**4**). Polymerization data are presented in Table 3.1.

**Table 3.1:** Polymerization of  $\epsilon$ -Caprolactone (0.17 g, 1.5 mmol using Catalysts **1**, **2**, and **4** (0.015 mmol) without BnOH in toluene (3 mL)

Entry	Cat.	[M] <sub>0</sub> : [Al] <sub>0</sub> : [BnOH]	T (°C)	t (h)	<i>M<sub>n</sub></i> (obsd)	<i>M<sub>n</sub></i> (calcd)	Conv. (%)	<i>M<sub>w</sub></i> / <i>M<sub>n</sub></i>
1	1	100:1:0	25	2	nd		1	
2	1	100:1:0	25	3	nd		5	
3	1	100:1:0	25	4	nd		25	
4	2	100:1:0	25	1	nd		12	
5	2	100:1:0	25	2	nd		22	
6	2	100:1:0	25	3	26070	3840	33	1.08
7	2	100:1:0	25	4	32660	5096	44	1.02
8	4	100:1:0	25	1	15090	2214	19	1.01
9	4	100:1:0	25	2	19390	3618	32	1.00
10	4	100:1:0	25	3	29850	4622	41	1.00
11	1	100:1:0	50	1	22360	5250	47	1.15
12	1	100:1:0	50	2	31700	9353	81	1.01
13	1	100:1:0	50	3	31900	10951	95	1.02
14	1	100:1:0	50	4	33470	11345	99	1.02

nd: not determined

As shown in Table 3.1, experiments were carried out at both room temperature and at 50 °C. Complex **1** showed low catalytic activity toward the ROP of  $\epsilon$ -CL in the absence of BnOH, with conversions of 1%, 5%, and 25%, at 25 °C within 2, 3, 4 hours respectively (Table 3.1; entries 1, 2, and 3). In contrast, complexes **2** and **4** showed a higher conversion than **1** after 4 hours (Entries 7 and 10). The reason for the low conversion with **1** is unclear, but it may be due to the lack of sterically demanding groups that may protect the catalyst from side reactions or redistribution processes during the catalytic reaction. For example, the 5-coordinate complex may be generally more open to decomposition as a result of its low coordination number, which is offset by sterically demanding flanking groups on the phenoxide ligands; this effective stabilization will be minimal for complex **1**, and may therefore result in a less stable complex when the pyridyl is not coordinated to the metal centre. Whether or not the varying coordination number affects the stability of these complexes, it is clear from polymerization data (see below) that the hemilabile character of these ligands plays a crucial factor in their reactivity in the ROP of  $\epsilon$ -CL. A high coordination number decreases the electrophilic character at the metal and as a result reduces the reactivity of the catalyst, moreover the increase in coordination number renders it less likely for a substrate to coordinate to the metal prior to reaction. The ratio between 6 and 5 coordinate species is varied, and there is no guarantee that both are catalytically active. In catalysts **2** and **4**, the presence of bulky groups in the ligand may increase the preference for forming the 5-coordinate isomers, disfavoring the corresponding 6-coordinate isomer. With **1**, in which there is less steric demand, the 6-coordinate isomer could be preferred, thereby reducing the reactivity of the catalyst. It should be noted that this is necessarily speculative, since the relative proportion of the isomers in **1** is highly unlikely to match those present within the catalytic cycle, which are, by definition, impossible to determine experimentally. It is perhaps more likely, given the observations in Chapter 2, that the coordinative state of the pyridyl varies throughout the catalytic cycle; this has been probed computationally below.

Although these preliminary experiments gave rather poor catalytic activity, it is unusual for complexes, especially aluminium complexes, to effect this reaction under ambient conditions. It was therefore prudent to study the reactivity of

### Chapter 3 - Ring opening polymerization of $\epsilon$ -Caprolactone and rac-Lactide

catalyst **1** as a function of temperature. To this end, complex **1** was used as for entries 1-3, but at 50 °C instead of room temperature (entries 11-14). A dramatic change was observed, even without using a co catalyst. An approximately total conversion of the monomer to polymer was obtained after 4 hours, with high molecular weight polymer produced with narrow polydispersity index (PDI) of 1.02, consistent with a highly controlled polymerization process with few side-reactions (termination events such as transesterification and back-biting of the polymer chain). The experimental molecular weights determined by GPC (corrected using the appropriate Mark-Houwink parameters, due to the use of poly(styrene) standards) are 3-4 times higher than those calculated based upon conversions and catalyst : monomer ratios, indicating that only a part of the aluminium catalyst is active (about 34% for entry 14, assuming one polymer chain per active metal centre). This suggests that the rate of propagation is fast compared to the rate of initiation.

**Table 3.2:** Polymerization of  $\epsilon$ -Caprolactone (0.17 g, 1.5 mmol using Catalysts **1-4** and **11** (0.015 mmol) with BnOH in toluene (3 mL)

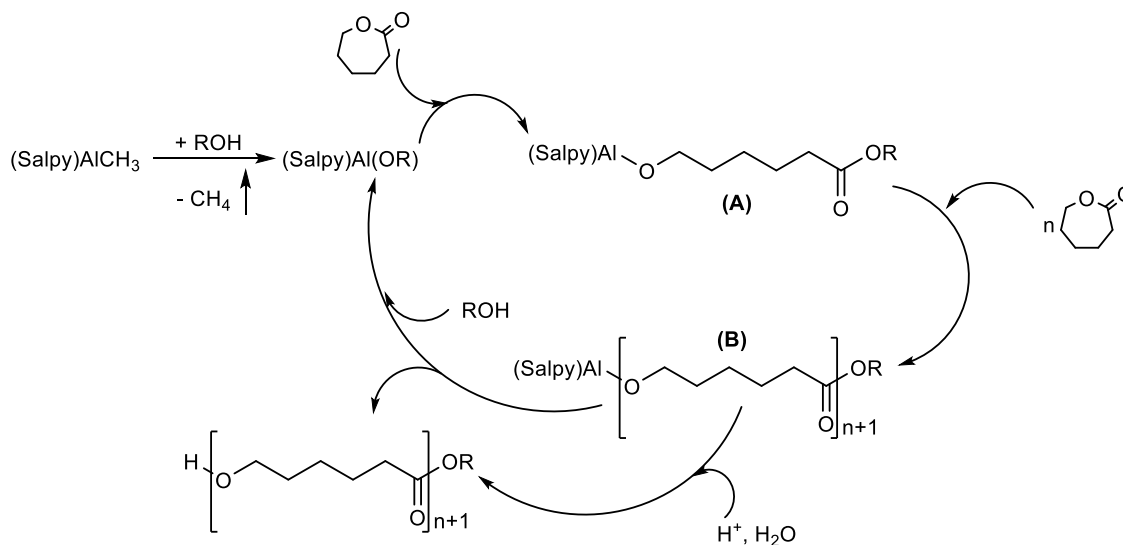
Entry	Cat.	[M] <sub>0</sub> : [Al] <sub>0</sub> : [BnOH]	T (°C)	t (h)	<i>M<sub>n</sub></i> (obsd)	<i>M<sub>n</sub></i> (calcd)	Conv. (%)	<i>M<sub>w</sub></i> / <i>M<sub>n</sub></i>
15	1	100:1:1	25	1	4140	6842	59	1.09
16	1	100:1:1	25	2	5270	8500	74	
17	1	100:1:1	25	3	8840	9354	82	1.06
18	1	100:1:1	25	4	9070	10838	94	1.04
19	2	100:1:1	25	1	8320	10097	88	1.02
20	2	100:1:1	25	2	8900	11186	98	1.02
21	2	100:1:1	25	3	9230	11300	99	1.01
22	2	100:1:1	25	4	9570	11500	100	1.01
23	3	100:1:1	25	1	nd		34	

### Chapter 3 - Ring opening polymerization of $\epsilon$ -Caprolactone and *rac*-Lactide

24	3	100:1:1	25	2	4700	6950	61	1.0
25	3	100:1:1	25	3	6960	8332	73	1.10
26	3	100:1:1	25	4	10800	9240	83	1.05
27	3	100:1:1	25	6	12540	10946	94	1.05
28	4	100:1:1	25	0.5	7300	8100	70	1.02
29	4	100:1:1	25	1	11580	10000	87	1.01
30	4	100:1:1	25	1.5	13010	11236	98	1.01
31	4	100:1:1	25	2	13670	11500	100	1.00
32	11	100:1:1	25	1	nd		6	
33	11	100:1:1	25	2	nd		9	
34	11	100:1:1	25	3	nd		13	
35	11	100:1:1	25	4	nd		19	

nd: not determined

Complexes [Al(Salpy)Me] (**1**), [Al(<sup>t</sup>Bu,<sup>t</sup>Bu-Salpy)Me] (**2**), [Al(Naphpy)Me] (**3**) and [Al(<sup>t</sup>Bu,OMe-Salpy)Me] (**4**) exhibit efficient catalytic activity in the polymerization of  $\epsilon$ -CL in the presence of BnOH (Table 3.2). The *in situ* formation of an alkoxide species [Al(R,R-Salpy)(OBn)] under the reaction conditions employed was confirmed by <sup>1</sup>H NMR spectroscopy for the 1:1 reaction of each complex with BnOH. The signal of the methyl ligand at  $< 0$  ppm disappeared, and new resonances for the alkoxide group grew in. These benzyloxy complexes were isolated (see Chapter 2) and their spectroscopic data were identical to *in situ* NMR tube scale reactions. Redshaw and co-workers reported the *in situ* formation of active aluminium alkoxide complexes for ROP for dialkylaluminium amidates,<sup>34</sup> and this procedure has become standard practice for various metal complexes.<sup>35,36</sup> The formation of an alkoxide species is so successful since it gives a good balance between the rate of initiation and the rate of propagation, which suggests that the polymerization mechanism is via a coordination–insertion mechanism (Scheme 3.1).



**Scheme 3.1:** Suggested mechanism for the ROP of  $\epsilon$ -CL initiated by **1**/ROH

The  $^1\text{H}$  NMR spectra of the PCL (Figure 3.2, above) synthesized using complex **1** with  $\text{BnOH}$  (Table 3.2, entry 18) confirmed the presence of the methylene signals from both benzylalkoxyl  $\text{PhCH}_2\text{O}$  (**b**) at around 5.1 ppm, and hydroxyl  $\text{HOCH}_2$  (**g**) at around 3.6 ppm, chain ends, which correlate well with the expected character of the catalytically active species. The intensity ratio between **H<sub>b</sub>** ( $\text{CH}_2$  from PCL at the benzyloxy chain end) and **H<sub>g</sub>** ( $\text{CH}_2$  from PCL at the hydroxy end) is close to 1, thus it is reasonable to assume that the initiation step proceeds through a monomer insertion into the  $\text{Al}-\text{O}$  bond of the aluminium benzyloxy intermediate **b**, which is formed *in situ* with the concomitant evolution of methane (Scheme 3.1). The intensity ratio of 1 indicates that the ring cleavage of the lactone occurs between the acyl-oxygen bond to form an aluminium alkoxide intermediate, which further reacts with excess lactones to form polyesters. Consequently, the quenching of these aluminum active bonds by hydrolysis results in the hydroxyl end group.

Generally, It is believed that ROP of cyclic esters by alkoxide complexes operates by a 'coordination-insertion' mechanism<sup>37-39</sup> (Figure 3.3).

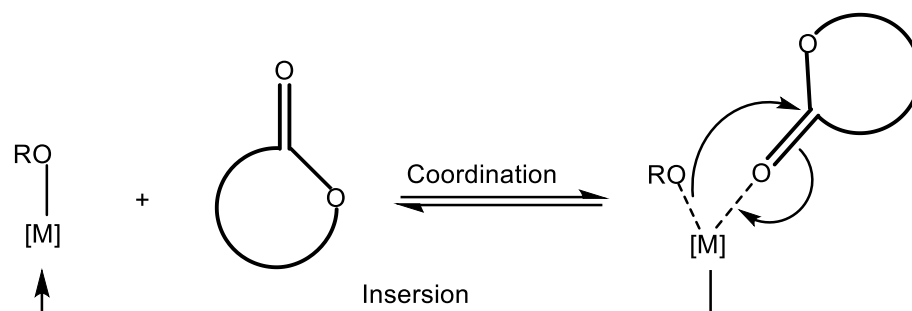


**Figure 3.3:** Coordination–insertion mechanism for the ring opening polymerization of cyclic esters.

A study of the kinetics of the ROP of  $\epsilon$ -CL initiated by aluminium complexes was conducted by Tolman and co-workers (Figure 3.4). They suggested that ROP involves reversible binding of a cyclic ester to the metal ( $k_1/k_{-1}$ ), the activated carbonyl is then attacked by an alkoxide ligand ( $k_2/k_{-2}$ ), and finally the cyclic monomer is ring-opened to generate a new propagating alkoxide ( $k_3/k_{-3}$ ). In the study the latter two steps were reversible, and  $k_3$  was probably post rate determining, although the barrier for the ring-opening ( $k_3$ ) would be lower than that of the ring-closing ( $k_{-3}$ ) and alkoxide deinsertion ( $k_{-2}$ ). They therefore simplified the mechanistic description to involve only  $k_1$ ,  $k_{-1}$ , and  $k_2$ ; when  $k_{-1} \gg k_2$ ,  $k_M = k_{-1}/k_1$  (Figure 3.4).<sup>40</sup>

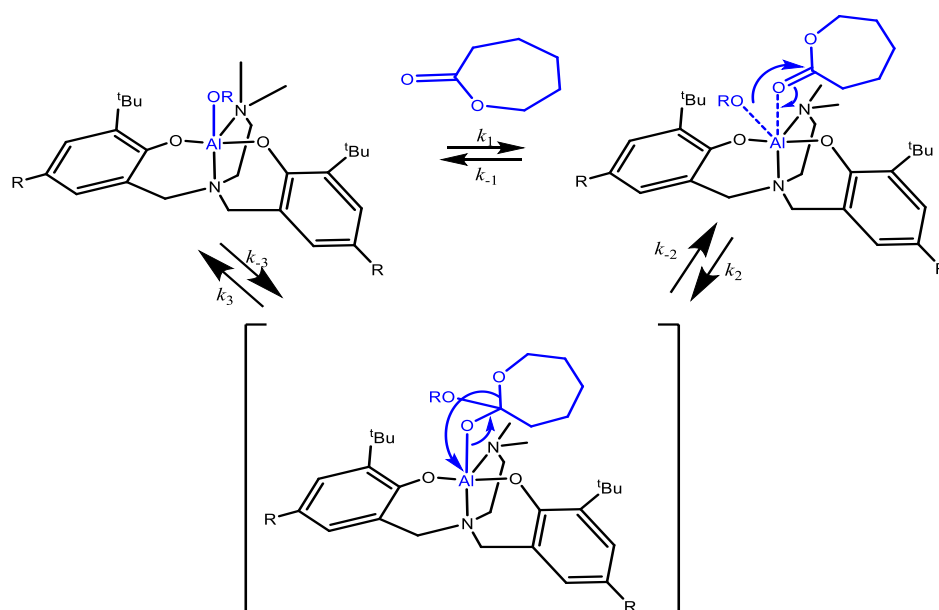
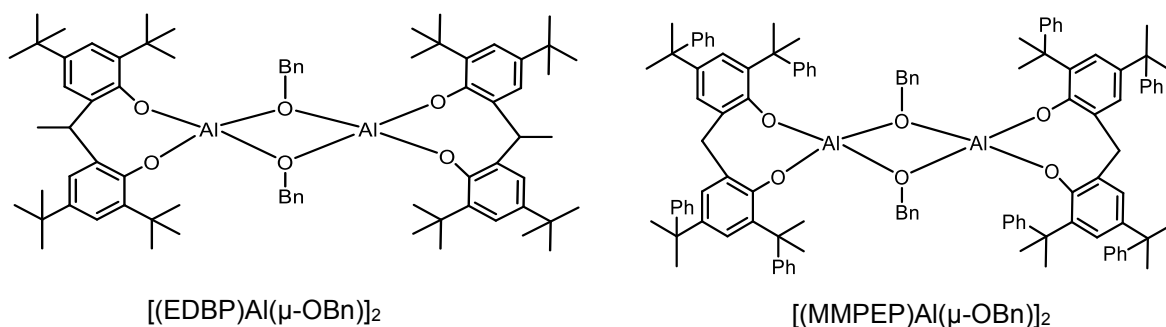


**Figure 3.4:** Proposed mechanism for CL polymerization by aluminium complexes.

Complexes **2** and **4** showed higher reactivity than complexes **1** or **3**, in the polymerization of CL in the presence of BnOH. With **2** and **4**, the reaction reaches maximum conversion after 2 hours at room temperature, whereas at least 4 hours were needed to obtain comparable conversions using **1** and **3**. The substituents on the phenoxide ring contribute to an acceleration of the polymerization reaction. The steric effect is less easy to quantify with complex **3**; the naphthyl derivative contains a fused ring with the phenol, and although there are no sterically demanding groups on the planar ring system, the relatively rigid ring system could be considered as sterically demanding. If this were the case, then the lower reactivity of complex **3** arises from the bulky naphthyl group in the ligand which hinders the monomer from reaching the catalyst, thus a longer time was needed to complete the reaction. The same argument cannot be made for **1**, which might be expected to give the highest reactivity based upon steric arguments. The low reactivity in this case may result from a lower stability arising from lower steric protection against decomposition processes. Assessing the overall data for catalysts **1–4**, it is likely that this argument is more likely to apply to both **1** and **3**, where the naphthyl is actually *less* sterically demanding than other derivatives probed. In the case of **4** as an initiator, the measured number average molecular weights of the polymers were higher than those obtained using **1–3**, suggesting that the initiation is slow for **4**, possibly on steric grounds. In all cases the molecular weight increases with the conversion, as expected.

There are two effects of the sterically demanding groups or ligands on the polymerization rate. The first effect is when there is more than one coordination mode. In this case the preferred coordination mode depends on the steric hindrance around the metal; greater steric demand favours a lower coordination number, and this in turn enhances the reactivity of the catalyst, if the substrate can still coordinate to the metal ion. Liu and co-workers examined the reactivity of two benzyloxy complexes toward  $\epsilon$ -CL polymerization. They concluded that the ligand of  $[(\text{MMPEP})\text{Al}(\mu\text{-OBn})_2]$  is more sterically hindered than the ligand of  $[(\text{EDBP})\text{Al}(\mu\text{-OBn})_2]$ . The authors suggested that the reactivity would be higher with greater steric demand because the intermediate will be four-coordinate instead of five-coordinate during the polymerization process.<sup>41</sup>



The second effect of the sterically hindered group pertains to the insertion of the monomer to the metal-alkoxide bond; a bulky group reduces the space around the metal centre and as a result, reduce the reactivity of the catalyst.

As a means of probing the effect of introducing some conformational flexibility into the ligand backbone, other ROP experiments were conducted using an amine-based ligand (instead of the imine congener).  $[\text{Al}(\text{Salpy-Me})\text{Me}]$  (**11**) was compared with  $[\text{Al}(\text{Salpy})\text{Me}]$  (**1**). Entries 32-35 were conducted using complex **11** at room temperature, with each entry corresponding to a different reaction time. In stark contrast to **1**, **11** gave slow conversion with no isolated yield even after 4 hours. The structures of **11** and **1** are shown in Figure 3.5, which may help to explain the low reactivity of **11**.

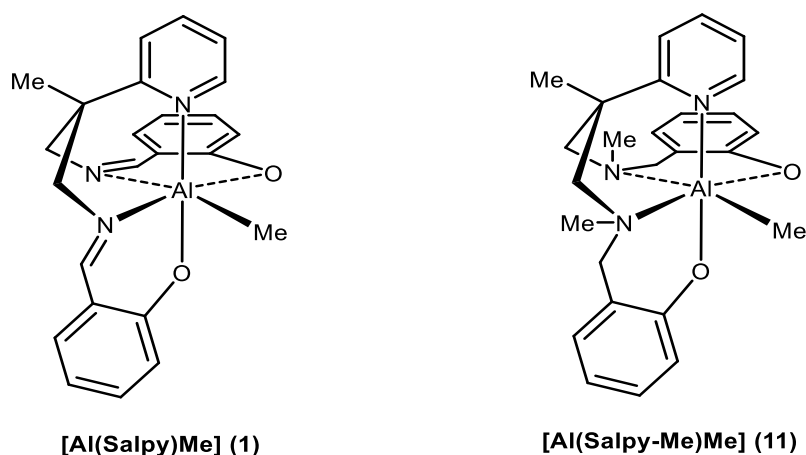


**Figure 3.5:** the structures of complexes **1** and **11**

One possibility is that the different reactivities could result from different donor abilities of imines vs. amines. The presence of imine groups coordinated to the aluminium could promote higher ROP activity due to an enhancement of the

Lewis acidity of the aluminium centre; this character is not found in complex **11** which makes the aluminium less Lewis acidic and as a result of that reducing the reactivity of the catalyst. Another explanation could be the presence of the additional N-methyl substituent, which introduces increased steric demand into the proximity of the coordination sphere and hinders the approach of the  $\epsilon$ -CL substrate.

In order to better understand the role of the pyridyl donor and its effect on the polymerization of  $\epsilon$ -caprolactone, parallel studies were performed using [Al(<sup>t</sup>Bu,OMe-Salpy)Me] (**4**) and [Al(<sup>t</sup>Bu,OMe-Salpn)Me] (**6**) in the presence of BnOH; these complexes differ only in the backbone pyridyl and methyl substituents, whilst keeping the phenoxide substituents identical. Experiments with complex **6** were performed under the same conditions as complex **4** in entries 28-31 (Table 3.2).

A plot of monomer conversion *versus* time showed higher conversion with catalyst **4**, compared to **6** after comparable reaction times (Figure 3.6). After 2 hours both catalysts showed approximately equal conversion while after only 30 minutes the difference was clearer. This indicates a positive effect of the pyridyl group on the polymerization rate. The precise mechanistic details of this effect are not yet clear, since the pyridyl also introduces additional steric encumbrance, and could easily hinder the polymerization process. Nevertheless, this phenomenon is clearly of interest in reactivity studies of aluminium complexes within and beyond the scope of this thesis.

The kinetic studies of  $\epsilon$ -CL polymerization expressed as semilogarithmic plots of  $\ln[\text{CL}]_0/[\text{CL}]_t$  versus time for the polymerizations initiated by **4** and **6**, in the presence of 1 equivalent of BnOH, are shown in Figure 3.7. These plots are linear with an induction period, indicating a first order dependence of reaction rate with respect to monomer concentration. The induction period indicates that complex **4** and **6** reacted with BnOH to form the benzyloxy aluminium complexes as the actual active species to initiate the polymerization. In addition, the increase in rate with the pyridyl donor is evident from the greater gradient of the fitted line.

Monomer conversion was observed to follow first-order kinetics in the form of (1):

$$-d[\text{CL}] / dt = k_{\text{app}}[\text{CL}] \quad (1)$$

where  $k_{\text{app}}$  is the apparent polymerization rate constant, which were obtained from the slope of these linear plots.

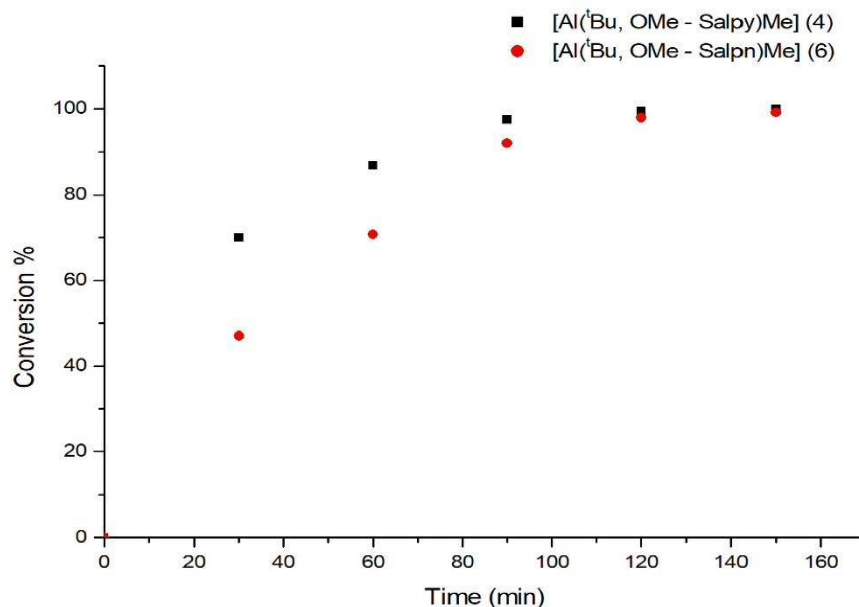


Figure 3.6: conversion *versus* time for the ROP of  $\epsilon$ -CL initiated by **4** and **6**

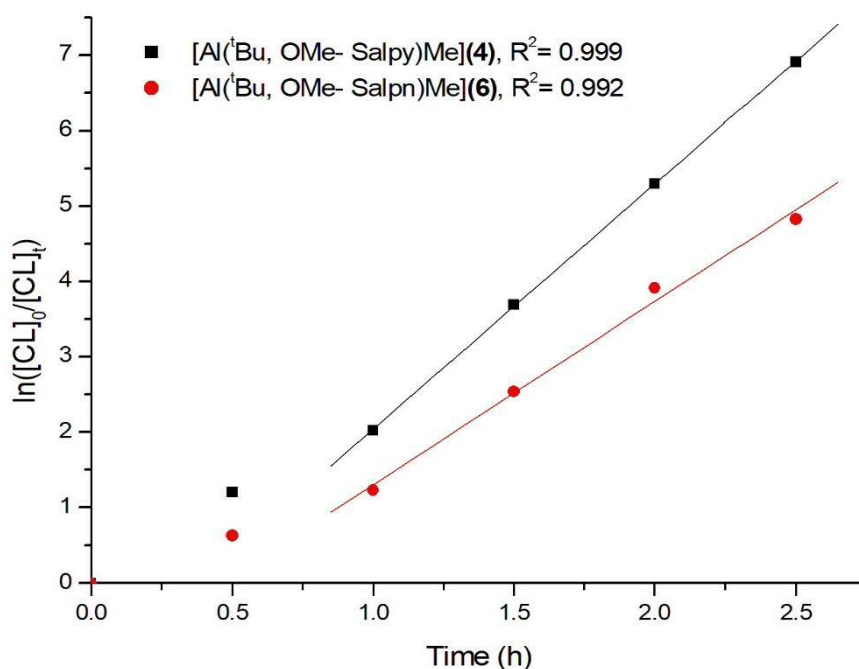


Figure 3.7: Monomer conversion stated as  $\ln([\text{CL}]_0/[\text{CL}]_t)$  *versus* reaction time for the polymerization of  $\epsilon$ -caprolactone using **4** and **6** / BnOH,  $k_{\text{app}} = 3.251 \pm 0.018$  and  $2.434 \pm 0.144 \text{ h}^{-1}$  for complexes **4** and **6** respectively.

### Chapter 3 - Ring opening polymerization of $\epsilon$ -Caprolactone and *rac*-Lactide

The polymerization of  $\epsilon$ -CL using catalyst **2** was studied in the presence of isopropanol (instead of benzyl alcohol); these experiments were conducted under the same conditions as entries 19-22 (Table 3.2). The isopropanol co-initiated data are provided in Table 3.3. Polymerization reactions were probed at both room temperature (entries 36-39) and 50 °C (Entries 40-43), to examine the rate of the reaction and the reactivity of the catalyst. In terms of the conversion, the reactions at 50 °C show essentially quantitative conversions after 1-2 hours, whereas the reactions at room temperature required 4 hours. The polymers produced at room temperature had slightly higher molecular weight than the polymers produced at 50 °C (for equivalent conversion), but the differences are not thought to be significant. However, for both temperatures the molecular weights are higher than the corresponding theoretical values, consistent with a slow initiation and not all of the catalyst participating in the polymerization process.

**Table 3.3:** Polymerization of  $\epsilon$ -Caprolactone Catalyzed by  $[Al(tBu,^tBu-Salpy)Me]$  (**2**) In the presence of isopropanol

Entry	Cat.	[M] <sub>0</sub> : [Al] <sub>0</sub> : [iPrOH]	T (°C)	t (h)	$M_n$ (obsd)	$M_n$ (calcd)	Conv. (%)	$M_w/M_n$
36	2	100:1:1	25	1	8720	4054	35	1.18
37	2	100:1:1	25	2	14980	7821	68	1.13
38	2	100:1:1	25	3	16120	9761	85	1.12
39	2	100:1:1	25	4	18780	11245	98	1.10
40	2	100:1:1	50	1	13540	10446	91	1.18
41	2	100:1:1	50	2	14110	11245	98	1.19
42	2	100:1:1	50	3	14930	11359	99	1.27
43	2	100:1:1	50	4	15600	11474	100	1.22

#### **3.1.2.4 Polymerization of $\epsilon$ -CL Using aluminium benzyloxy complexes**

There are many advantages of using pre-prepared aluminium benzyloxy complexes, over preparing them *in situ* by reacting aluminium organometallic complexes with benzyl (or any other) alcohol. Whilst the active catalyst should be identical, it is much easier to manipulate aluminium alkoxide complexes than the corresponding organometallic complexes because of the high reactivity of aluminium–hydrocarbonyl ligands towards air and moisture; aluminium alkoxide complexes are much less sensitive and can sometimes be handled in air, without recourse to a glove box. There is additionally no need to add further reactant to the reaction vessel, (e.g. benzyl alcohol), thus ensuring that a consistent and accurate amount of initiating ligand is present in all batches of catalyst. The preparation of alkoxide complexes *in situ*, by definition, does not involve purifying the complex and an excess (or slight sub-stoichiometric amount) of alcohol may affect the catalytic performance. Another consideration, which may be a problem for some complexes where steric demand results in slow protonation chemistry, is that it may be desirable to allow the *in situ reaction* to stand for a period of time, to ensure the complete removal of the initial organometallic complex. This is particularly important when, as discussed above, not all of the catalyst may be involved in the polymerization propagation step. This consideration is obsolete for pre-prepared complexes; such complexes can be used immediately without such time delays. The following discussion relates to pre-prepared benzyloxy complexes; the benzyl derivatives were selected on the basis of their superior reactivity when prepared *in situ* above.

Further consideration should be given to the overall performance parameters of (salen)Al systems. In other studies, it has been reported that the rate of polymerization is affected by the nature of substituents about the phenoxide donor. Such effects may be electronic, for example by appending electron-withdrawing or donating substituents, or else they may be steric in nature.<sup>42</sup> It is also possible, even likely, that truly fine-tuning the reactivity of such catalysts will involve a subtle interplay of both factors that may be difficult to completely deconvolute. We therefore initiated a systematic investigation into the  $\epsilon$ -CL polymerization behaviour of a family of Al(Salpy) initiator systems, in which the phenoxy substituents are varied, to obtain an improved understanding of the

influence of this class of salen-type ligands on catalyst performance in polymer production. Since several aluminium bridged-phenoxide derivatives have demonstrated efficient catalytic activities towards the ROP of lactones,<sup>43,44,41</sup> the benzyloxy derivatives **12**, **15**, **17**, **19** and **23** were expected to work as initiators in the ROP of  $\epsilon$ -caprolactone.

Kinetic studies for the  $\epsilon$ -CL polymerization using **12**, **15**, **17**, **19** and **23** in the absence of BnOH were studied. The kinetic studies for the polymerization of CL in the ratio  $[CL]_0/[Al]_0 = 100$  was performed at 25 °C. The results are depicted in Figure 3.8. The plots suggest that there is a first-order dependence of the rate of polymerization on monomer concentration, as judged by the linear relationship of  $\ln([CL]_0/[CL]_t)$  versus time (Figure 3.8).

The apparent polymerization rate constant ( $k_{app}$ ) are given in Table 3.4. Among the five aluminium benzyloxy complexes, the apparent first-order rate constants follow the order **15** > **12** > **19** > **17** > **23**. The trend can be understood, at least in part, by steric and electronic considerations. In **12**, **15** and **19**, where the ligand framework is the same (i.e. differing only in the  $\sigma$ -substituents around the phenoxide ring), the electron-donating groups at phenoxide result in lowered reactivity, which may suggest a delicate sensitivity of reactivity towards the Lewis acidity of the metal centre. A purely steric argument would give the lowest activity to  $[Al(tBu,^iBu-Salpy)(OBn)]$  (**15**), which gave the highest rate constant. The practice of modifying ancillary ligands has allowed for additional investigations in which electron donating and withdrawing groups are used to tune catalyst reactivity. Thus, studies of aluminium complexes of tetradentate salen- and salen-type ligands have shown enhanced LA polymerization rates with ligands that incorporate electron-withdrawing substituents such as chlorine.<sup>24,45</sup> In **17** and **23** there is a steric effect that has an impact on the reactivity of the catalyst. By introducing a bulky naphthyl group on the ligand moiety or by adding more groups in close proximity to the metal centre, such as by introducing two methyl groups onto the imine in **23**, there is a reduction in the reactivity of the catalyst.

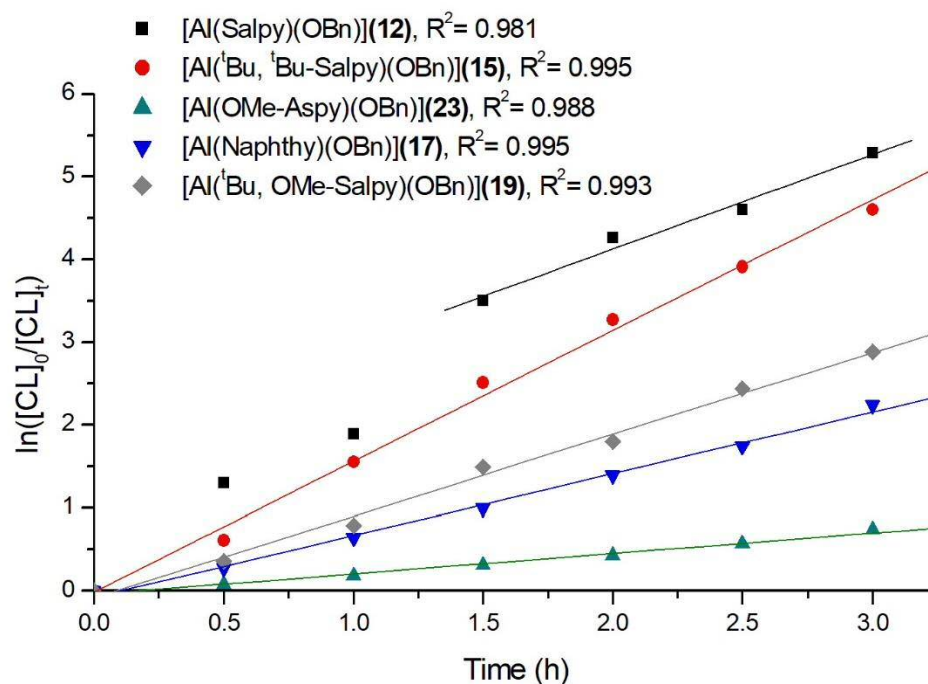


**Figure 3.8:** First-order kinetic plots for CL polymerizations initiated by **12**, **15**, **17**, **19** and **23**:  $[CL]_0/[Al]_0 = 100$  in toluene at 25 °C

**Table 3.4:** Apparent Rate Constants ( $k_{app}$ ) for the Polymerization of  $\epsilon$ -CL

Entry	Catalyst	$k_{app}$ ( $h^{-1}$ )
44	[Al(Salpy)(OBn)] ( <b>12</b> )	1.142±0.111
45	[Al( <sup>t</sup> Bu, <sup>t</sup> Bu-Salpy)(OBn)] ( <b>15</b> )	1.580±0.048
46	[Al( <sup>t</sup> Bu,OMe-Salpy)(OBn)] ( <b>19</b> )	0.986±0.034
47	[Al(Naphpy)(OBn)] ( <b>17</b> )	0.743±0.023
48	[Al(OMe-Acpy)(OBn)] ( <b>23</b> )	0.246±0.011

Data for the polymers obtained from these reactions are summarized in Table 3.5. The molecular weights of the polymers increase linearly with an increase in monomer conversion; the PDIs of these polymers are kept in a narrow range (1.01-1.19). Both of these features are manifest of living behaviour of the catalytic system.

**Table 3.5:** Ring-opening polymerization of  $\epsilon$ -CL catalyzed by complexes **12,15,17** and **23**

Entry	Cat.	t (h)	Mn (obsd)	Mn (calcd)	Conv. (%)	Mw/Mn
44	12	1	16040	9701	85	1.05
45	12	2	20140	11254	99	1.12
46	12	3	31400	11402	100	1.01
47	15	1	13520	9005	79	1.01
48	15	2	15090	10980	96	1.04
49	15	3	16890	11299	99	1.05
50	19	1	13810	6243	55	1.01
51	19	2	14660	9542	84	1.00
52	19	3	15960	10843	95	1.07
53	17	1	15630	5398	47	1.19
54	17	2	18870	8594	75	1.18
55	17	3	19040	10204	89	1.17
56	17	4	19280	11242	99	1.18
57	23	1	n.d	-	17	-
58	23	2	5690	4040	35	1.03
59	23	3	7770	6003	53	1.02
60	23	4	9050	7213	63	1.02

Polymerization conditions: T = 25 °C, Toluene,  $[\epsilon\text{-CL}]_0 = 0.5 \text{ mol/L}$ ,  $[\epsilon\text{-CL}]_0/[\text{Al}]_0 = 100/1$ .

From Table 3.5, catalyst **12** shows high reactivity toward the polymerization, represented by high conversion between 2-3 hours and high molecular weight. The lower steric demand may be the main reason for the higher reactivity in this case. Catalyst **23**, with the methyl groups at the imine carbon, shows slow conversion with time, and moreover produces a polymer with low molecular weight. This suggests that the two methyl groups attached to the imine groups have a detrimental effect on the reactivity of the catalyst. The effect of the phenoxide substituent (methoxy) in **23** probably hinders the reactivity further, since it is an electron donating group. At 50 °C, the reaction reaches full conversion between 90-120 min (Figure 3.9).

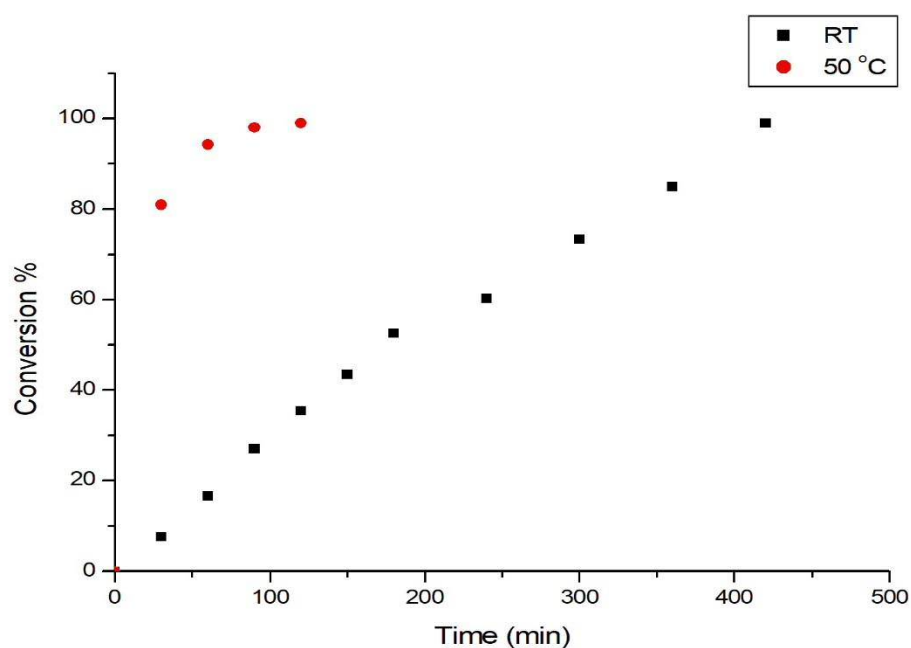


**Figure 3.9:** Plot of Conversion % versus time (min) for the polymerization of  $\epsilon$ -CL by [Al(OMe-Acpy)(OBn)] (**23**) at room temperature and 50 °C

### 3.1.2.5 Ring opening polymerization of Caprolactone using phenoxide complexes.

Structural characterization of the aluminium complexes was aided by preparing phenoxide derivatives,  $[\text{Al}(\text{R,R}'\text{-Salpy})(\text{OTol})]$  (Tol = 4-C<sub>6</sub>H<sub>4</sub>Me) (see Chapter 2 for details). It was therefore of interest to test these complexes in the ring-opening polymerization of  $\epsilon$ -caprolactone, to see if they exhibited similar behaviour to the benzyloxy complexes detailed above. In all cases, the phenoxide complexes showed poor catalytic activity at room temperature, in stark contrast to the data obtained for the benzyloxy complexes. The reaction conditions were varied by changing the catalyst concentration and the reaction time. However, no conversion was observed after 24 hours.

With phenoxide aluminium complexes  $[\text{Al}(\text{Salpy})(\text{OTol})]$  (**13**),  $[\text{Al}(\text{<sup>t</sup>Bu,<sup>t</sup>Bu-Salpy})(\text{OTol})]$  (**16**),  $[\text{Al}(\text{Naphpy})(\text{OTol})]$  (**18**) and  $[\text{Al}(\text{<sup>t</sup>Bu,OMe-Salpy})(\text{OTol})]$  (**20**), which were used in CL polymerization (*vide infra*), there are three factors that may effect the polymerization rate: steric, electronic and the coordination mode of the metal centre. Steric effects could be important since the phenyl ring is directly attached to the Al-O bond, thereby increasing the steric crowding of the metal centre; since the polymerization follows the coordination-insertion mechanism, placing a relatively large group closer to the metal centre is likely to hinder the monomer's access to the metal, thereby disfavoured coordination. With benzyloxy complexes, the phenyl group is distanced from the metal by virtue of the methylene linker between it and the aluminium-bound oxygen; moreover, the methylene linker provides a degree of flexibility, allowing the phenyl ring orient away from the incoming CL monomer (Figure 3.10)

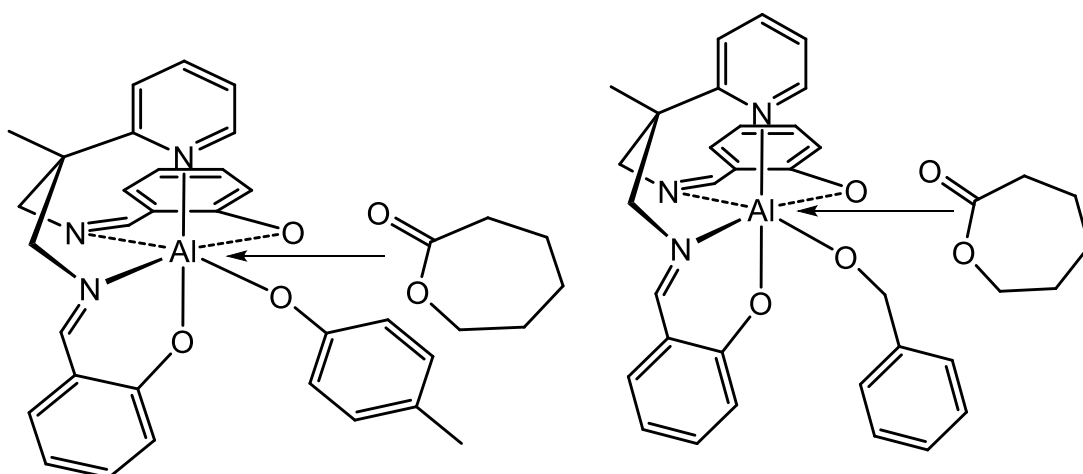


**Figure 3.10:** Coordination approach of CL monomer in both benzyloxy and tolyloxy aluminium complexes

The second effect relates to the electronic properties of the benzyl and tolyl groups. The difference between an aliphatic and an aromatic group directly bonded to the coordinating oxygen of the initiating co-ligand is likely to have an effect on the polymerization process. It would be unsurprising to find that the difference in partial atomic charge on the oxygen, and/or  $\pi$ -bonding effects with the oxygen lone pairs, would have an effect on the transition state energy of the carbonyl insertion step.

The third factor that may affect the reactivity of the initiator is the coordination mode of the metal centre. It is likely that the hemilabile pyridyl plays an important role in the insertion step. It is unlikely that the six-coordinate isomer is able to coordinate the  $\epsilon$ -CL prior to the insertion step, and so a co-ligand that disfavours de-coordination of the pyridyl may prevent the polymerization reaction from proceeding. Whilst all three of these factors may play a part in the observed reactivity, it is likely that the first two are the more significant.

Although the phenoxide complexes were found to be inactive in  $\epsilon$ -CL polymerization at room temperature, this should be considered in the context that  $\epsilon$ -CL polymerization catalysts normally operate at elevated temperatures, and activity at room temperature is unusual, especially for aluminium. Therefore, the phenoxide complexes were probed using higher reaction temperatures. To this

end, [Al(Salpy)(OTol)] (**13**) was tested for the polymerization of  $\epsilon$ -CL at 50 °C, using different reaction times; under these conditions the conversion reaches 32% after 5 hours (Figure 3.11). At 70 °C, the reaction attains full conversion after 5 hours, and since these higher temperatures gave improved conversions, all reactions were henceforth studied at 80 °C (Table 3.6).

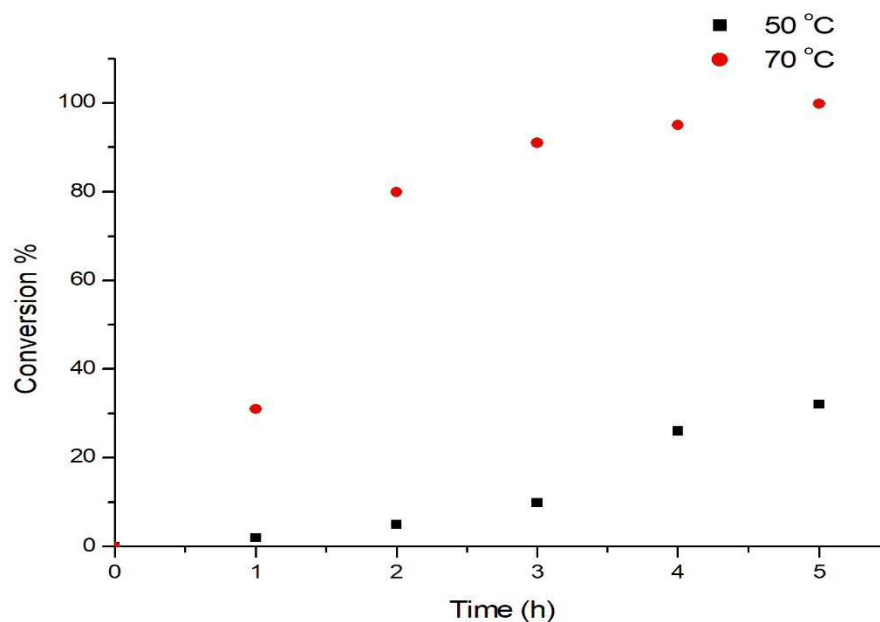


**Figure 3.11:** Plots of conversion versus time for the ROP of  $\epsilon$ -CL initiated by [Al(Salpy)(OTol)] (**13**) at 50 °C and 70 °C.

**Table 3.6:** Ring-opening polymerization of  $\epsilon$ -caprolactone initiated by complexes **13**, **16**, **18** and **20** at 80 °C for 4 h.

Entry	Cat.	[M] <sub>0</sub> : [Al] <sub>0</sub>	M <sub>n</sub> (obsd)	M <sub>n</sub> (calcd)	M <sub>w</sub> /M <sub>n</sub>
61	<b>13</b>	50:1	5800	5650	1.04
62	<b>13</b>	100:1	6020	11300	1.04
63	<b>13</b>	150:1	6180	16950	1.03
64	<b>13</b>	200:1	6380	22600	1.04
65	<b>13</b>	250:1	6530	28250	1.04
66	<b>16</b>	50:1	5280	5650	1.02
67	<b>16</b>	100:1	5380	11300	1.02
68	<b>16</b>	150:1	5450	16950	1.02
69	<b>16</b>	200:1	5510	22600	1.02
70	<b>16</b>	250:1	5630	28250	1.02
71	<b>18</b>	50:1	5750	5650	1.03
72	<b>18</b>	100:1	5910	11300	1.04
73	<b>18</b>	150:1	6090	16950	1.03
74	<b>18</b>	200:1	6140	22600	1.03
75	<b>18</b>	250:1	6300	28250	1.03
76	<b>20</b>	50:1	5180	5650	1.02
77	<b>20</b>	100:1	5280	11300	1.02
78	<b>20</b>	150:1	5370	16950	1.02
79	<b>20</b>	200:1	5540	22600	1.02
80	<b>20</b>	250:1	5610	28250	1.02

Conversions all > 99%

In all cases, the polymers were produced with very narrow molecular weight distributions (1.02–1.04), indicating that all of the aluminium complexes **13**, **16**, **18** and **20** behave in a highly-controlled manner. Monitoring of the polymerization reactions indicated a linear relationship between the number-average molecular weight ( $M_n$ ) and the monomer : initiator ratio  $[M]_0:[I]_0$ , as shown in Figure 3.12 (entries 61-65), Figure 3.13 (entries 66-70), Figure 3.14 (entries 71-75) and Figure 3.15. (entries 76-80); these data are consistent with a ‘living’ character of the polymerization process. This is further supported by the observation that the polydispersity indices (PDIs) are constant, regardless of monomer : initiator ratio.

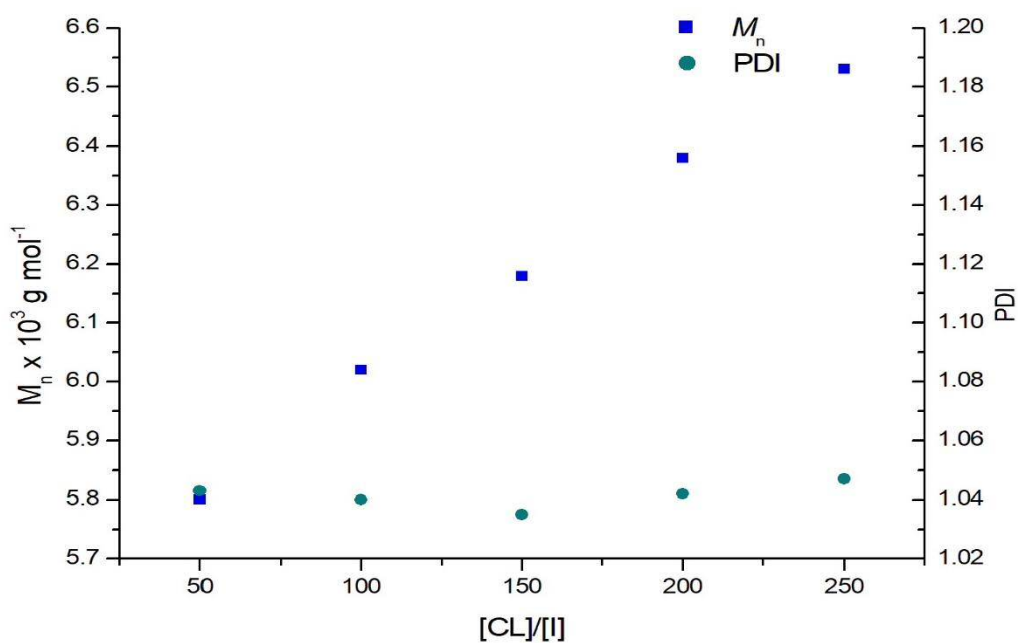


**Figure 3.12:** Polymerization of  $\epsilon$ -CL initiated by **13** in toluene at 80 °C.

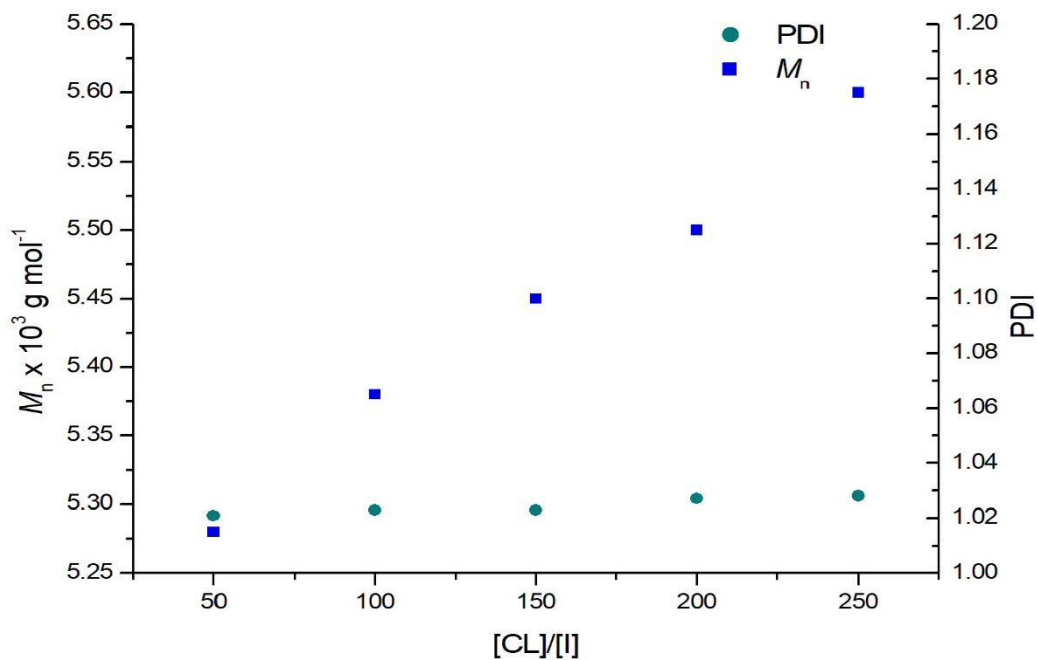


Figure 3.13: Polymerization of  $\epsilon$ -CL initiated by **16** in toluene at 80 °C.

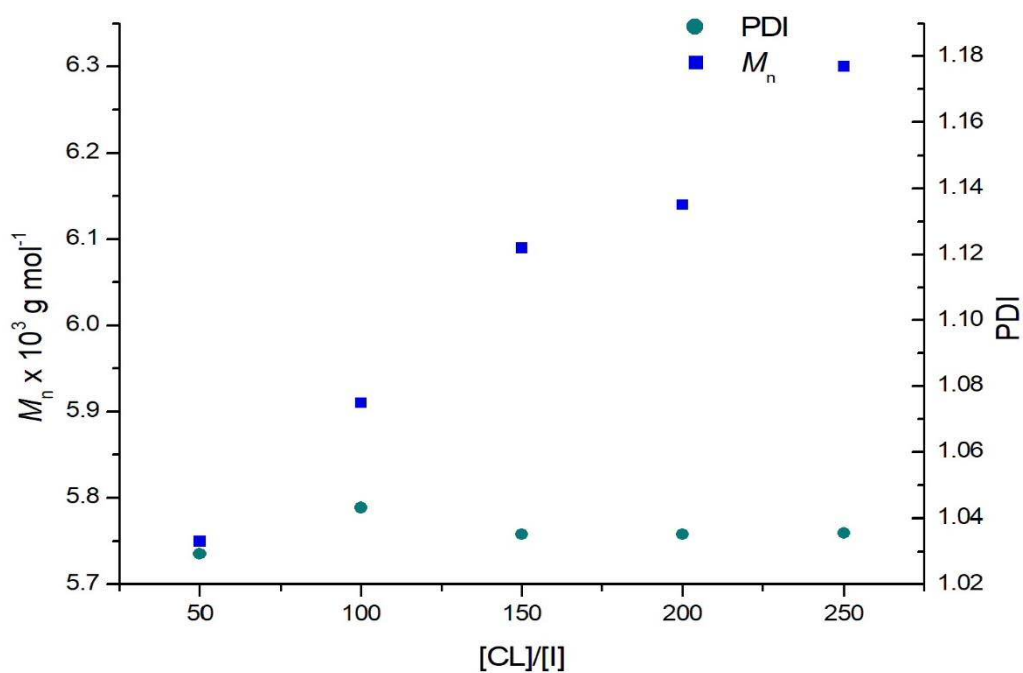
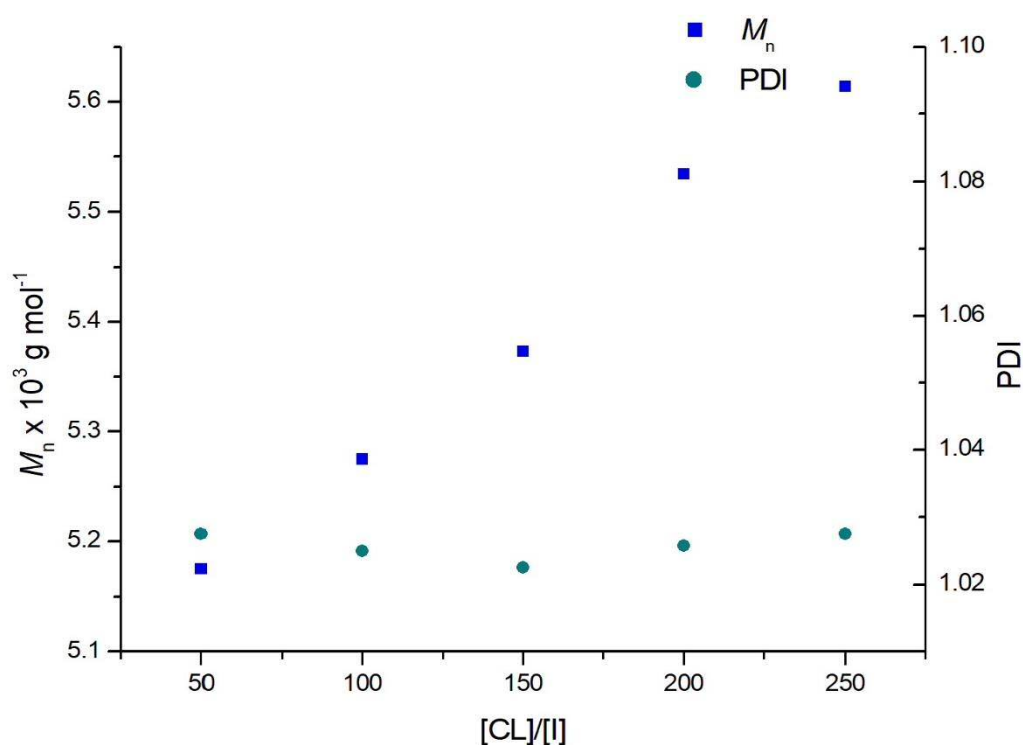


Figure 3.14: Polymerization of  $\epsilon$ -CL initiated by **18** in toluene at 80 °C.



**Figure 3.15:** Polymerization of  $\epsilon$ -CL initiated by **20** in toluene at 80 °C.

Polymerization reactions using all of the complexes show full conversion after 4 hours under these conditions, however the  $M_n$  values for all entries were lower than the theoretical values. Lower than expected  $M_n$  values can be caused by transesterification or back-biting termination processes during the polymerization process.<sup>46</sup> Interestingly, termination processes often result in an increase in PDI, which is not the case with these catalysts.

### 3.1.2.6 The effect of cocatalyst on the ROP of $\epsilon$ -CL using [Al(Salpy)Me] (**1**)

The above observations, that the tolyloxide complexes gave substantially different catalytic activity to the benzyloxide ones, prompts a question: which alcohol is the most efficient at promoting this reaction? Benzyl alcohol is ubiquitously used throughout the literature; one would assume this to be for good reason, but nevertheless, are there others that can give competitive reactivities? To answer these questions, the catalytic efficiency of [Al(Salpy)Me] (**1**) toward  $\epsilon$ -caprolactone ( $\epsilon$ -CL) in the presence of different phenols and alcohols have been

studied. Six types of phenol and three types of alcohol were utilised, to encompass a range of steric and electronic factors (Table 3.7).

**Table 3.7:** Ring-opening polymerization of  $\epsilon$ -caprolactone initiated by complex **1** with different cocatalysts

Entry	Phenol/Alcohol	T (°C)	t (h)	Conv. (%)	$M_n$ (obsd)	$M_n$ (calcd)	$M_w/M_n$
81	p-Cresol	80	6	36	7850	4262	1.18
82	p-tBu-Phenol	80	6	34	7780	4053	1.18
83	p-Cl-Phenol	80	6	13	9120	1612	1.04
84	p-NO <sub>2</sub> -Phenol	80	6	2	-	3674	-
85	p-Ph-Phenol	80	6	18	8390	2224	1.14
86	Hydroquinone	80	6	Nil	-	-	-
87	Benzyl alcohol	25	5	96	7570	11111	1.12
88	Isopropanol	25	5	87	7620	10013	1.20
89	1-Adamantanol	25	5	12	22270	1556	1.17

The differences in reactivity for the benzyloxide and tolyloxide complexes meant that the polymerization studies were performed at different temperatures, 25 °C and 80 °C respectively (*vide supra*). Therefore, these polymerization studies, aimed at probing the effectiveness of different cocatalysts, were carried out at 25 °C for alcohols and at 80 °C for the phenols. All reactions were carried out in toluene (3 mL) using **1** (0.015 mmol) as the pre-catalyst. The initiator was stirred with the alcohol / phenol (ROH) for 30 min to form initiating species [Al(Salpy)(OR)]. Afterwards, 1.5 mmol of  $\epsilon$ -CL was added and the mixture was stirred at constant temperature for 5 hours for alcohol and 6 hours for phenols. The polymerization reaction was quenched after the prescribed time (5 or 6 h) by

adding a few drops of an acetic acid solution. The solvent was removed and the  $^1\text{H}$  NMR spectra recorded of the crude product to calculate the conversion. The polymerization mixture was thereafter dissolved in THF and the polymer precipitated as a white solid by adding hexane. The polymers were further purified by repeating this procedure a further two times. After precipitation, the polymer product was collected by filtration and dried under vacuum to constant weight. The ratio of the reactants  $[\text{M}]:[\text{Al}]:[\text{ROH}]$  was  $[100]:[1]:[1]$ , comparable to the studies discussed above.

The polymerization results are shown in Table 3.7. As expected, based upon prior observations, the phenoxide catalysts are much less reactive towards the ring-opening polymerization of  $\epsilon$ -caprolactone than the aliphatic congeners. None of the phenols tested gave any conversion when the reaction was conducted at room temperature, within 24 hours. This suggests that it is the aromatic nature of the initiator ligand that hinders the initiation step (the first  $\epsilon$ -CL insertion) since this is not a tolyl-specific observation. Both steric and electronic factors of the initiating ligand play important roles in the polymerization, especially the migratory insertion to the carbonyl of the monomer. The electronic structure of the aromatic ligand may render the oxygen-based lone pair less susceptible to attack the carbonyl carbon, thus increasing the activation barrier to insertion.<sup>47</sup> This arises since oxygen of the phenol is bonded directly to the aromatic ring, and there is a possibility that the lone pairs may be, to some extent, delocalized over the  $\pi$ -system, increasing the stability of this bond complex by resonance. This resonance effect is not available with alcohols, so when a methylene group separates the oxygen and the aromatic ring the oxygen-based lone pairs become more nucleophilic towards the substrate. This effect is in addition to the relief of steric crowding mentioned above.

In contrast to the aromatic derivatives, the alcohol-derived catalysts were active at room temperature, with high conversion attained after five hours for two of the alcohols used; the conversion for adamantanol was significantly lower than benzyl alcohol or isopropanol.

The effect of the substituents on the polymerization performance was most marked with the phenoxide complexes. Entries 81-86 were conducted using

phenols containing different substituents, ranging from small to bulky, to electron donating and electron withdrawing. The temperature of the reaction was increased to 80 °C and reaction time was 6 hours in all cases. In general, even with a high reaction temperature, a low conversion was observed with all phenol cocatalysts. Catalysts containing electron-withdrawing substituents, nitro and chloro, gave the lowest conversions. A plot of the conversion vs. the Hammett parameter,  $\sigma_p$ , for entries 81-85 (Figure 3.16) shows a clear correlation between the electron donating/withdrawing ability of the *para*- substituent and the conversion; since the molecular weight of the polymers are comparable in all cases, the lower conversion would appear to equate to less catalyst being active, but where the active catalyst, once initiated, has a comparable rate. In all cases, the  $M_n$  is lower than expected, showing that initiation is slow. This is expected, since after the first  $\epsilon$ -CL has been opened, the initiating ligand resides at the terminal end of the polymer chain and should have little influence over the propagation of the polymerization process.

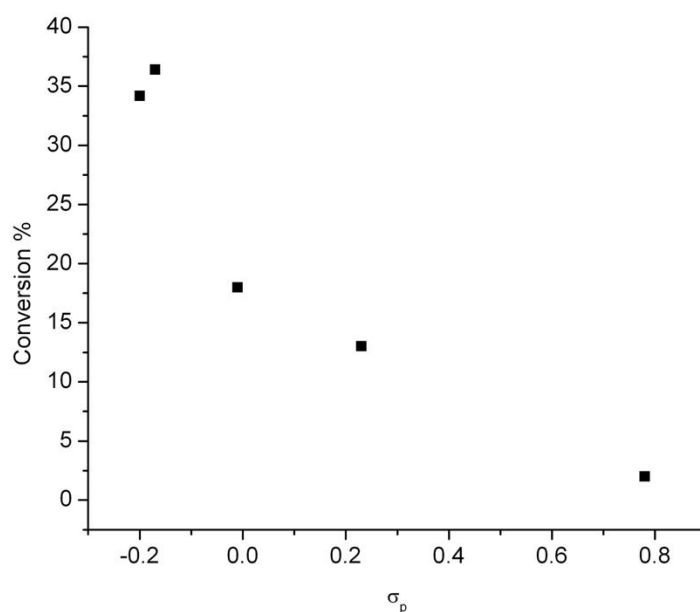


**Figure 3.16:** Plot of PCL conversion vs. Hammett parameter of the co-catalyst

The electronic effect of the initiating group can be understood by considering that the lone pair of the initiating group oxygen attacks the carbonyl carbon of the

monomer (see the computational analysis below); an electron withdrawing group on the phenyl group is likely to make it harder for the lone pair to be donated, thereby slowing down the initiating step. Naturally this explanation is somewhat simplified, since probing a correlation with the Hammett parameter ignores subtle steric effects, e.g. of the *tert*-butyl group. The plot in Figure 3.16 is not a perfectly linear correlation as a result.

Entries 87-89 show the effect of the alcohols on the polymerization. Benzyl and isopropyl alcohols show effectively the same reactivity, there being approximately the same conversion and molecular weight of the polymers. 1-adamantanol was different, the low conversion was recorded after five hours at room temperature; the steric effect of the bulky adamantyl group restricts the insertion of the monomer into the metal-oxygen bond. Hermanova *et al.* suggested that for a particular alkoxide ligand, the steric influence has a more significant effect on the activity of catalytic species, compared to its electronic contribution as a Lewis acidic centre.<sup>48</sup> They found that the catalytic system of the triazole-based aluminium complex in the presence of methanol and isopropanol produced polymers with high conversion (81–85%) but broader distribution ( $M_w/M_n = 1.5$ – $1.8$ ) after a polymerization period of 8 hours. A prolonged period of 20 hours was necessary to reach a comparable conversion of 85% when bifunctional poly(ethylene glycol) was used.<sup>48</sup>

The PDIs of poly(caprolactone)s are quite narrow, ranging from 1.04 to 1.2. In these experiments, the corrected experimental value of  $M_n$  ( $M_n(\text{obsd})$ ) obtained from the GPC analysis was always higher than the theoretical  $M_n$  value ( $M_n(\text{calcd})$ ). There are two possible reasons for the unexpected high value of  $M_n(\text{obsd})$ . First, the activity of intermediate B (as shown in Scheme 3.1) is higher than the catalyst **b**; therefore only part of catalyst **b** participates in the catalytic cycle. Secondly, during the polymerization process, inter- or intra-transesterification reaction occurs.<sup>43</sup> In these cases, as discussed above, it is more likely that the higher than expected values correspond to a slowing of the initiation rate.

### 3.1.2.7 Density functional calculations of polymerization mechanism

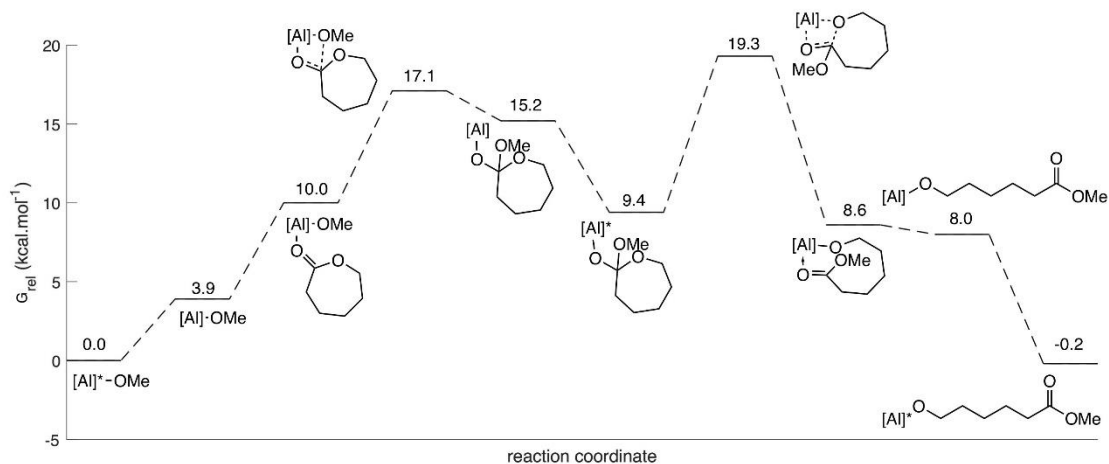


**Figure 3.17:** Calculated free energy profile for the polymerization of CL. [Al]<sup>+</sup> denotes the Al Salpy core with coordinated pyridyl, [Al] denotes a de-coordinated pyridyl

A possible mechanism for the polymerization of  $\epsilon$ -caprolactone was computed using density functional calculations. All calculations were undertaken by Dr. Benjamin Ward using the Gaussian 09 software package. In all cases, the M06-2X functional was used, employing the cc-pV(D+d)Z basis set for Al, and cc-pVDZ basis set for all other atoms. The hypothetical complex [Al(Salpy)(OMe)] was used as the catalyst complex, representing the alkoxide resting state.

Assuming that a coordination-insertion mechanism operates, which seems viable based upon experimental and literature evidence, the calculated energy profile is shown in Figure 3.17.<sup>49</sup> Calculation of the reaction pathway whilst keeping the pyridyl permanently coordinated were unsuccessful, for both substrate coordination and the transition states. Given the discussion earlier, regarding the hemi-lability of the pyridyl donor, the calculations considered the energy of pyridyl de-coordination; this was found to be 3.9 kcal.mol<sup>-1</sup> and so readily achievable under ambient conditions, consistent with the proposed equation and the experimentally determined values ( 4.8 kJ.mol<sup>-1</sup> = 1.1 kcal.mol<sup>-1</sup>. Thus having reduced the coordination number from 6 to 5, the  $\epsilon$ -caprolactone monomer was found to coordinate to the aluminium centre, and the reaction proceed within readily-accessible energy limits.

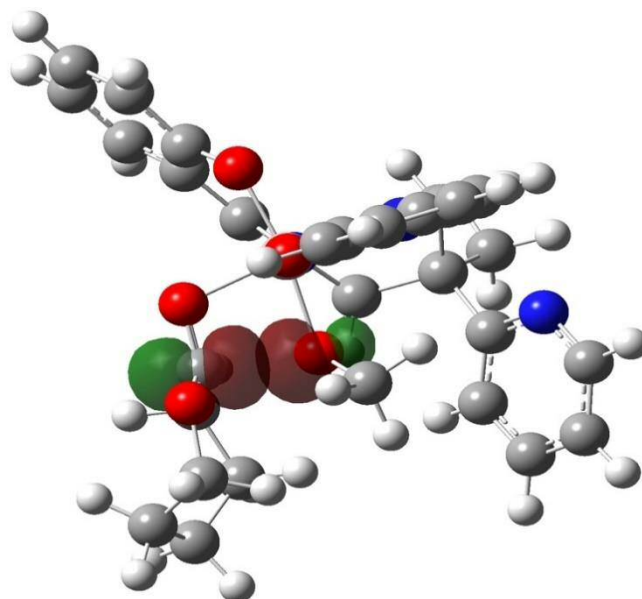


**Figure 3.18:** Calculated structure of the carbonyl-insertion transition state for the polymerization of  $\epsilon$ -caprolactone, showing the donor-acceptor NBO interactions.

The transition state corresponding to the OMe ligand inserting into the monomer carbonyl group is shown in Figure 3.18, and as expected, corresponds to a four-centre 1,2-migratory insertion transition state structure. A Natural Bonding Orbital (NBO) analysis indicates the principal donor-acceptor interactions associated with the transition state core are effectively the  $\pi_p$  of the OMe oxygen to  $\pi_p^*$  of the carbonyl carbon. This is particularly informative, when considered in conjunction with the different initiation rates found for various co-catalysts (Section 3.1.6); electron-withdrawing alkoxide substituents will disfavour facile donation of the oxygen  $\pi_p$  electrons whereas electron-donating substituents will promote this process.

After the insertion, the energy after the transition state is 15.2 kcal.mol<sup>-1</sup>; upon re-coordination of the pyridyl the energy reduces further to 9.4 kcal.mol<sup>-1</sup>. It is likely that the coordinated pyridyl intermediate corresponds to a short-lived resting state in the catalytic cycle; decoordination of the pyridyl allows the coordination of the ring-oxygen as part of the ring-opening step.

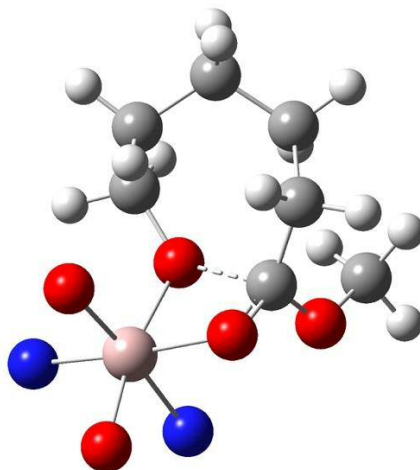


**Figure 3.19:** Calculated structure of the ring-opening transition state for the polymerization of  $\epsilon$ -caprolactone. For clarity, only the donor atoms of the Salpy ligand are shown

The transition state for the ring-opening step (Figure 3.19) corresponds to the highest point on the potential energy surface; this corresponds to  $\Delta G = +19.3$  kcal.mol<sup>-1</sup>, and should therefore be accessible at room temperature (as a rule of thumb, values of  $\leq 25$  kcal.mol<sup>-1</sup> / 100 kJ.mol<sup>-1</sup> correspond to viable room temperature reactions). The calculations are therefore consistent with the experimental data.

After the ring-opening, it is possible that the ring-opened species is formed with the newly-formed ester linkage coordinated to the aluminium. Whilst this is a viable species, de-coordination of the polymer chain gives a significant reduction in the energy level, which is further reduced upon re-coordination of the pyridyl, giving an overall (slightly) exothermic process.

### 3.1.3 Racemic lactide (Rac-LA) Polymerization

#### 3.1.3.1 General procedure for Rac-LA polymerization

Since the catalysts discussed in this chapter were active in the ROP of  $\epsilon$ -caprolactone, it was also of interest to probe their reactivity with *rac*-lactide; these studies were conducted using complexes **1–4** as initiators in the presence of BnOH (Table 3.8). The initiators were generated by *in situ* alcoholyses of the

aluminium methyl complexes using benzyl alcohol, as is common for aluminium complexes.<sup>24,50–54</sup> Toluene solutions (3 mL) of the aluminium methyl complexes **1-4** were treated with one equivalent of benzyl alcohol. After stirring for 10 min. at room temperature, the *rac*-lactide was added. The ring-opening polymerization of *rac*-lactide was conducted at 80 °C, the ratio of [LA]:[Al]:[BnOH] was 100:1:1, and the lactide concentration in all experiments were 0.5 mol L<sup>-1</sup>.

After the appropriate reaction time, the polymerization was quenched by addition of wet THF (10% water, 90% THF). After removal of the volatiles, the residue was subjected to <sup>1</sup>H NMR analysis for monomer conversion calculation. The polymer was purified by dissolving the crude samples in methylene chloride and precipitating the polymer with methanol. The polymers were further dried in a vacuum oven at 50 °C for accurate mass measurement.

### 3.1.3.2 Characterization and evaluation of the polymer products

Monomer conversions were determined by observing the methine resonance integrations of monomer vs. polymer in the <sup>1</sup>H NMR (CDCl<sub>3</sub>, 400 MHz) spectra (Figure 3.20).

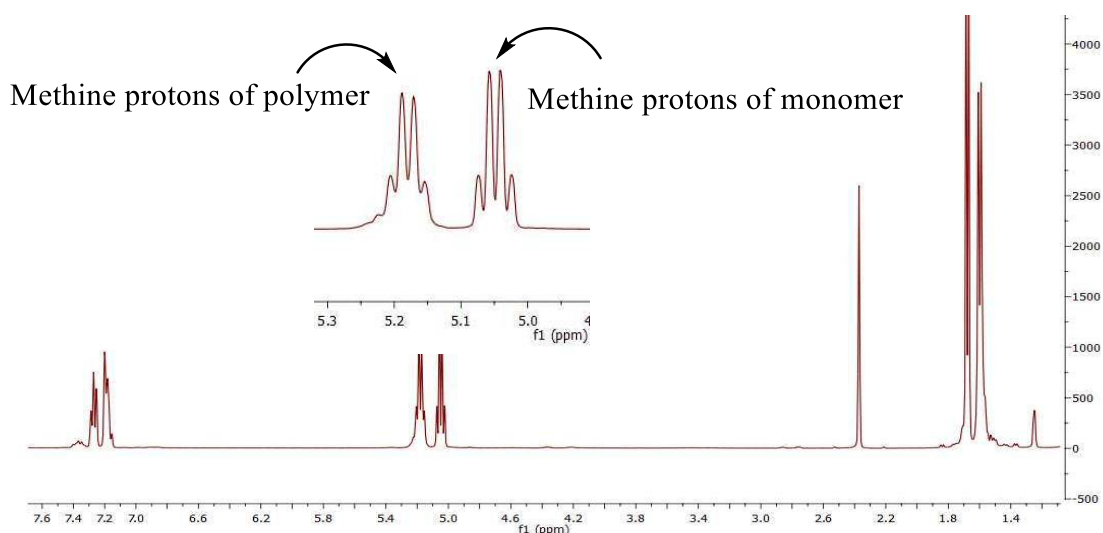


**Figure 3.20:** *rac*-lactide conversion to PLA using **15** as catalyst

The theoretical molecular weight was calculated according to the following equation:<sup>55</sup>

$$M_{n,Cal} = ([LA]_0 / [Al]_0) \times 144.13 \times \text{conversion} + 108.14$$

The observed  $M_n$  was determined by GPC in THF relative to Polystyrene standards. A more accurate value of  $M_n$  was obtained after the correction of the  $M_n$  from the GPC data using the Mark-Houwink equation. Homonuclear decoupled  $^1\text{H}$  NMR spectra were measured to examine the stereochemical microstructures of the poly(lactic acid) (PLA) samples.

### **3.1.3.3 Aluminium methyl complexes as initiator for ROP of *rac*-lactide**

Experimental results indicate that complexes **1–4** are inactive toward the ROP of *rac*-lactide at 25 °C in the presence of BnOH, as the conversions were less than 5% after 22 hours. The conversion was increased to 96% with the temperature raised to 80 °C in toluene (entries 1-16). At 80 °C all the four complexes showed high reactivity toward *rac*-lactide after 6 hours. For complete conversion, a long reaction time was used. Even with 22 hours of stirring at 80 °C, a maximum conversion of 96% was obtained. Catalysts **1** and **3** showed higher conversion (83% and 86% respectively) after 1 hour reaction time, whereas complexes **2** and **4** showed low conversion after the same time; for complex **2**, 6 hours were needed to reach 83% (Entry 7). The number average molecular weight obtained using **1** for 22 hours was the highest among all complexes (Entry 4) while **3** gave a polymer with a lowest molecular weight. Even though catalysts **2** and **4** showed lower reactivity than **1** and **3**, the low polydispersity indices were characteristic of controlled propagation. Relatively high (in comparison to many in this thesis) PDI values were recorded which may be caused by side reactions, such as transesterification; however, the values are still relatively small. Interestingly, the  $M_n$  values obtained from GPC (and corrected using Mark-Houwink parameters) are lower than the theoretical values which again may refer that transesterification to the monomer take place under such conditions.

The modifications in the auxiliary ligand exhibited a dramatic influence on the catalytic performance. Complexes [Al(Salpy)(Me)] (**1**), [Al(<sup>t</sup>Bu,<sup>t</sup>Bu-Salpy)(Me)] (**2**), [Al(Naphpy)(Me)] (**3**) and [Al(<sup>t</sup>Bu,OMe-Salpy)(Me)] (**4**) have the same diimine backbone, but different phenoxide substituents; the electron-withdrawing or

donating ability and the bulkiness of the groups at the ortho positions of the phenoxide may be responsible for the subtle differences in reactivity and selectivity. On the other hand, introducing a methyl group to the imine group (complex **9**) significantly reduced the reactivity of the catalyst. Complex **9** contains a ligand prepared from substituted 2-hydroxyacetophenone while the other ligands are derived from salicylaldehydes. It is possible that the two imine methyl groups restrict the approach of a *rac*-LA monomer, hindering the reaction; entries 17-20 show the polymerization data. Low conversions were observed in comparison to the salpy complexes: the conversion only reached 56% after 6 hours. This was improved by increasing the reaction time to 22 hours, after which 88% conversion was obtained, which suggests that steric hindrance is the principal factor affecting the reactivity of this catalyst.

Generally, the ROP of *rac*-LA initiated by these complexes is well-controlled. By using complexes **1**, **2** and **9** as the initiator to catalyze the ROP of *rac*-LA in toluene, the relationship of  $M_n$  of the obtained PLA sample versus conversion was plotted (Figures 3.21, 3.22 and 3.23), showing a linear increase of  $M_n$  with conversion.

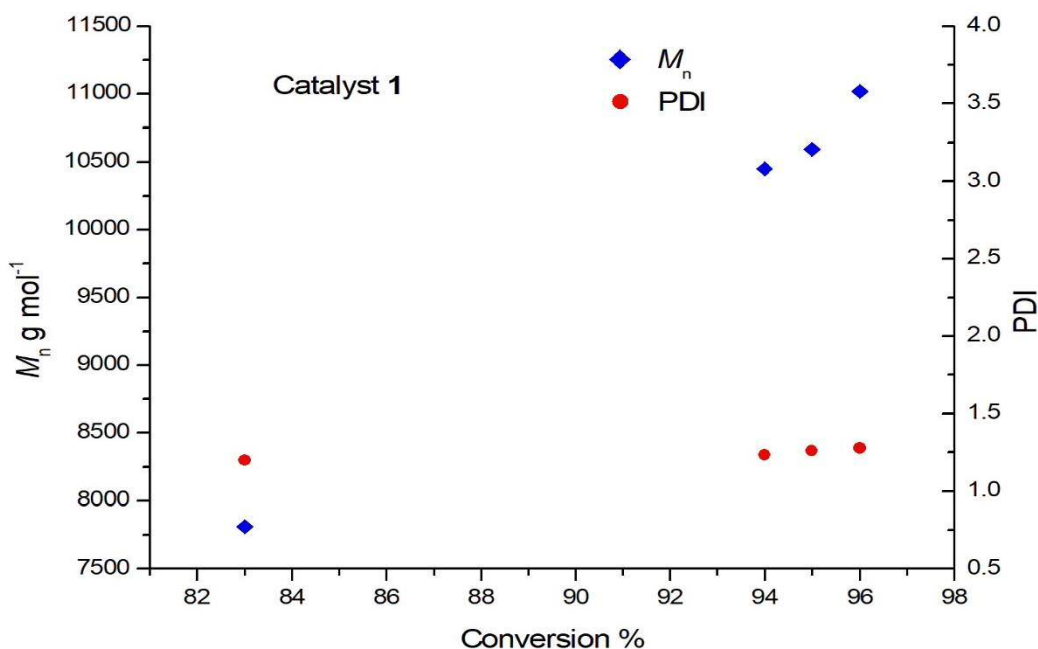


Figure 3.21: Relationship of  $M_n$  and PDI versus conversion catalyzed by **1**

**Chapter 3 - Ring opening polymerization of  $\epsilon$ -Caprolactone and *rac*-Lactide**

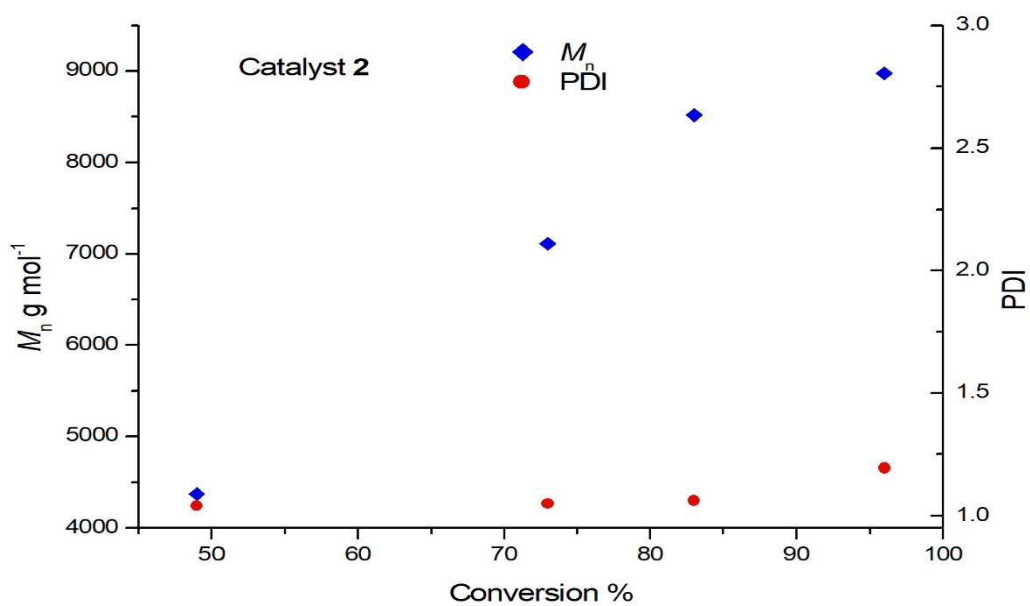


Figure 3.22: Relationship of  $M_n$  and PDI versus conversion catalyzed by **2**

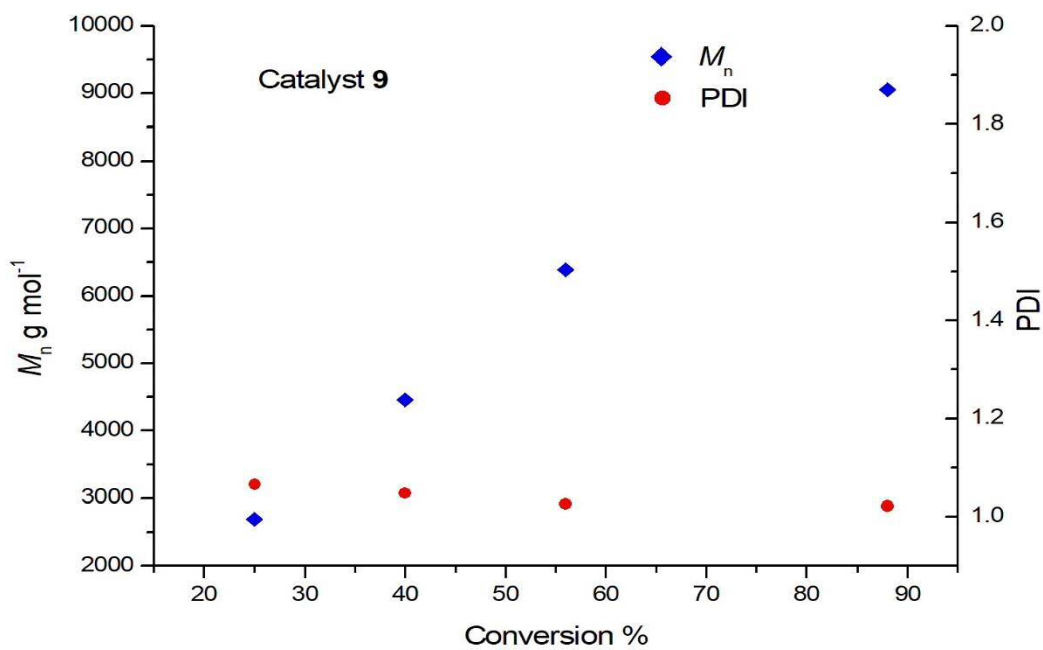
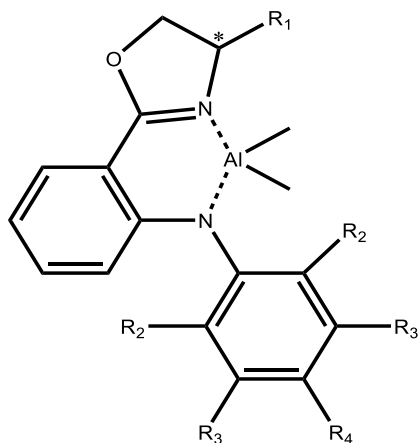


Figure 3.23: Relationship of  $M_n$  and PDI versus conversion catalyzed by **9**

**Table 3.8:** Polymerization of rac-Lactide with Al complexes 1-4 and 9.

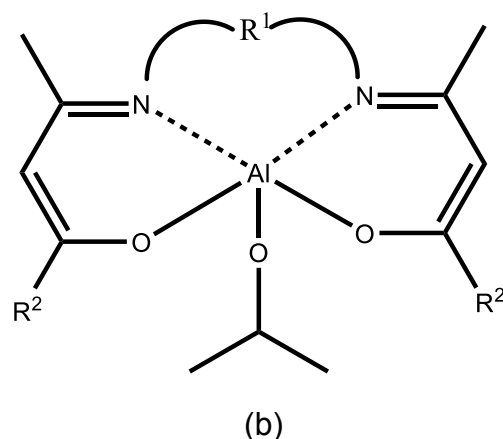
Entry	Cat.	t (h)	$M_n$ (obsd)	$M_n$ (calcd)	Conv. (%)	$M_w/M_n$	$P_i$
1	1	2	7810	12070	83	1.09	0.81
2	1	4	10450	13656	94	1.23	0.84
3	1	6	10600	13858	95	1.26	0.84
4	1	22	11020	13944	96	1.27	0.81
5	2	2	4380	7098	49	1.04	0.69
6	2	4	7110	10629	73	1.05	0.80
7	2	6	8520	12099	83	1.06	0.81
8	2	22	8970	14000	96	1.19	0.81
9	3	2	-	-	86	-	0.74
10	3	4	-	-	92	-	0.77
11	3	6	-	-	94	-	0.79
12	3	22	7850	-	95	1.29	0.81
13	4	2	-	7602	52	-	-
14	4	4	-	10197	70	-	0.82
15	4	6	7800	10918	75	1.03	0.93
16	4	22	8880	13757	94	1.04	0.85
17	9	2	2700	3711	25	1.06	-
18	9	4	4460	5873	40	1.04	0.73
19	9	6	6390	8180	56	1.02	0.73
20	9	22	9050	12790	88	1.02	-

Du *et al.* synthesized a series of dimethyl aluminum complexes (a) bearing chiral bidentate anilido-oxazolinato ligands, and they found that in the presence of benzyl alcohol, these complexes are active initiators for the stereoselective ring-opening polymerization of *rac*-lactide in toluene solution and under bulk conditions, yielding poly(lactic acid) with a range of tacticities from slightly isotactic to moderately heterotactic. Among all the studied complexes and when R = Ph they obtained PLA with the highest isoselectivity. They suggested that the electron-withdrawing ability and the bulkiness of the phenyl group at R<sub>1</sub> may be responsible for the increase in isoselectivity.<sup>56</sup>

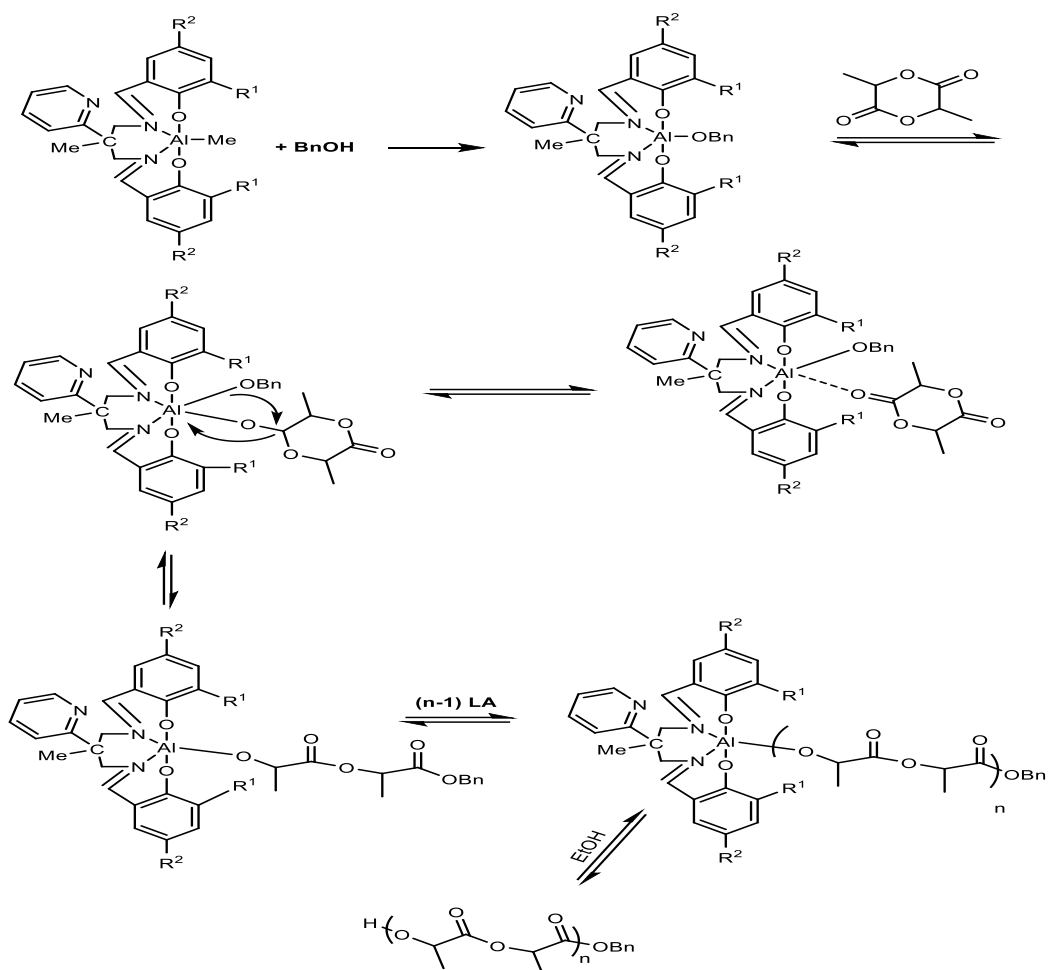


(a)

Jing *et al.* prepared series of enolic Schiff base aluminium complexes (b) containing ligands that differ in their steric and electronic properties. They revealed that introducing electron-withdrawing substituents in the diketone ( $R^2 = CF_3$ ) significantly improved the catalyst activity and the stereoselectivity of the PLA.<sup>57</sup> Gibson *et al.* came to a similar conclusion; they reported that chloro substituents in the phenoxide unit had higher activity and higher stereoselectivity than their dimethyl analogues for salan-type catalysts.<sup>24</sup>



The  $^1\text{H}$  NMR spectrum of the PLA indicated that the polymer chains were end-capped with a benzyl ester and a hydroxyl group,<sup>58</sup> suggesting that the ring-opening occurred through a coordination insertion mechanism<sup>59</sup> as described in Scheme 3.2.



**Scheme 3.2:** proposed mechanism for the ROP of lactide using salen type aluminium benzyloxide complexes

### 3.1.3.4 Aluminium benzyloxy complexes as initiators for the ROP of *rac*-lactide

Complexes [Al(Salpy)(OBn)](**12**), [Al(<sup>t</sup>Bu,<sup>t</sup>Bu-Salpy)(OBn)](**15**), [Al(Naphpy)(OBn) (**17**) and [Al(<sup>t</sup>Bu,OMe-Salpy)(OBn)] (**19**) were tested for the ROP of *rac*-lactide without added BnOH. The same polymerization conditions of the aluminium methyl complexes were applied with benzyloxy complexes. The successful entries are listed in Table 3.9. Maximum conversion was achieved after 2 hours when complexes **12** and **17** were used (Entries 21 and 22). Half the monomer was converted to polymer after 4 hours at 80 °C when complexes **15** and **19** were used (Entries 24 and 32). Many researchers have reported that introducing electron-withdrawing groups leads to enhanced catalyst reactivity, whilst electron-donating groups accordingly reduce catalyst reactivity by reducing the Lewis acidity of the metal centre.<sup>60</sup> Such observations are consistent with the data obtained for these Salpy complexes.

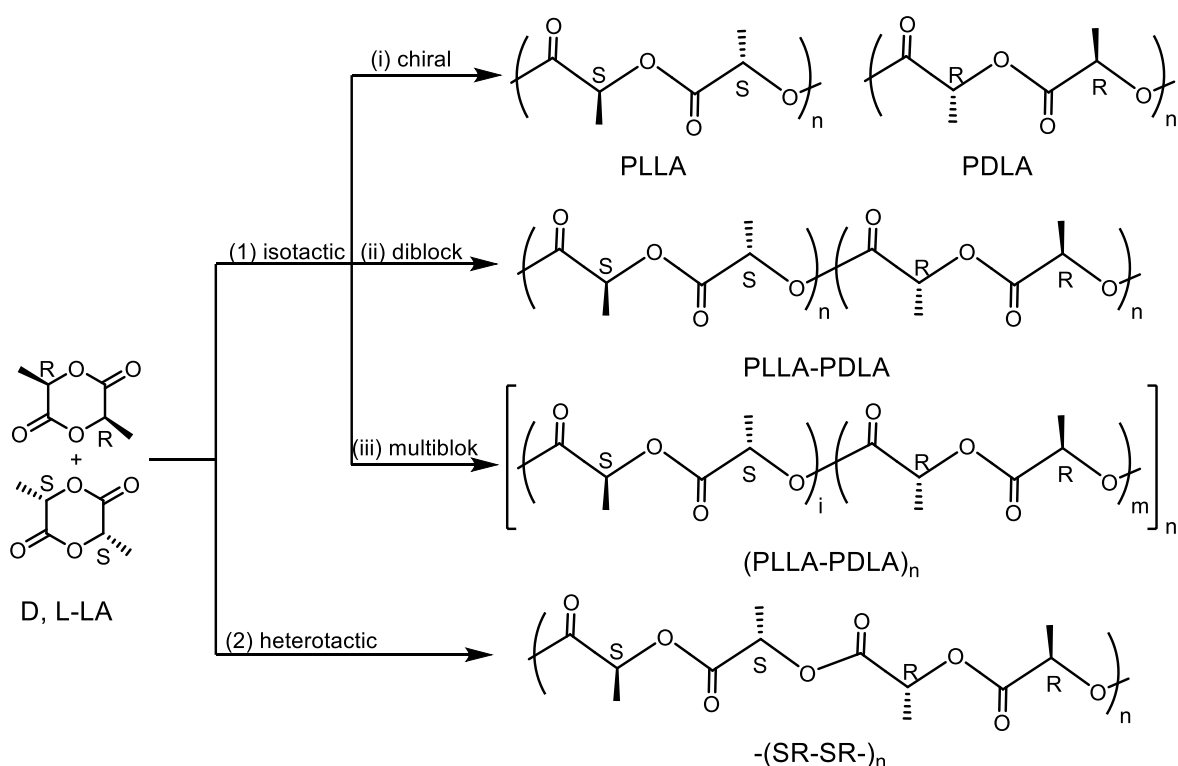
Since the groups in *ortho* position of the phenoxide rings in both **15** and **19** are the same, *tert*-butyl, so the reactivity becomes less in comparison to complexes **12** and **17**, which have only hydrogen in *ortho* position and are therefore less sterically crowded at the metal centre. Regarding the polydispersity indices, both **15** and **19** showed low PDI ranging from (1.00-1.03) which are lower than the values obtained with complexes **12** and **17**. Generally, low PDI values (close to 1.0) correspond to a highly controlled polymerization process.<sup>27,61,62</sup> Duda *et al.* reported that any increase of the bulkiness of ligands of aluminium alkoxide species leads to a suppression of transesterification, hence lower PDI,<sup>63–65</sup> in agreement with the results in this thesis. Although the PLA  $M_n$  values obtained using aluminium methyl complexes in the presence of BnOH was lower than the calculated values, a higher molecular weight than predicted was afforded when aluminium benzyloxy complexes were used, indicating fewer chains are initiated relative to the number of metal centres (some of the catalyst is not involved in propagation);<sup>66</sup> this could suggest that the preparation of a benzyloxy complex *in situ* is incomplete under the activation conditions employed.

**Table 3.9:** Polymerization data of rac-LA using complexes **12**, **15**, **17** and **19**  
at 80 °C in toluene

Entry	Cat.	t (h)	$M_n$ (obsd)	$M_n$ (calcd)	Conv. (%)	$M_w/ M_n$	$P_i$
21	12	2	12580	12294	85	1.13	0.86
22	12	4	15430	13173	91	1.13	0.81
23	12	6	16130	13807	96	1.24	0.86
24	15	4	8660	7206	50	1.03	0.84
25	15	6	12540	8863	62	1.02	0.87
26	15	22	19360	13303	92	1.01	0.92
27	17	1	13690	10293	71	1.08	0.72
28	17	2	18240	13159	91	1.23	0.73
29	17	3	18800	13259	92	1.23	0.69
30	17	4	20284	13951	97	1.28	0.67
31	19	2	7220	4900	34	1.03	0.88
32	19	4	11740	8143	57	1.02	0.82
33	19	6	15690	10449	73	1.01	0.90
34	19	22	27290	13750	95	1.00	0.86

### 3.1.3.5 Stereochemistry of the prepared polylactides

As discussed in Chapter 1, lactide exists as three different stereoisomers: L-lactide, D-lactide and meso-lactide. When D and L lactide are present as a 50:50 mixture, the lactide is called *rac*-LA. If the ring opening polymerization reaction of *rac*-LA occurs via a coordination–insertion mechanism without racemization, the *rac*-LA may produce two ultimate stereoregular patterns, isotactic and heterotactic polymers (Scheme 3.3). The isotactic PLA obtained from *rac*-LA can be divided into three kinds of PLA: i) each polymer molecule is homochiral; ii) a diblock stereocopolymer which is formed when the ROP of one enantiomer of monomer is highly favoured in comparison with ROP of the other enantiomer, resulting in a block copolymer of D-LA and L-LA and iii) a multiblock stereocopolymer. The alternate polyadditions of LLA and DLA produce heterotactic PLA.



**Scheme 3.3:** PLA microstructure obtained from ROP of *rac*-LA via the coordination-insertion mechanism.

The stereochemical microstructures of the PLA samples prepared in this thesis were determined through inspection of the methine group of the homonuclear decoupled  $^1\text{H}$  NMR spectra (Figure 3.24). We anticipate that stereoselectivity in

the polymerization of *rac*-LA takes place via the chain-end control mechanism because all the prepared Schiff base ligands were achiral. Thus, the initiator system will be achiral as well.

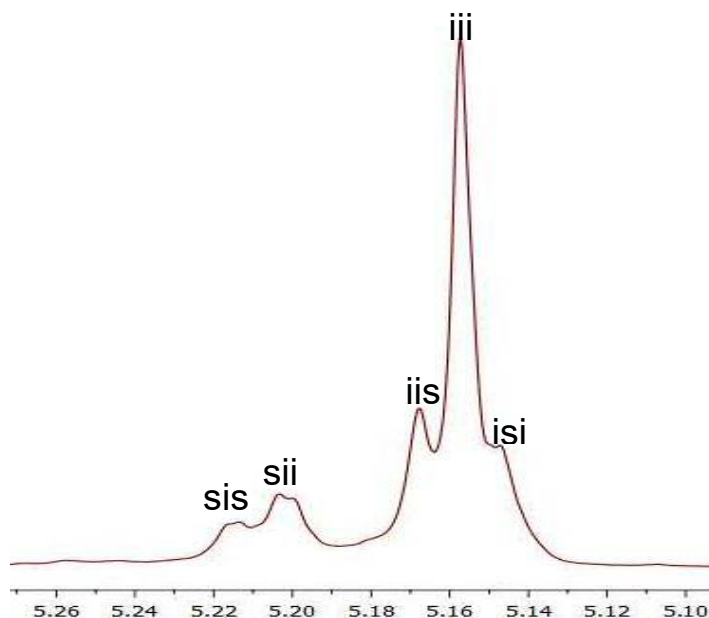


**Figure 3.24:** Methine region of homonuclear decoupled  $^1\text{H}$  NMR spectra of PLA produced using **17** as a catalyst.

The PLA produced with complexes **1–4** and **9** in the presence of BnOH as a cocatalyst, in toluene at 80 °C, are substantially isotactic. The isotactic enrichment represents by  $P_i$ , ranging from 0.69 to 0.93 (Table 3.8, entries 1-20). The ratio of the tetrad signals can be related to *the*  $P_i$  value according to the formulae given in Table 3.10;<sup>67</sup> the tetrads correspond to the stereosequences of PLA shown in Figure 3.25.

**Table 3.10:** probability to form tetrades in polymer chain resulting from ROP of *rac*-Lactide as a function of  $P_i$

Tetrads	iii	isi	iis	sii	sis
Ratio	$P_i(P_i + 1)/2$	$(1 - P_i)/2$	$P_i(1 - P_i)/2$	$P_i(1 - P_i)/2$	$(1 - P_i)^2/2$

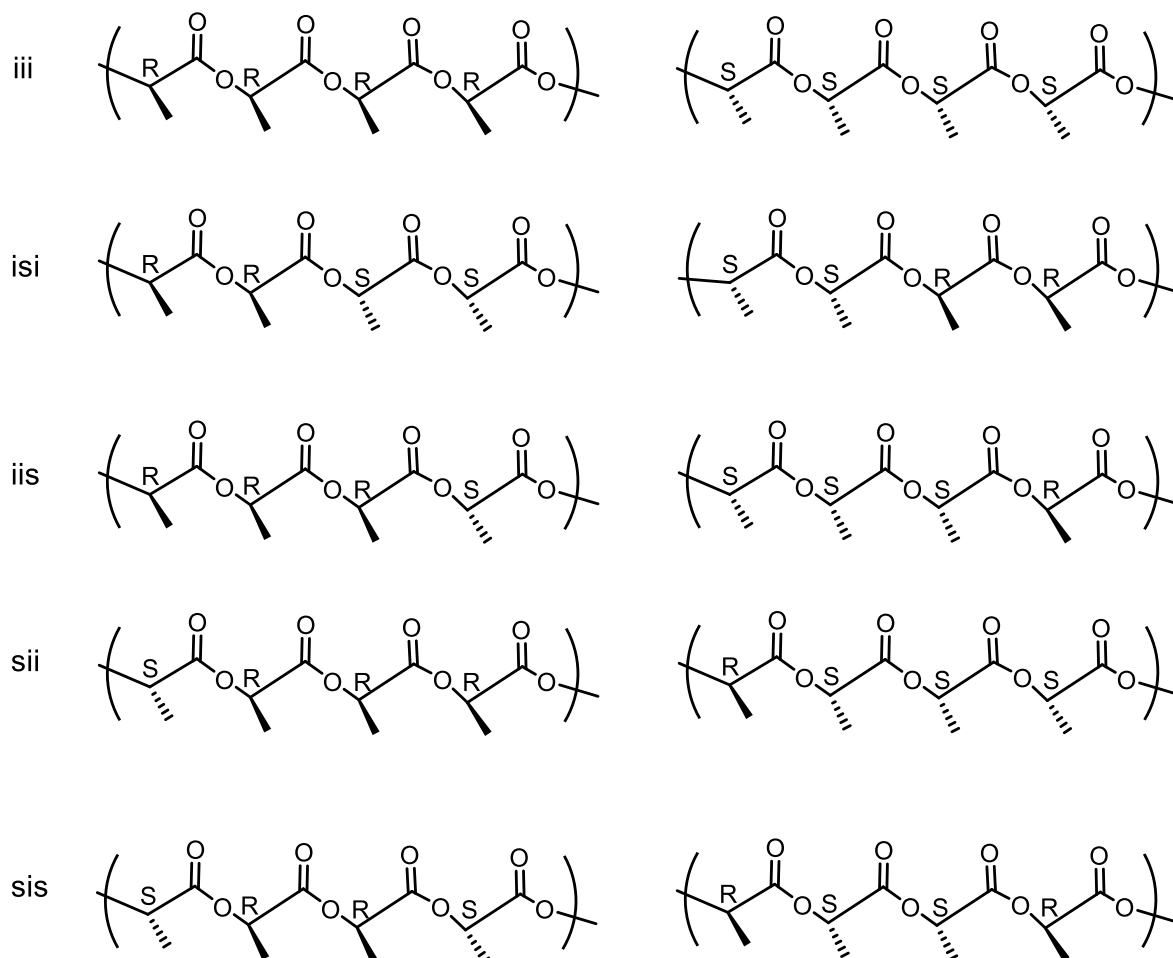


**Figure 3.25:** The tetrads from stereosequences of PLA.

An analysis of the  $P_i$  values indicates that the *ortho*-substituents of the phenoxide rings exert influence on the ability of corresponding catalysts to control monomer insertion. However, a clearer influence was observed when another substituent was introduced on the imine group or phenoxy ring. On comparison of the structures of complexes **1**, **3** and **9** (Figure 3.26), it can be seen that complexes **3** and **9** have a significant effect on the microstructure of the PLA by decreasing the degree of stereocontrol over the polymerization. For instance, changing the phenyl group in complex **1** (Table 3.8, Entry 3,  $P_i = 0.84$ ) to the naphthyl group in complex **3** (Table 3.8, Entry 11) results in a decrease in isotactic bias ( $P_i = 0.79$ ).

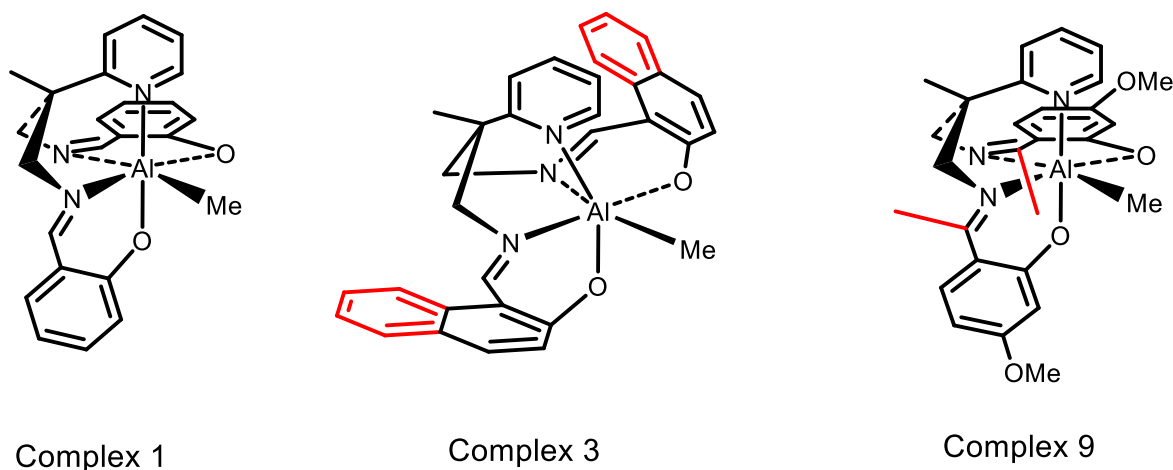


**Figure 3.26:** The structures of complexes **1**, **3** and **9**

The same behaviour was obtained with the pre-prepared benzyloxy complexes; it was found that PLA produced using complex **12** (Table 3.9, Entry 22) ( $P_i = 0.81$ ) had higher isotactic enrichment than the PLA produced using complex **17** (Table 3.9, Entry 30) ( $P_i = 0.67$ ). The methyl group on the imine bond appears to reduce the stereocontrol over the polymerization. Complex **9** gives polymer with  $P_i$  values that are lower than those obtained for complex **1** (see Table 3.8, Entries 1-4, 18 and 19). Some studies suggest that introducing a bulky group in the *ortho* position of the phenyl ring enhance the stereocontrol and increases the  $P_i$  values. They suggested that the sterically demanding groups in the *ortho* positions may block the coordination sphere of the metal centre, thereby restricting the direction of monomer insertion which in turn leads to higher regularity in the PLA microstructure. However, this may also lower the activities of the complexes towards polymerization.<sup>50,58,68</sup>

The methine signals in the  $^1\text{H}$  NMR spectra give a preliminary expectation of the microstructure of the produced PLA. Nomura and co-workers examined two series of substituted catalysts **3.1** and **3.2** (Figure 3.27).<sup>52</sup> They found the order of isotactic selectivity to be **3.1b** < **3.1a** < **3.1c** < **3.1d**  $\leq$  **3.1e**; **3.2b** < **3.2a** < **3.2c** < **3.2d** < **3.2e**, using the methine region of the  $^1\text{H}$  NMR spectra of crude PLA (Figures 3.28 and 3.29).

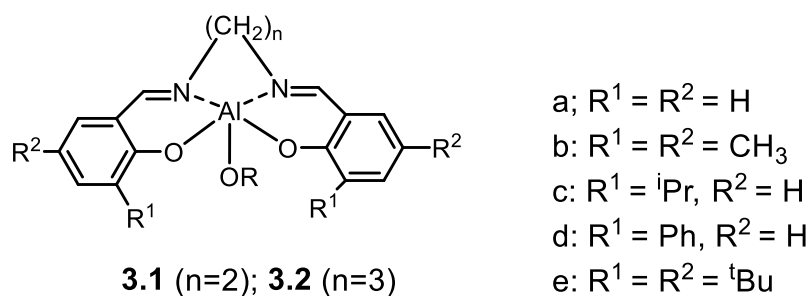


Figure 3.27: Catalysts prepared by Nomura and co-workers for stereoregular PLA

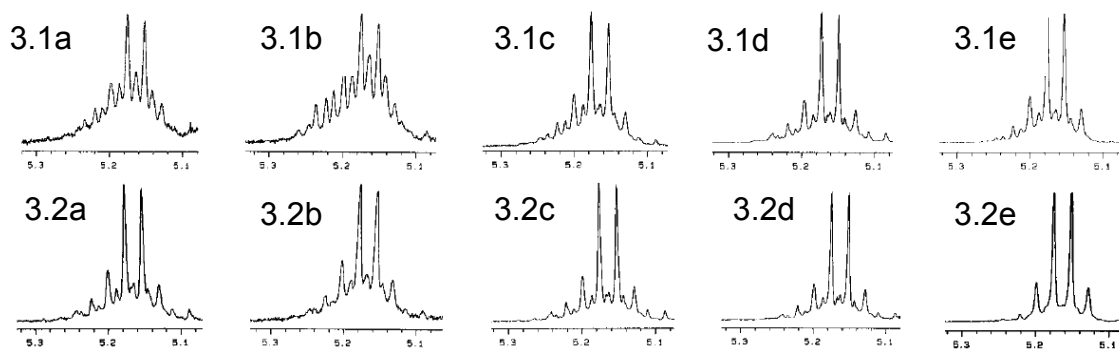


Figure 3.28:  $^1H$  NMR spectra of methine region of crude PLA prepared by Nomura and coworkers

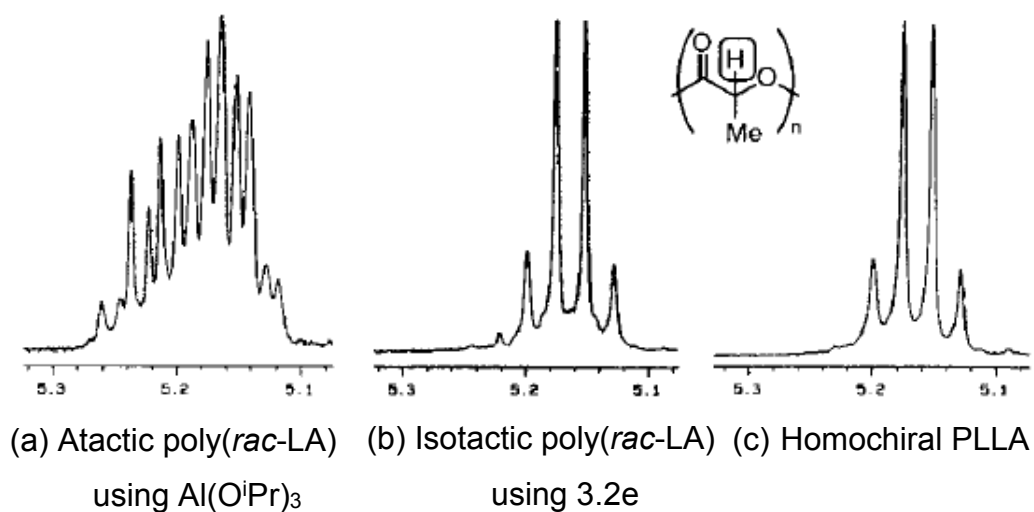
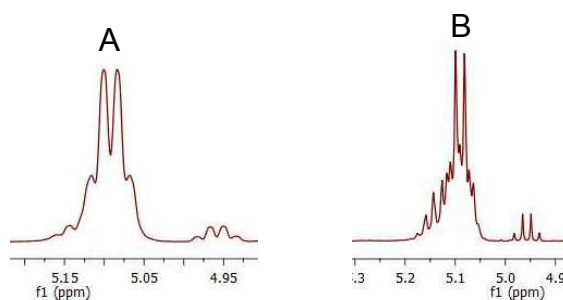


Figure 3.29:  $^1H$  NMR spectra of the methine region of PLA

Figure 3.30 shows the  $^1\text{H}$  NMR spectra of methine region of crude PLA prepared using catalysts **15** (A) and **17** (B) which reveal that the isotactic enrichment of the PLA prepared using **15** is higher than for **17**.



**Figure 3.30:**  $^1\text{H}$  NMR spectra (400 MHz, 293 K,  $\text{CDCl}_3$ ) of the methine region of crude PLA prepared using **15** and **17**

## 3.2 Ring-opening polymerisation using titanium complexes

### 3.2.1 Introduction

Group 4 metal complexes are known to be active in various types of polymerization reaction. For example, titanium complexes have been used for the polymerization of olefins,<sup>69–72</sup> and in the ROP of cyclic esters.<sup>73–77</sup> Recently, metal complexes bearing salen-type ligands have been widely used in ring-opening polymerization of cyclic esters.<sup>78–81</sup> In particular, titanium salen complexes have been widely investigated as initiators for the ROP of cyclic esters.<sup>82–84</sup> Numerous complexes of titanium with varying coordination number were prepared, and evaluated as an initiator for  $\epsilon$ -caprolactone and lactide.

Kostjuk and co-workers prepared a series of complexes affording five and six coordinate titanium complexes, dialkanolamines-titanocanes and spirobititanocanes respectively. Both sets of Ti(IV) complexes were screened for the bulk ROP of  $\epsilon$ -CL in the monomer:initiator ratio 300:1, at 80 °C. they found that the polymerisation of  $\epsilon$ -CL with spirobititanocanes proceeds with lower reaction rate than with titanocanes.<sup>85</sup>

### **3.2.2. General polymerisation procedure**

Titanium complexes, [Ti(Salpy)(O<sup>i</sup>Pr)<sub>2</sub>] (**31**), [Ti(Naphpy)(O<sup>i</sup>Pr)<sub>2</sub>] (**33**), [Ti(<sup>t</sup>Bu,OMe-Salpy)(O<sup>i</sup>Pr)<sub>2</sub>] (**34**), [Ti(<sup>t</sup>Bu,OMe-Salpn)(O<sup>i</sup>Pr)<sub>2</sub>] (**36**) and [Ti(Cl,Cl-Salpy)(O<sup>i</sup>Pr)<sub>2</sub>] (**37**) were studied as initiators for the ROP of  $\epsilon$ -CL. The general procedure of the polymerization was carried in a screw-cap vial equipped with a magnetic stirrer bar. The vial was charged with the initiator solution in toluene (2.5 mL, 0.01 M). The required amount of  $\epsilon$ -CL was added to the reactor, then the reaction vessel was immersed in an oil bath preheated to 80 °C. After 20 hours, aliquots were withdrawn from the flask and subjected to <sup>1</sup>H NMR spectroscopy to determine the conversion. The solution was quenched with a methanolic solution of hydrochloric acid. The solid thus precipitated was washed with hexane, isolated, and dried under reduced pressure to constant weight. The polymerization was conducted at different feed ratios ([CL]:[Ti], Table 3.11). As with the aluminium complexes, the conversion was determined from the ratio of the integral of methylene protons adjacent to the ester oxygen, which were well-separated in the monomer and polymer.

Two types of calculation were made to obtain the theoretical molecular weight, depending on the number of isopropoxide groups that participate in the growing of polymer chains. When titanium isopropoxide complexes initiate the polymerization reaction by only one of the isopropoxide groups the theoretical molecular weight,  $M_n^b$ , is calculated according to the following equation:

$$M(\epsilon\text{-CL}) \times [\epsilon\text{-CL}]_0 / [\text{Ti}]_0 \times \text{conversion}$$

While if the reaction is initiated with both isopropoxide groups attached to the titanium the theoretical molecular weight,  $M_n^a$ , is given by:

$$M(\epsilon\text{-CL}) \times ([\epsilon\text{-CL}]_0 / 2 \times [\text{Ti}]_0) \times \text{conversion}$$

In both cases all the  $M_n$  values obtained from GPC analyses were corrected using Mark-Houwink parameters.

### **3.2.3 Result and discussion**

At 25 °C, all the above complexes were found to be extremely inactive toward the polymerisation of  $\epsilon$ -CL. No conversion was observed after 28 hours, which is in stark contrast with the results obtained for five coordinate titanium isopropoxide complexes; in these cases high monomer conversion at room temperature has been reported.<sup>77,86,87</sup> Considering the polymerization reaction follows the coordination-insertion mechanism, the first step, which is the initiation step, involves the coordination of the monomer to the metal centre; in the case of our complexes this would afford seven-coordinate titanium (IV) intermediates, which are unlikely to be favourable given the relatively small ionic radius of Ti(IV). It should be noted that seven-coordinate Ti(IV) is rare; 358 X-ray structures of seven-coordinate Ti(IV) complexes have been recorded in the Cambridge Structure Database, which is a small number compared to 6 coordinate (3203), 5 coordinate (4195) and 4 coordinate (5435), suggesting that seven coordinate intermediates are unlikely, without invoking forcing conditions.

In contrast to the data obtained at room temperature, high to moderate conversions were obtained by increasing the temperature to 80 °C. It is evidence that activity of six-coordinate titanium complexes in the polymerisation of  $\epsilon$ -CL strongly depends on the polymerization temperature, and that moderately high temperatures are required to overcome a high activation barrier, no doubt originating from the high coordination number of the pre-catalyst complexes.

Liu and co-workers prepared a six coordinate titanium (IV) complexes derived from diamine-bis(benzotriazole phenolate) (DiBTP) ligands. They reported that the  $\epsilon$ -CL conversion initiated by the titanium isopropoxide complex could reach 95% within 40 hours at 110 °C with a monomer-to-initiator ratio of 200/1.<sup>88</sup> These observations are consistent with those reported in this thesis, but the experiments described herein did not require such high temperatures to achieve comparable activities.

The phenol substituents were varied from hydrogen (no substituent), electron donating, and electron withdrawing. The diamine backbone was changed to probe any effect of the pyridyl group on the polymerization reaction.

**Chapter 3 - Ring opening polymerization of  $\epsilon$ -Caprolactone and *rac*-Lactide**

The catalytic activities of **31**, **33**, **34**, **36** and **37** were examined with various equivalents of monomer (Table 3.11). Notably, the number average molecular weights ( $M_n$ ) of PCL increase proportionally to the monomer-to-catalyst ratios. The PDI values in these cases decrease gradually with an increase in the monomer-to-catalyst ratios. Changing the catalyst and the monomer-to-catalyst ratios had a strong effect on the rate of the polymerization, and on the molecular weight of the resulting polymers.

**Table 3.11:** polymerisation of  $\epsilon$ -CL with different  $[\epsilon\text{-CL}]_0:[\text{Ti}]_0$  ratios at 80 °C for 20 h

Entry	Cat.	$[\text{M}]_0:[\text{Ti}]_0$	$M_n$ (obsd)	$M_n^a$ (calcd)	$M_n^b$ (calcd)	Conv. (%)	$M_w/M_n$
1	31	50:1	2780	1908	3816	66.88	1.22
2	31	100:1	3870	3192	6384	55.94	1.18
3	31	150:1	5730	4738	9476	55.35	1.15
4	31	200:1	6920 <sup>c</sup>	5438	10875	47.64	1.15
			6220 <sup>d</sup>				1.06
			9590 <sup>d</sup>				1.07
5	31	250:1	7930 <sup>c</sup>	6677	13354	46.80	1.13
			7090 <sup>d</sup>				1.05
			11610 <sup>d</sup>				1.02
6	31	300:1	8520 <sup>c</sup>	6867	13734	40.11	1.12
			7680 <sup>d</sup>				1.04
			11550 <sup>d</sup>				1.03

**Chapter 3 - Ring opening polymerization of  $\epsilon$ -Caprolactone and rac-Lactide**

7	31	400:1	8300 <sup>c</sup>	7190	14381	31.50	1.10
			7570 <sup>d</sup>				1.04
			11730 <sup>d</sup>				1.03
8	33	50:1	3190	2565	5128	89.87	1.44
9	33	100:1	7660	5230	10459	91.64	1.43
10	33	150:1	10630	7563	15126	88.35	1.36
11	33	200:1	12360	9850	19700	86.30	1.30
12	33	250:1	12730	11291	22582	79.14	1.22
13	33	300:1	13840 <sup>c</sup>	10940	21880	63.09	1.15
			11500 <sup>d</sup>				
			13900 <sup>d</sup>				
14	33	400:1	15180 <sup>c</sup>	14014	28028	61.39	1.14
			12490 <sup>d</sup>				1.02
			13970 <sup>d</sup>				1.00
15	34	50:1	11490	2570	5139	90.06	1.27
16	34	100:1	18.760	5492	10984	96.24	1.21
17	34	150:1	19.380	8396	16793	98.09	1.22
18	34	200:1	20.300	10935	21871	95.81	1.19
19	34	250:1	20.820	13315	26631	93.33	1.19
20	34	300:1	21.900	15756	31512	92.03	1.16
21	34	400:1	23080	19061	38122	83.5	1.20
22	36	50:1	4160	2401	4802	84.15	1.29

**Chapter 3 - Ring opening polymerization of  $\epsilon$ -Caprolactone and rac-Lactide**

23	36	100:1	16.400	5298	10596	92.84	1.24
24	36	150:1	17.720	8203	16407	95.83	1.27
25	36	200:1	18.500	11072	22145	97.01	1.23
26	36	250:1	19.530	13796	27593	96.7	1.21
27	36	300:1	19.910	16407	32814	95.83	1.20
28	36	400:1	21000	19531	39063	85.56	1.18
29	37	50:1	2500	2368	4736	83	1.34
30	37	100:1	7370	5506	11012	96.48	1.32
31	37	150:1	14270	8227	16454	96.11	1.24
32	37	200:1	17590	10946	21892	95.9	1.20
33	37	250:1	20150	13653	27307	95.7	1.15
34	37	300:1	21560	15840	31680	92.52	1.12
35	37	400:1	22158	18650	37300	81.7	1.10

$M_n^a$  calculated from  $M(\epsilon\text{-CL}) \times ([\epsilon\text{-CL}]_0/2 \times [\text{Ti}]_0) \times \text{conversion}$

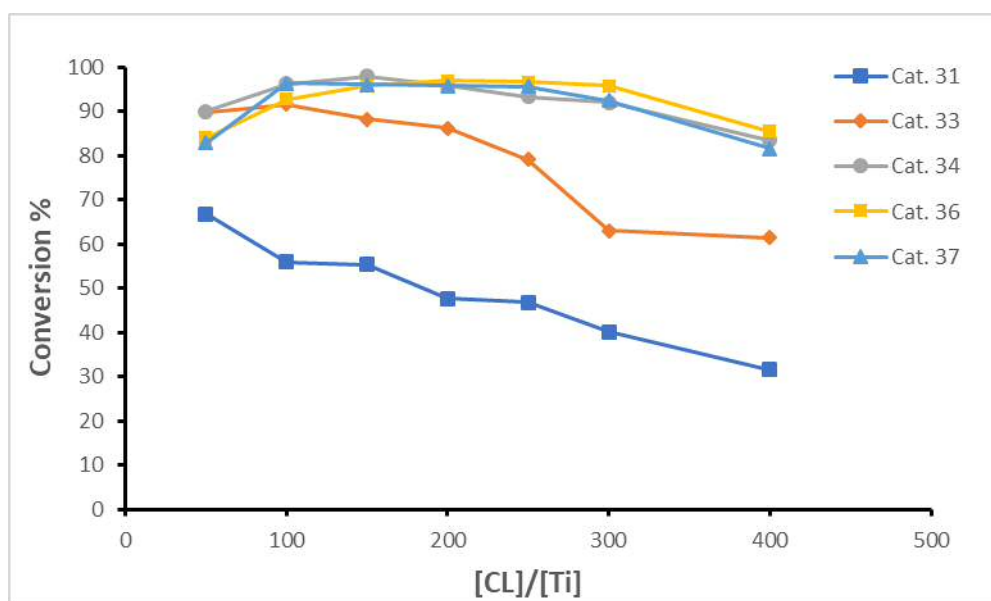
$M_n^b$  calculated from  $M(\epsilon\text{-CL}) \times ([\epsilon\text{-CL}]_0 \times [\text{Ti}]_0) \times \text{conversion}$

<sup>c</sup> Combined values from the GPC data when the peak is bimodal

<sup>d</sup> Deconvoluted values from the GPC data when the peak is bimodal

Interestingly, as we can see from the Table 3.11,  $[\text{Ti}(\text{Salpy})(\text{OiPr})_2]$  (**31**) gave lower conversions compared with the other titanium complexes; only 67% conversion was recorded after 20 hours at 80 °C with a monomer:feed ratio of 50:1 (Entry 1). The quantity of polymer produced increased upon increasing the amount of the monomer, however the percentage conversion decreased, to reach only 32% at a feed ratio of 400:1 (Entry 7) under otherwise identical conditions. If the catalyst were decomposing, thus halting the reaction, then at

400 equivalents one might expect the conversion to be eight times less than at 50 equivalents; the fact that it is higher than this suggests that the catalyst exhibits slow reactivity towards the polymerization, with a slight increase in absolute rate upon increasing the monomer concentration. A similar observation was obtained, albeit with slight differences, with the other complexes probed in this study. An increase in the percentage conversion was observed with an increase in the feed ratio up to 200:1; further increases in the feed ratio gave a reduction in the percentage conversion (Figure 3.31).



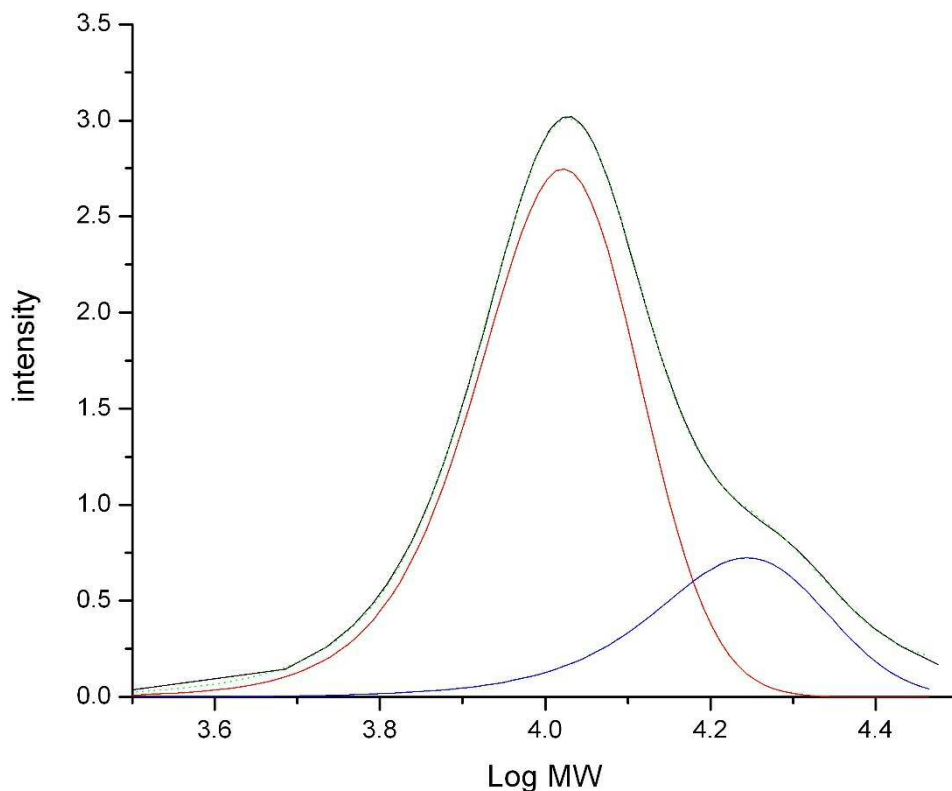
**Figure 3.31:** conversion vs [CL]/[Ti] feed ratio using catalysts **31**, **33**, **34**, **36** and **37** at 80 °C for 20 h.

Figure 3.31 shows that catalysts **34**, **36**, and **37** (i.e. those with alkyl substituents on the phenol) give higher conversion in comparison to those with only hydrogen (phenol, **31**, or naphthol, **33**). The subtle differences between the conversions with catalysts **34**, **36**, and **37** are likely to be within experimental error. The pyridyl group on the ligand backbone appears to have little effect on the polymerization rate, since complexes **34** and **36**, which have identical substituents on the phenoxide rings and differ only in the substituents on the propylene backbone, give essentially identical performances. It is possible that the addition of steric demand on the phenol rings prevents catalyst deactivation (but not necessarily

decomposition, see discussion above), thus increasing the observed conversions, and by inference, the reaction rates.

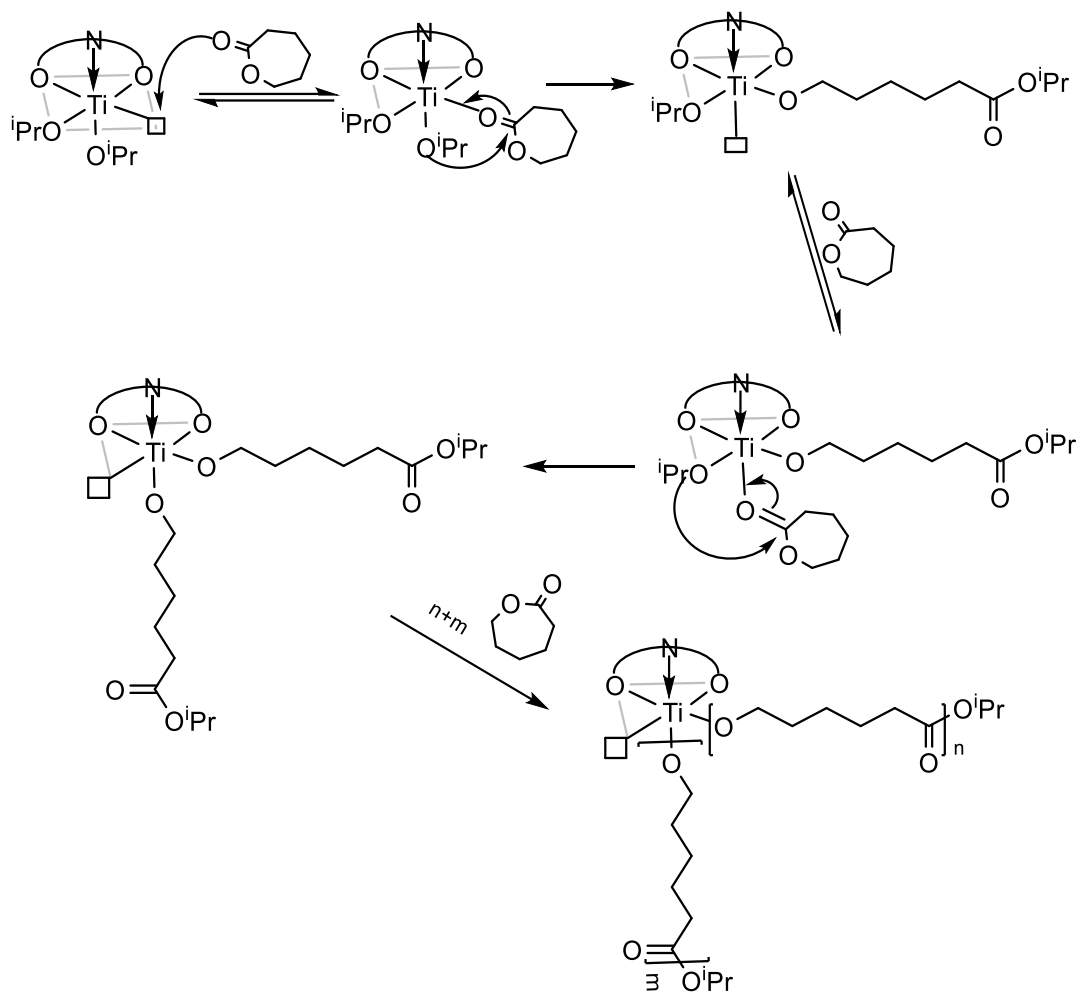
Increasing the feed ratio leads to an increased polymer molecular weight, even when the conversion decreases. As mentioned above, this is because the turnover number (TON) increases, but not proportionately to the increase in feed ratio, hence higher *absolute* conversion but lower *percentage* conversion. The number-average molecular obtained from GPC analyses of PCL prepared with **31** and **33** are close to the calculated  $M_n^a$  values and half the calculated  $M_n^b$  (Table 1), which suggests that each catalyst molecule generates two polymer chains (i.e. one per isopropoxide ligand). The  $M_n$  values obtained using catalyst **34** were higher than expected, entries 15-21, being approximately twice the highest theoretical values (i.e. with one chain per metal) at feed ratios of 50 and 100. At a feed ratio 200:1, the experimental  $M_n$  was close to that expected for one polymer chain per metal. Further increasing the feed ratio resulted in a slight increase in  $M_n$ , but with values that became progressively disparate from the theoretical values. Complex **34** is arguably the most sterically demanding of the catalysts tested, which therefore renders it less likely to obtain two polymer chains per metal centre. In addition, the higher than expected  $M_n$  values indicate that not all of the catalyst is actively participating in the polymerization process, again possibly due to sterics which can prevent effective initiation. A similar, but less pronounced, behaviour to complex **34** was seen for complexes **36** and **37**.

Interestingly, at high feed ratios, catalysts **31** and **33** gave bimodal molecular weight distributions; these have been deconvoluted using the PeakFit software with an exponentially modified gaussian curve. The deconvoluted data are given in Table 3.11, and are depicted in Figure 3.32. Each component was found to possess a low PDI. It is possible that the bimodal molecular weight distribution arises as a result of transesterification processes at high monomer concentrations.



**Figure 3.32** : GPC data obtained for PCL prepared using [Ti(Salpy)(OiPr)<sub>2</sub>] (**31**). Green: combined data; red, blue: deconvoluted curves

Two possible polymerization mechanisms were suggested by Kostjuk and co-workers.<sup>85</sup> The first, suggested for five coordinate titanium complexes, is where the first step involves coordination of  $\epsilon$ -CL to the titanium through a vacant site. The ring-opening of lactone occurs between the acyl-oxygen bond in such a way that the growing chain remains attached to titanium through alkoxide bond, while the alkoxide group of the initiator is moved to the end of the polymer chain. Linear polymers are yielded by continuous coordination and insertion of the monomer (Scheme 3.4).



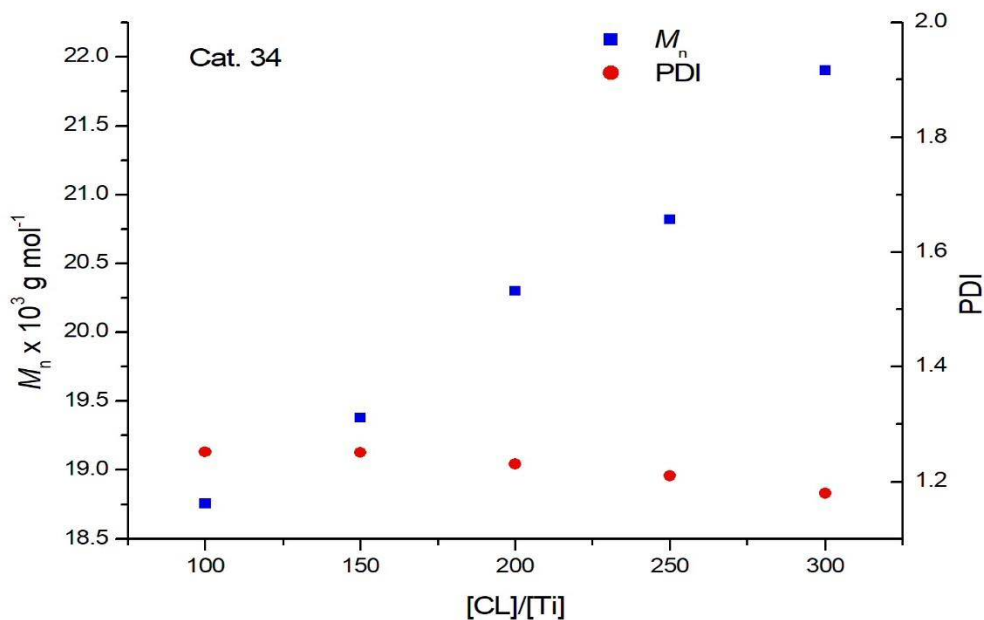
**Scheme 3.4:** suggested mechanism for ROP of  $\epsilon$ -CL using penta-coordinated titanium complexes

For six-coordinate titanium complexes the suggested mechanism involves a reversible formation of penta-coordinated titanium ion, followed by insertion of the first molecule of caprolactone into the Ti-O bond.

The polydispersity index (PDI) decreases gradually with an increase in the feed ratio. Low PDI values refer to greater control (less catalytically active components and less chain-termination events) over the polymerization reaction.

The living manner of the ROP of  $\epsilon$ -CL using **34**, **36** and **37** was supported by the linear relationship between the  $M_n$  and a wide range of feed ratios, and is further supported by narrow polydispersity. The number-average molecular weights ( $M_n$ ) of PCL produced increased proportionally with the monomer:catalyst ratio

(Figures 3.33, 3.34, and 3.35). The PDI values consistently decreased with increasing feed ratio.



e

at 80 °C for 20 h. The plot of  $M_n$  and PDI as a function of  $[\epsilon\text{-CL}]_0/[\text{Ti}]_0$  is shown.

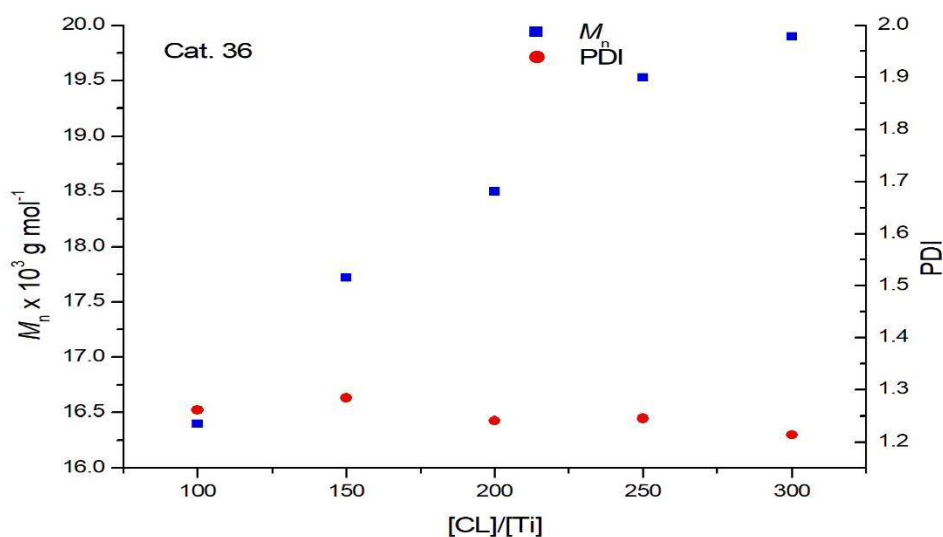


**Figure 3.34:** Polymerization of  $\epsilon$ -CL initiated by titanium complex **36** in toluene at 80 °C for 30 h. The plot of  $M_n$  and PDI as a function of  $[\epsilon\text{-CL}]_0/[\text{Ti}]_0$  is shown.

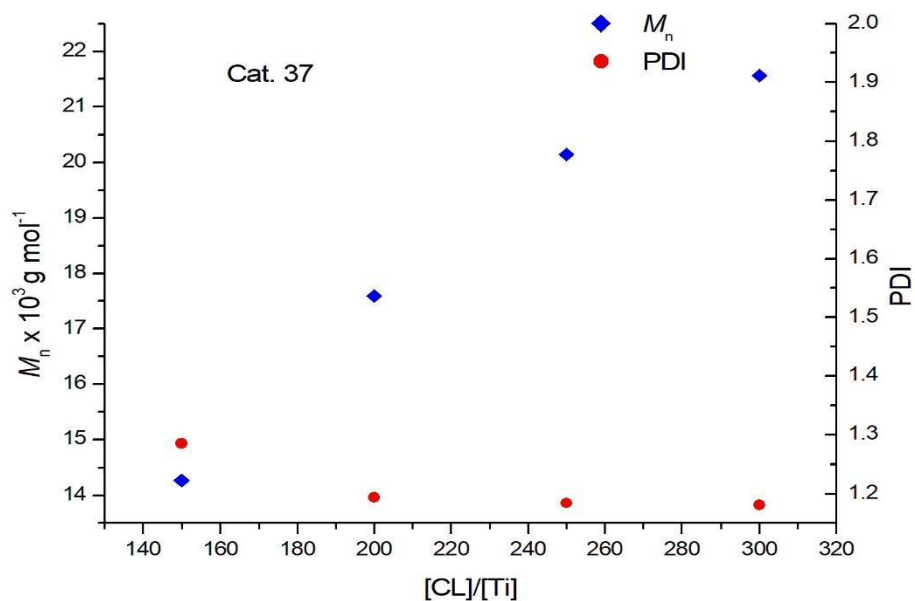


**Figure 3.35:** Polymerization of  $\epsilon$ -CL initiated by titanium complex **37** in toluene at 80 °C for 30 h. The plot of  $M_n$  and PDI as a function of  $[\epsilon\text{-CL}]_0/[\text{Ti}]_0$  is shown.

The polymerization kinetics were studied for complexes **31**, **34**, **36** and **37** with  $[\epsilon\text{-CL}]_0/[\text{Ti}]_0 = 100$  and  $[\text{Ti}] = 0.01 \text{ M}$  at 80 °C using benzene- $d_6$  as solvent. In a nitrogen-filled glove box, both initiator and monomer were dissolved in dry benzene- $d_6$ , and transferred to an NMR tube fitted with J. Young valve. The sample was placed in a preheated oil bath (80 °C) and monitored by  $^1\text{H}$  NMR spectroscopy after the prescribed times. At each data point, the conversion was determined by comparing the integrations of the  $\alpha$ -methylene proton signals of the monomer and polymer (Figure 3.36).

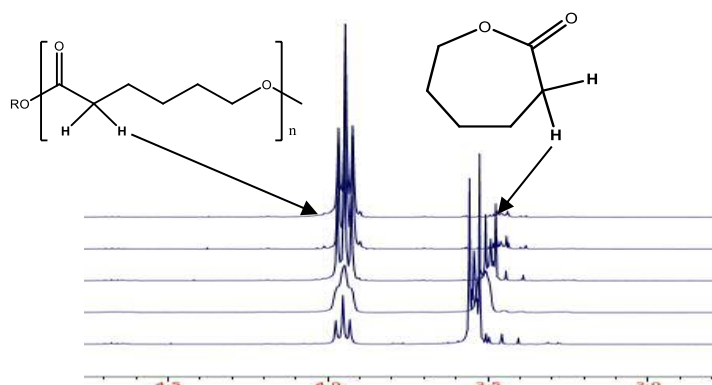


**Figure 3.36:** calculating the conversion of  $\epsilon$ -CL to PCL by monitoring  $^1\text{H}$  NMR spectra of the polymerisation reaction in  $\text{C}_6\text{D}_6$  at 80 °C

Semilogarithmic plots of  $\ln([\epsilon\text{-CL}]_0/[\epsilon\text{-CL}]_t)$  versus reaction time are shown in Figures 3.37, 3.38, 3.39 and 3.40 where  $[\epsilon\text{-CL}]_0$  is the initial lactone monomer concentration and  $[\epsilon\text{-CL}]_t$  the lactone concentration at a given reaction time  $t$ . In the case of catalyst **31**, the plot shows a linear increase with time after an initial induction period, which may indicate a slow initiation of the catalyst. Generally, in all cases, the linearity of the plot shows that the propagation was first order with respect to lactone monomer (Figures 3.37, 3.38, 3.39 and 3.40 ).

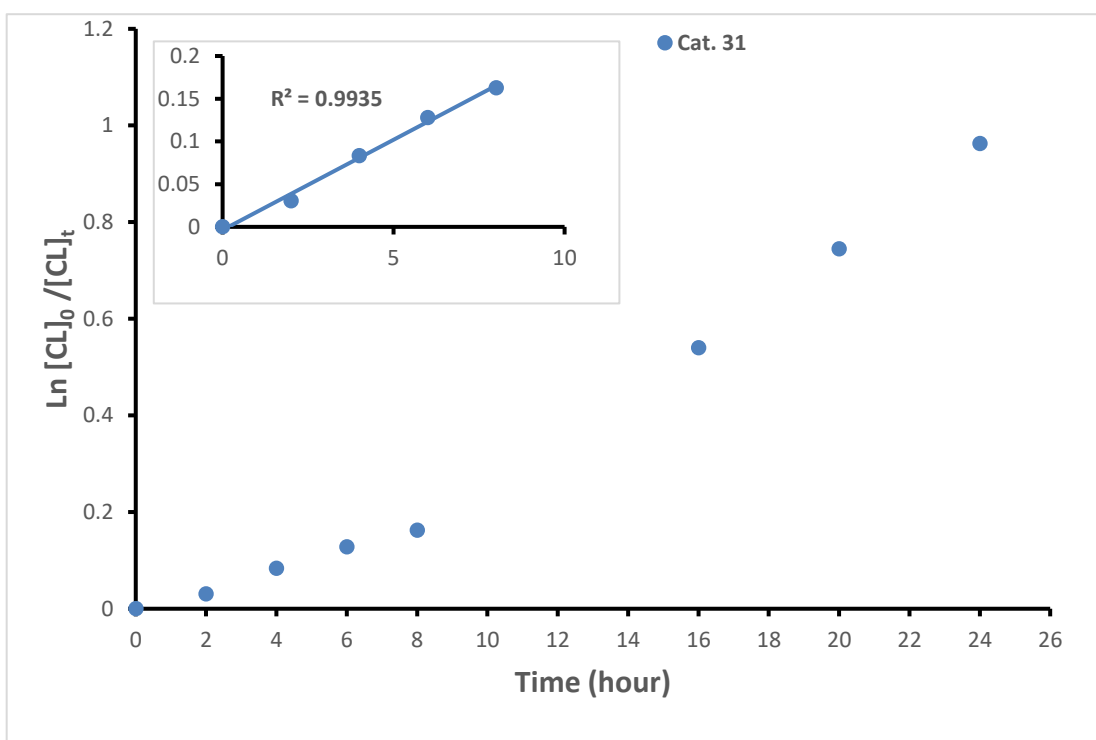


**Figure 3.37:** Plot of  $\ln([CL]_0/[CL]_t)$  vs. time for the polymerization of  $\epsilon$ -CL catalysed by **31**.

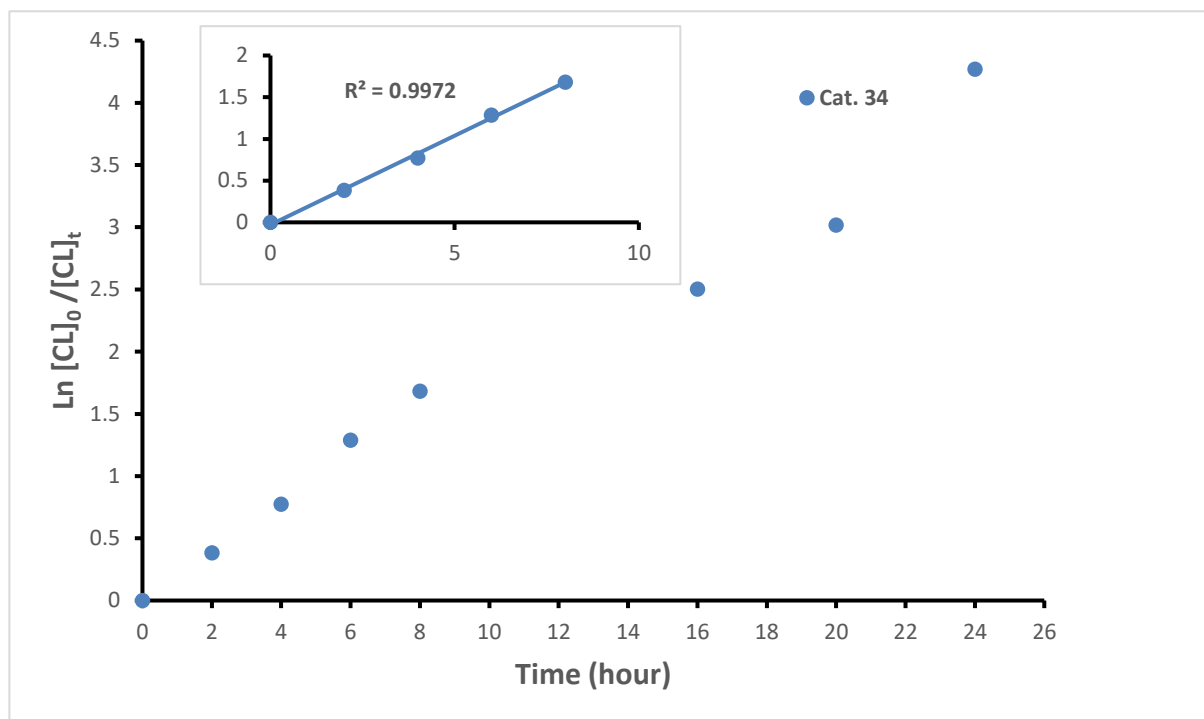


Figure 3.38: Plot of  $\ln([CL]_0/[CL]_t)$  vs. time for the polymerization of  $\epsilon$ -CL catalysed by **34**

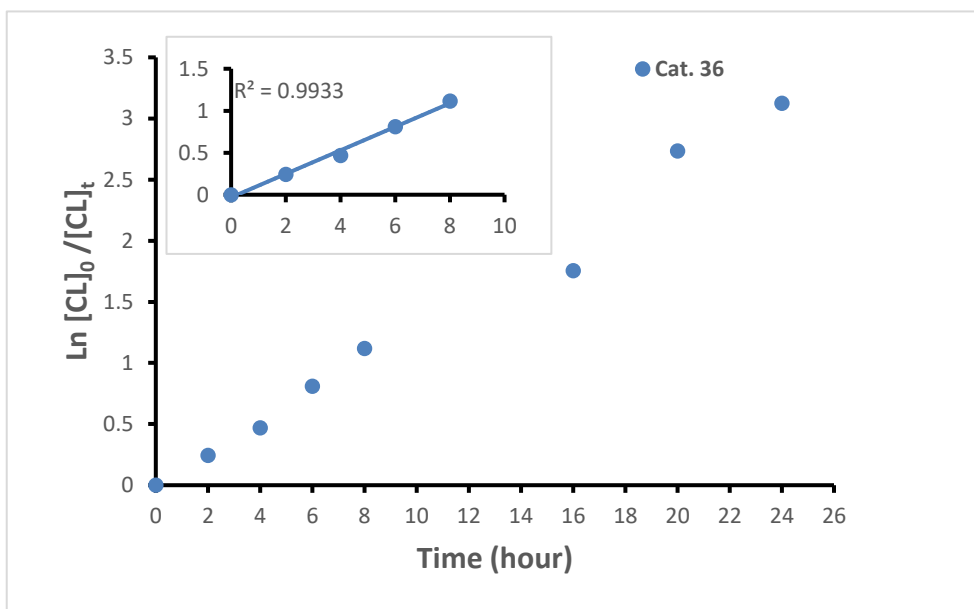
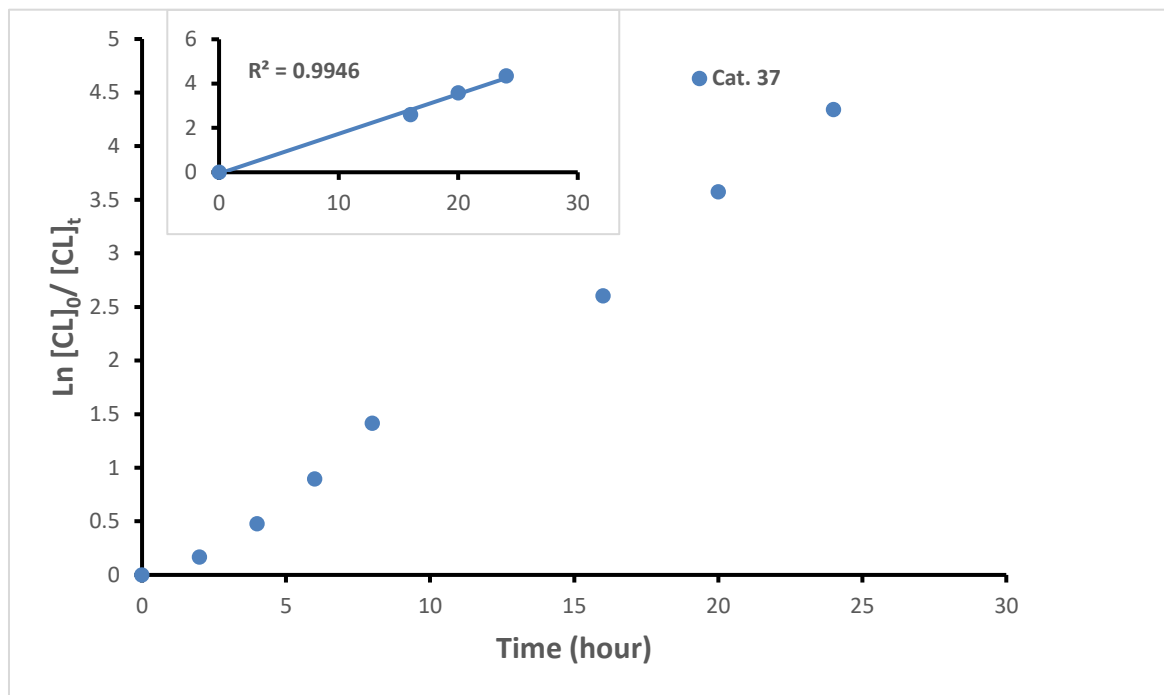


Figure 3.39: Plot of  $\ln([CL]_0/[CL]_t)$  vs. time for the polymerization of  $\epsilon$ -CL catalysed by **36**.



**Figure 3.40:** Plot of  $\ln([CL]_0/[CL]_t)$  vs. time for the polymerization of  $\epsilon$ -CL catalysed by **37**.

The coordination-insertion mechanism dictates that the polymer end groups will correspond to the initiating alkoxide ligand, in this case isopropoxide, and hydroxide (from the quenching procedure). End-group analysis of PCL initiated by these titanium isopropoxide complexes was performed by analyzing the  $^1\text{H}$  NMR spectra of PCL, which show signals corresponding to isopropyl ester (signals f and g) and methylene hydroxy (peak h) chain ends (Figure 3.41), suggesting that ROP was initiated by insertion of the coordinated  $\epsilon$ -CL into the  $\text{Ti}-\text{O}^i\text{Pr}$  bond followed by ring opening to cleave the acyl–oxygen bond for chain propagation, as expected for the coordination-insertion mechanism.

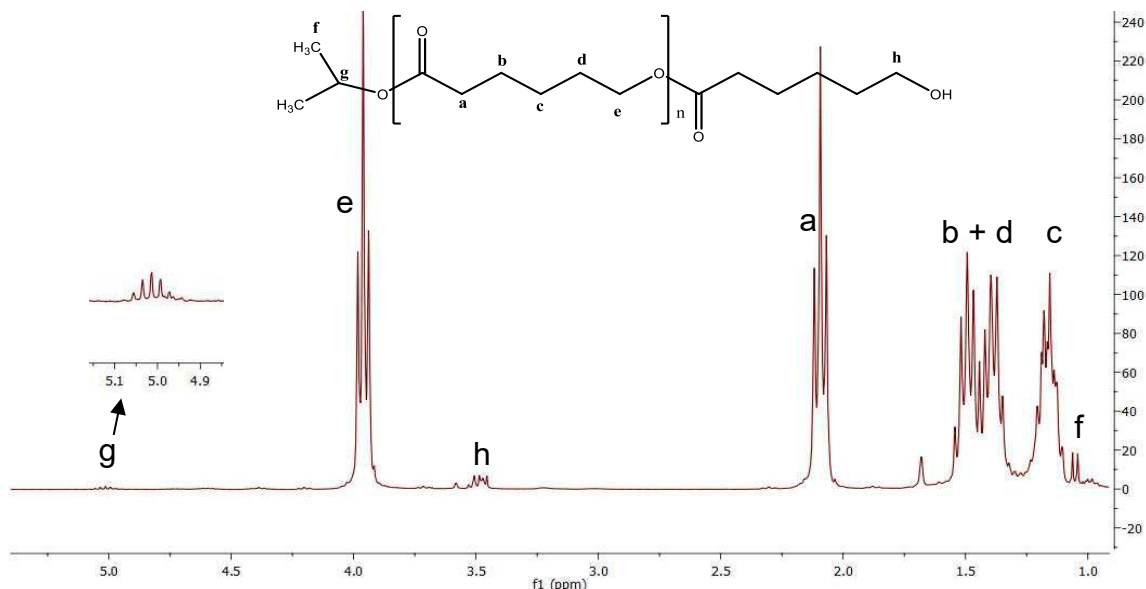


Figure 3.41:  $^1\text{H}$  NMR spectrum of PCL (in  $\text{C}_6\text{D}_6$ ) obtained with **34** at  $80^\circ\text{C}$ .

### 3.3 Conclusions

In this chapter, the efficacy of the Salpy aluminium complexes towards the ring-opening polymerization of cyclic esters has been probed and discussed. In many cases, aluminium has a reputation for giving rather slow reactivity in this manner, but on the contrary, the complexes described herein have been shown to be highly active at room temperature for the polymerization of  $\epsilon$ -caprolactone. On comparison with the pyridyl-free derivative, a subtle but convincing positive effect was attributed to the pyridyl donor, despite the potential for this additional donor to add steric demands to the coordination sphere and to compete with the substrate for metal binding. The complexes were less active in the polymerization of *rac*-lactide, but nevertheless gave competitive activities and with substantial isotactic enrichment to the polymer microstructures. The effect of the co-catalyst was probed; benzyl and isopropyl alcohols were found to be the most active initiating ligands, whereas phenol derivatives were substantially less active. A correlation between the electron-withdrawing or -donating ability of the phenol

initiator group and the activity of the catalyst in the ROP of  $\epsilon$ -caprolactone was observed.

It has also been shown that the Salpy family of ligands are suitable for supporting titanium catalysts for ring-opening polymerization of  $\epsilon$ -caprolactone. Since the titanium is tetravalent, the complexes are 6-coordinate without the intervention of the pyridyl arm, which remains pendant (Chapter 2); the data herein show that the role of this donor in the polymerization reactions is minimal. However, it is noteworthy that the greater the steric demand of the ligand at the phenoxide arm, the greater the catalytic efficacy; ligands based upon salicylaldehyde and hydroxynaphthalene are poorly active in comparison to their substituted congeners. Future studies involving Ti(III) will be an interesting avenue to probe, since this would give the metal ion one less labile initiating ligand and would afford complexes with a comparable coordination sphere to that observed for aluminium, in previous chapters. In such cases, there may be a greater role for the hemilabile pyridyl donor.

### 3.4 References

- 1 K. E. Uhrich, S. M. Cannizzaro, R. S. Langer and K. M. Shakesheff, *Chem. Rev.*, 1999, **99**, 3181–3198.
- 2 M. Shen, Y. Peng, W. Hung and C. Lin, *Dalt. Trans.*, 2009, 9906–9913.
- 3 V. Poirier and T. Roisnel, *Dalt. Trans.*, 2009, 9820–9827.
- 4 M. H. Chisholm, J. C. Gallucci and K. Phomphrai, *Inorg. Chem.*, 2005, **44**, 8004–8010.
- 5 M. H. Chisholm, J. C. Gallucci and K. Phomphrai, *Inorg. Chem.*, 2004, **43**, 6717–6725.
- 6 S. Ho, C. Hsiao, A. Datta, C. Hung and L. Chang, *Inorg. Chem.*, 2013, **48**, 8004–8011.
- 7 L. Piao, M. Deng, X. Chen, L. Jiang and X. Jing, *Polymer (Guildf.)*, 2003,

- 44**, 2331–2336.
- 8 R. R. Gowda, D. Chakraborty and V. Ramkumar, *Eur. J. Inorg. Chem.*, 2009, 2981–2993.
- 9 F. Gornshtein, M. Kapon, M. Botoshansky, M. S. Eisen and R. V August, *Org. Lett.*, 2007, **26**, 497–507.
- 10 L. Postigo, S. Javier, P. Royo and M. E. G. Mosquera, *Dalt. Trans.*, 2009, 3756–3765.
- 11 C. Cai, A. Amgoune, W. Lehmann, J. Carpentier, U. M. R. C. De Rennes, I. D. C. De Rennes, R. Cedex, F. E-mail, M. Kohlenforschung and M. Ruhr, *Chem. Commun.*, 2004, 330–331.
- 12 R. H. Platel, A. J. P. White and C. K. Williams, *Inorg. Chem.*, 2008, **47**, 6840–6849.
- 13 H. Ma and J. Okuda, *Macromolecules*, 2005, **38**, 2665–2673.
- 14 B. J. O. Keefe, L. E. Breyfogle, M. A. Hillmyer and W. B. Tolman, *J. Am. Chem. Soc.*, 2002, **124**, 4384–4393.
- 15 M. Chen, H. Sun, W. Li, Z. Wang, Q. Shen and Y. Zhang, *J. Organomet. Chem.*, 2006, **691**, 2489–2494.
- 16 B. M. Chamberlain, M. Cheng, D. R. Moore, T. M. Ovitt, E. B. Lobkovsky, G. W. Coates, C. U. V, N. York, V. Recci and V. No, *J. Am. Chem. Soc.*, 2001, **123**, 3229–3238.
- 17 H. Chen, B. Huang and C. Lin, *Macromolecules*, 2005, **38**, 5400–5405.
- 18 A. P. Dove, V. C. Gibson, E. L. Marshall, H. S. Rzepa, A. J. P. White and D. J. Williams, *J. Am. Chem. Soc.*, 2006, **128**, 9834–9843.
- 19 N. Nimitsiriwat, V. C. Gibson, E. L. Marshall and M. R. J. Elsegood, *Inorg. Chem.*, 2008, **47**, 5417–5424.
- 20 N. Lu, Z. Jiang, H. Pei, W. Liu, Y. Li and Y. Dong, *Eur. J. Inorg. Chem.*, 2017, 1320–1327.

**Chapter 3 - Ring opening polymerization of  $\epsilon$ -Caprolactone and rac-Lactide**

- 21 A. Pilone, N. De Maio, K. Press, V. Venditto and M. Lamberti, *Dalt. Trans.*, 2015, **44**, 2157–2165.
- 22 K. Bakthavachalam, A. Rajagopal and N. D. Reddy, *Dalt. Trans.*, 2014, **43**, 14816–14823.
- 23 E. D. Cross, L. E. N. Allan, A. Decken and M. P. Shaver, *J. Polym. Sci. Part A Polym. Chem.*, 2013, **51**, 1137–1146.
- 24 P. Hormnirun, E. L. Marshall, V. C. Gibson, A. J. P. White, D. J. Williams, I. C. London, S. K. Campus and L. Sw, *J. Am. Chem. Soc.*, 2004, **126**, 2688–2689.
- 25 H. Du, A. H. Velders, P. J. Dijkstra and J. Sun, *Chem. Eur. J.*, 2009, **15**, 9836–9845.
- 26 P. Mckeown, M. G. Davidson, G. Kociok-ko and M. D. Jones, *Chem. Commun.*, 2016, **52**, 10431–10434.
- 27 J. S. Klitzke, T. Roisnel, E. Kirillov, O. D. L. Casagrande and J. F. Carpentier, *Organometallics*, 2014, **33**, 5693–5707.
- 28 M. Bouyahyi, E. Grunova, N. Marquet, E. Kirillov, C. M. Thomas and T. Roisnel, *Organometallics*, 2008, **27**, 5815–5825.
- 29 F. Ge, Y. Dan, Y. Al-khafaji, T. J. Prior, L. Jiang, M. R. J. Elsegood and C. Redshaw, *RSC Adv.*, 2016, **6**, 4792–4802.
- 30 A. Otero, A. Lara-Sánchez, J. Fernández-Baeza, C. Alonso-Moreno, J. A. Castro-Osma, I. Márquez-Segovia, L. F. Sánchez-Barba, A. M. Rodríguez and J. C. Garcia-Martinez, *Organometallics*, 2011, **30**, 1507–1522.
- 31 S. Rojas, D. Osorio and A. Otero, *J. Polym. Sci. Part A Polym. Chem.*, 2017, **55**, 2397–2407.
- 32 D. Li, Y. Peng, C. Geng, K. Liu and D. Kong, *Dalt. Trans.*, 2013, **42**, 11295–11303.
- 33 J. Liu and H. Ma, *J. Polym. Sci. Part A Polym. Chem.*, 2014, **52**, 3096–3106.

**Chapter 3 - Ring opening polymerization of  $\epsilon$ -Caprolactone and rac-Lactide**

- 34 D. A. Links, *Dalt. Trans.*, 2011, **40**, 2645–2653.
- 35 L. Mata-mata and J. A. Gutie, *J. Polym. Sci. Part A Polym. Chem.*, 2006, **44**, 6926–6942.
- 36 Y. Tai, C. Li, C. Lin, Y. Liu, B. Ko and Y. Sun, *J. Polym. Sci. Part A Polym. Chem.*, 2011, **49**, 4027–4036.
- 37 E. L. Marshall, V. C. Gibson and H. S. Rzepa, *J. Am. Chem. Soc.*, 2005, **127**, 6048–6051.
- 38 A. P. Dove, V. C. Gibson, E. L. Marshall, H. S. Rzepa, A. J. P. White and D. J. Williams, *J. Am. Chem. Soc.*, 2006, **128**, 9834–9843.
- 39 M. H. Chisholm, J. C. Gallucci, K. T. Quisenberry and Z. Zhou, *Inorg. Chem.*, 2008, **47**, 2613–2624.
- 40 K. Ding, M. O. Miranda, B. Moscato-Goodpaster, N. Ajellal, L. E. Breyfogle, E. D. Hermes, C. P. Schaller, S. E. Roe, C. J. Cramer, M. A. Hillmyer and W. B. Tolman, *Macromolecules*, 2012, **45**, 5387–5396.
- 41 Y. C. Liu, B. T. Ko and C. C. Lin, *Macromolecules*, 2001, **34**, 6196–6201.
- 42 P. a Cameron, D. Jhurry, V. C. Gibson, A. J. P. White, D. J. Williams and S. Williams, *Macromol. Rapid Commun.*, 1999, **20**, 616–618.
- 43 B.-T. Ko and C.-C. Lin, *Macromolecules*, 1999, **32**, 8296–8300.
- 44 H. Chen, B. Ko, B. Huang and C. Lin, *Organometallics*, 2001, **20**, 5076–5083.
- 45 D. Jhurry and N. Spassky, *Polym. Bull.*, 2000, **44**, 31–38.
- 46 N. Ikpo, S. M. Barbon, M. W. Drover, L. N. Dawe and F. M. Kerton, *Organometallics*, 2012, **31**, 8145–8158.
- 47 R. T. Morrison and R. N. Boyd, *Organic Chemistry*, Prentice Hall, Englewood Cliffs, NJ, 6th. ed., 1992.
- 48 S. Hermanová, M. M. M. Cabrera, Z. Vyroubalová and L. Vojtová, *Polym. Bull.*, 2011, **67**, 1751–1760.

**Chapter 3 - Ring opening polymerization of  $\epsilon$ -Caprolactone and rac-Lactide**

- 49 E. E. Marlier, J. A. MacAranas, D. J. Marell, C. R. Dunbar, M. A. Johnson, Y. DePorre, M. O. Miranda, B. D. Neisen, C. J. Cramer, M. A. Hillmyer and W. B. Tolman, *ACS Catal.*, 2016, **6**, 1215–1224.
- 50 H. Du, X. Pang, H. Yu, X. Zhuang, X. Chen, D. Cui, X. Wang and X. Jing, *Macromol. Rapid Commun.*, 2007, **40**, 1904–1913.
- 51 N. Nomura, R. Ishii, Y. Yamamoto and T. Kondo, *Chem. - A Eur. J.*, 2007, **13**, 4433–4451.
- 52 N. Nomura, R. Ishii, M. Akakura and K. Aoi, *J. Am. Chem. Soc.*, 2002, **124**, 5938–5939.
- 53 Z. Tang, X. Chen, X. Pang, Y. Yang, X. Zhang and X. Jing, *Biomacromolecules*, 2004, **5**, 965–970.
- 54 J. Wu, X. Pan, N. Tang and C. C. Lin, *Eur. Polym. J.*, 2007, **43**, 5040–5046.
- 55 S. Tabthong, T. Nanok, P. Sumrit, P. Kongsaree, S. Prabpai, P. Chuawong and P. Hormnirun, *Macromolecules*, 2015, **48**, 6846–6861.
- 56 S. Bian, S. Abbina, Z. Lu, E. Kolodka and G. Du, *Organometallics*, 2014, **33**, 2489–2495.
- 57 X. Pang, H. Du, X. Chen, X. Wang and X. Jing, *Chem. - A Eur. J.*, 2008, **14**, 3126–3136.
- 58 F. Qian, K. Liu and H. Ma, *Dalt. Trans.*, 2010, **39**, 8071–8083.
- 59 D. Cheshmedzhieva, I. Angelova, S. Ilieva, G. S. Georgiev and B. Galabov, *Comput. Theor. Chem.*, 2012, **995**, 8–16.
- 60 U. Herber, K. Hegner, D. Wolters, R. Siris, K. Wrobel, A. Hoffmann, C. Lochenie, B. Weber, D. Kuckling and S. Herres-pawlis, *Eur. J. Inorg. Chem*, 2017, 1341–1354.
- 61 D. J. Darensbourg and O. Karroonnirun, *Inorg. Chem.*, 2010, **49**, 2360–2371.

**Chapter 3 - Ring opening polymerization of  $\epsilon$ -Caprolactone and rac-Lactide**

- 62 M. Hsiao, G. Wu, B. Huang and C. Lin, *Inorg. Chem. Commun.*, 2013, **36**, 90–95.
- 63 T. Biela, A. Kowalski, J. Libiszowski and A. Duda, *Makromol. Chem., Macromol. Symp.*, 2006, **240**, 47–55.
- 64 S. Penczel, A. Duda and S. Slomkowski, *Makromol. Chem., Macromol. Symp.*, 1992, **54/55**, 31–40.
- 65 J. Baran, A. Duda, A. Kowalski, R. Szymanski and S. Penczek, *Makromol. Chem., Macromol. Symp.*, 1997, **123**, 93–101.
- 66 P. Mckeown, J. Brown-humes, M. G. Davidson, M. F. Mahon, T. J. Woodman and M. D. Jones, *Dalt. Trans.*, 2017, **46**, 5048–5057.
- 67 J. Coudane, G. Schwach and M. Vert, *J. Polym. Sci. Part A Polym. Chem.*, 1997, **35**, 1651–1658.
- 68 S. Gong and H. Ma, *Dalt. Trans.*, 2008, 3345–3357.
- 69 M. K. Panda, S. Kaur, A. R. Reddy, M. M. Shaikh, R. J. Butcher, V. Gupta and P. Ghosh, *Dalton Trans.*, 2010, **39**, 11060–8.
- 70 D. Shoken, M. Sharma, M. Botoshansky, M. Tamm and M. S. Eisen, *J. Am. Chem. Soc.*, 2013, **135**, 12592–12595.
- 71 M. Sharma, H. S. Yameen, B. Tumanskii, S. Filimon, M. Tamm and M. S. Eisen, *J. Am. Chem. Soc.*, 2012, **134**, 17234–17244.
- 72 M. Bia and E. Bisz, *J Polym Res*, 2013, **164**, 1–9.
- 73 Y. Sarazin, R. H. Howard, D. L. Hughes, S. M. Humphrey and M. Bochmann, *Dalt. Trans.*, 2006, 340–350.
- 74 B. Gao, X. Li, R. Duan and X. Pang, *New J. Chem.*, 2015, **39**, 2404–2408.
- 75 C. Li, C. Yu and B. Ko, *Organometallics*, 2013, **32**, 172–180.
- 76 H. Tseng, H. Chen, Y. Huang, W. Lu, Y. Chang, M. Y. Chiang, Y. Lai and H. Chen, *Inorg. Chem.*, 2016, **55**, 1642–1650.

**Chapter 3 - Ring opening polymerization of  $\epsilon$ -Caprolactone and rac-Lactide**

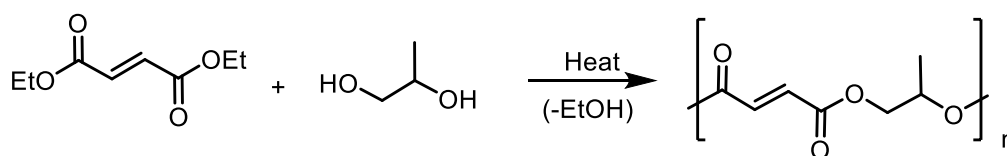
- 77 D. Takeuchi, T. Nakamura and T. Aida, *Macromolecules*, 2000, **33**, 725–729.
- 78 C. Agatemor, A. E. Arnold, E. D. Cross, A. Decken and M. P. Shaver, *J. Organomet. Chem.*, 2013, **745–746**, 335–340.
- 79 D. J. Darensbourg, O. Karroonnirun and S. J. Wilson, *Inorg. Chem.*, 2011, **50**, 6775–6787.
- 80 P. Hormnirun, E. L. Marshall, V. C. Gibson, R. I. Pugh and A. J. P. White, *Proc. Natl. Acad. Sci. U. S. A.*, 2006, **103**, 15343–8.
- 81 B. Gao, D. Li, Y. Li, Q. Duan, R. Duan and X. Pang, *New J. Chem.*, 2015, **39**, 4670–4675.
- 82 X. C. X. Pang, R Duan, X. Li, *Polym. Chem.*, 2014, **5**, 3894–3900.
- 83 C. K. A. Gregson, I. J. Blackmore, V. C. Gibson, N. J. Long, E. L. Marshall and A. J. P. White, *Dalt. Trans.*, 2006, 3134–3140.
- 84 R. Duan, Z. Qu, X. Pang, Y. Zhang, Z. Sun and H. Zhang, *Chin. J. Chem.*, 2017, **35**, 640–644.
- 85 Y. A. Piskun, I. V Vasilenko, S. V Kostjuk, K. V Zaitsev and G. S. Zaitseva, *J. Polym. Sci. Part A Polym. Chem.*, 2010, **48**, 1230–1240.
- 86 L. Liang, S. Lin and C. Chien, *Inorg. Chem.*, 2013, **52**, 1780–1786.
- 87 Y. Takashima, Y. Nakayama and T. Hirao, *J. Organomet. Chem.*, 2004, **689**, 612–619.
- 88 Z. Liu, C. Li, J. Chen, W. Liu, C. Tsai and B. Ko, *J. Mol. Struct.*, 2017, **1134**, 395–403.

# **Chapter 4**

## **Copolymerization of Epoxides with Cyclic Anhydrides**

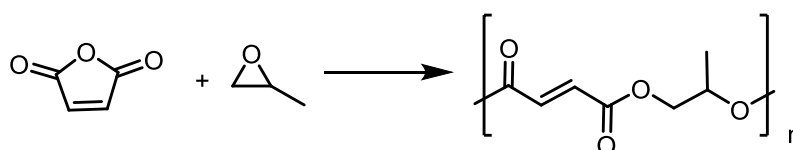
## 4.1 Introduction

Polyesters are commonly produced by the condensation polymerization of diacids or diesters with diols.<sup>1</sup> This type of polymerization is called step-growth polymerization; an example is the preparation of poly(propylenefumarate) by the condensation of propylene glycol and diethyl fumarate (Equation 4.1).<sup>2</sup> However, this method of producing polyesters requires high energy input; high temperature and long reaction times are commonplace. To afford high molecular weight polymers, the alcohol or water byproduct needs to be removed during the reaction.<sup>3</sup>



**Equation 4.1:** step-growth polymerization

Many of the disadvantages of step-growth routes could be circumvented via catalytic chain-growth copolymerization, which requires milder conditions and provides the polymer with higher  $M_n$ ; in addition this method is much more atom efficient.<sup>4</sup> An example of this type of polymerization is the reaction of cyclic anhydrides and epoxides, such as propylene oxide (PO) and cyclohexene oxide (CHO) (Equation 4.2).<sup>5-9</sup>



**Equation 4.2:** chain-growth polymerization

The third important method for the production of aliphatic polyesters is the ring-opening polymerization of cyclic esters. The ROP of cyclic esters, especially caprolactone and lactide, has been studied extensively. A wide range of initiators, including metal alkoxides and various metal complexes, have been explored, and was the subject of Chapter 3.<sup>10-17</sup>

## Chapter 4 - Copolymerization of Epoxides with Cyclic Anhydrides

The copolymerization of oxiranes (epoxides) with carbon dioxide or anhydrides, using organometallic compounds, was reported for the first time approximately 50 years ago by Inoue and co-workers.<sup>18</sup> The formation of polycarbonate by the copolymerization of epoxides with carbon dioxide, or the formation of polyesters by the copolymerization of epoxide with anhydrides, has attracted significant attention during recent years.<sup>19–22</sup> The majority of copolymerization research has focused on PO and CHO; other epoxides have received much less attention, for instance styrene oxide (SO) is less reactive than CHO and PO and it is hard to convert to polycarbonate when reacting with carbon dioxide. The less reactive  $\beta$ -carbon and the tendency to form the cyclic styrene carbonate is the main reason for its lower reactivity;<sup>23–26</sup> the lack of success in CO<sub>2</sub>-copolymerization is possibly why it has also been less studied for copolymerization with anhydrides.

A variety of metal complexes have been used as catalysts for the copolymerization of epoxides and anhydrides. Examples have been based upon chromium,<sup>27–30</sup> cobalt,<sup>9,31,32</sup> magnesium,<sup>32,33</sup> zinc,<sup>19,32–36</sup> and aluminium.<sup>29,37–42</sup> Most of these catalysts are based upon salen (**4.1**) and porphyrin (**4.2**) architectures (Figure 4.1).

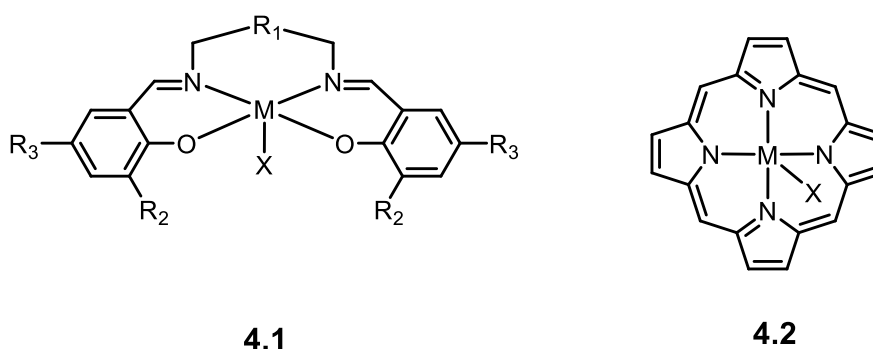


**Figure 4.1:** Salen and Porphyrin catalysts

Coates and co-workers reported that  $\beta$ -diketiminato zinc acetate [(BDI)ZnOAc] catalysts (**4.3**) (Figure 4.2) are effective catalysts for the copolymerization of a

number of epoxides and cyclic anhydrides.<sup>3</sup> The same catalysts had previously been used for epoxide/CO<sub>2</sub> copolymerization.

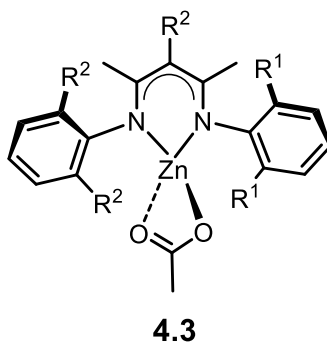
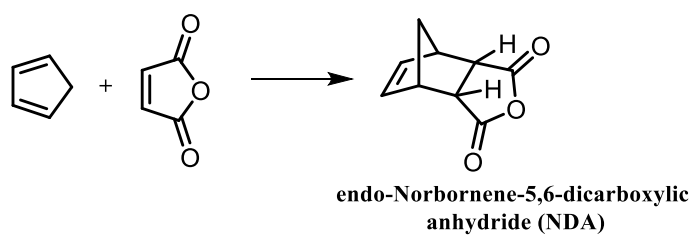


**Figure 4.2:**  $\beta$ -diketiminato zinc acetate complexes

The catalysts in this thesis are a derivative of salen type complexes, the first type of catalyst used in the copolymerization of cyclic anhydride and epoxide. However, these catalysts contain a pendant hemi-labile pyridyl donor. In this chapter their use in the copolymerization of epoxides and cyclic anhydrides will be discussed; the effect of the pyridyl donor, compared to literature precedence, will be the principal point of interest.

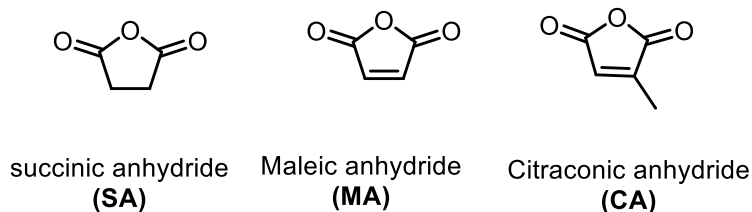
## 4.2 Anhydrides, Epoxide and cocatalysts

In this thesis, the ring-opening copolymerization of cyclohexene oxide with various anhydrides containing different ring strain is described (Figure 4.3). Previously reported examples often include cocatalysts, and therefore these studies have been performed with and without cocatalysts. The anhydrides used in this study were carefully selected to provide a range of structural motifs, including aliphatic, unsaturated, aromatic; substituted and unsubstituted alicyclic; mono- and dianhydrides; one ring and fixed ring. All anhydrides except NDA, which was prepared from the Diels-Alder Reaction of MA and cyclopentadiene according to a literature procedure (Equation 4.3),<sup>43</sup> were commercially available; all anhydrides were purified by recrystallization followed by sublimation to obtain pure (acid-free) anhydrides.

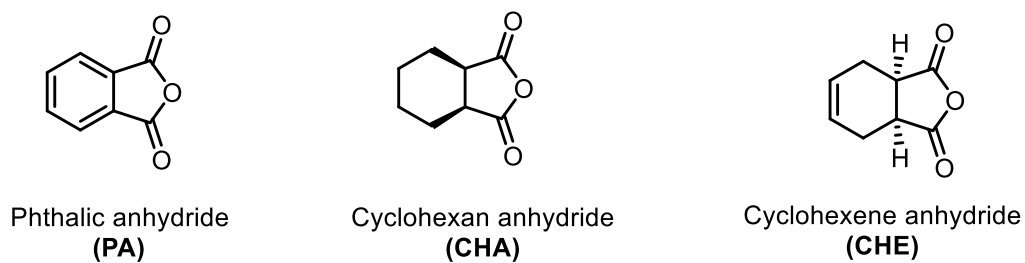


Equation 4.3: Synthesis of NDA

### 1. Monocyclic Anhydride



### 2. Bicyclic Anhydride



### 3. Tricyclic Anhydride

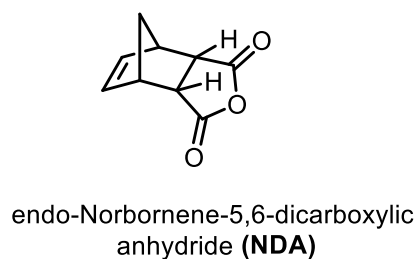
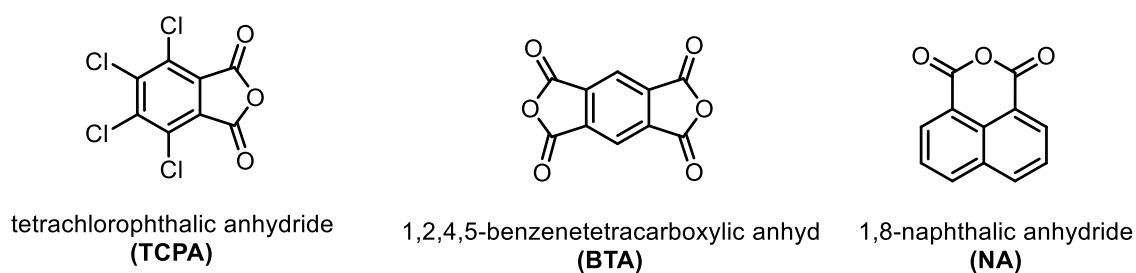


Figure 4.3: The anhydrides used for copolymerization catalysis

#### Chapter 4 - Copolymerization of Epoxides with Cyclic Anhydrides

Unfortunately, co-polymerization with the anhydrides in Figure 4.4 were not successful. The two main reason for the failure of copolymerization with these types of anhydride is the solubility and reactivity. The high molecular weight of these anhydrides means that a greater mass is required, which means that the solubility limit is easily reached. The majority of the anhydrides are still insoluble and separate from the reaction, even when toluene or high temperatures are used. The second reason is the high reactivity of such anhydrides. For example, the dianhydride BTA is more reactive than PA; a solid mass that defied characterization was formed immediately after a few minutes. In the same manner, TCPA and NA failed to afford a copolymer with CHO; with TCPA the reactivity of the anhydride, which results from the presence of four chloro groups, forms a solid product that again defied characterization. The lack of solubility of NA restricts the continuing study of this in copolymerization reactions.



**Figure 4.4:** the unsuccessful anhydrides in the copolymerization reaction

Among all epoxides shown in Figure 4.5, the CHO showed the highest reactivity towards the copolymerization with anhydrides using our catalysts. Most studies are focused on propylene oxide (PO) and CHO. Preliminary tests with different epoxides were unsuccessful, and gave copolymers with low molecular weight. Harsh conditions are required to increase the reactivity of these epoxides; oligomers were obtained during the polymerization of PO, SO or IBO with an anhydride. It was therefore decided to focus on cyclohexene oxide, and leave the other epoxides for further studies to achieve successful results.

## Chapter 4 - Copolymerization of Epoxides with Cyclic Anhydrides

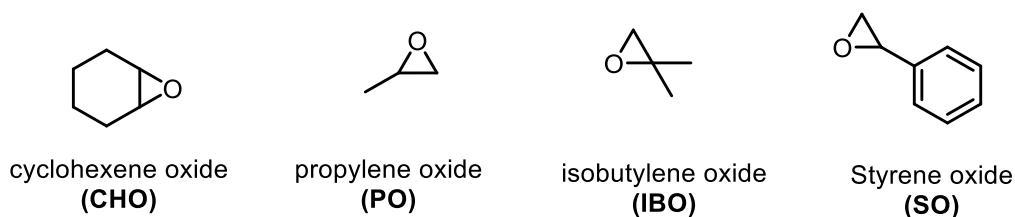


**Figure 4.5:** The epoxides tested in copolymerization reactions

In this study, two cocatalysts were probed: bis(triphenylphosphine)iminium chloride (PPNCl) and 4-dimethylaminopyridine (DMAP); these are two of the most commonly reported cocatalysts in the literature (Figure 4.6).

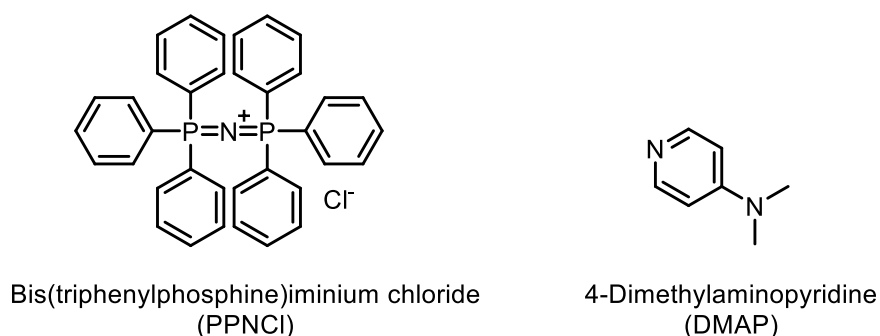


**Figure 4.6:** The structure of the two cocatalysts used in this study

### 4.3 General procedure for Copolymerization of Anhydrides and CHO

The copolymerization was performed at different temperatures, and with two sets of oxirane : anhydride : catalyst : cocatalyst feed ratios, in both bulk (no solvent) and in solution (toluene), with or without a cocatalyst. The polymerization data are summarized in Table 4.1.

**Table 4.1:** Feed ratio of CHO : anhydride : catalyst : cocatalyst in copolymerization reaction

	<b>CHO</b>	<b>Anhydride</b>	<b>Catalyst</b>	<b>Cocatalyst</b>
<b>set 1 feed ratio</b>	1000 eq. (6.4 mmol)	200 eq. (1.3 mmol)	1 eq. (6.4 $\mu$ mol)	1 eq. (6.4 $\mu$ mol)
<b>set 2 feed ratio</b>	250 eq. (2.5 mmol)	250 eq. (2.5 mmol)	1 eq. (0.01 mmol)	1 eq. (0.01 mmol)

In the glovebox, catalyst and cocatalyst (if needed) were placed in an oven-dried screw cup vial equipped with a magnetic stir bar. Cyclic anhydride was then added, followed by the epoxide. The vial was sealed, removed from the glovebox, and placed in an aluminium heating block preheated to the appropriate temperature. After the appropriate amount of time, an aliquot was taken for  $^1\text{H}$  NMR spectroscopic analysis to determine the conversion. The reaction mixture was then diluted with approx. 1 mL dichloromethane and the polymer precipitated by adding 10 mL of methanol with vigorous stirring, after which the solvents were decanted. Precipitation was repeated three times to remove the excess of monomer and catalyst. The polymer was dried under vacuum at 50 °C.

The polyether linkage in the produced polymers was determined by the comparison the methine resonance in both poly(CHO) and polyester. The poly(CHO) was prepared according to literature procedure.<sup>44</sup> The  $^1\text{H}$  NMR spectrum of poly(CHO) is shown in Figure 4.7. Polyether linkages in the copolymers are expected to exhibit  $^1\text{H}$  NMR resonances in the same regions as for pure poly(cyclohexene oxide). The diagnostic  $^1\text{H}$  NMR signals are at 3.4 ppm (CH) and 1.2–1.9 ppm for (CH<sub>2</sub>).

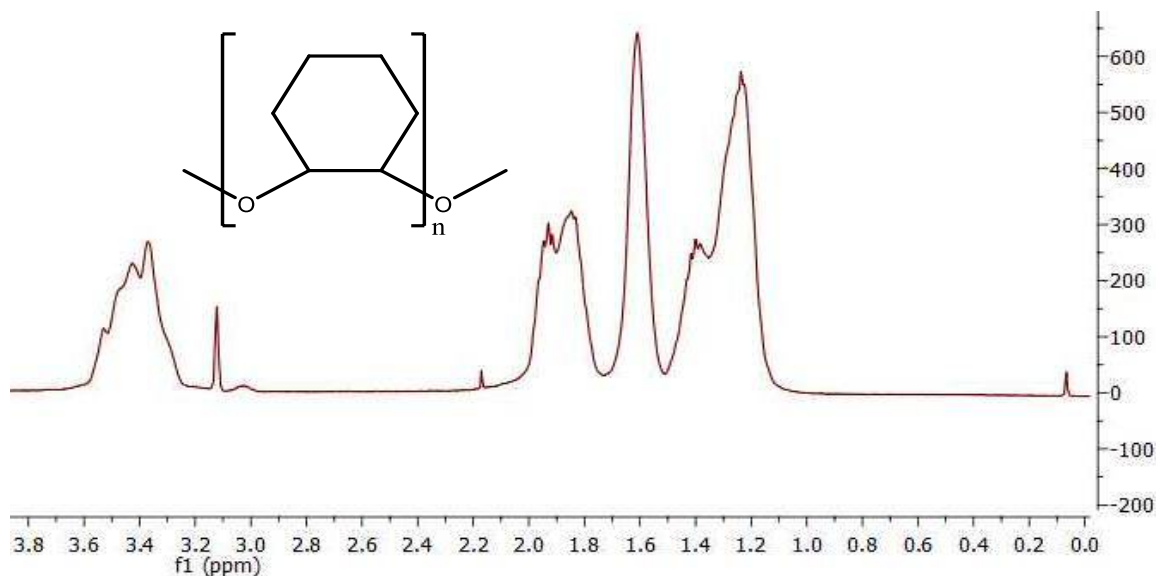


**Figure 4.7:**  $^1\text{H}$  NMR spectrum (400 MHz,  $\text{CDCl}_3$ ) of poly(cyclohexene oxide)

#### 4.4 Result and discussion

Initially we investigated the copolymerization of succinic anhydride (SA), maleic anhydride (MA) and phthalic anhydride (PA) with cyclohexene oxide (CHO), employing  $[\text{Al}(\text{tBu}, \text{tBu-Salpy})\text{Cl}]$  (**25**) as a catalyst and PPNCI as a cocatalyst. The experiments were conducted at 100 °C for 4 h using set 2 feed ratio, in toluene solvent. Table 4.2 shows the results of the polymerization experiments. No  $^1\text{H}$  NMR spectra were recorded for these entries since the purpose was to probe viability in catalysis. Some unexpected observations were made in the course of performing these experiments: all copolymerization experiments between SA and CHO in the presence of PPNCI give black solutions, which may correspond to a complicated, unidentified reaction between the reactants. Upon replacing the SA with MA, the anhydride was found to be much more soluble and the copolymerization reaction colour changed to yellow. No change in colour was observed with PA. As shown in entries 1-5, catalyst **25** showed low activity toward the ring opening copolymerization of the three anhydrides with CHO in toluene, giving oligomers rather than polymers. Extending the reaction time to 20 hours increased the molecular weight but only slightly. Although low molecular weight oligomers were obtained, they were formed with good polydispersity indices, suggesting good control over the copolymerization reaction.

**Table 4.2:** CHO–anhydride solution copolymerization catalyzed by [Al(<sup>t</sup>Bu,<sup>t</sup>Bu-Salpy)Cl] (**25**) in the presence of PPNCI cocatalyst using set 2 feed ratio

Entry	Catalyst	Cocatalyst	Anhydride	Time (h)	$M_n$ (g/mol)	PDI
1	25	PPNCI	SA	4	1340	1.00
2	25	PPNCI	MA	4	1390	1.00
3	25	PPNCI	PA	4	1280	1.00
4	25	PPNCI	SA	20	2120	1.06
5	25	PPNCI	PA	20	1420	1.00

To study the effect of the steric and electronic environment imposed by the Salpy ligands, six aluminium chloride complexes bearing various Salpy derivatives, and one titanium chloride complex, were tested in the copolymerization of CHO with SA using set 1 feed ratio. The complexes used were [Al(Salpy)Cl] (**24**), [Al(<sup>t</sup>Bu,<sup>t</sup>Bu-Salpy)Cl] (**25**), [Al(Naphpy)Cl] (**26**), [Al(<sup>t</sup>Bu,OMe-Salpy)Cl] (**27**), [Al(Ad,Me-Salpy)Cl] (**28**), [Al(Cl,Cl-Salpy)Cl] (**30**) and [Ti(<sup>t</sup>Bu,OMe-Salpn)Cl] (**40**). The copolymerization reactions were conducted at 100 °C for 5 hours. As shown in Table 4.3, a noticeable change in the molecular weight was observed upon changing the catalyst. In all cases, the alternating selectivity in the copolymer microstructure was rather low, the proportion of ether linkage being between 68 and 90%. With these entries, extending the reaction time did not affect the yield or molecular weight of the resulting polymer. This can be attributed to the highly viscous solution, which is formed after 1-2 hours, and which prevents adequate stirring. Figure 4.8 shows the <sup>1</sup>H NMR spectrum of the copolymer of CHO and SA; the methine protons of CHO in both polyether and polyester are displayed. Scheme 4.1 shows the structure of the polymers produced by the copolymerization reaction of cyclic anhydride and cyclohexene oxide.

#### Chapter 4 - Copolymerization of Epoxides with Cyclic Anhydrides

In contrast to the Set 2 conditions, polymerization experiments under set 1 feed ratios (Table 4.3) gave consistently higher molecular weights. The titanium catalyst (**40**) afforded a polymer with the highest molecular weight and a moderate proportion of ester linkages. This catalyst not only differs from the other catalysts in the metal centre, but also in the coordination number, which is 6 without the intervention of the pyridyl donor; the presence of a non-interacting Lewis base could be beneficial since it could fulfil the role of the co-catalyst (akin to DMAP). All of the aluminium complexes provided copolymers with molecular weights ranging from 4170-5710 g.mol<sup>-1</sup>.

**Table 4.3:** CHO–SA Copolymerization Catalyzed by **24-28**, **30** and **40** using set 1 feed ratio

Entry	Cat.	CHO conv. (%)	Ester (%)	Ether (%)	$M_n$ (g/mol)	PDI
6	<b>24</b>	85	16	84	5710	1.38
7	<b>25</b>	78	12	88	4430	1.59
8	<b>26</b>	80	25	76	5049	1.47
9	<b>27</b>	82	13	87	5320	1.33
10	<b>28</b>	80	32	68	4740	1.41
11	<b>30</b>	75	10	90	4170	1.43
12	<b>40</b>	87	23	77	6580	1.43

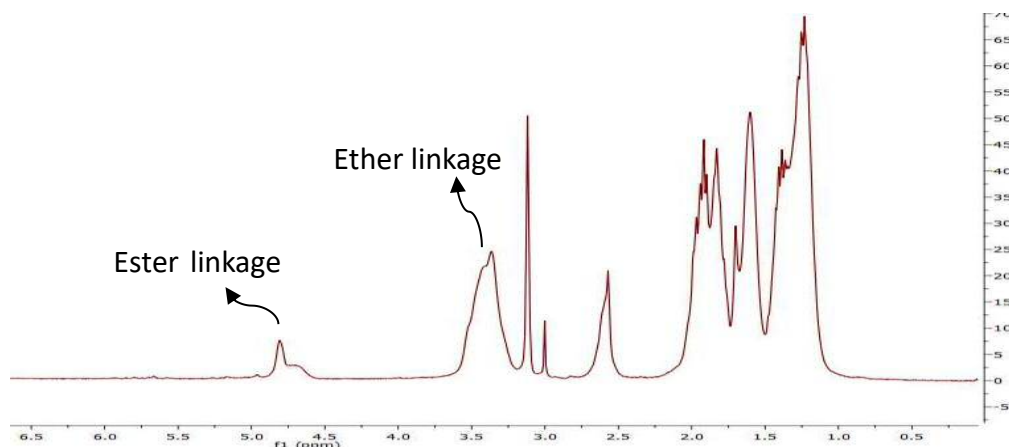
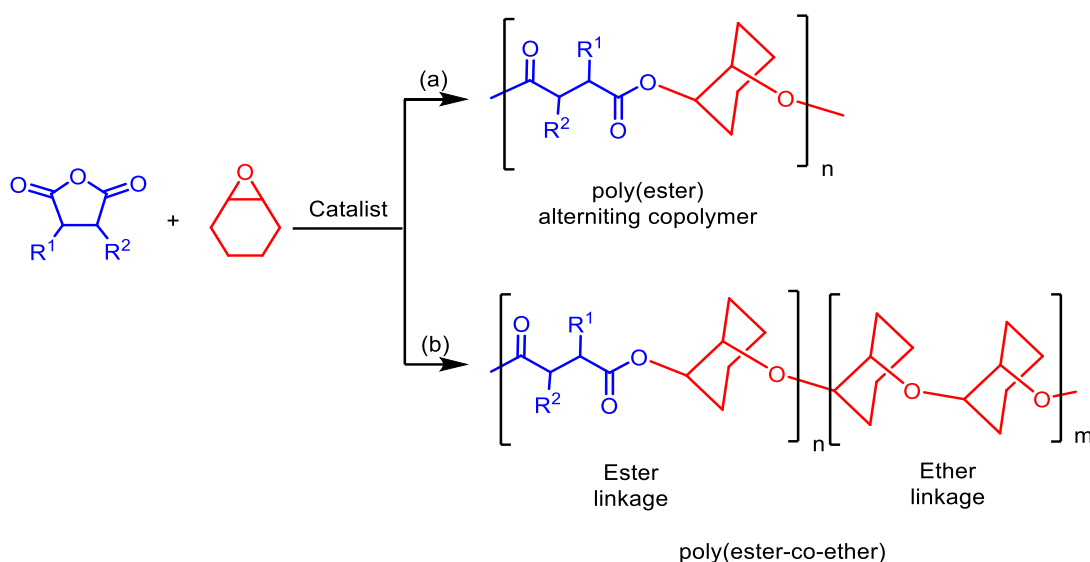


**Figure 4.8:**  $^1\text{H}$  NMR spectrum of the SA/CHO copolymer produced using  $[\text{Al}(\text{Salpy})\text{Cl}]$  (**24**) as a catalyst

The general equation for the synthesis of polyester using chain-growth polymerization is represented in Scheme 4.1. The repeating unit  $m$  and  $n$  are varied, so that  $n$  represents the number of ester linkages in the polymer chains, whereas  $m$  refers to the number of ether linkages. When  $m=0$ , a perfectly alternating copolymer will be obtained (route a); when  $m$  is high, a poly(ester-co-ether) will dominate the structure of the resulting polymer (route b). It is noteworthy that the experiments summarised in Table 4.3 give modestly alternating microstructures with selectivities of up to 32%.



**Scheme 4.1:** Synthesis of polyesters from cyclohexene oxide and cyclic anhydrides

An increasing viscosity during the polymerization reaction appears to affect the molecular weight of the resulting polyester, presumably due to the catalyst being immobilized in the reaction medium. This is a greater problem for the set 1 feed ratio when the reaction is carried out in effectively pure reactant. Performing the reaction using a solvent is one method of reducing the viscosity of the reaction medium. On the other hand, using a solvent will reduce the concentration of the reactants, thereby reducing the reaction rate; some studies reveal that bulk polymerizations (without solvent) show higher conversion rates compared to solution polymerization conditions.<sup>40</sup> In order to probe this effect, dichloroethane was used with entries 13-16, using the set 2 feed ratio at 100 °C, for 25 hours. Under these conditions, an improvement in the content of ester linkage was found, however the polyesters were formed with low molecular weights, an indication of a reduction in the catalyst reactivity (Table 4.4).

**Table 4.4:** CHO–SA copolymerization data using set 2 conditions

Entry	Catalyst	CHO conv. (%)	Ester (%)	Ether (%)	$M_n$ (g/mol)	PDI
13	25	96	30	70	2300	1.21
14	27	92	28	72	3400	1.19
15	29	83	27	73	4170	1.14
16	30	81	21	79	3500	1.15

The reactivity of the catalysts was enhanced by increasing the reaction temperature by 15 °C; the new entries were conducted at 115 °C instead of 100 °C. A higher molecular weight was obtained when the set 1 feed ratio was used. As we can see from Table 4.5, the number average molecular weight  $M_n$  initiated by **24** did not vary significantly with increasing the reaction time, possibly due to an increase in the viscosity of the reaction within the first hour of the reaction. The set 2 feed ratio was found to give copolymers with lower molecular weights than obtained using the set 1 conditions. Again, the viscosity had the greatest

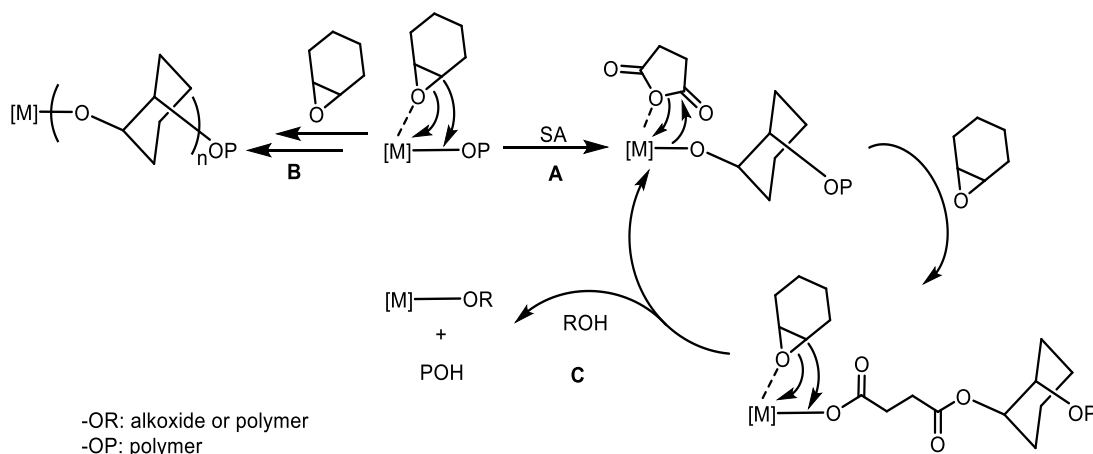
effect on the polymerization performance; one equivalent of each anhydride and CHO, without any solvent, gave reactions that increased in viscosity, which lowered the  $M_n$ . A slight decrease in the conversion was observed with entries 17-28 in comparison with entries 13-16.

**Table 4.5:** CHO–SA Copolymerization Catalyzed by **24** at 115 °C

Entry	Time (h)	CHO conv. (%)	Ester (%)	Ether (%)	$M_n$ (g/mol)	PDI
<b>Set 1</b>						
17	0.5	63	12	88	7880	1.42
18	1	66	12	88	8430	1.37
19	1.5	67	15	85	8490	1.48
20	2	75	17	83	8580	1.46
21	3	78	17	83	8690	1.47
22	4	80	18	82	8810	1.45
<b>Set 2</b>						
23	0.5	62	8	92	4690	1.29
24	1	63	10	90	4700	1.31
25	1.5	65	10	90	4760	1.31
26	2	67	11	89	5080	1.29
27	3	68	15	85	5120	1.30
28	4	83	15	85	5610	1.26

The generally accepted mechanism for the alternating copolymerization of cyclohexene oxide (CHO) and succinic anhydride (SA) (or another anhydride)

was suggested by Chisholm and co-workers.<sup>30</sup> As we can see from Scheme 4.2 there are three suggested pathways. Path **A** involves two main steps: coordination and insertion of anhydride into the M–O bond of the metal alkoxide to provide a metal carboxylate intermediate, which then reacts to ring-open of the epoxide, thereby reforming the metal alkoxide. When the metal-alkoxide bond reacts with the anhydride to form the carboxylate faster than the metal-alkoxide ring-opens the CHO, poly(cyclohexene succinate) is obtained as the major product, otherwise homopolymerization of CHO or the formation of polyether blocks is observed, as shown in path **B**. Path **C** shows that a rapid displacement of the growing polymer chain can be formed by a traces water or alcohol impurities. Thus, this a new metal-alkoxide or hydroxide bond formed in this “chain transfer” process can initiate a new polymer chain, thereby decreasing the molecular weight of the polymer. The modest selectivities observed in the above data suggests that there is insufficient kinetic differentiation between the reaction of the alkoxide with the CHO, vs the rate of SA opening by the alkoxide.



**Scheme 4.2:** Coordination-insertion mechanism for the copolymerization of CHO and SA

A polyester with higher molecular weight was obtained by the copolymerization of *endo*-Norbornene-5,6-dicarboxylic anhydride (NDA) with CHO using set 1 feed

ratio without cocatalysts. Table 4.6 shows that, although the ester incorporation is still low, catalysts **24** and **26** (Entries 29 and 30 respectively) afforded higher ester content in comparison with **27** (Entry 31) and **28** (Entry 32). The higher molecular weight of the NDA copolymer compared to the SA copolymer may be because the reaction is less viscous after a comparable time with SA, which is therefore less susceptible to catalyst immobilization. It was assumed that an increase in the ring strain of the anhydride backbone would also increase the reactivity and possibly also increase the molecular weight of the products.<sup>45</sup>

**Table 4.6:** CHO–NDA Copolymerization Catalyzed by **24**, **26**, **27** and **28** using set 1 feed ratio

Entry	Catalyst	Time (h)	Ester (%)	Ether (%)	$M_n$ (g/mol)	PDI
29	<b>24</b>	15	18	82	12400	1.67
30	<b>26</b>	15	20	80	12310	1.56
31	<b>27</b>	15	10	90	13270	1.42
32	<b>28</b>	15	10	90	14880	1.49

The copolymerization of PA and CHO without cocatalysts and solvent were conducted at 100 °C for 15 minutes with different catalyst complexes using set 1 feed ratio (Table 4.7). In each case, the experiments afforded polymers with high ether content, the precise amount being dependent on the catalyst identity. The molecular weights ranged from 4600–5100 g/mol<sup>-1</sup> and both catalyst **24** (Entry 34) and **26** (Entry 35) showed low PDI, which may be because the steric demands of the Salpy ligands in **24** and **26** are less than for the other catalysts which have substituents on the phenol rings. An increasing in the viscosity during the reaction has an effect of hindering the growth of the polymer chain and in turn lowers the resulting molecular weight of the polymer. The result of the polymerization is represented in Table 4.7

**Table 4.7:** CHO–PA copolymerization Catalyzed by **24**, **25**, **26**, **27** and **28** using set 1 feed ratio

Entry	Catalyst	Time (h)	Ester (%)	Ether (%)	$M_n$ (g/mol)	PDI
33	<b>25</b>	15	10	90	5140	1.48
34	<b>24</b>	15	11	89	4670	1.16
35	<b>26</b>	15	18	82	4680	1.14
36	<b>27</b>	15	14	86	4630	1.47
37	<b>28</b>	15	13	87	4980	1.58

The copolymerization of PA and CHO catalyzed by  $[Al(tBu,OMe-Salpy)Cl]$  (**27**) was probed with different (or without) a cocatalyst (Table 4.8). The set 2 feed ratio was used, with a reaction temperature of 100 °C. In the beginning PA, CHO and **27** were stirred at 100 °C. A highly viscous, turbid solution was formed after 15 minutes, and solid PA started to separate from the reaction (Entry 38). Without solvent, and with an equimolar amount of CHO, the proportion of PA is relatively high, and therefore the CHO was unable to dissolve all the PA under these conditions. After 50 minutes, the reaction turned to a solid mass and stopped stirring. The  $^1H$  NMR spectrum showed a high proportion of ether linkage (80%) and only 20% ester linkage. Introducing a cocatalyst, such as PPNCI or DMAP, to the reaction made a significant change in both solubility and structure of the resulting polymers. Regarding the solubility, during the reaction a clear solution was observed when PPNCI or DMAP was added. When PPNCI was used, the PA completely dissolved in CHO. Between 40-50 minutes the viscosity of the solution reached its maximum, and the stirrer bar was not able to rotate freely. A high conversion of the CHO was obtained (94%) using this cocatalyst, which decreased slightly when DMAP was used (83%). Interestingly, the presence of a cocatalyst made a big difference to the polymer structure, in comparison to the polymer produced without using any cocatalyst. A high ester content (ca. 80%) (Entries 39, 40, Table 4.8) was obtained, which is a significant improvement in

the selectivity for an alternating copolymer. In contrast to an improvement in the microstructure, the the presence of a cocatalyst gave polymers with low molecular weight, albeit with excellent polydispersity indices. At this point one suggestion is that the formation of the highly viscous polymer affects the polymer molecular weight, by immobilizing the catalyst; a low molecular weight caused by chain termination events would be expected to exhibit a higher PDI. One possible solution was to add 1 mL of toluene, and repeat the reaction (entry 41). Adding the toluene increases the solubility of the polymer, but the increased dilution can lower the reaction rate. In this case, the molecular weight was almost identical after 23 hours, after all the CHO was consumed giving 99% conversion.

**Table 4.8:** CHO–PA Copolymerization Catalyzed by [Al(<sup>t</sup>Bu,OMe-Salpy)Cl] (**27**) with various cocatalysts using set 2 feed conditions

Entry	Cocatalyst	Time (h)	CHO conv. (%)	Ester (%)	Ether (%)	$M_n$ (g/mol)	PDI
38	-	1	73	20	80	-	-
39	PPNCl	1	94	81	19	2970	1.05
40	DMAP	1	83	80	20	2740	1.04
41	PPNCl	23	99	87	13	2980	1.04

Using the set 1 feed ratio, with different catalysts and PPNCl or DMAP, at 100 °C for 3 hours yielded copolymers with high ester proportions. Figure 4.9 shows that DMAP consistently afforded higher conversion (albeit only slightly) than PPNCl. On the other hand, the  $M_n$  values for all the entries in Table 4.9 are between 3120-3550 g/mol<sup>-1</sup> with narrow PDIs, and these values are subtly influenced by the catalyst identity as well as the cocatalyst (Figure 4.10).

It is possible that the low reactivity of these catalysts is attributable to the pyridine group in the Salpy ligand, which affords 6-coordinate complexes, as shown in

solid state studies (Chapter 2). This coordination mode could reduce the reactivity of the catalyst by coordinatively saturating the metal centre. Even despite the previous studies in Chapter 2, in which the hemi-lability of the Salpy ligand is asserted with compelling evidence (which would render the complexes with the same coordination number as other Salen-type ligands), this suggestion cannot be true. Entries 44 and 46 (Table 4.9) correspond to identical catalyst substituents except the presence of the pyridyl donor; entry 44 describes  $[Al(tBu,OMe-Salpy)Cl]$  (**27**) whereas entry 46 describes  $[Al(tBu,OMe-Salpn)Cl]$  (**29**). These entries give almost identical polymers (comparable molecular weight and polyester content). The same comparison can be made with entries 49 and 51, which describe polymerization experiments using DMAP as the cocatalyst. These data suggest that the pyridyl is not the only reason for the low reactivity.

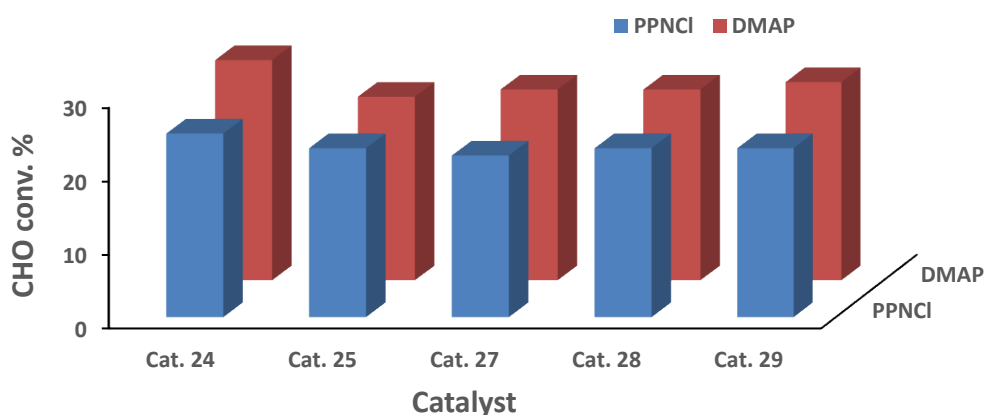


**Figure 4.9:** CHO conversion for the copolymerization of CHO and PA catalyzed by **24**, **25**, **27**, **28** and **29**

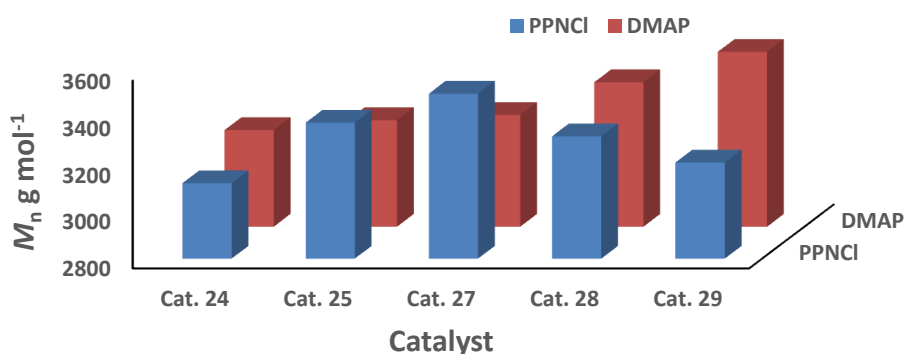


**Figure 4.10:**  $M_n$  values for the copolymerization of CHO and PA catalyzed by **24**, **25**, **27**, **28** and **29**

**Table 4.9:** CHO–PA copolymerization catalyzed by **24**, **25**, **27**, **28** and **29** using set 1 feed ratio

Entry	Cat.	Cocat.	CHO conv. (%)	Ester (%)	Ether (%)	$M_n$ (g/mol)	PDI
42	<b>24</b>	PPNCI	25	75	25	3120	1.08
43	<b>25</b>	PPNCI	23	83	17	3380	1.17
44	<b>27</b>	PPNCI	22	84	16	3500	1.20
45	<b>28</b>	PPNCI	23	83	17	3320	1.18
46	<b>29</b>	PPNCI	23	81	19	3210	1.10
47	<b>24</b>	DMAP	30	81	19	3210	1.16
48	<b>25</b>	DMAP	25	75	25	3260	1.11
49	<b>27</b>	DMAP	26	77	23	3280	1.13
50	<b>28</b>	DMAP	26	77	23	3420	1.14
51	<b>29</b>	DMAP	27	78	22	3550	1.16

Upon changing the anhydride to those containing unsaturated backbones, maleic or citraconic anhydride, different behaviour was observed in the copolymerization with CHO. The presence of a side-reaction was suggested by the observation that the reaction mixture changed colour at room temperature, at which temperature experiments established that no polymerization occurred. The copolymerization of maleic anhydride (MA) and CHO, conducted at 100 °C, afforded a solid black mass, which was insoluble in all common solvents. This could possibly be accounted for if the double bonds of MA (whether part of a copolymer or not) are cross-linked, although since the black solid defied characterization, this could not be verified or falsified. Decreasing the temperature to 60 °C lead to the formation of soluble polymers, more consistent

with the formation of a linear polymer chains (Table 4.10). For all polymerization experiments with MA the reaction solidified between 0.5-1 hour. Regarding the structure of the resulting polymers, the catalytic behaviour of all catalysts was essentially identical, affording polymers with comparable molecular weights. Interestingly, no ester linkage was observed in the NMR spectra, which suggests that homopolymerization of CHO occurs. The signal corresponding to the maleic anhydride at ca. 7 ppm is very sharp, and therefore inconsistent with the MA being incorporated in a polymer chain; the <sup>1</sup>H NMR spectrum is shown in Figure 4.11. In comparison to succinic anhydride, the reactions with maleic anhydride yielded polymers with much higher molecular weight, approximately three-fold higher than the polymers produced using SA.

**Table 4.10:** CHO–MA copolymerization catalyzed by **24**, **26**, **27** and **28** using set 1 feed ratio

Entry	Catalyst	Time (h)	CHO conv. (%)	Ester (%)	Ether (%)	<i>M<sub>n</sub></i> (g/mol)	PDI
52	<b>24</b>	5	92	0	100	13390	1.61
53	<b>26</b>	5	88	0	100	12960	1.68
54	<b>27</b>	5	93	0	100	14470	1.56
55	<b>28</b>	5	81	0	100	15600	1.57

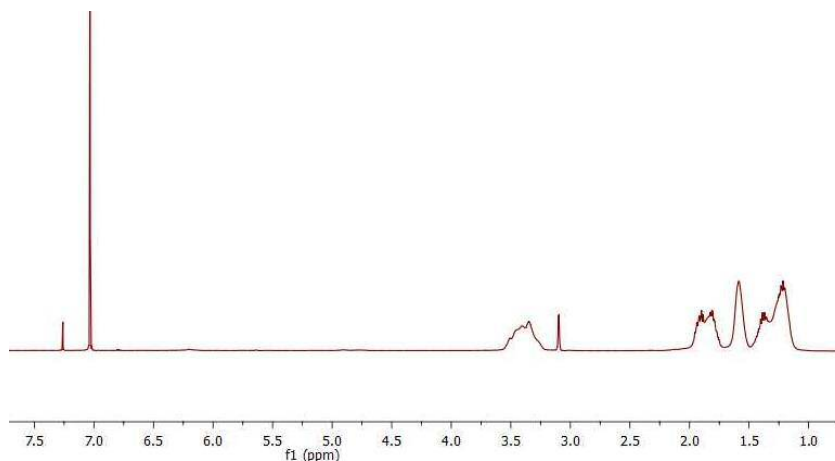
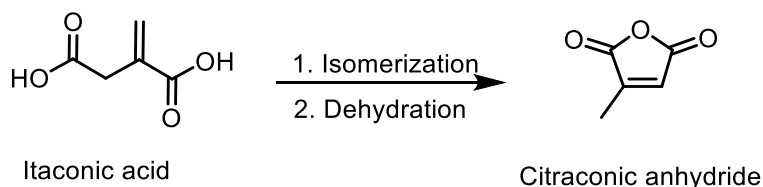


**Figure 4.11:**  $^1\text{H}$  NMR spectrum (400 MHz,  $\text{CDCl}_3$ , 293 K) of the crude polymerization product of MA and CHO using **24** as a catalyst

Citraconic anhydride (CA) is no less interesting than maleic anhydride; it is an important monomer for chain growth copolymerization. This anhydride is normally produced by the isomerization and dehydration of itaconic acid (Equation 4.4).<sup>46</sup> The acid in turn is generally produced commercially by the fermentation of carbohydrates; this naturally occurring acid, produced industrially by such a process.



**Equation 4.4:** Synthesis of citraconic anhydride

The presence of a methyl group on the double bond of the anhydride makes it more sterically hindered. Regarding the copolymerization with CHO, CA shows the same behaviour of MA; no ester resonances were observed in the  $^1\text{H}$  NMR spectra (Figure 4.12), again consistent with the formation of poly(cyclohexene oxide). The resulting polymers were found to be pale red in colour, but since the polymers consist of only poly(CHO), the colouration must be due to minor impurities, which could be explained by strongly coloured copolymers that lie beyond the detection limits of the NMR spectra, or else minor compounds arising

from the decomposition of CA under the catalytic reaction conditions (Figure 4.13). Again, the molecular weight of the polymers (Table 4.11) were higher than the polymer produced from SA. In general, the poly(MA) samples show higher  $M_n$  values than the poly(CA) samples (Figure 4.14) while the PDI of the poly(CA) samples were higher than the poly(MA) samples.

**Table 4.11:** CHO–CA copolymerization catalyzed by **24**, **26**, **27** and **28** using set 1 feed ratio

Entry	Catalyst	Time (h)	CHO conv. (%)	Ester (%)	Ether (%)	$M_n$ (g/mol)	PDI
56	<b>24</b>	5	94	0	100	10030	1.78
57	<b>26</b>	5	94	0	100	8810	1.80
58	<b>27</b>	5	88	0	100	11570	1.81
59	<b>28</b>	5	90	0	100	11140	1.80

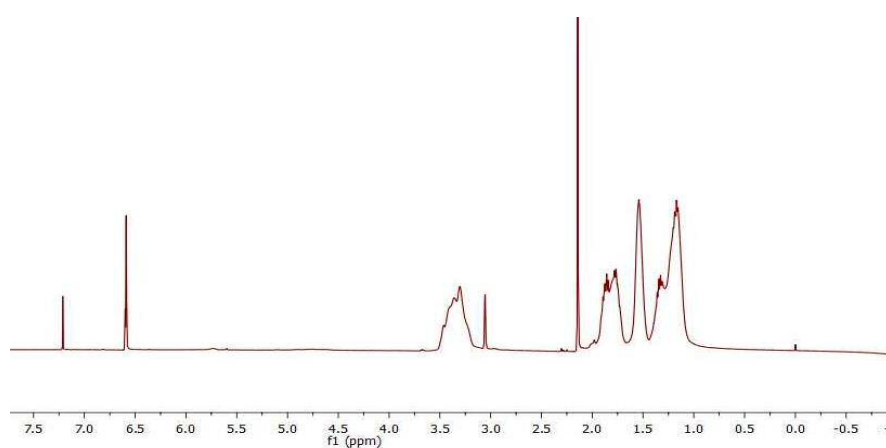


**Figure 4.12:**  $^1\text{H}$  NMR spectrum (400 MHz,  $\text{CDCl}_3$ , 203 K) of the crude polymerization product of CA and CHO using **24** as a catalyst

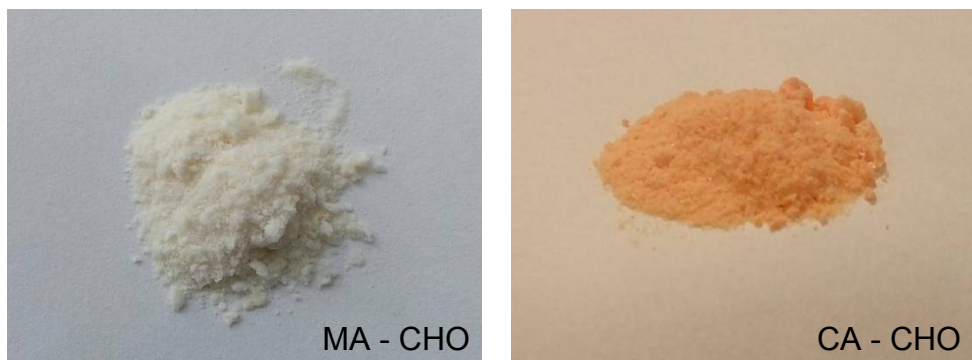


Figure 4.13: Polymer produced from attempted ROCOP of MA- CHO and CA- CHO

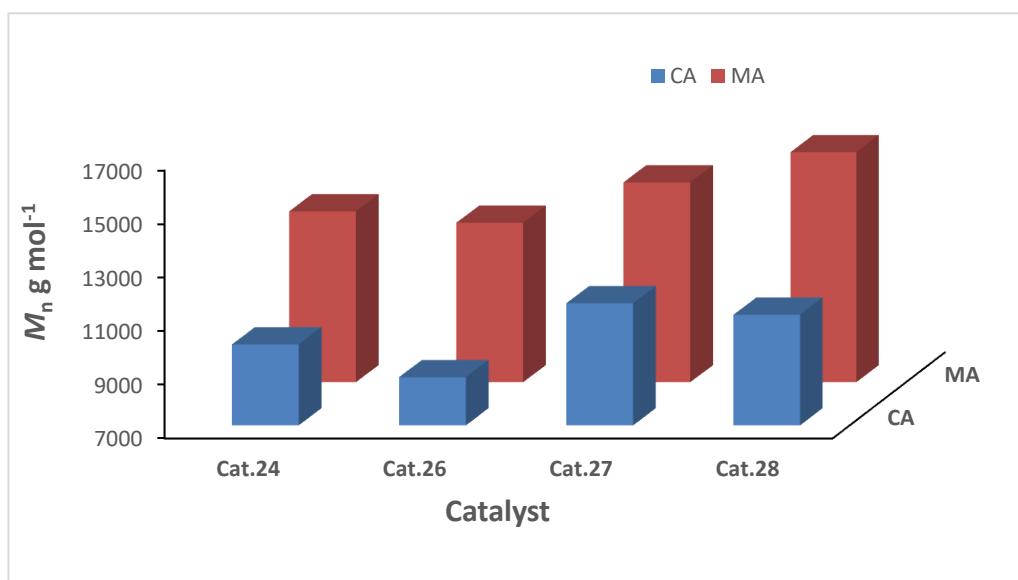


Figure 4.14:  $M_n$  values for the polymer produced in the CHO/ anhydride experiments catalyzed by **24**, **26**, **27** and **28**.

The cyclohexane anhydride (CHA) is the aliphatic version of phthalic anhydride. As expected, there was no change in the copolymerization behaviour. In the same way as found for the previous entries, a polyester-co-polyether was obtained when no cocatalyst was added. When the reaction was conducted at 115 °C for 20 hours, applying set 1 feed ratio with four different catalysts, listed in Table 4.12, without cocatalysts, a relatively high ether content was observed in the <sup>1</sup>H NMR spectra (entries 60-63). However, the GPC analyses showed a broad multimodal peak (more than one overlapping peak), or else two separate

peaks in the same chromatogram. For instance, when **25** was used as a catalyst (entry 60), two separate peaks were obtained, the first peak was showed a significantly higher molecular weight (62850 g/mol), however the second peak exhibited a molecular weight of 10607. With the entries 61, 62 and 63 (Table 4.12), the  $M_n$  values fluctuate because of the multiplicity of peaks in the same curve.

**Table 4.12:** CHO–CHA copolymerization catalyzed by **25**, **26**, **27** and **28** at 115 °C applying set 1 feed ratio

Entry	Catalyst	Time (h)	Ester (%)	Ether (%)	$M_n$ (g/mol)	PDI
60	25	20	27	73	62850	1.00
					10610	1.33
61	26	20	22	78	2530	1.35
62	27	20	20	80	12100	1.06
					11010	1.24
63	28	20	36	64	2170	1.21

Reducing the temperature to 100 °C and using one selected catalyst, **27**, with or without cocatalyst gave alternating polymer with high selectivity when PPNCI or DMAP was added. The copolymerization was performed using set 1 feed ratio at 100 °C for 23 hours. An enormous difference was observed in molecular weights between the three experiments (entries 64-66) (Figure 4.15). A higher molecular weight was obtained with this anhydride compared to many of the others. Running the reaction for a longer time did not give any improvement in the molecular weight. The polydispersity indices were reasonably low (Table 4.13)

Using set 2 feed ratio and without using cocatalysts, with the same conditions as in the set 1 experiments above, afforded polymers with lower  $M_n$  than with the set

#### Chapter 4 - Copolymerization of Epoxides with Cyclic Anhydrides

1 conditions. This was attributed to the amount of CHO in the polymerization reaction. In the case of set 1, the excess of CHO worked as a solvent for the reactant and improved the solubility. However, adding PPNCI caused a lowering of the  $M_n$  values, but simultaneously improved the alternating microstructure in the copolymer (Entries 67-69 in Table 4.13).

**Table 4.13:** CHO-CHA copolymerization catalyzed by **27** at 100 °C

Entry	Catalyst	Cocatalyst	Time (h)	CHO conv. (%)	Ester (%)	Ether (%)	$M_n$ (g/mol)	PDI
<b>Set 1</b>								
64	<b>27</b>	-	20	-	15	85	25020	1.22
65	<b>27</b>	PPNCI	20	-	84	16	2350	1.24
66	<b>27</b>	DMAP	20	-	85	15	4220	1.15
<b>Set 2</b>								
67	<b>27</b>	-	20	-	26	74	5300	1.38
68	<b>27</b>	PPNCI	20	-	86	14	2020	1.11
69	<b>27</b>	DMAP	20	-	84	16	1910	1.07

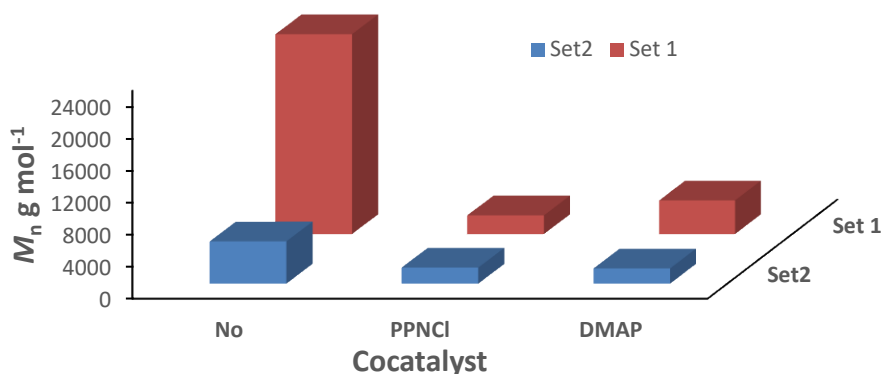


**Figure 4.15:**  $M_n$  values for the copolymerization of CHA and CHO catalyzed by **27**

Introducing a double bond to CHA gave a new anhydride, cyclohexene anhydride (CHE). As with CHA, the copolymerization experiments using CHE afforded high molecular weight polymers under set 1 conditions without cocatalyst (Figure 4.16), but with very low ester content (entry 70, Table 4.14). By introducing the cocatalysts, the ester linkage content increased dramatically (entries 71, 72). Repeating the experiments under the set 2 feed ratio give data showing a similar trend, albeit with lower molecular weights. In these experiments, the CHO conversion could not be calculated since the CHO signals in the <sup>1</sup>H NMR spectra overlap with those attributed to CHE.

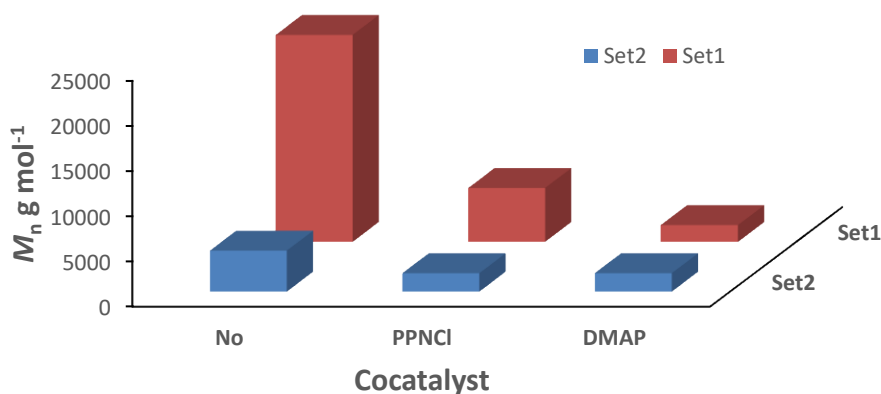


**Figure 4.16:**  $M_n$  values for the copolymerization of CHE and CHO catalyzed by **27**

Table 4.14: CHO–CHE Copolymerization Catalyzed by 27

Entry	Catalyst	Cocatalyst	Time (h)	CHO conv. (%)	Ester (%)	Ether (%)	$M_n$ (g/mol)	PDI
<b>Set 1</b>								
70	27	-	20	-	6	94	22900	1.35
71	27	PPNCl	20	-	80	20	5990	1.17
72	27	DMAP	20		78	22	1870	1.10
<b>Set 2</b>								
73	27	-	20		-Ove	-ove	4560	1.34
74	27	PPNCl	20		82	18	2050	1.08
75	27	DMAP	20		80	20	2060	1.07

Tables 4.15 and 4.16 show the results of performing the CHA/CHO copolymerization experiments over different times at 105 °C. In each case, no cocatalyst was used. Table 4.15 describes the experiments under set 1 feed ratio conditions, whereas Table 4.16 describes the corresponding experiments using set 2 conditions. In both cases an increase in  $M_n$  values was observed with time; the polymerization using set 1 showed higher  $M_n$  values than for set 2, possibly because of catalyst immobilization under set 2 conditions which affords highly viscous reaction mixtures, and as described above.

**Table 4.15:** CHO–CHA Copolymerization Catalyzed by **24** using set 1 conditions (no cocatalyst)

Entry	Time	CHO conv. (%)	Ester (%)	Ether (%)	$M_n$ (g/mol)	PDI
76	1	-	21	79	5460	1.48
77	2	-	11	89	5990	1.42
78	4	99	21	79	6200	1.40
79	6	99	16	84	6480	1.41

**Table 4.16:** CHO–CHA Copolymerization Catalyzed by **24** using set 2 conditions (no cocatalyst)

Entry	Time (h)	CHO conv. (%)	Ester (%)	Ether (%)	$M_n$ (g/mol)	PDI
80	1	96	23	77	4530	1.50
81	2	98	14	86	5380	1.29
82	4	99	30	70	5540	1.36
83	6	99	27	73	5990	1.42

Other experiments were conducted for copolymerization of CHO and NDA using the set 1 feed ratio, to probe the effect of added solvent. The reactions were conducted at 110 °C using [Al(<sup>t</sup>Bu,<sup>t</sup>Bu-Salpy)Cl] (**25**) as a catalyst. No solvent was used for entry 84, whilst 1 mL of toluene was added for entry 85; the results of the polymerization experiments are illustrated in Table 4.17. The reaction

mixture for entry 84 was homogeneous at the beginning of the reaction; upon consumption of the monomer, the viscosity increased gradually. Using solvent in entry 85 enhanced the solubility of the reactant, and reduced the viscosity of the reaction mixture as the preaction progressed. However, as described above for other monomers, the reaction rate is expected to decrease when using solvent due to the lower concentration of the CHO, which may well reduce the molecular weight of the polymer under otherwise identical conditions. In this case, a higher molecular weight polymer chain can be achieved by increasing the reaction time. As seen in Table 4.17, to afford a comparable molecular weight polymer, the reaction with solvent required significantly longer than the reaction without solvent. Both conditions afforded poly(ester-co-ether)s with a high ether linkage, as expected in the absence of a cocatalyst.

**Table 4.17:** CHO-NDA Copolymerization Catalyzed by **25** with or without solvent using set 1 feed ratio

Entry	Anhydride	Time (h)	Ester (%)	Ether (%)	$M_n$ (g/mol)	PDI
84	NDA	5	10	90	9650	1.86
85	NDA	23	7	93	9940	1.36

Entry 48 without toluene, entry 85 with 1 mL toluene.

#### 4.5 Density functional calculations

A plausible mechanism<sup>47</sup> for the ring-opening copolymerization of succinic anhydride and ethylene oxide, as models for the substrates described in this chapter, was probed using density functional theory. Calculations were performed by Dr. Benjamin Ward using the Gaussian 09 program. The M06-2X functional was used, employing the cc-pV(D+d)Z basis set on Al and cc-pVDZ on all other centres. The calculated energy profile is shown in Figure 4.17. The initial complex used in the calculations was the hypothetical species [Al(Salpy)(OMe)].

## Chapter 4 - Copolymerization of Epoxides with Cyclic Anhydrides

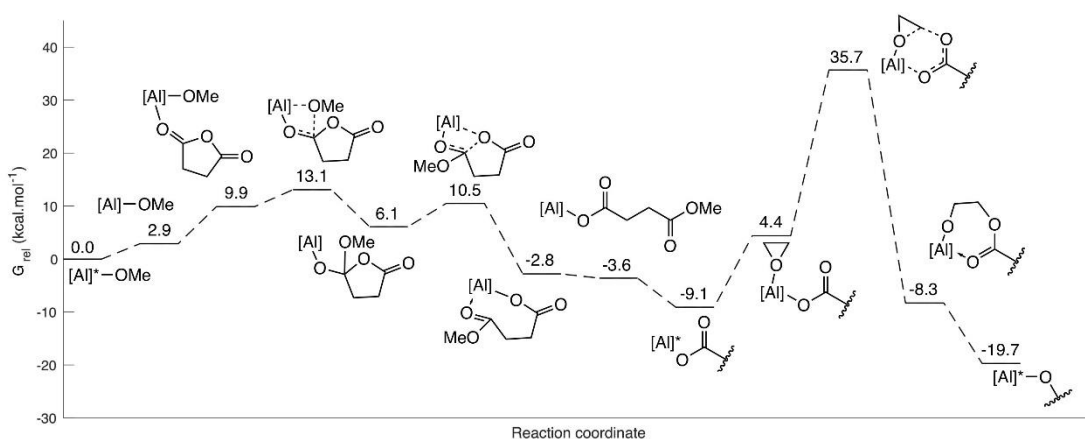


**Figure 4.17:** Calculated free energy profile for the copolymerization of succinic anhydride and ethylene oxide by  $[Al(\text{Salpy})(\text{OMe})]$ . Species in which the pyridyl is coordinated are denoted by \*

Since experimental studies and DFT studies suggest that the coordinated-pyridyl isomer is the most stable form, this was chosen as the zero-point energy on the energy profile. Subsequent calculations failed to give viable structures unless the pyridyl was de-coordinated; this is therefore proposed as the first step in the catalytic reaction, and involves a small increase of  $2.9 \text{ kcal.mol}^{-1}$ .

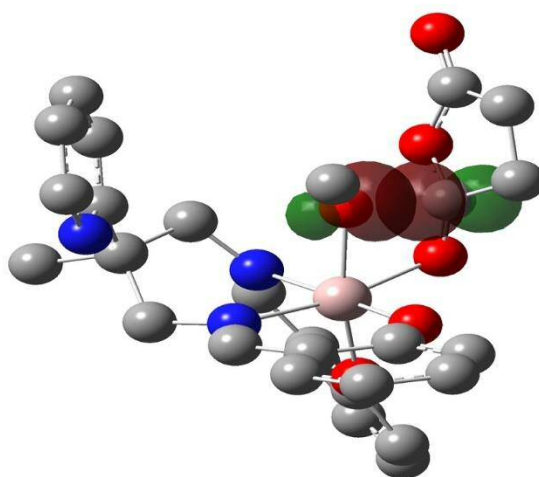


**Figure 4.18:** Calculated structure of the carbonyl-insertion transition state showing the donor-acceptor NBOs. H atoms omitted for clarity

The calculated mechanism is based upon that suggested by Chisholm *et al.*,<sup>30</sup> and involves the migratory insertion of an alkoxide ligand (OMe in the calculations, representing the growing polymer chain). This step is essentially identical to the first step in the ring-opening polymerization of cyclic esters and involves a four-membered transition state between the Al–OMe and the C=O. The transition state structure is shown in Figure 4.18, showing the principal donor-acceptor interactions derived from an NBO analysis. The donor-acceptor interactions are as expected, the donor orbital corresponds to a  $\pi_p$  orbital of the coordinated oxygen, which is donated into a  $\pi^*_p$ -type orbital of the carbonyl group. This, and the ring-opening step, closely resemble the calculations associated with the ROP of  $\epsilon$ -caprolactone in Chapter 3, and the associated energies suggest that this should be viable at room temperature.

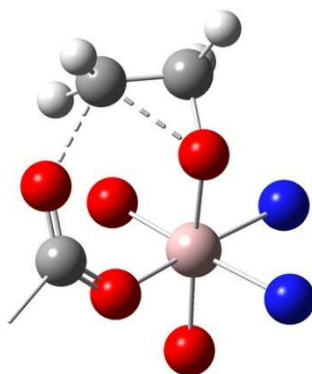


**Figure 4.19:** Calculated transition state structure for the opening of epoxide.

Only the transition state core and coordinating atoms are shown; the forming/breaking bonds are shown as dashed lines

The highest point on the energy profile is associated with the insertion of the epoxide; at  $35.7 \text{ kcal.mol}^{-1}$  ( $149 \text{ kJ.mol}^{-1}$ ), this step is not expected to be viable under ambient conditions, and is consistent with experimental observations, since this polymerization reaction requires elevated temperatures. The transition state core is shown in Figure 4.19; the ligand has been removed for clarity and only the donor atoms remain. The pendant carbonyl resulting from the opened-anhydride attacks the epoxide, whilst the bond forms this carbon to the epoxide oxygen is simultaneously broken. This forms a 6-membered transition state. This is crucial for understanding the possible selectivity in this type of reaction; the

homo-polymerization by a single metal centre will normally proceed via an energetically higher 4-membered transition state between a coordinated alkoxide and the epoxide. This is the reason for the higher successes normally enjoyed by Salen and porphyrin complexes, since they can circumvent this high energy transition state by adopting a bimetallic mechanism where the polymer chain (alkoxide) is transferred to an epoxide on a different metal centre.<sup>48</sup> Successful ROCOP catalysts therefore operate via kinetic control by virtue of a lower energy 6-membered transition state. The principal donor-acceptor interactions from an NBO analysis are shown in Figure 4.20.

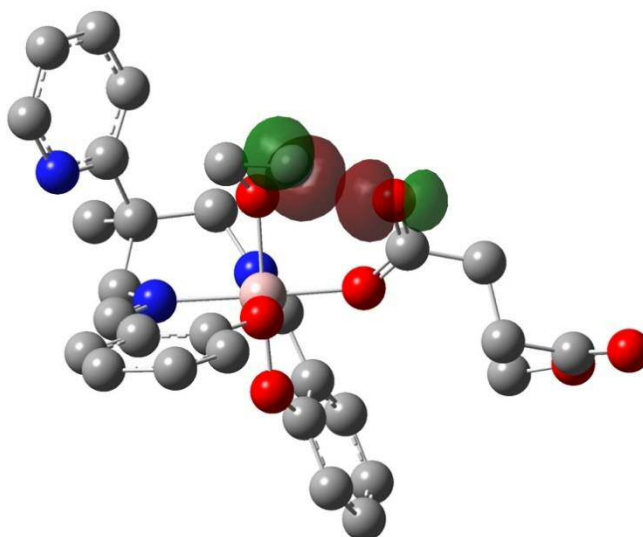


**Figure 4.20:** Calculated transition state structure for the opening of epoxide showing the donor-acceptor NBOs. H atoms omitted for clarity

The calculated mechanism suggests that the rate-limiting step should be the coordination and ring-opening of the epoxide, and since the steps involving anhydride are expected to be facile at room temperature, the resting state of the catalyst is expected to be the carboxylate derived from the opened anhydride. If this were the case, this would certainly be consistent with some of the high selectivities reported previously in this chapter, but it would be hard to explain the high polyether content in the absence of the cocatalyst.

It is thought that the cocatalyst acts as an external nucleophile, effectively transforming the initial chloride complexes to an alkoxide by ring-opening the first epoxide (initiation step).<sup>49</sup> It is possible that any catalyst complex that remains a chloride (i.e. not initiated) could be an active catalyst for the homopolymerization of epoxides, but inactive for the copolymerization of anhydrides and epoxides; this would explain why the systems without cocatalyst give poorly alternating copolymers, whereas only those with cocatalyst give high selectivities. There are problems with this suggestion, in that once the first epoxide has been ring-opened, regardless of how this occurs mechanistically, an alkoxide is formed and it is hard to imagine how this could therefore have such a profound effect on the selectivity. The answer undoubtedly lies in a fuller understanding of the role of the cocatalyst, and it is in this direction that future research should lie.

## **4.6 Conclusion**

In this chapter the aluminium Salpy complexes have been probed for catalytic activity in the ring-opening copolymerization (COCOP) of cyclic anhydrides and epoxides. This area of copolymerization is much less understood than the related CO<sub>2</sub>-epoxide copolymerization process. As such, the data presented herein should be regarded as an attempt to establish some fundamental operating parameters by which we may further understand how this reaction functions; lessons learned from these data should serve to produce catalysts that can afford copolymers with high molecular weights and simultaneously high ester content.

As with many studies of this nature, many of the observations in this chapter raise more questions than they answer, but some conclusions are clear:

1. Catalyst immobilization by viscous reaction mixtures makes it more difficult to adequately control the reaction. Future studies would do well to use a solvent system to reduce this problem.
2. Since the rate-limiting step is likely to be the epoxide ring-opening, using a solvent-free system, or using the epoxide as the solvent, is likely to enhance the rate of the reaction. A compromise is therefore likely, of using high epoxide

concentration vs using a reaction medium that prevents a rapidly increasing viscosity.

3. The cocatalyst makes a significant difference to the selectivity. Polymers formed without the cocatalyst were mostly comprised of polyether, and little polyester. In this chapter, competitive polyester selectivities were obtained, but only in the presence of a cocatalyst. The role of the cocatalyst requires further investigation; cocatalysts such as PPNCI are often discussed in epoxide homopolymerization, and are thought to offer an external nucleophile to assist the ring-opening step. Such a role may be expected to give *lower* selectivities by facilitating the homopolymerization of epoxide, but this is not observed. The role of the cocatalyst is therefore intriguing and further studies should focus on this aspect of the research.

4. Whilst the pyridyl had a profound effect on the ROP of  $\epsilon$ -CL, it appears to be less important in ROCOP catalysis.

Further studies, in addition to probing the role of the cocatalyst, should include probing the precise reaction conditions (e.g. different concentrations, solvents, temperatures) to determine the optimum conditions to obtain highly selective polyesters. There is also much scope for probing epoxides other than CHO, and more importantly, ligand environments that move away from the ubiquitous Salen framework.

## 4.7 References

- 1 G. Odian, *Principles of Polymerization*, John Wiley & Sons, Hoboken, New Jersey, 4th ed., 2004.
- 2 A. M. Diccio and G. W. Coates, *J. Am. Chem. Soc.*, 2011, **133**, 10724–10727.
- 3 R. C. Jeske, A. M. DiCiccio and G. W. Coates, *J. Am. Chem. Soc.*, 2007, **129**, 11330–11331.
- 4 S. Huijser, E. Hosseinejad, R. Sablong, C. De Jong, C. E. Koning and R. Duchateau, *Macromolecules*, 2011, **44**, 1132–1139.

#### Chapter 4 - Copolymerization of Epoxides with Cyclic Anhydrides

- 5 B. Han, L. Zhang, M. Yang, B. Liu, X. Dong and P. Theato, *Macromolecules*, 2016, **49**, 6232–6239.
- 6 J. Liu, R. Zhou, L. Jia, D. Fan and X. Lü, *Inorg. Chem. Commun.*, 2017, **79**, 86–88.
- 7 A. Thevenon, J. A. Garden, A. J. P. White and C. K. Williams, *Inorg. Chem.*, 2015, **54**, 11906–11915.
- 8 M. J. Sanford, L. Peña Carrodegua, N. J. Van Zee, A. W. Kleij and G. W. Coates, *Macromolecules*, 2016, **49**, 6394–6400.
- 9 C.-Y. Yu, H.-J. Chuang and B.-T. Ko, *Catal. Sci. Technol.*, 2016, **6**, 1779–1791.
- 10 D. J. Darensbourg and O. Karroonnirun, *Macromolecules*, 2010, **43**, 8880–8886.
- 11 D. J. Darensbourg, O. Karroonnirun and S. J. Wilson, *Inorg. Chem.*, 2011, **50**, 6775–6787.
- 12 R. Duan, Z. Qu, X. Pang, Y. Zhang, Z. Sun and H. Zhang, *Chin. J. Chem.*, 2017, **35**, 640–644.
- 13 M. Oshimura, T. Tang and A. Takasu, *J. Polym. Sci. Part A Polym. Chem.*, 2011, **49**, 1210–1218.
- 14 H. Chen, W. Lu, Y. Chen, S. C. N. Hsu, S. Ou, W. Peng, N. Jheng, Y. Lai, B. Wu, H. Chung, Y. Chen and T. Huang, 2012, **1**, 327–333.
- 15 H. Chen, B. Huang and C. Lin, *Macromolecules*, 2005, **38**, 5400–5405.
- 16 B. Gao, D. Li, Y. Li, Q. Duan, R. Duan and X. Pang, *New J. Chem.*, 2015, **39**, 4670–4675.
- 17 W. Yi and H. Ma, *Inorg. Chem.*, 2013, **52**, 11821–11835.
- 18 S. Tsurutat, T.; Matsuura, K.; Inoue, *Makromol. Chem.*, 1964, **75**, 211–214.
- 19 R. L. Paddock and S. T. Nguyen, *J. Am. Chem. Soc.*, 2001, **123**, 11498–

#### Chapter 4 - Copolymerization of Epoxides with Cyclic Anhydrides

- 11499.
- 20 S. Matsumura, A. R. Hlil, C. Lepiller, J. Gaudet, D. Guay, Z. Shi, S. Holdcroft and A. S. Hay, *Am. Chem. Soc. Polym. Prepr. Div. Polym. Chem.*, 2008, **49**, 511–512.
- 21 D. J. Darensbourg, R. M. Mackiewicz, J. L. Rodgers, C. C. Fang, D. R. Billodeaux and J. H. Reibenspies, *Inorg. Chem.*, 2004, **43**, 6024–6034.
- 22 J. E. Seong, S. J. Na, A. Cyriac, B. W. Kim and B. Y. Lee, *Macromolecules*, 2010, **43**, 903–908.
- 23 F. Jutz, J. D. Grunwaldt and A. Baiker, *J. Mol. Catal. A Chem.*, 2008, **279**, 94–103.
- 24 A. Barbarini, R. Maggi, A. Mazzacani, G. Mori, G. Sartori and R. Sartorio, *Tetrahedron Lett.*, 2003, **44**, 2931–2934.
- 25 R. L. Paddock, Y. Hiyama, J. M. McKay and S. T. Nguyen, *Tetrahedron Lett.*, 2004, **45**, 2023–2026.
- 26 V. Caló, A. Nacci, A. Monopoli and A. Fanizzi, *Org. Lett.*, 2002, **4**, 2561–2563.
- 27 N. D. Harrold, Y. Li and M. H. Chisholm, *Macromolecules*, 2013, **46**, 692–698.
- 28 J. Liu, Y.-Y. Bao, Y. Liu, W.-M. Ren and X.-B. Lu, *Polym. Chem.*, 2013, **4**, 1439–1444.
- 29 C. Robert, F. de Montigny and C. M. Thomas, *Nat. Commun.*, 2011, **2**, 586.
- 30 A. Bernard, C. Chatterjee and M. H. Chisholm, *Polymer (Guildf.)*, 2013, **54**, 2639–2646.
- 31 E. H. Nejad, A. Paoniasari, C. G. W. van Melis, C. E. Koning and R. Duchateau, *Macromolecules*, 2013, **46**, 631–637.
- 32 M. Winkler, C. Romain, M. A. R. Meier and C. K. Williams, *Green Chem.*,

**Chapter 4 - Copolymerization of Epoxides with Cyclic Anhydrides**

- 2015, **17**, 300–306.
- 33 P. K. Saini, C. Romain, Y. Zhu and C. K. Williams, *Polym. Chem.*, 2014, **5**, 6068–6075.
- 34 Y. Liu, M. Xiao, S. Wang, L. Xia, D. Hang, G. Cui and Y. Meng, *RSC Adv.*, 2014, **4**, 9503–9508.
- 35 D. F. Liu, L. Y. Wu, W. X. Feng, X. M. Zhang, J. Wu, L. Q. Zhu, D. Di Fan, X. Q. Lü and Q. Shi, *Inorg. Chem. Commun.*, 2013, **37**, 182–185.
- 36 D. F. Liu, L. Y. Wu, W. X. Feng, X. M. Zhang, J. Wu, L. Q. Zhu, D. Di Fan, X. Q. Lü and Q. Shi, *J. Mol. Catal. A Chem.*, 2014, **382**, 136–145.
- 37 A. Takasu, T. Bando, Y. Morimoto, Y. Shibata and T. Hirabayashi, *Biomacromolecules*, 2005, **6**, 1707–1712.
- 38 T. Aida, K. Sanuki and S. Inoue, *Macromolecules*, 1985, **18**, 1049–1055.
- 39 D.-F. Liu, L.-Q. Zhu, J. Wu, L.-Y. Wu and X.-Q. Lü, *RSC Adv.*, 2015, **5**, 3854–3859.
- 40 E. Hosseini Nejad, C. G. W. Van Melis, T. J. Vermeer, C. E. Koning and R. Duchateau, *Macromolecules*, 2012, **45**, 1770–1776.
- 41 N. J. Van Zee and G. W. Coates, *Angew. Chemie - Int. Ed.*, 2015, **54**, 2665–2668.
- 42 N. J. Van Zee, M. J. Sanford and G. W. Coates, *J. Am. Chem. Soc.*, 2016, **138**, 2755–2761.
- 43 K. L. W. Louis F. Fieser, *Organic Experiments*, 1992.
- 44 R. Bacskai, *J. Polym. Sci. Part A Gen. Pap.*, 1963, **1**, 2777–2790.
- 45 R. C. Jeske, J. M. Rowley and G. W. Coates, *Angew. Chemie - Int. Ed.*, 2008, **47**, 6041–6044.
- 46 *The Merck Index*, Merck & Co., Inc.: Whitehouse Station, NJ, 14th ed., 2006.

**Chapter 4 - Copolymerization of Epoxides with Cyclic Anhydrides**

- 47 Y. Z. Hua, X. C. Yang, M. M. Liu, X. Song, M. C. Wang and J. B. Chang, *Macromolecules*, 2015, **48**, 1651–1657.
- 48 M. I. Childers, J. M. Longo, N. J. Van Zee, A. M. Lapointe and G. W. Coates, *Chem. Rev.*, 2014, **114**, 8129–8152.
- 49 G. Trott, P. K. Saini and C. K. Williams, *Philos. Trans. R. Soc.*, 2016, **A374:20150**.

# Chapter 5

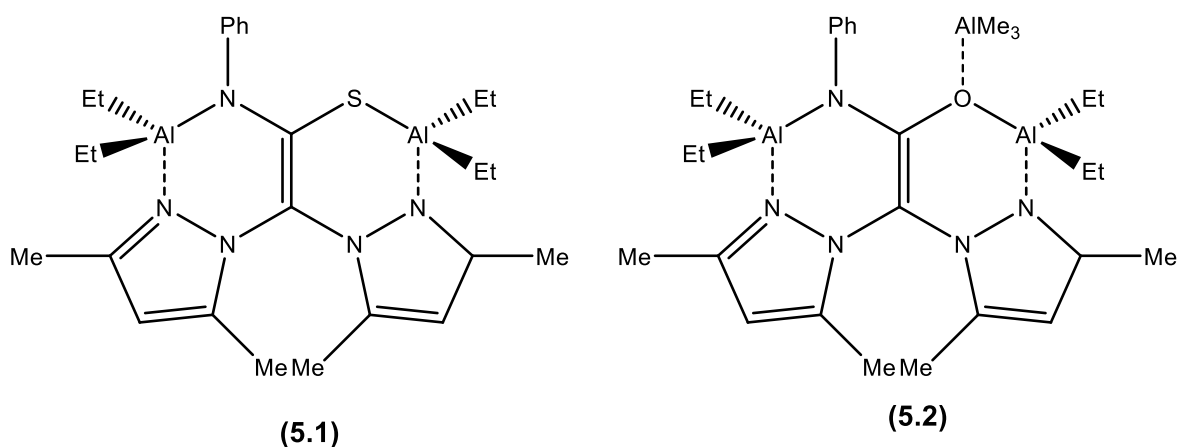
**Bimetallic aluminium complexes:  
Synthesis, characterization, X-ray  
crystal structures and ring opening  
polymerization**

## 5.1 Introduction

Salen type complexes based on five-coordinate aluminium ions are among the most successful catalysts in the ring opening polymerization (ROP) of cyclic esters, such as lactide<sup>1-3</sup> and caprolactone.<sup>4-6</sup>

There has been recent interest in the preparation of bimetallic catalysts, with the hope there will be beneficial cooperativity between the metal centres, and a corresponding enhancement in the catalytic performance. Such bimetallic complexes can have different catalytic behaviour in comparison to their related monometallic congeners because of the presence of two proximal reactive centres within the same complex that can act in a concerted mode.<sup>7-10</sup> Different types of bimetallic aluminium complexes have been prepared and tested for various types of polymerization.

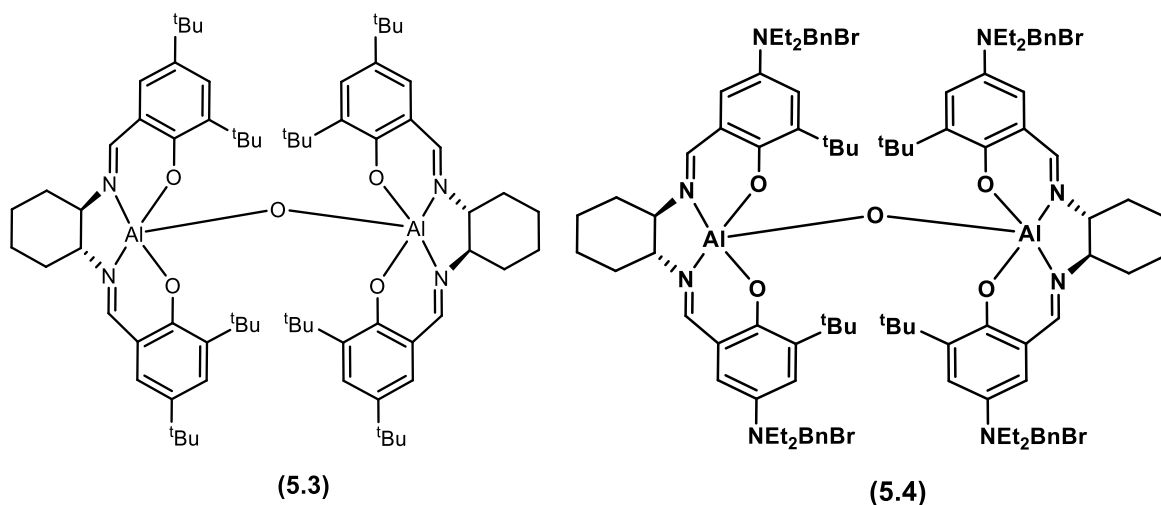
Rodriguez-Dieguez *et al.* reported the use of a range of thioacetamidate (**5.1**) or acetamidate (**5.2**) heteroscorpionate aluminium complexes in combination with quaternary ammonium salts, as highly active catalyst systems for the synthesis of cyclic carbonates at room temperature under one bar pressure of carbon dioxide.<sup>11,12</sup>



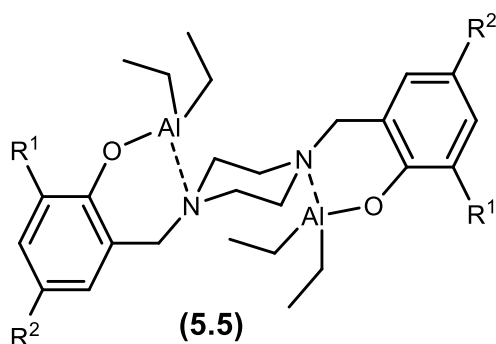
The same authors reported a different type of bimetallic complexes. They revealed that complex **5.3**, in combination with tetrabutylammonium bromide (TBAB), is the most active catalyst system for the synthesis of cyclic carbonates from terminal epoxides and carbon dioxide (1 bar) at room temperature.<sup>13,14</sup> Complex **5.4** show the same behaviour after incorporation of the cocatalyst into

**Chapter 5 - Bimetallic aluminium complexes: Synthesis, characterization, X-ray crystal structures and ring opening polymerization**

the salen ligand, to afford one-component immobilised aluminium(salen) catalysts.<sup>15</sup>

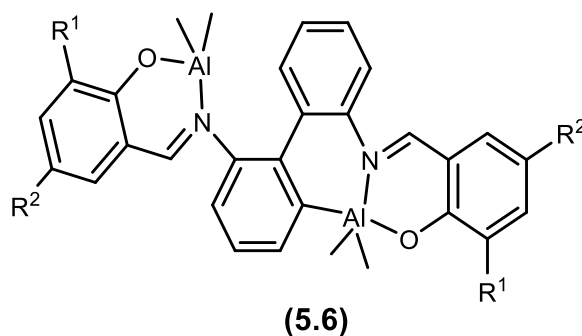


A series of tetradentate bimetallic aluminium complexes derived from piperazine-bridged bis(phenolato) ligands were investigated by Yao and co-workers, for initiating the ring-opening polymerization (ROP) of  $\epsilon$ -caprolactone.<sup>9</sup> They found from kinetic studies that the activity of dinuclear complexes (5.5) is around 2–8 times of that of their mononuclear counterparts, which provides evidence for the cooperation between two metal centres in the former complexes.



When racemic 6,6'-dimethylbiphenyl-bridged salen-type ligands were reacted with 2 equivalents of  $\text{AlMe}_3$ , bimetallic complexes of the general formula 5.6 were formed. These complexes were reported, alongside the corresponding monometallic versions, by Ma and Kan as initiators for ROP of *rac*-lactide. They

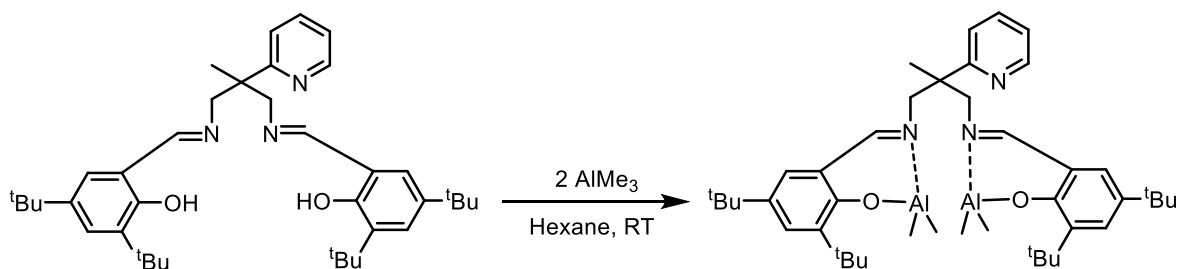
concluded that the dinuclear aluminium complexes enabled an increase in activity with comparison with the mononuclear counterparts, but gave atactic PLAs with broadened PDIs.



In this study, three novel bimetallic aluminium complexes were synthesised from the Salpy and related proligands, to afford a tetradentate coordination site to give binuclear four-coordinate aluminium complexes, with and without the hemilabile pyridyl group.

## 5.2 Synthesis and characterization of bimetallic aluminium methyl complexes $[Al_2(^tBu, ^tBu\text{-Salpy})Me_4]$ (**41**), $[Al_2(Ad, Me\text{-Salpy})Me_4]$ (**42**), and $[Al_2(^tBu, OMe\text{-salpn})Me_4]$ (**43**)

Three dinuclear aluminium alkyl complexes  $[Al_2(^tBu, ^tBu\text{-Salpy})Me_4]$  (**41**),  $[Al_2(Ad, Me\text{-Salpy})Me_4]$  (**42**), and  $[Al_2(^tBu, OMe\text{-salpn})Me_4]$  (**43**) have been prepared through alkane elimination reactions between each protio-ligand and two equivalents of  $AlMe_3$ . Complex **41** precipitated from hexane solution upon the reaction of  $^tBu, ^tBu\text{-Salpy}$  with 2 equivalents of trimethyl aluminium, allowing the product to be easily isolated by filtration as a yellow solid (Equation 5.1). This was the only derivative prepared using hexane as a solvent; the presence of four *tert*-butyl groups in the ligand enhances the solubility of this ligand in hexane whereas the other ligand derivatives studied were insoluble in this medium.



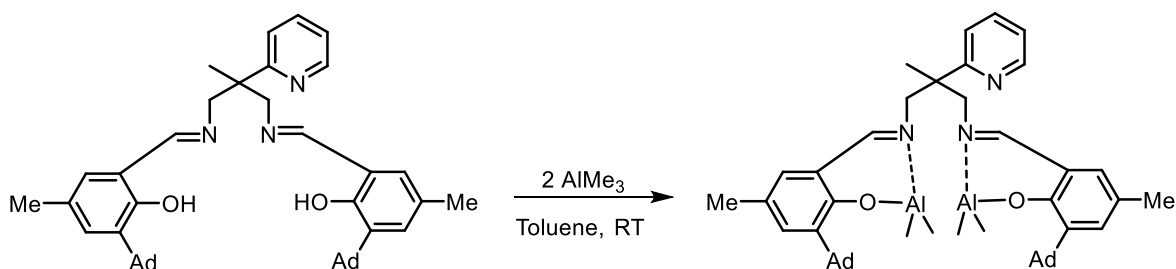
**Equation 5.1**

The <sup>1</sup>H NMR spectrum of [Al<sub>2</sub>(<sup>t</sup>Bu,<sup>t</sup>Bu-Salpy)Me<sub>4</sub>] (**41**) in C<sub>6</sub>D<sub>6</sub> is consistent with the presence of two aluminium ions per Salpy ligand, and pointed to symmetrical structures in solution, on the basis of there being one set of signals for the two iminophenol “arms”. Diagnostic resonances in the proton spectra are detected, for instance, the OH peak of the free ligands in the very downfield region 14.04 ppm disappeared upon reaction, suggesting the deprotonation of both phenol groups. The signals corresponding to the aluminum methyl protons were observed in the upfield region between  $\delta = -0.20$  and  $-0.55$  ppm as two separate singlets, each integrating to 6 H relative to the pyridyl H<sup>6</sup> (1 H integration). This is consistent with the presence of four methyl groups (two per aluminium), and for which the two methyl groups on the same aluminium are inequivalent (having also duly considered the fact that the Salpy ligand is symmetrical, from which it can be inferred that the two aluminium ions are also in equivalent environments). In the low-field region, singlets ( $\delta = 6.93$  ppm) are observed for the equivalent CH=N moieties. Interestingly, the H<sup>6</sup> of the pyridyl group has approximately the same chemical shift as the free ligand (8.48 ppm), and as mention in the previous chapter, the chemical shift corresponding to H<sup>6</sup> can be indicative of the coordinative state of the pyridyl moiety; no change in the chemical shift indicates that the pyridyl is not coordinated to the metal ion. The methylene groups of the complex **41** appear as two doublet in the region 3.86 and 3.19 ppm.

The complex [Al<sub>2</sub>(Ad,Me-Salpy)Me<sub>4</sub>] (**42**) was prepared by the treatment of the ligand Ad,Me-Salpy with two equivalent of AlMe<sub>3</sub> in toluene. Unlike the

**Chapter 5 - Bimetallic aluminium complexes: Synthesis, characterization, X-ray crystal structures and ring opening polymerization**

monometallic complex of this ligand, which is hard to form, the bimetallic complex was obtained easily as a pure product (equation 5.2).



**Equation 5.2**

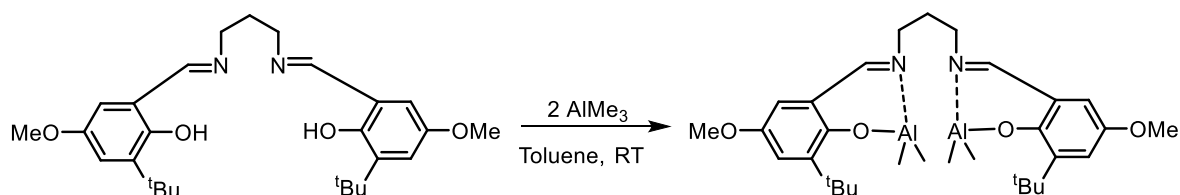
The steric hindrance of the large adamantyl substituents in the *ortho* positions of the phenol rings makes it a challenge for the two arms of the ligand to exist in close proximity, and therefore disfavoring the formation of a monometallic complex. However, in the bimetallic arrangement, these groups are necessarily further apart and are therefore not subject to such steric clashes.

$^1\text{H}$  NMR spectroscopy of the reaction product indicated that the proligand was deprotonated by two metal alkyls of trimethylaluminium with the concomitant release of two equivalents of methane. The disappearance of the OH signal of the protio-ligand and the appearance of two singlet resonances for the protons of the methyl groups at -0.2 and -0.4 ppm (6 H integration each) bound to the two Al ions suggests the formation of the proposed bimetallic Al complexes. The complex is sensitive to moisture and air and each of two methyl groups attached to the same aluminium are inequivalent. The  $\text{CH}_2$  protons appear as two AB doublets. No substantial change in the chemical shift of the pyridyl  $\text{H}^6$  was observed, in comparison to the value of the free ligand. The  $^{13}\text{C}$  NMR signals of the aluminium methyl ligands appear at -7.5 and -8.9 ppm; all other  $^{13}\text{C}$  signals were in the expected regions based upon the coordination chemistry discussed in Chapter 2.

In order to probe the role of the pyridyl donor in these bimetallic complexes,  $[\text{Al}_2(\text{}^t\text{Bu,OMe-salpn})\text{Me}_4]$  (**43**) was prepared by the treatment of the free ligand  $\text{}^t\text{Bu,OMe-salpn}$  with two equivalents of trimethyl aluminium (Equation 5.3). The

**Chapter 5 - Bimetallic aluminium complexes: Synthesis, characterization, X-ray crystal structures and ring opening polymerization**

solvent used with this ligand affects the orientation of the reaction towards the mono- or bimetallic complex. As mentioned in the previous chapter, when THF used as a solvent, the complex was isolated as a pure monometallic compound. To obtain the bimetallic complex, toluene was the best choice to afford the desired product. A good indication that the bimetallic complex had formed was given by NMR analysis, which is consistent with the proposed structure.



**Equation 5.3**

Unlike the other two bimetallic complexes, which have a pyridyl pendant on the diamine backbone, complex **43** exhibits a higher symmetry, exemplified by the Al-Me ligands, which are all equivalent, appearing as a singlet at -0.3 ppm, integrating to 12 H (Figure 5.1).

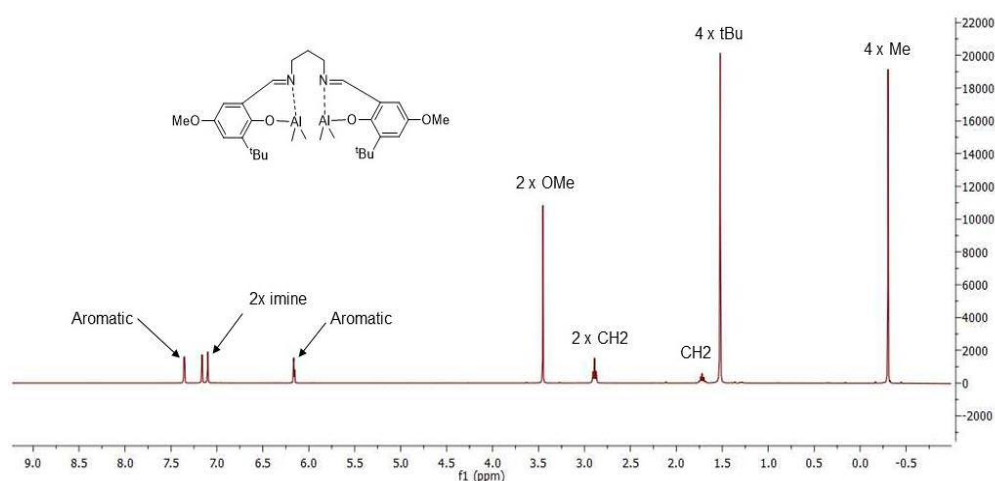


**Figure 5.1:**  $^1\text{H}$  NMR spectrum (400 MHz,  $\text{C}_6\text{D}_6$ , 293 K) of  $[\text{Al}_2(\text{tBu}, \text{OMe-salpn})\text{Me}_4]$  (**43**)

### 5.3 Crystallographic studies of bimetallic aluminium methyl complexes

Crystals of complex **41** suitable for X-ray crystal structure determination were crystallized from hexanes at room temperature, and under a nitrogen atmosphere. The crystals of complexes **42** and **43** were grown from concentrated solutions in benzene at room temperature. The crystal structure analyses of complexes **41**, **42** and **43** (Figures 5.2, 5.3, 5.4 respectively) show that the three complexes adopt four-coordinate distorted tetrahedral geometries, and that the salpy / salpn ligands bond to the central aluminium ions in a bidentate manner. In all cases, each of the two aluminium ions are coordinated to the phenolate, imine and two methyl ligands. The six-membered chelating ring is nearly planar, with the Aluminium atom lying out of the plane by 0.279 and 0.077 Å in **41** and 0.175 and 0.191 Å in **43** (Figure 5.5)

Selected bond distances and bond angles are given in Tables 5.1, 5.2 and 5.3.

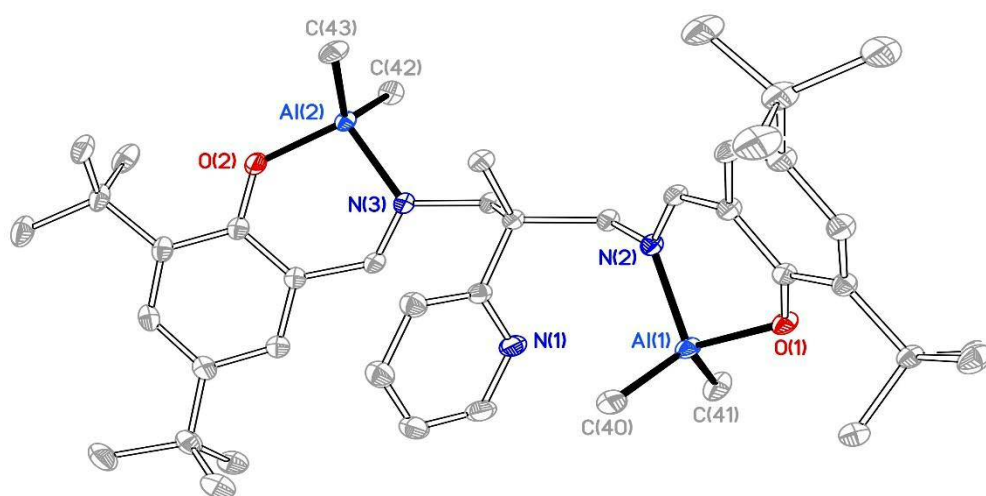


**Figure 5.2:** Solid state structure of  $[Al_2(^tBu,^iBu\text{-Salpy})Me_4]$  (**41**). Ellipsoids are shown at the 30% probability level. Hydrogen atoms are omitted for clarity

**Table 5.1:** Selected bond lengths (Å) and bond angles (°) for [Al<sub>2</sub>(<sup>t</sup>Bu,<sup>t</sup>Bu-Salpy)Me<sub>4</sub>] (**41**)

Al(1)-O(1)	1.7862(13)	Al(2)-O(2)	1.7755(13)
Al(1)-C(41)	1.950(2)	Al(2)-C(43)	1.9539(19)
Al(1)-C(40)	1.963(2)	Al(2)-C(42)	1.9557(19)
Al(1)-N(2)	1.9805(15)	Al(2)-N(3)	1.9650(14)
O(1)-Al(1)-C(41)	109.56(8)	O(2)-Al(2)-C(43)	109.63(8)
O(1)-Al(1)-C(40)	107.29(8)	O(2)-Al(2)-C(42)	112.59(7)
C(41)-Al(1)-C(40)	122.24(10)	C(43)-Al(2)-C(42)	118.00(9)
O(1)-Al(1)-N(2)	92.78(6)	O(2)-Al(2)-N(3)	95.03(6)
C(41)-Al(1)-N(2)	110.24(8)	C(43)-Al(2)-N(3)	113.33(7)
C(40)-Al(1)-N(2)	110.66(7)	C(42)-Al(2)-N(3)	105.91(7)

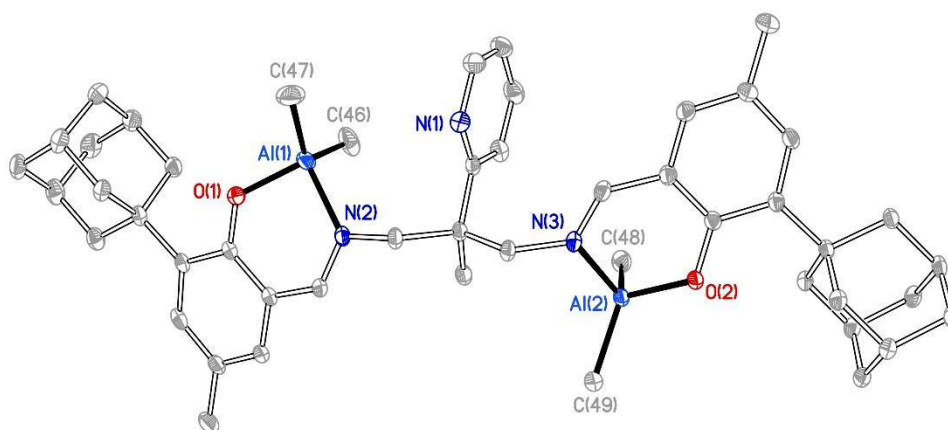


**Figure 5.3 :** Solid state structure of [Al<sub>2</sub>(Ad,Me-Salpy)Me<sub>4</sub>] (**42**). Ellipsoids are shown at the 30% probability level. Hydrogen atoms are omitted for clarity

**Table 5.2:** Selected bond lengths (Å) and bond angles (°) for [Al<sub>2</sub>(Ad,Me-Salpy)Me<sub>4</sub>] (**42**)

Al(1)-O(1)	1.7764(13)	Al(2)-O(2)	1.7833(13)
Al(1)-C(47)	1.944(3)	Al(2)-C(49)	1.9493(19)
Al(1)-C(46)	1.969(3)	Al(2)-C(48)	1.961(2)
Al(1)-N(2)	1.9759(16)	Al(2)-N(3)	1.9706(15)
O(1)-Al(1)-C(47)	108.91(10)	O(2)-Al(2)-C(49)	114.15(8)
O(1)-Al(1)-C(46)	110.14(9)	O(2)-Al(2)-C(48)	107.15(7)
C(47)-Al(1)-C(46)	119.20(13)	C(49)-Al(2)-C(48)	120.96(9)
O(1)-Al(1)-N(2)	93.58(6)	O(2)-Al(2)-N(3)	93.69(6)
C(47)-Al(1)-N(2)	113.70(10)	C(49)-Al(2)-N(3)	109.10(7)
C(46)-Al(1)-N(2)	108.32(10)	C(48)-Al(2)-N(3)	108.27(8)

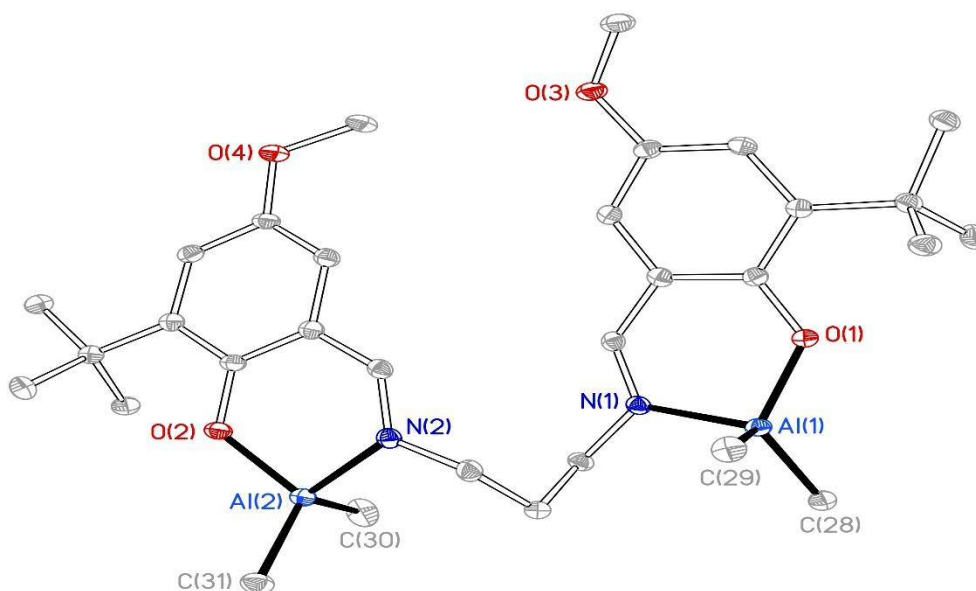


**Figure 5.4 :** Solid state structure of [Al<sub>2</sub>(<sup>t</sup>Bu,OMe-salpn)Me<sub>4</sub>] (**43**). Ellipsoids are shown at the 30% probability level. Hydrogen atoms are omitted for clarity

**Chapter 5 - Bimetallic aluminium complexes: Synthesis, characterization, X-ray crystal structures and ring opening polymerization**

**Table 5.3:** Selected bond lengths (Å) and bond angles (°) for  $[\text{Al}_2(\text{tBu,OMe-salpn})\text{Me}_4]$  (**43**)

Al(1)-O(1)	1.7702(13)	Al(2)-O(2)	1.7683(14)
Al(1)-C(28)	1.9568(19)	Al(2)-C(31)	1.954(2)
Al(1)-C(29)	1.9638(19)	Al(2)-C(30)	1.959(2)
Al(1)-N(1)	1.9727(15)	Al(2)-N(2)	1.9693(15)
O(1)-Al(1)-C(28)	114.62(7)	O(2)-Al(2)-C(31)	113.04(8)
O(1)-Al(1)-C(29)	110.94(8)	O(2)-Al(2)-C(30)	111.50(9)
C(28)-Al(1)-C(29)	118.63(9)	C(31)-Al(2)-C(30)	117.12(10)
O(1)-Al(1)-N(1)	94.20(6)	O(2)-Al(2)-N(2)	93.85(6)
C(28)-Al(1)-N(1)	106.37(7)	C(31)-Al(2)-N(2)	110.37(7)
C(29)-Al(1)-N(1)	108.97(7)	C(30)-Al(2)-N(2)	108.41(8)

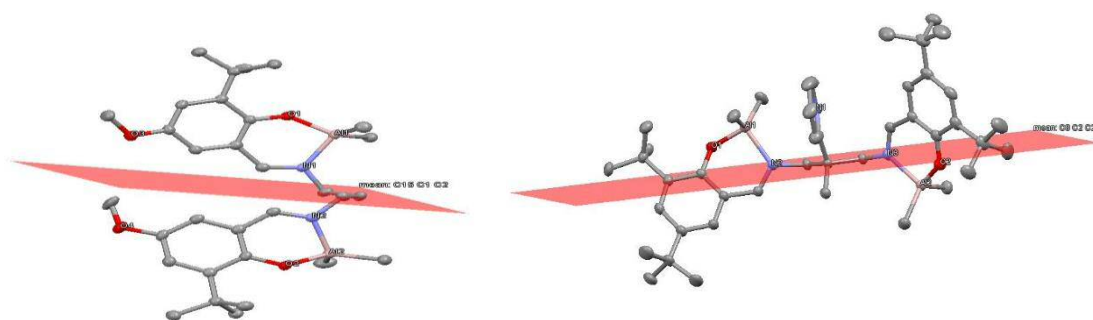


**Figure 5.5:** relative location of Al centres in  $[\text{Al}_2(\text{tBu,tBu-Salpy})\text{Me}_4]$  (**41**, right) and  $[\text{Al}_2(\text{tBu,OMe-salpn})\text{Me}_4]$  (**43**, left)

**Chapter 5 - Bimetallic aluminium complexes: Synthesis, characterization, X-ray crystal structures and ring opening polymerization**

One of the most interesting features of these structures is the relative location of the two aluminium centres. For example, an analysis of the C<sub>3</sub> plane formed by the propylene fragment of the Salpy ligand in [Al<sub>2</sub>(<sup>t</sup>Bu,<sup>t</sup>Bu-Salpy)Me<sub>4</sub>] (**41**) shows that the aluminium centres are oriented on opposite sides of this plane. This gives an Al(1)⋯Al(2) distance of 7.970 Å. This configuration is presumably necessary to minimise steric clashes between the bulky <sup>t</sup>Bu substituents. The same behaviour was observed with [Al<sub>2</sub>(Ad,Me-Salpy)Me] (**42**), which gives an Al(1)⋯Al(2) distance of 7.537 Å. However, for [Al<sub>2</sub>(<sup>t</sup>Bu,OMe-salpn)Me<sub>4</sub>] (**43**) the corresponding Al⋯Al distance is 6.672 Å, which is shorter than complexes **41** and **42**. This shorter distance derives from the free rotation of the C<sub>3</sub> propylene unit, which being free of hydrocarbyl substituents is more flexible in **43** which allows the ligand to adopt an alternative configuration in which the Al centres are mutually *cis*, whilst still avoiding steric conflict between the two <sup>t</sup>Bu substituents.

Regarding the bond lengths and angles, there were no significant differences between the three complexes. As we can see from the bond angles in the above tables, the C-Al-C angles are more obtuse than the other angles subtended at Al (involving O or N donors). From these data the distortions in the angles can be explained by considering only the electronic effects. The more acute angles are generated with more electronegative atoms, which possess more *p*-orbital character in their bonds and so generally have more acute angles than for less electronegative donors, such as carbon.<sup>16</sup>

The C-Al-C bond angles range from 117.12(10)° to 122.24(10)°. The Al-C, Al-O and Al-N distances range from 1.944(3)–1.969(3) Å, 1.768(14)–1.786(13) Å and 1.9965(14)–1.980(15) Å respectively, which within the expected ranges for four-coordinate methyl aluminium complexes.<sup>17–20</sup>

#### **5.4. Ring opening polymerization using Bimetallic aluminium complexes**

Owing to the success of the monometallic Al-Salpy complexes in the ring-opening polymerization of  $\epsilon$ -caprolactone ( $\epsilon$ -CL), complexes **41-43** were tested for catalytic efficacy in this type of polymerization reaction. The most interesting feature is the role, if any, of the pyridyl donor; it may be expected that this group will have little influence, since there is no evidence that the pyridyl coordinates to the aluminium ions in the methyl complexes, *vide supra*.

In a typical polymerization experiment, the appropriate bimetallic aluminium complex and benzyl alcohol were stirred in toluene at room temperature for 15 minutes in a glove box. The reaction was charged with the required amount of  $\epsilon$ -CL, the screw-cap vial sealed, then placed in an oil bath thermostated at the required temperature for the prescribed time. After the experiment was completed, the polymer was isolated by precipitation with cold methanol. The precipitate was collected by filtration and dried under vacuum. For polymerization experiments where conversion was required, aliquot samples were taken directly from the reaction mixture and the conversion determined by  $^1\text{H}$  NMR spectroscopy.

In Chapter 3, it was noted that the monometallic complexes were, unusually, active for the ROP of  $\epsilon$ -CL at room temperature. A meaningful comparison was therefore made by testing the bimetallic congeners under similar conditions. The experiments showed that the pyridyl-free complex  $[\text{Al}_2(\text{tBu}, \text{OMe-salpn})\text{Me}_4]$  (**43**) exhibited only very low activity at room temperature in the presence of 4 equivalents of BnOH, whereas the pyridyl-containing complexes  $[\text{Al}_2(\text{tBu}, \text{tBu-Salpy})\text{Me}_4]$  (**41**) and  $[\text{Al}_2(\text{Ad}, \text{Me-Salpy})\text{Me}_4]$  (**42**) exhibited high activities.

Both complexes **41** and **42** showed high conversion (92-99%) after 4 hours at room temperature. Conversely complex **43** gave only 11% conversion after five hours at the same temperature (Figure 5.6); even when the reaction time was increased to 24 hours, the conversion was still only 62%.

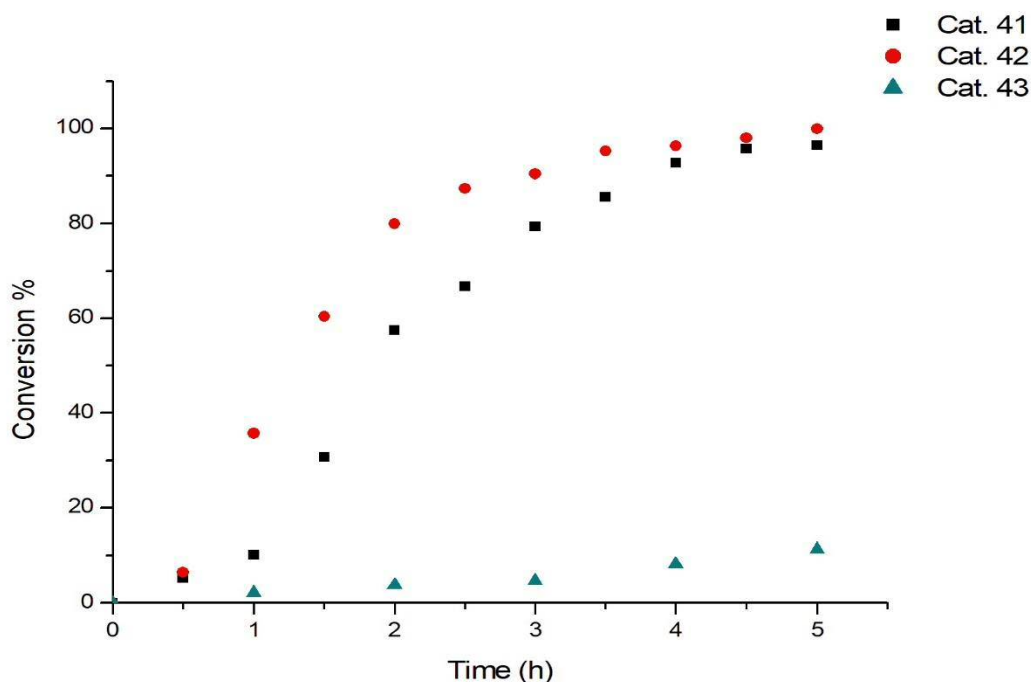


**Figure 5.6:** Conversion versus time for the ROP of  $\epsilon$ -CL by **41**, **42** and **43** at 25 °C in the presence of BnOH.

It should be noted that any catalytic activity in this reaction at room temperature is impressive for aluminium. However, the reactivity of **43** is clearly substantially lower than for **41** and **42**, the reasons for which are not entirely clear. One possible explanation is that the different reactivity levels may be attributed to the structure of the complex in both solid states and the solution; specifically, it has been shown that the Al...Al distance in bimetallic complexes affects the polymerization process. Hughes and co-workers explained that a shorter Al...Al distance hinders the polymerization process. In their study, complex **5.7** (Figure 5.7) has an Al...Al distance of 5.7818(10) Å whereas complex **5.8** has corresponding distances of 3.2129(13) and 3.2270(14) Å. Complex **5.7** showed higher reactivity in contrast to complex **5.8**.<sup>21</sup>

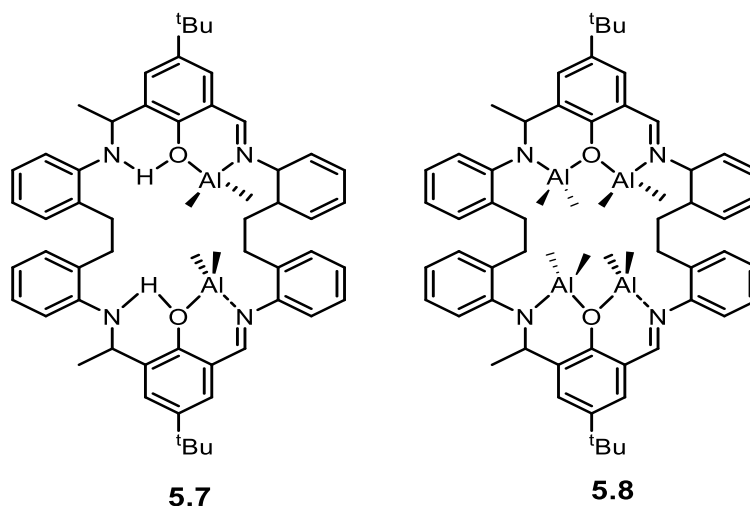


**Figure 5.7:** Bimetallic complexes reported by Hughes

As described above, in the crystal structure analyses of **41**, **42** and **43**, the distances between the aluminium centres in the complexes containing a pyridyl group are larger than the distance in the complex without a pyridyl, presumably due to a greater degree of conformational flexibility in the propylene backbone. It is possible that this may equate to the observations by Hughes *et al.*, and a shorter Al...Al distance is responsible for the lower activity. However, the inherent flexibility in the propylene backbone necessarily means that the Al...Al distance need not be the same in both solid state and in solution. Indeed, one would expect that in solution the two Al-containing moieties would have an average structure in which the Al ions are as far apart as possible. If true, this would undermine the applicability of Hughes' interpretation to the system described in this thesis.

An alternative interpretation is worth considering in these systems, which pertains to the role of the pyridyl donor. In the solid state structures, the pyridyl donors in **41** and **42** are apparently pendant, and have no discernable interaction with either of the aluminium centres. The danger of equating this observation to the molecular structure during a catalytic reaction is that the coordination spheres in the catalytic intermediates will be necessarily different to those in the pre-catalyst complexes. It would therefore be erroneous to assume that the pyridyl must be pendant in the corresponding alkoxide complexes (which are expected

to the propagating catalytic species); indeed, preliminary DFT calculations by Dr. B. Ward of the hypothetical complex  $[\text{Al}_2(\text{Salpy})_2(\text{OMe})_4]$  indicates that the pyridyl coordinates to one of the Al centres. It therefore seems a distinct possibility that the pyridyl donor of the Salpy ligands has a role to play in the reactivity enhancement of complexes **41** and **42**, compared to **43**.

In order to study the mechanism of  $\epsilon$ -CL polymerization, kinetic investigations were conducted at 25 °C, with  $[\epsilon\text{-CL}]_0/[I]_0 = 200:1$ . For all complexes the polymerization reactions obeyed first-order kinetic in the monomer after an initial induction period. For the three complexes, the *pseudo*-first-order rate constants  $k_{\text{app}}$  were different, being  $0.855 \pm 0.034$ ,  $0.997 \pm 0.031$  and  $0.023 \pm 0.002 \text{ h}^{-1}$  for complexes **41**, **42** and **43** respectively, thus indicating that differences in ligand structure affects the catalytic activity. As expected, the values of  $k_{\text{app}}$  are of a similar order of magnitude for the two pyridyl-containing complexes **41** and **42**, and significantly lower for the pyridine-free complex **43**. Representative kinetic plots for complexes **41** and **42** are reported in figure 5.8, and for complex **43** in Figure 5.9.

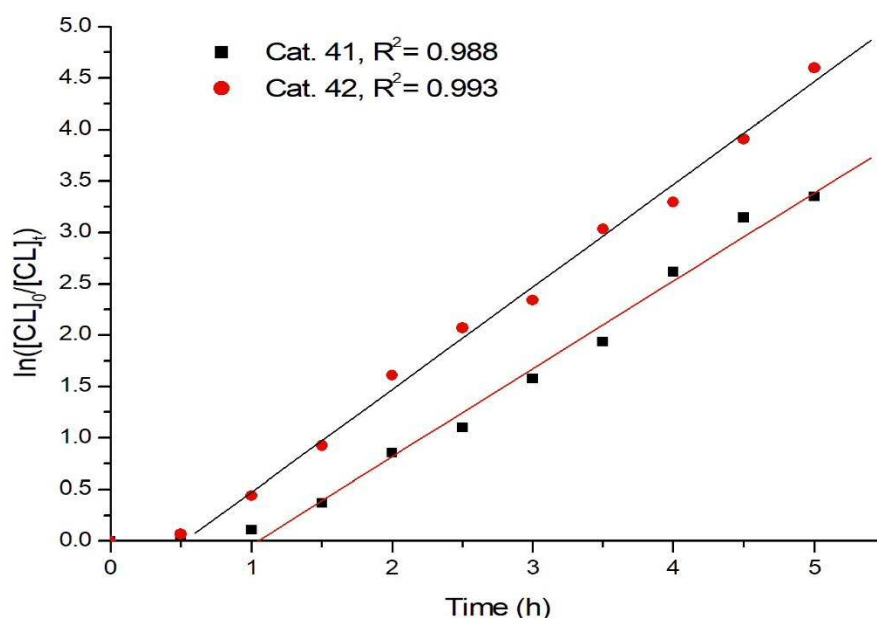


**Figure 5.8:** *Pseudo*-first-order kinetic plots for ROP of  $\epsilon$ -CL promoted by **41** and **42**. The *pseudo*-first-order rate constant are  $0.855 \pm 0.034$  and  $0.997 \pm 0.031 \text{ h}^{-1}$  for **41** and **42** respectively. Reaction conditions:  $[\epsilon\text{-CL}]_0 = 0.5 \text{ M}$ ;  $[\epsilon\text{-CL}]_0/[I]_0 = 200$ ; toluene 3 mL;  $T = 25 \text{ }^\circ\text{C}$

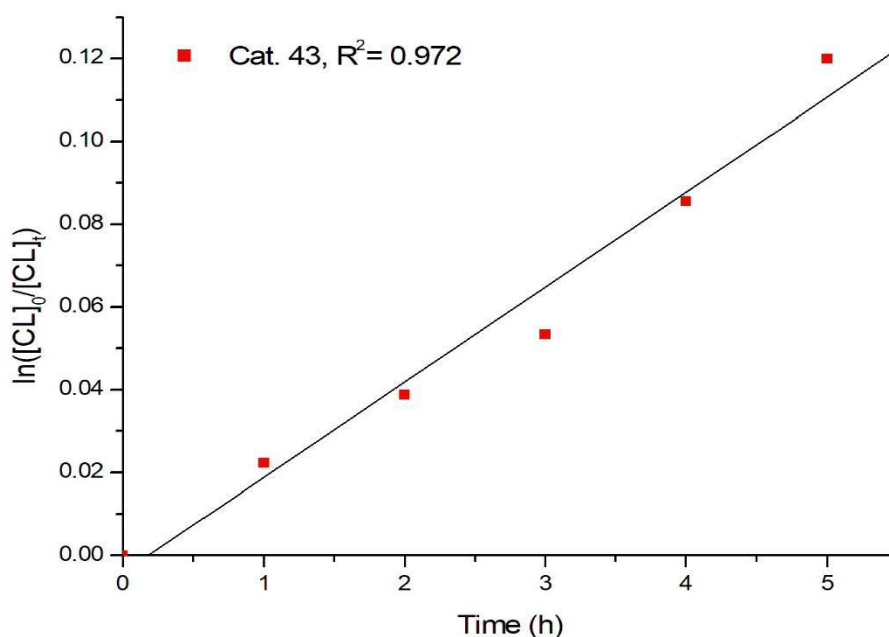


**Figure 5.9:** Pseudo-first-order kinetic plots for ROP of  $\epsilon$ -CL promoted by **43**.

The pseudo-first-order rate constant is  $0.023 \pm 0.002 \text{ h}^{-1}$ . Reaction conditions:  $[\epsilon\text{-CL}]_0 = 0.5 \text{ M}$ ;  $[\epsilon\text{-CL}]_0/[I]_0 = 200$ ; toluene 3 mL;  $T = 25 \text{ }^\circ\text{C}$

Increasing the reaction temperature led to a dramatic improvement in the polymerization rates; catalytic activity was enhanced with the increase in polymerization temperature, which is expected for a catalyst that has good thermal stability. For example, complex **43** gave 8% conversion at  $25 \text{ }^\circ\text{C}$  within 4 h, whereas it gave 100% conversion at  $50 \text{ }^\circ\text{C}$  in the same time under otherwise identical conditions, a rate increase of 12 times than that at  $25 \text{ }^\circ\text{C}$  (Figure 5.10). Complex **41** gave 79% conversion of at  $25 \text{ }^\circ\text{C}$  in 3 h. By contrast, it led to 91% monomer conversion at  $50 \text{ }^\circ\text{C}$  in the same time. The data suggest that there is a high activation barrier to polymerization propagation with **43** that requires temperature elevation to proceed with an acceptable rate; a lower activation barrier for **41** and **42** results in a high propagation rate at room temperature. Whilst elevated temperature gives higher reaction rates for **41** and **42**, it is not necessary for these catalysts. The differences in  $k_{\text{app}}$  for **41** and **42** presumably reflect the differences in steric demands of the Salpy ligand. Whilst **42** has the largest substituent (adamantyl), the second group is small (methyl); complex **41** has two bulky groups (two *tert*-butyl groups).

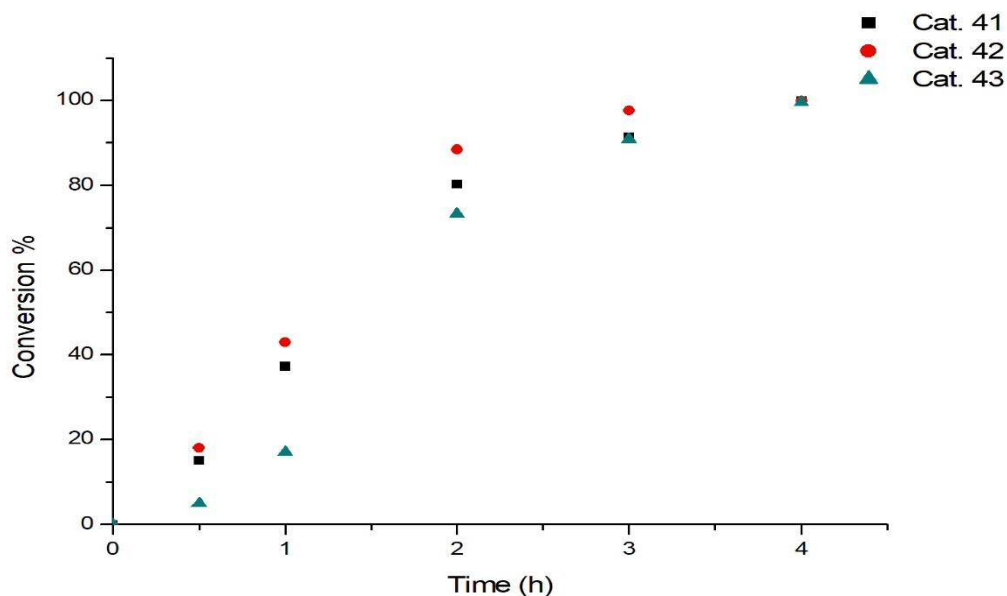


**Figure 5.10:** Conversion versus time for the ROP of  $\epsilon$ -CL by **41**, **42** and **43** at 50 °C in the presence of BnOH.

The kinetic study additionally involved the effect of [CL][Cat] molar ratio on the molecular weight and PDI of the polymer. The number average molecular weight versus monomer to initiator ratio (Figures 5.11, 5.12 and 5.13) showed a linear dependence of molecular weight with monomer concentration, which is one of the indications of “living” character of polymerization processes. The PDI showed a very slight decrease upon increasing the monomer to initiator ratio, but was invariably found between 1.4 and 1.1, indicating that the polymerization was well controlled; the values for **41** are slightly high for a truly “living” polymerization process (typically < 1.1), but those of **42** and **43** approach such values that could be classified as living-type behaviour.

**Chapter 5 - Bimetallic aluminium complexes: Synthesis, characterization, X-ray crystal structures and ring opening polymerization**

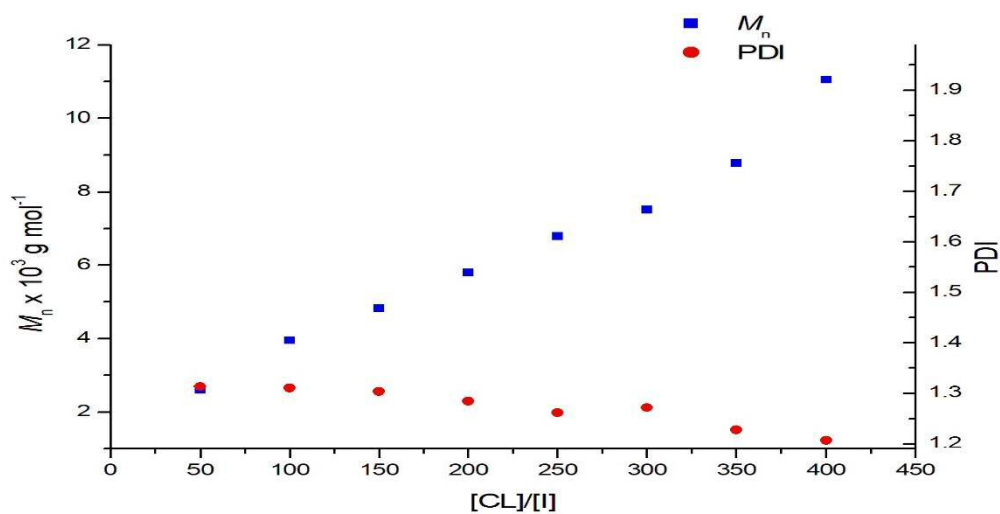


**Figure 5.11:** Plot of  $M_n$  vs.  $[CL]/[I]$  for the polymerization of  $\epsilon$ -CL catalysed by complex **41** and BnOH in toluene at 50 °C. All conversions >97%.

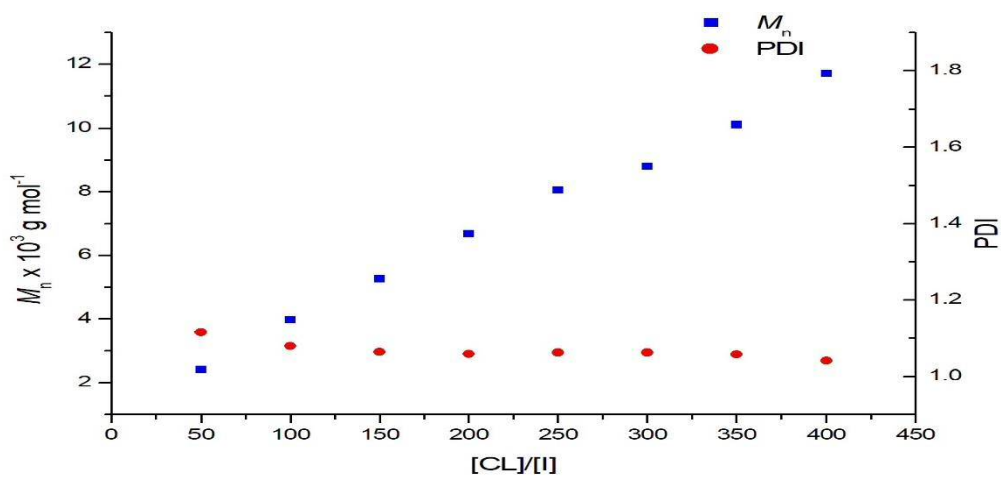


**Figure 5.12:** Plot of  $M_n$  vs.  $[CL]/[I]$  for the polymerization of  $\epsilon$ -CL catalysed by complex **42** and BnOH in toluene at 50 °C. All conversions >97%.

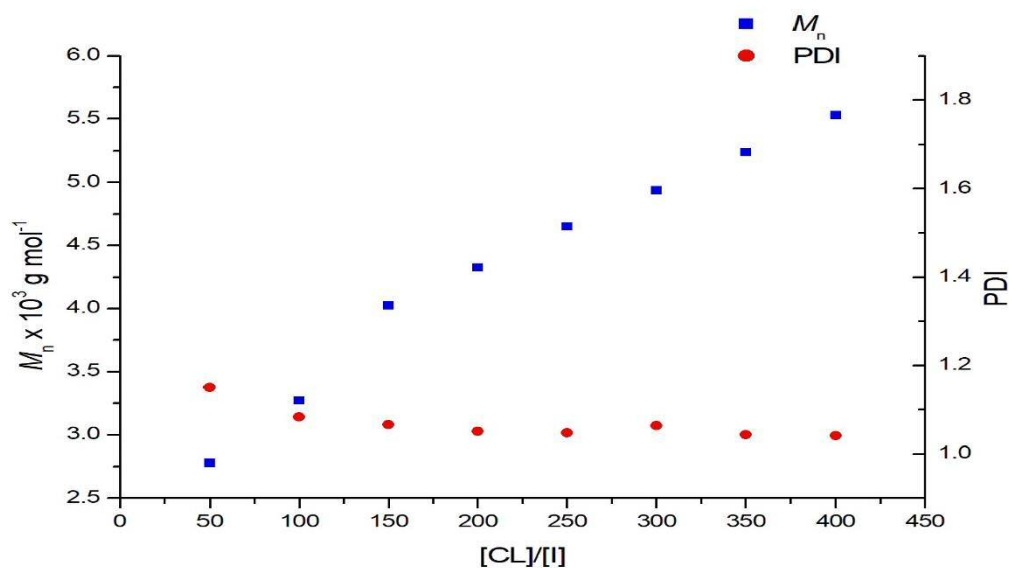


**Figure 5.13:** Plot of  $M_n$  vs.  $[CL]/[I]$  for the polymerization of  $\epsilon$ -CL catalysed by complex **43** and BnOH in toluene at 50 °C. All conversions >97%.

The polymerization data at 50 °C are summarized in Table 5.4. Entries 1-16, which involve using **41** and **42** as a catalyst at different molar ratio of  $[CL]_0:[Al]_0$  showed that the molecular weights determined by GPC, and corrected using Mark-Houwink equation, approximately match the theoretical values calculated on the basis of four initiating groups in each complex molecule (i.e. two chains per metal centre). This implies that all four BnO groups in each complex are active for the polymerization. However, the PDIs of the polymers formed by using complex **41** are a little large, especially when the monomer-to-catalyst ratio is low. Whereas the PDIs of the polymers using **42** and **43** as the catalysts are narrow throughout the range of monomer to initiator ratios studied.

**Chapter 5 - Bimetallic aluminium complexes: Synthesis, characterization, X-ray crystal structures and ring opening polymerization**

**Table 5.4:** Ring-opening polymerization of  $\epsilon$ -caprolactone initiated by complexes **41**, **42** and **43** at 50 °C for 4 h.

Entry	Cat.	[M] <sub>0</sub> : [Al] <sub>0</sub>	<i>M<sub>n</sub></i> (obsd)	<i>M<sub>n</sub></i> (calcd)	<i>M<sub>w</sub></i> / <i>M<sub>n</sub></i>
1	<b>41</b>	50:1:4	2590	1520	1.23
2	<b>41</b>	100:1:4	3950	2933	1.31
3	<b>41</b>	150:1:4	4830	4345	1.30
4	<b>41</b>	200:1:4	5810	5758	1.28
5	<b>41</b>	250:1:4	6800	7170	1.26
6	<b>41</b>	300:1:4	6810	8583	1.27
7	<b>41</b>	350:1:4	8790	9995	1.22
8	<b>41</b>	400:1:4	11210	11408	1.20
9	<b>42</b>	50:1:4	2420	1520	1.11
10	<b>42</b>	100:1:4	3970	2933	1.07
11	<b>42</b>	150:1:4	5270	4345	1.06
12	<b>42</b>	200:1:4	6680	5758	1.05
13	<b>42</b>	250:1:4	8060	7170	1.06
14	<b>42</b>	300:1:4	8800	8583	1.06
15	<b>42</b>	350:1:4	10110	9995	1.05
16	<b>42</b>	400:1:4	11700	11408	1.04
17	<b>43</b>	50:1:4	2270	1520	1.15
18	<b>43</b>	100:1:4	3270	2933	1.08
19	<b>43</b>	150:1:4	4020	4345	1.06

**Chapter 5 - Bimetallic aluminium complexes: Synthesis, characterization, X-ray crystal structures and ring opening polymerization**

20	<b>43</b>	200:1:4	4580	5758	1.05
21	<b>43</b>	250:1:4	4650	7170	1.04
22	<b>43</b>	300:1:4	4940	8583	1.06
23	<b>43</b>	350:1:4	5240	9995	1.04
24	<b>43</b>	400:1:4	5530	11408	1.04

Polymerization reactions in the presence of a different ratios of BnOH were also evaluated (entries 25-28, Table 5.5). Complex **42** was used at 50 °C for 4 h (monomer : initiator = 200 : 1). The catalytic activity of the complex increased upon increasing the ratio of BnOH : pre-catalyst. In the presence of 1 equivalent of BnOH 67% conversion was obtained (entry 25), whereas under the same reaction conditions in the presence of 4 equivalents of BnOH, the reaction gave 99% conversion (entry 28, Table 5.5).

It has been suggested that the added BnOH molecules act as chain-transfer agents in the polymerization reaction. They result in the formation of new benzyloxy-metal complexes along with hydroxy-terminated polymer chains. Each new formed benzyloxy-metal complex molecule is a new initiator for the lactone polymerization. Hence the total number of PCL molecules is greater than the initial number of metal complex molecules introduced and is directly set by the initial amount of chain-transfer agents introduced.<sup>22,23</sup> However increasing the number of chain-termination events in the catalytic reaction would result in an increase in PDI, which was not observed in these bimetallic complexes. It was nevertheless observed that there was a direct effect of the amount of added benzyl alcohol on the  $M_n$  values of the obtained polymer. As we can see from Table 5.5, the  $M_n$  values obtained from GPC measurement dropped gradually with increasing BnOH equivalents, with a relatively constant PDI. It is therefore likely that each added benzyl alcohol results in one alkoxide ligand by the *in situ* alcoholysis of a methyl ligand; the alkoxide ligand acts as an initiating group, which is more efficient than the original methyl ligand. In particular, the methyl

ligand is likely to have a slow initiating rate compared to the alkoxide. Therefore to a first approximation, the number of polymer chains per metal equates to the number of alkoxide ligands; adding four BnOH equivalents results in 4 polymer chains/complex which results in a lower molecular weight. These data with an agreement with results obtained by Ma and Wang, who used isopropanol as a cocatalyst and found that  $M_n$  value dropped from 9800 to 5500 when the feed ratio  $[CL]_0:[Cat]_0:[iPrOH]$  changed from  $[200][1][2]$  to  $[200][1][4]$ .<sup>24</sup> Generally, the amount of added BnOH has a great influence in both the conversion and molecular weight of the resulting polymer.

**Table 5.5:** polymerization of  $\epsilon$ - CL using complex 42 and different concentration of BnOH.

Entry	Cat.	$[M]_0:[Al]_0:[BnOH]$	Conv. (%)	$M_n$ (obsd)	$M_n$ (calcd)	$M_w/M_n$
25	42	200:1:1	67	19700	15377	1.06
26	42	200:1:2	86	17080	9830	1.08
27	42	200:1:3	92	9530	7091	1.07
28	42	200:1:4	99	6680	5758	1.05

## 5.5 Lactide polymerization

Preliminary experiments were conducted to investigate the reactivity of the bimetallic aluminium complexes **41**, **42** and **43** as initiators for the ROP of *rac*-lactide. The reactivity of these complexes towards *rac*-lactide polymerization was much lower than for  $\epsilon$ -caprolactone, and therefore these experiments were carried out in toluene at 80 °C for 20 h in the presence of BnOH. The feed ratio of  $[LA]_0:[Al]_0$  was 100:1 in all experiments with two different equivalents of BnOH. The concentration of *rac*-lactide  $[rac\text{-lactide}]_0$  was 1.0 mol L<sup>-1</sup>. The polymerization results are summarized in Table 5.6.

**Chapter 5 - Bimetallic aluminium complexes: Synthesis, characterization, X-ray crystal structures and ring opening polymerization**

In all cases, the polymerization reactions gave near quantitative conversion, with narrow PDIs, but which were higher than the values obtained for the PCL experiments above. Upon increasing the amount of BnOH from 2 to 4 equivalents, the measured number-averaged molecular weight ( $M_n$ ) was found to decrease, as expected, but not as dramatically as for PCL. Kinetic studies were not performed owing to time constraints, but this is a promising area for further study.

**Table 5.6:** polymerization of *rac*-lactide using complex **41**, **42** and **43** with different amounts of BnOH.

Entry	Cat.	[M] <sub>0</sub> : [Al] <sub>0</sub> : [BnOH]	Conv. (%)	$M_n$ (obsd)	$M_n$ (calcd)	$M_w/M_n$
29	<b>41</b>	100:1:2	97.9	4920	7163	1.19
30	<b>41</b>	100:1:4	97.4	4120	3509	1.25
31	<b>42</b>	100:1:2	97.5	7830	7134	1.21
32	<b>42</b>	100:1:4	97.7	4060	3628	1.24
33	<b>43</b>	100:1:2	97.8	9970	7156	1.28
34	<b>43</b>	100:1:4	97.4	9400	3653	1.17

## 5.6 Conclusion

Three New dinuclear aluminum methyl complexes of the general formula  $LAl_2Me_4$ , where L are salpy or salpn ligands with a propyl (Complex **43**) or substituted propyl (Complexes **41** and **42**) backbone have been prepared through alkane elimination reactions between each ligand and two equivalents of  $AlMe_3$ .

The activities of these aluminium complexes in the ring-opening polymerization (ROP) of  $\epsilon$ -CL, and some preliminary experiments with *rac*-LA have been

investigated and compared. The dinuclear complexes **41** and **42**, bearing the salpy ligand with the pyridyl and methyl groups on the propyl backbone, were the most active in the ROP of  $\epsilon$ -CL at room temperature showing high conversion between 3-4 h reaction time. Conversely, the salpn complex (**43**), showed very poor activity at room temperature. increasing the temperature to 50 °C dramatically enhanced the reactivity of **43**, and moderately for **41** and **42**.

## 5.7 References

- 1 T. M. Ovitt and G. W. Coates, *J. Polym. Sci. Part A Polym. Chem.*, 2000, **38**, 4686–4692.
- 2 J. Wu, X. Pan, N. Tang and C. C. Lin, *Eur. Polym. J.*, 2007, **43**, 5040–5046.
- 3 B. Gao, D. Li, Y. Li, Q. Duan, R. Duan and X. Pang, *New J. Chem.*, 2015, **39**, 4670–4675.
- 4 M. O. Miranda, Y. Deporre, H. Vazquez-Lima, M. A. Johnson, D. J. Marell, C. J. Cramer and W. B. Tolman, *Inorg. Chem.*, 2013, **52**, 13692–13701.
- 5 D. J. Darensbourg, O. Karroonnirun and S. J. Wilson, *Inorg. Chem.*, 2011, **50**, 6775–6787.
- 6 M. P. F. Pepels, M. Bouyahyi, A. Heise and R. Duchateau, *Macromolecules*, 2013, **46**, 4324–4334.
- 7 E. Bukhaltsev, L. Frish, Y. Cohen and A. Vigalok, *Org. Lett.*, 2005, **7**, 5123–5126.
- 8 H. Chen, M. Liu, A. K. Sutar and C. Lin, *Inorg. Chem.*, 2010, **49**, 665–674.
- 9 L. Chen, W. Li, D. Yuan, Y. Zhang, Q. Shen and Y. Yao, *Inorg. Chem.*, 2015, **54**, 4699–4708.
- 10 H. Tseng, H. Chen, Y. Huang, W. Lu, Y. Chang, M. Y. Chiang, Y. Lai and

**Chapter 5 - Bimetallic aluminium complexes: Synthesis, characterization, X-ray crystal structures and ring opening polymerization**

- H. Chen, *Inorg. Chem.*, 2016, **55**, 1642–1650.
- 11 A. Lara-sa, M. North and P. Villuendas, *Catal. Sci. Technol.*, 2012, **2**, 1021–1026.
- 12 J. Martínez and A. Otero, *Catal. Sci. Technol.*, 2014, **4**, 1674–1684.
- 13 W. Clegg, R. W. Harrington, M. North and R. Pasquale, *Chem. Eur. J.*, 2010, **16**, 6828–6843.
- 14 M. North and R. Pasquale, *Angew. Chemie - Int. Ed.*, 2009, **48**, 2946–2948.
- 15 M. North, P. Villuendas and C. Young, *Tetrahedron Lett.*, 2012, **53**, 2736–2740.
- 16 M. A. Van Aelstyn, T. S. Keizer, D. L. Klopotek, S. Liu, P. Wei and D. A. Atwood, *Organometallics*, 2000, **19**, 1796–1801.
- 17 J. Lewin, J. Zachara, K. B. Starowieyski, Z. Ochal, I. Justyniak, T. Kopec and P. Stolarzewicz, *Organometallics*, 2003, **22**, 3773–3780.
- 18 Y. Liu, W. Dong, J. Liu and Y. Li, *Dalt. Trans.*, 2014, **43**, 2244–2251.
- 19 P. A. Cameron, V. C. Gibson, C. Redshaw, J. A. Segal, G. A. Solan, A. J. P. White and D. J. Williams, *J. Chem. Soc., Dalt. Trans.*, 2001, 1472–1476.
- 20 S. Milione, F. Grisi, R. Centore and A. Tuzi, *Eur. J. Inorg. Chem.*, 2008, 5532–5539.
- 21 A. Arbaoui, C. Redshaw and D. L. Hughes, *Chem. Commun.*, 2008, 4717–4719.
- 22 M. Hsueh, B. Huang and C. Lin, *Macromolecules*, 2002, **35**, 5763–5768.
- 23 M. Helou, O. Miserque, J. Brusson, J. Carpentier and S. M. Guillaume, *Chem. Eur. J.*, 2008, **14**, 8772–8775.
- 24 Y. Wang and H. Ma, *Chem. Commun.*, 2012, **48**, 6729–6731.

# **Chapter 6**

## **Experimental**

## 6.1 General Methods and Instrumentation

All manipulations involving metal complexes and sample preparation for polymerization studies were carried out using standard Schlenk line or glove-box techniques under an atmosphere of argon or of dinitrogen. Solvents were predried over activated 4 Å molecular sieves and were refluxed over potassium (tetrahydrofuran and benzene) or sodium wire / benzophenone (diethyl ether) under a dinitrogen atmosphere and collected by distillation. Other solvents were dried by passing through a column of activated alumina incorporated into an Mbraun SPS800 solvent purification system (Toluene, pentane and hexanes). Solvents (other than dichloromethane and THF) were stored over potassium mirrors. Deuterated solvents were dried over potassium ( $C_6D_6$ , THF- $d_3$ ) or calcium hydride ( $CDCl_3$ ), distilled under reduced pressure and stored under dinitrogen in Teflon valve ampoules.

$\epsilon$ -Caprolactone, Cyclohexene oxide, Propylene oxide and styrene oxide were dried by stirring over fresh calcium hydride for 48 h and then distilled under reduced pressure. *Rac*-Lactide was purified using a three-step procedure involving a recrystallization from a hot, concentrated  $i$ PrOH (80 °C), followed by two subsequent recrystallizations from hot toluene (100 °C) and finally sublimed under vacuum and stored in refrigerator. All anhydrides used in copolymerization were purified by sublimation under reduced pressure. The pyridine-diamine precursor PPDA,<sup>1</sup> and the salicylaldehyde derivatives, 3-*tert*-Butyl-5-methoxysalicylaldehyde<sup>2</sup> and 3-(1-adamantyl)-5-methylsalicylaldehyde<sup>3</sup> were prepared according to published procedures. All other reagents were purchased from commercial suppliers and used as received, unless stated explicitly in the experimental text.

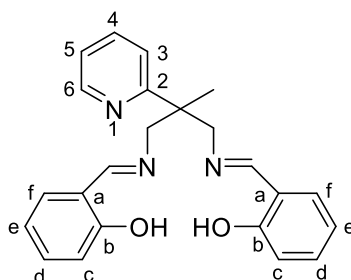
NMR samples of metal complexes were prepared under dinitrogen in 5 mm Wilmad 507-PP tubes fitted with J. Young Teflon valves.  $^1H$  and  $^{13}C$ - $\{^1H\}$  NMR spectra were recorded on Bruker Fourier 300, Bruker DPX 400 and Bruker Avance 500 spectrometers.  $^1H$  and  $^{13}C$  assignments were confirmed when necessary with the use of two dimensional  $^1H$ - $^1H$  and  $^{13}C$ - $^1H$  NMR experiments.  $^1H$  and  $^{13}C$  spectra were referenced internally to residual protio solvent ( $^1H$ ) or

## **Chapter 6 - Experimental**

solvent ( $^{13}\text{C}$ ) resonances, and are reported relative to tetramethylsilane ( $\delta = 0$  ppm). Chemical shifts are quoted in  $\delta$  (ppm) and coupling constants in Hertz. Infrared spectra were recorded on SHIMADZU IR AFFINITY-1S. Infrared data are quoted in wavenumbers ( $\text{cm}^{-1}$ ).

Mass Spectra were recorded at the EPSRC National Mass Spectrometry Service Centre, Swansea, UK or in-house at the School of Chemistry, Cardiff University using a Waters LCT Premier XE (oa-TOF) mass spectrometer. Elemental analyses were performed at the School of Human Sciences, London metropolitan University. Gel Permeation Chromatography data were obtained at Cardiff catalyst institute, Cardiff University using ACQUITY Advanced Polymer Chromatography System. X-ray data for single-crystal analyses were measured by the UK National Crystallography Service, School of Chemistry, University of Southampton;<sup>4</sup> the structures were subsequently solved using SHELXT,<sup>5</sup> and refined using SHELXL-2014,<sup>6</sup> by Dr. Benjamin Ward.

## 6.2 Ligand Synthesis

6.2.1 synthesis of Salpy<sup>(1)</sup>

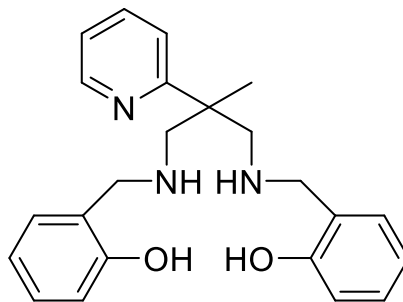
A solution of salicylaldehyde (2.21 g, 18.5 mmol) in methanol (15 mL) was added to a stirred solution of ppda (1.50 g, 9.07 mmol) in methanol (15 mL). The resulting yellow solution was stirred at 50 °C for 2 h. The pale-yellow solution was then allowed to cool to room temperature, whereupon a yellow precipitate formed, which was filtered and washed with cold methanol. The product was dried *in vacuo* for several hours. Yield: 2.97 g (88%). m.p = 118-120 °C.

<sup>1</sup>H NMR (400 MHz, CDCl<sub>3</sub>, 293 K): δ 13.21 (s, 2H, OH), 8.63 (ddd, <sup>3</sup>J = 4.8 Hz, <sup>4</sup>J = 1.9 Hz, <sup>5</sup>J = 0.9 Hz, 1 H, H<sup>6</sup>), 8.31 (s, 2 H, CH=N), 7.61 (td, <sup>3</sup>J = 7.6 Hz, <sup>4</sup>J = 1.9 Hz, 1 H, H<sup>4</sup>), 7.34 (dt, <sup>3</sup>J = 8.0 Hz, <sup>4</sup>J = 1.0 Hz, 1 H, H<sup>3</sup>), 7.28 (ddd, <sup>3</sup>J = 9.0 Hz, <sup>3</sup>J = 7.3 Hz, <sup>4</sup>J = 1.7 Hz, 2H, H<sup>d</sup>), 7.21 (dd, <sup>3</sup>J = 7.7 Hz, <sup>4</sup>J = 1.7 Hz, 2H, H<sup>c</sup>), 7.15 (ddd, <sup>3</sup>J = 7.5 Hz, <sup>3</sup>J = 4.8 Hz, <sup>4</sup>J = 1.0 Hz, 1 H, H<sup>5</sup>), 6.91 (dd, <sup>3</sup>J = 8.3 Hz, <sup>4</sup>J = 1.1 Hz, 2H, H<sup>f</sup>), 6.89 (td, <sup>3</sup>J = 7.4 Hz, <sup>4</sup>J = 1.1 Hz, 2H, H<sup>e</sup>), 4.13 (dd, <sup>2</sup>J = 12.2 Hz, <sup>4</sup>J = 1.1 Hz, 2H, CHH), 4.00 (dd, <sup>2</sup>J = 12.2 Hz, <sup>4</sup>J = 1.1 Hz, 2 H, CHH), 1.53 (s, 3 H, CH<sub>3</sub>).

<sup>13</sup>C{<sup>1</sup>H} NMR (101 MHz, CDCl<sub>3</sub>, 293 K): δ 166 (CH=N), 163.2 (C<sup>2</sup>), 161.07 (C<sup>b</sup>), 149.0 (C<sup>6</sup>), 136.4 (C<sup>4</sup>), 132.3 (C<sup>d</sup>), 131.3 (C<sup>c</sup>), 121.6 (C<sup>5</sup>), 121.16 (C<sup>3</sup>), 118.7 (C<sup>a</sup>), 118.5 (C<sup>e</sup>), 116.9 (C<sup>f</sup>), 67.11 (CH<sub>2</sub>), 46.13 (MeC), 21.71 (CH<sub>3</sub>).

FT-IR (cm<sup>-1</sup>): 3305 (O-H), 3055 (C-H aromatic), 2962 (s, C-H), 2920 (s, C-H), 2864 (s, CH), 1625 (s, C=N<sub>imine</sub>), 1496 (s, C=N<sub>py</sub>, C=C<sub>aromatic</sub>), 1452, 1422, 1377, 1334, 1273, 1209, 1155, 1038, 1019, 989, 949. HRMS for [M+H]<sup>+</sup> (ES): calcd. for (C<sub>23</sub>H<sub>24</sub>N<sub>3</sub>O<sub>2</sub>): 374.1869; found: 374.1887.

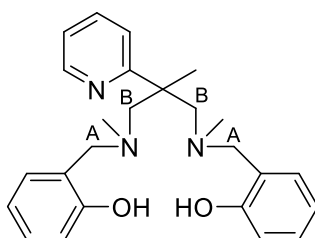
### 6.2.2 Synthesis of Salpy-H<sub>2</sub>



Following a modified literature procedure, ppda (0.684 g, 4.14 mmol) was dissolved in methanol (10 mL), to which a solution of salicylaldehyde (1.01 g, 8.27 mmol) in methanol (10 mL) was added. The resulting yellow solution was stirred at 50 °C for 2 h, and then the reaction mixture was treated carefully with sodium borohydride (0.46 g, 12.16 mmol) at 0 °C, stirred at room temperature for 5 h and the solvent removed under vacuum to give a white residue. The reaction was quenched by addition of aqueous saturated NaHCO<sub>3</sub> (100 mL), and the product extracted with diethyl ether (3 × 100 mL). The combined organic layers were washed with water (2 × 100 mL) and dried over MgSO<sub>4</sub>. The product was isolated after solvent evaporation. (1.29 g, 83% yield).

<sup>1</sup>H NMR (400 MHz, CDCl<sub>3</sub>, 293 K): δ 8.47 (ddd, <sup>3</sup>J = 4.8, <sup>4</sup>J = 1.9, <sup>5</sup>J = 0.9 Hz, 1H, H<sup>6</sup>), 7.61 (dt, <sup>3</sup>J = 7.7, <sup>4</sup>J = 1.9, 1H, H<sup>4</sup>), 7.23 (dt, <sup>3</sup>J = 8.1, <sup>4</sup>J = 0.9 Hz, 1H, H<sup>5</sup>), 7.11 – 7.10 (m, 3H), 6.91 (d, <sup>4</sup>J = 1.2 Hz, 1H), 6.89 (d, <sup>4</sup>J = 1.3 Hz, 1H), 6.72 – 6.66 (m, 4H), 3.88 (d, <sup>2</sup>J = 13.8 Hz, 2H, CH<sub>2</sub>), 3.81 (d, <sup>2</sup>J = 13.8 Hz, 2H, CH<sub>2</sub>), 3.05 (d, <sup>2</sup>J = 11.6 Hz, 2H, CH<sub>2</sub>), 2.81 – 2.78 (d, <sup>2</sup>J = 11.6 Hz, 2H, CH<sub>2</sub>), 1.39 (s, 3H, CH<sub>3</sub>). <sup>13</sup>C{<sup>1</sup>H} NMR (101 MHz, CDCl<sub>3</sub>, 293 K): δ 149.1(C-Py), 137.0 (Py-C), 128.7 (Ar-C), 128.4 (Ar-C), 121.9 (Py-C), 121.2 (Ar-C), 119.0 (Ar-C), 116.2 (Ar-C), 57.2 (CH<sub>2</sub>), 53.2 (CH<sub>2</sub>), 22.7 (CH<sub>3</sub>).

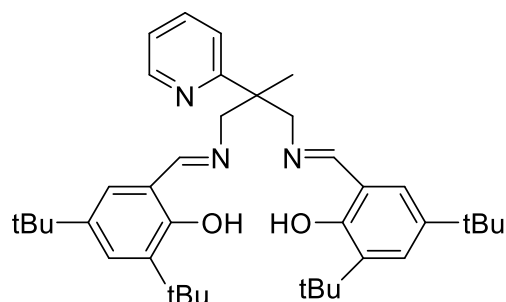
### 6.2.3 Synthesis of Salpy-Me



(0.85 g, 2.27 mmol) of Salpy-H<sub>2</sub> was dissolved in acetonitrile (20 mL) and aqueous formaldehyde (1.84 mL, 37% w/w, 22.75 mmol) was added. The reaction mixture was stirred for 15 min at room temperature and then sodium cyanoborohydride (0.43 g, 6.82 mmol) was added with constant stirring. After 15 min, glacial acetic acid (1.2 mL) was added to the mixture dropwise and stirring was continued for 5 h at room temperature. The solvent was then removed under reduced pressure and aqueous saturated NaHCO<sub>3</sub> (100 mL) was added to the residue. The product was extracted with diethyl ether (3 × 100 mL) and the combined organic layers were washed with water (2 × 100 mL) and dried over MgSO<sub>4</sub>. The solvent was evaporated under vacuum to give the crude product as a waxy solid compound which solidified after 3 days to give a white solid. The product was purified by recrystallization from methanol. (0.69 g, 75 % yield).

<sup>1</sup>H NMR (400 MHz, CDCl<sub>3</sub>, 293 K): δ 10.46 (s, 2H, OH), 8.60 (dd, *J* = 4.7, 0.9 Hz, 1H, H<sup>6</sup>), 7.74 (td, *J* = 7.8, 1.9 Hz, 1H, H<sup>4</sup>), 7.49 (d, *J* = 8.0 Hz, 1H, H<sup>3</sup>), 7.18 – 7.09 (overlapping, 3H, H<sup>5</sup>, H<sup>d</sup>), 6.88 (d, *J* = 6.3 Hz, 2H, H<sup>c</sup>), 6.73 (m, 4H, H<sup>f</sup>, H<sup>e</sup>), 3.65 (d, *J* = 13.7 Hz, 2H, (CHH<sup>A</sup>)), 3.56 (d, *J* = 13.7 Hz, 2H, CHH<sup>A</sup>), 3.26 (d, *J* = 13.2 Hz, 2H, CHH<sup>B</sup>), 2.62 (d, *J* = 13.2 Hz, 2H, CHH<sup>B</sup>), 1.94 (s, 6H, CH<sub>3</sub>N), 1.68 (s, 3H, CH<sub>3</sub>). <sup>13</sup>C{<sup>1</sup>H} NMR (101 MHz, CDCl<sub>3</sub>, 293 K): δ 163.7 (C<sup>2</sup>), 157.8 (C<sup>b</sup>), 149.4 (C<sup>6</sup>), 137.4 (C<sup>4</sup>), 129.1 (C<sup>d</sup>), 128.9 (C<sup>c</sup>), 122.5 (C<sup>5</sup>), 122.2 (C<sup>3</sup>), 119.6 ((C<sup>a</sup>), 119.0 (C<sup>e</sup>), 116.1 (C<sup>f</sup>), 68.2 (CH<sub>2</sub><sup>B</sup>), 64.31 (CH<sub>2</sub><sup>A</sup>), 47.03 (CH<sub>3</sub>N), 44.07 (CCH<sub>3</sub>), 20.94 (CH<sub>3</sub>C). HRMS (APCI): calcd. for (C<sub>25</sub>H<sub>31</sub>N<sub>3</sub>O<sub>2</sub>+H): 406.2495, found 406.2477.

### 6.2.4 Synthesis of <sup>t</sup>Bu, <sup>t</sup>Bu - Salpy

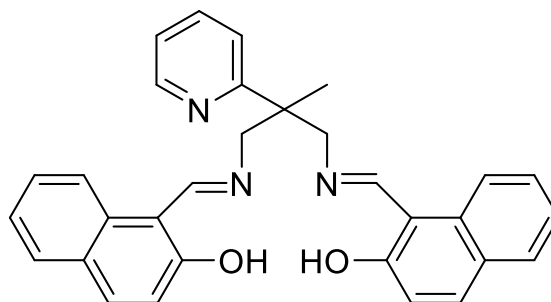


To a stirred solution of ppda (0.23 g, 1.39 mmol) in methanol (15 mL), a solution of 2, 4-di-tert-butyl-2-hydroxybenzaldehyde (0.655 g, 2.79 mmol) in methanol (15 mL) was added. The resulting yellow solution was stirred at 50 °C for 3 h. The pale yellow solution was then allowed to cool to room temperature, whereupon a yellow precipitate formed, which was filtered and washed with cold methanol. The product was dried *in vacuo*. Yield: 0.61 g (73%). m.p = 131-133 °C.

<sup>1</sup>H NMR (400 MHz, CDCl<sub>3</sub>, 293 K): δ 13.57 (s, 2 H, OH), 8.64 (dd, <sup>3</sup>J = 4.7 Hz, <sup>4</sup>J = 1.6 Hz, 1 H, H<sup>6</sup>), 8.36 (s, 2 H, CH=N), 7.66 (td, <sup>3</sup>J = 7.8 Hz, <sup>4</sup>J = 1.8 Hz, 1 H, H<sup>4</sup>), 7.35 (overlapping m, 3 H, H<sup>3</sup>, H<sup>d</sup>), 7.15 (ddd, <sup>3</sup>J = 7.4 Hz, <sup>4</sup>J = 4.8 Hz, <sup>5</sup>J = 0.7 Hz, 1 H, H<sup>5</sup>), 7.06 (d, <sup>4</sup>J = 2.4 Hz, 2 H, H<sup>f</sup>), 4.07 (s, 4 H, CH<sub>2</sub>), 1.58 (s, 3 H, CH<sub>3</sub>), 1.44 (s, 18 H, C(CH<sub>3</sub>)<sub>3</sub>), 1.30 (s, 18H, C(CH<sub>3</sub>)<sub>3</sub>).

<sup>13</sup>C{<sup>1</sup>H} NMR (101 MHz, CDCl<sub>3</sub>, 293 K): δ 167.3 (CH=N), 163.7 (C<sup>2</sup>), 158.2 (C<sup>b</sup>), 149.1 (C<sup>6</sup>), 137.0 (C<sup>4</sup>), 127.3 (Ar-C), 126.2 (Ar-C), 118.2 (Ar-C), 67.0 (CH<sub>2</sub>), 46.2 (Py-C-Me), 35.1 (C(CH<sub>3</sub>)), 34.2 (C(CH<sub>3</sub>)), 31.6 (C(CH<sub>3</sub>)), 29.5 (C(CH<sub>3</sub>)), 21.7 (CH<sub>3</sub>). FT-IR (cm<sup>-1</sup>): 3305 (O-H), 2956 (s, C-H), 2906 (s, C-H), 2864 (s, CH), 1620 (s, C=N<sub>imine</sub>), 1589, 1465 (s, C=N<sub>py</sub>, C=C<sub>aromatic</sub>), 1440, 1359, 1269, 1250, 1203, 1170, 1029, 948, 854, 825, 750. HRMS for [M+H]<sup>+</sup> (APCI): calcd. for (C<sub>40</sub>H<sub>55</sub>N<sub>3</sub>O<sub>2</sub>): 598.4373; found: 598.4365.

### 6.2.5 Synthesis of Naphpy



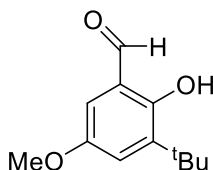
Under an argon atmosphere, to a stirred solution of ppda (2.02 g, 12.22 mmol) in dry ethanol (100 mL), 4.209 g, (24.44 mmol) of 2-hydroxy-1-naphthaldehyde was added in a small portions at 40 °C. After one hour, a yellow precipitate started to separate from the brown solution. The stirring was continued for further 4 h. After this time, the solution was cooled to room temperature and the precipitate was filtered, washed with cold ethanol (3 x 25 mL), and dried *in vacuo* to give the titled compound as a deep yellow solid. Yield (4.55 g, 78.6 %). m.p= 134-135 °C.

$^1\text{H}$  NMR (400 MHz,  $\text{CDCl}_3$ , 293 K):  $\delta$  14.42 (s, 2H, OH), 8.59 (d,  $^3J = 4.41$  Hz, 1H, H<sup>6</sup>), 8.54 (overlapping, 2H, CH=N), 7.58 – 7.48 (m, 5H), 7.43 (d,  $^3J = 7.7$  Hz, 2H), 7.22 – 7.09 (overlapping m, 3H), 7.04 (t,  $J = ^3J = 7.3$  Hz, 3H), 6.79 (d, 9.3 Hz, 2H), 3.98 (dd,  $J = 12.9, 3.9$  Hz, 2H, CH<sub>2</sub>H), 3.85 (dd,  $J = 12.9, 3.9$  Hz, 2H, CH<sub>2</sub>H), 1.48 (s, 3H, CH<sub>3</sub>).

$^{13}\text{C}\{^1\text{H}\}$  NMR (101 MHz,  $\text{CDCl}_3$ , 293 K):  $\delta$  174.01(CH=N), 161.63 (C<sup>2</sup>), 159.53 (Ar), 149.4 (C<sup>6</sup>), 136.97 (C<sup>4</sup>), 133.45 (Ar-C), 129.13 (Ar-C), 127.95 (Ar-C), 126.45 (Ar-C), 123.83 (Ar-C), 122.88 (Ar-C), 122.40 (C<sup>3</sup>), 121.42 (C<sup>5</sup>), 118.08 (Ar-C), 107.06 (Ar-C), 61.85 (CH<sub>2</sub>), 46.35 (Py-C-Me), 21.34 (CH<sub>3</sub>).

FT-IR ( $\text{cm}^{-1}$ ): 3050 (s, C-H<sub>Aromatic</sub>), 2960 (s, C-H), 2855 (s, CH), 1625 (s, C=N<sub>imine</sub>), 1530, 1445 (s, C=N<sub>py</sub>, C=C<sub>aromatic</sub>), 1440, 1350, 1135, 950. HRMS for  $[\text{M}+\text{H}]^+$  (ESI): calcd. for (C<sub>32</sub>H<sub>27</sub>N<sub>3</sub>O<sub>2</sub>): 474.2182; found 474.2173.

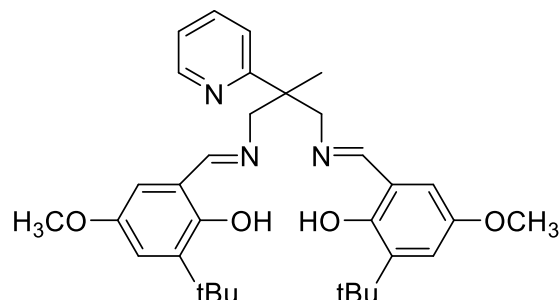
### 6.2.6 Synthesis of 3-*tert*-butyl-5-methoxy salicylaldehyde<sup>2</sup>



To a stirred solution of 3-*tert*-butyl-4-hydroxyanisole (2.26 g, 12.5 mmol) in glacial acetic acid, 12.5 mL, (3.51 g, 25 mmol) of hexamethylenetetramine was added. The resulting solution was heated at 110 °C for 2 hours and then aqueous solution of sulfuric acid (33%, 12.5 mL) was added at 75 °C. The solution was heated at 110 °C for further 3 hours. The mixture was extracted with diethyl ether (2 × 100 mL) and then the organic layer was washed with water (2 × 100 mL), a saturated solution of sodium bicarbonate (2 × 100 mL) and finally with a saturated solution of sodium chloride (1 × 100 mL). The organic layer was dried over MgSO<sub>4</sub>, filtered, and the solvent removed by evaporation under reduced pressure. The crude product was purified by using column chromatography using CH<sub>2</sub>Cl<sub>2</sub> as eluent to yield the title compound as yellow oil (2.24 g, 86% yield).

<sup>1</sup>H NMR (400 MHz, CDCl<sub>3</sub>, 293 K): δ 11.48 (s, 1H, OH), 9.81 (s, 1H, CHO), 7.15 (d, <sup>4</sup>J = 3.1 Hz, 1H, ArH), 6.79 (d, <sup>4</sup>J = 3.1 Hz, 1H, ArH), 3.79 (s, 3H, OCH<sub>3</sub>), 1.39 (s, 9H, C(CH<sub>3</sub>)<sub>3</sub>).

### 6.2.7 Synthesis of <sup>t</sup>Bu, OMe- Salpy



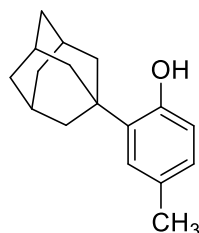
3-*tert*-butyl-5-methoxy salicylaldehyde (1.3 g, 6.24 mmol) was dissolved in methanol (20 mL). A solution of PPDA (0.515 g, 3.12 mmol) in methanol (20 mL) was added dropwise. The solution was stirred at room temperature for 4 hours; a precipitate started to form after 1 hour. The product was filtered and washed with cold methanol. The title compound was recrystallized from methanol to give <sup>t</sup>Bu, OMe- Salpy as a yellow powder. Yield: 1.29 g (76%). m.p = 151-152 °C.

<sup>1</sup>H NMR (400 MHz, CDCl<sub>3</sub>, 293 K): δ 13.31 (s, 2H, OH), 8.53 (d, <sup>3</sup>J = 4.8 Hz, 1H, H<sup>6</sup>), 8.19 (s, 2H, CH=N), 7.55 (t, <sup>3</sup>J = 7.8 Hz, 1H, H<sup>4</sup>), 7.26 (d, <sup>3</sup>J = 7.8 Hz, 1H, H<sup>3</sup>), 7.04 (t, <sup>3</sup>J = 6.20 Hz, 1H, H<sup>5</sup>), 6.86 (2H, H<sup>f</sup>), 6.46 (s, 2H, H<sup>d</sup>), 3.98 (2d, 4H, CH<sub>2</sub>), 3.66 (s, 6H, OCH<sub>3</sub>), 1.49 (s, 3H, CH<sub>3</sub>), 1.31 (s, 18H, C(CH<sub>3</sub>)<sub>3</sub>).

<sup>13</sup>C{<sup>1</sup>H} NMR (126 MHz, CDCl<sub>3</sub>, 293 K): δ 166.6 (CH=N), 163.5 (C<sup>2</sup>), 154.9 (C<sup>e</sup>), 151.1 (C<sup>b</sup>), 148.9 (C<sup>6</sup>), 139.0 (C<sup>c</sup>), 136.3 (C<sup>4</sup>), 121.5 (C<sup>3</sup>), 121.1 (C<sup>5</sup>), 118.2 (C<sup>f</sup>), 117.9 (C<sup>a</sup>), 111.3 (C<sup>d</sup>), 67.01 (CH<sub>2</sub>), 55.7 (OCH<sub>3</sub>), 46.3 (Py-C<sub>Me</sub>), 34.9 (C(CH<sub>3</sub>)<sub>3</sub>), 29.2 (C(CH<sub>3</sub>)<sub>3</sub>), 22.3 (CH<sub>3</sub>).

FT-IR (cm<sup>-1</sup>): 3000 (s, C-H<sub>Aromatic</sub>), 2953 (s, C-H), 2885 (s, CH), 1639 (s, C=N<sub>imine</sub>), 1593, 1465 (s, C=N<sub>py</sub>, C=C<sub>aromatic</sub>), 1423, 1325, 1259, 1201, 1149, 1049, 835. HRMS for [M+H]<sup>+</sup> (ESI): calcd. for (C<sub>33</sub>H<sub>44</sub>N<sub>3</sub>O<sub>4</sub>): 546.3332; found: 546.3314.

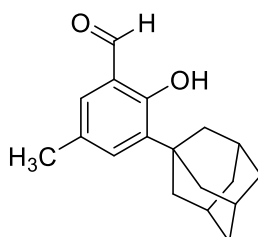
### 6.2.8 Synthesis of 2-Adamantyl-4-methylphenol<sup>3</sup>



p-cresol (1.08 g, 10 mmol) and 1-adamantanol (1.67g, 11 mmol) were dissolved in DCM (20 mL). The mixture was stirred to ensure complete dissolution of the reactants. 1.0 mL of concentrated sulfuric acid was added dropwise to the stirring mixture over 20 minutes. The mixture was allowed to stir for further 30 minutes. Water (30 mL) was added to the reaction mixture at which point a cloudy precipitate was observed. The solution was neutralized by adding sodium hydroxide (2 M) to a achieve pH=7. The crude product was extracted using ethyl acetate (3 × 30 mL). The combined organic phase were washed with brine (30 mL) and dried over magnesium sulfate. The solution was filtered and the solvent was removed under reduced pressure to give a waxy white compound which was dissolved in methanol (30 mL) and heated to reflux for one hour then allowed to cool to room temperature. The solution was kept at 4.0 °C overnight. The title compound was obtained as a white powder after concentration of the mother liquor. Yield: 1.73 g (72%).

<sup>1</sup>H NMR (300 MHz, CDCl<sub>3</sub>, 293 K): δ 7.05 (s, 1 H, ArH), 6.89 (d, <sup>3</sup>J = 7.9 Hz, 1 H, ArH), 6.56 (d, <sup>3</sup>J = 7.9 Hz, 1 H, ArH), 4.39 (s, 1H, OH), 2.30 (s, 3 H, ArCH<sub>3</sub>), 2.13 (d, J = 11.6 Hz 9 H, Ad), 1.81 (s, 6H, Ad).

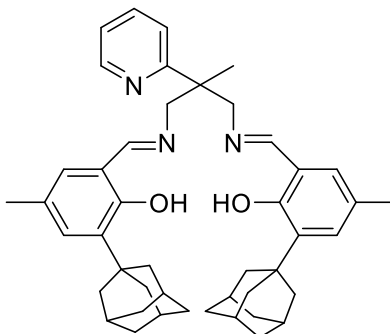
### 6.2.9 Synthesis of 3-adamantyl-2-hydroxy-5-methylbenzaldehyde<sup>3</sup>



2-adamantyl-*p*-cresol (2.26 g, 0.0093 mol) and hexamethylenetetraamine (2.61 g, 0.019 mol) were dissolved in glacial acetic acid (100 mL). The mixture was heated at 110 °C for 5 hours, becoming a yellow solution. The solution was allowed to cool to 90 °C. Water (150 mL) was added dropwise to the yellow solution over a period of 30 minutes while the mixture cooled to room temperature, forming an off-white suspension (large solid dark yellow chunks occasionally formed; they were removed from the mixture and discarded). The precipitate was filtered, and treated with methanol (50 mL) and stirred for 1 hour. The mixture was then filtered, and the precipitate was washed with methanol (50 mL) and dried *in vacuo*, the titled compound was afforded as an off-white solid (1.28 g, 51% yield).

<sup>1</sup>H NMR (300 MHz, CDCl<sub>3</sub>, 293 K): δ 11.67 (s, 1H, OH), 9.84 (s, 1H, CHO), 7.28 (s, 1 H, ArH), 7.18 (s, 1 H, ArH), 2.34 (s, 3H, ArCH<sub>3</sub>), 2.12 (m, 9 H, Ad), 1.80 (s, 6H, Ad).

### 6.2.10 Synthesis of Ad, Me- Salpy

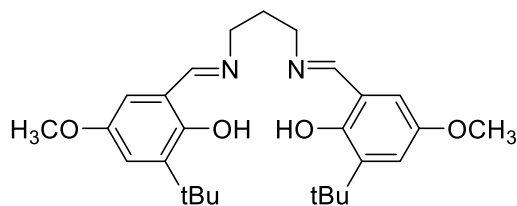


3-adamantyl-2-hydroxy-5-methylbenzaldehyde (0.63 g, 2.33 mmol) was dissolved in dichloromethane/methanol (15 mL/15 mL). A solution of ppda (0.19g, 1.15 mmol) in methanol (10 mL) was added dropwise. The solution was stirred at 40 °C for 5 hour, during which a precipitate formed. The solution was cooled to room temperature and the precipitate was filtered, washed with cooled methanol, and dried *in vacuo*. Yield: 0.57 g (74%). m.p = 178-180 °C.

$^1\text{H}$  NMR (400 MHz,  $\text{CDCl}_3$ , 203 K)  $\delta$  13.57 (s, 2H, OH), 8.62 (ddd,  $^3J = 4.75$  Hz,  $^4J = 1.04$  Hz,  $^5J = 0.92$  Hz, 1 H,  $\text{H}^6$ ), 8.27 (s, 2H, CH=N), 7.64 (td,  $J = 7.8, 1.8$  Hz, 1H,  $\text{H}^4$ ), 7.36 (d,  $J = 8.0$  Hz, 1H,  $\text{H}^3$ ), 7.14 (dd,  $J = 7.1, 5.0$  Hz, 1H,  $\text{H}^5$ ), 7.05 (d,  $^4J = 1.7$  Hz, 2H,  $\text{H}^f$ ), 6.85 (d,  $^4J = 1.4$  Hz, 2H,  $\text{H}^d$ ), 4.05 (q,  $^2J = 12.3$  Hz, 4H,  $\text{CH}_2$ ), 2.26 (s, 6H,  $\text{ArCH}_3$ ), 2.16 (s, 12H, Ad), 2.09 (s, 6H, Ad), 1.85 – 1.73 (m, 12H, Ad), 1.60 (s, 3H).

$^{13}\text{C}\{^1\text{H}\}$  NMR (101 MHz,  $\text{CDCl}_3$ , 293 K):  $\delta$  167.7 (CH=N), 164.1 ( $\text{C}^2$ ), 158.8, 137.7 ( $\text{C}^4$ ), 130.0, 126.9, 121.9, 118.7, 67.4 ( $\text{CH}_2$ ), 46.6 Py-C-Me), 40.6 (Ad), 37.5 (Ad), 37.3 (Ad), 29.5 (Ad), 21.1 ( $\text{CH}_3$ ). HRMS (ESI): calcd. for ( $\text{C}_{45}\text{H}_{55}\text{N}_3\text{O}_2+\text{H}$ ): 670.4373, found 670.4365.

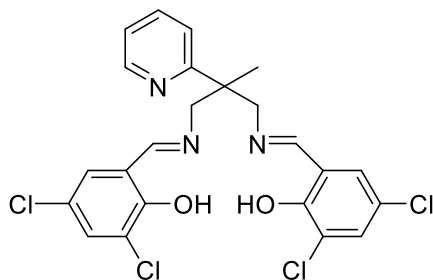
### 6.2.11 Synthesis of <sup>t</sup>Bu, OMe- Salpn



3-*tert*-butyl-5-methoxy salicylaldehyde (0.8 g, 3.8 mmol) was dissolved in methanol (15 mL). A solution of 1,3-diaminopropane (0.14 g, 1.92 mmol) was added dropwise. The solution was heated at 50 °C. The ligand was formed as a precipitate after 5 min. The reaction was stirred at 5- °C for 1 h, after which the reaction was cooled and filtered. The precipitate was washed with cold methanol to give <sup>t</sup>Bu, OMe- Salpn as a yellow solid. Yield: 0.67 g (78%). m.p = 125-126 °C. <sup>1</sup>H NMR (400 MHz, CDCl<sub>3</sub>, 293 K): δ 13.59 (s, 2H, OH), 8.36 (s, 2H, CH=N), 6.98 (d, <sup>4</sup>J = 3.1 Hz, 2H, Ar), 6.61 (d, <sup>4</sup>J = 3.1 Hz, 2H, Ar), 3.78 (s, 3H, OCH<sub>3</sub>), 3.73 (overlapping 2 d, <sup>2</sup>J = 12.6 Hz 4H, CH<sub>2</sub>), , 2.14 (p, <sup>3</sup>J = 6.6 Hz 2H, CH<sub>2</sub>), 1.44 (s, 18H, C(CH<sub>3</sub>)<sub>3</sub>).

<sup>13</sup>C{<sup>1</sup>H} NMR (126 MHz, CDCl<sub>3</sub>, 293 K): δ 165.7 (CH=N), 154.9 (C<sup>e</sup>), 151.0 (C<sup>b</sup>), 139.0 (C<sup>c</sup>), 118.0 (C<sup>f</sup>), 117.9 (C<sup>a</sup>), 111.4 (C<sup>d</sup>), 56.8 (N-CH<sub>2</sub>), 55.6 (OCH<sub>3</sub>), 35.0 (C(CH<sub>3</sub>)<sub>3</sub>), 31.6 (CH<sub>2</sub>CH<sub>2</sub>CH<sub>2</sub>), 28.9 (C(CH<sub>3</sub>)<sub>3</sub>). HRMS for [M+H]<sup>+</sup> (APCI): calcd. for (C<sub>27</sub>H<sub>38</sub>N<sub>2</sub>O<sub>4</sub>): 455.2910; found 455.2900.

### 6.2.12 Synthesis of Cl, Cl- Salpy

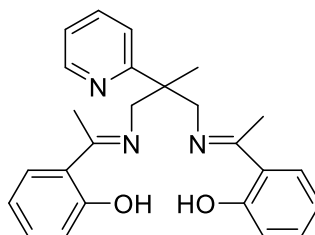


A solution of 3,5-dichlorosalicylaldehyde (1.73 g, 9.07 mmol) in a mixture of methanol/ dichloromethane (15 mL / 15 mL) was added dropwise to a stirred solution of ppda (0.75 g, 4.53 mmol) in methanol (10 mL). A dark orange solution was formed. The solution was stirred at 50 °C for 4 h. The solvent was removed and the resulting solid was washed with methanol, purified by recrystallization from DCM/petroleum ether, and dried *in vacuo* to give the titled compound as a deep orange solid. Yield: 1.96 g (84%). m.p = 63-65 °C.

$^1\text{H}$  NMR (400 MHz,  $\text{CDCl}_3$ , 293 K):  $\delta$  14.12 (s, 2H, OH), 8.60 (ddd,  $^3J = 4.8$ ,  $^4J = 1.8$ ,  $^5J = 0.8$  Hz, 1H, H<sup>6</sup>), 8.17 (s, 2H, CH=N), 7.65 (td,  $^3J = 7.8$ ,  $^4J = 1.9$  Hz, 1H, H<sup>4</sup>), 7.37 (d,  $^4J = 2.5$  Hz, 2H, H<sup>d</sup>), 7.29 (d,  $^3J = 8.0$  Hz, 1H, H<sup>3</sup>), 7.15 (ddd,  $^3J = 7.5$ ,  $^4J = 4.8$ ,  $^5J = 1.0$  Hz, 1H, H<sup>5</sup>), 7.08 (d,  $^4J = 2.5$  Hz, 2H, H<sup>f</sup>), 4.15 (d,  $^2J = 12.4$  Hz, 2H, CHH), 4.04 (dd,  $^2J = 12.4$ ,  $^4J = 1.0$  Hz, 2H, CHH), 1.55 (s, 3H, CH<sub>3</sub>). HRMS for  $[\text{M}+\text{H}]^+$  (ES): calcd. for (C<sub>23</sub>H<sub>20</sub>Cl<sub>4</sub>N<sub>3</sub>O<sub>2</sub>): 512.0280; found 512.0281.

$^{13}\text{C}\{^1\text{H}\}$  NMR (126 MHz,  $\text{CDCl}_3$ , 293 K):  $\delta$  164.8 (CH=N), 161.8, 156.9, 149.2 (Py-C), 136.8 (Py-C), 132.3, 129.1, 122.8, 122.4, 122.0 (Py-C), 121.0, 119.2, 66.2 (CH<sub>2</sub>), 46.0 (Py-C-CH<sub>3</sub>), 21.5 (CH<sub>3</sub>).

### 6.2.13 Synthesis of Acpy

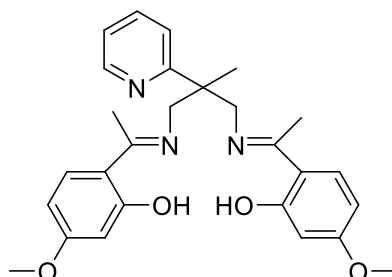


To a solution of ppda (1.02 g, 6.17 mmol) in dry ethanol (30 mL) was added dropwise to a solution of 2-hydroxyacetophenone (1.68 g, 12.34 mmol) in dry ethanol (5 mL) at 50 °C with stirring. After being stirred at 70 °C for 20 h, the solvent was removed under reduced pressure to afford a yellow oil. The oil was dissolved in small amount of DCM (ca. 5 mL), and then hexane (40 mL) was added with vigorous stirring. The resulted solution was left in freezer overnight, whereupon crystals were formed, which were filtered, washed with hexane, and dried *in vacuo* to yield the titled compound as a yellow solid. Yield: 2.098 g (85%). m.p = 85-87 °C.

$^1\text{H}$  NMR (400 MHz,  $\text{CDCl}_3$ , 293 K):  $\delta$  15.73 (s, 2H, OH), 8.50 (d,  $^3J = 4.0$  Hz, 1H, H<sup>6</sup>), 7.58 (td,  $^3J = 7.8$ ,  $^4J = 1.5$  Hz, 1H, H<sup>4</sup>), 7.34 (overlapping t, 3H, H<sup>3</sup>, H<sup>f</sup>), 7.13 (t,  $^3J = 7.7$  Hz, 2H, H), 7.03 (dd,  $^3J = 7.2$ ,  $^3J = 5.0$  Hz, 1H, H<sup>5</sup>), 6.76 (d,  $J = 8.2$  Hz, 1H, 2H), 6.63 (t,  $J = 7.5$  Hz, 2H, H),  $\delta$  4.19 (d,  $^2J = 14.5$  Hz, 2H, CHH), 4.05 (d,  $^2J = 14.5$  Hz, 2H, CHH), 2.18 (s, 6H, N=CCH<sub>3</sub>), 1.58 (s, 3H, CH<sub>3</sub>).

$^{13}\text{C}\{^1\text{H}\}$  NMR (126 MHz,  $\text{CDCl}_3$ , 293 K):  $\delta$  172.38 (CH=N), 163.42 (Ar-C), 149.18 (C<sup>6</sup>), 136.71 (C<sup>4</sup>), 132.36 (Ar-C), 128.04 (Ar-C), 121.76 (C<sup>3</sup>), 121.32 (C<sup>5</sup>), 119.43 (Ar-C), 118.45 (Ar-C), 117.15 (Ar-C), 57.67 (CH<sub>2</sub>), 45.96 (Py-C-CH<sub>3</sub>), 22.38 (CH<sub>3</sub>), 14.73 (CH<sub>3</sub>-C=N). HRMS for  $[\text{M}+\text{H}]^+$  (APCI): calcd. for (C<sub>25</sub>H<sub>28</sub>N<sub>3</sub>O<sub>2</sub>): 402.2182; found 402.2172.

### 6.2.14 Synthesis of OMe- Acpy

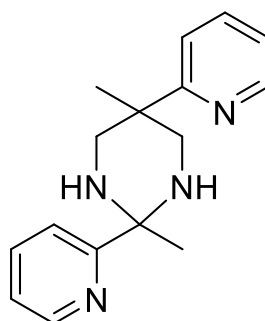


ppda (1.53 g, 9.26 mmol) and 2-hydroxy-4-methoxyacetophenone (3.0 g, 18.05 mmol) were dissolved in dry ethanol (30 mL). The solution was heated at 70 °C for 18 h. The solvent was removed completely to leave a pale yellow solid which was washed with petroleum ether and dried *in vacuo* to yield a pale yellow solid. Yield: 3.47 g (81%). m.p = 122-123°C.

<sup>1</sup>H NMR (400 MHz, CDCl<sub>3</sub>, 293 K): δ 16.6 (s, 2H, OH), 8.61 (ddd, <sup>3</sup>J = 4.5, <sup>4</sup>J = 1.9, <sup>5</sup>J = 0.9 Hz, 1H, H<sup>6</sup>), 7.70 (td, <sup>3</sup>J = 7.8, <sup>4</sup>J = 1.8 Hz, 1H, H<sup>4</sup>), 7.43 (d, <sup>3</sup>J = 8.0 Hz, 1H, H<sup>3</sup>), 7.32 (d, <sup>3</sup>J = 9.0 Hz, 2H, H<sup>f</sup>), 7.17 (m, 1H, H<sup>5</sup>), 6.31 (d, <sup>3</sup>J = 2.6 Hz, 2H, H<sup>c</sup>), 6.25 (dd, <sup>3</sup>J = 9.0, <sup>4</sup>J 2.6 Hz, 2H, H<sup>e</sup>) 4.15 (d, <sup>2</sup>J = 14.1 Hz, 2H, CH<sub>2</sub>H), 4.01 (d, <sup>2</sup>J = 14.1 Hz, 2H, CH<sub>2</sub>H), 3.74 (s, 6H, OCH<sub>3</sub>), 2.26 (s, 6H, N=CCH<sub>3</sub>), 1.70 (s, 3H, CH<sub>3</sub>).

<sup>13</sup>C{<sup>1</sup>H} NMR (101 MHz, CDCl<sub>3</sub>, 293 K): δ 171.9 (CH=N), 169.4 (C<sup>b</sup>), 163.8 (C<sup>d</sup>), 162.7 (C<sup>2</sup>), 149.2 (C<sup>6</sup>), 136.8 (C<sup>4</sup>), 129.5 (C<sup>f</sup>), 121.9 (C<sup>3</sup>), 121.3 (C<sup>5</sup>), 112.2 (C<sup>a</sup>), 105.4 (C<sup>e</sup>), 102.0 (C<sup>c</sup>), 55.7 (CH<sub>2</sub>), 55.2 (OCH<sub>3</sub>), 45.8 (Py-C-CH<sub>3</sub>), 21.8 (CH<sub>3</sub>), 14.4 (CH<sub>3</sub>-C=N). HRMS for [M+H]<sup>+</sup> (APCI): calcd. for (C<sub>27</sub>H<sub>32</sub>N<sub>3</sub>O<sub>4</sub>): 462.2393; found 462.2388.

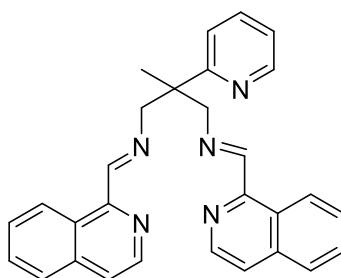
### 6.2.15 Synthesis of Pypy



To a stirred solution of ppda (1.04 g, 6.3 mmol) in methanol (25 mL), 2-acetylpyridine (1.52 g, 12.6 mmol) was added. The resulting colourless solution was stirred at 50 °C for 24 h, after which the colour of the solution had changed to yellow. The solvent was removed under reduced pressure and the resulting yellow solid washed with hexane (10 mL) and petroleum ether (10 mL). The product was dried *in vacuo* (0.17 g, 61% yield).

$^1\text{H}$  NMR (400 MHz,  $\text{CDCl}_3$ , 293 K):  $\delta$  8.61 (overlapping, 2H,  $\text{H}^6$ ), 7.85 (d,  $J = 7.9$  Hz, 1H, Py), 7.70 (m, 2H, Py), 7.47 (d,  $J = 8.0$  Hz, 1H, Py), 7.15 (m, 2H, Py), 3.52 (d,  $^2J = 12.6$  Hz, 2H,  $\text{CH}_2$ ), 2.64 (d,  $^2J = 13.5$  Hz, 2H,  $\text{CH}_2$ ), 2.61 – 2.50 (b, 2H, NH), 1.22 (s, 3H,  $\text{CH}_3$ ), 0.92 (s, 3H,  $\text{CH}_3$ ). HRMS for  $[\text{M}+\text{H}]^+$  (ESI): calcd. for ( $\text{C}_{16}\text{H}_{21}\text{N}_4$ ): 269.1766; found 269.1755.

### 6.2.16 Synthesis of Qupy



To a solution of ppda (0.55 g, 3.32 mmol) in methanol (20 mL) was added a solution of 2-Quenolinecarboxaldehyde (1.04 g, 6.6 mmol) in methanol (20 mL) dropwise at 50 °C with stirring. After being stirred at 50 °C for 18 h, the solvent was removed under reduced pressure to afford a brown solid. The solid was recrystallized from a mixture of petroleum ether and dichloromethane; the solid was dissolved in a minimum of DCM (*ca.* 5 mL) and then petroleum ether (40 mL) was

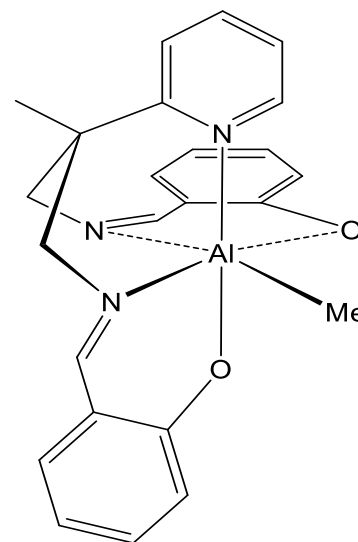
added with vigorous stirring. A precipitate was formed, which was filtered, washed with petroleum ether, and dried *in vacuo* to yield the titled compound as a brown solid. (0.98 g, 66% yield). This ligand could only be obtained as an inseparable mixture of compounds.

## 6.3 Aluminum complexes

### 6.3.1. Aluminum methyl complexes

#### 6.3.1.1 Synthesis of [Al(Salpy) Me] (1)

To a stirred solution of Salpy (1.37 g, 3.6 mmol) in toluene (20 mL), AlMe<sub>3</sub> 1.83 mL (2.0 M in toluene, 3.6 mmol) was added dropwise. The reaction mixture was heated at 80 °C overnight. After the stirring, the solvent was removed under reduced pressure. The residue was washed with hexanes (2 x 15 mL) to afford an off-white solid. Yield: 1.25 g (82%). Crystals of [Al(Salpy) Me] suitable for structural determination were obtained from a concentrated benzene solution.



<sup>1</sup>H NMR (400 MHz, THF-d<sub>8</sub>, 293 K): δ **Isomer 1**: 8.69 (d, <sup>3</sup>J = 4.6 Hz, 1H, H<sup>6</sup>), 8.18 (s, 2H, CH=N), 7.79 (t, <sup>3</sup>J = 7.9 Hz, 1H, H<sup>4</sup>), 7.52 (d, <sup>3</sup>J = 8.0 Hz, 1H), 7.13 (m, 4H), 6.72 (m, 2H), 6.55 (m, 3H), 4.52 (d, <sup>2</sup>J = 12.5 Hz, 2H, CHH), 3.65 (d, <sup>2</sup>J = 12.5 Hz, 2H, CHH), 1.38 (s, 3H, CH<sub>3</sub>), -0.89 (s, 3H, Al-CH<sub>3</sub>).

**Isomer 2**: 8.53 (d, <sup>3</sup>J = 4.2 Hz, 1H, H<sup>6</sup>), 8.34 (s, 2H, CH=N), 7.69 (t, <sup>3</sup>J = 7.6 Hz, 1H, H<sup>4</sup>), 7.46 (d, <sup>3</sup>J = 8.6 Hz, 1H), 7.26 (m, 4H), 6.77-6.43 (m, 5H), 4.34 (d, <sup>2</sup>J = 12.4 Hz, 2H, CHH), 4.02 (d, <sup>2</sup>J = 12.4 Hz, 2H, CHH), 1.44 (s, 3H, CH<sub>3</sub>), -0.89 (s, 3H, Al-CH<sub>3</sub>).

<sup>13</sup>C{<sup>1</sup>H} NMR (126 MHz, THF-d<sub>8</sub>, 293 K): δ, **Isomer 1**: 170.8 (CH=N), 166.8 (C<sup>2</sup>), 165.4 (C<sup>b</sup>), 149.1 (C<sup>6</sup>), 137.0 (C<sup>4</sup>), 134.6, 132.8, 132.6, 122.0, 121.1, 120.4, 119.2, 115.5, 68.0 (CH<sub>2</sub>), 45.5 (Py-C-CH<sub>3</sub>), 21.0 (CH<sub>3</sub>), Al-CH<sub>3</sub> (Not observed).

**Isomer 2**: 170.8 (CH=N), 166.4 (C<sup>2</sup>), 163.4 (C<sup>b</sup>), 149.0 (C<sup>6</sup>), 136.5 (Py-C), 134.8, 132.8, 122.5, 120.4, 119.3, 114.9, 67.0 (CH<sub>2</sub>), 44.2 (Py-C-Me), 21.0 (CH<sub>3</sub>), Al-CH<sub>3</sub> (Not observed). Anal. Calcd. for C<sub>24</sub>H<sub>24</sub>AlN<sub>3</sub>O<sub>2</sub> (%): C, 69.72; H, 5.85; N, 10.16. Found (%): C, 69.54; H, 5.92; N, 10.01. HRMS for [M-CH<sub>3</sub>]<sup>+</sup> (EI): calcd. for (C<sub>23</sub>H<sub>21</sub>AlN<sub>3</sub>O<sub>2</sub>): 398.14449; found 398.1444.

### 6.3.1.2 Synthesis of [Al(<sup>t</sup>Bu, <sup>t</sup>Bu-Salpy)Me] (2)

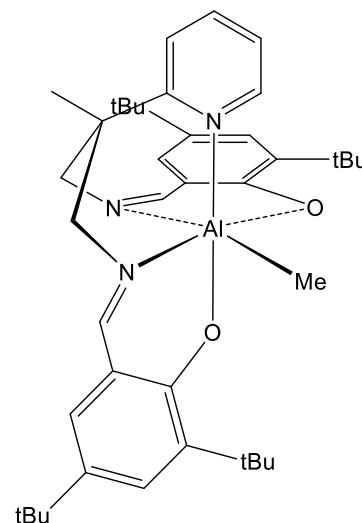
To a schlenk containing <sup>t</sup>Bu, <sup>t</sup>Bu-Salpy (1.37 g, 2.29 mmol) in toluene (10 mL), AlMe<sub>3</sub> (1.14 mL, 2.0 M in toluene, 2.29 mmol) was added dropwise. The reaction mixture was stirred for 6 hours. After the stirring, the solvent was removed under reduced pressure. The residue was washed twice with hexanes (ca. 15 mL) to afford a yellow solid. Yield: 1.08 g (74%).

<sup>1</sup>H NMR (400 MHz, C<sub>6</sub>D<sub>6</sub>, 293 K): δ **Isomer 1** : 8.49 (d, <sup>3</sup>J = 4.8 Hz, 1H, H<sup>6</sup>), , 7.75 (d, <sup>4</sup>J = 2.0 Hz, 2H, H<sup>d</sup>), 7.67 (s, 2H, CH=N), 7.01 (m, 1H, H<sup>4</sup>), , 6.95 (d, <sup>4</sup>J = 2.1 Hz, 2H, H<sup>f</sup>), 6.74 (d, <sup>3</sup>J = 8.0 Hz, 1H, H<sup>3</sup>), , 6.56 (m, 1H, H<sup>5</sup>), 4.05 (d, <sup>2</sup>J = 12.3 Hz, 2H, CHH), 3.00 (d, <sup>2</sup>J = 12.5 Hz, 2H, CHH), 1.83 (s, 18H, 2 x C(CH<sub>3</sub>)<sub>3</sub>), 1.36 (s, 18H, 2 x C(CH<sub>3</sub>)<sub>3</sub>), 0.85 (s, 3H, CH<sub>3</sub>), -0.32 (s, 3H, AlCH<sub>3</sub>),

**Isomer 2** : 8.29 (d, <sup>3</sup>J = 4.5 Hz, 1H, H<sup>6</sup>), 7.77 (d, <sup>4</sup>J = 2.0 Hz, 2H, H<sup>d</sup>), 7.74 (s, 2H, CH=N), 7.01 (m, 1H, H<sup>4</sup>), 6.98 (d, <sup>4</sup>J = 2.1 Hz, 2H, H<sup>f</sup>), 6.63 (d, <sup>3</sup>J = 8.0 Hz, 1H, H<sup>3</sup>), 6.56 (m, 1H, H<sup>5</sup>), 3.95 (d, <sup>3</sup>J = 12.3 Hz, 2H, CHH), 3.21 (d, <sup>2</sup>J = 12.5 Hz, 2H, CHH), 1.87 (s, 18H, 2 x C(CH<sub>3</sub>)<sub>3</sub>), 1.36 (s, 18H, 2 x C(CH<sub>3</sub>)<sub>3</sub>), 1.06 (s, 3H, CH<sub>3</sub>), -0.33 (s, 3H, AlCH<sub>3</sub>).

<sup>13</sup>C{<sup>1</sup>H} NMR (101 MHz, C<sub>6</sub>D<sub>6</sub>, 293 K): δ, **Isomer 1** : 170.4 (CH=N), 163.9 (C<sup>2</sup>), 148.8 (C<sup>6</sup>), 141.1, 137.0 (Py-C), 136.3, 130.0, 127.1, 121.3 (Py-C), 119.2, 118.8, 64.6 (CH<sub>2</sub>), 45.1 (Py-C-CH<sub>3</sub>), 35.6 (C(CH<sub>3</sub>)<sub>3</sub>), 33.7 (C(CH<sub>3</sub>)<sub>3</sub>), 31.3 (C(CH<sub>3</sub>)<sub>3</sub>), 29.8 (C(CH<sub>3</sub>)<sub>3</sub>), 24.7 (CH<sub>3</sub>), Al-CH<sub>3</sub> (Not observed).

**Isomer 2**: 171.2 (CH=N), 164.4 (C<sup>2</sup>), 148.8 (C<sup>6</sup>), 141.2, 137.2 (Py-C), 136.0, 130.2, 127.2, 121.5 (Py-C), 119.9, 118.9, 65.2 (CH<sub>2</sub>), 45.1 (Py-C-CH<sub>3</sub>), 35.6 (C(CH<sub>3</sub>)<sub>3</sub>), 33.7 (C(CH<sub>3</sub>)<sub>3</sub>), 31.3 (C(CH<sub>3</sub>)<sub>3</sub>), 29.8 (C(CH<sub>3</sub>)<sub>3</sub>), 23.8 (CH<sub>3</sub>), Al-CH<sub>3</sub> (Not observed). Anal. Calcd. for C<sub>40</sub>H<sub>56</sub>AlN<sub>3</sub>O<sub>2</sub> (%): C, 75.32; H, 8.85; N, 6.59. Found (%): C, 75.29; H, 8.61; N, 6.39. HRMS for [M-CH<sub>3</sub>]<sup>+</sup> (EI): calcd. for (C<sub>39</sub>H<sub>53</sub>AlN<sub>3</sub>O<sub>2</sub>): 622.3953; found 622.3954.



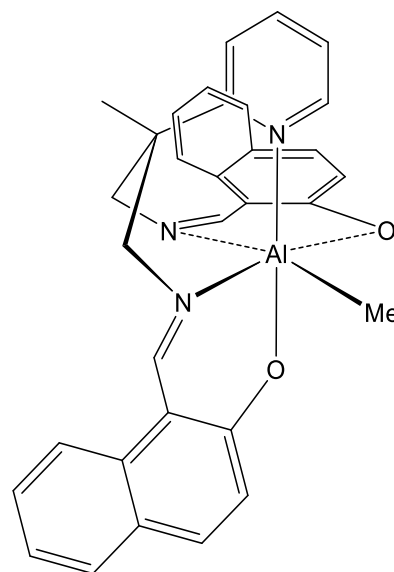
### 6.3.1.3 Synthesis of [Al(Naphpy)Me] (3)

To a schlenk containing Naphpy (1.22 g, 2.98 mmol) and 20 mL toluene, AlMe<sub>3</sub> (1.51 mL, 2.0 M in toluene, 3.02 mmol) was added at ambient temperature. The reaction mixture was allowed to stir for 20 hours at room temperature. After which, the solution was filtered and the volatiles were removed under reduced pressure. The residue was washed with hexanes (30 mL) to afford a pale brown solid Yield: 2.11 g (92%).

<sup>1</sup>H NMR (400 MHz, C<sub>6</sub>D<sub>6</sub>, 293 K): δ 8.66 (s, 1H, H<sup>6</sup>), 8.02 (s, 2H, CH=N), 7.44 – 6.63 (m, 16H, py and Ar), 3.73 (d, <sup>2</sup>J = 12.4 Hz, 2H, CHH), 3.45 (d, <sup>2</sup>J = 12.1 Hz, 2H, CHH), 1.44 (s, 3H, CH<sub>3</sub>), -0.30 (s, 3H, Al-CH<sub>3</sub>).

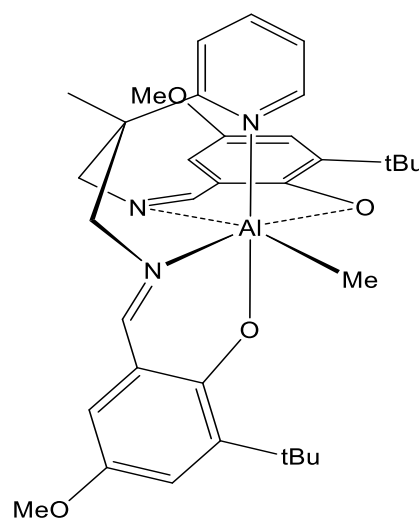
<sup>13</sup>C{<sup>1</sup>H} NMR (101 MHz, C<sub>6</sub>D<sub>6</sub>, 293 K): δ 169.1 (CH=N), 167.54 (Ar-C), 160.5 (Ar-C), 149.9 (Py-C), 138.7 (Ar-C), 137.7 (Ar-C), 137.3 (Py-C), 134.2 (Ar-C), 125.7 (Ar-C), 124.4 (Ar-C), 123.7 (Ar-C), 123.4 (Py-C), 119.3, 110.3, 66.3 (CH<sub>2</sub>), 47.4 (Py-C-Me), 21.43 (CH<sub>3</sub>), Al-CH<sub>3</sub> (Not observed).

Anal. Calcd. for C<sub>32</sub>H<sub>28</sub>AlN<sub>3</sub>O<sub>2</sub> (%): C, 74.84; H, 5.50; N, 8.18. Found (%): C, 74.65; H, 5.36; N, 8.04. HRMS for [M-CH<sub>3</sub>]<sup>+</sup> (EI): calcd. for (C<sub>31</sub>H<sub>25</sub>Al N<sub>3</sub>O<sub>2</sub>): 498.1762; found 498.1764.



### 6.3.1.4 Synthesis of [Al(<sup>t</sup>Bu, OCH<sub>3</sub> - Salpy)Me] (4)

To a solution of <sup>t</sup>Bu, OMe- Salpy (1.22 g, 2.25 mmol) in toluene (25 mL), AlMe<sub>3</sub> (1.23 mL, 2 M in toluene, 2.47 mmol) was added dropwise at room temperature. The colour of the solution immediately changed from yellow to dark yellow. The stirring was continued for 20 h. The solution was concentrated to minimum, and hexanes (20 mL) were added. The solution was stirred for 2 minutes and the precipitate was filtered. The washing process was repeated three times. The solid was dried under high reduce pressure to afford a yellow powder. Yield: 0.98 g (75%).



## Chapter 6 - Experimental

$^1\text{H}$  NMR (400 MHz,  $\text{C}_6\text{D}_6$ , 293 K):  $\delta$  **Isomer 1**: 8.49 (d,  $^4J = 4.7$  Hz, 1H,  $\text{H}^6$ ), 7.65 (s, 2H  $\text{CH}=\text{N}$ ), 7.43 (s, 2H,  $\text{H}^d$ ), 7.04 (m, , 1H,  $\text{H}^4$ ), 6.77 (d,  $^3J = 8.0$  Hz, 1H,  $\text{H}^3$ ), 6.60 (m, 1H,  $\text{H}^5$ ), 6.38 (m, 2H,  $\text{H}^f$ ), 4.06 (d,  $^2J = 12.3$  Hz, 2H,  $\text{CH}_2$ ), 3.47 (s, 6H,  $\text{OCH}_3$ ), 3.01 (d,  $^2J = 12.3$  Hz, 2H,  $\text{CH}_2$ ), 1.75 (s, 18H, 2 x  $\text{C}(\text{CH}_3)_3$ ), 0.90 (s, 3H,  $\text{CH}_3$ ), -0.35 (s, 3H,  $\text{Al-CH}_3$ ).

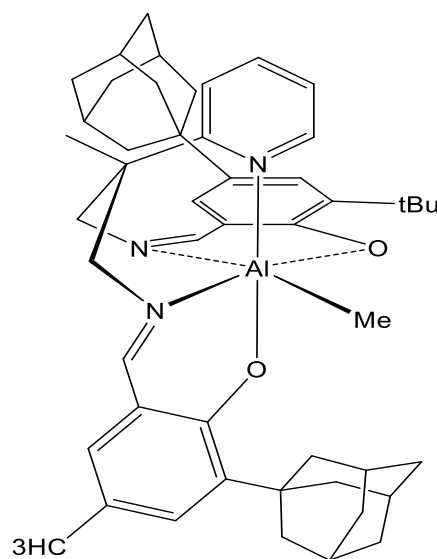
**Isomer 2** : 8.33 (d,  $^4J = 4.4$  Hz, 1H,  $\text{H}^6$ ), 7.71 (s, 2H,  $\text{CH}=\text{N}$ ), 7.43 (s, 2H,  $\text{H}^d$ ), 7.04 (m, , 1H,  $\text{H}^4$ ), 6.66 (d,  $^3J = 8.0$  Hz, 1H,  $\text{H}^3$ ), 6.60 (m, 1H,  $\text{H}^5$ ), 6.38 (m, 2H,  $\text{H}^f$ ), 3.93 (d,  $^2J = 12.3$  Hz, 2H,  $\text{CH}_2$ ), 3.47 (s, 6H,  $\text{OCH}_3$ ), 3.22 (d,  $^2J = 12.3$  Hz, 2H,  $\text{CH}_2$ ), 1.77 (s, 18H, 2 x  $\text{C}(\text{CH}_3)_3$ ), 1.10 (s, 3H,  $\text{CH}_3$ ), -0.36 (s, 3H,  $\text{Al-CH}_3$ ).

$^{13}\text{C}\{^1\text{H}\}$  NMR (101 MHz,  $\text{C}_6\text{D}_6$ , 293 K):  $\delta$  **Isomer 1**: 170.1 ( $\text{CH}=\text{N}$ ), 163.7 ( $\text{C}^2$ ), 161.4, 161.3, 150.1, 149.2 ( $\text{C}^6$ ), 143.6, 136.8 ( $\text{C}^4$ ), 123.1 ( $\text{C}^d$ ), 121.8 ( $\text{C}^5$ ), 120.4 ( $\text{C}^3$ ), 118.8, 111.8 ( $\text{C}^f$ ), 64.9 ( $\text{CH}_2$ ), 55.5 ( $\text{OCH}_3$ ), 45.6 ( $\text{Py-C-CH}_3$ ), 35.9 ( $\text{C}(\text{CH}_3)_3$ ), 29.9 ( $\text{C}(\text{CH}_3)_3$ ), 25.1 ( $\text{CH}_3$ ),  $\text{Al-CH}_3$  (Not observed).

**Isomer 2**: 170.9 ( $\text{CH}=\text{N}$ ), 164.6 ( $\text{C}^2$ ), 150.3, 149.2 ( $\text{C}^6$ ), 143.7, 136.5 ( $\text{C}^4$ ), 123.3 ( $\text{C}^d$ ), 121.9 ( $\text{C}^5$ ), 119.7 ( $\text{C}^3$ ), 118.7, 111.7 ( $\text{C}^f$ ), 65.4 ( $\text{CH}_2$ ), 55.4 ( $\text{OCH}_3$ ), 45.5 ( $\text{Py-C-CH}_3$ ), 35.9 ( $\text{C}(\text{CH}_3)_3$ ), 29.9 ( $\text{C}(\text{CH}_3)_3$ ), 24.1 ( $\text{CH}_3$ ),  $\text{Al-CH}_3$  (Not observed). Anal. Calcd. for  $\text{C}_{34}\text{H}_{44}\text{AlN}_3\text{O}_4$  (%): C, 69.72; H, 7.57; N, 7.17. Found (%): C, 69.49; H, 7.62; N, 6.98. HRMS for  $[\text{M-CH}_3]^+$  (EI): calcd. for ( $\text{C}_{33}\text{H}_{41}\text{Al N}_3\text{O}_4$ ): 570.2912; found 570.2918.

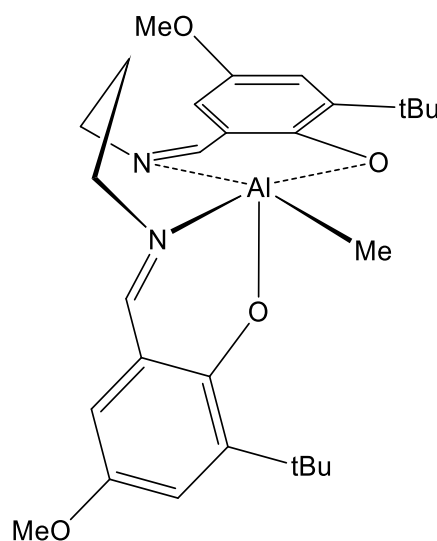
### 6.3.1.5 Synthesis of $[\text{Al}(\text{Ad}, \text{Me} - \text{Salpy})\text{Me}]$ (5)

Ad, Me-Salpy (0.2 g, 0.29 mmol) was dissolved in toluene (10 mL) and 0.15 mL of  $\text{AlMe}_3$  (0.15 mL of a 2 M solution in toluene, 0.29 mmol) was added dropwise. The solution was stirred overnight at room temperature. The solvent was concentrated to minimum, and hexanes (15 mL) were added with stirring. The resulting precipitate was filtered and dried *in vacuo*. HRMS for  $[\text{M-CH}_3]^+$  (EI): calcd. for ( $\text{C}_{45}\text{H}_{53}\text{Al N}_3\text{O}_2$ ): 694.3953; found 694.3954. The main product is bimetallic; the data for this major component are provided in the appropriate section, below.



6.3.1.6 Synthesis of [Al(<sup>t</sup>Bu, OCH<sub>3</sub> - Salpn)Me] (6)

AlMe<sub>3</sub> (0.85 mL, 2 M in toluene, 1.69 mmol) was added dropwise to a stirred solution of <sup>t</sup>Bu, OMe-Salpn (0.70 g, 1.54 mmol) in THF (15 mL) at room temperature. The mixture was left to stir overnight. The solution was concentrated and hexanes (15 mL) were added with vigorous stirring. The resulting precipitate was isolated *via* cannula filtration, washed with hexanes (2 x 15 mL), and dried under high vacuum (10<sup>-6</sup> mbar) to give the titled complex as a yellow solid. Yield: 0.54 g (70%).

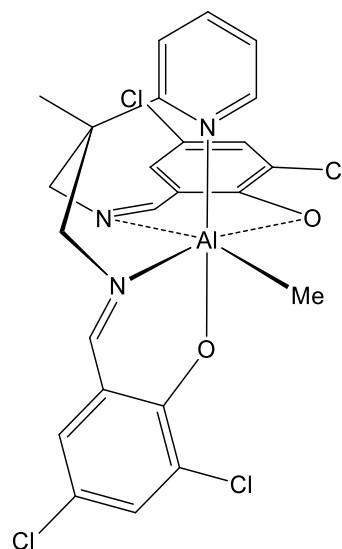


<sup>1</sup>H NMR (400 MHz, C<sub>6</sub>D<sub>6</sub>, 293 K): δ 7.26 (d, <sup>4</sup>J = 3.2 Hz, 2H, Ar), 7.00 (s, 2H, CH=N), 6.17 (d, <sup>4</sup>J = 3.2 Hz, 2H, Ar), 3.36 (s, 6H, OCH<sub>3</sub>), 2.91 (dt, <sup>2</sup>J = 12.0, <sup>3</sup>J = 5.8 Hz, 2H, CHH), 2.61 (dt, <sup>2</sup>J = 12.0, <sup>3</sup>J = 5.8 Hz, 2H, CHH), 1.56 (s, 18H, C(CH<sub>3</sub>)<sub>3</sub>), 1.35 (s, 3H, CH<sub>3</sub>), 1.04 (m, 2H, CH<sub>2</sub>), -0.53 (s, 3H, Al-CH<sub>3</sub>).

<sup>13</sup>C{<sup>1</sup>H} NMR (126 MHz, C<sub>6</sub>D<sub>6</sub>, 293 K): δ 169.0 (CH=N), 160.8 (C<sup>e</sup>), 149.5 (C<sup>b</sup>), 143.1 (C<sup>c</sup>), 122.6, 118.1, 111.0, 55.1 (N-CH<sub>2</sub>), 54.5 (OCH<sub>3</sub>), 35.4 (C(CH<sub>3</sub>)<sub>3</sub>), 29.8 (CH<sub>2</sub>CH<sub>2</sub>CH<sub>2</sub>), 27.0 (C(CH<sub>3</sub>)<sub>3</sub>), Al-CH<sub>3</sub> (Not observed). Anal. Calcd. for C<sub>28</sub>H<sub>39</sub>AlN<sub>2</sub>O<sub>4</sub> (%): C, 67.99; H, 7.95; N, 5.66. Found (%): C, 67.56; H, 7.43; N, 5.69. HRMS for [M-CH<sub>3</sub>]<sup>+</sup> (EI): calcd. for (C<sub>27</sub>H<sub>36</sub>Al N<sub>2</sub>O<sub>4</sub>): 479.2490; found 479.2499.

## 6.3.1.7 Synthesis of [Al(Cl, Cl - Salpy)Me] (7)

To a stirred deep orange solution of Cl, Cl-Salpy (0.86 g, 1.68 mmol) in toluene (20 mL), AlMe<sub>3</sub> (0.84 mL, 2M in toluene, 1.68 mmol) was added dropwise. The solution changed to yellow and the precipitate was formed after 15 min. The stirring was continued at room temperature for 6 h. After which time the solution was filtered and the precipitate was washed with hexanes (2 x 15 mL) and dried *in vacuo* to afford complex 7 as a deep yellow solid. Yield: 0.8 g, 1.45 mmol (86%).



## Chapter 6 - Experimental

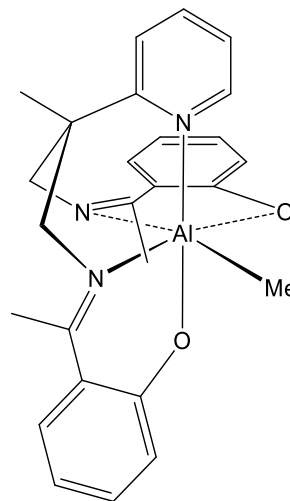
$^1\text{H}$  NMR (400 MHz, THF, 293 K): **Isomer 1**  $\delta$  8.95 (d,  $^3J = 4.3$  Hz, 1H, H<sup>6</sup>), , 8.02 (m, 1H, Py), 7.97 (s, 2H, CH=N), 7.90 (td,  $^3J = 7.8$ ,  $^4J = 1.7$  Hz, 1H, Py), 7.57 (d,  $^3J = 7.67$ , 1H, Py), 7.31 (d,  $^4J = 2.8$  Hz, 2H), 7.04 (d,  $^2J = 2.7$  Hz, 2H), 3.98 (d,  $^2J = 13.7$  Hz, 2H, CHH), 3.89 (d,  $^2J = 13.7$  Hz, 2H, CHH), 1.56 (s, 3H, CH<sub>3</sub>), -0.90 (s, 3H, Al-CH<sub>3</sub>).

**Isomer 2** 8.69 (d,  $^3J = 4.3$  Hz, 1H, H<sup>6</sup>), 7.97 (s, 2H, CH=N), 7.82 (m, 1H, Py), 7.67 (d,  $^3J = 8.2$  Hz, 1H, Py), 7.44 (d,  $^4J = 4.2$  Hz, 2H, Ar), 7.40 (m, 1H, Py), 7.17 (d,  $^4J = 4.3$  Hz, 2H, Ar), 4.30 (m, 4H, CH<sub>2</sub>), 1.63 (s, 3H, CH<sub>3</sub>), -0.96 (s, 3H, Al-CH<sub>3</sub>).

$^{13}\text{C}\{^1\text{H}\}$  NMR (126 MHz, THF, 293 K):  $\delta$  167.3 (CH=N), 162.0 (Ar-C), 150.9 (Py-C), 133.8 (Py-C), 130.7 (Ar-C), 129.8 (Ar-C), 129.0 (Ar-C), 127.9, 126.2, 123.8, 122.4, 120.9 (Py-C), 118.2 (Ar-C), 41.9 (Py-C-Me), 21.9 (CH<sub>3</sub>), Al-CH<sub>3</sub> (Not observed). Anal. Calcd. for C<sub>24</sub>H<sub>20</sub>AlCl<sub>4</sub> N<sub>3</sub>O<sub>2</sub> (%): C, 52.30; H, 3.66; N, 7.62. Found (%): C, 52.23; H, 3.50; N, 7.55. HRMS for [M-CH<sub>3</sub>]<sup>+</sup> (EI): calcd. for (C<sub>23</sub>H<sub>17</sub>Al Cl<sub>4</sub>N<sub>3</sub>O<sub>2</sub>): 535.9861; found 535.9739.

### 6.3.1.8 Synthesis of [Al(Acpy)Me] (8)

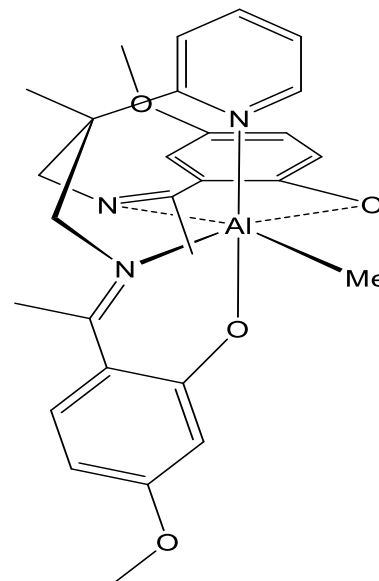
To a stirred solution of Acpy (0.3 g, 0.74 mmol) in toluene (10 mL), AlMe<sub>3</sub> (0.37 mL, 2M in toluene, 0.74 mmol) was added dropwise. The mixture was stirred at room temperature for 20 h. The toluene was removed under reduced pressure and the residue washed with hexanes (3 x 15 mL). The solvent was then removed by canula filtration and the product dried *in vacuo* at room temperature, affording the product as a yellow solid. Yield: 0.29 g, 0.65 mmol (88%). HRMS for [M-CH<sub>3</sub>]<sup>+</sup> (EI): calcd.



for (C<sub>25</sub>H<sub>25</sub>Al N<sub>3</sub>O<sub>2</sub>): 426.1762; found 426.1760. The NMR data comprised complex overlapping signals that could not be differentiated sufficiently to provide accurate characterization, although reaction with benzyl alcohol (below) gave clean conversion to an identifiable product. It is possible that some ligand redistribution occurs in this case.

### 6.3.1.9 Synthesis of [Al(OMe- Acpy)Me] (9)

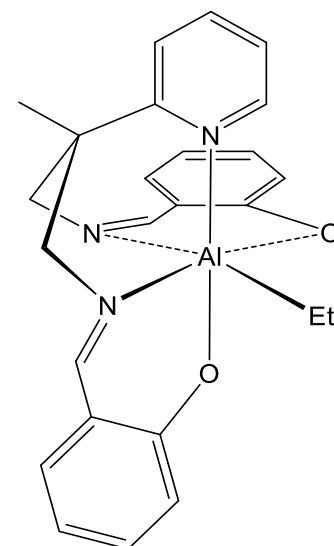
The OMe- Acpy protio-ligand (0.15 g, 0.34 mmol) was dissolved in toluene (15 mL) and AlMe<sub>3</sub> (0.17 mL, 2M in toluene, 0.34 mmol) was added dropwise. The mixture was stirred at room temperature for 18 h. After removal of toluene under reduced pressure, the resulting pale yellow residue was washed three times with dry hexanes. The solvent was then removed by canula filtration and the product dried *in vacuo* at room temperature, affording the product as a pale yellow powder. Yield: 0.14 g, 0.28 mmol (86%). HRMS for [M-CH<sub>3</sub>]<sup>+</sup> (EI): calcd. for (C<sub>27</sub>H<sub>29</sub>Al N<sub>3</sub>O<sub>4</sub>): 486.1973; found 486.1970. The NMR data comprised complex overlapping signals that could not be differentiated sufficiently to provide accurate characterization, although reaction with benzyl alcohol (below) gave clean conversion to an identifiable product. It is possible that some ligand redistribution occurs in this case.



### 6.3.1.10 Synthesis of [Al(Salpy)Et] (10)

To a solution of Salpy (0.4 g, 1.07 mmol) in toluene (25 mL), AlEt<sub>3</sub> (0.56 mL, 1.9 M in toluene, 1.07 mmol) was added dropwise at room temperature. The solution was stirred at ambient temperature for 24 h. The solution was concentrated to a minimum, and hexanes (20 mL) added. The solution was stirred for 2 minutes and the precipitate isolated by filtration. This process was repeated three times. The solid was dried under high vacuum (10<sup>-6</sup> mbar) to afford a yellow powder. Yield: 0.38 g (83%).

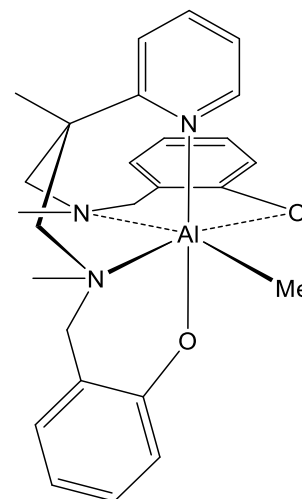
<sup>1</sup>H NMR (400 MHz, C<sub>6</sub>D<sub>6</sub>, 293 K): **Isomer 1** δ 8.58 (m, 1H, H<sup>6</sup>), , 7.46 (s, 2H, CH=N), 7.18 (m, 2H, Ar), 7.12 (overlapping, 3H, Py, Ar), 7.02 (m, , 1H, Py), 6.87 (overlapping, 3H, Ar, Py), (overlapping, 2H, Ar,) 4.10 (d, <sup>2</sup>J = 12.5 Hz, 2H, CHH), 2.92 (d, <sup>2</sup>J = 12.5 Hz, 2H, CHH), 1.46 (t, <sup>3</sup>J = 8.1 Hz 3H, AlCH<sub>2</sub>CH<sub>3</sub>), 0.79 (s, 3H, CH<sub>3</sub>), 0.55 (q, <sup>3</sup>J = 8.0 Hz, 2H, AlCH<sub>2</sub>CH<sub>3</sub>).



**Isomer 2**  $\delta$  8.25 (d,  $^3J = 4.6$  Hz 1H, H<sup>6</sup>), 7.70 (s, 2H, CH=N), 7.21 (m, 2H, Ar), 7.11 (overlapping, 1H, Ar), 7.02-650 (overlapping, 8H, Py, Ar), 3.80 (d,  $^2J = 12.6$  Hz, 2H, CHH), 3.42 (d,  $^2J = 12.5$  Hz, 2H, CHH), 1.54 (t,  $^3J = 8.1$  Hz 3H, AlCH<sub>2</sub>CH<sub>3</sub>), 0.98 (s, 3H, CH<sub>3</sub>), 0.44 (q,  $^3J = 8.0$  Hz, 2H, AlCH<sub>2</sub>CH<sub>3</sub>).

### 6.3.1.11 Synthesis of [Al(Salpy-Me)Me] (11)

The Salpy-Me protio-ligand (0.18 g, 0.44 mmol) was dissolved in tetrahydrofuran (15 mL). Trimethyl aluminium (0.22 mL, 2M in toluene, 0.44 mmol) was added dropwise to the ligand solution. The mixture was stirred at room temperature for 4 h. After removal of the volatiles under reduced pressure, the resulting white residue was washed three times with dry hexanes (15 mL). The solvent was then removed by canula filtration and the product was dried *in vacuo* at room temperature, affording the product as a white powder. Yield: 0.145 g, 0.28 mmol (73%). The NMR data comprised complex overlapping signals that could not be differentiated sufficiently to provide accurate characterization.

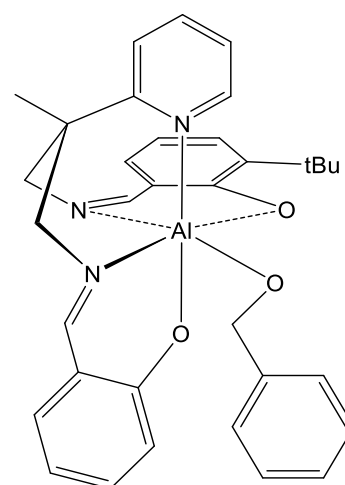


## 6.3.2. Aluminium alkoxide and aryloxide complexes

### 6.3.2.1 Synthesis of [Al(Salpy)(OBn)] (12)

A mixture of [Al(Salpy)Me] (1) (1.19 g, 2.87 mmol) and dry benzyl alcohol (0.3 mL, 2.9 mmol) were dissolved in toluene (30 mL), and the solution was stirred at room temperature for 24 h. the solvent was concentrated to half the original volume, the precipitate filtered, and washed with hexanes (2 x 20 mL) to give an off- white solid. Yield: 1.16 g, 2.29 mmol, (80%).

<sup>1</sup>H NMR (500 MHz, CDCl<sub>3</sub>, 293 K):  $\delta$  9.10 (s, 1H, H<sup>6</sup>), 7.84 (s, 2H, CH=N), 7.64 (t,  $^3J = 5.5$  Hz, 1H, H<sup>4</sup>), 7.16 (m, 5H), 6.96 (m, 6H), 6.76 (s, 2H, Ar), 6.48 (d,  $^3J = 6.4$  Hz, 2H, Ar), 4.68 (s, 2H,



## Chapter 6 - Experimental

OCH<sub>2</sub>Ph), 3.80 (d, <sup>2</sup>J = 12.9 Hz, 2H, CH<sub>2</sub>), 3.71 (d, <sup>2</sup>J = 12.9 Hz, 2H, CH<sub>2</sub>), 1.42 (s, 3H, CH<sub>3</sub>).

<sup>13</sup>C{<sup>1</sup>H} NMR (101 MHz, CDCl<sub>3</sub>, 293 K): δ 168.9 (CH=N), 167.4 (C<sup>2</sup>), 161.3 (C<sup>b</sup>), 151.2 (C<sup>6</sup>), 139.0 (C<sup>4</sup>), 135.3 (C<sup>d</sup>), 133.2, 129.4, 128.6, 127.7, 127.5, 123.3, 122.7, 120.2, 119.8, 115.3, 67.1 (CH<sub>2</sub>), 66.8 (OCH<sub>2</sub>Ph), 41.1(Py-C-Me), 22.9 (CH<sub>3</sub>).

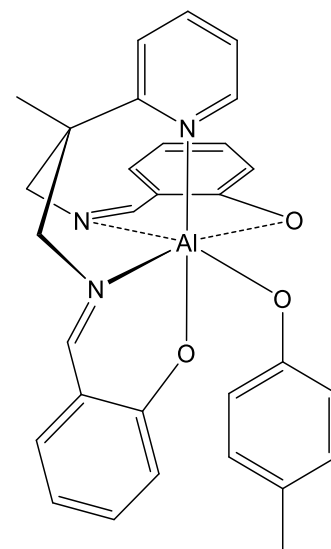
Anal. Calcd. for C<sub>30</sub>H<sub>28</sub>AlN<sub>3</sub>O<sub>3</sub> (%): C, 71.27; H, 5.58; N, 8.31. Found (%): C, 71.36; H, 5.99; N, 8.03. HRMS for [M-OBn]<sup>+</sup> (ES): calcd. for (C<sub>23</sub>H<sub>21</sub>AlN<sub>3</sub>O<sub>2</sub>): 398.1449; found: 398.1454.

### 6.3.2.2 Synthesis of [Al(Salpy)(OTol)] (13)

To a solution of [Al(Salpy)Me] (1) (0.2 g, 0.48 mmol) in toluene (10 mL), p-cresol (0.05 g, 0.48 mmol) was added at room temperature. The mixture was stirred for 20 hours. A precipitate formed during the reaction time. The solid was isolated by cannula filtration and washed with hexanes (3 x 20 mL) to remove any unreacted starting materials, affording the title compound as a white solid. Yield: 0.2 g, 0.39 mmol, (82%).

<sup>1</sup>H NMR (400 MHz, CDCl<sub>3</sub>, 293 K): δ 8.79 (d, <sup>3</sup>J = 3.9 Hz, 1H, H<sup>6</sup>), 7.59 (s, 2H, CH=N), 7.49 (td, <sup>3</sup>J = 7.8, <sup>4</sup>J = 1.7 Hz, 1H, H<sup>4</sup>), 7.08 (d, <sup>3</sup>J = 8.0 Hz, 1H, H<sup>3</sup>), 7.08 (t, <sup>3</sup>J = 6.4 Hz, 1H, H<sup>5</sup>), 6.91 (m, 2H, |Ar), 6.70 (dd, <sup>3</sup>J = 7.7, <sup>4</sup>J = 1.7 Hz, 2H, Ar), 6.48 (s, 2H, Ar), 6.45 (s, 2H, Ar), 6.25 (d, <sup>3</sup>J = 8.4 Hz, 2H, Ar), 6.21 (t, <sup>3</sup>J = 7.3 Hz, 2H, Ar), 3.53 (Overlapping d, 4H, CH<sub>2</sub>), 1.85 (s, 3H, OPh-CH<sub>3</sub>), 1.25 (s, 3H, CH<sub>3</sub>).

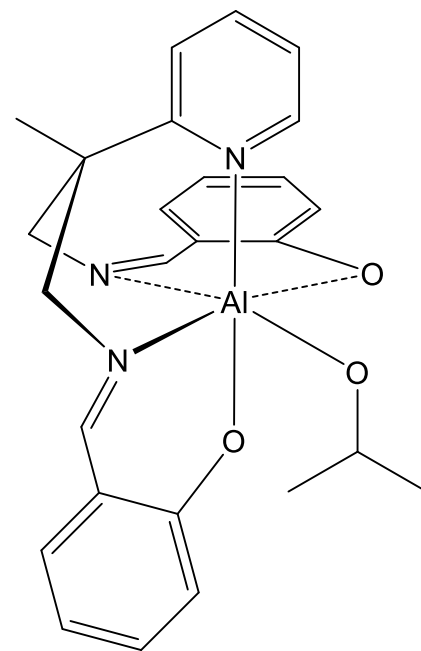
<sup>13</sup>C{<sup>1</sup>H} NMR (101 MHz, CDCl<sub>3</sub>, 293 K): δ 166.9 (C<sup>2</sup>), 161.6 (C<sup>b</sup>), 160.7, 151.1 (C<sup>6</sup>), 139.0, 135.0, 132.7 (C<sup>d</sup>), 128.7, 123.7, 123.1, 122.4, 120.1, 119.8, 119.3, 114.9, 66.9 (CH<sub>2</sub>), 40.1 (Py-C-Me), 22.0 (Ar-CH<sub>3</sub>), 20.5 (CH<sub>3</sub>). Anal. Calcd. for C<sub>30</sub>H<sub>28</sub>AlN<sub>3</sub>O<sub>3</sub> (%): C, 71.27; H, 5.58; N, 8.31. Found (%): C, 71.13; H, 5.33; N, 8.16. HRMS for [M]<sup>+</sup> (EI): calcd. for (C<sub>30</sub>H<sub>28</sub>AlN<sub>3</sub>O<sub>3</sub>): 505.1946; found: 505.1952 (M<sup>+</sup>).



### 6.3.2.3 Synthesis of [Al(Salpy)(OiPr)] (14)

The isopropoxide derivative **14** was prepared using the same procedure as described for **12**, using [Al(Salpy)Me] (**1**) (0.5 g, 1.2 mmol) and dry isopropyl alcohol (0.09 mL, 1.2 mmol) in toluene 15 mL. Yield: 0.45 g, 0.98 mmol, (81%). <sup>1</sup>H NMR (400 MHz, CDCl<sub>3</sub>, 293 K): δ 9.14 (ddd, <sup>3</sup>J = 5.4 Hz, <sup>4</sup>J = 1.8 Hz, <sup>5</sup>J = 0.8 Hz, 1H, H<sup>6</sup>), 7.87 (s, 2H, CH=N), 7.68 (td, <sup>3</sup>J = 7.5, <sup>4</sup>J = 1.7 Hz, 1H, H<sup>4</sup>), 7.19 (overlapping, 5H, Ar, Py), 7.00 (d, <sup>3</sup>J = 1.8 Hz, 1H, Ar), 6.99 (d, <sup>3</sup>J = 1.8 Hz, 1H, Ar), 6.76 (m, 1H, Ar), 6.74 (m, 1H, Ar), 6.50 (overlapping, 3H, Ar, Py), 3.95-3.73 (overlapping, 5H, CH(CH<sub>3</sub>)<sub>2</sub>, CH<sub>2</sub>), 1.46 (s, 3H, CH<sub>3</sub>), 0.8 (d, <sup>3</sup>J = 5.4 Hz, 6H, CH(CH<sub>3</sub>)<sub>2</sub>).

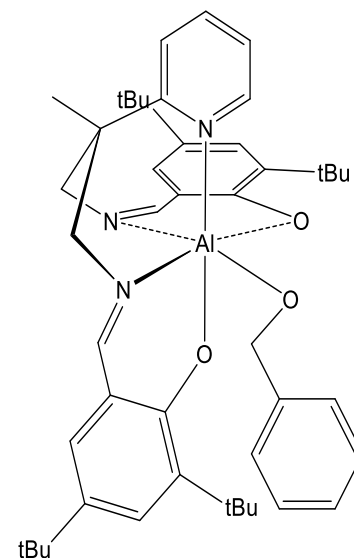
<sup>13</sup>C{<sup>1</sup>H} NMR (101 MHz, CDCl<sub>3</sub>, 293 K): δ 168.3 (CH=N), 167.1 (C<sup>2</sup>), 150.8 (C<sup>6</sup>), 147.9, 138.6 (C<sup>4</sup>), 134.7 (C<sup>d</sup>), 132.6, 129.0, 128.2, 123.0, 122.6, 120.0, 119.5, 114.8, 66.7 (CH<sub>2</sub>), 62.2 (CH(CH<sub>3</sub>)<sub>2</sub>), 40.0(Py-C-Me), 27.2 (CH(CH<sub>3</sub>)<sub>2</sub>), 22.5 (CH<sub>3</sub>). Anal. Calcd. for C<sub>26</sub>H<sub>28</sub>AlN<sub>3</sub>O<sub>3</sub> (%): C, 68.26; H, 6.17; N, 9.18. Found (%): C, 67.93; H, 5.99; N, 9.34. HRMS for [M-OiPr]<sup>+</sup> (ES): calcd. for (C<sub>23</sub>H<sub>21</sub>AlN<sub>3</sub>O<sub>2</sub>): 398.1449; found: 398.1448.



### 6.3.2.4 Synthesis of [Al(<sup>t</sup>Bu, <sup>t</sup>Bu-Salpy)(OBn)] (15)

Benzyl alcohol (33 μl, 0.32 mmol) was added to a stirred solution of [Al(<sup>t</sup>Bu, <sup>t</sup>Bu-Salpy)Me] (**2**) (0.2 g, 0.31 mmol) in toluene (20 mL) and the mixture stirred at room temperature for 24 h. The volatiles were removed under reduced pressure, the residue dissolved in toluene (5 mL), and the product precipitated by the addition of hexanes. The product was obtained as a yellow powder after filtration. Yield: 0.18 g, 0.24 mmol, (79%).

<sup>1</sup>H NMR (500 MHz, CDCl<sub>3</sub>, 293 K): δ 9.2 (dd, <sup>3</sup>J = 5.1 Hz, <sup>4</sup>J = 1.1 Hz, 1 H, H<sup>6</sup>), 7.82 (s, 2H, CH=N), 7.62 (td, <sup>3</sup>J = 7.8, <sup>4</sup>J = 1.8 Hz, 1H, H<sup>4</sup>), 7.31 (d, <sup>4</sup>J = 2.5 Hz, 2H, Ar), 7.25 – 7.18 (m, 2H), 7.05 (d, <sup>3</sup>J = 7.2 Hz, 2H, Benzyl), 6.96 (t, <sup>3</sup>J = 7.3 Hz, 2H, Benzyl), 6.92 (m, 1H, Py), 6.76 (d,



## Chapter 6 - Experimental

$^4J = 2.5$  Hz, 2H, Ar), 4.70 (s, 2H, OCH<sub>2</sub>Ph), 3.91 (d,  $^2J = 12.8$  Hz, 2H, CHH), 3.61 (d,  $^2J = 13.1$  Hz, 2H, CHH), 1.43 (s, 3H, CH<sub>3</sub>), 1.24 (s, 18H, 2 x (C(CH<sub>3</sub>)<sub>3</sub>)), 1.22 (s, 18H, 2 x (C(CH<sub>3</sub>)<sub>3</sub>)).

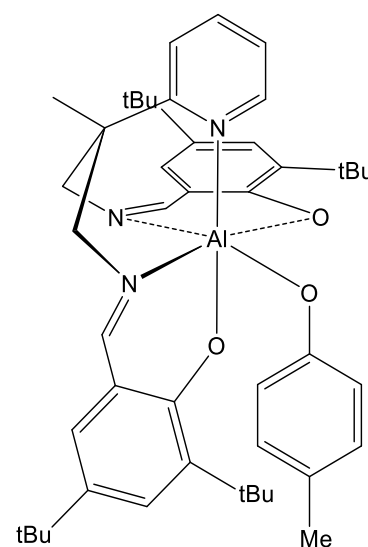
$^{13}\text{C}\{^1\text{H}\}$  NMR (126 MHz, CDCl<sub>3</sub>, 293 K):  $\delta$  168.8 (CH=N), 164.0 (C<sup>2</sup>), 161.9 (C<sup>b</sup>), 150.7 (C<sup>6</sup>), 147.9, 140.1, 138.0, 136.2, 129.7, 129.0, 127.1, 126.8, 126.3, 124.7, 122.3, 119.3, 118.7, 66.5 (CH<sub>2</sub>), 65.8 (OCH<sub>2</sub>Ph), 41.9 (Py-C-Me), 35.2 (C(CH<sub>3</sub>)<sub>3</sub>), 33.8 (C(CH<sub>3</sub>)<sub>3</sub>), 31.3 (C(CH<sub>3</sub>)<sub>3</sub>), 29.7 (C(CH<sub>3</sub>)<sub>3</sub>). Anal. Calcd. for C<sub>46</sub>H<sub>60</sub>AlN<sub>3</sub>O<sub>3</sub> (%): C, 75.69; H, 8.29; N, 5.76. Found (%): C, 75.59; H, 8.46; N, 5.87. HRMS for [M-OBn]<sup>+</sup> (ES): calcd. for (C<sub>39</sub>H<sub>53</sub>AlN<sub>3</sub>O<sub>2</sub>): 622.3953; found: 622.3958.

### 6.3.2.5 Synthesis of [Al(<sup>t</sup>Bu, <sup>t</sup>Bu-Salpy)(OTol)] (16)

In the glove box, [Al(<sup>t</sup>Bu, <sup>t</sup>Bu-Salpy)Me] (2) (0.5 g, 0.78 mmol) was dissolved in toluene (25 mL), and p-cresol (0.085 g, 0.79 mmol) added. The solution was stirred overnight at room temperature, during which time a precipitate formed. The solid was filtered, washed with hexanes (2 x 20 ml), and dried under high vacuum (10<sup>-6</sup> mbar) to leave a yellow solid. Yield: 0.44 g, 0.6 mmol, (77%).

$^1\text{H}$  NMR (400 MHz, CDCl<sub>3</sub>, 293 K):  $\delta$  9.27 (d,  $^3J = 4.3$  Hz, 1H, H<sup>6</sup>), 7.59 (s, 2H, CH=N), 7.53 (t,  $^3J = 7.2$  Hz, 1H, H<sup>4</sup>), 7.12 (m, 4H, Ar), 6.57 (d,  $^4J = 2.0$  Hz, 2H, Ar), 6.38 (d,  $^3J = 8.0$  Hz, 2H, Tol), 6.03 (d,  $^3J = 8.2$  Hz, 2H, Tol), 3.52 (overlapping d, 4H, 2 x CH<sub>2</sub>), 1.87 (s, 3H, OPhCH<sub>3</sub>), 1.31 (s, 3H, CH<sub>3</sub>), 1.02 (s, 36H, 4 x C(CH<sub>3</sub>)<sub>3</sub>).

$^{13}\text{C}\{^1\text{H}\}$  NMR (101 MHz, CDCl<sub>3</sub>, 293 K):  $\delta$  168.7 (CH=N), 165.3 (C<sup>2</sup>), 155.3 (C<sup>b</sup>), 151.1, 150.3, 149.4 (C<sup>6</sup>), 139.4, 137.3, 132.5, 130.1, 128.9, 128.7, 127.1, 123.3, 122.2, 121.4, 66.2 (CH<sub>2</sub>), 41.0 (Py-C-Me), 35.6 (C(CH<sub>3</sub>)<sub>3</sub>), 31.6 (C(CH<sub>3</sub>)<sub>3</sub>), 31.0 (C(CH<sub>3</sub>)<sub>3</sub>), 21.3 (CH<sub>3</sub>). Anal. Calcd. for C<sub>46</sub>H<sub>60</sub>AlN<sub>3</sub>O<sub>3</sub> (%): C, 75.69; H, 8.29; N, 5.76. Found (%): C, 75.55; H, 8.38; N, 5.82. HRMS for [M-OTol]<sup>+</sup> (ASAP): calcd. for (C<sub>39</sub>H<sub>53</sub>AlN<sub>3</sub>O<sub>2</sub>): 622.3953; found: 622.3950.

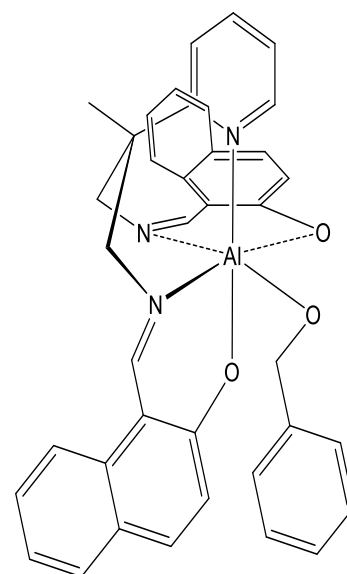


## 6.3.2.6 Synthesis of [Al(Naphpy)(OBn) (17)

To a stirred solution of [Al(Naphpy)Me] (**3**) (0.2 g, 0.39 mmol) in toluene (20 mL) was added benzyl alcohol (40  $\mu$ l, 0.4 mmol). The reaction mixture was stirred at room temperature for 20 h, before the solution was concentrated and filtered. The precipitate was washed with a mixture of toluene and hexane (1:4) (20 mL), with vigorous stirring. The precipitate was filtered and dried *in vacuo* to obtain an off-white solid. Yield: 0.19 g, 0.31 mmol, (81%).

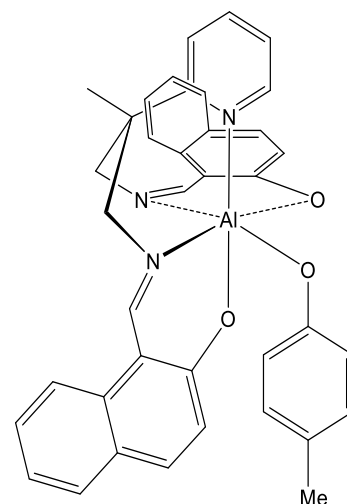
$^1\text{H}$  NMR (400 MHz,  $\text{CDCl}_3$ , 293 K):  $\delta$  9.13 (dd,  $^3J = 5.4$ ,  $^4J = 1.2$  Hz, 1H, H<sup>6</sup>), 8.70 (s, 2H, CH=N), 7.71 (overlapping d, 3H), 7.61 (d,  $^3J = 9.1$  Hz, 2H), 7.58 (dd,  $^3J = 8.0$ ,  $^4J = 1.0$  Hz, 2H), 7.33 (m, 3H), 7.28 (m, 2H), 7.12 (m, 5H), 6.92 (d,  $^3J = 9.1$  Hz, 2H), 6.86 (m, 3H), 4.70 (s, 2H, OCH<sub>2</sub>Ph), 4.01 – 3.87 (overlapping 2 d, 4H, CH<sub>2</sub>), 1.54 (s, 3H, CH<sub>3</sub>).

$^{13}\text{C}\{^1\text{H}\}$  NMR (101 MHz,  $\text{CDCl}_3$ , 293 K):  $\delta$  168.4 (CH=N), 163.2 (C<sup>2</sup>), 150.6 (Py-C), 138.8 (Ar-C), 135.7 (Py-C), 134.0 (Ar-C), 128.9 (Ar-C), 127.1 (Ar-C), 126.4, 125.5 (Ar-C), 123.02, 121.8 (Py-C), 119.5 (Ar-C), 118.9 (Ar-C), 110.4, 67.3 (CH<sub>2</sub>), 66.6 (OCH<sub>2</sub>Ph), 40.4 (Py-C-Me), 22.3 (CH<sub>3</sub>). Anal. Calcd. for C<sub>38</sub>H<sub>32</sub>AlN<sub>3</sub>O<sub>3</sub> (%): C, 75.36; H, 5.33; N, 6.94. Found (%): C, 74.89; H, 5.02; N, 6.83. HRMS for [M-OBn]<sup>+</sup> (ES): calcd. for (C<sub>31</sub>H<sub>25</sub>AlN<sub>3</sub>O<sub>2</sub>): 498.1762; found: 498.1774.



## 6.3.2.7 Synthesis of [Al(Naphpy)(OTol)] (18)

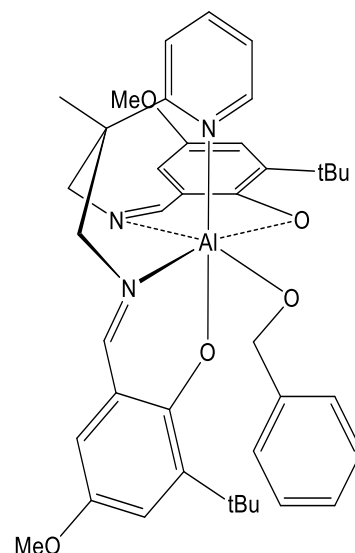
Complex **18** was prepared using the same procedure as described for [Al(<sup>t</sup>Bu,<sup>t</sup>Bu-Salpy)(OTol)], using [Al(Naphpy)Me] (**3**) (0.23 g, 0.44 mmol), P-cresol (0.05 g, 0.46 mmol). Yield: 0.23 g, 0.37 mmol, (85%). <sup>1</sup>H NMR (400 MHz, CDCl<sub>3</sub>, 293 K): δ 9.09 (dd, <sup>3</sup>J = 5.5, <sup>4</sup>J = 1.3 Hz, 1H, H<sup>6</sup>), 8.68 (s, 2H, CH=N), 7.77 (td, <sup>3</sup>J = 7.9, <sup>4</sup>J = 1.8 Hz, 1H, H<sup>4</sup>), 7.67 (d, <sup>3</sup>J = 8.4 Hz, 2H), 7.60 (d, <sup>3</sup>J = 9.2 Hz, 2H), 7.55 (d, <sup>3</sup>J = 7.7 Hz, 2H), 7.39 (d, <sup>3</sup>J = 8.0 Hz, 1H), 7.30 (m, 3H), 7.12 (t, <sup>3</sup>J = 7.4 Hz, 2H), 6.88 (d, <sup>3</sup>J = 9.1 Hz, 2H), 6.69 (d, <sup>3</sup>J = 8.2 Hz, 2H), 6.54 (d, <sup>3</sup>J = 8.4 Hz, 2H), 3.95 (Overlapping two d, <sup>2</sup>J = 12.4 Hz, 4H, CH<sub>2</sub>), 2.08 (s, 3H, OPhCH<sub>3</sub>), 1.57 (s, 3H, CH<sub>3</sub>).



<sup>13</sup>C{<sup>1</sup>H} NMR (101 MHz, CDCl<sub>3</sub>, 293 K): δ 168.3 (CH=N), 161.5 (C<sup>2</sup>), 160.6 (Ar-C), 150.6 (Ar-C), (Py-C), 139.2 (Ar-C), 135.9 (Py-C), 133.9 (Ar-C), 128.7 (Ar-C), 127.0 (Ar-C), 126.5, 123.8, 123.0, 121.8 (Py-C), , 120.0, 119.5, 118.9, 110.4, 67.3 (CH<sub>2</sub>), 40.1 (Py-C-CH<sub>3</sub>), 20.4 (CH<sub>3</sub>). Anal. Calcd. for C<sub>38</sub>H<sub>32</sub>AlN<sub>3</sub>O<sub>3</sub> (%): C, 75.36; H, 5.33; N, 6.94. Found (%): C, 75.14; H, 5.16; N, 6.76. HRMS for [M-OTol]<sup>+</sup> (ASAP): calcd. for (C<sub>31</sub>H<sub>25</sub>AlN<sub>3</sub>O<sub>2</sub>): 498.1762; found: 498.1770.

6.3.2.8 Synthesis of [Al(<sup>t</sup>Bu, OCH<sub>3</sub> - Salpy)(OBn)] (19)

Benzyl alcohol (35 μl, 0.32 mmol) was added to a stirred solution of [Al(<sup>t</sup>Bu, OCH<sub>3</sub> - Salpy)Me] (**4**) (0.2 g, 0.34 mmol) in toluene (20 mL), and the mixture stirred overnight. The solvent was removed under reduced pressure and redissolved in toluene (5 mL); a precipitate formed after the addition of hexanes (25 mL). The mixture was stirred for one minute, after which time the precipitate was isolated by filtration and washed twice with hexanes (15 mL), and dried *in vacuo* to afford the benzyl complex as a yellow powder. Yield: 0.2 g, 0.29 mmol, (86%).



<sup>1</sup>H NMR (400 MHz, CDCl<sub>3</sub>, 293 K): δ 9.21 (d, <sup>3</sup>J = 4.6 Hz, 1H, H<sup>6</sup>), 7.82 (s, 2H, CH=N), 7.64 (t, <sup>3</sup>J = 7.6 Hz, 1H, H<sup>4</sup>), 7.27 – 6.86 (m, 9H), 6.30 (s, 2H), 4.66 (s,

2H, OCH<sub>2</sub>Ph), 3.94 (d, <sup>2</sup>J = 13.0 Hz, 2H, CHH), 3.62 (Overlapping 8H ( 2 x OCH<sub>3</sub>, 2 x CHH), , 1.22 (s, 18H, 2 x C(CH<sub>3</sub>)<sub>3</sub>), 1.19 (s, 3H, CH<sub>3</sub>).

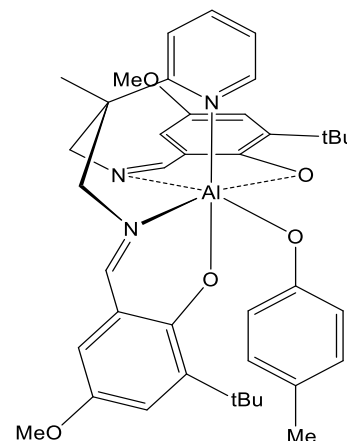
<sup>13</sup>C{<sup>1</sup>H} NMR (101 MHz, CDCl<sub>3</sub>, 293 K): δ 168.2 (CH=N), 162.8 (Ar-C), 150.7 (Ar-C), 149.1 (Py-C), 148.7 (Ar-C), 142.7(Ar-C), 139.7 (Ar-C), 136.7 (Py-C), 129.0 (Ar-C), 128.4 (Ar-C), 127.9 (Ar-C), 122.3 (py-C), 119.6 (Ar-C), 70.7 (CH<sub>2</sub>), 66.6 OCH<sub>2</sub>Ph), 56.1 (OCH<sub>3</sub>), 46.7 (Py-C-Me), 35.3 (C(CH<sub>3</sub>)<sub>3</sub>), 29.7 (C(CH<sub>3</sub>)<sub>3</sub>), 21.0 (CH<sub>3</sub>). Anal. Calcd. for C<sub>40</sub>H<sub>48</sub>AlN<sub>3</sub>O<sub>5</sub> (%): C, 70.88; H, 7.14; N, 6.20. Found (%): C, 70.77; H, 7.03; N, 6.05. HRMS for [M-OBn]<sup>+</sup> (ES): calcd. for (C<sub>33</sub>H<sub>41</sub>AlN<sub>3</sub>O<sub>4</sub>): 570.2912; found: 570.2901.

### 6.3.2.9 Synthesis of [Al(<sup>t</sup>Bu, OCH<sub>3</sub> - Salpy)(OTol)] (20)

The synthesis of complex **20** was carried out in a manner identical to that for [Al(<sup>t</sup>Bu, <sup>t</sup>Bu- Salpy)(OTol)], using [(<sup>t</sup>Bu, OCH<sub>3</sub> - Salpy)Me] (**4**) (0.2 g, 0.34 mmol), p-cresol (0.037 g, 0.34 mmol), and toluene (20 mL). Yield: 0.21 g, 0.30 mmol, (91%).

<sup>1</sup>H NMR (400 MHz, CDCl<sub>3</sub>, 293 K): δ 9.39 (d, <sup>3</sup>J = 5.5 Hz, 1H, H<sup>6</sup>), 7.71 (m, 2H (CH=N), 1H (H<sup>4</sup>)), 7.26 (m, 2H), 6.91 (d, <sup>4</sup>J = 1.2 Hz, 2H, Ar), 6.54 (d, <sup>3</sup>J = 7.7 Hz, 2H, Tol), 6.25 (s, 2H, Ar), 6.14 (d, <sup>3</sup>J = 7.5 Hz, 2H, Tol), 3.74(d, <sup>2</sup>J = 13.2 Hz, 2H, CHH), 3.66(d, <sup>2</sup>J = 13.2 Hz, 2H, CHH) 3.60 (s, 6H, OCH<sub>3</sub>), 1.45 (s, 3H, CH<sub>3</sub>), 1.15 (s, 18H, 2 x C(CH<sub>3</sub>)<sub>3</sub>).

<sup>13</sup>C{<sup>1</sup>H} NMR (101 MHz, CDCl<sub>3</sub>, 293 K): δ 167.7 (CH=N), 161.7 (C<sup>2</sup>), 161.4, 160.5, 151.1, 148.4, 142.7, 136.6 (Py-C), 128.8, 128.3, 123.6, 122.5, 122.2 (Py-C), 120.0, 119.1, 118.1, 111.1, 66.9 (CH<sub>2</sub>), 56.0 (OCH<sub>3</sub>), 40.8 (Py-C-CH<sub>3</sub>), 35.1(C(CH<sub>3</sub>)<sub>3</sub>), 29.4 (C(CH<sub>3</sub>)<sub>3</sub>), 22.3 (CH<sub>3</sub>). Anal. Calcd. for C<sub>40</sub>H<sub>48</sub>AlN<sub>3</sub>O<sub>5</sub> (%): C, 70.88; H, 7.14; N, 6.20. Found (%): C, 70.54; H, 7.53; N, 5.97. HRMS for [M-OTol]<sup>+</sup> (EI): calcd. for (C<sub>33</sub>H<sub>41</sub>AlN<sub>3</sub>O<sub>4</sub>): 570.2912; found: 570.2932.

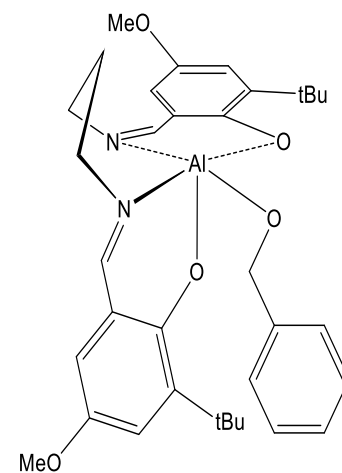


### 6.3.2.10 Synthesis of [Al(<sup>t</sup>Bu, OCH<sub>3</sub> - Salpn)(OBn)] (21)

The synthesis of this complex was carried out in a manner identical to that for [Al(<sup>t</sup>Bu, OCH<sub>3</sub> - Salpy)(OBn)], using [Al(<sup>t</sup>Bu, OCH<sub>3</sub> - Salpn)Me] (**6**) (0.3 g, 0.6 mmol), benzyl alcohol (63 μl, 0.61 mmol), and toluene (20 mL). Yield: 0.32 g, 0.85 mmol, (90%).

<sup>1</sup>H NMR (300 MHz, CDCl<sub>3</sub>, 293 K): δ 8.05 (s, 2H, CH=N), 7.19 (m, 3H), 7.03 (d, <sup>4</sup>J = 3.0 Hz, 2H), 6.88 (m, 2H) 6.40 (d, <sup>4</sup>J = 3.0 Hz, 2H), 4.62 (s, 2H, OCH<sub>2</sub>Ph), 3.91 (Quintet, 2H, CH<sub>2</sub>), 3.68 (s, 6H, OCH<sub>3</sub>), 3.50 (Quintet, 2H, CH<sub>2</sub>), 1.97 (ddd, <sup>2</sup>J = 19.1, <sup>2</sup>J = 13.8, <sup>3</sup>J = 6.6 Hz, 2H, CH<sub>2</sub>), 1.35 (s, 18H, C(CH<sub>3</sub>)<sub>3</sub>).

<sup>13</sup>C{<sup>1</sup>H} NMR (101 MHz, CDCl<sub>3</sub>, 293 K): δ 167.2 (CH=N), 162.4 (Ar-C), 155.4 (Ar-C), 148.6 (Ar-C), 139.3 (Ar-C), 136.7 (Ar-C), 129.5 (Ar-C), 128.2 (Ar-C), 127.6 (Ar-C), 118.5 (Ar-C), 65.7 (OCH<sub>2</sub>Ph), 57.7 (N-CH<sub>2</sub>), 55.9 (OCH<sub>3</sub>), 35.4 (C(CH<sub>3</sub>)<sub>3</sub>), 31.3 (CH<sub>2</sub>CH<sub>2</sub>CH<sub>2</sub>), (29.3 (C(CH<sub>3</sub>)<sub>3</sub>)).

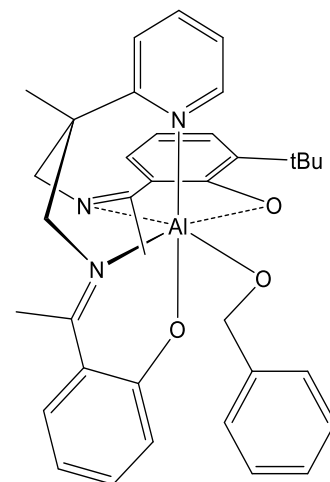


### 6.3.2.11 Synthesis of [Al(Acpy)(OBn)] (22)

The synthesis of this complex was carried out in a manner identical with that for [Al(<sup>t</sup>Bu, OCH<sub>3</sub> - Salpy)(OBn)], using [Al(Acpy)Me] (**8**) (0.72 g, 1.63 mmol), benzyl alcohol (0.17 mL, 1.64 mmol), and toluene (30 mL). Yield: 0.77 g, 1.44 mmol, (88%).

<sup>1</sup>H NMR (400 MHz, CDCl<sub>3</sub>, 293 K): δ 9.21 (dd, <sup>3</sup>J = 5.5, <sup>4</sup>J = 1.4 Hz, 1H, H<sup>6</sup>), 7.75 (td, <sup>3</sup>J = 7.8, <sup>4</sup>J = 1.8 Hz, 1H, H<sup>4</sup>), 7.42 (s, 2H), 7.35 (d, <sup>3</sup>J = 7.7 Hz, 1H), 7.28 (m, 1H), 6.97 (m, 14H), 6.53 (m, 2H), 6.33 (d, <sup>3</sup>J = 7.3 Hz, 1H), 4.72 (s, 2H, OPhCH<sub>3</sub>), 3.79 (m, 4H, CH<sub>2</sub>), 2.26 (s, 3H, CH<sub>3</sub>), 1.54 (s, 3H, CH<sub>3</sub>).

<sup>13</sup>C{<sup>1</sup>H} NMR (101 MHz, CDCl<sub>3</sub>, 293 K): δ 160.0 (Ar-C), 150.8 (Ar-C), 147.3 (Py-C), 139.3 (Ar-C), 133.3 (Py-C), 129.1 (Ar-C), 128.3 (Ar-C), 127.3 (Ar-C), 125.1 (Ar-C), 123.3 (py-C), 119.4 (Ar-C), 67.3 (CH<sub>2</sub>), 62.4 (OCH<sub>2</sub>Ph), 39.2 (Py-C-Me), 23.6 (CH<sub>3</sub>). Anal. Calcd. for C<sub>32</sub>H<sub>32</sub>AlN<sub>3</sub>O<sub>3</sub> (%): C, 72.03; H, 6.04; N, 7.87. Found (%): C, 71.87; H, 5.95; N, 7.76. HRMS for [M-OBn]<sup>+</sup> (EI): calcd. for (C<sub>25</sub>H<sub>25</sub>AlN<sub>3</sub>O<sub>2</sub>): 426.1762; found 426.1754.

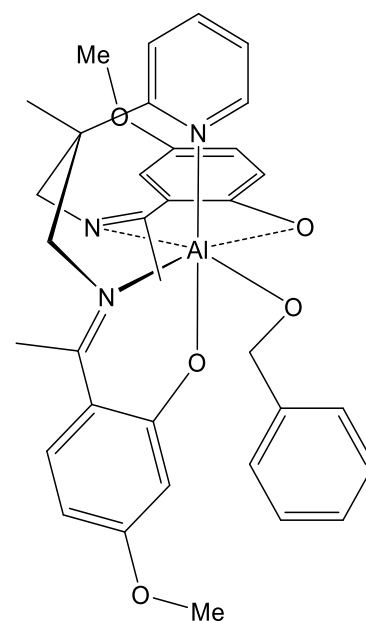


### 6.3.2.12 Synthesis of [Al(OCH<sub>3</sub>- Acpy)(OBn)] (23)

The synthesis of this complex was carried out in a manner identical to that for [Al(<sup>t</sup>Bu, OCH<sub>3</sub> - Salpy)(OBn)], using [Al(OCH<sub>3</sub>- Acpy)Me] (**9**) (0.48 g, 0.95 mmol), benzyl alcohol (98  $\mu$ l, 0.95 mmol), and toluene (25 mL). Yield: 0.51 g, 0.85 mmol, (90%).

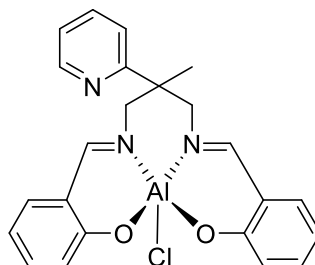
<sup>1</sup>H NMR (400 MHz, CDCl<sub>3</sub>, 293 K)  $\delta$  9.43 (d, <sup>3</sup>J = 5.2 Hz, 1H, H<sup>6</sup>), 7.92 (t, <sup>4</sup>J = 7.7 Hz, 1H), 7.57 – 7.43 (m, 4H), 7.38 (d, <sup>3</sup>J = 6.4 Hz, 2H), 7.31 (d, <sup>3</sup>J = 7.1 Hz, 2H), 7.18 (d, <sup>3</sup>J = 3.0 Hz, 1H), 6.63 (s, 1H), 6.35 (d, <sup>3</sup>J = 7.9 Hz, 2H), 6.12 (s, 1H), 4.92 (s, 2H, OCH<sub>2</sub>Ph), 3.87 (m, 4H, CH<sub>2</sub>), 3.76 (s, 6H, OCH<sub>3</sub>), 2.38 (s, 6H, 2 x CH<sub>3</sub>), 1.71 (s, 3H, CH<sub>3</sub>).

<sup>13</sup>C{<sup>1</sup>H} NMR (101 MHz, CDCl<sub>3</sub>, 293 K):  $\delta$  174.5 (CH<sub>3</sub>C=N), , 169.5 (Ar-C), 164.4, 160.2, 150.5, 148.9 (Py-C), 147.6, 139.2, 137.9 (Py-C), 130.9, 128.2, 125.3, 122.1 (Py-C), 119.4, 118.3, 105.1, 104.5, , 67.4 (CH<sub>2</sub>), 62.6 (OCH<sub>2</sub>Ph), 55.2 (OCH<sub>3</sub>), 39.4 (Py-C-Me), 23.6 (CH<sub>3</sub>C=N), ( 21.5 (CH<sub>3</sub>). Anal. Calcd. for C<sub>32</sub>H<sub>32</sub>AlN<sub>3</sub>O<sub>3</sub>.toluene (%): C, 68.79; H, 6.11; N, 7.08. Found (%): C, 69.93; H, 5.51; N, 6.21. HRMS for [M-OBn]<sup>+</sup> (EI): calcd. for (C<sub>27</sub>H<sub>29</sub>Al N<sub>3</sub>O<sub>4</sub>) : 486.1973; found 486.1984.



### 6.3.3. Aluminum Chloride complexes

#### 6.3.3.1 Synthesis of [Al(Salpy) Cl] (24)



A 100 mL Schlenk flask was charged with Salpy (0.25, 0.67 mmol) and 15 mL of toluene. Diethyl aluminium chloride (0.74 mL, 0.67 mmol, 0.9 M in toluene) was added dropwise over 2 min, resulting in a yellow solution and a pale yellow solid.

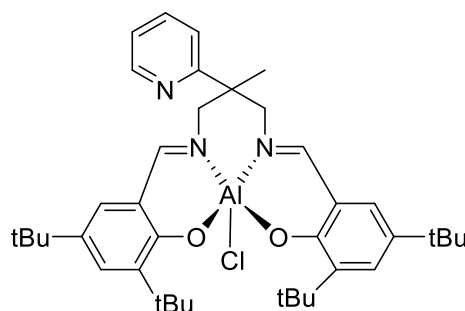
## Chapter 6 - Experimental

The mixture was allowed to stir for 3 h at 25 °C, after which time the solution was concentrated under reduced pressure to 5 mL, and 20 mL of hexane was added with stirring to completely precipitate the product. The precipitate was filtered, washed with hexanes (20 mL), and dried *in vacuo* to yield the titled complex as an off-white solid. Yield: 0.27 g, 0.62 mmol, (93%).

$^1\text{H}$  NMR (500 MHz,  $\text{CD}_2\text{Cl}_2$ , 293K)  $\delta$  9.14 (d,  $^3J = 5.3$  Hz, 1H,  $\text{H}^6$ ), 8.32 (s, 1H, CH=N), 7.79 (t,  $^3J = 7.7$  Hz, 1H, Pyridyl), 7.74 (s, 1H, CH=N), 7.43 (d,  $^3J = 8.0$  Hz, 1H, Aromatic), 7.33 (m, 3H, Aromatic), 7.05 (d,  $^3J = 7.5$  Hz, 1H, Aromatic), 6.74 (t,  $^3J = 7.2$  Hz, 1H, Pyridyl), 6.62 (m, 4H, Aromatic), 4.72 (d,  $^2J = 13.8$  Hz, 1H,  $\text{CH}_2$ ), 4.26 (d,  $^2J = 13.4$  Hz, 1H,  $\text{CH}_2$ ), 3.54 (d,  $^2J = 13.9$  Hz, 1H,  $\text{CH}_2$ ), 3.35 (d,  $^2J = 13.7$  Hz, 1H,  $\text{CH}_2$ ), 1.59 (s, 3H,  $\text{CH}_3$ ).

$^{13}\text{C}\{^1\text{H}\}$  NMR (101 MHz,  $\text{CD}_2\text{Cl}_2$ , 293 K):  $\delta$  171.5 (CH=N), 167.8 (CH=N), 165.8 (Ar-C), 164.6 (Ar-C), 160.1 (Ar-C), 150.7 (Py-C), 139.9 (Py-C), 135.8 (Ar-C), 135.5 (Ar-C), 133.8 (Ar-C), 133.1 (Ar-C), 125.2 (Ar-C), 123.9 (Ar-C), 121.7 (Py-C), 119.7 (Ar-C), 119.5 (Ar-C), 119.0 (Ar-C), 116.1 (Ar-C), 116.1 (Ar-C), 115.5 (Ar-C), 68.2 ( $\text{CH}_2$ ), 64.6 ( $\text{CH}_2$ ), 40.0 (Py-C-Me), 21.6 ( $\text{CH}_3$ ). Anal. Calcd. for  $\text{C}_{23}\text{H}_{21}\text{AlClN}_3\text{O}_2$  (%): C, 63.67; H, 4.88; N, 9.69 Found (%): C, 63.17; H, 5.12; N, 9.05. HRMS for  $[\text{M}-\text{Cl}]^+$  (ES): calcd. for  $(\text{C}_{23}\text{H}_{21}\text{AlN}_3\text{O}_2)$ : 398.1449; found: 398.1447.

### 6.3.3.2 Synthesis of $[\text{Al}(\text{tBu}, \text{tBu-Salpy})\text{Cl}]$ (25)



To a solution of  $\text{tBu}, \text{tBu-Salpy}$  (0.2 g, 0.33 mmol) in toluene (15 mL) was added a solution of diethylaluminum chloride (0.37 mL, 0.33 mmol, 0.9 M in toluene). The addition took place over 1-2 min, resulting in a yellow solution and a pale yellow precipitate, which began to form after 5 minutes. The mixture was stirred for 3 h at ambient temperature. The solution was then concentrated and 15 mL

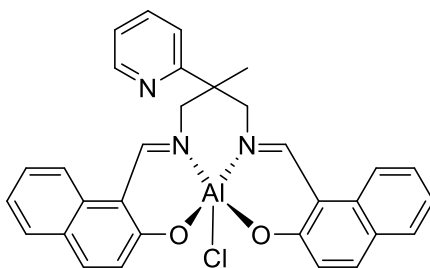
## Chapter 6 - Experimental

of hexanes added; the suspension was allowed to stir for 5 minutes and the solid isolated by filtration. The solid was washed a further two times to afford a yellow solid. Yield: 0.203 g, 0.303 mmol, (92%).  $^1\text{H}$  NMR (400 MHz,  $\text{CDCl}_3$ , 293 K):  $\delta$  9.66 (d,  $^3J = 4.6$  Hz, 1H,  $\text{H}^6$ ), 8.14-7.60 (b, 2H,  $\text{CH}=\text{N}$ ), 7.81 (t,  $^3J = 8.1$  Hz, 1H, Py), 7.41 (d,  $^4J = 1.9$  Hz, 1H, Ar), 7.41 – 7.34 (overlapping, 4H, Py, Ar), 6.99-6.71 (b, 2H, Ar), 4.45 – 3.11 (b, 4H,  $\text{CH}_2$ ), 1.62-0.95 (m,b, 39H,  $4\times(\text{CH}_3)_3$ ,  $\text{CH}_3$ ).

$^1\text{H}$  NMR (400 MHz,  $\text{CDCl}_3$ , 243 K):  $\delta$  9.66 (d,  $^3J = 4.5$  Hz, 1H,  $\text{H}^6$ ), 8.12 (s, 1H,  $\text{CH}=\text{N}$ ), 7.81 (t,  $^3J = 7.8$  Hz, 1H, Py-C), 7.68 (s, 1H,  $\text{CH}=\text{N}$ ), 7.41 (d,  $^4J = 1.9$  Hz, 1H, Ar-C), 7.41 – 7.36 (overlapping, 2H, Py-C), 7.34 (d,  $^4J = 1.9$  Hz, 1H, Ar-C), 6.97 (d,  $^4J = 1.9$  Hz, 1H, Ar-C), 6.82 (d,  $^4J = 1.9$  Hz, 1H, Ar-C), 4.37 (d,  $^2J = 13.0$  Hz, 1H,  $\text{CH}_2$ ), 4.15 (d,  $^2J = 14$  Hz, 1H,  $\text{CH}_2$ ), 3.47 (d,  $^2J = 13.4$  Hz, 1H,  $\text{CH}_2$ ), 3.30 (d,  $^2J = 14.0$  Hz, 1H,  $\text{CH}_2$ ), 1.59 (s, 3H,  $\text{CH}_3$ ), 1.52 (s, 9H,  $\text{C}(\text{CH}_3)_3$ ), 1.22 (s, 18H,  $2\times \text{C}(\text{CH}_3)_3$ ), 0.99 (s, 9H,  $\text{C}(\text{CH}_3)_3$ ).

$^{13}\text{C}\{^1\text{H}\}$  NMR (101 MHz,  $\text{CDCl}_3$ , 293 K):  $\delta$  163.7 ( $\text{CH}=\text{N}$ ), 160.9 (C2), 152.1 (Py-C), 139.1, 136.6 (C-Py), 129.0 (Ar), 128.2 (Ar), 125.3, 122.7 (Py-C), 118.9, 40.1 (Py-C-Me), 33.8 ( $\text{C}(\text{CH}_3)$ ), 31.3 ( $\text{C}(\text{CH}_3)$ ), 21.4( $\text{CH}_3$ ). Anal. Calcd. for  $\text{C}_{39}\text{H}_{53}\text{AlClN}_3\text{O}_2$  (%): C, 71.16; H, 8.12; N, 6.38 Found (%): C, 70.90; H, 7.91; N, 5.74. HRMS for  $[\text{M}+\text{Cl}]^+$  (ES): calcd. for  $(\text{C}_{39}\text{H}_{53}\text{AlCl}_2 \text{N}_3\text{O}_2)$ : 692.3330; found: 692.3315.

### 6.3.3.3 Synthesis of $[\text{Al}(\text{Naphpy})\text{Cl}]$ (**26**)



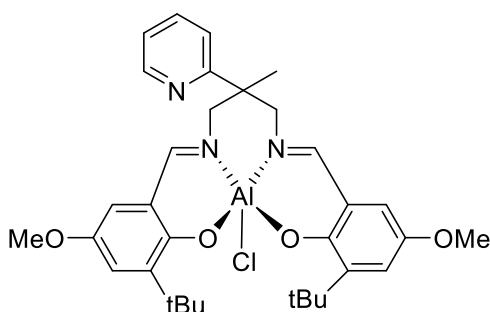
Complex **26** was prepared as described for  $[\text{Al}(\text{Salpy})\text{Cl}]$  using Naphpy (0.4 g, 0.84 mmol) in toluene (20 mL), and  $\text{Et}_2\text{AlCl}$  (0.94 mL, 0.84 mmol, 0.9 M in toluene). The complex was obtained as an off-white solid. Yield: 0.408 g, 0.76 mmol, (90%).

## Chapter 6 - Experimental

$^1\text{H}$  NMR (400 MHz,  $\text{CDCl}_3$ , 293 K):  $\delta$  9.34 (d,  $^3J = 5.0$  Hz, 1H,  $\text{H}^6$ ), 8.53 (overlapping m,  $\text{CH}=\text{N}$ , 2H), 7.75 (m, 2H) 7.63 (t,  $^3J = 7.75$  Hz, 2H), 7.56 (s, b, 2H), 7.48 (d,  $^3J = 7.6$  Hz, 2H), 7.28 (m, 3H), 7.13 (m, 4H), 3.30-4.16 (dd,b,  $^2J = 14.3$  Hz, 4H), 1.40 (s, 3H).

$^{13}\text{C}\{^1\text{H}\}$  NMR (101 MHz,  $\text{CDCl}_3$ , 293 K): 168.0 ( $\text{CH}=\text{N}$ ), 160.2 ( $\text{C}^2$ ), 151.4 ( $\text{C}^6$ ), 139.4, 133.6, 129.0, 127.4, 126.6, 125.6, 125.3, 123.1, 122.2 (Py-C), 119.5, 119.1, 40.1 (Py-C- $\text{CH}_3$ ), 22.0 ( $\text{CH}_3$ ). Anal. Calcd. for  $\text{C}_{31}\text{H}_{25}\text{AlClN}_3\text{O}_2$  (%): C, 69.73; H, 4.72; N, 7.87 Found (%): C, 69.43; H, 5.01; N, 7.22. HRMS for  $[\text{M}+\text{Cl}]^+$  (ES): calcd. for ( $\text{C}_{31}\text{H}_{25}\text{AlCl}_2\text{N}_3\text{O}_2$ ): 568.1139; found: 568.1136.

### 6.3.3.4 Synthesis of $[\text{Al}(\text{tBu}, \text{OCH}_3 - \text{Salpy})\text{Cl}]$ (27)



Diethyl aluminium chloride (0.69 mL, 0.62 mmol, 0.9 M in toluene) was added dropwise to a stirred yellow solution of  $\text{tBu}$ ,  $\text{OMe}$ - Salpy (0.34 g, 0.62 mmol) in toluene (15 mL) at room temperature. The colour of the solution changed to deep yellow and a precipitate started to form after 1 h. The stirring was continued for a further 2 h, after which the solvent was concentrated to minimum and hexanes (20 mL) added. The precipitate was filtered and washed with hexanes (2 x 15mL) and dried *in vacuo* to give the titled complex as a deep yellow solid. Yield: 0.243 g, 0.4 mmol, (91%).

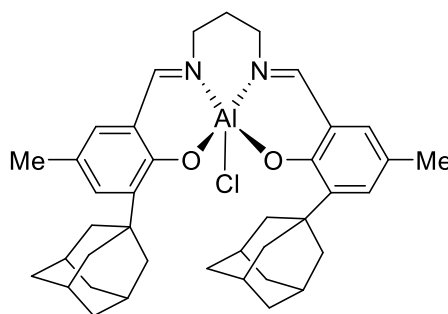
$^1\text{H}$  NMR (500 MHz,  $\text{CDCl}_3$ , 293 K)  $\delta$  9.66 (d,  $^3J = 5.5$  Hz, 1H,  $\text{H}^6$ ), 7.82 (t,  $^3J = 7.7$  Hz, 1H), 7.39 (m, 2H), 7.17 (t,  $^3J = 7.3$  Hz, 2H), 7.03 (s, 2H), 6.42 (s, 2H), 4.23 (d,  $^2J = 13.5$  Hz,  $\text{CH}_2$ , 2H), 3.70 (s,  $\text{OCH}_3$ , 3H) 3.46 (d,  $^2J = 13.5$  Hz, 2H), 1.57 (s,  $\text{CH}_3$ , 3H). 1.30 (m, 18H,  $\text{C}(\text{CH}_3)_3$ ).

$^{13}\text{C}\{^1\text{H}\}$  NMR (101 MHz,  $\text{CDCl}_3$ , 293 K):  $\delta$  161.2 ( $\text{CH}=\text{N}$ ), 160.7 ( $\text{C}^2$ ), 151.9, 148.8 ( $\text{C}^6$ ), 142.7, 139.3, 122.7, 119.1, 111.1, 56.0 ( $\text{OCH}_3$ ), 40.0 (Py-C-Me), 35.0 ( $\text{C}(\text{CH}_3)_3$ ), 29.6 ( $\text{C}(\text{CH}_3)_3$ ), 22.0 ( $\text{CH}_3$ ). Anal. Calcd. for  $\text{C}_{33}\text{H}_{41}\text{AlClN}_3\text{O}_4 \cdot 0.4\text{C}_7\text{H}_8$

## Chapter 6 - Experimental

(%): C, 66.87; H, 6.93 N, 6.54 Found (%): C, 66.66; H, 7.03; N, 6.21. HRMS for  $[M+Cl]^+$  (ES): calcd. for  $(C_{33}H_{41}AlCl_2N_3O_4)$ : 640.2290; found: 640.2316.

### 6.3.3.5 $[Al(Ad, Me - Salpy)Cl]$ (**28**)

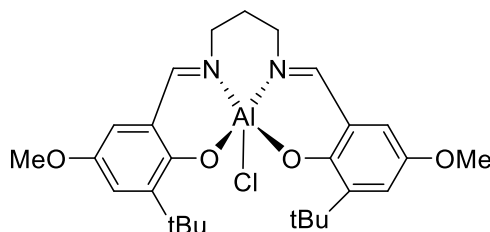


Complex **28** was prepared as described for  $[Al(Salpy)Cl]$  using Ad, Me-Salpy (0.4 g, 0.59 mmol) in toluene (20 mL), and  $Et_2AlCl$  (0.66 mL, 0.59 mmol, 0.9 M in toluene). The product was obtained as a yellow solid. Yield: 0.39 g, 0.53 mmol, (89%).

$^1H$  NMR (300 MHz,  $CDCl_3$ , 293 K)  $\delta$  9.65 (d,  $^3J = 4.2$  Hz, 1H,  $H^6$ ), 8.06 (s, 1H), 7.77 (td,  $^3J = 7.8$ ,  $^4J = 1.6$  Hz, 1H,  $H^4$ ), 7.63 (s, 1H), 7.33 (m, 2H), 7.05 (dd,  $J = 4.0$ ,  $J = 2.3$  Hz, 2H), 6.82 (s, 1H), 6.65 (s, 1H), 4.25 (d,  $^2J = 13.6$  Hz, 2H), 3.45 (d,  $^2J = 13.6$  Hz, 1H), 3.25 (d,  $^2J = 13.5$  Hz, 1H), 2.43 – 2.05 (m, 6H, 2 (Ar- $CH_3$ ), 9 H (Ad), 2.00 – 1.64 (m, 15H, Ad), 1.55 (s, 3H,  $CH_3$ ), 1.37 (d,  $^3J = 11.7$  Hz, 3H, Ad), 1.13 (d,  $^3J = 11.7$  Hz, 3H, Ad).

$^{13}C\{^1H\}$  NMR (101 MHz,  $CDCl_3$ , 293 K):  $\delta$  170.2 (CH=N), 166.4 ( $C^2$ ), 163.9, 163.2, 160.5, 151.8 (Py-C), 141.1, 140.7, 138.8, 134.1, 133.3, 130.5, 129.7, 123.5, 123.2, 122.4, 119.3, 119.0, 118.8, 68.16 ( $CH_2$ ), 63.9 ( $CH_2$ ), 40.0, 37.0, 36.7, 36.5, 31.4, 29.1, 28.9, 22.4, 21.7, 20.3. Anal. Calcd. for  $C_{45}H_{53}AlClN_3O_2$  (%): C, 74.00; H, 7.31; N, 5.75 Found (%): C, 74.14; H, 7.16; N, 5.66. HRMS for  $[M+Cl]^+$  (ES): calcd. for  $(C_{45}H_{53}AlCl_2N_3O_2)$ : 764.3330; found: 764.3320.

### 6.3.3.6 Synthesis of [Al(<sup>t</sup>Bu, OCH<sub>3</sub> - Salpn)Cl] (29)

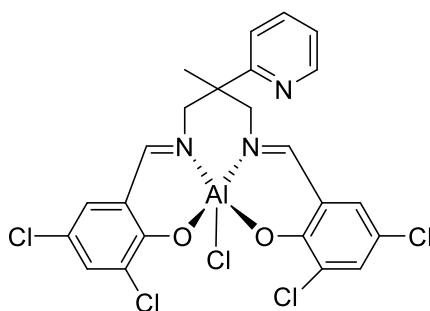


<sup>t</sup>Bu, OMe- Salpn (0.45 g, 0.99 mmol) was dissolved in toluene (25 mL). diethylaluminum chloride (1.1 mL, 0.99 mmol, 0.9 M in toluene) was added dropwise. The solution was stirred at room temperature for 4 h. During this time, the clear solution turned turbid. The solvent was concentrated to 10 mL and 25 mL of hexanes were added with vigorous stirring. The yellow precipitate was filtered and washed with hexanes (25 mL). Yield: 0.45 g, 0.87 mmol, (90%).

<sup>1</sup>H NMR (300 MHz, CDCl<sub>3</sub>, 293 K) δ 8.13 (s, 2H, CH=N), 7.08 (d, <sup>3</sup>J = 3.2 Hz, 2H, Ar), 6.45 (d, <sup>3</sup>J = 3.1 Hz, 2H, Ar), 3.94 (m, 2H, CH<sub>2</sub>), 3.67 (s, 6H, OCH<sub>3</sub>), 3.53 (q, 2H, CH<sub>2</sub>), 2.08 (m, 2H, CH<sub>2</sub>), 1.41 (s, 18H, 2 x (CH<sub>3</sub>)<sub>3</sub>).

<sup>13</sup>C{<sup>1</sup>H} NMR (101 MHz, CDCl<sub>3</sub>, 293 K): δ 171.1 (CH=N), 160.0, 150.1 (C<sup>b</sup>), 143.4, 123.5, 117.8 (C<sup>a</sup>), 110.8 (C<sup>d</sup>), 55.7 (CH<sub>2</sub>), 55.0 (OCH<sub>3</sub>), 35.4 (C(CH<sub>3</sub>)<sub>3</sub>), 29.4 (CH<sub>2</sub>CH<sub>2</sub>CH<sub>2</sub>), 27.2 (C(CH<sub>3</sub>)<sub>3</sub>). Anal. Calcd. for C<sub>25</sub>H<sub>36</sub>AlClN<sub>2</sub>O<sub>4</sub> (%): C, 62.97; H, 7.05; N, 5.44 Found (%): C, 62.89; H, 7.16; N, 5.53. HRMS for [M]<sup>+</sup> (EI): calcd. for (C<sub>27</sub>H<sub>36</sub>AlClN<sub>2</sub>O<sub>4</sub>): 514.2179; found: 514.2173.

### 6.3.3.7 Synthesis of [Al(Cl, Cl - Salpy)Cl] (30)



To the orange solution of Cl, Cl - Salpy (0.33 g, 0.64 mmol) in toluene (25 mL) was added a solution of diethylaluminum chloride (0.71 mL, 0.64 mmol, 0.9 M in

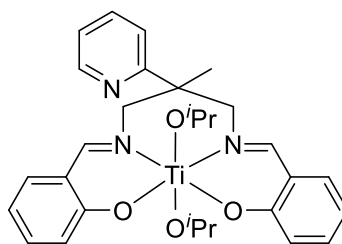
toluene). The precipitate was formed immediately and the stirring was continued for 5 h. at ambient temperature. The solution was filtered and washed three times with hexane (20 mL). The solid was dried *in vacuo* to obtain the titled complex as an off-white solid. Yield: 0.33 g (89.4%).

$^1\text{H}$  NMR (400 MHz, DMSO, 293 K)  $\delta$  8.67 (s, overlapping 2H, H<sup>6</sup>, CH=N), 8.23 (m, 2H, CH=N, Ar), 7.80 (d,  $^3J = 8.0$  Hz, 1H, Pyridyl), 7.73 (t,  $^3J = 6.0$  Hz, 1H, Pyridyl), 7.65 (m, 3H, Ar), 7.43 (s, 1H, Ar), 4.44 (d,  $^2J = 14.7$  Hz, 1H, CH<sub>2</sub>), 4.02 (overlapping, 2d, 2H, CH<sub>2</sub>), 3.71 (d,  $^2J = 14.7$  Hz, 1H, CH<sub>2</sub>), 1.59 (s, 3H, CH<sub>3</sub>).

$^{13}\text{C}$  NMR (126 MHz, DMSO, 293 K)  $\delta$  170.6 (CH=N), 167.6 (CH=N), 161.4 (Ar-C), 158.8 (Ar-C), 158.0 (Ar-C), 148.2 (Py-C), 141.5 (Ar-C), 133.7 (Ar-C), 133.1 (Ar-C), 131.1 (Ar-C), 130.9, 124.0 (Py-C), 121.8 (Ar-C), 121.4 (Ar-C), 120.9 (Ar-C), 118.8 (Ar-C), 118.4 (Ar-C), 66.4 (CH<sub>2</sub>), 61.8 (CH<sub>2</sub>), 20.6 (CH<sub>3</sub>). Anal. Calcd. for C<sub>23</sub>H<sub>17</sub>AlCl<sub>5</sub>N<sub>3</sub>O<sub>2</sub> (%): C, 48.33; H, 3.00; N, 7.35 Found (%): C, 48.12; H, 2.90; N, 7.26. HRMS for [M]<sup>+</sup> (EI): calcd. for (C<sub>23</sub>H<sub>17</sub>AlCl<sub>5</sub>N<sub>3</sub>O<sub>2</sub>): 570.9549; found: 570.9656. [M-Cl]<sup>+</sup> calcd. for (C<sub>23</sub>H<sub>17</sub>AlCl<sub>4</sub>N<sub>3</sub>O<sub>2</sub>) 535.9861 found 535.9999.

## 6.4 Titanium Isopropoxide complexes

### 6.4.1 Synthesis of [Ti(Salpy)(O<sup>i</sup>Pr)<sub>2</sub>] (31)



To a solution of Salpy (1.12 g, 3 mmol) in DCM (10 mL), was added a solution of Ti(O<sup>i</sup>Pr)<sub>4</sub> (0.85 g, 3 mmol) in DCM (5 mL). The resulting solution was stirred at room temperature for 4 h, after which the volatiles were removed under reduced pressure. The residue was washed with cold pentane (2 x 5 mL) and dried *in vacuo* to obtain the titled complex as a pale yellow solid. Yield: 1.36 g (84%).

$^1\text{H}$  NMR (500 MHz, CDCl<sub>3</sub>, 293 K):  $\delta$  **Isomer 1**: 8.63 (d,  $J = 4.1$  Hz, 1H, H<sup>6</sup>), 8.16-7.97 (s, br, 2H), 7.69 (t,  $J = 7.7$  Hz, 1H, H<sup>4</sup>), 7.48 (d,  $J = 8.0$  Hz, 1H, H<sup>3</sup>), 7.40-6.56 (overlapping, 8H, Aromatic), , 7.20 (t,  $J = 7.20$  Hz, 2H, H<sup>5</sup>), 5.51 (s, br, 1H,

## Chapter 6 - Experimental

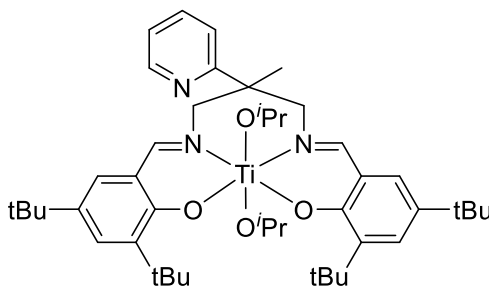
CH<sub>2</sub>), 4.81 (septet, 1H, CH(CH<sub>3</sub>)<sub>2</sub>), 4.57 (overlapping, 1H, CH<sub>2</sub>), 4.54 (septet, 1H, CH(CH<sub>3</sub>)<sub>2</sub>), 3.53 (d, <sup>2</sup>J = 11.4 Hz, 2H, CH<sub>2</sub>), 1.18 (s, 3H, CH<sub>3</sub>), 1.12 (d, <sup>3</sup>J = 5.9 Hz, 6H, CH(CH<sub>3</sub>)<sub>2</sub>), 1.08 – 0.66 (b, overlapping 6H, CH(CH<sub>3</sub>)<sub>2</sub>).

**Isomer 2:** δ 8.53 (d, J = 4.1 Hz, 1H, H<sup>6</sup>), 8.16-7.97 (s, br, 2H), 7.56 (t, <sup>3</sup>J = 7.8 Hz, 1H, H<sup>4</sup>), 7.29 (b, 1H, H<sup>3</sup>), 7.09 (t, <sup>3</sup>J = 6.19 Hz, 1H), 7.40-6.56 (overlapping, 8H, Aromatic), 7.20 (t, <sup>3</sup>J = 7.20 Hz, 2H, H<sup>5</sup>), 4.91 (s, br, 1H, CH<sub>2</sub>), 4.73 (septet, 1H, CH(CH<sub>3</sub>)<sub>2</sub>), 4.60 (septet, 1H, CH(CH<sub>3</sub>)<sub>2</sub>), 4.30 (d, <sup>2</sup>J = 11.3 Hz, 2H, CH<sub>2</sub>), 3.36 (s, br, 1H, CH<sub>2</sub>), 1.55 (s, 3H, CH<sub>3</sub>), 1.08 – 0.66 (b, overlapping, 6H, CH(CH<sub>3</sub>)<sub>2</sub>).

<sup>13</sup>C{<sup>1</sup>H} NMR (101 MHz, CDCl<sub>3</sub>, 293 K): δ 164.9 (CH=N), , 149.0 (Py-C), 136.5 (Py-C), 134.1 (Ar-C), 132.6 (Ar-C), 121.9 (Py-C), 121.6 (Ar-C), 120.6 (Ar-C), 77.7 (OCH(CH<sub>3</sub>)<sub>2</sub>), 70.9 (CH<sub>2</sub>), 46.6 (PyCCH<sub>3</sub>), 25.9 (OCH(CH<sub>3</sub>)<sub>2</sub>), 25.3 (OCH(CH<sub>3</sub>)<sub>2</sub>), 22.3 (CH<sub>3</sub>).

Anal. Calcd. for C<sub>29</sub>H<sub>35</sub>N<sub>3</sub>O<sub>4</sub>Ti (%): C, 64.81; H, 6.56; N, 7.82. Found (%): C, 64.75; H, 6.68; N, 7.77. HRMS for [M]<sup>+</sup> (EI): calcd. for (C<sub>29</sub>H<sub>35</sub>N<sub>3</sub>O<sub>4</sub>Ti): 537.2107; found: 537.2084 (M<sup>+</sup>), [M-O<sup>i</sup>Pr]<sup>+</sup>: calcd. for (C<sub>26</sub>H<sub>28</sub>N<sub>3</sub>O<sub>3</sub>Ti): 478.1610; found: 478.1674.

### 6.4.2 Synthesis of [Ti(<sup>t</sup>Bu, <sup>t</sup>Bu - salpy)(O<sup>i</sup>Pr)<sub>2</sub>] (32)



[Ti(<sup>t</sup>Bu, <sup>t</sup>Bu - salpy)(O<sup>i</sup>Pr)<sub>2</sub>] was synthesized similarly as a yellow solid in quantitative yield by treating Ti(O<sup>i</sup>Pr)<sub>4</sub> (0.41 g, 1.47 mmol) with <sup>t</sup>Bu, <sup>t</sup>Bu - Salpy (0.88 g, 1.47 mmol) in DCM (15 mL) for 5 h at room temperature. Yield: 0.91 g (81%).

<sup>1</sup>H NMR (500 MHz, C<sub>6</sub>D<sub>6</sub>, 293 K): δ **Isomer 1:** 8.50 (d, <sup>3</sup>J = 4.2 Hz, 1H, H<sup>6</sup>), 7.76 (s, 1H, CH=N), 7.70 (d, <sup>4</sup>J = 2.5 Hz, 1H, Aromatic), 7.60 (d, <sup>4</sup>J = 2.5 Hz, 1H, Aromatic), 7.59 (s, 1H, CH=N), , 7.17 (overlapping, 1H, Pyridyl), 7.13 (overlapping, 2H, pyridyl, Aromatic), 7.05 (d, <sup>4</sup>J = 2.4 Hz, 1H, Aromatic), 6.65 (ddd, <sup>3</sup>J = 7.1, <sup>4</sup>J = 4.8, <sup>4</sup>J = 1.1 Hz, 1H, pyridyl), 5.70 (d, <sup>2</sup>J = 10.3 Hz, 1H, CH<sub>2</sub>), 5.22 (septet, 1H,

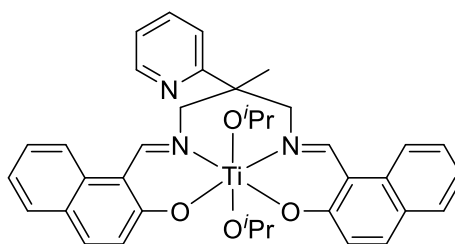
## Chapter 6 - Experimental

$\text{CH}(\text{CH}_3)_2$ , 4.72 (septet, 1H,  $\text{CH}(\text{CH}_3)_2$ ), 3.24 (second order triplet, 2H,  $\text{CH}_2$ ), 1.77 (s, 9H,  $\text{C}(\text{CH}_3)_3$ ), 1.46 (d,  $^3J = 6.0$  Hz, 6H,  $\text{CH}(\text{CH}_3)_2$ ), 1.08 (d,  $^3J = 6.1$  Hz, 3H,  $\text{CH}(\text{CH}_3)_2$ ), 1.05 (d,  $^3J = 6.1$  Hz, 3H,  $\text{CH}(\text{CH}_3)_2$ ). 0.96 (s, 3H,  $\text{CH}_3$ ).

**Isomer 2:** 8.31 (d,  $^3J = 4.0$  Hz, 1H,  $\text{H}^6$ ), 7.83 (s, 1H,  $\text{CH}=\text{N}$ ), 7.74 (d,  $^4J = 2.5$  Hz, 1H, Aromatic), 7.68 (s, 1H,  $\text{CH}=\text{N}$ ), 7.58 (overlapping d, 1H, Aromatic), 7.18 (overlapping, 1H, Aromatic), 7.11 (d,  $^4J = 1.8$  Hz, 1H, Aromatic), 6.98 (d,  $^3J = 7.0$ , 1H, pyridyl), 6.88 (td,  $^3J = 7.8$ ,  $^3J = 1.9$  Hz, 1H, pyridyl), 6.44 (m, 1H, pyridyl), 5.07 (Overlapping, 2H,  $\text{CH}_2$ ,  $\text{CH}(\text{CH}_3)_2$ ), 4.68 (septet, 1H,  $\text{CH}(\text{CH}_3)_2$ ), 4.12 (d,  $^2J = 12.3$  Hz, 1H,  $\text{CH}_2$ ), 4.06 (d,  $^2J = 10.6$  Hz, 1H,  $\text{CH}_2$ ), 3.37 (d,  $^2J = 12.4$  Hz, 1H,  $\text{CH}_2$ ), 1.81 (s, 9H,  $\text{C}(\text{CH}_3)_3$ ), 1.54 (s, 9H,  $\text{C}(\text{CH}_3)_3$ ), 1.49 (s, 3H,  $\text{CH}_3$ ), 1.37 (s, 9H,  $\text{C}(\text{CH}_3)_3$ ), 1.30 (d,  $^3J = 6.0$  Hz, 3H,  $\text{CH}(\text{CH}_3)_2$ ), 1.25 (d,  $^3J = 6.0$  Hz, 6H,  $\text{CH}(\text{CH}_3)_2$ ), 1.08 (overlapping 3H,  $\text{CH}(\text{CH}_3)_2$ ), 1.02 (d,  $^3J = 6.0$  Hz, 3H,  $\text{CH}(\text{CH}_3)_2$ ).

Anal. Calcd. for  $\text{C}_{45}\text{H}_{67}\text{N}_3\text{O}_4\text{Ti}$  (%): C, 70.94; H, 8.86 N, 5.52 Found (%): C, 70.98; H, 8.92; N, 5.59. HRMS for  $[\text{M}]^+$  (EI): calcd. for  $(\text{C}_{45}\text{H}_{67}\text{N}_3\text{O}_4\text{Ti})$ : 761.4611; found: 761.4556 ( $\text{M}^+$ ),  $[\text{M}-\text{O}^i\text{Pr}]^+$ : calcd. for  $(\text{C}_{42}\text{H}_{60}\text{N}_3\text{O}_3\text{Ti})$ : 702.4114; found: 702.3622.  $[\text{M}-2(\text{O}^i\text{Pr})]^+$ : calcd. for  $(\text{C}_{39}\text{H}_{53}\text{N}_3\text{O}_2\text{Ti})$ : 643.3617; found: 643.3571.

### 6.4.3 Synthesis of $[\text{Ti}(\text{Naphpy})(\text{O}^i\text{Pr})_2]$ (33)



A yellow solution of Naphpy (0.52 g, 1.11 mmol) was dissolved in 10 mL of dry DCM, which was added to  $\text{Ti}(\text{O}^i\text{Pr})_4$  (0.31 g, 1.1 mmol) in 5 mL of dry DCM with stirring. The reaction was left to stir at room temperature overnight. Volatiles were then removed under reduced pressure, and the solid washed with hexanes (ca. 5 mL) to give the desired product as yellow solid. Yield: 0.25 g (87%).

$^1\text{H}$  NMR (400 MHz,  $\text{CDCl}_3$ , 293 K):  $\delta$ : 8.81 (d,  $^3J = 4.3$  Hz, 1H,  $\text{H}^6$ ), 8.78 (s, 1H,  $\text{CH}=\text{N}$ ), 8.73 (s, 1H,  $\text{CH}=\text{N}$ ), 8.72 (m, 8H, Aromatic), 7.52 (m, 3H, Aromatic), 7.34 (m, 3H, Aromatic), 7.16 (d,  $^3J = 7.18$  Hz, 1H, Aromatic), 5.44 (d,  $^2J = 10.7$  Hz, 1H,  $\text{CH}_2$ ), 4.86 (d,  $^2J = 11.1$  Hz, 1H,  $\text{CH}_2$ ), 4.70 (septet, 1H,  $\text{CH}(\text{CH}_3)_2$ ), 4.51 (septet,

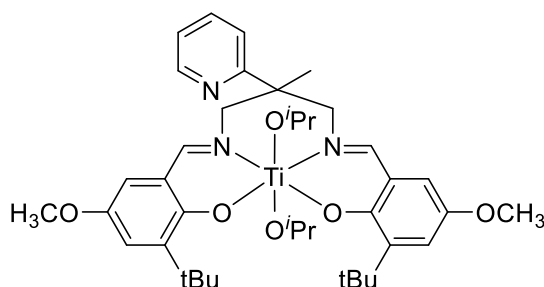
## Chapter 6 - Experimental

$^1\text{H}$ ,  $\text{CH}(\text{CH}_3)_2$ , 3.76 (d,  $^2J = 10.7$  Hz, 1H,  $\text{CH}_2$ ), 3.68(d,  $^2J = 11.3$  Hz, 1H,  $\text{CH}_2$ ), 1.27 (overlapping, 3H,  $\text{CH}_3$ ), 1.23 (d,  $^3J = 6.1$  Hz, 3H,  $\text{CH}(\text{CH}_3)_2$ ), 1.03 (d,  $^3J = 6.1$  Hz, 3H,  $\text{CH}(\text{CH}_3)_2$ ), 0.94 (d,  $^3J = 6.1$  Hz, 3H,  $\text{CH}(\text{CH}_3)_2$ ). 1.03 (d,  $^3J = 6.1$  Hz, 3H,  $\text{CH}(\text{CH}_3)_2$ ).

$^{13}\text{C}$  NMR (101 MHz,  $\text{CDCl}_3$ )  $\delta$  163.96 ( $\text{CH}=\text{N}$ ), 160.7 (Ar-C), 159.5 (Ar-C), 149.1 (Py-C), 136.4 (Py-C), 128.9 (Ar-C), 127.2 (Ar-C), 121.9 (Py-C), 120.5 (Ar-C), 77.8 ( $\text{OCH}(\text{CH}_3)_2$ ), 77.6 ( $\text{OCH}(\text{CH}_3)_2$ ), 46.9 (Py-C- $\text{CH}_3$ ), 26.0 ( $\text{OCH}(\text{CH}_3)_2$ ), 25.2 ( $\text{OCH}(\text{CH}_3)_2$ ), 21.5 ( $\text{CH}_3$ ).

Anal. Calcd. for  $\text{C}_{37}\text{H}_{39}\text{N}_3\text{O}_4\text{Ti}$  (%): C, 69.70; H, 6.17; N, 6.59. Found (%): C, 69.50; H, 6.44; N, 6.22. HRMS for  $[\text{M}]^+$  (EI): calcd. for ( $\text{C}_{37}\text{H}_{39}\text{N}_3\text{O}_3\text{Ti}$ ): 637.2420; found: 637.2370 ( $\text{M}^+$ ),  $[\text{M}-\text{O}^i\text{Pr}]^+$ : calcd. for ( $\text{C}_{34}\text{H}_{32}\text{N}_3\text{O}_3\text{Ti}$ ): 578.1923; found: 578.1410.  $[\text{M}-2(\text{O}^i\text{Pr})]^+$ : calcd. for ( $\text{C}_{31}\text{H}_{25}\text{N}_3\text{O}_2\text{Ti}$ ): 519.1426; found: 519.1094.

### 6.4.4 Synthesis of $[\text{Ti}(\text{tBu}, \text{OMe} - \text{Salpy})(\text{O}^i\text{Pr})_2]$ (**34**)



Following a procedure similar to that described for the preparation of  $[\text{Ti}(\text{Salpy})(\text{O}^i\text{Pr})_2]$ ,  $\text{Ti}(\text{O}^i\text{Pr})_4$  (0.29 g, 1.02 mmol) in DCM (5 mL) was reacted with  $\text{tBu}$ ,  $\text{OMe}$ -Salpy (0.56 g, 1.02 mmol) in DCM (10 mL). The reaction mixture was stirred at room temperature overnight, after which time volatiles were removed under reduced pressure. The residue was washed with cold pentane (ca. 5 mL) and dried *in vacuo* to obtain **34** as yellow solid. Yield: 0.25 g (86%)

$^1\text{H}$  NMR (500 MHz,  $\text{CDCl}_3$ , 293 K):  $\delta$  (1) **Isomer 1**: 8.56 (d,  $^3J = 4.7$  Hz, 1H,  $\text{H}^6$ ), 8.00 (s, 1H,  $\text{CH}=\text{N}$ ), 7.80 (s, 1H,  $\text{CH}=\text{N}$ ), 7.61 (t,  $^3J = 7.8$  Hz, 1H,  $\text{H}^4$ ), 7.46 (d,  $^3J = 8.0$  Hz, 1H,  $\text{H}^3$ ), 7.12 (m, 1H,  $\text{H}^5$ ), 6.99 (d,  $^4J = 2.7$  Hz, 1H, Ar), 6.91 (d,  $^4J = 2.8$  Hz, 1H, Ar), 6.51 (d,  $^4J = 2.7$  Hz, 2H, Ar), 5.42 (d,  $^2J = 10.4$  Hz, 1H,  $\text{CH}_2$ ), 4.83 (septet,  $^3J = 5.9$  Hz, 1H,  $\text{CH}(\text{CH}_3)_2$ ), 4.49 (d,  $^2J = 12.2$  Hz, 1H,  $\text{CH}_2$ ), 4.34 (septet,  $^3J = 6.4$  Hz, 1H,  $\text{CH}(\text{CH}_3)_2$ ), 3.69 (Overlapping 2 s, 6H,  $\text{OCH}_3$ ), 3.38 (dd,  $^2J = 11.2$ ,  $^4J = 4.2$  Hz, 2H,  $\text{CH}_2$ ), 1.39 (s, 3H,  $\text{CH}_3$ ), 1.37 (s, 9H,  $\text{C}(\text{CH}_3)_3$ ), 1.07

## Chapter 6 - Experimental

(Overlapping m, 6H, CH (CH<sub>3</sub>)<sub>2</sub>), 0.99 (s, 9H, C(CH<sub>3</sub>)<sub>3</sub>), 0.80 (d, <sup>3</sup>J = 6.0 Hz, 3H, CH (CH<sub>3</sub>)<sub>2</sub>), 0.74 (d, <sup>3</sup>J = 6.0 Hz, 3H, CH (CH<sub>3</sub>)<sub>2</sub>).

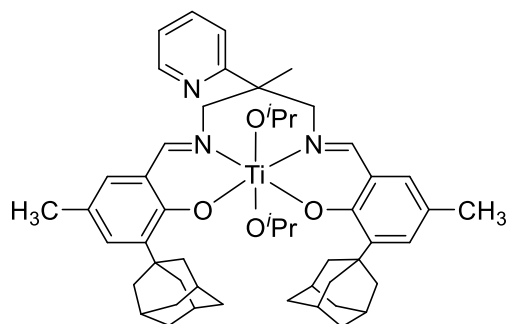
**Isomer 2** : 8.43 (d, <sup>3</sup>J = 4.6 Hz, 1H, H<sup>6</sup>), 7.99 (s, 1H, CH=N), 7.66 (s, 1H, CH=N), 7.28 (t, <sup>3</sup>J = 7.7 Hz, 1H, H<sup>4</sup>), 7.04 (d, <sup>3</sup>J = 8.0 Hz 1H, H<sup>3</sup>), 7.01 (d, <sup>4</sup>J = 2.8 Hz, 1H, Ar), 6.93 (dd, <sup>3</sup>J = 4.3, 3.2 Hz, 1H, H<sup>5</sup>), 6.85 (d, <sup>4</sup>J = 2.8 Hz, 1H, Ar), 6.60 (d, <sup>4</sup>J = 2.6 Hz, 1H, Ar), 6.31 (d, <sup>4</sup>J = 2.7 Hz, 1H, Ar), 4.93 (d, <sup>2</sup>J = 10.4 Hz, 1H, CH<sub>2</sub>), 4.75 (septet, <sup>3</sup>J = 6.0 Hz, 1H, CH (CH<sub>3</sub>)<sub>2</sub>), 4.33 (septet, <sup>3</sup>J = 6.5 Hz, 1H, CH (CH<sub>3</sub>)<sub>2</sub>), 4.0 (d, <sup>2</sup>J = 12.6 Hz, 1H, CH<sub>2</sub>), 3.96 (d, <sup>2</sup>J = 12.6 Hz, 1H, CH<sub>2</sub>) 3.73 (s, 3H, OCH<sub>3</sub>), 3.64 (s, 1H, CH<sub>2</sub>), 3.63 (s, 3H, OCH<sub>3</sub>), 1.48 (s, 3H, CH<sub>3</sub>), 1.08 (overlapping, 18H, 2 x C(CH<sub>3</sub>)<sub>3</sub>), 1.06 (d, <sup>3</sup>J = 4.3 Hz, 3H, CH (CH<sub>3</sub>)<sub>2</sub>), 1.00 (d, <sup>3</sup>J = 4.3 Hz, 3H, CH (CH<sub>3</sub>)<sub>2</sub>), 0.77 (d, <sup>3</sup>J = 6.0 Hz, 3H, CH (CH<sub>3</sub>)<sub>2</sub>), 0.71 (d, <sup>3</sup>J = 6.0 Hz, 3H, CH (CH<sub>3</sub>)<sub>2</sub>).

<sup>13</sup>C{<sup>1</sup>H} NMR (126 MHz, CDCl<sub>3</sub>, 293 K) δ (1) **Isomer 1**: 164.5 (CH=N), 163.9 (CH=N), 162.7 (Ar-C), 158.7 (Ar-C), 150.3 (Ar-C), 149.0 (Py-C), 148.8 (Ar-C), 141.2 (Ar-C), 139.2 (Py-C), 136.4 (Py-C), 122.9 (Ar-C), 121.8 (Py-C), 121.7 (Ar-C), 120.7 (Ar-C), 120.6 (Ar-C), 120.5 (Ar-C), 112.2 (Ar-C), 110.1 (Ar-C), 77.4 (OCH(CH<sub>3</sub>)<sub>2</sub>), 77.2 (OCH(CH<sub>3</sub>)<sub>2</sub>), 71.2 (CH<sub>2</sub>), 71.2 (CH<sub>2</sub>), 56.0 (OCH<sub>3</sub>), 55.7 (OCH<sub>3</sub>), 46.9 (Py-C-CH<sub>3</sub>), 35.3 (C(CH<sub>3</sub>)<sub>3</sub>), 34.7 (C(CH<sub>3</sub>)<sub>3</sub>), 29.8 (C(CH<sub>3</sub>)<sub>3</sub>), 29.3 (C(CH<sub>3</sub>)<sub>3</sub>), 26.6 (OCH(CH<sub>3</sub>)<sub>2</sub>), 26.3 (OCH(CH<sub>3</sub>)<sub>2</sub>), 25.7 (OCH(CH<sub>3</sub>)<sub>2</sub>), 21.4 (CH<sub>3</sub>).

**Isomer 2**: δ 165.1 (CH=N), 164.0 (CH=N), 162.2 (Ar-C), 159.0 (Ar-C), 150.2 (Py-C), 148.8 (Ar-C), 148.7 (Ar-C), 140.7 (Ar-C), 139.3 (Ar-C), 136.0 (Py-C), 122.5 (Ar-C), 121.4 (Py-C), 121.2 (Ar-C), 121.0 (Ar-C), 120.7 (Ar-C), 112.4 (Ar-C), 110.3 (Ar-C), 77.2 (OCH(CH<sub>3</sub>)<sub>2</sub>), 76.0 (OCH(CH<sub>3</sub>)<sub>2</sub>), 70.5 (CH<sub>2</sub>), 70.1 (CH<sub>2</sub>), 55.9 (OCH<sub>3</sub>), 55.7 (OCH<sub>3</sub>), 46.2 (Py-C-CH<sub>3</sub>), 35.2 (C(CH<sub>3</sub>)<sub>3</sub>), 34.9 (C(CH<sub>3</sub>)<sub>3</sub>), 29.7 (C(CH<sub>3</sub>)<sub>3</sub>), 29.3 (C(CH<sub>3</sub>)<sub>3</sub>), 26.6 (OCH(CH<sub>3</sub>)<sub>2</sub>), 26.3 (OCH(CH<sub>3</sub>)<sub>2</sub>), 25.7 (OCH(CH<sub>3</sub>)<sub>2</sub>), 25.3 (OCH(CH<sub>3</sub>)<sub>2</sub>), 24.9 (OCH(CH<sub>3</sub>)<sub>2</sub>), 21.4 (CH<sub>3</sub>).

Anal. Calcd. for C<sub>39</sub>H<sub>55</sub>N<sub>3</sub>O<sub>6</sub>Ti (%): C, 66.00; H, 7.81; N, 5.92. Found (%): C, 65.89; H, 7.82; N, 5.90. HRMS for [M]<sup>+</sup> (EI): calcd. for (C<sub>39</sub>H<sub>55</sub>N<sub>3</sub>O<sub>6</sub>Ti): 709.3570; found: 709.3597 (M<sup>+</sup>), [M-O'Pr]<sup>+</sup>: calcd. for (C<sub>36</sub>H<sub>48</sub>N<sub>3</sub>O<sub>5</sub>Ti): 650.3073; found: 650.2482. [M-2(O'Pr)]<sup>+</sup>: calcd. for (C<sub>33</sub>H<sub>41</sub>N<sub>3</sub>O<sub>4</sub>Ti): 591.2577; found: 591.2529.

### 6.4.5 Synthesis of [Ti(Ad, Me-Salpy)(O<sup>i</sup>Pr)<sub>2</sub>] (35)



A solution of Ad, Me-Salpy (0.25 g, 0.37 mmol) in DCM (8 ml) was added to a solution of Ti(O<sup>i</sup>Pr)<sub>4</sub> (0.1g, 0.37 mmol) in DCM (2 mL) and stirred at RT for 20 h. The mixture was then evaporated to dryness to afford a yellow residue. The residue was washed with pentane to give the titled complex as yellow solid. Yield: 0.24 g (77%).

<sup>1</sup>H NMR (500 MHz, C<sub>6</sub>D<sub>6</sub>, 293 K): δ **Isomer 1** : 8.33 (ddd, <sup>3</sup>J = 4.7, <sup>4</sup>J = 1.9, <sup>5</sup>J = 0.9 Hz, 1H, H<sup>6</sup>), 7.78 (s, 1H, CH=N), , 7.65 (s, 1H, CH=N), 7.32 (d, <sup>4</sup>J = 2.2 Hz, 1H, Aromatic), 7.19 (d, <sup>4</sup>J = 2.3 Hz, 1H, Aromatic), 6.94 (td, <sup>3</sup>J = 7.7 Hz, <sup>4</sup>J = 1.9 Hz 1H, pyridyl), 6.84 (d, <sup>3</sup>J = 8.0 Hz, 1H, pyridyl), 6.79 (d, <sup>4</sup>J = 1.7 Hz, 1H, Aromatic), 6.73 (d, <sup>4</sup>J = 1.7 Hz, 1H, Aromatic), 6.45 (ddd, <sup>3</sup>J = 7.4, <sup>4</sup>J = 4.8, <sup>5</sup>J = 1.0 Hz, 1H, Pyridyl), 5.07 (overlapping, 1H, CH(CH<sub>3</sub>)<sub>2</sub>, 1H, CH<sub>2</sub>), 4.65 (septet, 1H, CH(CH<sub>3</sub>)<sub>2</sub>), 4.12 (d, <sup>2</sup>J = 12.4 Hz, 1H, CH<sub>2</sub>), 4.00 (d, <sup>2</sup>J = 10.5 Hz, 1H, CH<sub>2</sub>), 3.32 (d, <sup>2</sup>J = 12.4 Hz, 2H, CH<sub>2</sub>), 2.54 (s, 3H, Ar-CH<sub>3</sub>), 2.51 (s, 3H, ArCH<sub>3</sub>), 2.40-1.46 (m, 33H, Adamantyl, CH<sub>3</sub>), 1.30 (d, <sup>3</sup>J = 6.0 Hz, 3H, CH(CH<sub>3</sub>)<sub>2</sub>), 1.21 (d, <sup>3</sup>J = 6.0 Hz, 3H, CH(CH<sub>3</sub>)<sub>2</sub>), 1.06 (d, <sup>3</sup>J = 6.0 Hz, 3H, CH(CH<sub>3</sub>)<sub>2</sub>), 1.03 (d, <sup>3</sup>J = 6.0 Hz, 3H, CH(CH<sub>3</sub>)<sub>2</sub>).

**Isomer 2**: 8.49 (ddd, <sup>3</sup>J = 4.8, <sup>4</sup>J = 1.9, <sup>5</sup>J = 0.9 Hz, 1H, H<sup>6</sup>), 7.79 (s, 1H, CH=N), , 7.55 (s, 1H, CH=N), 7.28 (overlapping , 1H, Aromatic, 1H, Pyridyl), 7.27 (d, <sup>4</sup>J = 2.3 Hz, 1H, Aromatic), 7.11 (td, <sup>3</sup>J = 6.95 Hz, <sup>4</sup>J = 1.88 Hz 1H, pyridyl), 6.90 (d, <sup>4</sup>J = 1.6 Hz, 1H, Aromatic), 6.69 (d, <sup>4</sup>J = 1.7 Hz, 1H, Aromatic), 6.63 (ddd, <sup>3</sup>J = 7.5, <sup>4</sup>J = 4.8, <sup>5</sup>J = 1.0 Hz, 1H, Pyridyl), 5.65 (d, <sup>2</sup>J = 10.3 Hz, 1H, CH<sub>2</sub>) 5.07 (overlapping, 1H, CH(CH<sub>3</sub>)<sub>2</sub>, 1H, CH<sub>2</sub>), 4.68 (septet, 1H, CH(CH<sub>3</sub>)<sub>2</sub>), 4.31 (d, <sup>2</sup>J = 12.4 Hz, 1H, CH<sub>2</sub>), 3.38 (d, <sup>2</sup>J = 12.4 Hz, 1H, CH<sub>2</sub>), 3.19 (d, <sup>2</sup>J = 10.5 Hz, 2H, CH<sub>2</sub>), 2.54 (s, 3H, ArCH<sub>3</sub>), 2.51 (s, 3H, ArCH<sub>3</sub>), 2.40-1.46 (m, 33H, Adamantyl, CH<sub>3</sub>), 1.34 (d, <sup>3</sup>J = 6.0 Hz, 3H, CH(CH<sub>3</sub>)<sub>2</sub>), 1.26 (d, <sup>3</sup>J = 6.0 Hz, 3H, CH(CH<sub>3</sub>)<sub>2</sub>), 1.11 (d, <sup>3</sup>J = 6.0 Hz, 3H, CH(CH<sub>3</sub>)<sub>2</sub>), 1.06 (d, <sup>3</sup>J = 6.0 Hz, 3H, CH(CH<sub>3</sub>)<sub>2</sub>).

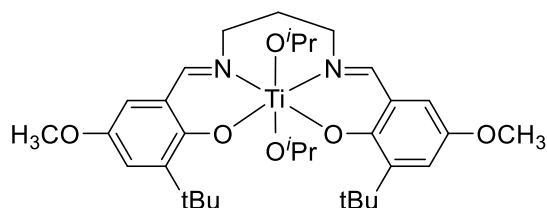
## Chapter 6 - Experimental

$^{13}\text{C}\{^1\text{H}\}$  NMR (126 MHz,  $\text{C}_6\text{D}_6$ , 293 K)  $\delta$  **Isomer 1** :  $\delta$  166.7 (CH=N), 166.0 (CH=N), 165.5 (Ar-C), 165.2 (Ar-C), 162.7 (Py-C), 149.4 (Py-C), 140.0 (Ar-C), 138.4 (Ar-C), 136.2 (Py-C), 133.9 (Ar-C), 133.1 (Ar-C), 131.7 (Ar-C), 130.7 (Ar-C), 126.2 (Ar-C), 125.9 (Ar-C), 124.4 (Ar-C), 124.1 (Ar-C), 121.9 (Py-C), 78.1 ( $\text{OCH}(\text{CH}_3)_2$ ), 76.9 ( $\text{OCH}(\text{CH}_3)_2$ ), 71.4 ( $\text{CH}_2$ ), 70.8 ( $\text{CH}_2$ ), 47.3 (Py-C- $\text{CH}_3$ ), 41.7 (Ad), 41.1 (Ad), 37.9 (Ad), 37.7 (Ad), 29.8 (Ad), 29.7 (Ad), 27.3 ( $\text{OCH}(\text{CH}_3)_2$ ), 26.9 ( $\text{OCH}(\text{CH}_3)_2$ ), 26.3 ( $\text{OCH}(\text{CH}_3)_2$ ), 24.9 ( $\text{OCH}(\text{CH}_3)_2$ ), 22.6 ( $\text{CH}_3$ ), 21.8 ( $\text{CH}_3$ ), 21.1 (Ar- $\text{CH}_3$ ), 21.1 (Ar- $\text{CH}_3$ ).

**Isomer 2:**  $\delta$  166.0 (CH=N), 165.3 (CH=N), 164.8 (Ar-C), 163.0 (Ar-C), 149.3 (Py-C), 139.6 (Ar-C), 138.4 (Ar-C), 136.3 (Py-C), 133.6 (Ar-C), 133.3 (Ar-C), 131.9 (Ar-C), 130.6 (Ar-C), 126.0 (Ar-C), 125.9 (Ar-C), 124.2 (Ar-C), 123.9 (Ar-C), 121.6 (Py-C), 78.0 ( $\text{OCH}(\text{CH}_3)_2$ ), 76.7 ( $\text{OCH}(\text{CH}_3)_2$ ), 70.8 ( $\text{CH}_2$ ), 70.3 ( $\text{CH}_2$ ), 46.5 (Py-C- $\text{CH}_3$ ), 41.1 (Ad), 41.0 (Ad), 37.8 (Ad), 37.6 (Ad), 30.1 (Ad), 29.9 (Ad), 27.3 ( $\text{OCH}(\text{CH}_3)_2$ ), 27.0 ( $\text{OCH}(\text{CH}_3)_2$ ), 26.5 ( $\text{OCH}(\text{CH}_3)_2$ ), 24.9 ( $\text{OCH}(\text{CH}_3)_2$ ), 21.8 ( $\text{CH}_3$ ), 21.1 (Ar- $\text{CH}_3$ ), 21.1 (Ar- $\text{CH}_3$ ).

Anal. Calcd. for  $\text{C}_{51}\text{H}_{67}\text{N}_3\text{O}_4\text{Ti}$  (%): C, 73.45; H, 8.10; N, 5.04 Found (%): C, 73.50; H, 8.45; N, 4.88. HRMS for  $[\text{M}]^+$  (EI): calcd. for ( $\text{C}_{51}\text{H}_{67}\text{N}_3\text{O}_4\text{Ti}$ ): 833.4611; found: 833.4476 ( $\text{M}^+$ ),  $[\text{M}-\text{O}^i\text{Pr}]^+$ : calcd. for ( $\text{C}_{48}\text{H}_{60}\text{N}_3\text{O}_3\text{Ti}$ ): 774.4114; found: 774.4081.  $[\text{M}-2(\text{O}^i\text{Pr})]^+$ : calcd. for ( $\text{C}_{45}\text{H}_{53}\text{N}_3\text{O}_2\text{Ti}$ ): 715.3617; found: 715.3530.

### 6.4.6 Synthesis of $[\text{Ti}(\text{tBu}, \text{OMe} - \text{Salpn})(\text{O}^i\text{Pr})_2]$ (36)



$[\text{Ti}(\text{tBu}, \text{OMe} - \text{Salpn})(\text{O}^i\text{Pr})_2]$  was synthesized similarly as a yellow solid in quantitative yield by treating  $\text{Ti}(\text{O}^i\text{Pr})_4$  (0.33 g, 1.18 mmol) with tBu, OMe- Salpn (0.53 g, 1.18 mmol) in DCM (10 mL) for 20 h at room temperature. Yield: 0.63 g (87.3%)

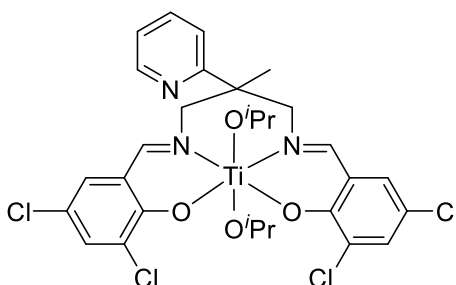
## Chapter 6 - Experimental

$^1\text{H}$  NMR (400 MHz,  $\text{CDCl}_3$ , 293 K):  $\delta$  8.09 (s, 1H, CH=N), 7.95 (s, 1H, CH=N), 7.06 (d,  $^4J = 3.1$  Hz, 1H, Ar), 6.96 (d,  $^4J = 3.2$  Hz, 1H, Ar), 6.59 (d,  $^4J = 3.1$  Hz, 1H, Ar), 6.55 (d,  $^4J = 3.2$  Hz, 1H, Ar), 4.85 (septet, 1H,  $\text{CH}(\text{CH}_3)_2$ ), 4.48 (septet, 1H,  $\text{CH}(\text{CH}_3)_2$ ), 3.82 (m, 2H, N- $\text{CH}_2$ ), 3.76 (s, 3H, OCH<sub>3</sub>), 3.74 (s, 3H, OCH<sub>3</sub>), 3.58 (m, 2H, N- $\text{CH}_2$ ), 2.32 (m, 1H,  $\text{CH}_2\text{CH}(\text{CH}_3)\text{CH}_2$ ), 1.87 (m, 1H,  $\text{CH}_2\text{CH}(\text{CH}_3)\text{CH}_2$ ), 1.45 (s, 9H,  $\text{C}(\text{CH}_3)_3$ ), 1.18 (d,  $^3J = 6.0$  Hz, 3H,  $\text{CH}(\text{CH}_3)_2$ ), 1.13 (d,  $^3J = 6.1$  Hz, 3H,  $\text{CH}(\text{CH}_3)_2$ ), 1.08 (s, 9H,  $\text{C}(\text{CH}_3)_3$ ), 0.88 (d,  $^3J = 6.1$  Hz, 3H,  $\text{CH}(\text{CH}_3)_2$ ), 0.83 (d,  $^3J = 6.0$  Hz, 3H,  $\text{CH}(\text{CH}_3)_2$ ).

$^{13}\text{C}\{^1\text{H}\}$  NMR (101 MHz,  $\text{CDCl}_3$ , 293 K):  $\delta$ : 164.4 (N=CH), 162.2 (N=CH), 158.4 ( $\text{C}^b$ ), 150.2 ( $\text{C}^e$ ), 148.8 ( $\text{C}^e$ ), 141.0 ( $\text{C}^c$ ), 122.4 (Ar-C), 121.5 (Ar-C), 120.5 (Ar-C), 112.4 (Ar-C), 110.4 (Ar-C), 76.2 ( $\text{OCH}(\text{CH}_3)_2$ ), 60.7 (N- $\text{CH}_2$ ), 60.3 (N- $\text{CH}_2$ ), 55.9 (OCH<sub>3</sub>), 55.8 (OCH<sub>3</sub>), 35.3 ( $\text{C}(\text{CH}_3)_3$ ), 34.8 ( $\text{C}(\text{CH}_3)_3$ ), 30.8 ( $\text{CH}_2$ ), 29.8 ( $\text{C}(\text{CH}_3)_3$ ), 29.3 ( $\text{C}(\text{CH}_3)_3$ ), 26.6 ( $\text{OCH}(\text{CH}_3)_2$ ), 26.2 ( $\text{OCH}(\text{CH}_3)_2$ ).

Anal. Calcd. for  $\text{C}_{33}\text{H}_{50}\text{N}_2\text{O}_6\text{Ti}$  (%): C, 64.07; H, 8.15; N, 4.53. Found (%): C, 63.85; H, 8.35; N, 4.58. HRMS for  $[\text{M}]^+$  (EI): calcd. for ( $\text{C}_{33}\text{H}_{50}\text{N}_2\text{O}_6\text{Ti}$ ): 618.3148; found: 618.3101 ( $\text{M}^+$ ),  $[\text{M}-\text{O}^i\text{Pr}]^+$ : calcd. for ( $\text{C}_{30}\text{H}_{43}\text{N}_2\text{O}_5\text{Ti}$ ): 559.2651; found: 559.2299.  $[\text{M}-2(\text{O}^i\text{Pr})]^+$ : calcd. for ( $\text{C}_{27}\text{H}_{36}\text{N}_2\text{O}_4\text{Ti}$ ): 500.2155; found: 500.2155.2084.

### 6.4.7 Synthesis of $[\text{Ti}(\text{Cl}, \text{Cl} - \text{Salpy})(\text{O}^i\text{Pr})_2]$ (37)



This complex was prepared as an orange solid from reaction of Cl, Cl- Salpy (0.26 g, 0.5 mmol) in DCM (10 mL) with  $\text{Ti}(\text{O}^i\text{Pr})_4$  (0.14 g, 0.5 mmol) in DCM (2 mL) at room temperature for 24 h. The volatiles were removed under reduced pressure

## Chapter 6 - Experimental

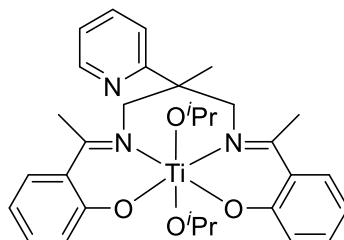
and the residue washed with hexanes (2 x ca. 5 mL), filtered and dried *in vacuo*.

Yield: 0.28 g (81.5%).

$^1\text{H}$  NMR (400 MHz,  $\text{CDCl}_3$ , 243 K (low temperature)):  $\delta$  **Isomer 1** : 8.73 (m, 1H,  $\text{H}^6$ ), 8.11 (s, 1H,  $\text{CH}=\text{N}$ ), , 8.10 (s, 1H,  $\text{CH}=\text{N}$ ), 7.84 (td,  $J = 7.8$  Hz, 1H, Py), 7.58 (d,  $^4J = 2.6$  Hz, 1H, Ar), 7.47 (d,  $^3J = 8.8$  Hz, 1H, py), 7.43 (d,  $^4J = 2.7$  Hz, 1H, Ar), 7.36 (m, 1H, Py), 7.29 (d,  $^4J = 2.6$  Hz, 1H, Ar), 7.20 (d,  $^4J = 2.7$ , 1H, Ar), 5.53 (d,  $^2J = 10.4$  Hz, 1H,  $\text{CH}_2$ ), 5.25 (d,  $^2J = 11.7$  Hz, 1H,  $\text{CH}_2$ ), 5.16 (septet, 1H,  $\text{CH}(\text{CH}_3)_2$ ), 4.62 (septet, 1H,  $\text{CH}(\text{CH}_3)_2$ ), 3.57 (d,  $^2J = 10.6$  Hz, 1H,  $\text{CH}_2$ ), 3.49 (d,  $^2J = 12.3$  Hz, 1H,  $\text{CH}_2$ ), 1.50 (d,  $^3J = 6.2$  Hz, 3H,  $\text{CH}(\text{CH}_3)_2$ ), 1.44 (d,  $^3J = 6.1$  Hz, 3H,  $\text{CH}(\text{CH}_3)_2$ ), 1.21 (d,  $^3J = 6.0$  Hz, 3H,  $\text{CH}(\text{CH}_3)_2$ ), 1.15 (s, 3H,  $\text{CH}_3$ ), 0.74 (d,  $^3J = 6.1$  Hz, 3H,  $\text{CH}(\text{CH}_3)_2$ ).

**Isomer 2**: 8.50 (m, 1H,  $\text{H}^6$ ), 8.24 (s, 1H,  $\text{CH}=\text{N}$ ), , 8.04 (s, 1H,  $\text{CH}=\text{N}$ ), 7.64 (td,  $J = 7.7$  Hz, 1H, Py), 7.55 (d,  $^4J = 2.6$  Hz, 1H, Ar), 7.36 (overlapping, 1H, pyridyl), 7.15 (overlapping, 1H, Py, 2H, Ar), 7.05 (d,  $^4J = 2.5$  Hz, 1H, Ar), 5.07 (septet, 1H,  $\text{CH}(\text{CH}_3)_2$ ) 5.18 (overlapping, 2H,  $\text{CH}_2$ ), 5.0 (d,  $^2J = 10.7$  Hz, 1H,  $\text{CH}_2$ ) 4.62 (septet, 1H,  $\text{CH}(\text{CH}_3)_2$ ), 4.46 (d,  $^2J = 10.7$  Hz, 1H,  $\text{CH}_2$ ), 4.29 (d,  $^2J = 12.6$  Hz, 1H,  $\text{CH}_2$ ), 1.36 (d,  $^3J = 6.0$  Hz, 3H,  $\text{CH}(\text{CH}_3)_2$ ), 1.30 (overlapping, 3H,  $\text{CH}_3$ , 3H,  $\text{CH}(\text{CH}_3)_2$ ), 1.19 (d,  $^3J = 6.0$  Hz, 3H,  $\text{CH}(\text{CH}_3)_2$ ), 0.71 (d,  $^3J = 6.2$  Hz, 3H,  $\text{CH}(\text{CH}_3)_2$ ).

$^{13}\text{C}\{^1\text{H}\}$  NMR (101 MHz,  $\text{CDCl}_3$ , 293 K):  $\delta$ : 162.6 ( $\text{N}=\text{CH}$ ), 149.3, 149.1, 136.9, 122.3, 120.4, 119.7, 79.3 ( $\text{OCH}(\text{CH}_3)_2$ ), 78.7 ( $\text{OCH}(\text{CH}_3)_2$ ), 46.7 ( $\text{PyCCH}_3$ ) 25.3 ( $\text{OCH}(\text{CH}_3)_2$ ), 19.9 ( $\text{CH}_3$ ). Anal. Calcd. for  $\text{C}_{29}\text{H}_{31}\text{Cl}_4\text{N}_3\text{O}_4\text{Ti}$  (%): C, 51.58; H, 4.63; N, 6.22 Found (%): C, 49.95; H, 4.87; N, 5.78. HRMS for  $[\text{M}]^+$  (EI): calcd. for ( $\text{C}_{29}\text{H}_{31}\text{Cl}_4\text{N}_3\text{O}_4\text{Ti}$ ): 675.0519; found: 675.0428 ( $\text{M}^+$ ),  $[\text{M}-\text{O}^i\text{Pr}]^+$ : calcd. for ( $\text{C}_{26}\text{H}_{24}\text{Cl}_4\text{N}_3\text{O}_3\text{Ti}$ ): 616.0022; found: 615.9994.

6.4.8 Synthesis of [Ti(Aspy)(O<sup>i</sup>Pr)<sub>2</sub>] (38)

To a solution of Acpy (0.8 g, 1.99 mmol) in dichloromethane (15 mL), was added Ti(O<sup>i</sup>Pr)<sub>4</sub> (0.56 g, 1.99 mmol) in dichloromethane (2 mL). The resulting solution was stirred at room temperature for 20 h, after which the volatiles were removed under reduced pressure. The residue was washed with pentane (ca. 2 x 5 mL) and dried *in vacuo* to obtain the product as yellow solid. Yield: 0.91 g (81.2%).

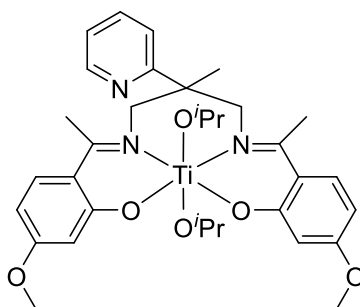
<sup>1</sup>H NMR (500 MHz, C<sub>6</sub>D<sub>6</sub>, 293 K) **Isomer 1 and 2** δ 8.51 (d, <sup>3</sup>J = 4.0 Hz, 1H, H<sup>6</sup>), 8.32 (d, <sup>3</sup>J = 3.6 Hz, 1H, H<sup>6</sup>), 7.44 (s,br, 1H), 7.29 (overlapping, 4H), 6.92 (s,br, 1H), 6.75 (qoverlapping, 2H), 6.69 (m, 2H), 6.65 – 6.54 (m, 3H), 6.50 (m, 1H), 5.69 (d, <sup>2</sup>J = 11.6 Hz, 1H, CH<sub>2</sub>), 5.17 (m, 2H, CH<sub>2</sub>), 4.78 (septet, 2H, CH(CH<sub>3</sub>)<sub>2</sub>), 4.67 (septet, 1H, CH(CH<sub>3</sub>)<sub>2</sub>), 4.61 (d, <sup>2</sup>J = 11.7 Hz, 1H, CH<sub>2</sub>), 4.53 (m, 1H, CH<sub>2</sub>), 3.85 (m, 2H, CH<sub>2</sub>), 3.48 (d, <sup>2</sup>J = 11.8 Hz, 1H, CH<sub>2</sub>), 1.83 (s, 3H, CH<sub>3</sub>-C=N), 1.77 (s, 3H, CH<sub>3</sub>-C=N), 1.41-1.34 (overlapping, 12H, 6H x CH<sub>3</sub>-C=N, 3H x CH<sub>3</sub>, 3H, CH(CH<sub>3</sub>)<sub>2</sub>), 1.27 (m, 6H, CH(CH<sub>3</sub>)<sub>2</sub>), 1.20 (s, 3H, CH<sub>3</sub>), 1.08 (m, 6H, CH(CH<sub>3</sub>)<sub>2</sub>), 0.98 (d, <sup>3</sup>J = 5.8 Hz, 3H, CH(CH<sub>3</sub>)<sub>2</sub>), 0.94 (m, 6H, CH(CH<sub>3</sub>)<sub>2</sub>).

<sup>13</sup>C{<sup>1</sup>H} NMR (126 MHz, C<sub>6</sub>D<sub>6</sub>, 293 K): δ 169.0 (CH=N), 168.7 (CH=N), 167.5 (CH=N), 166.7 (Ar-C), 166.4 (Ar-C), 164.4 (Ar-C), 164.2 (Ar-C), 163.7 (Ar-C), 163.4 (Ar-C), 148.4 (Py-C), 148.1 (Py-C), 135.0 (Py-C), 134.7 (Py-C), 132.3 (Ar-C), 132.1 (Ar-C), 131.2 (Ar-C), 131.2 (Ar-C), 128.6 (Ar-C), 128.2 (Ar-C), 124.8 (Ar-C), 120.6 (Py-C), 120.5 (Py-C), 120.3 (Ar-C), 119.0 (Ar-C), 117.9 (Ar-C), 117.8 (Ar-C), 116.1 (Ar-C), 114.5 (Ar-C), 114.4 (Ar-C), 76.3 (OCH(CH<sub>3</sub>)<sub>2</sub>), 76.2 (OCH(CH<sub>3</sub>)<sub>2</sub>), 75.7 (OCH(CH<sub>3</sub>)<sub>2</sub>), 75.5 (OCH(CH<sub>3</sub>)<sub>2</sub>), 60.5 (CH<sub>2</sub>), 56.1 (CH<sub>2</sub>), 47.0 (Py-C-CH<sub>3</sub>), 45.7 (Py-C-CH<sub>3</sub>), 25.6 (OCH(CH<sub>3</sub>)<sub>2</sub>), 25.4 (OCH(CH<sub>3</sub>)<sub>2</sub>), 25.2 (OCH(CH<sub>3</sub>)<sub>2</sub>), 25.1 (OCH(CH<sub>3</sub>)<sub>2</sub>), 24.9 (OCH(CH<sub>3</sub>)<sub>2</sub>), 24.6 (OCH(CH<sub>3</sub>)<sub>2</sub>), 24.3 (OCH(CH<sub>3</sub>)<sub>2</sub>), 23.6 (CH<sub>3</sub>), 17.4 (CH<sub>3</sub>-C=N), 16.8 (CH<sub>3</sub>-C=N), 16.7 (CH<sub>3</sub>-C=N), 15.9 (CH<sub>3</sub>-C=N).

## Chapter 6 - Experimental

Anal. Calcd. for  $C_{31}H_{39}N_3O_4Ti$  (%): C, 65.84; H, 6.95 N, 7.43 Found (%): C, 65.68; H, 7.03; N, 7.22. HRMS for  $[M]^+$  (EI): calcd. for  $(C_{31}H_{39}N_3O_4Ti)$ : 565.2420; found: 565.2403 ( $M^+$ ),  $[M-O'Pr]^+$ : calcd. for  $(C_{28}H_{32}N_3O_3Ti)$ : 506.1923; found: 506.1572.  $[M-2(O'Pr)]^+$ : calcd. for  $(C_{25}H_{25}N_3O_4Ti)$ : 447.1426; found: 447.1300.

### 6.4.9 Synthesis of $[Ti(OMe-Aspy)(O'Pr)_2]$ (39)



A solution of  $Ti(O'Pr)_4$  (0.37 g, 1.92 mmol) dissolved in (2 mL) of DCM was added to OMe-Aspy (0.6 g, 1.92 mmol) dissolved in of DCM (10 mL) at room temperature. The reaction mixture was left to stir overnight. The volatiles were then removed under reduced pressure, and the resultant yellow solid washed with cold pentane to give the desired product as a pale yellow solid. Yield: 0.68 g (84%).

$^1H$  NMR (500 MHz,  $C_6D_6$ , 293 K) **Isomer 1 and 2**  $\delta$  8.52 (dd,  $^4J = 4.7$ ,  $^3J = 1.0$  Hz, 1H, H<sup>6</sup>), 8.36 (d,  $^3J = 3.6$  Hz, 1H, H<sup>6</sup>), 7.50 (s,br, 1H, H<sup>5</sup>), 7.26 (m, 2H, pyridyl), 7.18 – 7.10 (overlapping m, 3H), 6.82 (td,  $^3J = 7.8$ ,  $^4J = 1.8$  Hz, 1H, pyridyl), 6.69 (overlapping m, 4H), 6.66 (d,  $^4J = 2.6$  Hz, 1H, Aromatic), 6.56 (dd,  $^3J = 8.9$ ,  $^4J = 2.6$  Hz, 1H, Pyridyl), 6.54 – 6.47 (overlapping m, 3H), 6.44 (d,  $^4J = 2.6$  Hz, 1H, Aromatic), 6.42 (d,  $^4J = 2.7$  Hz, 1H, Aromatic), 5.65 (d,  $^2J = 11.8$  Hz, 1H, CH<sub>2</sub>), 5.18 (septet, 1H, CH(CH<sub>3</sub>)<sub>2</sub>), 5.11 (d,  $^2J = 12.0$  Hz, 1H, CH<sub>2</sub>), 4.89 (septet, 1H, CH(CH<sub>3</sub>)<sub>2</sub>), 4.81 (septet, 2H, CH(CH<sub>3</sub>)<sub>2</sub>), 4.61 (d,  $^2J = 12.0$  Hz, 1H, CH<sub>2</sub>), 4.53 (d,  $^2J = 11.9$  Hz, 1H, CH<sub>2</sub>), 3.88 (d,  $^2J = 12.4$ , 1H, CH<sub>2</sub>), 3.87 (d,  $^2J = 12.0$ , 1H, CH<sub>2</sub>), 3.51 (d,  $^2J = 12.0$  Hz, 1H, CH<sub>2</sub>), 3.35 (s, 6H, 2 x OCH<sub>3</sub>), 3.28 (s, 3H, OCH<sub>3</sub>), 3.23 (s, 3H, OCH<sub>3</sub>), 1.87 (s, 3H, CH<sub>3</sub>), 1.79 (s, 3H, CH<sub>3</sub>), 1.38 (d,  $^3J = 6.1$  Hz, 6H, CH(CH<sub>3</sub>)<sub>2</sub>), 1.28 (d,  $^3J = 6.0$  Hz, 3H, CH(CH<sub>3</sub>)<sub>2</sub>), 1.15 (d,  $^3J = 6.0$  Hz, 3H, CH(CH<sub>3</sub>)<sub>2</sub>), 1.12 (d,  $^3J = 6.0$  Hz, 3H, CH(CH<sub>3</sub>)<sub>2</sub>), 1.09 (d,  $^3J = 6.0$  Hz, 3H, CH(CH<sub>3</sub>)<sub>2</sub>), 1.06 (overlapping, 6H, CH(CH<sub>3</sub>)<sub>2</sub>).

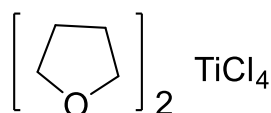
## Chapter 6 - Experimental

$^{13}\text{C}\{^1\text{H}\}$  NMR (126 MHz,  $\text{C}_6\text{D}_6$ , 293 K):  $\delta$  169.2 (CH=N), 168.9 (CH=N), 168.3 (CH=N), 168.0 (CH=N), 167.3 (Ar-C), 166.9 (Ar-C), 166.5 (Ar-C), 166.2 (Ar-C), 163.6 (Ar-C), 162.7 (Ar-C), 148.4 (Py-C), 148.1 (Py-C), 134.9 (Py-C), 134.7 (Py-C), 129.9 (Ar-C), 129.6 (Ar-C), 120.4 (Py-C), 120.2 (Py-C), 119.0 (Ar-C), 118.7 (Ar-C), 104.9 (Ar-C), 104.8 (Ar-C), 101.9 (Ar-C), 100.8 (Ar-C), 76.3 ( $\text{OCH}(\text{CH}_3)_2$ ), 76.2 ( $\text{OCH}(\text{CH}_3)_2$ ), 75.7 ( $\text{OCH}(\text{CH}_3)_2$ ), 75.5 ( $\text{OCH}(\text{CH}_3)_2$ ), 62.6 ( $\text{CH}_2$ ), 60.4 ( $\text{CH}_2$ ), 55.9 ( $\text{CH}_2$ ), 53.55 ( $\text{OCH}_3$ ), 53.53 ( $\text{OCH}_3$ ), 53.52 ( $\text{OCH}_3$ ), 53.49 ( $\text{OCH}_3$ ), 47.2 (Py-C- $\text{CH}_3$ ), 45.9 (Py-C- $\text{CH}_3$ ), 25.5 ( $\text{OCH}(\text{CH}_3)_2$ ), 25.3 ( $\text{OCH}(\text{CH}_3)_2$ ), 25.2 ( $\text{OCH}(\text{CH}_3)_2$ ), 25.1 ( $\text{OCH}(\text{CH}_3)_2$ ), 24.8 ( $\text{OCH}(\text{CH}_3)_2$ ), 24.5 ( $\text{OCH}(\text{CH}_3)_2$ ), 24.3 ( $\text{OCH}(\text{CH}_3)_2$ ), 23.7 ( $\text{CH}_3$ ), 17.3 ( $\text{CH}_3\text{-C=N}$ ), 16.6 ( $\text{CH}_3\text{-C=N}$ ), 15.6 ( $\text{CH}_3\text{-C=N}$ ).

Anal. Calcd. for  $\text{C}_{33}\text{H}_{43}\text{N}_3\text{O}_6\text{Ti}$  (%): C 63.36; H, 6.93; N, 6.72. Found (%): C, 63.11; H, 7.35; N, 6.34. HRMS for  $[\text{M}]^+$  (EI): calcd. for ( $\text{C}_{33}\text{H}_{43}\text{N}_3\text{O}_6\text{Ti}$ ): 625.2631; found: 625.2633 ( $\text{M}^+$ ),  $[\text{M}-\text{O}^i\text{Pr}]^+$ : calcd. for ( $\text{C}_{30}\text{H}_{36}\text{N}_3\text{O}_5\text{Ti}$ ): 566.2134; found: 566.1689.  $[\text{M}-2(\text{O}^i\text{Pr})]^+$ : calcd. for ( $\text{C}_{27}\text{H}_{29}\text{N}_3\text{O}_4\text{Ti}$ ): 507.1638; found: 507.1506.

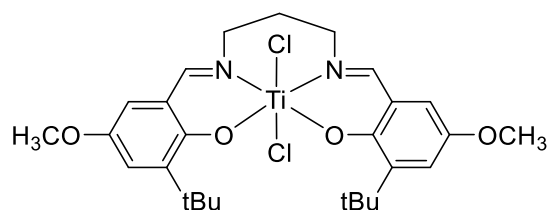
## 6.5 Titanium Chloride complex

### 6.5.1 Synthesis of $\text{TiCl}_4(\text{thf})_2$ <sup>7</sup>



A Schlenk equipped with a magnetic stirring bar was charged with 2.9 mL (26.4 mmol) titanium tetrachloride dissolved in 30 mL dichloromethane. Dry tetrahydrofuran (9 mL, 111.1 mmol) was added dropwise over 1 h. The solution was stirred at room temperature under argon for 15 minutes. Pentane (60 mL) was added. The solution was cooled to  $-30\text{ }^\circ\text{C}$  for 24 h. the bright yellow crystalline solid was recovered by filtration, and dried *in vacuo*. Yield: 8.1 g (92%).

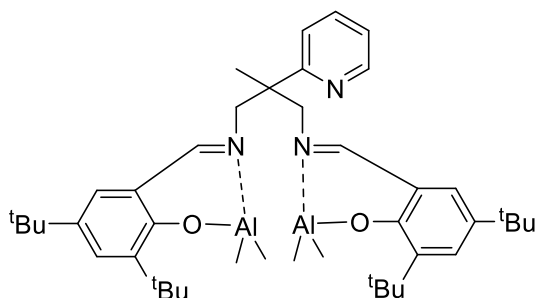
### 6.5.2 Synthesis of [Ti(<sup>t</sup>Bu, OMe - Salpn)Cl] (40)



A solution of  $\text{TiCl}_4 \cdot 2\text{THF}$  (0.146 g, 0.43 mmol) in THF (10 mL) was added slowly to a solution of <sup>t</sup>Bu, OMe- Salpn (0.2 g, 0.43 mmol) in THF (5 mL), resulting in a red solution. The reaction mixture was stirred and refluxed at 70 °C for 1 h, then cooled to room temperature. The solvent was removed under reduced pressure and the brown solid was washed with  $\text{Et}_2\text{O}$  (20 mL), filtered *via* cannula, washed with additional  $\text{Et}_2\text{O}$ , and dried under high vacuum ( $10^{-6}$  mbar) at 50 °C for 5 h, to yield a brown solid. Yield: 0.235 g (94%).  $^1\text{H}$  NMR (500 MHz,  $\text{CDCl}_3$ , 293 K):  $\delta$  8.13 (s, 2H, CH=N), 7.04 (d,  $^4J = 3.06$  Hz, 2H, Ar), 6.72 (d,  $^4J = 3.06$  Hz, 2H, Ar), 4.04 (t,  $^3J = 5.03$  Hz, 4H, 2 x  $\text{CH}_2$ ), 3.73 (s, 6H, 2 x  $\text{OCH}_3$ ), 2.29 (m, 2H), 1.46 (s, 18H).  $^{13}\text{C}\{^1\text{H}\}$  NMR (126 MHz,  $\text{CDCl}_3$ , 293 K):  $\delta$  165.6 (CH=N), 157.1 ( $\text{C}^e$ ), 154.2 ( $\text{C}^b$ ), 139.3 ( $\text{C}^c$ ), 127.5 ( $\text{C}^f$ ), 120.9 ( $\text{C}^a$ ), 114.5 ( $\text{C}^d$ ), 62.5 (N- $\text{CH}_2$ ), 55.7 ( $\text{OCH}_3$ ), 35.6 ( $\text{C}(\text{CH}_3)_3$ ), 30.1 ( $\text{CH}_2$ ), 27.6 ( $\text{C}(\text{CH}_3)_3$ ). Anal. Calcd. for  $\text{C}_{27}\text{H}_{36}\text{Cl}_2\text{N}_2\text{O}_4\text{Ti}$  (%): C, 56.76; H, 6.35; N, 4.90. Found (%): C, 56.61; H, 6.47; N, 4.91.

## 6.6. Bimetallic aluminum complexes

### 6.6.1 Synthesis of [Al<sub>2</sub>(<sup>t</sup>Bu, <sup>t</sup>Bu - Salpy)Me<sub>4</sub>] (41)



A 100 mL Schlenk flask was charged with <sup>t</sup>Bu, <sup>t</sup>Bu - Salpy (0.52, 0.87 mmol) and 45 mL of dry hexanes. The solution was stirred for 2-3 minutes until all the ligand dissolved completely.  $\text{AlMe}_3$  (0.87 mL, 2 M in toluene, 1.74 mmol) was added

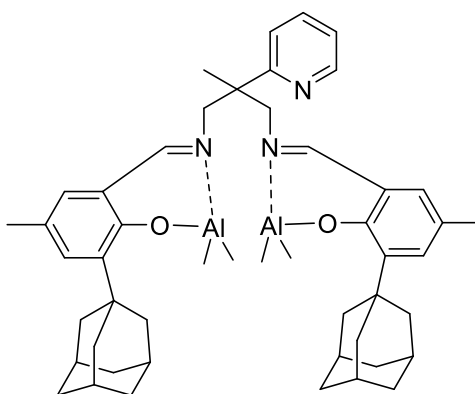
## Chapter 6 - Experimental

dropwise over 3 min. The mixture was allowed to stir for 6 h at ambient temperature. The precipitate was formed during the reaction period. After which time the solvent was removed by filtration and the solid was washed with hexanes (3 x 20 mL), filtered and dried in vacuo to give a yellow solid of bimetallic complex. Yield: 0.44 g, 0.62 mmol, (71%).

$^1\text{H}$  NMR (400 MHz,  $\text{C}_6\text{D}_6$ , 293 K):  $\delta$  8.48 (dd,  $^3J = 4.8$ ,  $^4J = 1.0$  Hz, 1H, H<sup>6</sup>), 7.64 (Overlapping 2 s, 2H, CH=N), 6.93 (s, 2H, Ar), 6.74 (td,  $^3J = 7.8$ ,  $^4J = 1.9$  Hz, 1H, H<sup>4</sup>), 6.56 (m, 1H, H<sup>5</sup>), 6.52 (d,  $^4J = 2.5$  Hz, 2H, Ar), 6.45 (d,  $^3J = 7.9$  Hz, 1H, H<sup>3</sup>), 3.86 (d,  $^2J = 12.1$  Hz, 2H), 3.19 (d,  $^2J = 12.1$  Hz, 2H), 1.56 (s, 18H, C(CH<sub>3</sub>)<sub>3</sub>), 1.28 (s, 18H, C(CH<sub>3</sub>)<sub>3</sub>), 1.24 (s, 3H, CH<sub>3</sub>), -0.20 (s, 6H, Al(CH<sub>3</sub>)<sub>2</sub>), -0.55 (s, 6H, Al(CH<sub>3</sub>)<sub>2</sub>).

$^{13}\text{C}\{^1\text{H}\}$  NMR (126 MHz,  $\text{CDCl}_3$ , 293 K)  $\delta$  175.3 (CH=N), 162.1 (C<sup>6</sup>), 159.9, 149.3 (C<sup>6</sup>), 140.5, 138.4, 136.7, 131.8, 128.3, 123.3, 122.0, 118.3, 65.0 (CH<sub>2</sub>), 47.3 (C-Py), 35.2 (C(CH<sub>3</sub>)<sub>3</sub>), 33.7 (C(CH<sub>3</sub>)<sub>3</sub>), 31.1 (C(CH<sub>3</sub>)<sub>3</sub>), 29.2 (C(CH<sub>3</sub>)<sub>3</sub>), 20.1 (CH<sub>3</sub>), -8.0 (Al(CH<sub>3</sub>)<sub>2</sub>), -9.3 (Al(CH<sub>3</sub>)<sub>2</sub>). Anal. Calcd. for  $\text{C}_{43}\text{H}_{65}\text{Al}_2\text{N}_3\text{O}_2$  (%): C, 72.75; H, 9.23; N, 5.92. Found (%): C, 72.61; H, 9.36; N, 5.88. HRMS for  $[\text{M}-\text{CH}_3]^+$  (ASAP): calcd. for  $\text{C}_{42}\text{H}_{62}\text{Al}_2\text{N}_3\text{O}_2$ : 694.4473; found 694.4490

### 6.6.2 Synthesis of $[\text{Al}_2(\text{Ad}, \text{Me} - \text{Salpy})\text{Me}_4]$ (42)



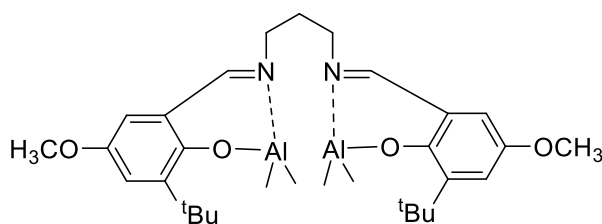
To a stirred turbid solution of Ad, Me - Salpy (0.5 g, 0.74 mmol) in toluene (15 mL) was added, dropwise over 1-2 minutes, a solution of  $\text{AlMe}_3$  (0.74 mL, 2 M in toluene, 1.49 mmol). The reaction turned to a clear solution upon the addition. The stirring was continued overnight at ambient temperature, after which the solvent was removed and the precipitate washed twice with hexanes (20 mL) to afford a yellow solid. Yield: 0.40 g, 0.51 mmol, (69%).

## Chapter 6 - Experimental

$^1\text{H}$  NMR (400 MHz,  $\text{C}_6\text{D}_6$ , 293 K):  $\delta$  8.66 (dd,  $^3J = 4.8$ ,  $^4J = 1.1$  Hz, 1H,  $\text{H}^6$ ), 7.34-7.29 (m, 4H, (2H  $\text{N}=\text{CH}_2$ ), (2H Py)), 6.89 (td,  $^3J = 7.8$ ,  $^4J = 1.8$  Hz, 1H,  $\text{H}^4$ ) 6.67 (m, 2H, Ar), 6.42 (d,  $^4J = 1.5$  Hz, 2H, Ar), 3.88 (d,  $^2J = 12.2$  Hz, 2H,  $\text{CH}_2$ ), 3.39 (d,  $^2J = 12.2$  Hz, 2H,  $\text{CH}_2$ ), 2.48 (s, 12H, 6 x Ar- $\text{CH}_3$ , 6 x Ad), 2.25 (m, 12H, Ad), 1.99 (d,  $^3J = 12$  Hz, 6H, Ad), 1.90 (d,  $^3J = 12$  Hz, 6H, Ad), 1.44 (s, 2H,  $\text{CH}_3$ ), -0.06 (s, 6H,  $\text{Al}(\text{CH}_3)_2$ ), -0.32 (s, 6H,  $\text{Al}(\text{CH}_3)_2$ ).

$^{13}\text{C}\{^1\text{H}\}$  NMR (126 MHz,  $\text{CDCl}_3$ , 293 K)  $\delta$  175.3 ( $\text{CH}=\text{N}$ ), 162.8 ( $\text{C}^2$ ), 160.3 ( $\text{C}^b$ ), 149.67 ( $\text{C}^6$ ), 141.4, 136.08, 132.0, 123.3, 122.6, 119.3, 65.7 ( $\text{CH}_2$ ), 47.4 ( $\text{C}$ -Py), 40.61 (Ad), 37.59 (Ad), 29.5 (Ad), 23.0 ( $\text{CH}_3$ ), 20.6 (Ar- $\text{CH}_3$ ), -7.6 ( $\text{Al}-\text{CH}_3$ ), -9.0 ( $\text{AlCH}_3$ ). Anal. Calcd. for  $\text{C}_{49}\text{H}_{65}\text{Al}_2\text{N}_3\text{O}_2$  (%): C, 75.26; H, 8.38; N, 5.37. Found (%): C, 75.16; H, 8.66; N, 5.39. HRMS for  $[\text{M}]^+$  (ASAP): calcd. for  $\text{C}_{49}\text{H}_{65}\text{Al}_2\text{N}_3\text{O}_2$ : 781.4708; found 781.7682

### 6.6.3 Synthesis of $[\text{Al}_2(\text{tBu}, \text{OMe} - \text{salpn})\text{Me}_4]$ (43)



$\text{AlMe}_3$  (1.54 mL, 2 M in toluene, 3.08 mmol) was added dropwise to a stirred solution of  $\text{tBu}$ ,  $\text{OMe} - \text{salpn}$  (0.70 g, 1.54 mmol) in toluene (15 mL) at room temperature. The mixture was left to stir for 6 h, after which time the solvent was removed under reduced pressure and the solid washed with hexanes (2 x 15 mL). The hexane was removed by filtration and the precipitate dried under high vacuum ( $10^{-6}$  mbar) to give the titled complex as a yellow solid. Yield: 0.75 g, 1.3 mmol (86%).

$^1\text{H}$  NMR (400 MHz,  $\text{C}_6\text{D}_6$ , 293 K):  $\delta$  7.36 (d,  $^4J = 3.2$  Hz, 2H, Ar), 7.10 (s, 2H,  $\text{CH}=\text{N}$ ), 6.17 (d,  $^4J = 3.2$  Hz, 2H, Ar), 3.46 (s, 6H,  $\text{OCH}_3$ ), 2.89 (t,  $^3J = 6.9$  Hz, 4H,  $\text{N}=\text{CH}_2$ ), 1.78 (p,  $^3J = 6.8$  Hz, 2H), 1.52 (s, 18H,  $\text{C}(\text{CH}_3)_3$ ), -0.30 (s, 12H,  $2\text{Al}(\text{CH}_3)_2$ ).

## Chapter 6 - Experimental

$^{13}\text{C}\{^1\text{H}\}$  NMR (126 MHz,  $\text{CDCl}_3$ , 293 K)  $\delta$  171.9 (CH=N), 159.4 ( $\text{C}^e$ ), 151.2 ( $\text{C}^b$ ), 143.3 ( $\text{C}^c$ ), 124.7, 118.3 ( $\text{C}^f$ ), 113.1 ( $\text{C}^d$ ), 55.6 (N- $\text{CH}_2$ ), 55.1 ( $\text{OCH}_3$ ), 35.6 ( $\text{C}(\text{CH}_3)_3$ ), 29.4 ( $\text{CH}_2\text{CH}_2\text{CH}_2$ ), 29.3 ( $\text{C}(\text{CH}_3)_3$ ), -8.7 ( $\text{AlCH}_3$ ).

Anal. Calcd. for  $\text{C}_{31}\text{H}_{48}\text{Al}_2\text{N}_2\text{O}_4$  (%): C, 65.70; H, 8.54; N, 4.94. Found (%): C, 65.52; H, 8.60; N, 5.02. HRMS for  $[\text{M}-\text{CH}_3]^+$  (ASAP): calcd. for  $\text{C}_{30}\text{H}_{45}\text{Al}_2\text{N}_2\text{O}_4$ : 551.3010; found 551.3010; for  $[\text{M}-4\text{CH}_3]^+$ : calcd. for  $\text{C}_{27}\text{H}_{36}\text{AlN}_2\text{O}_4$ : 479.2490; found 479.2506

## 6.7 References

- 1 S. Friedrich, M. Schubarta, L. H. Gade, I. J. Scowenb, A. J. Edwardsb and M. Mcpartlinb, *Chem. Ber/ Recl.*, 1997, **130**, 1751–1759.
- 2 T. Kurahashi and H. Fujii, *J. Am. Chem. Soc.*, 2011, **133**, 8307–8316.
- 3 A. Sattler, J. A. Labinger and J. E. Bercaw, *Organometallics*, 2013, **32**, 6899–6902.
- 4 Simon J. Coles and Philip A. Gale, *Chem. Sci.*, 2012, **3**, 683.
- 5 G. M. Sheldrick, *Acta Cryst.*, 2015, **A71**, 3–8.
- 6 G. M. Sheldrick, *Acta Cryst.*, 2015, **C71**, 3–8.
- 7 E. Manzer, *Inorg. Synth*, 1982, **21**, 135.

# **Chapter 7**

## **General Conclusions**

## **7 General Conclusions**

A series of salen type ligands have been prepared, bearing pyridyl donors. These salen ligands have been divided into three groups. The first group are the Salpy ligands, which were obtained by the condensation of two equivalents of a salicylaldehyde derivative and 2-Methyl-2-(2-pyridyl)propane-1,3-diamine (ppda). The second group are the Acpy ligands, which were prepared by the Schiff base condensation of two equivalents of an acetophenone derivative with one equivalent of ppda; the last category is the Salpn ligand obtained from the treatment of 3-tert-butyl-5-methoxysalicylaldehyde with 1,3-diaminopropane. Only one derivative of the Salpn ligand was prepared, as its purpose was to provide a comparison with the Salpy ligands, but without the pyridyl.

All ligands were characterized by  $^1\text{H}$  and  $^{13}\text{C}\{^1\text{H}\}$  NMR spectroscopy, and where necessary, 2D NMR spectroscopy, mass spectrometry and IR spectroscopy. As expected, the NMR data revealed that all three ligand groups are symmetrical, with both “arms” being identical. For all ligands, no bands for the OH groups of the phenol were observed in the IR spectra, reflecting the strong hydrogen bonding between the imine and phenol groups.

All the attempts to prepare neutral ligands from the condensation of ppda and 2-pyridine carboxaldehyde, 2-acetyl pyridine and 2-quinoline carboxaldehyde were unsuccessful, a cyclic compound was isolated as a main product, as identified by NMR spectroscopy and X-ray crystallography. Attempts to prepare asymmetric ligands from the condensation of ppda with two different aldehydes were equally unsuccessful; competitive redistribution of the iminophenol arms afforded only the symmetrical ligands.

A range of aluminium complexes bearing different co-ligands were synthesized. These complexes are divided into three groups. The first group are a series of methyl aluminium complexes, which were prepared for use in the ring-opening polymerization of cyclic esters. The presence of the pyridyl group has a significant effect on the reaction products, with more than one species being detected in

## Chapter 7 - General Conclusions

solution. These species have been attributed to two conformational isomers, bearing either coordinated or pendant pyridyl donors.

The second set of complexes are alkoxide and phenoxide aluminium derivatives. These complexes were obtained from the reaction of the corresponding methyl aluminium complexes with benzyl alcohol or p-cresol; a single product was obtained from these reactions, although in one case a second species was detected in a very small quantity, analogous to those observed for the methyl complexes.

The third type of aluminium complex was a series of chloride aluminium complexes, designed for use as catalysts for the co-polymerization of epoxides and anhydrides. A single product was evident in solution, but their NMR spectra were invariably broad, and reflect the fast exchange of the two ligand "arms". Variable temperature NMR spectra were measured to study their dynamic behaviour, and to calculate the activation parameters  $\Delta G^\ddagger$ ,  $\Delta H^\ddagger$  and  $\Delta S^\ddagger$  for this process.

Single crystal X-ray diffraction was used extensively to examine the solid state structures of the aluminium complexes. Both  $\kappa^4$  and  $\kappa^5$  Salpy ligands were found for the methyl and alkoxide/phenoxide complexes; all chloride complexes exhibited a  $\kappa^5$  Salpy ligand.

A series of titanium isopropoxide complexes and one titanium chloride complex were prepared, fully characterized, and evaluated as a catalyst for the ROP of caprolactone. Two conformational isomers were observed in solution for both Salpy and Aspy titanium complexes. The iminophenoxide arms were inequivalent in the  $^1\text{H}$  and  $^{13}\text{C}$  NMR spectra, consistent with  $C_1$ -symmetric complexes. In all cases the pyridyl donor remained pendant. These complexes exhibit a  $\beta$ -cis geometry rather than trans or -cis geometries.

The most novel feature of the aluminium complexes is almost certainly the role of a hemi-labile pyridyl donor, and its effect on the performance of the complexes in a variety of polymerization and co-polymerization reactions.

The Salpy aluminium complexes have been probed as catalysts towards the ring-opening polymerization of cyclic esters. These complexes showed high reactivity at room temperature for the polymerization of  $\epsilon$ -caprolactone. In comparison with the pyridyl-free derivative, a subtle but convincing positive effect was attributed to the pyridyl donor, despite the potential for this additional donor to add steric demands to the coordination sphere and to compete with the substrate for metal binding. The complexes were less active in the polymerization of *rac*-lactide, but nevertheless gave competitive activities and with substantial isotactic enrichment to the polymer microstructures. The effect of the co-catalyst was studied by the comparison of the catalyst reactivity after the addition of benzyl and isopropyl alcohols, or phenols. The alcohols were found to be the most active initiating ligands, whereas phenol derivatives were substantially less active. A correlation between the electron-withdrawing or -donating ability of the phenol initiator group and the activity of the catalyst in the ROP of  $\epsilon$ -caprolactone was observed.

The titanium complexes have been probed as initiators for the ring-opening polymerization of  $\epsilon$ -caprolactone. Since the titanium is tetravalent, the complexes are 6-coordinate without the intervention of the pyridyl arm, which remains pendant; the data herein show that the role of this donor in the polymerization reactions is minimal. However, it is noteworthy that the greater the steric demand of the ligand at the phenoxide arm, the greater the catalytic efficacy; ligands based upon salicylaldehyde and hydroxynaphthalene are poorly active in comparison to their substituted congeners. Future studies involving Ti(III) will be an interesting avenue to probe, since this would give the metal ion one less labile initiating ligand and would afford complexes with a comparable coordination sphere to that observed for aluminium. In such cases, there may be a greater role for the hemilabile pyridyl donor.

The aluminium chloride Salpy complexes have been tested for catalytic activity in the ring-opening copolymerization (ROCOP) of cyclic anhydrides and epoxides. This area of copolymerization is much less understood than the related CO<sub>2</sub>-epoxide copolymerization process. As such, the data presented herein should be regarded as an attempt to establish some fundamental operating parameters by which we may further understand how this reaction functions;

## Chapter 7 - General Conclusions

lessons learned from these data should serve to produce catalysts that can afford copolymers with high molecular weights and simultaneously high ester content.

As with many studies of this nature, many of the observations raise more questions than they answer, but some conclusions are clear:

1. Catalyst immobilization by viscous reaction mixtures makes it more difficult to adequately control the reaction. Future studies would do well to use a solvent system to reduce this problem.
2. Since the rate-limiting step is likely to be the epoxide ring-opening, using a solvent-free system, or using the epoxide as the solvent, is likely to enhance the rate of the reaction. A compromise is therefore likely, of using high epoxide concentration vs using a reaction medium that prevents a rapidly increasing viscosity.
3. The cocatalyst makes a significant difference to the selectivity. Polymers formed without the cocatalyst were mostly comprised of polyether, and little polyester. In this chapter, competitive polyester selectivities were obtained, but only in the presence of a cocatalyst. The role of the cocatalyst requires further investigation; cocatalysts such as PPNCI are often discussed in epoxide homopolymerization, and are thought to offer an external nucleophile to assist the ring-opening step. Such a role may be expected to give *lower* selectivities by facilitating the homopolymerization of epoxide, but this is not observed. The role of the cocatalyst is therefore intriguing and further studies should focus on this aspect of the research.

Further studies, in addition to probing the role of the cocatalyst, should include probing the precise reaction conditions (e.g. different concentrations, solvents, temperatures) to determine the optimum conditions to obtain highly selective polyesters. There is also much scope for probing epoxides other than CHO, and more importantly, ligand environments that move away from the ubiquitous Salen framework.

Three new dinuclear aluminum methyl complexes of the general formula  $LA_2Me_4$ , where L are salpy or salpn ligands with a propyl (Complex **43**) or substituted

## Chapter 7 - General Conclusions

propyl (Complexes **41** and **42**) backbone have been prepared through alkane elimination reactions between each ligand and two equivalents of AlMe<sub>3</sub>.

The activities of these complexes as initiators for the ring-opening polymerization (ROP) of  $\epsilon$ -CL, and some preliminary experiments with *rac*-LA have been investigated and compared. The dinuclear complexes **41** and **42**, bearing the salpy ligand with the pyridyl and methyl groups on the propyl backbone, were the most active in the ROP of  $\epsilon$ -CL at room temperature showing high conversion after 3-4 h reaction time. Conversely, the salpn complex (**43**), showed very poor activity at room temperature. increasing the temperature to 50 °C dramatically enhanced the reactivity of **43**, and moderately for **41** and **42**.

Overall, the complexes reported herein have been shown to be active in a number of polymerization processes, with the pyridyl having an effect for the trivalent metal (Al), but not for the tetravalent metal (Ti). Future work could focus on other trivalent metals, such as Cr(III) and Co(III).

# **Appendices: x-ray crystal structure data**

**Appendices: x-ray crystal structure data****Table 1:** Crystal data and structure refinement for Pypy<sup>b</sup>.

Identification code	mb9a		
Empirical formula	C <sub>32</sub> H <sub>40</sub> N <sub>8</sub>		
Formula weight	536.72		
Temperature	100(2) K		
Wavelength	0.71073 Å		
Crystal system	Monoclinic		
Space group	P 2 <sub>1</sub> /c		
Unit cell dimensions	$a = 7.8208(5) \text{ \AA}$	$\alpha = 90^\circ$	
	$b = 12.3905(9) \text{ \AA}$	$\beta = 96.775(2)^\circ$	
	$c = 7.1609(5) \text{ \AA}$	$\gamma = 90^\circ$	
Volume	689.07(8) Å <sup>3</sup>		
Z	1		
Density (calculated)	1.293 Mg/m <sup>3</sup>		
Absorption coefficient	0.080 mm <sup>-1</sup>		
F(000)	288		
Crystal size	0.290	0.250	0.040 mm <sup>3</sup>
$\theta$ range for data collection	3.096 to 27.553 °		
Index ranges	-9 h 10, -14 k 16, -9 l 9		
Reflections collected	9224		
Independent reflections	1594 [R(int) = 0.0457]		
Completeness to $\theta = 25.242^\circ$	99.8 %		
Absorption correction	Semi-empirical from equivalents		
Max. and min. transmission	1.000 and 0.702		
Refinement method	Full-matrix least-squares on F <sup>2</sup>		
Data / restraints / parameters	1594 / 60 / 112		
Goodness-of-fit on F <sup>2</sup>	1.055		
Final R indices [ $I > 2\sigma(I)$ ]	R <sub>1</sub> = 0.0516, wR <sub>2</sub> = 0.1433		
R indices (all data)	R <sub>1</sub> = 0.0572, wR <sub>2</sub> = 0.1473		
Extinction coefficient	n/a		
Largest diff. peak and hole	0.479 and -0.395 e.Å <sup>-3</sup>		

**Appendices: x-ray crystal structure data****Table 2:** Crystal data and structure refinement for Salpy.

Identification code	mb1	
Empirical formula	C <sub>23</sub> H <sub>23</sub> N <sub>3</sub> O <sub>2</sub>	
Formula weight	373.44	
Temperature	100(2) K	
Wavelength	0.71073 Å	
Crystal system	Monoclinic	
Space group	C c	
Unit cell dimensions	$a = 19.1233(13) \text{ \AA}$	$\alpha = 90^\circ$
◦	$b = 11.8499(8) \text{ \AA}$	$\beta = 108.5430(10)$
	$c = 8.8509(6) \text{ \AA}$	$\gamma = 90^\circ$
Volume	1901.6(2) Å <sup>3</sup>	
Z	4	
Density (calculated)	1.304 Mg/m <sup>3</sup>	
Absorption coefficient	0.085 mm <sup>-1</sup>	
F(000)	792	
Crystal size	0.220 0.210 0.150 mm <sup>3</sup>	
Theta range for data collection	2.894 to 27.499 °	
Index ranges	-23<=h<=24, -15<=k<=15, -9<=l<=11	
Reflections collected	10893	
Independent reflections	3659 [R(int) = 0.0227]	
Completeness to $\theta = 25.242^\circ$	99.7%	
Absorption correction	Semi-empirical from equivalents	
Max. and min. transmission	1.000 and 0.903	
Refinement method	Full-matrix least-squares on F <sup>2</sup>	
Data / restraints / parameters	3659 / 4 / 262	
Goodness-of-fit on F <sup>2</sup>	1.068	
Final R indices [ $I > 2\sigma(I)$ ]	R <sub>1</sub> = 0.0309, wR <sub>2</sub> = 0.0784	
R indices (all data)	R <sub>1</sub> = 0.0312, wR <sub>2</sub> = 0.0786	
Absolute structure parameter	n/a	
Extinction coefficient	n/a	
Largest diff. peak and hole	0.175 and -0.220 e.Å <sup>-3</sup>	

**Appendices: x-ray crystal structure data**

**Table 3:** Crystal data and structure refinement for [Al(Salpy)Me] (**1**).

Identification code	mb11	
Empirical formula	C <sub>30</sub> H <sub>30</sub> Al N <sub>3</sub> O <sub>2</sub> (C <sub>24</sub> H <sub>24</sub> Al N <sub>3</sub> O <sub>2</sub> · C <sub>6</sub> H <sub>6</sub> )	
Formula weight	491.55	
Temperature	100(2) K	
Wavelength	0.71073 Å	
Crystal system	Triclinic	
Space group		
Unit cell dimensions	$a = 8.9816(6) \text{ \AA}$	$\alpha = 71.196(3)^\circ$
	$b = 10.2889(7) \text{ \AA}$	$\beta = 84.480(3)^\circ$
	$c = 14.1189(10) \text{ \AA}$	$\gamma = 88.775(3)^\circ$
Volume	1229.31(15) Å <sup>3</sup>	
Z	2	
Density (calculated)	1.328 Mg/m <sup>3</sup>	
Absorption coefficient	0.117 mm <sup>-1</sup>	
F(000)	520	
Crystal size	0.175 0.106 0.098 mm <sup>3</sup>	
$\theta$ range for data collection	2.091 to 27.544 °	
Index ranges	-11 $h$ 11, -13 $k$ 12, -18 $l$ 18	
Reflections collected	26329	
Independent reflections	5623 [R(int) = 0.0377]	
Completeness to $\theta = 25.242^\circ$	99.3%	
Absorption correction	Semi-empirical from equivalents	
Max. and min. transmission	1.000 and 0.642	
Refinement method	Full-matrix least-squares on F <sup>2</sup>	
Data / restraints / parameters	5623 / 72 / 327	
Goodness-of-fit on F <sup>2</sup>	1.007	
Final R indices [ $I > 2\sigma(I)$ ]	R <sub>1</sub> = 0.0385, wR <sub>2</sub> = 0.1051	
R indices (all data)	R <sub>1</sub> = 0.0396, wR <sub>2</sub> = 0.1062	
Extinction coefficient	n/a	
Largest diff. peak and hole	0.383 and -0.294 e.Å <sup>-3</sup>	

**Appendices: x-ray crystal structure data****Table 4:** Crystal data and structure refinement for [Al(<sup>t</sup>Bu,OMe-Salpy)Me] (**4**).

Identification code	mb16	
Empirical formula	C <sub>37</sub> H <sub>47</sub> Al N <sub>3</sub> O <sub>4</sub>	
Formula weight	624.75	
Temperature	100(2) K	
Wavelength	0.71073 Å	
Crystal system	Monoclinic	
Space group	C2/c	
Unit cell dimensions	$a = 30.203(2) \text{ \AA}$	$\alpha = 90^\circ$
°	$b = 9.1454(6) \text{ \AA}$	$\beta = 103.9920(10)$
	$c = 25.4425(18) \text{ \AA}$	$\gamma = 90^\circ$
Volume	6819.2(8) Å <sup>3</sup>	
Z	8	
Density (calculated)	1.217 Mg/m <sup>3</sup>	
Absorption coefficient	0.102 mm <sup>-1</sup>	
F(000)	2680	
Crystal size	0.100 × 0.090 × 0.010 mm <sup>3</sup>	
θ range for data collection	2.530 to 27.496 °	
Index ranges	-39 ≤ h ≤ 39, -11 ≤ k ≤ 11, -33 ≤ l ≤ 32	
Reflections collected	49433	
Independent reflections	7832 [R(int) = 0.0716]	
Completeness to θ = 25.242 °	99.9%	
Absorption correction	Semi-empirical from equivalents	
Max. and min. transmission	1.000 and 0.689	
Refinement method	Full-matrix least-squares on F <sup>2</sup>	
Data / restraints / parameters	7832 / 147 / 445	
Goodness-of-fit on F <sup>2</sup>	1.013	
Final R indices [I > 2σ(I)]	R <sub>1</sub> = 0.0481, wR <sub>2</sub> = 0.1261	
R indices (all data)	R <sub>1</sub> = 0.0653, wR <sub>2</sub> = 0.1390	
Extinction coefficient	n/a	
Largest diff. peak and hole	0.416 and -0.434 e.Å <sup>-3</sup>	

**Appendices: x-ray crystal structure data****Table 5:** Crystal data and structure refinement for [Al(Ad,Me-Salpy)Me] (**5**).

Identification code	mb15	
Empirical formula	C <sub>64</sub> H <sub>74</sub> Al N <sub>3</sub> O <sub>2</sub> (C <sub>46</sub> H <sub>56</sub> Al N <sub>3</sub> O <sub>2</sub> 3 C <sub>6</sub> H <sub>6</sub> )	
Formula weight	944.24	
Temperature	100(2) K	
Wavelength	0.71073 Å	
Crystal system	Triclinic	
Space group		
Unit cell dimensions	$a = 12.5028(9) \text{ \AA}$	$\alpha = 77.700(3)^\circ$
	$b = 14.5636(10) \text{ \AA}$	$\beta = 81.306(3)^\circ$
	$c = 14.9075(10) \text{ \AA}$	$\gamma = 89.792(3)^\circ$
Volume	2620.5(3) Å <sup>3</sup>	
Z	2	
Density (calculated)	1.197 Mg/m <sup>3</sup>	
Absorption coefficient	0.087 mm <sup>-1</sup>	
F(000)	1016	
Crystal size	0.220 x 0.120 x 0.090 mm <sup>3</sup>	
$\theta$ range for data collection	2.545 to 27.503 °	
Index ranges	$-16 \leq h \leq 16, -15 \leq k \leq 18, -19 \leq l \leq 19$	
Reflections collected	47233	
Independent reflections	12009 [R(int) = 0.0464]	
Completeness to $\theta = 25.242^\circ$	99.8%	
Absorption correction	Semi-empirical from equivalents	
Max. and min. transmission	1.000 and 0.717	
Refinement method	Full-matrix least-squares on F <sup>2</sup>	
Data / restraints / parameters	12009 / 0 / 635	
Goodness-of-fit on F <sup>2</sup>	1.021	
Final R indices [ $I > 2\sigma(I)$ ]	$R_1 = 0.0402, wR_2 = 0.1073$	
R indices (all data)	$R_1 = 0.0480, wR_2 = 0.1131$	
Extinction coefficient	n/a	
Largest diff. peak and hole	0.360 and $-0.258 \text{ e.\AA}^{-3}$	

**Appendices: x-ray crystal structure data****Table 6:** Crystal data and structure refinement for [Al(<sup>t</sup>Bu,OMe-Salpn)Me] (**6**).

Identification code	mb27	
Empirical formula	C <sub>28</sub> H <sub>39</sub> Al N <sub>2</sub> O <sub>4</sub>	
Formula weight	494.59	
Temperature	100(2) K	
Wavelength	0.71073 Å	
Crystal system	Triclinic	
Space group		
Unit cell dimensions	$a = 10.3309(2) \text{ \AA}$	$\alpha = 92.4820(10)$
	$b = 16.2796(2) \text{ \AA}$	$\beta = 105.7550(10)$
	$c = 16.8875(3) \text{ \AA}$	$\gamma = 93.2930(10)^\circ$
Volume	2723.84(8) Å <sup>3</sup>	
Z	4	
Density (calculated)	1.206 Mg/m <sup>3</sup>	
Absorption coefficient	0.109 mm <sup>-1</sup>	
F(000)	1064	
Crystal size	0.170 × 0.070 × 0.040 mm <sup>3</sup>	
θ range for data collection	2.511 to 27.482 °	
Index ranges	-13 ≤ h ≤ 13, -21 ≤ k ≤ 21, -21 ≤ l ≤ 21	
Reflections collected	54820	
Independent reflections	12341 [R(int) = 0.0332]	
Completeness to θ = 25.242 °	99.2%	
Absorption correction	Semi-empirical from equivalents	
Max. and min. transmission	1.00000 and 0.91786	
Refinement method	Full-matrix least-squares on F <sup>2</sup>	
Data / restraints / parameters	12341 / 0 / 649	
Goodness-of-fit on F <sup>2</sup>	1.109	
Final R indices [I > 2σ(I)]	R <sub>1</sub> = 0.0593, wR <sub>2</sub> = 0.1718	
R indices (all data)	R <sub>1</sub> = 0.0656, wR <sub>2</sub> = 0.1760	
Extinction coefficient	n/a	
Largest diff. peak and hole	0.688 and -0.529 e.Å <sup>-3</sup>	

**Appendices: x-ray crystal structure data**

**Table 7:** Crystal data and structure refinement for [Al(Salpy)(OBn)] (**13**).

Identification code	mb8	
Empirical formula	C <sub>30</sub> H <sub>28</sub> Al N <sub>3</sub> O <sub>3</sub>	
Formula weight	505.53	
Temperature	100(2) K	
Wavelength	0.71073 Å	
Crystal system	Triclinic	
Space group		
Unit cell dimensions	$a = 13.4154(6) \text{ \AA}$	$\alpha = 79.454(4)^\circ$
	$b = 13.5031(6) \text{ \AA}$	$\beta = 76.691(4)^\circ$
	$c = 14.8493(7) \text{ \AA}$	$\gamma = 75.227(4)^\circ$
Volume	2509.0(2) Å <sup>3</sup>	
Z	4	
Density (calculated)	1.338 Mg/m <sup>3</sup>	
Absorption coefficient	0.119 mm <sup>-1</sup>	
F(000)	1064	
Crystal size	0.140 × 0.030 × 0.030 mm <sup>3</sup>	
θ range for data collection	1.600 to 27.634 °	
Index ranges	-15 ≤ h ≤ 17, -17 ≤ k ≤ 17, -19 ≤ l ≤ 19	
Reflections collected	17593	
Independent reflections	17593 [R(int) = 0]	
Completeness to θ = 25.242 °	99.9%	
Absorption correction	Semi-empirical from equivalents	
Max. and min. transmission	1.000 and 0.614	
Refinement method	Full-matrix least-squares on F <sup>2</sup>	
Data / restraints / parameters	17593 / 0 / 672	
Goodness-of-fit on F <sup>2</sup>	1.043	
Final R indices [ $I > 2\sigma(I)$ ]	R <sub>1</sub> = 0.0756, wR <sub>2</sub> = 0.1837	
R indices (all data)	R <sub>1</sub> = 0.1095, wR <sub>2</sub> = 0.2050	
Extinction coefficient	n/a	
Largest diff. peak and hole	1.362 and -0.358 e.Å <sup>-3</sup>	

**Appendices: x-ray crystal structure data****Table 8:** Crystal data and structure refinement for [Al(<sup>t</sup>Bu,<sup>i</sup>Bu-Salpy)(OTol)] (**16**).

Identification code	mb7	
Empirical formula	C <sub>46</sub> H <sub>60</sub> Al N <sub>3</sub> O <sub>3</sub>	
Formula weight	729.95	
Temperature	100(2) K	
Wavelength	0.71073 Å	
Crystal system	Triclinic	
Space group		
Unit cell dimensions	$a = 12.3805(9) \text{ \AA}$	$\alpha = 69.942(5)^\circ$
	$b = 12.7662(9) \text{ \AA}$	$\beta = 70.557(5)^\circ$
	$c = 15.1887(11) \text{ \AA}$	$\gamma = 81.330(5)^\circ$
Volume	2124.6(3) Å <sup>3</sup>	
Z	2	
Density (calculated)	1.141 Mg/m <sup>3</sup>	
Absorption coefficient	0.090 mm <sup>-1</sup>	
F(000)	788	
Crystal size	0.240 0.040 0.030 mm <sup>3</sup>	
θ range for data collection	2.595 to 27.518 °	
Index ranges	-15 h 16, -16 k 16, -19 l 19	
Reflections collected	38267	
Independent reflections	9712 [R(int) = 0.0843]	
Completeness to theta = 25.242 °	99.9%	
Absorption correction	Semi-empirical from equivalents	
Max. and min. transmission	1.000 and 0.622	
Refinement method	Full-matrix least-squares on F <sup>2</sup>	
Data / restraints / parameters	9712 / 0 / 492	
Goodness-of-fit on F <sup>2</sup>	1.021	
Final R indices [I>2σ(I)]	R <sub>1</sub> = 0.0567, wR <sub>2</sub> = 0.1451	
R indices (all data)	R <sub>1</sub> = 0.0791, wR <sub>2</sub> = 0.1596	
Extinction coefficient	n/a	
Largest diff. peak and hole	0.505 and -0.301 e.Å <sup>-3</sup>	

**Appendices: x-ray crystal structure data****Table 9:** Crystal data and structure refinement for [Al(<sup>t</sup>Bu,OMe-Salpy)(OTol)] (**20**).

Identification code	mb12	
Empirical formula	C <sub>47</sub> H <sub>56</sub> Al N <sub>3</sub> O <sub>5</sub> (C <sub>40</sub> H <sub>48</sub> Al N <sub>3</sub> O <sub>5</sub> · C <sub>7</sub> H <sub>8</sub> )	
Formula weight	769.92	
Temperature	100(2) K	
Wavelength	0.71073 Å	
Crystal system	Triclinic	
Space group		
Unit cell dimensions	$a = 10.2831(3) \text{ \AA}$	$\alpha = 100.711(3)^\circ$
	$b = 11.9848(5) \text{ \AA}$	$\beta = 95.699(2)^\circ$
	$c = 18.1958(6) \text{ \AA}$	$\gamma = 106.971(3)^\circ$
Volume	2079.12(13) Å <sup>3</sup>	
Z	2	
Density (calculated)	1.230 Mg/m <sup>3</sup>	
Absorption coefficient	0.099 mm <sup>-1</sup>	
F(000)	824	
Crystal size	0.190 × 0.060 × 0.060 mm <sup>3</sup>	
θ range for data collection	2.545 to 27.485 °	
Index ranges	-12 ≤ h ≤ 13, -15 ≤ k ≤ 15, -20 ≤ l ≤ 23	
Reflections collected	26372	
Independent reflections	9484 [R(int) = 0.0219]	
Completeness to θ = 25.242 °	99.9%	
Absorption correction	Semi-empirical from equivalents	
Max. and min. transmission	1.00000 and 0.76027	
Refinement method	Full-matrix least-squares on F <sup>2</sup>	
Data / restraints / parameters	9484 / 0 / 516	
Goodness-of-fit on F <sup>2</sup>	0.917	
Final R indices [I > 2σ(I)]	R <sub>1</sub> = 0.0356, wR <sub>2</sub> = 0.1088	
R indices (all data)	R <sub>1</sub> = 0.0398, wR <sub>2</sub> = 0.1136	
Extinction coefficient	n/a	
Largest diff. peak and hole	0.347 and -0.248 e.Å <sup>-3</sup>	

**Appendices: x-ray crystal structure data****Table 10:** Crystal data and structure refinement for [Al(OMe-Acpy)(OBn)] (**23**).

Identification code	mb21	
Empirical formula	C <sub>41</sub> H <sub>44</sub> Al N <sub>3</sub> O <sub>5</sub>	
Formula weight	685.77	
Temperature	100(2) K	
Wavelength	0.71073 Å	
Crystal system	Triclinic	
Space group		
Unit cell dimensions	$a = 10.7965(5) \text{ \AA}$	$\alpha = 105.402(3)^\circ$
	$b = 13.0415(3) \text{ \AA}$	$\beta = 106.483(4)^\circ$
	$c = 13.9563(6) \text{ \AA}$	$\gamma = 98.493(3)^\circ$
Volume	1762.98(13) Å <sup>3</sup>	
Z	2	
Density (calculated)	1.292 Mg/m <sup>3</sup>	
Absorption coefficient	0.108 mm <sup>-1</sup>	
F(000)	728	
Crystal size	0.180 × 0.070 × 0.040 mm <sup>3</sup>	
θ range for data collection	2.294 to 27.485 °	
Index ranges	-14 ≤ h ≤ 12, -16 ≤ k ≤ 16, -18 ≤ l ≤ 18	
Reflections collected	30392	
Independent reflections	8046 [R(int) = 0.0337]	
Completeness to θ = 25.242 °	99.9%	
Absorption correction	Semi-empirical from equivalents	
Max. and min. transmission	1.00000 and 0.89491	
Refinement method	Full-matrix least-squares on F <sup>2</sup>	
Data / restraints / parameters	8046 / 0 / 457	
Goodness-of-fit on F <sup>2</sup>	1.021	
Final R indices [I > 2σ(I)]	R <sub>1</sub> = 0.0419, wR <sub>2</sub> = 0.0939	
R indices (all data)	R <sub>1</sub> = 0.0577, wR <sub>2</sub> = 0.1007	
Extinction coefficient	n/a	
Largest diff. peak and hole	0.292 and -0.274 e.Å <sup>-3</sup>	

**Table 11:** Crystal data and structure refinement for [Al(salpy)Cl] (**24**).

**Appendices: x-ray crystal structure data**

Identification code	mb14
Empirical formula	C <sub>27</sub> H <sub>29</sub> Al Cl N <sub>3</sub> O <sub>3</sub>
Formula weight	505.96
Temperature	100(2) K
Wavelength	0.71073 Å
Crystal system	Monoclinic
Space group	<i>P</i> 2 <sub>1</sub> / <i>c</i>
Unit cell dimensions	$a = 13.0125(9) \text{ \AA}$ $\alpha = 90^\circ$ $b = 16.6777(9) \text{ \AA}$ $\beta = 96.739(6)^\circ$ $c = 11.2050(6) \text{ \AA}$ $\gamma = 90^\circ$
Volume	2414.9(2) Å <sup>3</sup>
Z	4
Density (calculated)	1.392 Mg/m <sup>3</sup>
Absorption coefficient	0.231 mm <sup>-1</sup>
F(000)	1064
Crystal size	0.042 × 0.024 × 0.015 mm <sup>3</sup>
θ range for data collection	2.200 to 27.509 °
Index ranges	-16 ≤ h ≤ 16, -21 ≤ k ≤ 21, -13 ≤ l ≤ 14
Reflections collected	29147
Independent reflections	5521 [R(int) = 0.2451]
Completeness to θ = 25.242 °	99.7%
Absorption correction	Semi-empirical from equivalents
Max. and min. transmission	1.000 and 0.862
Refinement method	Full-matrix least-squares on F <sup>2</sup>
Data / restraints / parameters	5521 / 0 / 317
Goodness-of-fit on F <sup>2</sup>	1.010
Final R indices [I > 2σ(I)]	R <sub>1</sub> = 0.0839, wR <sub>2</sub> = 0.1539
R indices (all data)	R <sub>1</sub> = 0.1738, wR <sub>2</sub> = 0.1816
Extinction coefficient	n/a
Largest diff. peak and hole	0.399 and -0.364 e.Å <sup>-3</sup>

**Appendices: x-ray crystal structure data****Table 12:** Crystal data and structure refinement for [Al(<sup>t</sup>Bu, OCH<sub>3</sub> - salpy)Cl] (**27**).

Identification code	mb18	
Empirical formula	C <sub>33</sub> H <sub>41</sub> AlClN <sub>3</sub> O <sub>4</sub>	
Formula weight	606.12	
Temperature	100(2) K	
Wavelength	0.71073 Å	
Crystal system	Monoclinic	
Space group	P2 <sub>1</sub> /n	
Unit cell dimensions	$a = 13.7831(5) \text{ \AA}$	$\alpha = 90^\circ$
	$b = 15.9862(6) \text{ \AA}$	$\beta = 111.000(5)^\circ$
	$c = 14.7018(7) \text{ \AA}$	$\gamma = 90^\circ$
Volume	3024.2(2) Å <sup>3</sup>	
Z	4	
Density (calculated)	1.331 Mg/m <sup>3</sup>	
Absorption coefficient	0.199 mm <sup>-1</sup>	
F(000)	1288	
Crystal size	0.190 × 0.110 × 0.010 mm <sup>3</sup>	
θ range for data collection	1.956 to 25.027 °	
Index ranges	-16 ≤ h ≤ 16, -16 ≤ k ≤ 19, -17 ≤ l ≤ 17	
Reflections collected	28025	
Independent reflections	5330 [R(int) = 0.0560]	
Completeness to θ = 25.027 °	99.9%	
Absorption correction	Semi-empirical from equivalents	
Max. and min. transmission	1.00000 and 0.91360	
Refinement method	Full-matrix least-squares on F <sup>2</sup>	
Data / restraints / parameters	5330 / 78 / 408	
Goodness-of-fit on F <sup>2</sup>	1.259	
Final R indices [I > 2σ(I)]	R <sub>1</sub> = 0.0683, wR <sub>2</sub> = 0.1318	
R indices (all data)	R <sub>1</sub> = 0.0911, wR <sub>2</sub> = 0.1387	
Extinction coefficient	n/a	
Largest diff. peak and hole	0.327 and -0.331 e.Å <sup>-3</sup>	

**Table 13:** Crystal data and structure refinement for [Al(Ad, CH<sub>3</sub> - salpy)Cl] (**28**).

**Appendices: x-ray crystal structure data**

Identification code	mb19	
Empirical formula	C <sub>59</sub> H <sub>69</sub> Al Cl N <sub>3</sub> O <sub>2</sub>	
Formula weight	914.60	
Temperature	100(2) K	
Wavelength	0.71073 Å	
Crystal system	Triclinic	
Space group		
Unit cell dimensions	$a = 12.1910(2) \text{ \AA}$	$\alpha = 109.5180(10)$
°	$b = 20.0085(3) \text{ \AA}$	$\beta = 91.0170(10)$
°	$c = 23.1399(3) \text{ \AA}$	$\gamma = 102.3010(10)$
Volume	5173.59(14) Å <sup>3</sup>	
Z	4	
Density (calculated)	1.174 Mg/m <sup>3</sup>	
Absorption coefficient	0.135 mm <sup>-1</sup>	
F(000)	1960	
Crystal size	0.150 × 0.090 × 0.030 mm <sup>3</sup>	
θ range for data collection	1.820 to 27.484 °	
Index ranges	-15 ≤ h ≤ 15, -25 ≤ k ≤ 25, -30 ≤ l ≤ 30	
Reflections collected	67370	
Independent reflections	23548 [R(int) = 0.0238]	
Completeness to θ = 25.242 °	99.9%	
Refinement method	Full-matrix least-squares on F <sup>2</sup>	
Data / restraints / parameters	23548 / 558 / 1323	
Goodness-of-fit on F <sup>2</sup>	0.999	
Final R indices [I > 2σ(I)]	R <sub>1</sub> = 0.0519, wR <sub>2</sub> = 0.1434	
R indices (all data)	R <sub>1</sub> = 0.0685, wR <sub>2</sub> = 0.1564	
Extinction coefficient	n/a	
Largest diff. peak and hole	0.670 and -0.411 e.Å <sup>-3</sup>	

**Appendices: x-ray crystal structure data****Table 14:** Crystal data and structure refinement for [Al(<sup>t</sup>Bu, OCH<sub>3</sub> - salpn)Cl] (**29**).

Identification code	mb29	
Empirical formula	C <sub>27</sub> H <sub>36</sub> Al Cl N <sub>2</sub> O <sub>4</sub>	
Formula weight	515.01	
Temperature	100(2) K	
Wavelength	0.71073 Å	
Crystal system	Triclinic	
Space group		
Unit cell dimensions	$a = 10.1805(2) \text{ \AA}$	$\alpha = 92.552(2)^\circ$
	$b = 16.4737(4) \text{ \AA}$	$\beta = 104.599(2)^\circ$
	$c = 16.5861(4) \text{ \AA}$	$\gamma = 90.782(2)^\circ$
Volume	2688.29(11) Å <sup>3</sup>	
Z	4	
Density (calculated)	1.272 Mg/m <sup>3</sup>	
Absorption coefficient	0.210 mm <sup>-1</sup>	
F(000)	1096	
Crystal size	0.250 × 0.110 × 0.100 mm <sup>3</sup>	
θ range for data collection	2.068 to 27.484 °	
Index ranges	-13 ≤ h ≤ 11, -21 ≤ k ≤ 20, -21 ≤ l ≤ 21	
Reflections collected	33003	
Independent reflections	12110 [R(int) = 0.0289]	
Completeness to θ = 25.242 °	99.2%	
Absorption correction	Semi-empirical from equivalents	
Max. and min. transmission	1.00000 and 0.79467	
Refinement method	Full-matrix least-squares on F <sup>2</sup>	
Data / restraints / parameters	12110 / 0 / 647	
Goodness-of-fit on F <sup>2</sup>	1.001	
Final R indices [I > 2σ(I)]	R <sub>1</sub> = 0.0414, wR <sub>2</sub> = 0.1107	
R indices (all data)	R <sub>1</sub> = 0.0505, wR <sub>2</sub> = 0.1164	
Extinction coefficient	n/a	
Largest diff. peak and hole	0.385 and -0.377 e.Å <sup>-3</sup>	

**Appendices: x-ray crystal structure data****Table 15:** Crystal data and structure refinement for [Ti(Ad, CH<sub>3</sub> - salpy)(OiPr)<sub>2</sub>] (**35**).

Identification code	mb38	
Empirical formula	C <sub>51</sub> H <sub>67</sub> N <sub>3</sub> O <sub>4</sub> Ti	
Formula weight	833.97	
Temperature	150(2) K	
Wavelength	1.54184 Å	
Crystal system	Triclinic	
Space group		
Unit cell dimensions	$a = 13.0164(5) \text{ \AA}$	$\alpha = 106.603(3)^\circ$
	$b = 13.1649(6) \text{ \AA}$	$\beta = 95.619(3)^\circ$
	$c = 14.8850(4) \text{ \AA}$	$\gamma = 109.641(4)^\circ$
Volume	2248.34(16) Å <sup>3</sup>	
Z	2	
Density (calculated)	1.232 Mg/m <sup>3</sup>	
Absorption coefficient	1.980 mm <sup>-1</sup>	
F(000)	896	
Crystal size	0.251 × 0.105 × 0.087 mm <sup>3</sup>	
θ range for data collection	3.692 to 67.062 °	
Index ranges	-15 ≤ h ≤ 15, -15 ≤ k ≤ 15, -17 ≤ l ≤ 17	
Reflections collected	34157	
Independent reflections	7955 [R(int) = 0.1080]	
Completeness to θ = 67.062 °	99.1%	
Absorption correction	Gaussian	
Max. and min. transmission	0.983 and 0.948	
Refinement method	Full-matrix least-squares on $F^2$	
Data / restraints / parameters	7955 / 0 / 539	
Goodness-of-fit on $F^2$	1.037	
Final R indices [ $I > 2\sigma(I)$ ]	$R_1 = 0.0677$ , $wR_2 = 0.1746$	
R indices (all data)	$R_1 = 0.0952$ , $wR_2 = 0.2045$	
Extinction coefficient	n/a	
Largest diff. peak and hole	0.991 and -0.696 e.Å <sup>-3</sup>	

**Appendices:** x-ray crystal structure data

**Table 16:** Crystal data and structure refinement for [Ti(<sup>t</sup>Bu, OCH<sub>3</sub> - salpn)(O<sup>i</sup>Pr)<sub>2</sub>] (**36**).

Identification code	mb35	
Empirical formula	C <sub>33</sub> H <sub>50</sub> N <sub>2</sub> O <sub>6</sub> Ti	
Formula weight	618.65	
Temperature	150(2) K	
Wavelength	1.54178 Å	
Crystal system	Triclinic	
Space group		
Unit cell dimensions	$a = 10.4827(4) \text{ \AA}$	$\alpha = 95.229(3)^\circ$
	$b = 11.7094(5) \text{ \AA}$	$\beta = 96.206(3)^\circ$
	$c = 15.2881(5) \text{ \AA}$	$\gamma = 115.427(4)^\circ$
Volume	1664.96(12) Å <sup>3</sup>	
Z	2	
Density (calculated)	1.234 Mg/m <sup>3</sup>	
Absorption coefficient	2.531 mm <sup>-1</sup>	
F(000)	664	
Crystal size	0.359 x 0.283 x 0.102 mm <sup>3</sup>	
$\theta$ range for data collection	4.230 to 74.092 °	
Index ranges	$-13 \leq h \leq 13, -14 \leq k \leq 14, -18 \leq l \leq 18$	
Reflections collected	28293	
Independent reflections	6592 [R(int) = 0.0450]	
Completeness to $\theta = 67.679^\circ$	99.9%	
Absorption correction	Semi-empirical from equivalents	
Max. and min. transmission	1.00000 and 0.70041	
Refinement method	Full-matrix least-squares on $F^2$	
Data / restraints / parameters	6592 / 0 / 391	
Goodness-of-fit on $F^2$	1.010	
Final R indices [ $I > 2\sigma(I)$ ]	$R_1 = 0.0417, wR_2 = 0.1139$	
R indices (all data)	$R_1 = 0.0462, wR_2 = 0.1208$	
Extinction coefficient	n/a	
Largest diff. peak and hole	0.511 and -0.484 e.Å <sup>-3</sup>	

**Appendices: x-ray crystal structure data****Table 17:** Crystal data and structure refinement for [Ti(Cl, Cl - salpy)(O<sup>i</sup>Pr)<sub>2</sub>] (**37**).

Identification code	mb37	
Empirical formula	C <sub>29</sub> H <sub>29</sub> Cl <sub>4</sub> N <sub>3</sub> O <sub>4</sub> Ti	
Formula weight	673.25	
Temperature	150(2) K	
Wavelength	1.54184 Å	
Crystal system	Monoclinic	
Space group	<i>P</i> 2 <sub>1</sub> / <i>n</i>	
Unit cell dimensions	<i>a</i> = 12.6861(5) Å	$\alpha = 90^\circ$
	<i>b</i> = 17.9892(7) Å	$\beta = 114.100(4)^\circ$
	<i>c</i> = 14.8598(5) Å	$\gamma = 90^\circ$
Volume	3095.6(2) Å <sup>3</sup>	
Z	4	
Density (calculated)	1.445 Mg/m <sup>3</sup>	
Absorption coefficient	5.843 mm <sup>-1</sup>	
F(000)	1384	
Crystal size	0.064 × 0.045 × 0.023 mm <sup>3</sup>	
$\theta$ range for data collection	3.877 to 74.294 <sup>∞</sup> .	
Index ranges	-14 ≤ <i>h</i> ≤ 15, -22 ≤ <i>k</i> ≤ 16, -17 ≤ <i>l</i> ≤ 18	
Reflections collected	12364	
Independent reflections	6091 [R(int) = 0.0705]	
Completeness to $\theta = 67.684^\circ$	99.6%	
Absorption correction	Semi-empirical from equivalents	
Max. and min. transmission	1.00000 and 0.65422	
Refinement method	Full-matrix least-squares on <i>F</i> <sup>2</sup>	
Data / restraints / parameters	6091 / 142 / 417	
Goodness-of-fit on <i>F</i> <sup>2</sup>	0.880	
Final R indices [ <i>I</i> > 2 $\sigma$ ( <i>I</i> )]	<i>R</i> <sub>1</sub> = 0.0563, <i>wR</i> <sub>2</sub> = 0.1355	
R indices (all data)	<i>R</i> <sub>1</sub> = 0.0888, <i>wR</i> <sub>2</sub> = 0.1469	
Extinction coefficient	<i>n/a</i>	
Largest diff. peak and hole	0.526 and -0.423 e.Å <sup>-3</sup>	

**Appendices: x-ray crystal structure data****Table 18:** Crystal data and structure refinement for [Ti(Acpy)(O<sup>i</sup>Pr)<sub>2</sub>] (**38**).

Identification code	mb36	
Empirical formula	C <sub>31</sub> H <sub>39</sub> N <sub>3</sub> O <sub>4</sub> Ti	
Formula weight	565.55	
Temperature	150(2) K	
Wavelength	0.71073 Å	
Crystal system	Monoclinic	
Space group	<i>P</i> 2 <sub>1</sub> / <i>c</i>	
Unit cell dimensions	<i>a</i> = 12.3143(4) Å	$\alpha = 90^\circ$
	<i>b</i> = 11.4904(3) Å	$\beta = 100.758(4)^\circ$
	<i>c</i> = 21.2264(8) Å	$\gamma = 90^\circ$
Volume	2950.67(17) Å <sup>3</sup>	
Z	4	
Density (calculated)	1.273 Mg/m <sup>3</sup>	
Absorption coefficient	0.329 mm <sup>-1</sup>	
F(000)	1200	
Crystal size	0.472 x 0.422 x 0.285 mm <sup>3</sup>	
$\theta$ range for data collection	3.425 to 29.890 °	
Index ranges	-17 ≤ <i>h</i> ≤ 15, -15 ≤ <i>k</i> ≤ 15, -21 ≤ <i>l</i> ≤ 26	
Reflections collected	28050	
Independent reflections	7416 [R(int) = 0.0417]	
Completeness to $\theta = 25.242^\circ$	99.8%	
Absorption correction	Gaussian	
Max. and min. transmission	0.995 and 0.991	
Refinement method	Full-matrix least-squares on <i>F</i> <sup>2</sup>	
Data / restraints / parameters	7416 / 212 / 419	
Goodness-of-fit on <i>F</i> <sup>2</sup>	0.993	
Final R indices [ <i>I</i> > 2 $\sigma$ ( <i>I</i> )]	<i>R</i> <sub>1</sub> = 0.0537, <i>wR</i> <sub>2</sub> = 0.1393	
R indices (all data)	<i>R</i> <sub>1</sub> = 0.0757, <i>wR</i> <sub>2</sub> = 0.1591	
Extinction coefficient	n/a	
Largest diff. peak and hole	0.692 and -0.622 e.Å <sup>-3</sup>	

**Appendices: x-ray crystal structure data****Table 19:** Crystal data and structure refinement for [Ti(OCH<sub>3</sub>-Acpy)(O<sup>i</sup>Pr)<sub>2</sub>] (**39**).

Identification code	mb31	
Empirical formula	C <sub>33</sub> H <sub>43</sub> N <sub>3</sub> O <sub>6</sub> Ti	
Formula weight	625.60	
Temperature	100(2) K	
Wavelength	0.71073 Å	
Crystal system	Monoclinic	
Space group	<i>P</i> 2 <sub>1</sub> / <i>n</i>	
Unit cell dimensions	<i>a</i> = 14.0305(4) Å	$\alpha = 90^\circ$
	<i>b</i> = 11.8806(2) Å	$\beta = 104.217(2)^\circ$
	<i>c</i> = 19.1826(5) Å	$\gamma = 90^\circ$
Volume	3099.63(13) Å <sup>3</sup>	
Z	4	
Density (calculated)	1.341 Mg/m <sup>3</sup>	
Absorption coefficient	0.325 mm <sup>-1</sup>	
F(000)	1328	
Crystal size	0.110 × 0.050 × 0.020 mm <sup>3</sup>	
$\theta$ range for data collection	2.276 to 27.485 °	
Index ranges	-18 ≤ <i>h</i> ≤ 18, -15 ≤ <i>k</i> ≤ 14, -24 ≤ <i>l</i> ≤ 24	
Reflections collected	45054	
Independent reflections	7091 [R(int) = 0.0469]	
Completeness to $\theta = 25.242^\circ$	99.8 %	
Absorption correction	Semi-empirical from equivalents	
Max. and min. transmission	1.00000 and 0.71858	
Refinement method	Full-matrix least-squares on F <sup>2</sup>	
Data / restraints / parameters	7091 / 0 / 397	
Goodness-of-fit on F <sup>2</sup>	1.012	
Final R indices [ <i>I</i> > 2 $\sigma$ ( <i>I</i> )]	<i>R</i> <sub>1</sub> = 0.0394, <i>wR</i> <sub>2</sub> = 0.0894	
R indices (all data)	<i>R</i> <sub>1</sub> = 0.0550, <i>wR</i> <sub>2</sub> = 0.0962	
Extinction coefficient	<i>n/a</i>	
Largest diff. peak and hole	0.361 and -0.379 e.Å <sup>-3</sup>	

**Appendices: x-ray crystal structure data****Table 20:** Crystal data and structure refinement for [Al<sub>2</sub>(<sup>t</sup>Bu,<sup>t</sup>Bu-Salpy)Me<sub>4</sub>] (**41**).

Identification code	mb40	
Empirical formula	C <sub>43</sub> H <sub>65</sub> Al <sub>2</sub> N <sub>3</sub> O <sub>2</sub>	
Formula weight	709.94	
Temperature	100(2) K	
Wavelength	1.54178 Å	
Crystal system	Monoclinic	
Space group	<i>P</i> 2 <sub>1</sub> / <i>c</i>	
Unit cell dimensions	<i>a</i> = 15.4806(2) Å	$\alpha = 90^\circ$
°	<i>b</i> = 22.1794(3) Å	$\beta = 103.3290(10)$
	<i>c</i> = 12.9741(2) Å	$\gamma = 90^\circ$
Volume	4334.66(11) Å <sup>3</sup>	
Z	4	
Density (calculated)	1.088 Mg/m <sup>3</sup>	
Absorption coefficient	0.874 mm <sup>-1</sup>	
F(000)	1544	
Crystal size	0.200 × 0.200 × 0.050 mm <sup>3</sup>	
$\theta$ range for data collection	3.547 to 70.103 °	
Index ranges	-18 ≤ <i>h</i> ≤ 18, -27 ≤ <i>k</i> ≤ 27, -15 ≤ <i>l</i> ≤ 15	
Reflections collected	14798	
Independent reflections	14798 [R(int) = 0.0508]	
Completeness to $\theta = 67.679^\circ$	100.0%	
Absorption correction	Semi-empirical from equivalents	
Max. and min. transmission	1.00000 and 0.67291	
Refinement method	Full-matrix least-squares on <i>F</i> <sup>2</sup>	
Data / restraints / parameters	14798 / 0 / 469	
Goodness-of-fit on <i>F</i> <sup>2</sup>	1.017	
Final R indices [ <i>I</i> > 2 $\sigma$ ( <i>I</i> )]	<i>R</i> <sub>1</sub> = 0.0456, <i>wR</i> <sub>2</sub> = 0.1300	
R indices (all data)	<i>R</i> <sub>1</sub> = 0.0485, <i>wR</i> <sub>2</sub> = 0.1321	
Extinction coefficient	n/a	
Largest diff. peak and hole	0.341 and -0.293 e.Å <sup>-3</sup>	

**Appendices: x-ray crystal structure data****Table 21:** Crystal data and structure refinement for [Al<sub>2</sub>(Ad,Me-Salpy)Me<sub>4</sub>] (**42**).

Identification code	mb28	
Empirical formula	C <sub>52</sub> H <sub>68</sub> Al <sub>2</sub> N <sub>3</sub> O <sub>2</sub>	
Formula weight	821.05	
Temperature	100(2) K	
Wavelength	0.71073 Å	
Crystal system	Triclinic	
Space group		
Unit cell dimensions	$a = 10.8773(2) \text{ \AA}$	$\alpha = 101.810(2)^\circ$
	$b = 12.7104(3) \text{ \AA}$	$\beta = 95.097(2)^\circ$
	$c = 18.7371(3) \text{ \AA}$	$\gamma = 111.723(2)^\circ$
Volume	2316.67(9) Å <sup>3</sup>	
Z	2	
Density (calculated)	1.177 Mg/m <sup>3</sup>	
Absorption coefficient	0.106 mm <sup>-1</sup>	
F(000)	886	
Crystal size	0.240 × 0.150 × 0.060 mm <sup>3</sup>	
θ range for data collection	1.784 to 27.484 °	
Index ranges	-14 ≤ h ≤ 13, -16 ≤ k ≤ 16, -24 ≤ l ≤ 23	
Reflections collected	34806	
Independent reflections	10468 [R(int) = 0.0242]	
Completeness to θ = 25.242 °	99.4%	
Absorption correction	Semi-empirical from equivalents	
Max. and min. transmission	1.00000 and 0.96002	
Refinement method	Full-matrix least-squares on F <sup>2</sup>	
Data / restraints / parameters	10468 / 0 / 539	
Goodness-of-fit on F <sup>2</sup>	1.031	
Final R indices [I > 2σ(I)]	R <sub>1</sub> = 0.0547, wR <sub>2</sub> = 0.1480	
R indices (all data)	R <sub>1</sub> = 0.0703, wR <sub>2</sub> = 0.1588	
Extinction coefficient	n/a	
Largest diff. peak and hole	0.455 and -0.292 e.Å <sup>-3</sup>	

**Appendices: x-ray crystal structure data****Table 22:** Crystal data and structure refinement for [Al<sub>2</sub>(<sup>t</sup>Bu,OMe-salpn)Me<sub>4</sub>] (**43**).

Identification code	mb39	
Empirical formula	C <sub>31</sub> H <sub>48</sub> Al <sub>2</sub> N <sub>2</sub> O <sub>4</sub>	
Formula weight	566.67	
Temperature	100(2) K	
Wavelength	1.54178 Å	
Crystal system	Monoclinic	
Space group	<i>P</i> 2 <sub>1</sub> / <i>n</i>	
Unit cell dimensions	<i>a</i> = 11.9678(2) Å	$\alpha = 90^\circ$
	<i>b</i> = 12.4409(2) Å	$\beta = 92.799(2)^\circ$
	<i>c</i> = 21.5489(4) Å	$\gamma = 90^\circ$
Volume	3204.59(10) Å <sup>3</sup>	
Z	4	
Density (calculated)	1.175 Mg/m <sup>3</sup>	
Absorption coefficient	1.101 mm <sup>-1</sup>	
F(000)	1224	
Crystal size	0.200 × 0.050 × 0.020 mm <sup>3</sup>	
$\theta$ range for data collection	4.104 to 70.112 °	
Index ranges	-14 ≤ <i>h</i> ≤ 14, -15 ≤ <i>k</i> ≤ 15, -26 ≤ <i>l</i> ≤ 25	
Reflections collected	10499	
Independent reflections	10499 [R(int) = 0.1401]	
Completeness to $\theta = 67.679^\circ$	100.0%	
Absorption correction	Semi-empirical from equivalents	
Max. and min. transmission	1.00000 and 0.89848	
Refinement method	Full-matrix least-squares on <i>F</i> <sup>2</sup>	
Data / restraints / parameters	10499 / 0 / 365	
Goodness-of-fit on <i>F</i> <sup>2</sup>	1.044	
Final R indices [ <i>I</i> > 2σ( <i>I</i> )]	<i>R</i> <sub>1</sub> = 0.0356, <i>wR</i> <sub>2</sub> = 0.1103	
R indices (all data)	<i>R</i> <sub>1</sub> = 0.0388, <i>wR</i> <sub>2</sub> = 0.1147	
Extinction coefficient	<i>n/a</i>	
Largest diff. peak and hole	0.288 and -0.270 e.Å <sup>-3</sup>	